THE JOURNAL
OF
CHEMICAL PHYSICS

VOLUME 32, NUMBER 6 JUNE, 1960

Comparison of n and s as Fall-Off Parameters in the Slater and Rice-Ramsperger-Kassel Classical Theories of Unimolecular Reaction

E. W. SCHLAG

Yerkes Research Laboratory, E. I. du Pont de Nemours and Company, Inc., Buffalo, New York

AND

B. S. RABINOVITCH AND F. W. SCHNEIDER

Department of Chemistry, University of Washington, Seattle, Washington

(Received November 12, 1959)

The classical Rice-Ramsperger-Kassel integral for the unimolecular rate constant has been evaluated over a range of s values at the several values of $b=32$, 36, 40 and 44. Equivalent values of s and of the Slater theory parameter n have been found by comparison of the shape of the fall-off behavior predicted by both theories in the upper region of fall-off. The equivalence diverges from the limiting relation $n=2s-1$ even below $n=8$. The findings are discussed briefly.

IN this paper we consider a formal correspondence between the conventional classical formulations of the Rice-Ramsperger-Kassel[1] and Slater[2] equations for the unimolecular rate constant, and the description of fall-off behavior which they afford. Despite any theoretical inadequacies, these treatments are of particular practical importance as representing the form in which these theories have been most widely applied to the interpretation of experimental data. The comparison to be made here is not possible for the quantum formulations of these theories.

The Kassel equation may be written

$$I_s(\theta')=k/k_\infty=[\Gamma(s)]^{-1}\int_0^\infty \frac{x^{s-1}e^{-x}dx}{1+[x/(b+x)]^{s-1}\theta'^{-1}}; \quad (1)$$

and the Slater equation (for the conventional "random-gap" assumption) is

$$I_n(\theta)=k/k_\infty=\{\Gamma[(n+1)/2)]\}^{-1}\int_0^\infty \frac{x^{(n-1)/2}e^{-x}dx}{1+x^{(n-1)/2}\theta^{-1}}, \quad (2)$$

where $s=$ the effective number of oscillators contributing to dissociation in Kassel theory; $n=$ the effective number of normal vibration modes which contribute to extension of the reaction coordinate in Slater theory; $\theta'=\omega/A$, where A may be identified with ν; $\theta=(\omega/\nu)\cdot b^{(n-1)/2}\cdot f_n$; $b=E_0/RT$; and all other quantities have their customary significance. As was pointed out by Slater, these equations are of the same form when $(b+x)$ is replaced in (1) by the approximation b; and (if b^{s-1} were formally incorporated into θ') the equations have equal magnitude apart from a small effect in f_n when $s=(n+1)/2$; the approximation to $(b+x)$ and the correspondence between the equations is accurate for large b, small s, and hence small n, and not too small ω and hence not too small $I_n(\theta)$.[2a]

It is noted from (1) and (2) that s and n constitute parameters whose magnitude determines the *shape* of the fall-off with pressure p (although not the absolute value of a particular fall-off pressure). For Eq. (1) the shape of the fall-off predicted by the s parameter must be calculated anew for each possible value of b (unless the condition $b\gg sRT$ holds). The correspondence of Eqs. (1) and (2) with respect to shape of the predicted fall-off is independent of quantity f_n, which only affects the absolute correspondence between p and θ.

Experimental studies of unimolecular reactions have, unfortunately, their well-known inaccuracies, and the shape of fall-off curves is not the quality most accurately determined. Nonetheless, as a matter both of principle and of practical import, it appears worthwhile

[1] L. S. Kassel, *Kinetics of Homogeneous Gas Reactions* (Reinhold Publishing Corporation, New York, 1932).

[2] (a) N. B. Slater, Phil. Trans. Roy. Soc. (London) **A246**, 57 (1953); (b) N. B. Slater, *Theory of Unimolecular Reactions* (Cornell University Press, Ithaca, New York, 1959), pp. 150, 157, 174.

Copyright © 1960 by the American Institute of Physics

TABLE I. $I_s(\theta')$.

$-\log\theta'$ \ s / b	3				7				11			
	32	36	40	44	32	36	40	44	32	36	40	44
11.0											0.0029	0.0053
10.0									0.0037	0.0077	0.0144	0.0245
9.0							0.0022	0.0034	0.0186	0.0348	0.0587	0.0908
8.0					0.0051	0.0085	0.0131	0.0191	0.0751	0.124	0.186	0.258
7.0					0.0283	0.0439	0.0633	0.0867	0.232	0.332	0.437	0.538
6.0					0.122	0.170	0.224	0.281	0.516	0.637	0.737	0.814
5.0	0.0046	0.0057	0.0069	0.0083	0.367	0.454	0.536	0.609	0.809	0.882	0.929	0.957
4.0	0.0387	0.0467	0.0551	0.0637	0.713	0.786	0.841	0.883	0.959	0.979	0.989	0.994
3.0	0.209	0.239	0.268	0.297	0.934	0.957	0.972	0.981	0.995	0.997		
2.0	0.620	0.660	0.695	0.725	0.991	0.995	0.997	0.998				
1.0	0.924	0.937	0.947	0.954								
0	0.991	0.993	0.994	0.995								

$-\log\theta'$ \ s / b	15				21				26			
	32	36	40	44	32	36	40	44	32	36	40	44
14.0											0.0133	0.0333
13.0							0.0146	0.0324		0.0176	0.0463	0.0988
12.0				0.0132		0.0224	0.0513	0.0992	0.0219	0.0610	0.133	0.240
11.0		0.0131	0.0270	0.0494	0.0322	0.0761	0.148	0.246	0.0757	0.171	0.307	0.465
10 0	0.0243	0.0509	0.0922	0.149	0.106	0.208	0.339	0.482	0.210	0.378	0.559	0.716
9 0	0.0879	0.158	0.248	0.352	0.276	0.441	0.602	0.738	0.448	0.647	0.800	0.897
8.0	0.248	0.376	0.507	0.628	0.544	0.714	0.836	0.913	0.724	0.865	0.941	0.976
7.0	0.520	0.664	0.778	0.860	0.806	0.906	0.958	0.982	0.913	0.968	0.989	0.996
6.0	0.799	0.887	0.940	0.968	0.951	0.982	0.993	0.997	0.984	0.995		
5.0	0.951	0 978	0.990	0.995	0.992							
4.0	0.993	0.997										

to explore the relation of s and n as fall-off parameters in more detail, and to clarify the region of validity of the approximation noted by Slater, as far as fall-off behavior is concerned.

$I_s(\theta')$ has been evaluated over a range of θ' for various s by numerical integration using quadrature with a Bendix G-15 digital computer; some values were checked by an independent program on an IBM 650 computer. The values are tabulated in Table I. Previously,[3] $I_n(\theta)$ has been evaluated for various n and θ supplemental to values given by Slater.[2a] Plots of log k/k_∞ vs log ω in the two theories were compared by superposition. Confining attention to comparison of the shape of fall-off predicted by both equations[4,5] in the upper region of $k/k_\infty > 0.08$ encountered most frequently experimentally, (and without regard to the matter of the theoretically predicted magnitudes of p for a particular region of fall-off), the following relation between n and s is found. For $b=40$, a value within the limited range commonly observed in conventional thermal studies, $s=(n+1)/2$ up to $s\sim 4$; above this s increases more rapidly for the same fall-off behavior, and at s around 18, $n=s$. Comparisons were not extended appreciably beyond this value; the approximations inherent in the Slater equation itself[2b] make the exact numerical values derived from it uncertain at n values appreciably above 15; although the qualitative conclusion that $n<s$ for higher s cannot be in doubt, and has its basis primarily in the $(b+x)^{s-1}$ term of Eq. (1).

The comparison of the two parameters is usefully accentuated, despite the reduced reliability of Eq. (2) at low b values,[2a] by comparing the s and n equivalent fall-off values at $b=10$. The relationship between s and n for the various values of b is summarized in Fig. 1.

Formal criteria of a gross nature concerning the relative validity of the classical Slater and Kassel treatments, applicable to certain cases and based on these fall-off considerations, may be stated. For simple molecules, hence n small, Kassel's s is constrained to be $\leq(t+1)/2$ (where t is the total number of vibration modes of the molecule) according to the Slater prediction; an experimental finding of $s>(t+1)/2$ would require $n>t$ and signify failure of the Slater postulates, according to this criterion. For complex molecules, on the other hand, a value of $n\sim t$ where t is large, if found experimentally,[6] could force $s>t$.

An additional criterion suitable for complex molecules exists in the variation of fall-off behavior with change in temperature. Both theories predict a shift in

[3] E. W. Schlag, Ph.D. thesis, University of Washington, 1958; see reference 2(b), p. 169.

[4] The curvature given by the two equations is not identical, of course, but substantial equivalence over the range of k/k_∞ concerned may be readily found; the correspondence between s and n is of accuracy ± 1 in n.

[5] Use of values computed at several n, including $n=11$ given by Slater, for the "gamma-type" gap distribution of Slater theory [reference 2(b), p. 201], reveals an increase in curvature with respect to the conventional theory which corresponds uniformly to a value of n_T which is 1–2 units larger.

[6] For possible example see B. S. Rabinovitch and K. W. Michel, J. Am. Chem. Soc. 81, 5065 (1959). Although $n=28$ was found formally, all that can probably be asserted with confidence is that $n>20$.

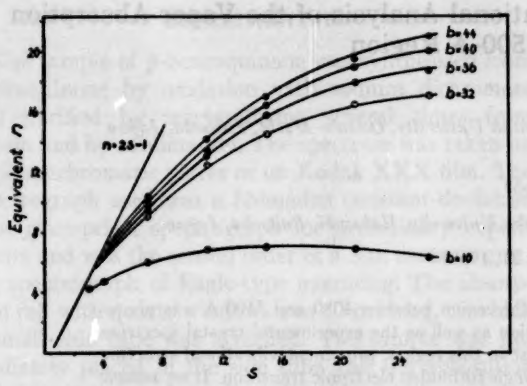

FIG. 1. Relation between the values of s and n which give comparable fall-off behavior, as compared in the upper region of k/k_∞. Deviation of some points of comparison from the smooth curves reflects comparison error.

the pressure corresponding to a given fall-off point, with change of temperature. In addition, the RRK equation predicts a change in curvature with change of temperature or b; increased temperature results in enhanced curvature of the fall-off plot. Unfortunately, there is as yet no data sufficiently extensive or accurate for test.

The comparison of n and s is relevant to the semi-theoretical values of the low-pressure limiting rate constant predicted from fall off, measured in the high-pressure region. The predicted magnitudes are similar in both theories when $s=(n+1)/2$, apart from small factors.[2] For complex molecules in the case of large n, the low-pressure rate constants calculated in both theories will diverge quite appreciably if values of fall-off parameters of the high-pressure region are utilized. N_2O_5 is the only complex molecule for which reasonably accurate measurements of the low-pressure rate, as well as for the higher-pressure region, exist.[7] If[8] n_{exp} is ~14–15, then the Slater formulation gives much better agreement with experiment for calculated values of k_0.[8] If[9] n_{exp} ~11–12, the calculations tend to be more inconclusive.

ACKNOWLEDGMENT

We thank the National Science Foundation for partial support of this work.

[7] H. S. Johnston and J. R. White, J. Chem. Phys. 22, 1969 (1954).
[8] Compare E. K. Gill and K. J. Laidler, Proc. Roy. Soc. (London), 250A, 121 (1959).
[9] R. E. Powell, J. Chem. Phys. 30, 724 (1959).

Electronic States of *p*-Benzoquinone. V. Vibrational Analysis of the Vapor Absorption Spectrum around 4500-A Region

TOSINOBU ANNO*

Chemical Laboratory, General Education Department, Kyushu University, Ootsubo-Machi, Fukuoka, Japan

AND

AKIRA SADÔ†

Department of Chemistry, Faculty of Science, Kyushu University, Hakozaki, Fukuoka, Japan

(Received August 21, 1959)

The absorption spectrum of *p*-benzoquinone vapor in the region between 4080 and 5100 A was photographed and measured. Although the theoretical calculation as well as the experimental crystal spectrum indicate that two singlet-singlet electronic transitions exist in this region, prominent vibrational structure of the vapor spectrum can be interpreted as caused by a single forbidden electronic transition. If we assume that the hydrogen vibrations are not effective as perturbing vibrations which make the forbidden electronic transitions allowed through the vibrational-electronic interaction, this fact suggests the following two sets of assignments for the symmetries of the forbidden transition and the perturbing allowed transition: (1) the spectrum is a superposition of ^1A_u, $^1B_{2u}\leftarrow{}^1A_g$ transitions perturbed by a $^1B_{2u}\leftarrow{}^1A_g$ transition, (2) the spectrum is caused by a *single* $^1B_{1g}\leftarrow{}^1A_g$ transition being allowed through vibrational-electronic interaction with the allowed $^1B_{1u}\leftarrow{}^1A_g$ transition. Vibrational structure alone cannot exclude the second possibility, but a discussion supporting the first assignment is given. This assignment (1) is in agreement with the theoretical calculation of the energy levels. Most prominent bands are assigned to particular vibronic transitions. Fundamental frequencies in the excited electronic state 436, 796, 1109, and 1220 cm^{-1} are obtained corresponding probably to the ground-state values of 444, 770, 1144, and 1667 cm^{-1}.

INTRODUCTION

IN the first[1] and second[2] parts of this series we have calculated the energy levels of the *p*-benzoquinone molecule by extending the semiempirical molecular-orbital method of Pariser and Parr to take the nonbonding electrons localized at the oxygen atoms, as well as π electrons, explicitly into the interaction term in the Hamiltonian. These calculations show that the weak absorption band of this molecule, appearing around 4500 A, is a superposition of two transitions, ^1A_u, $^1B_{2g}\leftarrow{}^1A_g$, both of which are n–π transitions forbidden by molecular symmetry but allowed through vibronic interaction with the allowed $^1B_{2u}\leftarrow{}^1A_g$ transition. If this assignment were correct, the spectrum should appear with the transition moment along the long molecular axis (connecting two oxygen atoms). This is in agreement with the spectroscopic studies of crystalline *p*-benzoquinone by Fixl and Schauenstein,[3] Brand and Goodwin,[4] and Sidman.[5] Among these workers Sidman,[5] who used a low temperature of 20°K, found three different n–π transitions in this region and assigned two of them to singlet-singlet transitions However, he has left the symmetries of these transitions unassigned.

The vapor spectrum in the visible region has been studied by Light.[6] He observed about 140 bands between 4000~5000 A and represented it by the following formula:

$$1/\lambda = 21\,013.2 + n\cdot 1110 + p\cdot 662 + q\cdot 35,$$

where n, p, and q are integers running $n=-1\sim+3$, $p=-3\sim+2$ and $q=-11\sim+8$. He considered that all the coefficients of n, p, and q in this formula represented vibrational frequencies of *p*-benzoquinone. However, he was forced to be satisfied by rough considerations on the nature of the vibrations concerned and nothing was mentioned in his paper on the nature of the electronic transitions concerned. More recently, the visible absorption spectrum of *p*-benzoquinone vapor was reinvestigated by Asundi and Singh,[7] but only the brief report containing description of the gross features and the results of analysis has been published.[7] They assigned the absorption to a *single* $^1A_u\leftarrow{}^1A_g$ transition in disagreement with our theoretical calculation and with the low temperature crystal-spectral data.[5] For these reasons, it seems to the present authors that a reinvestigation of the vapor spectrum in the visible region is necessary. It is the purpose of this paper to report the results of this work.

* Present address: Mathematical Institute, Oxford, England.
† Present address: Department of Chemistry, Faculty of Science, Kanazawa University, Kanazawa, Japan.

[1] T. Anno, I. Matubara, and A. Sadô, Bull. Chem. Soc. Japan **30**, 168 (1957).
[2] T. Anno, A. Sadô, and Matubara, J. Chem. Phys. **26**, 967 (1957).
[3] J. O. Fixl and E. Schauenstein, Monatsh. **81**, 598 (1950); Chem. Abstr. **45**, 4136f (1951).
[4] J. C. D. Brand and T. H. Goodwin, Trans. Faraday Soc. **53**, 295 (1957).
[5] J. W. Sidman, J. Am. Chem. Soc. **78**, 2363 (1956); J. Chem. Phys. **27**, 820 (1957).
[6] L. Light, Z. physik. Chem. **122**, 414 (1926).
[7] R. K. Asundi and R. S. Singh, Nature **176**, 1223 (1955).

EXPERIMENTAL

The sample of *p*-benzoquinone was synthesized from hydroquinone by oxidation with sodium dichromate and purified by recrystallizing several times from ligroin and by sublimation. The spectrum was taken on Fuji panchromatic plates or on Kodak XXX film. The spectrograph used was a Shimadzu constant-deviation type glass-prism spectrograph for preliminary experiments and was the second order of a 3-m concave grating spectrograph of Eagle-type mounting. The absorption cell with quartz windows was 40 cm long, to which a small side tube was attached. The sample was immediately placed in the side tube and the absorption cell was evacuated, cooling the side arm by using a freezing mixture of ice and sodium chloride to prevent the *p*-benzoquinone sample from sublimation, and sealed off. The temperature of the absorption cell was controlled between 80° and 160°C in the manner described elsewhere.[8] A tungsten lamp was used as a continuous light source, and an iron arc supplied a comparison spectrum. The wavelength was determined by using a comparator supplied by Rikagaku Kenkyusho (Institute for Physical and Chemical Research). The relative intensities of absorption bands were determined visually or by using a microphotometer supplied by the Institute.

RESULTS

The "visible" absorption spectrum of *p*-benzoquinone appears in the region between 4080–5100 A. Figure 1 shows the microphotometer tracing of the spectrogram, and Table I contains the measured frequencies and relative intensities of main absorption bands together with their interpretation. From the comparion of this table with Table 24 in Light's paper,[6] it can be seen that the present observation extends through a wider region than that of Light.[6] The bands near the "origin" of the absorption system are fairly sharp and have heads on the violet side. Our observation concerning the band degradation confirms the description of Light[6] but is in contradiction with that of Asundi and Singh.[7] The measured wave number values of stronger bands agree with those reported by Light[6] to within 2∼5 cm^{-1}. On a plate taken at 80°C six band groups appear. Each of these groups consists of several absorption bands probably forming pairs, although some components of these pairs are missing, probably on account of their low intensities. The band pairs (or stronger components of band pairs) of longest wavelength of these six groups are: 22 034/043 (A_0), 22 470/480 (B_0), 22 839 (C_0), 23 152 (A_1), 23 586 (B_1), 23 954 cm^{-1} (C_1). With increasing temperature of the absorption cell another group of bands appear on the red side of A_0 with the separation of 1068 cm^{-1} (D_0). On further increasing the temperature, the bands become very much broadened and overlapped, so that the spectrum appears almost continuous.

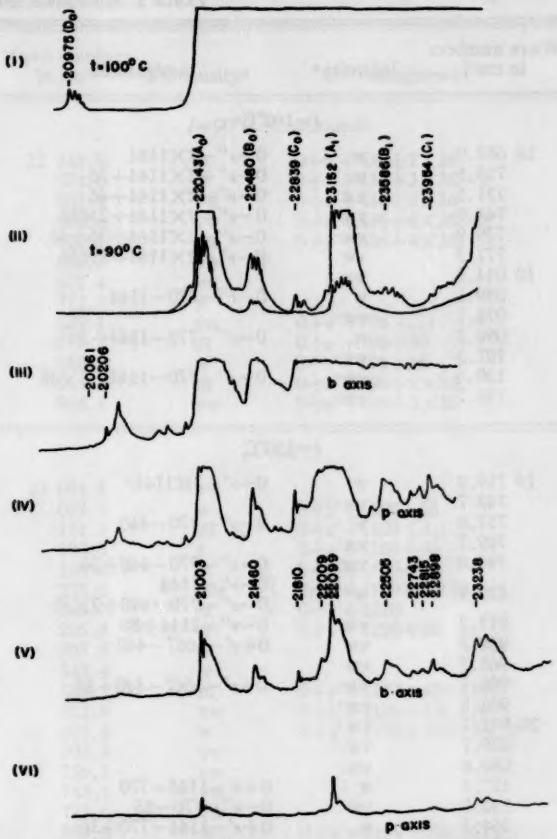

FIG. 1. Microphotometer tracings of the visible absorption spectrum of *p*-benzoquinone. (I) and (II) are in vapor; (III)–(VI) are in crystalline state (from reference 5, error in selecting crystal axes having been corrected).

THEORETICAL CONSIDERATIONS

Assuming the V_h structure of *p*-benzoquinone,[9,10] we take the axis connecting the two oxygen atoms as the *y* axis and the molecular plane as the *xy* plane. Then the symmetry notations are the same as those given by Herzberg.[11] This system of designation of coordinate axes differs from that recommended by Mulliken[12] but is adopted here for consistency with previous parts of this series.

Transitions from the ground A_g state to B_{2u} and B_{3u} states are allowed to appear with transition moments along the *y* and the *x* axes (both lying in the molecular plane), respectively, while the transitions to the B_{1u} state appear with moment along the *z* axis (perpendicu-

[8] T. Anno and I. Matubara, J. Chem. Phys. **23**, 796 (1955).

[9] J. M. Robertson, Proc. Roy. Soc. (London) **A150**, 106 (1935).
[10] S. M. Swingle, J. Am. Chem. Soc. **76**, 1409 (1954).
[11] G. Herzberg, *Infrared and Raman Spectra of Polyatomic Molecules* (D. Van Nostrand Company, New York, 1945), p. 108.
[12] R. S. Mulliken, J. Chem. Phys. **23**, 1997 (1955), **24**, 1118 (1956).

TABLE I. Absorption bands of *p*-benzoquinone vapor.

Wave numbers in cm^{-1}	Intensity[a]	Assignment
	$t=160°C$	
18 682.0	w	$0-\nu''-2\times1144$
713.5	w	$0-\nu''-2\times1144+36$
731.5	vw	$0-\nu''-2\times1144+46$
744.0	vw	$0-\nu''-2\times1144+2\times36$
759.9	vw	$0-\nu''-2\times1144+36+46$
777.2	vw	$0-\nu''-2\times1144+3\times36$
19 044.5	vw	
059.1	w	$0-\nu''-770-1144$
074.1	vw	
096.2	w	$0-\nu''-770-1144+36$
107.3	vw	
130.6	vw	$0-\nu''-770-1144+2\times36$
138.7	vw	
	$t=150°C$	
19 719.9	w	$0+\nu'-2\times1144$?
742.7	vw	
757.0	w	$0-\nu''-770-440$
769.7	vw	
794.0	vw	$0-\nu''-770-440+36$
829.9	w	$0-\nu''-1144$ and $0-\nu''-770-440+2\times36$
917.2	vw	$0-\nu''-1144+80$
950.3	vw	$0+\nu'-1667-440$
961.5	vw	
986.8	vw	$0+\nu'-1667-440+36$
994.8	vw	
20 032.7	vw	
039.7	vw	
086.6	vw	
127.1	w	$0+\nu'-1144-770$
136.0	vw	$0-\nu''-770-65$
164.3	w	$0+\nu'-1144-770+36$
174.4	w	$0-\nu''-770-65+36$
201.6	m	$0-\nu''-770$
237.1	w	$0-\nu''-770+36$
246.8	w	$0-\nu''-770+46$
271.8	w	$0-\nu''-770+2\times36$
281.5	w	$0-\nu''-770+80$
306.9	w	$0-\nu''-770+3\times36$
316.8	w	$0-\nu''-770+36+80$ and $0-\nu''-770+46+2\times36$
323.5	vw	
343.3	vw	
348.7	vw	
386.8	vw	$0+\nu'-1667$
	$t=140°C$	
20 422.2	vw	$0+\nu'-1667+36$
427.2	vw	
449.5	vw	
475.2	vw	
	$t=100°C$	
20 534.9	vw	$0-\nu''-440$
586.6	vw	
623.7	vw	$0-800$
651.9	vw	$0-\nu''+436-770$
658.8	vw	$0-800+36$
686.6	vw	$0-\nu''+436-770+36$
695.9	vw	$0-800+2\times36$
723.1	vw	$0-\nu''+436-770+2\times36$
729.3	vw	$0-800+3\times36$
738.1	vw	
764.5	vw	$0-800+4\times36$
785.8	vw	

Wave numbers in cm^{-1}	Intensity[a]	Assignment
	$t=120°C$	
20 824.5	vw	
828.9	vw	
853.2	vw	
863.0	vw	
872.9	vw	
890.7	vw	
	$t=100°C$	
20 900.2	w	$0+\nu'-1144$
910.2	w	$0-\nu''-65$
936.1	vw	$0+\nu'-1144+36$
941.4	vw	
965.8	w	$0-\nu''-9$
974.9	vs	$0-\nu''$ (D_0)
981.1	vw	
21 009.9	s	$0-\nu''+36$
015.8	w	
021.8	w	$0-\nu''+46$
045.4	m	$0-\nu''+2\times36$
051.8	m	$0-\nu''+80$
059.2	w	$0-\nu''+46+36$
080.3	w	$0-\nu''+3\times36$
086.5	w	$0-\nu''+80+36$
095.8	w	$0-\nu''+46+2\times36$
107.3	vw	
114.6	w	$0-\nu''+4\times36$
121.1	w	$0-\nu''+80+2\times36$
132.7	w	
154.4	w	
169.9	vw	
190.0	w	
228.3	vw	
242.0	vw	
269.3	vw	$0+\nu'-770-9$
278.5	w	$0+\nu'-770$
296.5	vw	
305.6	vw	$0+\nu'-770-9+36$
315.4	vw	$0+\nu'-770+36$
326.1	w	
336.5	vw	$0+\nu'-770+2\times36-9$
352.7	vw	$0+\nu'-770+2\times36$
363.0	vw	
380.7	vw	$0+\nu'-770+3\times36-9$
388.4	vw	$0+\nu'-770+3\times36$
410.7	w	$0-\nu''+436$
416.4	vw	
419.0	vw	
446.5	w	$0-\nu''+436+36$
458.0	vw	
483.6	vw	$0-\nu''+436+2\times36$
494.8	vw	
520.7	vw	$0-\nu''+436+3\times36$
530.9	vw	
532.8	vw	
538.4	vw	
566.7	vw	
573.8	vw	
594.1	vw	$0+\nu'-440-9$
602.8	vw	$0+\nu'-440$
627.5	vw	$0+\nu'-440-9+36$
639.1	vw	$0+\nu'-440+36$
663.1	vw	$0+\nu'-440-9+2\times36$
674.6	vw	$0+\nu'-440+2\times36$
692.6	vw	
706.4	vw	$0+\nu'-440+3\times36$
734.0	vw	$0+\nu'-440-9+4\times36$
744.4	vw	$0+\nu'-440+4\times36$
774.7	w	$0-\nu''+796$

TABLE I. (Continued).

Wave numbers in cm^{-1}	Intensity[a]	Assignment
	t=100°C (Continued)	
21 794.3	vw	
807.4	w	$0-\nu''+796+36$
844.0	vw	$0-\nu''+796+2\times36$
851.7	vw	
867.6	vw	
882.3	vw	$0-\nu''+796+3\times36$
913.4	w	
922.5	w	
966.0	w	$0+\nu'-65-9$
978.4	w	$0+\nu'-65$
22 015.5	w	$0+\nu'-65+36$
026.9	w	
	t=90°C	
22 034.2	vs	$0+\nu'-9$
042.7	vs	$0+\nu'$ (A_0)
051.2	w	
060.5	w	
069.5	s	$0+\nu'-9+36$
078.8	vs	$0+\nu'+36$
087.0	mw	$0+\nu'+46$
104.4	w	$0+\nu'-9+2\times36$
113.9	s	$0+\nu'+2\times36$
124.7	m	$0+\nu'+80$
149.2	s	$0+\nu'+3\times36$
161.2	m	$0+\nu'+80+36$
176.7	w	
184.0	m	$0+\nu'+4\times36$
200.5	w	
209.4	w	
219.7	w	$0+\nu'+5\times36$
239.4	vw	
255.0	w	$0+\nu'+6\times36$
291.5	vw	$0+\nu'+7\times36$
314.7	vw	
363.6	w	
399.0	w	
423.0	vw	
433.5	w	
469.5	w	$0+\nu'+436-9$
480.2	m	$0+\nu'+436$ (B_0)
504.6	w	$0+\nu'+436+36-9$
515.5	w	$0+\nu'+436+36$
537.6	w	$0+\nu'+436+2\times36-9$

Wave numbers in cm^{-1}	Intensity[a]	Assignment
	t=90°C (Continued)	
22 548.9	w	$0+\nu'+436+2\times36$
573.0	w	$0+\nu'+436+3\times36-9$
583.4	vw	$0+\nu'+436+3\times36$
608.6	vw	$0+\nu'+436+4\times36-9$
620.1	vw	$0+\nu'+436+4\times36$
662.0	vw	
672.4	vw	
712.7	w	
839.1	ms	$0+\nu'+796$ (C_0)
875.2	m	$0+\nu'+796+36$
886.6	w	$0+\nu'+796+46$
912.4	m	$0+\nu'+796+2\times36$
946.1	vw	$0+\nu'+796+3\times36$
	t=100°C	
23 084.4	vw	
089.5	w	$0+\nu'+1109-65$
151.5	vs	$0+\nu'+1109$ (A_1)
190.0	s	$0+\nu'+1109+36$
198.0	w	$0+\nu'+1109+46$
225.6	mw	$0+\nu'+1109+2\times36$
262.7	m	$0+\nu'+1220$
295.8	w	$0+\nu'+1220+36$
307.0	w	
345.4	w	
586.1	m	$0+\nu'+1109+436$ (B_1)
623.8	vw	$0+\nu'+1109+436+36$
651.4	w	$0+\nu'+1109+436+2\times36$
702.2	vw	
736.5	vw	
745.1	vw	
773.6	vw	
953.8	w	$0+\nu'+1109+796$ (C_1)
990.5	w	$0+\nu'+1109+796+36$
24 027.0	w	$0+\nu'+1109+796+2\times36$
065.3	vw	$0+\nu'+1109+796+3\times36$
105.5	vw	$0+\nu'+1109+796+4\times36$
141.3	vw	
269.7	vw	$0+\nu'+2\times1109$
305.6	vw	$0+\nu'+2\times1109+36$
352.8	vw	
382.8	vw	$0+\nu'+1109+1220$
501.8	vw	$0+\nu'+2\times1220$
592.8	vw	

[a] v=very, w=weak, m=medium, s=strong.

lar to the molecular plane). The other transitions are forbidden by molecular symmetry but allowed through the vibrational-electronic interaction.[13,14] Table II shows possible combinations of perturbed and perturbing states of this molecule. The second column of this table includes the symmetry species of perturbing vibrations which permit the forbidden transitions from the ground A_g state to the states of symmetry listed in the first column through interactions with the allowed transitions to the states of symmetry listed in the last column. The boldface letters used for the species notations, and the numbers given immediately after them in parentheses, in the second column of the table, will be explained in a later section.

[13] G. Herzberg and E. Teller, Z. physik. Chem. B21, 410 (1933).
[14] H. Sponer and E. Teller, Revs. Modern Phys. 13, 75 (1941).

Undoubtedly, the absorption spectra lying in the visible or in the near ultraviolet region are due to excitation of an electron from a bonding π molecular orbital (MO) or nonbonding MO to an antibonding π MO (designated as $\pi-\pi$ and $n-\pi$ transitions, respectively). In the case of p-benzoquinone, a $\pi-\pi$ transition from the ground state produces a state of symmetry of A_g, B_{1g}, B_{2u}, or B_{3u}, while an $n-\pi$ transition produces a state of symmetry A_u, B_{1u}, B_{2g}, or B_{3g}. Moreover, one can show that an A_u state is always in accidental degeneracy with a B_{2g} state and that the same applies to a B_{1u} and B_{3g} states, by MO calculation.[1,2] This statement holds even if all the multiply excited configurations are taken into CI calculation. This is the reason why the species notations A_u and B_{2g} of perturbed states in the first column of Table II are com-

TABLE II. Possible combinations of perturbed and perturbing states of *p*-benzoquinone.

Perturbed state	Perturbing vibration	Perturbing state
$\left\{\begin{matrix}A_u\\B_{2g}\end{matrix}\right.$	$\left\{\begin{matrix}b_{1g}\ (3)\\b_{3u}\ (3)\end{matrix}\right.$	B_{1u}
$\left\{\begin{matrix}A_u\\B_{2g}\end{matrix}\right.$	$\left\{\begin{matrix}b_{2g}\ (0)\\a_u\ (1)\end{matrix}\right.$	B_{2u}
$\left\{\begin{matrix}A_u\\B_{2g}\end{matrix}\right.$	$\left\{\begin{matrix}b_{3g}\ (2)\\b_{1u}\ (2)\end{matrix}\right.$	B_{3u}
B_{1g}	$a_u\ (1)$	B_{1u}
B_{1g}	$b_{3u}\ (3)$	B_{2u}
B_{1g}	$b_{2u}\ (3)$	B_{3u}
B_{2g}	$b_{2u}\ (3)$	B_{1u}
B_{2g}	$b_{1u}\ (2)$	B_{2u}
B_{2g}	$a_u\ (1)$	B_{2u}
A_g	$b_{1u}\ (2)$	B_{1u}
A_g	$b_{2u}\ (3)$	B_{2u}
A_g	$b_{3u}\ (3)$	B_{3u}

bined into a group by curly brackets.[15] The reason for this accidental degeneracy is the fact that two oxygen atoms, each of which has a pair of nonbonding electrons, lie rather remotely from each other in the *p*-benzoquinone molecule.

ANALYSIS AND DISCUSSIONS

A complete, although more or less tentative, assignment of fundamental frequencies of this molecule in its ground electronic state to modes of vibrations suggested in part IV[16] of this series are reproduced in Table III and will be used in the following discussions.

As mentioned in a previous section, the only groups of bands which appear in the spectrum at lower vapor pressures are those around A_0, B_0, C_0, A_1, B_1, and C_1, and all of them may be considered to be due to transitions from the vibrationless ground state by comparison with a low-temperature crystal spectrum,[5] the microphotometer tracings of which are reproduced in the lower part of Fig. 1. In Fig. 1 one can see that the pattern of the vapor spectrum formed by $A_0 \sim C_1$ is well exhibited in the low temperature crystal spectrum. On the other hand, the band D_0, which commences to appear in the vapor spectrum with increasing temperature of the absorption cell, has no counterpart in the low temperature crystal spectrum, as may also be seen in Fig. 1. The band D_0 must, therefore, result from a transition in which a certain kind (or kinds) of vibration is excited in the ground electronic state. Then, if the electronic transition with which we are concerned were allowed by the molecular symmetry, it would be natural to expect that the frequency separation 1068 cm^{-1} between A_0 and D_0 should represent a fundamental frequency in the ground electronic state. However, as can be seen in Table III, there is no appropriate fundamental to be assigned to this frequency separation. Therefore, the authors favor assigning D_0 and A_0 to vibronic transitions in which a perturbing vibration is superimposed by one quantum on the forbidden 0, 0 transition in the ground and the excited state, respectively.

The bands B_0, C_0, and A_1 lie on the violet side of A_0, the frequency separations from A_0 being 436, 796, and 1109 cm^{-1}, respectively. These frequency separations may all be considered to represent fundamental frequencies in the excited state belonging to species a_g, as will be discussed later. The frequency interval of 1109 cm^{-1} appears also between B_1–B_0 and C_1–C_0, and forms progressions of bands as can be seen in Table I. Another frequency interval constituting band progressions is 1220 cm^{-1} and may also be assigned to an a_g fundamental in the excited state as will be discussed later.

Since the main features of the spectrum have been described and since the remaining bands are relatively weak and may be interpreted as combinations of the aforementioned bands and fundamental frequencies in either or both of the electronic states as may be seen in Table I, one can say that the spectrum looks like the one caused by a *single* forbidden electronic transition, only one vibration being effective as a perturbing vibration. The assignment of the absorption in this region to a forbidden transition (or transitions) is also supported by the fact that it has only a small value of the extinction coefficient ($\log\epsilon = 1.2$) in a hexane solution.

Now let us consider the symmetry assignment of the forbidden transitions and the perturbing allowed transitions. Since the A_0–D_0 interval is 1068 cm^{-1}, we consider that the (single) perturbing vibration has a frequency of about 500 cm^{-1} in the ground electronic state. The boldface letters used for the species notations of perturbing vibration, given in the second column of Table II, show that the species contain ground-state frequencies of 400~600 cm^{-1}, as derived from Table III. Moreover, it may be natural to assume that only vibrations which are effective as perturbing vibrations are carbon or oxygen vibrations, since the electronic transitions with which we are concerned are due to excitation of a π electron or of a nonbonding electron localized at the oxygen atom. The figures given in parentheses immediately after the species notation of perturbing vibration in the second column of Table II represent the number of carbon or oxygen vibrations belonging to that species as derived also from Table III. These considerations together with the fact that the spectrum looks like the one caused by a single forbidden electronic transition and only one vibration is effective as a perturbing vibration show that only the second or the fourth combination may be the case.[17]

[15] Although a B_{1g} state is in accidental degeneracy with a B_{1u} state as described above, the "partner" B_{1u} of B_{3g} is not given in the first column of Table II, since the $B_{1u} \leftarrow A_g$ transition is allowed by the molecular symmetry and we are concerned only with states transitions to which are forbidden by molecular symmetry there.

[16] T. Anno and A. Sadô, Bull. Chem. Soc. Japan **31**, 734 (1958).

[17] The ninth combination is excluded since the forbidden $^1B_{3g} \leftarrow\!\!\!\!\!- ^1A_g$ transition should always be superimposed by an *allowed* $^1B_{1u} \leftarrow\!\!\!\!\!- ^1A_g$ transition.

TABLE III. Fundamental frequencies of p-benzoquinone[a](ground electronic state) (cm^{-1})[a,b]

	a_g	b_{1g}	b_{2g}	b_{3g}	a_u	b_{1u}	b_{2u}	b_{3u}
C—H stretching	3058	3058					3049	3049
C=O stretching	1667						1667	
C—C stretching	1688	610					1715	944
C—C breathing	770						730	1064
C=O bending		[~400][c]		243(···)		···(533)		370
C—H bending	1149	1360	794(839)	932(959)	···(962)	876(871)	1298	1356
Ring bending	444	540		···(790)	533(403)	99(98)		

[a] Calculated values of nonplanar vibrational frequencies are enclosed in parentheses.
[b] Experimental values in bold type are obtained from combination bands or electronic spectral data.
[c] Estimated.

The vibrational analysis of the vapor spectrum in this visible region alone cannot exclude the fourth combination, but the authors favor the second combination. The perturbing allowed transition $^1B_{1u}\leftarrow{}^1A_g$ for the fourth case is an n–π transition and an n–π transition for carbonyl-containing molecule is weak even if it is allowed by molecular symmetry.[18,19] Therefore, if the latter is the case, the "forbidden transition" should be much lower in intensity. For this reason the authors consider that the vapor spectrum lying in the visible region is a superposition of the $^1A_u\leftarrow{}^1A_g$ and $^1B_{2g}\leftarrow{}^1A_g$ transitions permitted through the vibrational-electronic interaction with the $^1B_{2u}\leftarrow{}^1A_g$ transition, although the $^1A_u\leftarrow{}^1A_g$ transition is much less important than $^1B_{2g}\leftarrow{}^1A_g$ transition. This conclusion should be compared with that of Asundi and Singh[7] who considered that the visible absorption of p-benzoquinone is due to a single $^1A_u\leftarrow{}^1A_g$ transition. Our conclusion confirms the energy levels of theoretical calculation[1,2] and is in agreement with the spectroscopic studies of crystalline p-benzoquinone[3–5] in that the vibronic transitions in this visible region appear with transition moment along the long axis of the molecule.

In connection with the symmetry assignment of the visible vapor absorption, the symmetry assignment of the corresponding absorption of p-benzoquinone crystal will be discussed. As already referred to in the Introduction, Sidman[5] found three different n–π transitions in the visible absorption spectrum of the p-benzoquinone crystal by using a low temperature of 20°K and assigned two of them to singlet-singlet transitions, although the symmetries remain unassigned.

The crystal structure of p-benzoquinone has been determined by Robertson.[9] The crystal belongs to the monoclinic system, and the space group symmetry is $C_{2h}^5(P_{21}/a)$ with two molecules per unit cell. Table IV shows the symmetry species and the character of the factor group (C_{2h}) of the space group and the symmetry species of molecular states which go over into the factor group species when the molecules gather into a crystal. In this table E, C_2^b, and σ^b denote the identity operation, the twofold screw rotation with respect to the crystal b axis, and the glide reflection with respect to the ac plane, respectively, while i represents an inversion about the center of symmetry at which the screw axis and the glide plane cross. $\mathbf{r}_a$, $\mathbf{r}_b$ and $\mathbf{r}_c$, included in the parentheses after the species notation of C_{2h}, indicate that a vecter along the b axis or in the ac plane belongs to the species A_u or B_u of C_{2h}, respectively. From this table we can expect that the molecular $^1B_{2g}\leftarrow{}^1A_g$ transition is still forbidden electronically in crystal while the molecular $^1A_u\leftarrow{}^1A_g$ transition becomes, in principle, an electronically allowed transition in crystal, the intensity of the crystal spectrum being determined by the strength of the crystal field. Although the molecular $^1B_{2g}\leftarrow{}^1A_g$ transition is still forbidden electronically even in crystal, it can be allowed through vibrational-electronic interaction, as in the case of the free molecule. Since the dichroic (Davydov) splitting[20] is undetectable in the visible absorption spectrum of crystalline p-benzoquinone,[5] the crystal perturbation which permits the molecular $^1A_u\leftarrow{}^1A_g$ transition is expected to be small

TABLE IV. Irreducible representations of C_{2h}

	E	C_2^b	i	σ^b	Associated species of molecular point group V_h
A_g	1	1	1	1	A_g, B_{1g}, B_{2g}, B_{3g}
A_u ($\mathbf{r}_b$)	1	1	−1	−1	A_u, B_{1u}, B_{2u}, B_{3u}
B_g	1	−1	1	1	A_g, B_{1g}, B_{2g}, B_{3g}
B_u ($\mathbf{r}_a$, $\mathbf{r}_c$)	1	−1	−1	1	A_u, B_{1u}, B_{2u}, B_{3u}

[18] J. R. Platt, J. Chem. Phys. **19**, 101 (1951).
[19] The referee of this article suggested that there is a possibility that the $^1B_{1u}\leftarrow{}^1A_g$ transition of the Rydberg type behaves as a perturbing transition. Indeed a Rydberg transition can give some amount of intensity through vibrational-electronic interaction to a forbidden transition if the former interacts fairly strongly with the latter, because the intensity of the former is large, but we neglect such a possibility here because the energy separation between Rydberg transitions and the forbidden transition with which we are concerned is expected to be large.
[20] A. S. Davydov, Zhur. Eksp. i Teoret. Fiz. **18**, 210 (1948).

TABLE V. Calculated and observed frequencies of totally symmetrical vibrations of *p*-benzoquinone.

Mode	No.	Calc[a]			Obs		
		Ground state	Excited state	Drop(%)[b]	Ground state[c]	Excited state	Drop(%)[b]
CH stretching	ν_1	3069	3068	0.03	3058	...	...
CC stretching	ν_2	1983	1920	3.1	1688	...	...
CO stretching	ν_3	1655	1470	11.2	1667	1220	26.8
CH bending	ν_4	1157	1152	0.43	1144	1109	3.1
CC bending	ν_5	782	810	−3.6	770	796	−3.4
Ring bending	ν_6	(444)	(436)	(1.8)	444	436	1.8

[a] See reference 23.
[b] Drop (%) = (Ground-state frequency − excited-state frequency)/ground-state frequency.
[c] See reference 16.

and this transition is expected to be allowed only weakly. In Sidman's[5] notation transition (*c*) has the origin of the anlysis at 21 003 cm^{-1} and is most intense among the three transitions observed by him. The fact that the spectrum caused by this transition is closely resembled by the vapor spectrum has already been mentioned. From these considerations Sidman's transition (*c*) may be assigned to the molecular $^1B_{2g} \leftarrow {}^1A_g$ transition which is still forbidden electronically even in crystal but is allowed through vibrational-electronic interaction. On the other hand, Sidman's transition (*b*) may be assigned to the molecular $^1A_u \leftarrow {}^1A_g$ transition allowed electronically in crystal and should have 0,0 band even if weak. The "forbidden part" of this crystal-allowed transition is expected to be absent or only weak since it can appear only through the vibrational perturbation as in the free molecule and the molecule has no "effective" vibration as mentioned before. Therefore, in Sidman's transition (*b*), the 20 206 cm^{-1} band, which is taken as the origin of the analysis, or a stronger band at 20 289 cm^{-1} may be taken as the 0,0 band of the transition.

In our molecular-orbital calculation of the energy levels of the free molecule of this substance,[1,2] the ^1A_u and $^1B_{2g}$ molecular states under consideration are shown to be in accidental degeneracy with each other, separation between the lowest ^1A_u and the lowest $^1B_{2g}$ state being calculated as 0.35 cm^{-1}, if we neglect CI. Such circumstances have been shown to exist also for gaseous pyrazine experimentally[21] as well as theoretically.[22] If ^1A_u and $^1B_{2g}$ molecular states were still in accidental degeneracy in crystal, the separation 21 003–20 289/20 206=714/797 cm^{-1} would represent the upper-state frequency of the a_u ring-bending vibration, which makes the molecular $^1B_{2g} \leftarrow {}^1A_g$ transition allowed, and the corresponding ground-state frequency would be equal to 1068 (A_0–D_0 separation in vapor) − 714/797=354/271 cm^{-1}. Then, the frequency of this vibration would increase to double or more upon electronic excitation which does not seem to be the case in comparing the result of the theoretical calculation of the frequency change[23] (calculated value of this frequency is equal to 404 and 438 cm^{-1} in the ground and the excited electronic states, respectively) and the case of pyrazine.[24] Therefore, it may be considered that the molecular ^1A_u and $^1B_{2g}$ states are no more in accidental degeneracy in crystal and that the crystal state derived from the ^1A_u molecular state is lower than that derived from the $^1B_{2g}$ molecular state, although the quantitative discussions cannot be given at present.

Let us turn to the discussions on the vapor spectrum. The suggestion that the frequency separations 436, 796, 1109, and 1220 cm^{-1} may be assigned to a_g vibrations in the excited state has already been mentioned. These frequencies may correspond to the ground-state frequency of 444, 770, 1149, and 1667 cm^{-1}, in that order, assigned to ring bending, ring breathing, CH bending, and CO stretching modes, respectively. The ground-state frequencies 444, 770, 1149, and 1667 cm^{-1} (Raman value[16]) occur also in the electronic spectrum as 22 043−21 603=20 975−20 535=440, 22 043−21 279=20 975−20 202=770, 22 043−20 900 =20 975−19 830=1144 and 22 043−20 387=1667 cm^{-1}. The aforementioned correlations of the upper-state frequencies with the ground-state frequencies are based partly on the estimation of the frequency change, brought about by the electronic excitation, by using the method proposed by the present authors.[25] The detail of these calculations will be described in another paper[23] on the application of the Franck-Condon principle to this transition. It is to be noted, however,

[21] M. Ito, R. Shimada, T. Kuraishi, and W. Mizushima, J. Chem. Phys. **26**, 1508 (1957). For some comments on the analysis see reference 22.
[22] T. Anno and A. Sadô, J. Chem. Phys. **29**, 1170 (1958).
[23] T. Anno and A. Sadô, J. Chem. Phys. **32**, 1611 (1960), following paper.
[24] If we take the separation between bands at 30 545 and 31 260 cm^{-1} as the sum of the ground- and excited-state frequencies of a_u ring-bending vibration (for further detail on this point see references 21 and 22) and the ground-state frequency of this vibration to be 340 cm^{-1} [Lord, Marston, and Miller, Spectrochim. Acta **9**, 113 (1957) and see also the discussion given in reference 22], we obtain as the upper-state frequency 375 cm^{-1}.
[25] T. Anno, A. Sadô, and I. Matubara, Bull. Chem. Soc. Japan **29**, 703 (1956).

that the CH stretching and the CH bending force constants are transferred for both states from the benzene moleucle in its ground electronic state and that the ground-state frequency of 444 cm^{-1} or the excited-state frequency of 436 cm^{-1} are used to obtain the ring-deformation force constant. The calculated value of the totally symmetrical frequencies are given in the third and the fourth column of Table V for the ground and the excited states, respectively. The sixth and the seventh column of this table contain the observed frequencies. Although we can see that the correlations 796 to 770 and 1109 to 1149 cm^{-1} are reasonable, by comparison of the figures in the fifth and the last columns of the table, the correlation 1220 to 1667 cm^{-1} would produce a frequency drop too great as compared with the "calculated" drop. The authors believe, however, that the correlation 1220 to 1667 cm^{-1} is nevertheless reasonable for the following reason.

In Table VI the changes of bond length caused by the electronic excitation, as derived from bond order-bond length relation, are compared with those derived from the Franck-Condon principle. Of course, the bond-length changes as derived from bond order take account only of the change in the π-electronic structure, while those derived from the Franck-Condon principle include the other effects, such as the change of the σ-electronic structure, as well. From this table we can see that the change of the CO bond length as derived from the Franck-Condon principle is 1.6 times that derived from bond order. Since ν_3 is due mainly to the CO stretching, this fact suggests that we may expect for this vibration a frequency drop larger than that derived from bond order. From similar reasoning using Table VI, ν_2, whose mode is mainly stretching of nominal CC double bond, is expected to increase its frequency upon electronic excitation although we could not obtain its excited state frequency from the spectrum, and the bond-order change would give a contrary result. As to ν_5, both bond-order and the Franck-Condon principle may give a similar change, as can be easily inferred from Table VI, since ν_5 is due mainly to stretching of the nominal CC single bond.

The remaining main feature of the vapor spectrum is the occurrence of small frequency intervals. Under a fairly high resolution of the second order of the concave-gration spectrograph, stronger bands are shown to be double with the separation of 8 cm^{-1}. We cannot say at present whether it really represents an unresolved rotational structure or whether it is only a difference (v–v) frequency of some kind. One remarkable feature of the spectrum is the appearance of the satellite bands with a separation of 36 cm^{-1} accompanying the main bands on their violet side. This frequency interval has also been reported by Asundi and Singh.[7] The 36 cm^{-1} progressions can be seen in many cases as shown in Table I. The authors thought at the outset that this frequency separation would represent a fundamental

TABLE VI. Comparison of the changes of bond lengths as derived from bond order-bond length relation with those derived from the Franck-Condon principle (from reference 23).

Bond	From bond order A	From Franck-Condon principle A
CO	0.07	0.1104
CC (nominal double)	0.015	−0.0294
CC (nominal single)	−0.032	−0.0294

frequency in the excited state. As in Table III, the lowest frequencies of *p*-benzoquinone in its ground state are 99 (b_{1u}) and 243 (b_{3g}) cm^{-1}. From the fact that no prominent bands can be found with frequency separations of these magnitudes on the red side of stronger bands we rejected this interpretation. The authors believe, therefore, that this is caused by v–v transitions. The fact that it forms long progressions (up to seven quanta, see Table I) suggests that it must be caused by a vibration of very low frequency. A vibration of torsion around the CC "single" bond belongs to species b_{1u} and has the ground-state frequency of 99 cm^{-1}. Since a molecular-orbital calculation shows that the π order of this bond increases from 0.226 to 0.414 in the excited state, it is probable that this vibration increases its frequency in the excited state. If we calculate it by the same manner as used in the calculation of the a_u ring-bending frequency in the excited state,[23] we obtain 105 cm^{-1} as compared with 98 cm^{-1} calculaged for the ground state.[26]

On the other hand, the ground-state frequency of 243 cm^{-1} (b_{3g}) is expected to decrease upon electronic excitation for the following reason. The vibration having the ground-state frequency of 243 cm^{-1} is of the CO out-of-plane bending mode. Although the out-of-plane deviation of the oxygen atom from the molecular plane decreases the overlap of the σ AO of the oxygen atom with the σ AO of the carbon atom to which the oxygen atom in question is attached, the increase of the potential energy which thus results will be partially compensated by the increase in the overlap of π AO of the oxygen atom with σ AO of the carbon atom. Compensation of such a kind in potential energy is expected to be larger in the excited state than in the ground state since the "electron population" to be assigned to the AO of the oxygen atom is larger in the excited state than in the ground state.[27] Therefore, the out-of-plane bending force constant is expected to *decrease* upon electronic excitation and the 36-cm^{-1} progression to the violet side of the stronger bands

[26] T. Anno and A. Sadô, Bull. Chem. Soc. Japan 31, 728 (1958).

[27] Since the electronic transition with which we are concerned is $\phi_{n1}\rightarrow\phi_4$ or $\phi_{n2}\rightarrow\phi_5$, in the notation of reference 1, if we neglect CI, the increase of "electron population" in the πAO of the oxygen atom is calculated to be $0.35339^2=0.12488$ from the molecular orbitals in LCAO listed in Table II of reference 1.

may not be assigned to v–v transitions of this vibration. For this reason we suggest with some reservation that 36 cm^{-1} frequency separation is assigned to v–v transitions of the lowest b_{1u} frequency.

Other small frequency intervals appearing less prominently are 46 and 80 cm^{-1} on the violet side and 65 cm^{-1} on the red side. We will not interpret them in order not to be too speculative. These frequency intervals are to be compared with the description of Asundi and Singh[7] who reported that stronger bands are accompanied by satellites on the red side with the separations of 37, 64, and 92 cm^{-1}.

Although the main feature of the spectrum may be interpreted by the superposition of the totally symmetrical vibrational frequencies and difference frequencies upon the 20 975- and 22 043-cm^{-1} bands, some comments will be given on the band at 20 624 cm^{-1}. This band is somewhat weak and diffuse but prominent in its neighborhood. We have failed to interpret it as a combination of the aforementioned frequencies. It may represent the vibronic transition from a state in which the b_{2g} hydrogen vibration is excited by one quantum in the ground electronic state to the vibrationless upper ^1A_u state. If so, the energy of the forbidden 0, 0 transition would amount to 20 624+800= 21 424 cm^{-1}, since the b_{2g} hydrogen vibrational frequency in the ground electronic state is about 800 cm^{-1}. Then, by considering the fact that the ^1A_u–$^1B_{2g}$ separation is negligible, it would be concluded that the a_u ring-bending frequency is equal to 449 (=21 424–20 975) and 619(=22 043–21 424) cm^{-1} in the ground and the excited electronic states, respectively.

In conclusion, it should be emphasized that the greatest difficulty encountered in the analysis of this spectrum is our ignorance of the exact value of the a_u ring-bending frequency even in the ground state. For this reason, in the analysis given in Table I, this frequency is merely indicated by ν'' and ν' for the ground and the excited states, respectively.

ACKNOWLEDGMENTS

This work was started in collaboration with Mr. I. Matubara, now at the Research Department of Toyo Rayon Company, Ltd. The authors express their hearty thanks to him for this collaboration. It is a pleasure of the authors to express their sincere thanks to Professor S. Imanishi and to Dr. Y. Kanda for their encouragement throughout this research.

Electronic States of *p*-Benzoquinone. VI. Molecular Geometry in the Excited Electronic State of the 4500-A Absorption System as Derived from the Franck-Condon Principle

TOSINOBU ANNO*
Chemical Laboratory, General Education Department, Kyushu University, Ootsubo-machi, Fukuoka, Japan
AND
AKIRA SADÔ†
Department of Chemistry, Faculty of Science, Kyushu University, Hakozaki, Fukuoka, Japan

(Received September 21, 1959)

The method used for evaluating the Condon overlap integral associated with any vibronic band of an electronic absorption system of an XY_2 molecule, as developed by J. B. Coon and his co-workers, is applied to more complex molecules. Thus, some information about the geometry of the excited electronic state of a complex molecule may be determined if the geometry in the ground state, the intensities of vibronic bands of the associated electronic absorption system, and normal coordinates and frequencies in both electronic states are known. The method is applied to the 4500-A absorption system of *p*-benzoquinone. Since the normal coordinate treatment for this molecule is only qualitatively valid, especially in its excited state, the results are expected to be more or less qualitative. If we take the resulting change of bond angles into account, the ring-bending frequency of species A_u in the excited electronic state is calculated to be 438 cm^{-1} by the method described in Part III of this series [T. Anno and A. Sadô, Bull. Chem. Soc. Japan **31**, 728 (1958)].

1. INTRODUCTION

IN Part III[1] of this series the present authors have calculated the nonplanar vibrational frequencies of the *p*-benzoquinone molecule in its ground electronic state by using the method described in another paper.[2] As to the vibrations for which observed frequencies are available,[3] the agreement between calculated and observed frequencies is fairly good except for $\nu_2(A_u)$ (the lower of the two frequencies belonging to species A_u of the molecular point group V_h). The assumption that the bond angles remain the same in the course of electronic excitation may be one reason for the disagreement between calculated and experimental values of $\nu_2(A_u)$, since the "experimental" value of $\nu_2(A_u)$ is obtained on the basis of this assumption and some interaction constants are sensitive to the change of the bond angles, as discussed in previous papers.[1,2]

The molecular geometry in the excited electronic state can be determined from the rotational structure of the electronic spectrum concerned. However, this is the case only for simple molecules. A method of obtaining information about the geometry of an excited electronic state is provided by the Franck-Condon principle.

The general theory of the Franck-Condon principle as applied to polyatomic molecules has been discussed.[4] This principle states that the relative intensities of the vibronic bands of a given electronic band system depend on the difference in the molecular geometries of the two states at vibrational equilibrium. In principle, therefore, measurement of the relative band intensities leads to information about the change in molecular geometry and hence to information about excited-state geometry. The Franck-Condon principle has often been used qualitatively in discussing the electronic spectra of polyatomic molecules.[5] The quantitative application of the principle has been confined to the case of the diatomic molecule[6] or to the simple case of the 2600-A system of benzene.[7] In both of these cases the number of normal coordinates whose origins are different in the ground and in the excited electronic states is only one (one-dimensional case).

Very recently, Coon and his co-workers[8] have extended the application of the principle to the bent XY_2 molecule and determined the structure of the sulfur-dioxide molecule in its excited state of the 3800-A absorption system. Of the four excited-state models consistent with the observed intensities, that model was chosen which was most consistent with the partially resolved rotational structure. It is the purpose of the present paper to describe how Coon's method applies to more complex molecules, to apply the method to the determination of the structure of the *p*-benzoquinone molecule in its excited state associated with the 4500-A absorption system, and to investigate how the consideration of change of bond angles in the course

* Present address: Mathematical Institute, Oxford, England.
† Present address: Department of Chemistry, Faculty of Science, Kanazawa University, Kanazawa, Japan.

[1] T. Anno and A. Sadô, Bull. Chem. Soc. Japan **31**, 728 (1958).
[2] T. Anno, J. Chem. Phys. **28**, 944 (1958).
[3] As to the assignment of vibrational frequencies in the ground electronic state, by using the infrared and Raman data, see T. Anno and A. Sadô, Bull. Chem. Soc. Japan **31**, 734 (1958).
[4] G. Herzberg and E. Teller, Z. physik. Chem. **B21**, 410 (1933); H. Sponer and E. Teller, Revs. Modern Phys. **13**, 85 (1941).
[5] See, for example, Sponer, Nordheim, Sklar, and Teller, J. Chem. Phys. **7**, 207 (1939).
[6] E. Hutchisson, Phys. Rev. **36**, 410 (1930).
[7] D. P. Craig, J. Chem. Soc. **1950**, 2146.
[8] J. K. Ward and J. B. Coon, AF Tech. Note (July, 1954) ASTIA Document No. AD38-856; Coffman, Corgan, Loyd, and Coon, AF Tech. Note (August, 1956) ASTIA Document No. AD95-806 (ASTIA Document Service Center, Knott Building, Dayton 2, Ohio).

TABLE I. Main absorption bands of λ 4500-A system of *p*-benzoquinone vapor.

Wave number (cm^{-1})	Relative molar extinction coefficient	Interpretation
22 043	1.0000	0, $\nu_2'(A_u)$
23 152	0.5239	0, $\nu_2'(A_u)$+1109
23 263	0.6387	0, $\nu_3'(A_u)$+1220
24 270	0.0744	0, $\nu_2'(A_u)$+2×1109
24 502	0.1295	0, $\nu_3'(A_u)$+2×1220

of electronic excitation affects the "experimental value" of $\nu_2(A_u)$.

For two absorption bands having wave numbers ν_i and ν_j and arising from the same vibrational level of the ground electronic state

$$R_i^2/R_j^2=(\epsilon_i/\nu_i)/(\epsilon_j/\nu_j), \tag{1}$$

where R_i is the Condon overlap integral of the ith band. These integrals are evaluated on the basis of harmonic approximation. ϵ_i is the intensity of the ith band and may be taken to be proportional to the molar extinction coefficient at the peak of the ith band. It is assumed that all bands of a given absorption system have the same envelope, and that the pressure of the absorbing gas is sufficient to wash out the rotational structure.

2. ABSORPTION SPECTRUM OF *p*-BENZOQUINONE VAPOR IN THE 4500-A REGION

The absorption system of *p*-benzoquinone around 4500 A is considered to be a superposition of two electronic transitions $^1B_{2g}\leftarrow{}^1A_g$ and $^1A_u\leftarrow{}^1A_g$.[9] The vibrational analysis of this system shows, however, that all the prominent bands seem to belong to only one transition $^1B_{2g}\leftarrow{}^1A_g$.[10] The application of the Franck-Condon principle to this absorption system leads, therefore, to information about the geometry in the $^1B_{2g}$ state. The molecular geometry in the ^1A_u state is expected to be nearly the same as that in the $^1B_{2g}$ state, since the electronic structure is nearly the same in both of these states.[9]

The absorption spectrum at 4500 A was described and analyzed in a previous paper.[10] Totally symmetrical vibrational frequencies in the excited state 1109 and 1220 cm^{-1} form progressions.[10] In Table I, wave numbers, molar extinction coefficients at band peak, and analyses are given for prominent bands of this system. The molar extinction coefficient at the peak of each band was determined from the logarithm of transmittance which was simply determined by using the microphotometer tracing curve of the spectrogram. No care was taken of the wavelength dependence of photographic emulsion sensitivity. This crude procedure of photometry does not seem to have serious effects on our final result, since the predicted intensity distribution is fairly sensitive to the model.

3. NORMAL COORDINATES

The normal coordinate was calculated by using the method of Wilson.[11] Let **S** be the column matrix formed by the internal coordinate. Then, a matrix equation

$$(\mathbf{GF}-\lambda\mathbf{I})\mathbf{S}=0 \tag{2}$$

is obtained. **G** and **F** are the inverse kinetic energy matrix and the force constant matrix, respectively, and **I** is the unit matrix. In the case of a symmetrical molecule, each one of symmetry species can be treated separately, and in such a case **S** represents the matrix formed by the internal symmetry coordinates. Equation (2) gives a matrix **L** which, when normalized by $\mathbf{LL}^*=\mathbf{G}$ ($\mathbf{L}^*$ is the transpose of **L**), relates the internal symmetry coordinates to the normal coordinates **Q** in such a way that

$$\mathbf{S}=\mathbf{LQ}. \tag{3}$$

The external symmetry coordinate **X** is related to the internal symmetry coordinate **S** by the equation

$$\mathbf{S}=\mathbf{NX}, \tag{4}$$

which defines a matrix **N**. From Eqs. (3) and (4) it follows that

$$\mathbf{Q}=\mathbf{L}^{-1}\mathbf{NX}. \tag{5}$$

Similarly, for the excited state,

$$\mathbf{Q}'=(\mathbf{L}^{-1})'\mathbf{N}'\mathbf{X}', \tag{6}$$

where the prime refers to the excited state.

Since the main progressions of the spectrum are formed by the totally symmetrical vibrations, the calculation of the normal coordinate belonging to species A_g will be described.

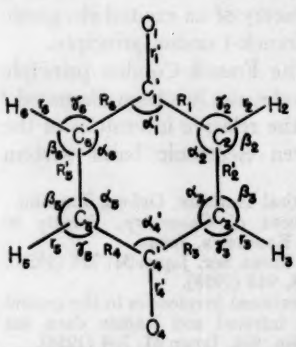

FIG. 1. Notations describing various atoms, bond lengths, and bond angles in the *p*-benzoquinone molecules.

[9] T. Anno, I. Matubara, and A. Sadô, Bull. Chem. Soc. Japan **30**, 168 (1957); T. Anno, A. Sadô, and I. Matubara, J. Chem. Phys. **26**, 967 (1957).

[10] T. Anno and A. Sadô, J. Chem. Phys. **32**, 1602 (1960), preceding paper. See also L. Light, Z. physik. Chem. **122**, 414 (1926); R. K. Asundi and R. S. Singh, Nature **176**, 1223 (1955).

[11] E. B. Wilson, Jr., J. Chem. Phys. **7**, 1047 (1939); **9**, 76 (1941); E. B. Wilson, Jr., J. C. Decius, and P. C. Cross, *Molecular Vibrations* (McGraw-Hill Book Company, Inc., New York, 1955).

Notations describing various atoms, bond lengths, and bond angles in the *p*-benzoquinone molecule are shown in Fig. 1. Denoting the *increase* of bond lengths and angles by placing Δ in front of notations for these quantities, internal symmetry coordinates belonging to species A_g are

$$\begin{aligned}
S_1 &= (1/2)(\Delta R_1+\Delta R_3+\Delta R_4+\Delta R_6)\\
S_2 &= (1/\sqrt{2})(\Delta R_2'+\Delta R_5')\\
S_3 &= (1/2)(\Delta r_2+\Delta r_3+\Delta r_5+\Delta r_6)\\
S_4 &= (1/\sqrt{2})(\Delta r_1'+\Delta r_4')\\
S_5 &= (1/2)(\Delta\alpha_2+\Delta\alpha_3+\Delta\alpha_5+\Delta\alpha_6)\\
S_6 &= (1/\sqrt{2})(\Delta\alpha_1'+\Delta\alpha_4')\\
S_7 &= (1/2)(\Delta\phi_2+\Delta\phi_3+\Delta\phi_5+\Delta\phi_6) \qquad (7)
\end{aligned}$$

where $\phi_i=(1/2)(\Delta\gamma_i-\Delta\beta_i)$ $(i=2, 3, 5, \text{and } 6)$.

In calculating the numerical value of G-matrix elements, the following values of the CH distance and the bond angles were assumed for the ground and the excited state: $r_i=1.08$ A, $\alpha_i=122°$, $\alpha_i'=116°$ and $\gamma_i=\beta_i=119°$. The source of these data may be found in a previous paper[1] and will not be repeated here. Although the CO distance of 1.23 A, determined by the electron-diffraction experiment, was used for the ground state, the corresponding quantity in the excited state was obtained by using the bond order calculated for both states and by assuming a linear relation between bond order and bond length for carbon-oxygen bonds. The values of CC bond length were obtained from bond order for both the electronic states. The values of bond orders used were those calculated by a semiempirical molecular-orbital method as described in a previous paper.[1] Bond orders and bond lengths are thus obtained are given in Table II.

The potential function assumed was a simple valence-force field type, all the interaction constants being neglected. Badger's relation[12] was used to obtain the CC and CO stretching force constants from bond lengths described in the preceding in the same manner as used in previous papers.[12,3] As for CH stretching and bending force constants, the corresponding quantities

TABLE II. Bond orders and bond lengths.

Bond	Bond order: Ground state	Bond order: Excited state	Bond length (in A): Ground state	Bond length (in A): Excited state	Bond length (in A): change
$C_1'O_1$	0.827	0.533	1.230	1.300	0.07
$C_1'C_2$	0.226	0.414	1.461	1.429	−0.032
C_3C_5	0.946	0.825	1.349	1.364	0.015

[12] R. M. Badger, J. Chem. Phys. **2**, 128 (1934); **3**, 710 (1935).
[13] T. Anno, A. Sadô, and I. Matubara, Bull. Chem. Soc. Japan **29**, 703 (1956).

TABLE III. Calculated and observed frequencies of totally symmetrical vibration of *p*-benzoquinone (cm^{-1}).

	Ground state: Calc	Ground state: Obs[a]	Excited state: Calc	Excited state: Obs[b]
ν_1	3069	3058	3068	3058
ν_2	1983	1688	1920	1688
ν_3	1655	1667	1470	1220
ν_4	1157	1149	1152	1109
ν_5	782	770	810	796
ν_6	(444)	444	(436)	436

[a] See reference 3.
[b] See reference 10 and the description given in text.

of the benzene molecule[14] in its ground electronic state were transferred to *p*-benzoquinone in both electronic states. The ring-deformation force constant was determined in such a way that a calculated value of frequency agrees to the experimental frequency assigned to the A_g ring-deformation vibration (444 and 436 cm^{-1} in the ground and in the excited states, respectively). The calculated value of totally symmetrical frequencies are given in Table III together with experimental values. The experimental frequencies are taken from Part IV[3] for the ground state, while the excited-state value are obtained from the analysis of the vapor electronic spectrum,[10] except for the highest two frequencies, which are assumed to be the same in the ground state.

The external symmetry coordinates are defined by using the Cartesian displacement coordinates of various atoms as

$$\left.\begin{aligned}
X_1 &= y_{O_1}-y_{O_4}\\
X_2 &= y_{C_1'}-y_{C_4'}\\
X_3 &= y_{C_2}-y_{C_3}-y_{C_5}+y_{C_6}\\
X_4 &= x_{C_2}+x_{C_3}-x_{C_5}-x_{C_6}\\
X_5 &= y_{H_2}-y_{H_3}-y_{H_5}+y_{H_6}\\
X_6 &= x_{H_2}+x_{H_3}-x_{H_5}-x_{H_6}
\end{aligned}\right\}. \qquad (8)$$

A right-handed Cartesian coordinate system at each atom is defined in such a way that the positive direction of the *y* axis runs parallel to the direction running from the atom O_4 to O_1 and the *xy* plane coincides with the molecular plane. From Eqs. (7) and (8), the N matrix, defined by Eq. (4), is obtained and is given in Table IV. It is to be noted that N matrix is not square. This is caused by the fact that there are six external symmetry coordinates and six vibrations of species A_g, while there are seven internal symmetry coordinates, as shown in Eq. (7). In other words, there is one redundancy in the internal symmetry coordinates defined in Eq. (7)

[14] B. L. Crawford, Jr., and F. A. Miller, J. Chem. Phys. **17**, 249 (1949).

TABLE IV. N matrix for the totally symmetrical vibrations of *p*-benzoquinone.[a]

	X_1	X_2	X_3	X_4	X_5	X_6
S_1	0	A	$-A/2$	$B/2$	0	0
S_2	0	0	$1/\sqrt{2}$	0	0	0
S_3	0	0	$-C/2$	$-D/2$	$C/2$	$D/2$
S_4	$1/\sqrt{2}$	$-1/\sqrt{2}$	0	0	0	0
S_5	0	B/R	$-B/2R$	$-A/2R$	0	0
S_6	0	$-\sqrt{2}B/R$	$B/\sqrt{2}R$	$A/\sqrt{2}R$	0	0
S_7	0	$-B/2R$	$(D/2r)+(B/4R)$	$-(C/2r)+(A/4R)$	$-D/2$	$C/2$

[a] $A=\cos(\alpha'/2)$, $B=\sin(\alpha'/2)$, $C=\cos(\pi-\beta)$, $D=\sin(\pi-\beta)$.

TABLE V. The totally symmetrical normal coordinates of *p*-benzoquinone in its ground electronic state.[a]

	X_1	X_2	X_3	X_4	X_5	X_6
Q_1	−0.0010 9275	0.0057 8930	−0.1354 6244	−0.1770 6003	0.0952 0652	0.1681 9121
Q_2	0.3440 6114	−0.6110 2691	0.4797 6076	−0.1123 8838	−0.0247 8156	0.0373 1475
Q_3	−0.5541 7444	0.5595 8216	0.4508 1558	−0.0284 7963	−0.0198 9398	0.0381 0164
Q_4	0.0155 1296	−0.0017 0687	0.1896 0877	0.0256 7049	0.1766 6128	−0.0850 1755
Q_5	0.3975 3096	0.1421 3624	0.0844 7318	0.6203 7779	0.0100 2774	0.0542 9437
Q_6	0.8626 1432	0.5377 4676	0.0557 5213	−0.2600 5289	−0.0105 7300	−0.0136 8303

[a] The figures in this table show the part of the L^{-1} N matrix which relate totally symmetrical normal coordinates to the external symmetry coordinates and are expressed in units of 10^{-11} gr$^{\frac{1}{2}}$.

TABLE VI. The totally symmetrical normal coordinates of *p*-benzoquinone in its excited electronic state.[a]

	X_1'	X_2'	X_3'	X_4'	X_5'	X_6'
Q_1'	−0.0004 5281	0.0035 7245	−0.1309 9631	−0.1783 4818	0.0952 2233	0.1683 6626
Q_2'	−0.1880 1421	0.4951 7670	−0.5560 0947	0.1405 8134	0.0316 5023	−0.0419 9406
Q_3'	−0.5636 2165	0.6949 2439	0.3442 5775	0.0271 8080	−0.0181 7238	0.0343 3591
Q_4'	−0.0092 5464	0.0043 2148	0.2025 2854	0.0088 5899	0.1754 6200	−0.0853 2669
Q_5'	0.4222 2410	0.0625 4540	0.0934 7431	0.6202 5669	0.0145 8354	0.0525 4530
Q_6'	0.8924 5959	0.5136 4657	0.0580 8746	−0.2466 6113	−0.0098 4044	−0.0128 2121

[a] The figures in this table show the part of the $(L')^{-1}N'$ matrix which relate totally symmetrical normal coordinates to the external symmetry coordinates and are expressed in units of 10^{-11} gr$^{\frac{1}{2}}$.

contrary to the case of the external symmetry coordinates. The numerical value of the elements of the N matrix may be calculated by using the molecular geometry assumed in the calculation of G matrix.

Now that all the necessary matrices are evaluated we can calculate the normal coordinates of species A_g. The results are shown in Tables V and VI for the ground and excited state, respectively.

4. THE CONDON OVERLAP INTEGRALS

The Condon overlap integrals have the form

$$R(v', v)=\int \psi_{v'}'(Q')\psi_v(Q)dQ', \tag{9}$$

where v and v' denote sets of vibrational quantum numbers of the ground and the excited state, respectively, of the vibronic transitions concerned. Similarly, Q and Q' represent sets of normal coordinates of the ground and the excited electronic states, respectively. The vibrational eigenfunctions appearing in (9) are

$$\psi_v(Q)=\prod_i N_i(v_i)H_{v_i}(\alpha_i Q_i)\exp[-(1/2)\alpha_i^2 Q_i^2], \tag{10}$$

where $H_{v_i}(\alpha_i Q_i)$ is a Hermitian polynomial of v_ith degree in $\alpha_i Q_i$, $N_i(v_i)$ is a normalization constant

$$N_i(v_i)=(\alpha_i/\pi^{\frac{1}{2}}2^{v_i}v_i!)^{\frac{1}{2}}, \tag{11}$$

and

$$\alpha_i^2=4\pi^2 c\nu_i/h. \tag{12}$$

In Eq. (12) ν_i is the frequency in cm^{-1} of the ith mode of vibration, c the velocity of light, and h is Planck's constant. If the electronic transition does not change the symmetry of a molecule an excited-state normal coordinate belonging to any one of symmetry species of the molecule can be expressed only in terms of the ground-state normal coordinates belonging to that species and a constant. In such a case, we may treat the symmetry species to which the progression-forming

vibration belongs separately, if we are interested only in the *relative* intensities of bands in a progression. This is the case for the 4500-A transition of p-benzoquinone, since the prominent vibrational structure is made up only from totally symmetrical vibrations and the deviation from V_h structure in the excited state may be considered to be negligible.

Thus, we are concerning the Condon overlap integrals

$$R(v_1'v_2'v_3'v_4'v_5'v_6', v_1v_2v_3v_4v_5v_6). \quad (13)$$

Since a ground-state normal coordinate belonging to a given symmetry species of the molecular point group can be expressed in terms of the excited-state normal coordinates belonging to that species and a constant, the Condon overlap integrals take the following form if we are considering the vibrational progression corresponding to Q_1':

$$R(v_1'\,0\,0\cdots 0,\,0\,0\,0\cdots 0)$$
$$=N\int\cdots\int_{-\infty}^{+\infty}H_{v_1'}(\alpha_1'Q_1')\exp\{\sum a_{ii}^{(0)}Q_i'^2$$
$$+2\sum_{i>j}a_{ij}^{(0)}Q_i'Q_j'+2\sum_i a_i^{(0)}Q_i'+a_0^{(0)}\}dQ_1'\cdots dQ_n', \quad (14)$$

where $a^{(0)}$'s are constants related to the fundamental frequencies in both electronic states and the transformation constants relating the ground-state normal coordinates to the excited-state coordinates, and

$$N=(\prod_{i=1}^{n}\alpha_i\alpha_i'/\pi^n 2^{v_1'}v_1'!)^{\frac{1}{2}}. \quad (15)$$

It is assumed that there are n normal coordinates belonging to the symmetry species. Thus, i and j in Eq. (14) run from 1 to n. Performing the integration in (14), with respect to Q_2', it follows that

$$R(v_1'\,0\,0\cdots 0,\,0\,0\,0\cdots 0)$$
$$=(-\pi/a_{22}^{(0)})^{\frac{1}{2}}N\int\cdots\int H_{v_1}(\alpha_1'Q_1')\exp\{\sum_{i\neq 2}a_{ii}^{(2)}Q_i'^2$$
$$+\sum_{i>j;\,i,j\neq 2}a_{ij}^{(1)}Q_i'Q_j'+2\sum_{i\neq 2}a_i^{(1)}Q_i'+a_0^{(1)}\}$$
$$\times dQ_1'dQ_3'\cdots dQ_n', \quad (16)$$

where i and j run from 1 to n excepting 2, and

$$\left.\begin{aligned}a_{ij}^{(1)}&=a_{ij}^{(0)}-[a_{2i}^{(0)}a_{2j}^{(0)}/a_{22}^{(0)}]\\ a_i^{(1)}&=a_i^{(0)}-[a_{2i}^{(0)}a_2^{(0)}/a_{22}^{(0)}]\\ a_0^{(1)}&=a_0^{(0)}-[a_2^{(0)2}/a_{22}^{(0)}]\end{aligned}\right\}. \quad (17)$$

By performing the integration with respect to Q_3', Q_4', $\cdots$, in succession, one arrives at the expression:

$$R(v_1'\,0\,0\cdots 0,\,0\,0\,0\cdots 0)$$
$$=\left[\frac{(-\pi)^{n-1}}{a_{22}^{(0)}a_{33}^{(1)}\cdots a_{n-1\,n-1}^{(n-2)}}\right]^{\frac{1}{2}}N\int_{-\infty}^{+\infty}H_{v_1'}(\alpha_1'Q_1')$$
$$\times\exp\{a_{11}^{(n-1)}Q_1'^2+2a_1^{(n-1)}Q_1'+a_0^{(n-1)}\}dQ_1', \quad (18)$$

where

$$\left.\begin{aligned}a_{ij}^{(r)}&=a_{ij}^{(r-1)}-[a_{r+1\,i}^{(r-1)}a_{r+1\,j}^{(r-1)}/a_{r+1\,r+1}^{(r-1)}]\\ a_i^{(r)}&=a_i^{(r-1)}-[a_{r+1\,i}^{(r-1)}a_{r+1}^{(r-1)}/a_{r+1\,r+1}^{(r-1)}]\\ a_0^{(r)}&=a_0^{(r-1)}-[\{a_{r+1}^{(r-1)}\}^2/a_{r+1\,r+1}^{(r-1)}]\end{aligned}\right\}. \quad (19)$$

From Eq. (18) one arrives, finally, at

$$\left.\begin{aligned}R(00,00)&=\left[\frac{(-1)^n\alpha_1\alpha_1'\alpha_2\alpha_2'\cdots\alpha_n\alpha_n'}{a_{22}^{(0)}a_{33}^{(1)}\cdots a_{n-1\,n-1}^{(n-2)}a_{11}^{(n-1)}}\right]^{\frac{1}{2}}\exp\{a_0^{(n-1)}-(a_1^{(n-1)}/a_{11}^{(n-1)}\}\\ \frac{R(10,00)}{R(00,00)}&=-2^{-\frac{1}{2}}\alpha_1'(a_1^{(n-1)}/a_{11}^{(n-1)})\\ \frac{R(20,00)}{R(00,00)}&=-2^{-\frac{1}{2}}\left[\frac{\alpha_1'^2}{a_{11}^{(n-1)}}\left\{1-\frac{2(a_1^{(n-1)})^2}{a_{11}^{(n-1)}}\right\}+1\right]\\ \frac{R(30,00)}{R(00,00)}&=\frac{\alpha_1'}{\sqrt{3}}\frac{a_1^{(n-1)}}{a_{11}^{(n-1)}}\left[\frac{\alpha_1'^2}{a_{11}^{(n-1)}}\left\{3-\frac{2(a_1^{(n-1)})^2}{a_{11}^{(n-1)}}\right\}+3\right]\end{aligned}\right\}, \quad (20)$$

where we have used following abbreviation:

$$R(v_i'00000,000000)=R(v_i'0,00).$$

Since the geometry of the ground state is known and since the center of mass of the excited state must coincide with that of the ground state, parameters c_i describing the differences between the ground- and the excited-state external symmetry coordinates in such a way that

$$\mathbf{X}=\mathbf{X}'+\mathbf{c}, \quad (21)$$

where $\mathbf{c}^*=(c_1c_2c_3c_4c_5c_6)$,

are sufficient to determine the geometry of the excited

TABLE VII. The numerical form of Eq. (22) for species A_g.

	$L^{-1}N(N')^{-1}L'$					
	Q_1'	Q_2'	Q_3'	Q_4'	Q_5'	Q_6'
Q_1	0.9999 751	0.0067 091	−0.0013 368	−0.0014 864	0.0004 747	−0.0003 880
Q_2	0.0062 665	−0.9766 244	−0.2051 285	0.0065 655	0.0596 358	0.0220 850
Q_3	0.0027 432	−0.2084 542	0.9760 504	0.0266 743	−0.0506 615	−0.0242 012
Q_4	0.0013 534	0.0132 692	−0.0230 023	0.9992 809	0.0268 252	0.0033 225
Q_5	−0.0007 333	0.0479 103	0.0632 449	−0.0260 020	0.9962 217	0.0238 835
Q_6	0.0003 308	0.0153 494	0.0267 288	−0.0022 005	−0.0264 448	0.9991 722
	$L^{-1}N$					
	c_1	c_2	c_3	c_4	c_5	c_6
Q_1	−0.0010 9275	0.0057 8930	−0.1354 6244	−0.1770 6003	0.0952 0652	0.1681 9121
Q_2	0.3440 6114	−0.6110 2691	0.4797 6076	−0.1123 8838	−0.0247 8156	0.0373 1475
Q_3	−0.5541 7444	0.5595 8216	0.4508 1558	−0.0284 7963	−0.0198 9398	0.0318 0164
Q_4	0.0155 1296	−0.0017 0687	0.1896 0877	0.0256 7049	0.1766 6128	−0.0850 1755
Q_5	0.3975 3096	0.1421 3624	0.0844 7318	0.6203 7779	0.0100 2774	0.0542 9437
Q_6	0.8626 1432	0.5377 4676	0.0557 5213	−0.2600 5289	−0.0105 7300	−0.0136 8303

TABLE VIII. Values of $[R(00\nu_3'000)]^2$, corresponding to the bands of the ν_3' progression, for Q_3' models of the excited molecule.

$c_3(Q_3')$ A	0.08	0.10	0.12	0.14	0.16	0.18
$[R(000000)]^2$	0.8335	0.7580	0.6746	0.5882	0.5020	0.4185
$[R(001000)]^2$	0.1618	0.2299	0.2947	0.3497	0.3898	0.4113
$[R(002000)]^2$	0.0009	0.0090	0.0279	0.0584	0.0988	0.1341
$[R(003000)]^2$	0.0018	0.0008	0.0000	0.0013	0.0071	0.0173
ΣR^2	0.9980	0.9977	0.9973	0.9976	0.9977	0.9812

state. It follows from Eqs. (5), (6), and (21) that

$$\mathbf{Q}=\mathbf{L}^{-1}\mathbf{N}(\mathbf{N}')^{-1}\mathbf{L}'\mathbf{Q}'+\mathbf{L}^{-1}\mathbf{N}\mathbf{c}. \qquad (22)$$

An excited-state model is specified when values are assigned to c's. Corresponding values for the Condon overlap integrals may be evaluated by using Eqs. (20) and (22). Thus, by the use of Eq. (1) we may obtain the excited-state model consistent with the intensity distributions among band progressions.

5. CALCULATION

In the following discussion the abbreviated notation

$$R(v_1'v_2'v_3'v_4'v_5'v_6')=R(v_1'v_2'v_3'v_4'v_5'v_6', 000000)$$

will be used. By using the L, L′, N, and N′ matrices obtained as described previously, one can obtain the numerical form of Eq. (22) for species A_g, which is given in Table VII. The Condon overlap integrals involve fundamental frequencies, for which we use the experimental values rather than the computed ones. Experimental frequencies were given in a previous section.

We have performed two sets of calculations of the Condon overlap integrals. In one set of calculations the values of $R(00v_3'000)$ with $v_3'=0, 1, 2, 3$ are calculated for each of six different models of the excited state. In these models each atom, when referred to the equilibrium configuration in the ground state, is displaced in just the same way as when Q_3' is excited. This type of excited state model, which will be called a Q_3' model, is specified by the ratio

$$c_1(Q_3'):c_2(Q_3'):c_3(Q_3'):c_4(Q_3'):c_5(Q_3'):c_6(Q_3')$$

which is equal to the ratio

$$X_1':X_2':X_3':X_4':X_5':X_6' \quad \text{in } Q_3'.$$

The latter ratio may be obtained from a set of simultaneous equations obtained by setting $Q_1'=Q_2'=Q_4'=Q_5'=Q_6'=0$ in the equations of Table VI. The resulting ratio is

$$-0.6139\ 5514:1.0093\ 1226:1.0000\ 0000$$
$$:0.0789\ 5520:-0.6334\ 5101:1.1968\ 7154. \qquad (23)$$

The results of this set of calculations are shown in Table VIII. For these models the integrals $R(v_i'0)$ with $v_i'\neq 0$ ($i\neq 3$) were found to be very nearly zero as expected. A check on the calculation is furnished by the sum rule[15]

$$R^2=1,$$

where the summation is over all bands arising from a given ground-state level. The sums given at the bottom of each column of Table VIII compare favorably with this rule.

[15] G. Herzberg, *Spectra of Diatomic Molecules* (D. Van Nostrand Company, Inc., New York, 1950), 2nd ed., p. 203.

TABLE IX. Values of $[R(000v_4'00)]^2$, corresponding to the bands of the ν_4' progression, for Q_4' models of the excited molecule.

$c_3(Q_4')A$	0.04	0.06	0.08	0.10	0.12
$[R(000000)]^2$	0.8957	0.7917	0.6673	0.5353	0.4090
$[R(000100)]^2$	0.0878	0.1746	0.2616	0.3280	0.3608
$[R(000200)]^2$	0.0034	0.0176	0.0493	0.0987	0.1583
$[R(000300)]^2$	0.0001	0.0010	0.0028	0.0188	0.0445
ΣR^2	0.9869	0.9840	0.9840	0.9808	0.9736

In another set of calculations the values of $R(00v_4'00)$ with $v_4'=0, 1, 2, 3$ have been calculated for another five different models of the excited state. In these models each atom, when referred to the equilibrium configuration in the ground state, is displaced in just the same way as when Q_4' is excited. This type of excited-state model, which will be referred to as a Q_4' model, is specified by the ratio

$$-0.0171\ 3593:0.0106\ 6796:1.0000\ 0000$$
$$:0.0437\ 4319:10.3963\ 2516:-0.0557\ 0599 \quad (24)$$

which may be obtained in the same way as the ratio (23) is obtained, except for setting $Q_1'=Q_2'=Q_3'=Q_5'=Q_6'=0$. The results of this set of calculations are given in Table IX.

6. MODELS CONSISTENT WITH INTENSITY DISTRIBUTION AMONG THE TOTALLY SYMMETRICAL PROGRESSIONS

As mentioned in a previous section, the Condon overlap integrals R for the band progression are related to the peak extinction coefficient ϵ as follows:

$$R_{v_i'}^2/R_0^2=(\epsilon_{v_i'}/\nu_{v_i'})/(\epsilon_0/\nu_0), \quad (25)$$

where zero refers to a vibronic transition in the upper state of which the progression-forming vibrations is not excited, while v_i' refers to the vibronic transition in the upper state of which the progression-forming vibration is excited by v_i' quanta superimposing the vibronic transition indicated by subscript zero.

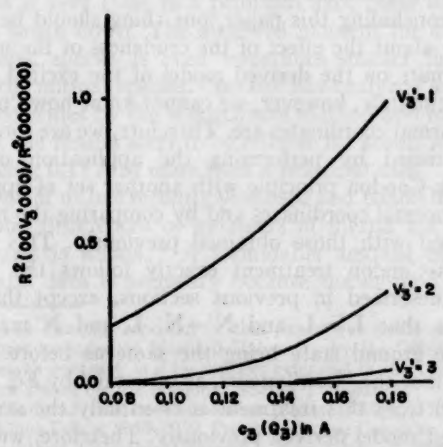

FIG. 2. Computed relative intensity of the first three of ν_3' progression vs the model of the excited state as specified by $c_3(Q_3')$.

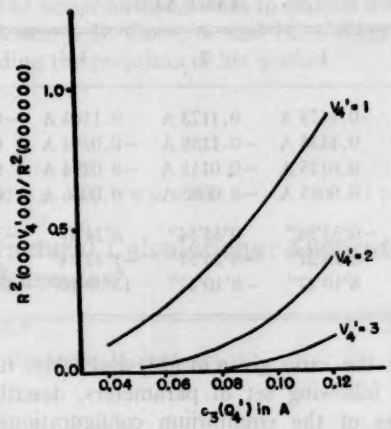

FIG. 3. Computed relative intensity of the first three of ν_4' progression vs the model of the excited state as specified by $c_3(Q_4')$.

In Fig. 2, values from Table VIII for the computed relative intensity $R^2(00v_3'000)/R^2(000000)$ of the first three bands of the ν_3' progression are plotted vs the model of the excited state as specified by $c_3(Q_3')$. Similarly, Fig. 3 shows the variation of computed intensity of bands of the ν_4' progression with variation of the Q_4' type model.

The results of comparing these computed intensities with the observed values, listed in Table I, are given in Table X. The first column gives the square of the ratio of the Condon overlap integrals as determined from experimental intensities by using Eq. (25), while the second column gives the parameter of the excited-state model which reproduces this ratio as determined by Figs. 2 and 3. From the results of Table X it is concluded that the best models of the excited state, consistent with the band intensities in the progressions of totally symmetrical vibrations, are those corresponding to

$$\left.\begin{aligned} &c_3(Q_3')=\pm 0.1430\ \text{A} \\ \text{and}\quad &c_3(Q_4')=\pm 0.0845\ \text{A} \end{aligned}\right\}. \quad (26)$$

TABLE X. Determination of the Q_3' and Q_4' model consistent with the observed intensities in the totally symmetric progressions.

Experimental intensity ratio from Table I	Resulting model from Figs. 2 and 3
$R^2(001000)/R^2(000000)=0.6050$	$c_3(Q_3')=0.141$
$R^2(002000)/R^2(000000)=0.1165$	$c_3(Q_3')=0.145$
$R^2(000100)/R^2(000000)=0.4986$	$c_3(Q_4')=0.090$
$R^2(000200)/R^2(000000)=0.0676$	$c_3(Q_4')=0.079$

TABLE XI.

Model	1	2	3	4
$r_{C'O}$	−0.1173 A	0.1173 A	0.1104 A	−0.1104 A
r_{CC}	0.1138 A	−0.1138 A	−0.0294 A	0.0294 A
$r_{C'C}$	0.0115 A	−0.0115 A	−0 0294 A	0.0294 A
r_{CH}	0.0085 A	−0.0085 A	−0.0046 A	0.0046 A
α'	−0°53′54″	0°53′54″	3°24′47″	−3°24′47″
α	0°26′57″	−0°26′57″	−1°42′24″	1°42′24″
β	8°10′47″	−8°10′47″	15°39′10″	−15°39′10″

By using the ratio given in (23) and (24), it follows that the following set of parameters, describing the differences of the equilibrium configurations of the molecule in the ground and the excited states, are consistent with the experimental intensity distribution among the band progressions of totally symmetrical vibrations:

$$\left.\begin{array}{ll} c_1(Q_3')=\mp 0.087\,796 & c_1(Q_4')=\mp 0.001\,448 \\ c_2(Q_3')=\pm 0.144\,332 & c_2(Q_4')=\pm 0.000\,901 \\ c_3(Q_3')=\pm 0.143\,000 & c_3(Q_4')=\pm 0.084\,500 \\ c_4(Q_3')=\pm 0.011\,291 & c_4(Q_4')=\pm 0.003\,696 \\ c_5(Q_3')=\mp 0.090\,583 & c_5(Q_4')=\pm 0.878\,489 \\ c_6(Q_3')=\pm 0.171\,153 & c_6(Q_4')=\mp 0.427\,207 \end{array}\right\}. \quad (27)$$

It is to be noted that the Franck-Condon principle cannot differentiate the two alternative signs for the value of c. For this reason, by pairing off each of the foregoing Q_3' models with each of the Q_4' models, four resultant models of the excited electronic state may be obtained. In Table XI the change of the molecular geometry brought about by the electronic excitation, corresponding to these four models of the excited molecule, is given. Since the four models of excited state are equally consistent with the intensity distribution, and the rotational structure of the electronic spectrum is not resolved even partially, we have selected one of these four models as the best model among four in the following manner. The changes of CC and CO bond lengths in the course of electronic excitation are estimated from the bond order by using the bond order-bond length relation as already mentioned in a previous section concerning the calculation of G-matrix elements. The results may be found in the last column of Table II. If we calculate the quantity

$$\sum_i \{(\Delta r_i)_{\text{order}} - (\Delta r_i)_{\text{FC}}\}^2, \quad (28)$$

we find that it is equal to 0.0467, 0.0192, 0.0036, and 0.0365, for models 1, 2, 3, and 4 of Table XI, respectively. In (28), Δr_i denotes the change of bond length caused by the electronic excitation. Subscripts "order" and "FC" denote that the Δr_i is derived from order-length relation and from the Franck-Condon principle, respectively, and that the summation extends over CC and CO bonds. We take model 3 as the "best" model, since the quantity (28) for this model is the smallest of the four.

7. DISCUSSIONS AND CONCLUSIONS

Now that the excited-state model has been derived the vibrational frequency, $\nu_2(A_u)$ may be calculated in order to determine whether the consideration of the change of bond angles brought about by the electronic excitation removes the disagreement between the calculated and "experimental" value of $\nu_2(A_u)$, as anticipated in Sec. 1. The bond orders mentioned in a previous section may be used to obtain the force constant of torsion around CC bonds by the method described previously.[2] The interaction constant between the wagging of the CH bond and the torsion around the CC bond may be obtained from the diagonal constant of torsion and the bond angles derived in the preceding section of this paper by using the method which has been described previously.[2] The other force constants were assumed to be equal to the values in the ground state.[1] The G-matrix elements were calculated by using the excited-state geometries derived in the previous section of this paper. The result is $\nu_2(A_u)=438$ cm^{-1} in the excited state showing that this frequency should increase upon electronic excitation. Therefore, the ground-state frequency should be smaller than one-half of the A_0-D_0 separation (1068 cm^{-1}), in the notation of Part V,[10] and we may say that a part of discrepancy between the calculated value and "experimental" value of $\nu_2(A_u)$ in the ground state can be removed by considering the planar changes of bond angles in the course of electronic excitation.

In concluding this paper, one thing should be mentioned about the effect of the crudeness of the normal coordinate on the derived model of the excited state. Unfortunately, however, we cannot know how "much" our normal coordinates are. Therefore, we are forced to be satisfied by performing the application of the Franck-Condon principle with another set of approximate normal coordinates and by comparing the results obtained with those obtained previously. This other Franck-Condon treatment exactly follows the treatment described in previous sections, except that we assume that $\mathbf{L}'=\mathbf{L}$ and $\mathbf{N}'=\mathbf{N}$, $\mathbf{L}$ and $\mathbf{N}$ matrices for the ground state being the same as before. It is found that the "best" model, as estimated by Eq. (28), derived from this treatment is essentially the same as the best model derived previously. Therefore, we may have some right to expect that the crudeness of our normal coordinates does not bring serious errors in the resulting model.

8. ACKNOWLEDGMENTS

The authors wish to thank Professor S. Imanishi and Dr. Y. Kanda for their encouragement throughout this work. The senior author wishes to express his gratitude to Professor J. B. Coon, A. and M. College of Texas, for sending the preprints of his works.

THE JOURNAL OF CHEMICAL PHYSICS VOLUME 32, NUMBER 6 JUNE, 1960

Second Differences of Moments of Inertia in Structural Calculations: Application to Methyl-Fluorosilane Molecules*

LAWRENCE C. KRISHER,†

Department of Chemistry, Harvard University, Cambridge, Massachusetts

AND

LOUIS PIERCE,

Department of Chemistry, University of Notre Dame, Notre Dame, Indiana

(Received December 3, 1959)

An extension and application of the method recently proposed by Pierce for the location of "near-axis atoms" from spectroscopically determined moments of inertia is made. Equations are derived which are required for the application of the method to asymmetric top molecules with C_s symmetry. The method is applied to the determination of silicon coordinates in the molecules CH_3SiH_2F and CH_3SiHF_2. The experimental results are combined with results of previous microwave investigations of these molecules in order to determine their structures. Addition of each fluorine atom lowers the SiC distance. The SiF distance is lowered on adding the second fluorine. In the case of CH_3SiHF_2 the equilibrium conformation (staggered) is also determined.

I. INTRODUCTION

MICROWAVE spectroscopists have long been faced with the problem of making use of data from isotopic substitution of an atom which is very close to one or more principal axes. Fitting the structure to the observed moments of inertia is inaccurate because of zero-point vibrational effects. Kraitchman[1] has developed formulas employing differences of moments of inertia for isotopic substitution which tend to cancel these effects. However, when a substituted atom is very close to a principal axis, these equations also break down. The observed moment for a heavier isotopic species is even sometimes smaller than that for the normal species. Costain[2] has analyzed a number of molecules by the Kraitchman method and has found that the results seem to be reliable for atoms which are roughly 0.15 A or more from a principal axis.

One of us has recently proposed and tested the use of second differences of moments of inertia for locating "near-axis atoms."[3] A formidable amount of experimental data is necessary because the method requires moments of inertia of doubly isotopically substituted molecules. Fortunately, the excellent results obtained in the test case of NNO suggest that the labor involved in the use of second differences is well rewarded.[3]

In the present paper the treatment of reference 3 is extended. Equations are derived which are appropriate for location, by the second-difference method, of atoms near principal axes in asymmetric rotors with a plane of symmetry. We have also undertaken the experimental study of two methyl fluorosilane molecules. In both of these molecules, the silicon atom lies less than 0.02 A from a principal axis. The "near-axis" coordinate in both cases is determined by the second-difference method. As for the linear molecule case[3] the method requires four isotopic species, with substitution in two different frameworks, e.g., $CH_3Si^{28}H_2F$, $CH_3Si^{29}H_2F$, $CD_3Si^{28}H_2F$, and $CD_3Si^{29}H_2F$. The method assumes that the transformation from one framework to the other is known (in the example the molecule $CH_3Si^{28}H_2F$ forms one framework and $CD_3Si^{28}H_2F$ forms the second).

We have also studied the rotational spectrum of CH_2DSiHF_2 in order to determine the equilibrium conformation of this molecule.

II. THEORY OF SECOND DIFFERENCES OF MOMENTS OF INERTIA

A. Atom Near One Principal Axis

An an example of substitution of an atom near *one* principal axis consider the calculation of the "a"

* The research reported in this paper was made possible by support extended to Harvard University by the Office of Naval Research contract, and by support extended to the University of Notre Dame by the National Science Foundation.

† National Science Foundation Fellow 1955–1958; National Distillers Fellow 1958–1959. Present address: Columbia Radiation Laboratory, Columbia University, New York 27, New York.

[1] J. Kraitchman, Am. J. Phys. **21**, 17 (1953).

[2] C. C. Costain, J. Chem. Phys. **29**, 864 (1958).

[3] L. Pierce, J. Mol. Spectroscopy **3**, 575 (1959).

coordinate of the silicon atom in methyl monofluorosilane. Here the four species are $CH_3Si^{28}H_2F$, $CH_3Si^{29}H_2F$, $CD_3Si^{28}H_2F$, and $CD_3Si^{29}H_2F$. The problem is to calculate "a_{Si}" from $\Delta I_b(CD_3)-\Delta I_b(CH_3)$ where

$$\Delta I_b(CD_3)=I_b(CD_3Si^{29}H_2F)-I_b(CD_3Si^{28}H_2F),$$

$$\Delta I_b(CH_3)=I_b(CH_3Si^{29}H_2F)-I_b(CH_3Si^{28}H_2F),$$

and a_{Si} is the coordinate of the silicon atom in the $CH_3Si^{28}H_2F$ system. Note that here b_{Si} is already known; it can safely be calculated from ΔI_a, ΔI_b using Kraitchman's equations.

It remains to express $\Delta I_b(CD_3)-\Delta I_b(CH_3)$ in terms of a_{Si} (hereafter called simply "a"). From Kraitchman's equations we can write

$$\Delta I_b(CH_3)=\mu a^2\{1+[\Delta I_a(CH_3)/(I_a-I_b)]\}^{-1}=ka^2 \quad (1)$$

where I_a, I_b are the principal moment of $CH_3Si^{28}H_2F$, $\mu=M\Delta m/M+\Delta m$ with M = mass of $CH_3Si^{28}H_2F$, $\Delta m=m(Si^{29})-m(Si^{28})$, and "$a$" is the coordinate of the silicon atom in the $CH_3Si^{28}H_2F$ system. Here k is a directly calculable quantity.

There will be a similar expression for $\Delta I_b(CD_3)$

$$\Delta I_b(CD_3)=\mu'(a')^2\{1+[\Delta I_a(CD_3)/(I_a'-I_b')]\}^{-1}=k'(a')^2 \quad (2)$$

where I_a', I_b' are moments of $CD_3Si^{28}H_2F$, $\mu'=M'\Delta m/M'+\Delta m$, M' = mass of $CD_3Si^{28}H_2F$, $\Delta m=m(Si^{29})-m(Si^{28})$ and a' is the coordinate of the silicon atom in the $CD_3Si^{28}H_2F$ system.

But a', b' and a, b are related by the known transformation[4] between the $CH_3Si^{28}H_2F$ and $CD_3Si^{28}H_2F$ frameworks:

$$a'=(a-A)\cos\theta-(b-B)\sin\theta$$

$$b'=(a-A)\sin\theta+(b-B)\cos\theta \quad (3)$$

where A, B are the coordinates of the center of mass of $CD_3Si^{28}H_2F$ in the CH_3 system, and θ is the angle of rotation from the CH_3 to the CD_3 system. Note that

$$a'=a\cos\theta+C \quad (4)$$

where C is a calculable constant.

Thus we can set up the required relation connecting the second difference of the I_b's and the "a" coordinate of the silicon:

$$\Delta\Delta I_b=\Delta I_b(CD_3)-\Delta I_b(CH_3)=k'(a')^2-ka^2$$

$$=(k'\cos^2\theta-k)a^2+(2k'C\cos\theta)a+k'C^2 \quad (5)$$

[4] In principle, this transformation depends only on the coordinates of the atoms on which substitutions are made, i.e., the methyl hydrogens. In this example the position of each hydrogen was not independently determined, and we assume that they are placed symmetrically around the C—Si bond. Thus the hydrogen coordinates and the CH_3 to CD_3 transformation are affected by the still undetermined silicon coordinate. Here this uncertainty in a_{Si} has a negligible effect on the result.

In the case where an atom is very close to the "a" principal axis, there is a similar relation connecting $\Delta\Delta I_a$ and the "b" coordinate of the atom.

It may sometimes be inconvenient to use one or the other of the preceding relations. Often, for example, an accurate spectroscopic determination of I_a is difficult, and location of an atom which is close to the "b" axis will be correspondingly inaccurate using the above formulas. In such cases, the use of I_c's may prove valuable. Since I_c refers to the radial distance of an atom from the center of mass in the plane of symmetry (here assumed to be the ab plane), the second difference equation takes the form

$$\Delta\Delta I_c=\Delta I_c(CD_3)-\Delta I_c(CH_3)=\mu'[(b-B)^2+(a-A)^2]-\mu[a^2+b^2]. \quad (6)$$

Since all other quantities are assumed to be calculable, we can thus find "b" from the ΔI_c's.

B. Atom near Center of Mass

In the preceding section, second differences of moments of inertia were used to calculate one near-axis coordinate of an atom whose other in-plane coordinate was assumed to be large, i.e., calculable from the Kraitchman formula. In this section we shall discuss the case of an atom near the center of mass, where neither the a nor b coordinates can be directly calculated.

In principle, the method of Sec. IA could be used, and we could solve a simultaneous system of two second-difference equations for the two unknowns, a and b. The algebra involved, however, is formidable. Fortunately, for the case where an atom is near the center of mass, certain simplifications are sometimes possible.

If it is possible, to a good approximation, to ignore the effect of rotation for the two species having the same "framework," this is equivalent to ignoring the second term in the expression for ΔI_b from Sec. IA, so that it becomes simply

$$\Delta I_b\simeq\mu a^2. \quad (7)$$

Similarly

$$\Delta I_b'\simeq\mu'(a')^2 \quad (8)$$

where a' is the "a" coordinate of the substituted atom in the second framework. Thus

$$\Delta\Delta I_b=\mu'(a')^2-\mu a^2. \quad (9)$$

This type of expression is analogous to that of Pierce[3] for the linear molecule case, and has been used by the authors for calculating the coordinate of the central carbon atom of CH_3COF.[5]

It is important to notice that this approximation is not always valid. For example, in a near-oblate top,

[5] L. Pierce and L. C. Krisher, J. Chem. Phys. 31, 875 (1959).

TABLE I. Observed spectra.[a]

Transition	CH_3SiH_2F molecules		
	$CH_3Si^{28}H_2F$	$CH_3Si^{29}H_2F$	$CH_3Si^{30}H_2F$
$1_{1,1}-2_{1,2}$	23 389.50 Mc	23 342.66	23 298.30
$1_{0,1}-2_{0,2}$	24 519.10	24 484.70	24 451.59
$1_{1,0}-2_{1,1}$	25 806.77	25 791.38	25 776.55
	CD_3SiH_2F molecules		
Transition	$CD_3Si^{28}H_2F$	$CD_3Si^{29}H_2F$	$CD_3Si^{30}H_2F$
$1_{1,1}-2_{1,2}$	20 326.70	20 284.02	20 243.40
$v=1$	20 319.39	20 276.44	20 236.06
$1_{0,1}-2_{0,2}$	21 211.54	21 179.40	21 148.76
$v=1$	21 197.28	21 165.26	21 134.95
$1_{1,0}-2_{1,1}$	22 206.50	22 189.69	22 173.46
$v=1$	22 183.99	22 167.26	22 151[b]
$2_{0,2}-3_{0,3}$	31 681.20	31 628.73	31 577.4[b]
$2_{1,1}-3_{1,2}$	33 274.15		33 224.40
$2_{1,2}-3_{1,3}$		30 391.14	30 328.58
$2_{2,1}-3_{2,2}$		31 854.5[a]	31 813.56

[a] Estimated accuracy ±0.10 Mc except where otherwise indicated.
[b] ±1 Mc.

I_a and I_b are nearly equal, and a considerable rotation of the principal axes can occur on substitution even though a and b are small.

III. EXPERIMENTAL

Extensive microwave data on CH_3SiH_2F and CH_3SiHF_2 have already been reported.[6,7] The preparations of CH_3SiH_2F and CD_3SiH_2F are described in reference 6. We used these samples and observed the Si^{29} and Si^{30} transitions in natural abundance.

Table I lists the observed transitions of $CH_3Si^{29}H_2F$ and $CH_3Si^{30}H_2F$ along with the corresponding transitions of $CH_3Si^{28}H_2F$ (for comparison). Rotational constants and moments of inertia for these species are listed in Table II. The observed spectra of $CD_3SiH_2F(Si^{28,29,30})$ are also listed in Table I. The low-J lines of these species have nearby satellites, nearly half as intense as the main lines, and these were used to confirm the assignments. Derived rotational constants and moments of inertia are listed in Table II.

TABLE II. Rotational constants and moments of inertia.[a]

	CH_3SiH_2F		
	Si^{28}	Si^{29}	Si^{30}
A	20 050 Mc	[19 848]	[19 657]
B	6753.80	6753.94	6753.92
C	5545.26	5529.58	5514.79
I_a	25.214 amu A²	[25.470]	[25.718]
I_b	74.8513	74.8498	74.8500
I_c	91.1645	91.4230	91.6682
	CD_3SiH_2F		
	Si^{28}	Si^{29}	Si^{30}
A	17 412 Mc	[17 248]	[17 087]
B	5786.60	5785.63	5784.62
C	4846.70	4832.80	4819.59
I_a	29.033 amu A²	[29.310]	[29.586]
I_b	87.3624	87.3770	87.3923
I_c	104.3042	104.6042	104.8909

[a] Conversion factor $h/8\pi^2=5.05531\times10^5$ amu A² Mc.

[6] L. Pierce, J. Chem. Phys. 29, 383 (1958).
[7] J. D. Swalen and B. P. Stoicheff, J. Chem. Phys. 28, 671 (1958).

TABLE III. Observed spectra of CD_3SiDF_2 molecules.

Transition	$CD_3Si^{28}DF_2$[a]	$CD_3Si^{29}DF_2$[b]	$CD_3Si^{30}DF_2$[b]
$1_{1,1}-2_{1,1}$	15 135.65 Mc	[c]	[c]
$1_{0,1}-2_{0,2}$	15 903.16	15 894.60	15 885.81
$1_{1,0}-2_{1,1}$	18 385.27	18 367.14	18 349.40
$2_{1,1}-3_{1,2}$	22 255.23	22 247.70	22 240.68
$2_{0,2}-3_{0,3}$	22 627.94	22 620.04	[c]
$2_{2,1}-3_{2,2}$	25 140.47	25 122.39	25 103.39
$2_{1,1}-3_{1,2}$	26 796.36		
$2_{2,0}-3_{2,1}$	27 653.13		
$1_{0,1}-2_{1,1}$	21 292.84		
$1_{1,0}-2_{2,0}$	23 091.31		
$1_{1,1}-2_{2,1}$	23 858.82		

[a] Estimated uncertainty ±0.1 Mc.
[b] Estimated uncertainty ±0.2 Mc.
[c] Buried by a strong line.

The sample of CD_3SiDF_2 was prepared by reacting CD_3SiD_3, kindly provided by Professor M. K. Wilson, with a double-molar amount of HCl in the presence of an $AlCl_3$ catalyst. The resulting CD_3SiDCl_2 was then passed over SbF_3 in a vacuum apparatus, and thereby converted to CD_3SiDF_2. The spectra of CD_3SiDF_2-$(Si^{28,29,30})$ are listed in Table III, and derived moments of inertia are given in Table IV. The results for normal $CH_3SiHF_2(Si^{28,29,30})$ were taken from reference 7.

TABLE IV. Rotational constants and moments of inertia.[a]

	CH_3SiHF_2[b]	
	Si^{28}	Si^{29}
A	6846.63 Mc	6835.39
B	6120.40	6111.15
C	3755.61	3755.66
I_a	73.836 amu A²	73.958
I_b	82.598	82.723
I_c	134.607	134.605
	CD_3SiDF_2	
	Si^{28}	Si^{29}
A	6258.43 Mc	6276.31
B	5002.52	4996.50
C	3377.71	3377.63
I_a	80.429 amu A²	80.546
I_b	101.055	101.177
I_c	149.667	149.670

[a] Conversion factor $h/8\pi^2=5.05531\times10^5$ amu A² Mc.
[b] Derived from the data of reference 7.

TABLE V. Silicon coordinates by second-difference method; Si—C bond distances.

	CH_3SiH_2F	
a_{Si}	From $Si^{29,28}$ data 0.0179 A Si—C bond distance = 1.849 A	From $Si^{30,28}$ data 0.0164 A
	CH_3SiHF_2	
a_{Si}	From $Si^{29,28}$ data −0.0090 A ($\Delta\Delta I_c$) −0.0107 A ($\Delta\Delta I_b$) Si—C bond distance = 1.840 A	

CH_2DSiHF_2 was prepared by similar reactions, starting with CH_2DSiH_3.[8] The observed spectra for the *sym* and *asym* species, and other data are listed in Tables VI and VII.

Rotational transitions were measured at either the Harvard or Notre Dame laboratories with typical Hughes-Wilson microwave spectrometers, employing 100 kc Stark modulation. Frequency measurements were made with multiples of 5 Mc standards, which were monitored by signals from the Cruft Laboratories of Harvard University, or the 10 Mc WWV signal, respectively.

IV. SILICON COORDINATES AND Si-C DISTANCE IN CH_3SiH_2F

A. Second-Difference Calculation

The "*b*" coordinate of the silicon atom of CH_3SiH_2F can be directly calculated from the Kraitchman formula, by considering the change in moments for the pair $CH_3Si^{29,28}H_2F$ or for $CH_3Si^{30,28}H_2F$. The agreement is excellent, and we have used the average of the two values. Both coordinates of the carbon atom can be accurately calculated by the standard Kraitchman method.

The "*a*" coordinate of the silicon atom is very small and a direct Kraitchman treatment is clearly inadequate, e.g., I_b for $CH_3Si^{29}H_2F$ was observed to be slightly less than I_b for $CH_3Si^{28}H_2F$. The silicon "*a*" was calculated by the second-differences method described in detail in Sec. II of this paper. We have enough data for two independent calculations; we can use $CD_3Si^{29,28}$, $CH_3Si^{29,28}$ as well as the set $CD_3Si^{30,28}$, $CH_3Si^{30,28}$. This calculation employs the ΔI_b's which were accurately determined. The values of a_{Si} for the two independent calculations are given in Table V. The agreement is excellent and the average of the two values was used for the Si–C bond distance calculation.

Note that the transitions measured do not allow a good determination of I_a. The bracketed values listed in the tables were obtained from the "*a*" moments of the normal species and the calculated isotopic shift. The second-difference calculation for a_{Si} depends primarily on the ΔI_b's, and this approximate calculation of the isotopic I_a values has a negligible effect on this result.

B. Complete Structure of CH_3SiH_2F

The foregoing calculations required the transformation from the CH_3SiH_2F to CD_3SiH_2F principal axis system, and this in turn required a considerable amount of structural information. The structure as reported by Pierce[6] was determined by a least square fit of moments of inertia using assumed values of two parameters, the HSiH and CSiH angles. Since publication of Costain's work,[2] it has been generally accepted that structures are best determined by fitting *differences* of moments of inertia. In view of this we felt that a recalculation of the structure of CH_3SiH_2F would be desirable. In the recalculation no assumed values of structural parameters were used.[9] All atom coordinates, except those of fluorine and the "*a*" coordinate of silicon, were determined by making use of differences of moments of inertia. The remaining three coordinates were obtained from the first moment equations and the principal axis condition. With this recalculated structure the method of second differences was then used to obtain the "*a*" coordinate of silicon directly as described in Sec. IVA. Finally the fluorine coordinates were recomputed using only the first moment equations. The resulting structural parameters are listed in Table VI. It is noteworthy that they differ only slightly from the ones reported in reference 6 with the exception of the CSiH angle. The results seem to suggest that for heavy atoms the least squares method of fitting moments of inertia to obtain structures should give results about as good as the method of fitting differences of moments. However, the latter method is much to be preferred since it requires much less computational work, especially when Kraitchman's equations can be used.

TABLE VI. "Structures" of methyl-fluorosilanes.

	CH_3SiH_2F		
Si—C	1.849±0.005	<	HSiH 110° 0′±30′
Si—F	1.597±0.005	<	CSiH 112° 28′±1° 30′
Si—H	1.477±0.005	<	HCH 108° 29′±30′
C—H	1.099±0.005	<	CSiF 108° 53′±30′
	CH_3SiHF_2		
Si—C	1.840 A±0.010	<	FSiF 107°6′±30′
Si—F	1.580±0.008	<	CSiH 115° 32′±1°
Si—H	1.471±0.010	<	CSiF 109°22′±30′
C—H	1.094±0.005	<	HCH 108°32′±30′

[8] R. W. Kilb and L. Pierce, J. Chem. Phys. **27**, 108 (1957).

[9] It was however assumed that the methyl group is symmetrical and coaxial with the CSi bond. The same assumption was made for CH_3SiHF_2.

With regard to the preceding structural calculations, it is important to note that experimental values of differences in the "a" moments of inertia were *not* used in locating the in-plane atoms. The differences were calculated from the relation

$$\Delta I_a = \Delta I_c - \Delta I_b \qquad (10)$$

which holds for in-plane substitutions if changes in inertial defects are neglected. Use of Eq. (10) was necessary because only "a"-type transitions which are insensitive to the "a" rotational constants have been observed for CH_3SiH_2F molecules. The "a" rotational constants reported in reference 6 are uncertain by about 10 Mc.

In order to locate the out-of-plane silyl hydrogens it was of course necessary to make use of the "a" moments. Because of this, the small (0.17 A) "a" coordinate of these atoms is uncertain by about ±0.03 A. This results in a rather large uncertainty of ±1.5° for the CSiH angle.

The two C-H parameters were obtained in the same manner as described in the following for CH_3SiHF_2. This involved the use of "a" moments but essentially the same results were obtained by fitting only the "b" and "c" moments.

V. Si COORDINATES AND Si-C DISTANCE IN CH_3SiHF_2

A. Coordinate by Second-Difference Method

CH_3SiHF_2 presents a similar case, except that the plane of symmetry for this molecule is the a, c plane. Both coordinates of the carbon atom as well as the "c" coordinate of the silicon can be calculated by the Kraitchman method.

The "a" coordinate of silicon is again very small and the method of second-differences was employed for its determination. The four species $CH_3Si^{29,28}HF_2$ and $CD_3Si^{29,28}DF_2$ were used. A determination using the

TABLE VII. Observed spectra (Mc).[a]

Rotational transition	*sym*-CH_2DSiHF_2 obs	*asym*-CH_2DSiHF_2 obs	*asym*-CH_2DSiHF_2 calc[b]
$0_{0,0}-1_{0,1}$	9 437.10	9 334.73	9 334.60
$1_{1,1}-2_{1,2}$	16 763.72	16 528.39	16 528.38
$1_{0,1}-2_{0,2}$	17 447.21	17 281.36	17 281.13
$1_{1,0}-2_{1,1}$	20 985.49	20 810.02	20 810.02
$2_{1,2}-3_{1,3}$	24 417.34	24 078.27 24 083.22	24 081.45
$2_{0,2}-3_{0,3}$	24 620.48	24 325.20 24 328.18	24 329.44
$2_{2,1}-3_{2,2}$	28 311.60	28 004.28	28 003.80
$2_{1,1}-3_{1,2}$	29 966.89	29 787.24 29 789.34	29 787.52
$2_{2,0}-3_{2,1}$	32 002.61	31 678.18	31 678.20
$3_{1,3}-4_{1,4}$	31 824.00	31 370.12	31 372.45

[a] ±0.20 Mc.
[b] Calculated from the rotational constants of Table VIII.

TABLE VIII. Rotational constants and principal moments of inertia.[a]

	sym-CH_2DSiHF_2	*asym*-CH_2DSiHF_2
A	6704.16 Mc	6796.64
B	5774.09	5737.71
C	3663.21	3596.89
I_a	75.406 amu A²	74.380
I_b	87.552	88.107
I_c	138.002	140.547
$I_a+I_c-I_b$	125.856	

[a] The conversion factor $h/8\pi^2=5.05531\times10^5$ amu A² Mc was used.

$Si^{30,28}$ system was not possible in this case. Swalen and Stoicheff found that the spectrum of $CH_3Si^{30}HF_2$ was largely "buried" by stronger lines and they were unable to get an accurate I_c for this species. We experienced similar difficulties with $CD_3Si^{30}DF_2$.

Two independent determinations of "a_{Si}" were made using $\Delta\Delta I_c$ and $\Delta\Delta I_b$. The two values of "a_{Si}" listed in Table V are seen to be in excellent agreement. Unfortunately, the agreement is not a good measure of the accuracy of the "a_{Si}" determination. Unlike the case of CH_3SiH_2F, the second differences of moments of inertia are for CH_3SiHF_2 quite small. Accordingly, because of experimental uncertainties in the moments of inertia, the values of "a_{Si}" quoted in Table V for CH_3SiHF_2 may be in error by as much as ±0.01A. Absolute errors for the I_b's are considerably less than for the I_c's. Consequently, in calculating the SiC distance we used "a_{Si}" as determined from $\Delta\Delta I_b$.

B. Complete Structure of CH_3SiHF_2

The new isotopic data reported here, when combined with that of Swalen and Stoicheff[7] allow a complete determination of the structure of methyl difluorosilane by the difference of moments methods (except for the fluorine coordinates). Accurate "a" moments are available for most isotopic species and because of this there are various ways of using the experimental data for calculating the coordinates of in-plane atoms by virtue of the relation

$$\Delta I_a + \Delta I_c - \Delta I_b = 0. \qquad (11)$$

Because inertial defects change slightly upon isotopic substitution, Eq. (11) is not satisfied exactly. When a coordinate is 1 A or larger, the various Kraitchman expressions give, in the present case, essentially the same result (±0.002 A variation or less). For small coordinates, (the "c" coordinates of carbon and silicon, and the "a" coordinate of the silyl hydrogen in the present case), discrepancies of 0.01 A and larger are encountered. In the case of the "c" coordinate of carbon we chose to use the average value of ΔI_a and $\Delta I_b - \Delta I_c$, simply because there is at present no sound theoret-

TABLE IX. Molecular parameters of fluorosilanes and methyl fluorosilanes.[a]

	CH	<HCH	SiC	SiH	<HSiH	<CSiH	<CSiF	SiF	<FSiF
CH_3SiH_3[b]	1.092	107°53′	1.867	1.483	108°20′	110°36′			
CH_3SiH_2F	1.099	108°29′	1.849	1.477	110°0′	112°28′	108°53′	1.597	
CH_3SiHF_2	1.094	108°32′	1.840	1.471		115°32′	109°22′	1.580	107°6′
SiH_3F[c]				1.453	110°11′			1.593	
SiH_2F_2[d]				1.467	114°54′			1.578	107°50′
$SiHF_3$[e]				1.455				1.565	108°16′

[a] Bond distances are in A. Many of the parameters in this table have been recalculated using data taken from the references listed below. Details of the calculations are in the text.
[b] Reference 8.
[c] Sharbaugh, Thomas, and Pritchard, Phys. Rev. **78**, 64 (1950); Bak, Bruhn, and Rastrup-Anderson, J. Chem. Phys. **21**, 752 (1953).
[d] V. Laurie, J. Chem. Phys. **26**, 1359 (1957).
[e] Sheridan and Gordy, Phys. Rev. **77**, 719 (1950), and J. Chem. Phys. **19**, 965 (1952); Heath, Thomas, and Sheridan, Trans. Faraday Soc. **50**, 779 (1954).

ical reason for choosing one value in preference to the other. Similarly, in calculating the "a" coordinate of the silyl hydrogen we used the average value of ΔI_c and $\Delta I_b - \Delta I_a$. The "c" coordinate of silicon on the other hand was calculated using the experimental value of $\Delta I_b - \Delta I_c$ rather than ΔI_a. The reason for this choice is that transitions of $CH_3Si^{29}HF_2$ which are sensitive to I_a are doublets, and only one such doublet was resolved,[7] leaving considerably more uncertainty in I_a for this species than for other species of methyl difluorosilane. The out-of-plane methyl hydrogen coordinate was determined from the species $CD_3Si^{28}DF_2$ and $CH_3Si^{28}DF_2$ by the method described by Laurie.[10] The remaining methyl hydrogen parameter was obtained by fitting the observed differences of moments of inertia for the pair CD_3SiDF_2, CH_3SiDF_2; the value C−H=1.094 A gives an excellent fit to the three observed ΔI's.

The "a" coordinate of the silicon atom was then determined by the method of second differences described above.

This leaves only the fluorine, for which there are no stable isotopes. The out-of-plane F coordinate was calculated from the relation

$$I_a + I_c - I_b = 4m_H r_H^2 + 4m_F r_F^2 \qquad (12)$$

where the r's are the out-of-plane coordinates of the methyl hydrogens (determined before) and of the fluorines. In this calculation we also assumed a typical "inertial defect," Δ', of 0.10 amu A^2 for this molecule.[10] The remaining fluorine coordinates were then calculated from the first-moment equations.

The results of this structural calculation are given in Table VI.

In view of the uncertainty in a_{Si}($\pm$0.01 A), we also determined a_{Si} and the fluorine coordinates from the first moment equations and the principal axis condition. This method gives a C–Si bond distance of 1.829 A and Si–F distance of 1.589 A.

[10] V. W. Laurie, J. Chem. Phys. **28**, 704 (1958).

VI. MICROWAVE SPECTRUM AND EQUILIBRIUM CONFIGURATION OF CH_2DSiHF_2

The microwave spectrum of CH_2DSiHF_2 arises from two distinct rotational isomers, one having a plane of symmetry containing the D atom (*sym*), and one having the D atom out-of-plane (*asym*). Rotational constants were predicted for the two orientations (staggered and eclipsed). The observed spectra are listed in Table VII, and require a staggered configuration, analogous to that found for methyl silane[8] and methyl-monofluorosilane.[6]

The observed frequencies for the *sym* species fit a rigid rotor spectrum within the accuracy of measurement. Rotational constants derived from the *sym* spectrum are given in Table VIII. For this species, the quantity $I_a + I_c - I_b$ should be the same as that found for the normal CH_3 species,[7] and the agreement here is excellent.

For the *asym* species, there are two equilibrium positions of identical potential energy, so that doublets due to the tunnel effect might be expected, and were observed. The individual members of the doublets do not fit pseudorigid rotor spectra very well. The rotational constants listed in Table VIII for the *asym* species are the result of a best fit of the observed spectrum. The spectrum calculated from these constants is listed in Table VII along with the observed transitions.

Characteristic Stark effects were used to confirm the assignments where possible. However, the spectrum of CH_2DSiHF_2 is very dense and observation of Stark effects often proved difficult, especially for the *asym*-CH_2D doublets.

VII. DISCUSSION

The calculations for the small silicon coordinates in CH_3SiH_2F and CH_3SiHF_2 demonstrate the usefulness of the double substitution technique, since in both cases, the first-difference or Kraitchman method for the $CH_3Si^{29,28}$ data gives an imaginary coordinate. Costain[2] points out that the Kraitchman method is accurate only if the substituted atom is some distance

from the principal axis in question. There is an analogous criterion[3] which one should apply for the use of the second-difference technique, namely that the principal axis system of the second "framework" should be shifted as far as possible with respect to the first "framework" along the direction in question. Thus for CH_3SiH_2F, where the "a" coordinate of the Si is small, it is desirable that the second isotopic framework (CD_3SiH_2F in our case) cause a large shift in the "a" direction. We feel that a shift of 0.03 A or more is desirable.

The additional isotopic data reported here have allowed considerably more reliable determination of the structures of these two molecules. The previously reported[6,7] shortening of the SiC bond distance on fluorination of the silyl group of methyl silane has been confirmed here. It is also apparent from Table VI that certain other structural parameters undergo progressive changes with fluorination of the silyl group. Thus the CSiH angle increases markedly while the SiF distance decreases with progressive fluorination. Table IX gives a comparison of structural parameters of the methyl fluorosilane series and the series[11] SiH_3F, SiH_2F_2, and $SiHF_3$. It is interesting to note that similar trends with progressive fluorination are found in both series.

ACKNOWLEDGMENTS

The authors are indebted to Professor E. B. Wilson, Jr., for many helpful discussions on this material, and to Professor M. K. Wilson for the sample of CD_3SiD_3.

[11] By using data from references listed in footnotes of Table IX, the structures of these molecules have been recalculated in the following manner: SiH_3F—Differences of moments of inertia were used to calculate the Si coordinate in both the SiH_3F and SiD_3F principal axis systems. The difference between the two values then was used to obtain the z coordinate of the hydrogens. The center of mass condition fixed the fluorine coordinate and the difference in moments of inertia for SiD_3F and SiH_3F fixed the remaining hydrogen coordinates; SiH_2F_2 and $SiHF_3$—The silicon and hydrogen coordinates for both molecules were determined by the difference of moments method. In both cases the center of mass condition yields one of the fluorine parameters, however the remaining fluorine coordinate required the use of one or more moments of inertia for its determination. (The structure of methyl silane was also recalculated. All atoms in this case were located by the difference of moments method. The results differed so slightly from those reported in reference 8 that we did not feel justified in making any changes.)

Rotational Diffusion Constant of a Cylindrical Particle*

S. BROERSMA

Department of Physics, University of Oklahoma, Norman, Oklahoma

(Received April 8, 1959)

The torque constant of a closed cylinder rotating in a viscous medium has been calculated for length (2a) over width (2b) ratios larger than 3.5 to within a first order in b/a. The analysis demonstrates how the contributions to the viscous dissipation tend to be underestimated in hydrodynamic considerations so that the geometrical values deduced from them come out too high. Experimental results for the torque on cylindrical rods and ellipsoids for a/b values from 3.5 to 30 are close to the theoretical results. For $a/b>10$ the difference is about 10%; for shorter molecules 20%. With the rotational diffusion constant given by $3kT(\sigma-\gamma)/8\pi\eta a^3\omega$, where $\sigma=\log 2a/b$ we obtain best fit with $\gamma(\sigma>2)=1.57-7\ (1/\sigma-0.28)^3\pm 0.2^5$. Experimental data for the rotational diffusion constant of a cylindrical virus ($a/b=20$) in water, obtained by O'Konski and Haltner agree with this result within 10%. The length of the protein fits within 3%.

1. INTRODUCTION

PERFORMING a transient electric birefringence experiment, O'Konski and Haltner[1] were able to measure the rotational diffusion constant D, (of a monomer unit) of Tobacco Mosaic Virus (TMV) in water. Their results were found to be independent of the concentration for a relative solute volume in the range of 2.10^{-6} to 3.10^{-4}. Also, varying the buffer concentration showed no dependence upon the thickness of the ionic atmosphere. An experimental accuracy as high as 3% in D, 1.5% in the length $2a$, could be achieved.

Now according to Burgers[2,3] the torque constant of a cylinder would be

$$T/\omega=8\pi\eta a^3/3(\log_e 2a/b-0.80). \qquad (1)$$

Here ω is the angular velocity, b is the half-width of the particle, and η is the viscosity of the solvent. Substituting the experimentally known value $2b=150$ A, which enters only in the logarithm, O'Konski thus obtains $2a=3416\pm 50$ A. Evidently the third power dependence upon a makes D a sensitive measure of this quantity. As O'Konski states, the problem presents itself how to reconcile this result with other physical methods which give 2980 ± 30 A for the length of the (relatively rigid rodlike) TMV molecule![1] Evidently, a is off by 15% and D is off by a factor of 1.44.

Adsorption of solvent upon the outside of the virus cannot cause an increase in size exceeding a few water layers, hence 5–10 A.[1,4] Then both through its dependence upon a^3 and upon b in log 2 a/b, D will be changed by less than 4%. (O'Konski does not expect swelling to explain the discrepancy, either.) This same fact, that the solvent molecule is small by comparison with the moving particle, leads us to expect that continuum hydrodynamics must apply. It is assumed that in these experiments[1] a single mode of motion, the rotation around a minor axis, is detected.

It is certainly fortunate that no concentration effect is observed in the concentration range for which experiments can still be performed.[1] As a matter of fact, for rotating *spheres* the diffusion constant would decrease with $1-\phi$ where ϕ is the volume concentration of the solute.[5] Even considering a sphere with a radius equal to the *major* axis of the rod, this is not excessive. Evidently, it holds that

$$\phi<\text{vol conc}\cdot(a/b)^2\ll 3.10^{-4}\cdot 400=12\%$$

as an upper limit. This cannot possibly cause the 40% decrease in D, in agreement with the experimental evidence.

While one can neglect $(b/a)^2$ terms as Burgers does, there are still b/a terms to be included. In the mathematical expansions to be discussed later in terms of x/a, where x is measured along the outer surface of the rod, one can neglect $(x/a)^n\approx\exp -n[(a-x)/a]$. For $a-x\geq b$ if $n>N=a/b$. Hence, one would expect that the first N terms have to be used, rather than the first two (1, 3) as Burgers does. This still leaves as a second and additional effect the force contribution of the top and bottom region of linear dimension b, an effect also hinted at by O'Konski and Haltner.[1]

Having reduced the discrepancy to a purely geometric problem, torque experiments on a laboratory scale immediately suggest themselves. These are described in Sec. 7.

2. OSEEN-BURGERS METHOD

In the Oseen-Burgers method[2] the velocity of a fluid element is related to force centers, the effect of which decreases with the distance [see, for example, Eq. (3)].

* Supported by the National Science Foundation.

[1] C. T. O'Konski and A. J. Haltner, J. Am. Chem. Soc. **78**, 3604 (1956). I thank Dr. O'Konski for calling this problem to my attention.

[2] J. M. Burgers, Verh. Kon. Ned. Akad. Wet., (1) **16**, 113 (1938).

[3] C. W. Oseen, *Hydrodynamik* (Akademische Verlagsgesellschaft m.b.H., Leipzig, 1927), p. 35.

[4] S. Broersma, J. Chem. Phys. **28**, 1158 (1958).

[5] S. Broersma, J. Chem. Phys. **30**, 707 (1959).

The mathematical technique entails finding the force distribution in a moving object that produces a certain velocity at its surface. In our case the velocity is ωx, where ω is the angular velocity. Once the force density is known the torque can be calculated.

Extending the Burgers formalism we use a linear force density $g(\xi)$ distributed along the axis of the cylinder as given by

$$g(\xi)/8\pi\eta\omega a=\sum_{k=0,1}^{\infty}B_k(\xi/a)^k. \tag{2}$$

Here ξ is measured along the axis of the rod. The velocity at point x of the surface then is[2]

$$v(x)=\sum_{k=0,1}^{\infty}B_k\int_{-a}^{a}(\xi/a)^k d\xi[1/\{(x-\xi)^2+b^2\}^{\frac{1}{2}} +b^2/2\{(x-\xi)^2+b^2\}^{\frac{3}{2}}]. \tag{3}$$

The coefficients B_k are to be determined. In Sec. 3 we shall expand Eq. (3) in terms of x/a and integrate. This way we obtain

$$v(x)=\sum_{n=0,1}^{\infty}(x/a)^n\sum_{k=0,1}^{\infty}c_{kn}B_k \qquad (k-n=\text{even}). \tag{4}$$

With $\sigma=\log_e 2a/b$ the result for c_{kn} is

$$c_{kk}=2\sigma+1-\sum_{l=1,2}^{k}2/l,$$

$$c_{kn}=2/(k-n) \qquad (k\neq n). \tag{5}$$

In the present problem only the odd terms in n and k need be considered. Starting with

$$v(x)=x/a \tag{6}$$

the odd terms can satisfy Eq. (4). Furthermore, the torque depends upon the odd terms only.

3. VELOCITY INTEGRAL

In Eq. (3) we substitute $y=\xi-x$ and expand $(x+y)^k$. Thus we find

$$v(x)=\sum_{k=0,1}^{\infty}B_k(x/a)^k\sum_{l=0,1}^{k}k!/(k-l)!l!\cdot I_l, \tag{7}$$

where

$$I_l=\int_{-(a+x)}^{a-x}(y/x)^l f(y)dy,$$

while

$$f(y)=1/(y^2+b^2)^{\frac{1}{2}}+b^2/2(y^2+b^2)^{\frac{3}{2}}=f^1(y)+f^3(y),$$

if we designate the first term of $f(y)$ with the superscript 1, the second with 3. The integrals I_l can easily be calculated for $|x|<(a-b)$.

We obtain for the integrals based upon the $f^1(y)$ term

$$I_0{}^1=2\sigma+\log(1-x^2/a^2)=2\sigma-\sum_{l=2,4}^{\infty}2/l\cdot(x/a)^l, \tag{8}$$

$$I_{\triangleright 0}{}^1=|y|/y\cdot 1/l\cdot(y/x)^l\Big|_{-(a+x)}^{a-x}-(b/x)^2 I_{l-2}{}^1.$$

The second term of $I_{\triangleright 0}{}^1$ can be neglected. This is of the order $b^2/(a\pm x)^2$. In Eq. (7) the sum over l from 1 to k now is found to be equivalent with

$$|y|/y\sum_{l=1,2}^{k}1/l\cdot[(1+y/x)^l-1]\Big|_{-(a+x)}^{a-x}.$$

One easily checks, for example, that the *integrands* are the same for $y=0$, while also their derivatives with regard to y are the same. The sum over l thus simplifies to

$$-\sum_{l=1,2}^{k}2/l+\sum_{l=2,4}^{\leq k}2/l\cdot(x/a)^{-l}.$$

The integrals based upon the $f^3(y)$ terms are

$$I_0{}^3=1, \qquad I_{\triangleright 0}{}^3=0. \tag{9}$$

This follows from $I_1{}^3(=0)$ and

$$I_l{}^3=(b/x)^2(1/2I_{l-2}{}^1-I_{l-2}{}^3).$$

Hence, $I_l{}^3$ is of the order of $(b/a)^2$ unless $l=0$.

Combining the results, we have

$$v(x)=\sum_{k=0,1,2}^{\infty}B_k(x/a)^k[(2\sigma+1-\sum_{l=1,2}^{k}2/l) +\sum_{l=2,4}^{\infty}-2/l\cdot(x/a)^l+\sum_{l=2,4}^{\leq k}2/l\cdot(x/a)^{-l}]. \tag{10}$$

After substituting $n=k\pm l$ it follows that

$$v(x)=(\sum_{k,n=0,2}^{\infty}+\sum_{k,n=1,3}^{\infty})B_k c_{kn}(x/a)^n, \tag{11}$$

where the c_{kn} are given by Eq. (5).

4. FORCE EXPANSION COEFFICIENTS

Written out for the upper left corner, the determinant of the known coefficients c_{kn} (k horizontal, n vertical, both odd) is

$$\Delta=|c_{kn}|$$

$$=\begin{vmatrix} 2\sigma-1 & 1 & 1/2 & 1/3 & 1 \\ -1 & 2\sigma-8/3 & 1 & 1/2 & 0 \\ -1/2 & -1 & 2\sigma-107/30 & 1 & 0 \\ -1/3 & -1/2 & -1 & 2\sigma-293/70 & 0. \end{vmatrix}$$

The unknown force coefficients B_k can be obtained by combining Eq. (4) and Eq. (6). Thus the solution of the problem is given by

$$B_k=\Delta_k/\Delta, \tag{12}$$

where Δ_k is the cofactor. This quantity is examined most conveniently by transposing two adjoining rows upwards, next to the first row, and also two adjoining columns sideways to the extreme left. Neither step introduces a sign change. Then we arrive at

$$\begin{vmatrix} c_{k,1} & c_{k+2,1} & c_{1,1} & & 1 \\ c_{k,k} & c_{k+2,k} & c_{1,k} & & 0 \\ c_{k,k+2} & c_{k+2,k+2} & c_{1,k+2} & & 0 \\ & & & c_{3,3} & 0. \end{vmatrix}$$

Now considering the case that $a/b=20$, $2\sigma=7$, we see that the diagonal elements c_{kk} with small k are much larger than the other elements. Hence, when in the calculation of the determinant a term does not include, for example, c_{33}, it will also miss another diagonal element and consequently have its magnitude reduced by $1/\sigma^2$. Neglecting these terms just for the case of c_{33}, we can reduce Δ and Δ_k to the product of their corner determinants and the entire unlimited remainder. Evidently, the latter cancels in the ratio for B_k as given by Eq. (12). We then find

$$B_1=1/c_{11}=1/(2\sigma-1),$$

$$B_k=-c_{1k}/c_{11}c_{kk}\cdot t, \qquad k\geq 3 \tag{13}$$

where

$$t=(1-1/c_{k+2,k+2})/(1+1/c_{k,k}c_{k+2,k+2}).$$

B_{k+2} is given by this type expression if we substitute for the numerator of t: $(1+1/c_{k,k})$. For small k this correction factor is approximately $1\mp 1/\sigma$. Hence, here t oscillates around 1. Because B_k then is of the order $1/\sigma^2$, while B_1 is of the order $1/\sigma$, it is a good approximation to use the average value $t=1$. On increasing k, B_k will decrease with $-c_{1k}=2/(k-1)$, hence as $1/k$. At the same time c_{kk} approaches 1 so that t can become zero. Then half the number of B_k will become zero. Increasing k still further the sign of B_k starts to alternate. This suggests a cutoff of the series as given by

$$c_{N_1N_1}=1$$

which defines N_1. In the entire interval, k from 3 to N_1, we shall use $t=1$ so that it holds that

$$B_k/B_1=2/(k-1)c_{kk}, \qquad (3\leq k\leq N_1). \tag{14}$$

Equation (14) thus is the solution of the problem. Its precision is essentially limited by the omission of $1/\sigma^2$ terms. The omission of $(b/a)^2$ has always a smaller effect. Because the neglected terms tend to alternate and the major contribution to the torque is given by the first few terms a relative error of about $1/2\sigma$ can be expected. Inasmuch as B_1 represents the long ellipsoid, $1/2\sigma$ is the error in the differential effect of a cylinder and an ellipsoid.

Using Euler's constant we can evaluate N_1. It holds approximately that

$$\sum_{1,2}^{k}1/l=0.577+\log k.$$

Introducing Eq. (5) we find $\sigma=\log 1.78N_2$ or

$$N_2=a/b=0.89N_1.$$

This confirms the argument given in the Introduction.

5. END EFFECTS

As we discussed in the Introduction, on account of terminating the series at $k=N$ and because of the presence of flat lids, end effects will have to be considered. As Eq. (3) suggests, on approaching the center of the "lid," the radius vector goes to zero and the function can diverge. Hence the force poles will have to be distributed over the surface of the lid, rather than upon the axis of the rod. Along the rod proper this is not necessary. Any cylindrical distribution gives essentially the same field.

Experiences with the distributed capacity of coils[6] led us to suspect that the contributions due to sharp edges, for example, tend to be underestimated. At these points of large curvature the velocity gradient is large so that the dissipation can be considerable.

Now the computed velocity will be reasonably close to the actual value when we can neglect

$$(\xi/a)^N\approx\exp[-N(a-\xi)/a].$$

With $N=a/b$ this means that the result is acceptable for $a-\xi\geq b$. Recalling that a long ellipsoid is adequately described by just the first term, N terms must describe a cylinder which is slightly rounded off near the edge! Therefore, as a first approximation for the end effect, we shall push the round equivelocity surface out into a sharp edge. We add a single force pole $\mathfrak{G}$(pole) at $\xi\approx a-b$ so that in Eq. (3) the value for r can increase from b to $b\sqrt{2}$. Using for $\mathfrak{G}\approx 2bg(a)$ as the original effective pole placed at $x=a-b$ it must then hold

$$\mathfrak{G}(\text{pole})\approx(\sqrt{2}-1)\mathfrak{G}=0.8bg(a).$$

Inasmuch as the velocity difference computed for the points $x=a$ and $x=a-b$ of the mantle is determined by the extra force on the axis between them, one would expect $bg(a)$ to be the optimum value required for $\mathfrak{G}$(pole). On the other hand, for flow parallel to the end face, as considered here, one would expect the friction of the end to add at least according to the

[6] S. Broersma, *Magnetic Measurements on Organic Compounds* (Martinus Nyhoff, The Hague, 1947), p. 56.

TABLE I. Theoretical torque ratio of cylinder and ellipsoid of equal over-all size.

$1/\sigma$	σ	$N_1(c_{kk}=1)$	$N_2(a/b)$	$\alpha(N_1)$	$\alpha(N_2)$	$\alpha\sigma$	$c_{11}\sum_{1,3}^{N}B_k$	β(pole)	β(disk)	$1+\alpha+\beta$	γ(cyl)
0.56	1.79	3	3	0.65	0.65	1.16	2.08	1.56	0.55	2.58	1.29
0.48	2.08	4	4	0.56	0.56	1.18	1.96	1.09	0.50	2.30	1.40
0.43[5]	2.30	5	5	0.52	0.52	1.20	1.91	0.86	0.46	2.15	1.46
0.33	3.02	11	10	0.42	0.41	1.25	1.99	0.45	0.32	1.80	1.62
0.26	3.89	27	24.5	0.32	0.31	1.21	2.07	0.19	0.18	1.50	1.63
0.20	5.00	83	74	0.22	0.22	1.12	2.14	0.07	0.08	1.30	1.54
0.16	6.24	277	256	0.17	0.16	1.05	2.25	0.02	0.03	1.19	1.42
0.14[5]	6.94	559	512	0.14[5]	0.14[5]	1.01	2.31	0.01	0.02	1.16	1.39
0.05	20.0	2.6×10^{8}	2.4×10^{8}	0.035	0.03[5]	0.70	3.35	0.00	0.00	1.03[5]	1.20
0.00	∞	∞	∞	0.00	0.00	0.64		0.00	0.00	1.00	1.14

area of the "lid." Relative to a length l of the mantle this is

$$lg(a)\cdot\pi b^2/2\pi bl=0.5bg(a).$$

Therefore our first approximation will be

$$\mathfrak{G}(\text{pole})=0.75\pm0.25\cdot bg(a). \quad (15)$$

This solution accounts for the friction due to the extra area and large gradients near the edge.

When considering the mantle we ignored the lids. As a second alternative approximation we shall temporarily forget the cylinder and shrink the two lids together. This makes a flat disk. For this case the velocity pattern has been calculated in detail; all components are zero at the surface. The exact solution for the force on the disk with viscous flow parallel to it[7] is given by

$$2G(\text{disk})=32/3\cdot\eta\omega ab. \quad (16)$$

On separating the two parts of the disk, we also halve the force density. But because of the $bg(a)$, term related to the cylinder mantle the over-all surface velocity will be roughly maintained. Therefore G(disk) can be used as another approximation for the additional effect of each end. It is appropriate because the short range flow pattern of the disk is similar to that of the cylinder edge.

Inasmuch as these two approximations have a different analytical form we shall carry them through independently. Actually, for very short rods the end corrections, to be called β, are so large that linear superposition is quite crude. Therefore, in the figures we shall also indicate what the effect is of $\beta/(1+\beta)$. For large β this cannot exceed 1. Indeed, even if $a=b$ one would expect the end effect not to exceed that of the mantle.

[7] H. Lamb, *Hydrodynamics* (Dover Publications, New York, 1945), Sec. 339.

6. TORQUE ON CYLINDER

The main contribution to the torque is given by the cylinder mantle. With Eqs. (2) and (14) we find

$$T(\text{mantle})=\int_{-a}^{a}g(\xi)\xi d\xi=T(\text{ell})\cdot3c_{11}\sum_{1,3}^{N}B_k/(k+2)$$
$$=T(\text{ell})\cdot(1+\alpha). \quad (17)$$

Here

$$T(\text{ell})=8\pi\eta\omega a^3/3[\sigma-\gamma(\text{ell})]$$

is the torque on an ellipsoid with axes a and b; $\gamma(\text{ell})=0.50$ for $\sigma>1.8$, $a/b>3$. From Gans' result[8] we obtain in general

$$\gamma=0.50+1/4(b/a)^2[1-9/2\cdot\sigma(b/a)^2].$$

The expression for α is

$$\alpha=\sum_{3,5}^{N}6/(k-1)(k+2)c_{kk}.$$

Table I gives the result using either $N_1(c_{kk}=1)$ or $N_2=a/b$ as cutoff.

According to Eq. (15) the end effects depend upon

$$g(a)=8\pi\eta\omega a\sum_{1,3}^{N}B_k. \quad (18)$$

The even terms do not contribute to the torque. We tabulate

$$c_{11}\sum_{1,3}^{N}B_k=1+\sum_{3,5}^{N}2/(k-1)c_{kk},$$

averaging between N_1 and N_2. Also entering the estimate according to Eq. (16), we find for the contribution of the ends to the torque

$$T(\text{end})/T(\text{ell})=3b/a[0.75c_{11}\sum_{1,3}^{N}B_k \text{ or } 2c_{11}/3\pi]$$
$$=\beta(\text{pole}) \text{ or } \beta(\text{disk}). \quad (19)$$

[8] R. Gans, Ann. d. Physik (IV) 86, 654 (1928).

TABLE II. Experimental torque ratio of cylinder and ellipsoid of equal overall size.

$2a$ cm	a/b	σ	$T(\text{cyl})/T(\text{ell})$	$\gamma(\text{cyl})$
7	3.65	2.0	1.83	1.18
7	5.5	2.4	1.77	1.32
7	7.4	2.7	1.53	1.26
7	10.5	3.1	1.52	1.37
14	21.3	3.8	1.41	1.45
21	31.5	4.2	1.33	1.40

In Table I β(pole) Eq. (15) refers to the first approximation, β(disk) Eq. (16) to the second. Designating the geometric average with β the final result for the torque is

$$T(\text{cyl})/T(\text{ell})=1+\alpha+\beta=[\sigma-\gamma(\text{ell})]/[\sigma-\gamma(\text{cyl})]. \tag{20}$$

Here the parameter $\gamma(\text{cyl})$ is defined in analogy with the formula for the ellipsoid.

For $\sigma>2.3$ the computational uncertainty in $T(\text{cyl})/T(\text{ell})$ due to β is about 10%; for $\sigma>3.3$ this is less than 5%. The theoretical relative error in the difference of the cylinder and the ellipsoid was indicated under Eq. (14) to be about $1/2\sigma$. This is also about 10 and 5%, respectively, in these regions. Together this can be expressed as an error in γ of $\delta\gamma=\pm 0.2^5$ over the entire σ range.

7. MACROSCOPIC TORQUE MEASUREMENTS

If a purely geometric effect is responsible for the discrepancy as discussed in Sec. 1 a macroscopic experiment can be used for a check. Certainly in those cases where the mathematical analysis is too hard, such measurements can be helpful.

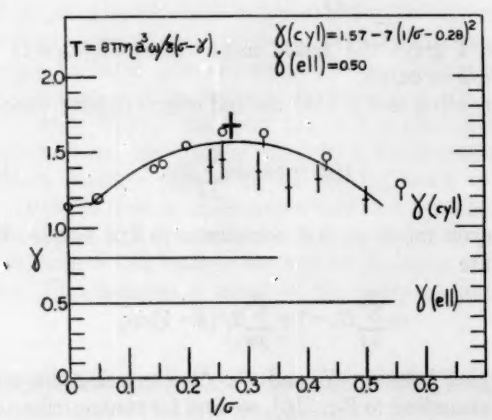

FIG. 1. γ values occurring in the expression for the torque on a cylinder, plotted against $1/\sigma$, $\sigma=\log 2a/b$. The theoretical values (circles) and the experimental data (vertical lines) are in essential agreement with O'Konski's value (+), $\gamma=1.67$ introducing $2a=2980$ A. The upper curve displays $\gamma(\sigma>2)$, Eq. (21). The middle line represents $\gamma=0.8$, Burgers' value for large σ. The lowest line gives $\gamma(\text{ell})=0.50$, correct for $\sigma>1.8$.

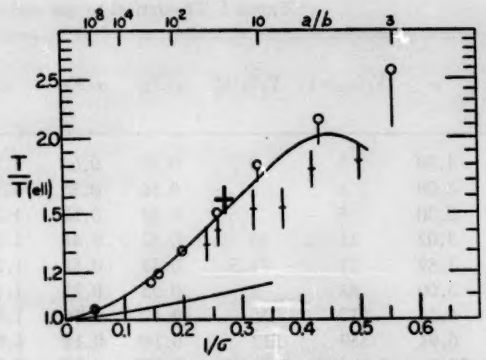

FIG. 2. Ratio of the torque (T) on a cylinder and on an ellipsoid (T(ell)) of equal over-all length ($2a$) and width ($2b$) against $1/\sigma$. The circles give our theoretical result (Table I), the lines extending downward connect to the points with $\beta/(1+\beta)$ as end correction. The vertical line segments give the experimental values using large scale models (Table II). The upper curve gives the torque using γ according to Eq. (21). The lower line uses Burgers' formula. The + mark represents O'Konski and Haltners' result for TMV, substituting the accepted value of $2a=2980$ A.

We used a stationary can with super cylinder oil: 25 poises at 20°C, height of fluid 20 cm, diameter of can 28 cm. The wooden models had lengths (2a) ranging from 7 to 21 cm and diameters from 0.6 to 1.9 cm (see Table II). For the ellipsoids the shape was approximated within 0.2 mm of the diameter. All the bodies were attached to and rotated by means of a thin vertical steel rod going through the wood. With a pulley system connected to this rod, weights permitted a measurement of the torque.

It is important that the Reynolds number does not exceed unity. In our case its numeric value was $\rho\omega a/\eta=0.3$. Actually, in the ratio $T(\text{cyl})/T(\text{ell})$ this is one of the effects which can cancel to a considerable degree.

Then there is the effect of the walls. For either shape, with $a/b=20$, the friction near the bottom was about 25% higher than at the center, where it was 35% higher than near the surface. The ratio $T/T(\text{ell})$ itself is a maximum at the center and decreases by less than 3% going in either direction. Evidently, in the torque ratio the effect of the can is relatively small for this shape. For the longest model the side wall of the can could have a larger effect.

TABLE III. Length of TMV according to various interpretations ($\sigma=3.7$).

Method		$2a$ A
Kerr effect	Eq. (1), Burgers	3416
Kerr effect	Present theory	3020
	Macroscopic experiment	3100
	Eq. (21), $\gamma=1.57$	3050
Electron microscope	Mass envelope	2980

From the torque on the various ellipsoids we derived a value for the viscosity of 23±4 poises. Independent flow checks gave 25 poises. Hence the method is essentially sound. In detail the ratios were determined as follows: We can write

$$T = T(\text{cyl}) + c\omega + c' = (m+m')gr,$$

where ω is the angular velocity, c the force constant for viscous friction caused by other parts, c' represents effects like solid friction, m' is the mass of the pan, and r the radius of the pulley driving the axle. Varying m, we can in principle eliminate the unknown c'. Then removing the body, c can be measured. Finally we calculate the ratio of the torques for cylinder and ellipsoid at a given ω. This helps to eliminate kinetic effects, among other things. The torque ratio reproduced well within a few percent, notwithstanding slight deviations in the linearity of ω and m probably due to a slight non-Newtonian behavior of the fluid.

Table II gives the results for $T(\text{cyl})/T(\text{ell})$ with an error of about 10% and γ with an absolute error of about 0.2. Mr. J. K. Furdyna assisted in the measurements and calculations.

Because molecules like TMV are only crudely approximated by a cylinder, it seemed to be of interest to check the effect of openings in the surface of the particle. Inasmuch as the torque ratios were found to be insensitive to a variety of influences we used a simple model. A short section of brass tubing 5 cm long and 3 cm in diam was connected sideways to an arm, 7 cm long, so that the cylinder wall was pushed against the fluid. The arm again was fastened at right angles to the axle and pulley system. The experimental result is interesting in that it shows that with 20 holes of 0.6 cm diam in the cylinder wall, hence 11% of the material removed, the torque is decreased by less than 3%. We come back to this in the next section.

8. CONCLUSION

In Fig. 1 the various results for γ have been plotted against $1/\sigma$. The theoretical values of Table I appear as circles; the vertical lines connect to the point derived with $\beta/(1+\beta)$ as end correction. The experimental values of Table II appear as vertical line segments. The uppermost curve is drawn according to the weighted average given by

$$\gamma(\text{cyl}, \sigma>2) = 1.57 - 7(1/\sigma - 0.28)^2 \pm 0.2^5, \quad (21)$$

For large σ the theoretical points are approximated, for very small σ the experimental data. O'Konski's result (+mark, $\gamma=1.67$), essentially agrees with this result. The magnitude of the scale factor, about 1 million, separating the experiments is rather considerable.

In Fig. 2 the various results for the torque ratios have been plotted against $1/\sigma$. The upper line represents Eqs. (20) and (21). For comparison we also plot $(\sigma-0.5)/(\sigma-0.8)$ which gives the ratio according to Burgers. O'Konski's result(+) is indicated as $(3416/2980)^3\,[\sigma(2980)-0.5]/[\sigma(3416)-0.8]$.

Table III expresses the results in terms of $2a$ values of the TMV molecule. Evidently, most of the discrepancy between the nonhydrodynamic value of 2980±30 A and the Kerr-effect-torque value of 3416±50 A ($\gamma=0.8$) has been removed.[9] The former is labeled mass envelope, because these experiments make use of the scattering of some type of rays by the material. Hydrodynamic measurements tend to give a geometric envelope. And, as the experiments in Sec. 7 indicate, the torque ratio does not decrease in proportion with the amount of material. It illustrates that rheological determinations can give larger geometric values than methods acting on the bulk matter.

[9] See also the independent experimental study of Haltner and Zimm, Nature 184, 265 (1959).

Viscous Force Constant for a Closed Cylinder*

S. BROERSMA

Department of Physics, University of Oklahoma, Norman, Oklahoma

(Received April 8, 1959)

The viscous force constant of a moving cylinder closed at the ends has been calculated including first-order effects in width $(2b)$/length $(2a)$. Experimental results, obtained for macroscopic models, are in essential agreement with this. For $a/b>20$ the discrepancy is about 8%, for shorter cylinders near 20%. With the force on a cylinder moving sideways given by $F=8\pi\eta av/(\sigma-\gamma)$, where $\sigma=\log 2a/b$, it is found that $\gamma(\sigma>2)=0.35-4(1/\sigma-0.43)^2\pm 0.2^5$. For a translation lengthwise, with $F=4\pi\eta av/(\sigma-\gamma)$, the relation $\gamma(\sigma>2)=1.30-8(1/\sigma-0.30)^2\pm 0.2^5$ holds.

1. INTRODUCTION

In a previous paper,[1] hereafter to be referred to as I, we were able to explain experimental data on the rotational diffusion constant of a rodlike molecule by including terms of the order b/a. Here b is the half width, a the half length of the cylinder. Macroscopic model experiments confirmed this geometric explanation.

Because formulas pertaining to other cases first examined by Burgers[2] may find application, we also computed the translational force constants of a cylinder within b/a terms. Fortunately, the integral occurring in the Oseen-Burgers' theory is so similar in the various problems that separate evaluations are required only in the final formulas.

Here we use as linear force density $g(\xi)$

$$g(\xi)/8\pi\eta v_0=\sum_{k=0,1,2}^{\infty} B_k(\xi/a)^k. \tag{1}$$

For a translational motion the velocity is independent of the coordinate along the cylinder, so that

$$v(x)=1. \tag{2}$$

This is the even analog of Eqs. (2), (3), and (6), in I. Therefore, we now select the system of B_k that is *even* in k and n, see Eqs. (10) and (11) in I. Moreover, only these B terms will contribute to the force integral. The B set is given by

$$B_0=1/c_{00}$$

$$B_{k\geq 2}=-c_{0k}/c_{00}c_{kk}. \tag{3}$$

For the straight part of the cylinder the correction for the force now is

$$\alpha=c_{00}\sum_{2,4}^{N} B_k/(k+1). \tag{4}$$

The end effects could be approximated by[1]

$$\beta(\text{pole})=0.75b/a\cdot c_{00}\sum_{0,2,4}^{N} B_k, \tag{5}$$

expressing the friction due to the edge in terms of a part of the cylinder mantle. In another estimate

$$\beta(\text{disk})=2/3\pi\cdot b/a\cdot c_{00}$$

or

$$\beta(\text{disk})=1/\pi\cdot b/a\cdot c_{00} \tag{6}$$

we add the resistance of a flat disk to that of the cylinder mantle. Here the former equation refers to the disk moving parallel to its surface. In this case either side represents the effect of a face of the cylinder which moves perpendicular to its major axis (Sec. 2). The latter equation refers to the resistance of a disk moving perpendicular to its plane, corresponding to the cylinder moving lengthwise (Sec. 3).

Combining both effects we have for the theoretical ratio of the force constants, or forces at equal velocity,

$$F(\text{cyl})/F(\text{ell},\gamma(\infty))=1+\alpha+\beta$$
$$=[\sigma-\gamma(\text{ell},\infty)]/(\sigma-\gamma). \tag{7}$$

The ellipsoid used for comparison has a major axis of $2a$ and a minor axis of $2b$. It should be kept in mind that α, in Eq. (4), and β express the difference between a cylinder and an ellipsoid, for the latter using the limiting expression of a *long* ellipsoid (c_{00}). The ratio of the force constants using the actual expression for $F(\text{ell})$ then is $(1+\alpha+\beta)[\sigma-\gamma(\text{ell})]/[\sigma-\gamma(\text{ell},\infty)]$. Only for lengthwise motion and σ near 2 is the σ factor different from 1 by as much as a few percent.

For short rods, i.e., large β values, linear superposition gives an upper limit. Therefore, we also indicate in the drawings the point obtained by adding $\beta/(1+\beta)$. This is the lower point of the vertical lines extending downward from the (theoretical) circles.

2. CYLINDER MOVING SIDEWAYS

The force integral for this case, Eq. (6.2) in Burgers' paper[2] is identical with the integral for the rotation,[2] Eq. (7.1) so that the velocity expansion in Eqs. (3),

* Supported by the National Science Foundation.

[1] S. Broersma, J. Chem. Phys. **32**, 1626 (1960); Fluid Dynamics Meeting, Am. Phys. Soc., paper C3 (1959).

[2] J. M. Burgers, Verhandel. Koninkl. Ned. Akad. Wetenschapp. Afdel. Natuurk, Sec. I **16**, 113 (1938).

TABLE I. Theoretical results for motion sideways.

σ	N(av)	α	β(pole)	β(disk)	$1+\alpha+\beta$	γ
2.08	4	0.26	0.37	0.27	1.57	0.44
2.30	5	0.27	0.29	0.24	1.53	0.46
3.02	11	0.18	0.15	0.14	1.33	0.37
3.89	26	0.13	0.06	0.08	1.20	0.23
5.00	79	0.10	0.02	0.03	1.12	0.08
6.94	535	0.06		0.01	1.07	−0.02
20.00	2.5×10^6	0.02			1.02	−0.15
∞	∞	$0.31/\sigma$			1.00	−0.19

(10) in I again applies. Therefore the expressions for c_{kn} are here also given by

$$c_{kk}=2\sigma+1-\sum_{l=1,2,3}^{k}2/l,$$

$$c_{kn}=2/(k-n). \qquad (k\neq n) \qquad (8)$$

This is to be substituted in the α and β equations. For N the two values $N_2=a/b$ and $N_1(c_{kk}=1)=1.1\,N_2$ can be used. Because the differences are small we averaged the results for α and β in this case.

The force upon the ellipsoid moving sideways can be written as

$$F(\text{sidew})=8\pi\eta a v/(\sigma-\gamma), \qquad (9)$$

where for an ellipsoid[3]

$$\gamma(\text{ell})=-0.50-1/4(b/a)^2. \qquad (10)$$

Table I lists the theoretical results for γ and $F/F(\text{ell})\approx1+\alpha+\beta$. Table II gives the experimental data. As Fig. 1 shows there is a reasonable agreement between theory and experiment. We, therefore, condensed the results in a simple expression, giving the theoretical values most weight for large σ, and the experimental data most weight for small σ. The final result is

$$\gamma(\text{cyl sidew}, \sigma>2)=0.35-4(1/\sigma-0.43)^2\pm0.2^5. \qquad (11)$$

While Eq. (11) is numerically meaningful, analytically it is too extended. It should be recalled that in the analysis higher order terms in $1/\sigma$ were neglected.

Figure 2 illustrates the results on the basis of the force ratio of cylinder and ellipsoid.

TABLE II. Experimental results for motion sideways.

$2a$(cm)	a/b	σ	F(cyl)/F(ell)	γ(cyl)
7	3.6^5	1.98	1.48	0.30
7	5.5	2.39	1.35	0.25
7	7.4	2.69	1.26	0.16
7	10.5	3.04	1.31	0.34
14	21.3	3.75	1.30	0.48
21	31.5	4.14	1.19	0.24

[3] C. W. Oseen, *Hydrodynamik* (Akademische Verlagsgesellschaft, m.b.H., Leipzig, 1927), pp. 137, 186–187.

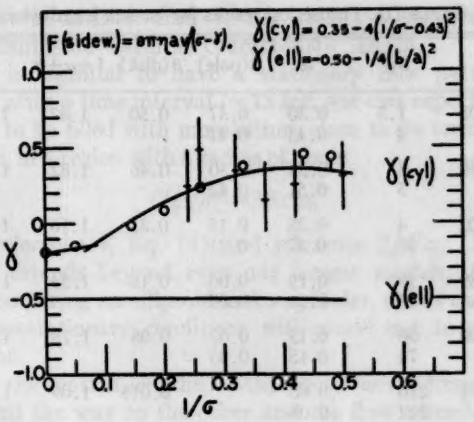

FIG. 1. Linear plot of γ, occurring in the expression for sideways motion $F=8\pi\eta av/(\sigma-\gamma)$ as a function of $1/\sigma$. The circles give the theoretical values. The vertical lines record the experimental results. The drawn curve represents the equation for γ (cyl), Eq. (11). The lower line gives γ for an ellipsoid.

3. CYLINDER MOVING LENGTHWISE

Burgers' force equation (5.2)[2] can be rewritten by using

$$(x-\xi)^2/r^3=1/r-b^2/r^3.$$

Then the integral will contain

$$g(y)=2\{f^1(y)-f^3(y)\}$$

instead of

$$f(y)=f^1(y)+f^3(y)$$

as defined in Eq. (7), of our previous paper.[1] Consequently, the integral I_0^3 given by Eq. (9) in I will now enter with the opposite sign while the c_{kn} doubles in value so that

$$\tfrac{1}{2}c_{kk}=2\sigma-1-\sum_{l=1,2}^{k}2/l \qquad (12)$$

and

$$\tfrac{1}{2}c_{kn}=2/(k-n), \qquad (k\neq n).$$

In this case

$$N_1(\tfrac{1}{2}c_{kk}=1)=0.4N_2.$$

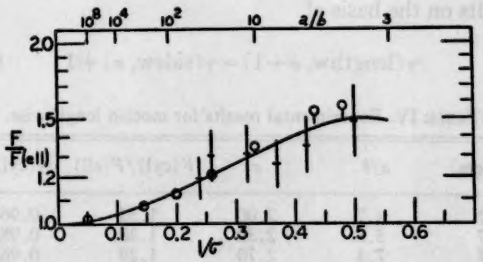

FIG. 2. Semilogarithmic plot of the ratio of the force constants, for motion sideways, in the case of a cylinder and of an ellipsoid of equal length and width, as a function of $1/\sigma$ ($\sigma=\log 2a/b$).

TABLE III. Theoretical results for motion lengthwise.

σ	N_2[1]	α	β(pole)	β(disk)	$1+\alpha+\beta$	γ
2.08	1.5	0.30	0.37	0.50	1.82	1.21
	4	0.43	0.47			
2.30	2	0.34	0.30	0.46	1.82	1.31
	5	0.51	0.42			
3.02	4	0.28	0.15	0.32	1.56	1.40
	10	0.37	0.21			
3.89	10	0.19	0.06	0.18	1.33	1.34
	25	0.24	0.09			
5.00	30	0.13	0.02	0.08	1.18	1.19
	74	0.15	0.03			
6.94	210	0.08		0.015	1.09	1.03
	512	0.08				
20.00	1×10^8	0.02			1.02	0.86
	2.4×10^8	0.02				
∞	∞	$0.31/\sigma$			1.00	0.81

The differences in the α's and β's terminating at either N_1 or N_2, keeping $c_{kk}(N_1<k<N_2)=1$, are not excessive. In Table III we list both estimates. The corresponding variation in γ does not exceed ±0.11.

The force necessary for moving the body lengthwise is given by

$$F(\text{lengthw})=4\pi\eta av/(\sigma-\gamma), \tag{13}$$

where for an ellipsoid[4]

$$\gamma(\text{ell})=0.50-(\sigma-3/4)\,(b/a)^2. \tag{14}$$

Table IV lists the experimental values for γ and $F/F(\text{ell})$. Figure 3 combines the γ values. Figure 4 gives the force ratios $(1+\alpha+\beta)\cdot[\sigma-\gamma(\text{ell})]/[\sigma-\gamma(\text{ell},\infty)]$. The results for $\gamma(\text{cyl})$ can be condensed as follows:

$$\gamma(\text{cyl lengthw},\sigma>2)=1.30-8(1/\sigma-0.30)^2\pm0.2^5. \tag{15}$$

It is of interest to notice that Eq. (12) permits a reduction to Eq. (8) in Sec. 2 by substituting $\sigma_l=\sigma_s+1$. Equation (6) which is averaged with Eq. (5) does not quite follow this rule. Still, a comparison of the results on the basis of

$$\gamma(\text{lengthw},\sigma+1)=\gamma(\text{sidew},\sigma)+1 \tag{16}$$

TABLE IV. Experimental results for motion lengthwise.

$2a$(cm)	a/b	σ	$F(\text{cyl})/F(\text{ell})$	γ(cyl)
7	3.7	2.00	1.53	0.96
7	5.5	2.39	1.38	0.98
7	7.5	2.70	1.29	0.96
30	24	3.85	1.32	1.30
30	46	4.52	1.26	1.33

[4] S. Broersma, J. Chem. Phys. **28**, 1158 (1959).

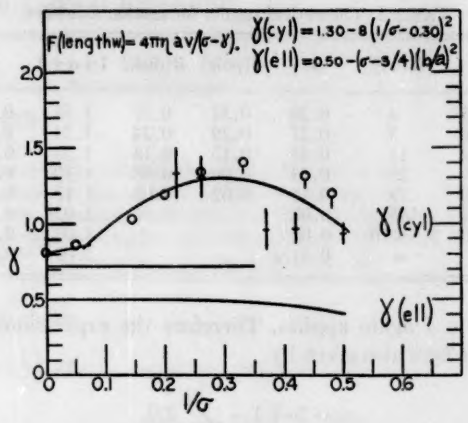

FIG. 3. Linear plot of γ as a function of $1/\sigma$, referring to lengthwise motion. The corresponding force is given by $F=4\pi\eta av/(\sigma-\gamma)$. The drawn line, based upon the equation for γ (cyl), Eq. (15), best approximates the theoretical results (circles) and experimental results (line segments). (The straight section near the ordinate represents a rigorous expansion of α in terms of $1/\sigma$). The middle line gives Burgers' value 0.72. The lower curve gives γ for an ellipsoid.

suggests itself. Evidently, $\gamma(\text{ell})$ and $\gamma(\infty)$ fit to a first order. The shape of the γ functions, given by Eqs. (11) and (15), also agree quite well. For example, their maxima differ by 0.95, which is close to unity. For the positions of the maxima one would also expect $\sigma(\text{lengthw})=\sigma(\text{sidew})+1$. From the brackets we see that indeed

$$1/0.43+1=3.33=1/0.30.$$

4. VISCOUS FORCE MEASUREMENTS

The force measurement with the rod moving sideways is performed most easily by suspending the models with a thin wire attached near the center. A small lead weight can keep them submerged. The motion is regulated by means of a pulley system varying the size of a counter weight.

The force required for moving the cylinder along its major axis was determined from the time of free ascent. The samples were brought down attached with a little wax to a stiff wire and released by pushing against a

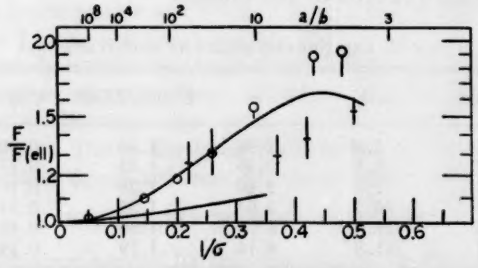

FIG. 4. Semilogarithmic plot of the ratio of the force constants, for motion lengthwise, of a cylinder and of an ellipsoid of equal length and width, as a function of $1/\sigma$. The middle curve represents Burgers' value $[\sigma-\gamma(\text{ell})]/(\sigma-0.72)$.

piece of gauze near the bottom. They escaped under the influence of the buoyant force. At the surface the "verticality" of alignment was checked. A trial experiment in a small flask with glycerin showed that the bodies, which are quite symmetric, will not change their alignment too readily.

In this case the ratio of the force *constants* is determined by

$$F(\text{cyl})/F(\text{ell}) = bf(c)/bf(e) \cdot t(c)/t(e), \qquad (17)$$

where bf is the buoyant force and t the time of travel over a fixed distance. For our initial set of measurements with fresh models of uniform density the bf ratio was exactly the volume ratio 3/2. Unfortunately, the samples soaked up some oil. After that the buoyant force was measured with a balance.

We used the same oil and samples as discussed in the paper on the torque constant.[1] Although the liquid is rather cumbersome in handling, its coefficient of viscosity has the right order of magnitude. Kinetic effects are small, while the viscous forces are relatively large.

When using a wide vat we found, for both lengthwise and sideways motion, that the experimental results for ellipsoids fit the theoretical formula substituting $\eta = 30 \pm 5$ poises. This is close to the value found before.[1] Again the ratios given in Tables II and IV were calculated for equal velocity. The experimental error in $\gamma(\text{cyl})$ is of the order of 0.2, assuming the γ values for the ellipsoid to be correct.

With a driving force of a few grams the velocity of the models is about 1 cm/sec. In that case the Reynolds number, given by

$$\text{Re} = \rho v 2b/\eta \approx 0.1,$$

indeed is smaller than 1. For sideways motion we substitute the width as characteristic length.

It is essential to have a stationary flow pattern. Now after a time interval $t \approx 15$ sec, one can expect the fluid to be filled with momentum, close to its terminal value, in a region with a radius of about

$$(3\eta t/\rho)^{\frac{1}{2}} = 30 \text{ cm},$$

see reference 4, Eq. (4) and reference 2, Eq. (3.6). This extends beyond even our largest models. Also, on comparing an ellipsoid and a cylinder, errors caused by nonstationary conditions will cancel out to some extent.

In the motion lengthwise the liquid moves from one end all the way to the other and the flow extends far sideways. This necessitates the use of a wide vat. Indeed, for a long ellipsoid even when moving in a rather wide tube, the "effective viscosity" is found doubled. Now we wish to recall that the friction per unit length of an infinitely long rod in a cylindrical container is determined by $\log R/b$. On the other hand, the force upon a rod in a very wide container is dependent upon $\log 2a/b$. Hence, it should hold

$$R > 2a > b.$$

Initial trials in which the rods were moved by means of a thread illustrated a significant aspect of rheological experiments. The force on a thin wire may well exceed that upon the rod! A slight increase in length easily makes up for a large decrease in thickness. The logarithmic dependence of the viscous force upon the width thus may be a reason that details in shape can be observed which do not show up in a linear mass average!

Analysis of the Nuclear Magnetic Resonance Spectrum of a Six-Spin System of Monofluorobenzene

SHIZUO FUJIWARA AND HIROSHI SHIMIZU
University of Electro-Communications, Chofu, Tokyo, Japan

(Received July 27, 1959)

This paper is concerned with the general analysis of a six-spin system belonging to the point group C_{2V}, using monofluorobenzene as an example. The apparatus used for the NMR measurements is the one constructed in this laboratory, operating at 27.030 Mc. The absorption lines calculated suggest the doublet structure of the spectrum, which is consistent with the observed spectrum. It was confirmed that this doublet structure is due to the spin-spin couplings of the ring protons with fluorine. More precise comparison of the calculated results with the observed spectrum was made by integrating the intensities of the lines having a suitable line shape and width. It was noted that this procedure for constructing the absorption spectrum from the calculated lines is useful in the discussion of the power of resolution of the apparatus and the type of line shape.

SEVERAL years ago, the hyperfine structures of the nuclear magnetic responance (NMR) spectra caused by the indirect nuclear spin couplings were observed experimentally.[1–4] Since then many efforts have been made to establish a theoretical basis for these phenomena[3,5–7] as well as to accumulate data.[8,9] Recently, the analyses of the multiplet structures of the complicated NMR spectra have aroused the deep interest of many workers[10–13] because many examples of complicated spectrum were encountered which can not be interpreted simply in terms of the chemical formula of the sample or by the low-order perturbation theory. Thus, McConnell, *et al.* showed a general method to deal with spin multiplets,[11] and analyses of three-[8,12,13] and four-spin systems[13] have also been performed.

This paper is concerned with the general analysis of a six-spin system belonging to the point group C_{2V} using monofluorobenzene as an example.

The proton magnetic resonance spectrum of monofluorobenzene was reported to be a doublet with components of almost equal intensity, and this result was interpreted in terms of the equal couplings of the fluorine nucleus with the ring protons having no chemical shift from each other.[14,15] Since this conclusion is a quite perplexing one to chemists, the authors continued efforts to resolve the spectrum further; and were able to show[16] that it has a more complicated multiplet structure which suggests not only the nonequivalence of the spin-spin couplings between the fluorine nucleus and the protons, but also the existence of chemical shifts among the protons, that is, nonequivalent couplings among protons. Thus, we started to make the analysis of this spectrum taking it as an example of a six-spin system. During our investigation,[17] Bak *et al.*[18] made extensive investigations on the structures of the NMR spectrum in deuterofluorobenzenes, and obtained the spin-spin coupling constants between fluorine and the protons at the ortho, meta, and para positions. They reported J_{FH^o}, J_{FH^m}, and J_{FH^p} to be 9.4 ± 0.2, 5.8 ± 0.2, and 0.0 ± 0.5 cps, respectively.[18] Thus, we made the numerical calculations with the use of these values of J, taking the chemical shifts of the ring protons as the variable parameter. For the calculation, the digital computer, FACOM, at the Calculation Center, Ichigaya, Tokyo, and the parametron digital computer PC–1 at the University of Tokyo, Hongo, Tokyo, were used. A method of approximation was used for the calculation of the secular equation, which will be shown in the Appendix.

APPARATUS FOR NMR MEASUREMENTS

The apparatus used[19] is composed[20] of an oscillator, a null-T bridge, a preamplifier, a Collins 51J–4 receiver,

[1] W. G. Proctor and F. C. Yu, Phys. Rev. **78**, 471 (1950); **81**, 20 (1951).
[2] S. S. Dharmatti and H. E. Weaver, Phys. Rev. **87**, 675 (1952).
[3] E. L. Hahn and D. E. Maxwell, Phys. Rev. **84**, 1246 (1951); **88**, 1070 (1952).
[4] E. B. McNeil, C. P. Slichter, and H. S. Gutowsky, Phys. Rev. **84**, 1245 (1951).
[5] N. F. Ramsey and E. M. Purcell, Phys. Rev. **85**, 143 (1952).
[6] N. F. Ramsey, Phys. Rev. **91**, 303 (1953).
[7] H. S. Gutowsky, D. W. McCall, and C. P. Slichter, Phys. Rev. **84**, 589 (1951); J. Chem. Phys. **21**, 279 (1953).
[8] H. S. Gutowsky, C. H. Holm, A. Saika, and G. A. Williams, J. Am. Chem. Soc. **79**, 4596 (1957).
[9] W. A. Anderson, Phys. Rev. **102**, 151 (1956).
[10] M. K. Banerjee, T. P. Das, and A. K. Saha, Proc. Roy. Soc. (London) **A226**, 490 (1954).
[11] H. M. McConnell, A. D. McLean, and C. A. Reilly, J. Chem. Phys. **23**, 1152 (1955).
[12] G. A. Williams, H. S. Gutowsky, J. Chem. Phys. **25**, 1288 (1956).
[13] H. J. Bernstein, W. G. Schneider, and J. A. Pople, Can. J. Chem. **35**, 65, 1060, 1487 (1957).
[14] E. B. Baker, J. Chem. Phys. **23**, 984 (1955).
[15] H. S. Gutowsky, L. H. Meyer, and D. W. McCall, J. Chem. Phys. **23**, 982 (1955).
[16] S. Fujiwara, M. Katayama, and H. Shimizu, Bull. Chem. Soc. Japan **32**, 103 (1959).
[17] We are indebted to Dr. Williams for a discussion of this work and for sending us a preprint of reference 18.
[18] B. Bak, J. N. Shoolery, and G. A. Williams, III, J. Mol. Spectroscopy **2**, 525 (1958).
[19] This apparatus is the same in almost every detail as the one built by Professor Gutowsky at the University of Illinois, and owes much of its setup to Professor Gutowsky's instruction which was given during one of the authors' (SF) stay at U. I. Thanks are also due to Mr. Shoichi Hayashi of this University for help in construction of the apparatus. The cost of this construction was defrayed by a Grant in Aid of the Ministry of Education in Japan.
[20] H. S. Gutowsky, L. H. Meyer, and R. E. McClure, Rev. Sci. Instr. **24**, 644 (1953).

a Sanborn recorder, a DuMont 504H oscilloscope, a magnet, and a sawtooth generator. The magnet is a permanent magnet of the Indiana Steel Product Company, with the same structure as the one previously described by Gutowksy.[20] Figure 1(a) shows the field distribution of the magnet when it was brought to this laboratory after the transpacific transportation. Homogeneity of the field could be very much improved, as shown in Fig. 1(b), by adjusting the six stainless steel tie rods fastening the pole caps and the pole to the yoke: the details of this procedure are the same as described by Gutowsky[20] including polishing the pole face with fine emery paper. No particular adjustment of the lateral alignment was made. In the measurements of the NMR spectrum, the sample was placed at the spot with best homogeneity.

The resonance coil is about 5 mm in diam and 3 mm in length. The sample was sealed in a thin-walled capillary with an inside diam of about 1.0 mm. The sample was spun[21] during the measurements.

ANALYSIS OF THE SPECTRUM

The scheme of the analysis is almost the same as given by McConnell *et al.*[11] and we will not show details of the calculation procedures. In Tables I and II, we show the zero-order spin functions and the matrix elements which will be applicable to the systems of not only AB_2C_2X but also of AB_2C_2D. (The notation is in accordance with the one used in the articles of Bernstein *et al.*[13])

The Hamiltonian to be taken here may be written as

$$\mathcal{H}=1/(2\pi)\sum_{i=A}^{D}\gamma_i H_i I_{iz}+\sum_{i,j=A}^{D} J_{ij}(1-\delta_{ij})\mathbf{I}_i\cdot\mathbf{I}_j, \quad (1)$$

where γ_i, H_i, and I_{iz} refer to the nuclear gyromagnetic ratio, the effective resonance field including the magnetic shielding effect, and the z component of the

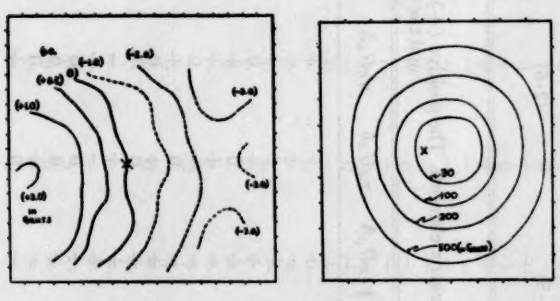

(a) (b)

FIG. 1. Contour maps of the variations in the magnetic field in the plane middle between the two pole faces: (a) before and (b) after the adjustments of the magnet to improve the field homogeneity. The figures given to each contour line represent decreases (minus sign) or increases (positive sign) of the field strength with respect to the center (marked as x). The distance scale is in cm.

[21] F. Bloch, Phys. Rev. **94**, 496 (1954).

TABLE I. Zero-order spin functions.

No.	$(R)_M$	A	B, B'	C, C'	D
1	$(A)_3$	α	$\alpha\alpha$	$\alpha\alpha$	α
2	$(A)_2$	β	$\alpha\alpha$	$\alpha\alpha$	α
3		α	$\alpha\alpha$	$\alpha\alpha$	β
4		α	$\alpha\alpha$	$\sqrt{2}^{-1}(\alpha\beta+\beta\alpha)$	α
5		α	$\sqrt{2}^{-1}(\alpha\beta+\beta\alpha)$	$\alpha\alpha$	α
6	$(A)_1$	β	$\alpha\alpha$	$\alpha\alpha$	β
7		β	$\alpha\alpha$	$\sqrt{2}^{-1}(\alpha\beta+\beta\alpha)$	α
8		β	$\sqrt{2}^{-1}(\alpha\beta+\beta\alpha)$	$\alpha\alpha$	α
9		α	$\alpha\alpha$	$\sqrt{2}^{-1}(\alpha\beta+\beta\alpha)$	β
10		α	$\sqrt{2}^{-1}(\alpha\beta+\beta\alpha)$	$\alpha\alpha$	β
11		α	$\alpha\alpha$	$\beta\beta$	α
12		α	$\beta\beta$	$\alpha\alpha$	α
13		α	$\sqrt{2}^{-1}(\alpha\beta+\beta\alpha)$	$\sqrt{2}^{-1}(\alpha\beta+\beta\alpha)$	α
14		α	$\sqrt{2}^{-1}(\alpha\beta-\beta\alpha)$	$\sqrt{2}^{-1}(\alpha\beta-\beta\alpha)$	α
15	$(A)_0$	β	$\alpha\alpha$	$\sqrt{2}^{-1}(\alpha\beta+\beta\alpha)$	β
16		β	$\sqrt{2}^{-1}(\alpha\beta+\beta\alpha)$	$\alpha\alpha$	β
17		β	$\alpha\alpha$	$\beta\beta$	α
18		β	$\beta\beta$	$\alpha\alpha$	α
19		β	$\sqrt{2}^{-1}(\alpha\beta+\beta\alpha)$	$\sqrt{2}^{-1}(\alpha\beta+\beta\alpha)$	α
20		β	$\sqrt{2}^{-1}(\alpha\beta-\beta\alpha)$	$\sqrt{2}^{-1}(\alpha\beta-\beta\alpha)$	α
21		α	$\alpha\alpha$	$\beta\beta$	β
22		α	$\beta\beta$	$\alpha\alpha$	β
23		α	$\sqrt{2}^{-1}(\alpha\beta+\beta\alpha)$	$\sqrt{2}^{-1}(\alpha\beta+\beta\alpha)$	β
24		α	$\sqrt{2}^{-1}(\alpha\rho-\beta\alpha)$	$\sqrt{2}^{-1}(\alpha\rho-\rho\alpha)$	β
25		α	$\beta\beta$	$\sqrt{2}^{-1}(\alpha\beta+\beta\alpha)$	α
26		α	$\sqrt{2}^{-1}(\alpha\beta+\beta\alpha)$	$\beta\beta$	α
27	$(A)_{-1}$	β	$\alpha\alpha$	$\beta\beta$	β
28		β	$\beta\beta$	$\alpha\alpha$	β
29		β	$\sqrt{2}^{-1}(\alpha\beta+\beta\alpha)$	$\sqrt{2}^{-1}(\alpha\beta+\beta\alpha)$	β
30		β	$\sqrt{2}^{-1}(\alpha\beta-\beta\alpha)$	$\sqrt{2}^{-1}(\alpha\beta-\beta\alpha)$	β
31		β	$\beta\beta$	$\sqrt{2}^{-1}(\alpha\beta+\beta\alpha)$	α
32		β	$\sqrt{2}^{-1}(\alpha\beta+\beta\alpha)$	$\beta\beta$	α
33		α	$\beta\beta$	$\sqrt{2}^{-1}(\alpha\beta+\beta\alpha)$	β
34		α	$\sqrt{2}^{-1}(\alpha\beta+\beta\alpha)$	$\beta\beta$	β
35		α	$\beta\beta$	$\beta\beta$	α
36	$(A)_{-2}$	β	$\beta\beta$	$\sqrt{2}^{-1}(\alpha\beta+\beta\alpha)$	β
37		β	$\sqrt{2}^{-1}(\alpha\beta+\beta\alpha)$	$\beta\beta$	β
38		β	$\beta\beta$	$\beta\beta$	α
39		α	$\beta\beta$	$\beta\beta$	β
40	$(A)_{-3}$	β	$\beta\beta$	$\beta\beta$	β
41	$(B)_2$	α	$\alpha\alpha$	$\sqrt{2}^{-1}(\alpha\beta-\beta\alpha)$	α
42		α	$\sqrt{2}^{-1}(\alpha\beta-\beta\alpha)$	$\alpha\alpha$	α
43	$(B)_1$	β	$\alpha\alpha$	$\sqrt{2}^{-1}(\alpha\beta-\beta\alpha)$	α
44		β	$\sqrt{2}^{-1}(\alpha\beta-\beta\alpha)$	$\alpha\alpha$	α
45		α	$\alpha\alpha$	$\sqrt{2}^{-1}(\alpha\beta-\beta\alpha)$	β
46		α	$\sqrt{2}^{-1}(\alpha\beta-\beta\alpha)$	$\alpha\alpha$	β
47		α	$\sqrt{2}^{-1}(\alpha\beta+\beta\alpha)$	$\sqrt{2}^{-1}(\alpha\beta-\beta\alpha)$	α
48		α	$\sqrt{2}^{-1}(\alpha\beta-\beta\alpha)$	$\sqrt{2}^{-1}(\alpha\beta+\beta\alpha)$	α
49	$(B)_0$	β	$\alpha\alpha$	$\sqrt{2}^{-1}(\alpha\beta-\beta\alpha)$	β
50		β	$\sqrt{2}^{-1}(\alpha\beta-\beta\alpha)$	$\alpha\alpha$	β
51		β	$\sqrt{2}^{-1}(\alpha\beta+\beta\alpha)$	$\sqrt{2}^{-1}(\alpha\beta-\beta\alpha)$	α
52		β	$\sqrt{2}^{-1}(\alpha\beta-\beta\alpha)$	$\sqrt{2}^{-1}(\alpha\beta+\beta\alpha)$	α
53		α	$\sqrt{2}^{-1}(\alpha\beta+\beta\alpha)$	$\sqrt{2}^{-1}(\alpha\beta-\beta\alpha)$	β
54		α	$\sqrt{2}^{-1}(\alpha\beta-\beta\alpha)$	$\sqrt{2}^{-1}(\alpha\beta+\beta\alpha)$	β
55		α	$\beta\beta$	$\sqrt{2}^{-1}(\alpha\beta-\beta\alpha)$	α
56		α	$\sqrt{2}^{-1}(\alpha\beta-\beta\alpha)$	$\beta\beta$	α
57	$(B)_{-1}$	β	$\sqrt{2}^{-1}(\alpha\beta+\beta\alpha)$	$\sqrt{2}^{-1}(\alpha\beta-\beta\alpha)$	β
58		β	$\sqrt{2}^{-1}(\alpha\beta-\beta\alpha)$	$\sqrt{2}^{-1}(\alpha\beta+\beta\alpha)$	β
59		β	$\beta\beta$	$\sqrt{2}^{-1}(\alpha\beta-\beta\alpha)$	α
60		β	$\sqrt{2}^{-1}(\alpha\beta-\beta\alpha)$	$\beta\beta$	α
61		α	$\beta\beta$	$\sqrt{2}^{-1}(\alpha\beta-\beta\alpha)$	β
62		α	$\sqrt{2}^{-1}(\alpha\beta-\beta\alpha)$	$\beta\beta$	β
63	$(B)_{-2}$	β	$\beta\beta$	$\sqrt{2}^{-1}(\alpha\beta-\beta\alpha)$	β
64		β	$\sqrt{2}^{-1}(\alpha\beta-\beta\alpha)$	$\beta\beta$	β

TABLE IIa. Off-diagonal matrix elements. H_{ij}'s are symbolized by (i, j) and $(i, j) = (j, i)$. For example, the off-diagonal elements of $(A)_1$ state are

$$a_{1,5}=a_{5,1}=a_{2,8}=a_{8,2}=a_{3,7}=a_{7,3}=\sqrt{2}^{-1}J_{AB},$$
$$a_{1,4}=a_{4,1}=\cdots=a_{8,3}=\sqrt{2}^{-1}J_{AC},$$
$$\cdots$$
$$\cdots$$
$$a_{6,9}=a_{9,6}=a_{7,9}=a_{9,7}=-\tfrac{1}{2}(J_{BC}-J_{BC'}),$$
$$a_{8,9}=a_{9,8}=\tfrac{1}{2}(J_{BC}-J_{BC'}).$$

$(R)_M$	$\sqrt{2}^{-1}J_{AB}$	$\sqrt{2}^{-1}J_{AC}$	$\frac{1}{2}J_{AD}$	$\sqrt{2}^{-1}J_{BD}$	$\sqrt{2}^{-1}J_{CD}$	$\frac{1}{2}(J_{BC}+J_{BC'})$	$\frac{1}{2}(J_{BC}-J_{BC'})$
$(A)_2$	(1·4)	(1·3)	(1·2)	(2·4)	(2·3)	(3·4)	
$(A)_1$	(1·5), (2·8), (3·7)	(1·4), (2·6), (3·8)	(2·4), (3·5)	(1·3), (4·8), (5·7)	(1·2), (4·6), (5·8)	(2·3), (4·5), (6·8), (7·8)	−(6·9), −(7·9), (8·9)
$(A)_0$	(1·9), (2·8), (3·12), (5·11)	(1·7), (2·9), (4·11), (5·12)	(3·7), (4·8), (5·9), (6·10)	(1·5), (2·4), (7·12), (9·11)	(1·3), (2·5), (8·11), (9·12)	(1·2), (3·5), (4·5), (7·9), (8·9), (11·12)	−(3·6), −(4.6), (5·6), −(7·10), −(8·10), (9·10)
$(A)_{-1}$	(1·8), (3·7), (6·9)	(2·7), (3·8), (5·9)	(5·7), (6·8)	(1·6), (3·5), (8·9)	(2·5), (3·6), (7·9)	(1·3), (2·3), (5·6), (7·8)	−(1·4), −(2·4), (3·4)
$(A)_{-2}$	(2·4)	(1·4)	(3·4)	(2·3)	(1·3)	(1·2)	
$(B)_2$							(1·2)
$(B)_1$	(1·5)	(2·6)	(1·3), (2·4)	(3·5)	(4·6)		(1·2), (3·4), (5·6)
$(B)_0$	(1·5), (3·7)	(2·6), (4·8)	(3·5), (4·6)	(1·3), (5·7)	(2·4), (6·8)		(1·2), (3·4), (5·6), (7·8)
$(B)_{-1}$	(1·5)	(2·6)	(3·5), (4·6)	(1·3)	(2·4)		(1·2), (3·4), (5·6)
$(B)_{-2}$							(1·2)

TABLE IIb. Diagonal matrix elements. The positive (+) or the negative (−) signs denote the procedures to add or reduce the numbers presented in the top line, respectively, and the sign −3 to reduce the figure three times of the number in the top line.

No.	$(R)_M$	$\frac{1}{2}\gamma_A H_A\hbar$	$\gamma_B H_B\hbar$	$\gamma_C H_C\hbar$	$\frac{1}{2}\gamma_D H_D\hbar$	$\frac{1}{2}J_{AB}$	$\frac{1}{2}J_{AC}$	$\frac{1}{2}J_{AD}$	$\frac{1}{2}J_{BC}$	$\frac{1}{2}J_{BC'}$	$\frac{1}{2}J_{BD}$	$\frac{1}{2}J_{CD}$	$\frac{1}{4}J_{BB'}$	$\frac{1}{4}J_{CC'}$
1	$(A)_2$	+	+	+	+	+	+	+	+	+	+	+	+	+
2	$(A)_2$	−	+	+	+	−	−	−	+	+	+	+	+	+
3		+	+	+	−	+	+	−	+	+	−	−	+	+
4		+	+	0	+	+	0	+	0	0	+	0	+	+
5		+	0	+	+	0	+	+	0	0	0	+	+	+
6	$(A)_1$	−	+	+	−	−	−	+	+	+	−	−	+	+
7		−	+	0	+	−	0	−	0	0	+	0	+	+
8		−	0	+	+	0	−	−	0	0	0	+	+	+
9		+	+	0	−	+	0	−	0	0	−	0	+	+
10		+	0	+	−	0	+	−	0	0	0	−	+	+
11		+	+	−	+	+	−	+	−	−	+	−	+	+
12		+	−	+	+	−	+	+	−	−	−	+	+	+
13		+	0	0	+	0	0	+	+	0	0	0	+	+
14		+	0	0	+	0	0	+	+	0	0	0	−3	−3
15	$(A)_0$	−	+	0	−	−	0	+	0	0	−	0	+	+
16		−	0	+	−	0	−	+	0	0	0	−	+	+

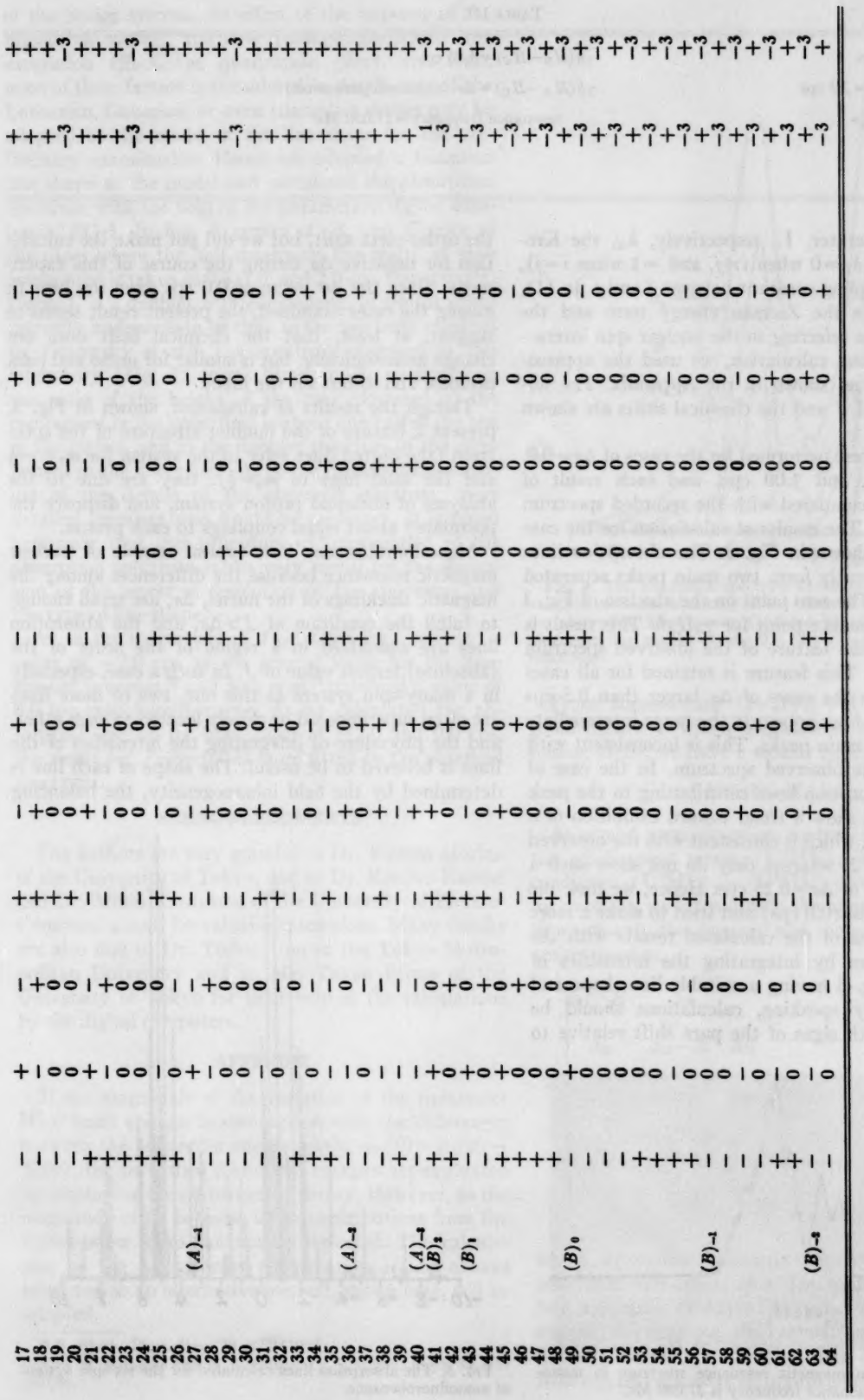
(A)-1
(A)-2
(A)2 (B)2
(B)1
(B)0
(B)-1
(B)-2
17 18 19 20 21 22 23 24 25 26 27 28 29 30 31 32 33 34 35 36 37 38 39 40 41 42 43 44 45 46 47 48 49 50 51 52 53 54 55 56 57 58 59 60 61 62 63 64

TABLE III.

$J_{BC}=J_{AB}=8.9$ cps	$\gamma h(H_B-H_C)=4.86$ cps
$J_{BB'}=J_{CC'}=J_{AC}=2.2$ cps	$\gamma h(H_A-H_C)=\Delta\sigma$ (unknown parameter)
$J_{BC'}=J_{AX}=0.0$ cps	resonance frequency = 27.030 Mc
$J_{XC}=9.4$ cps	
$J_{XB}=5.8$ cps	

nuclear spin operator, $\mathbf{I}_i$, respectively, δ_{ij}, the Kronecker symbol ($\delta_{ij}=0$ when $i\neq j$, and $=1$ when $i=j$), and J_{ij}, the coupling constant between i and j. In (1), the first term is the Zeeman energy term and the second is the one referring to the nuclear spin interaction. In the actual calculation, we used the approximation method as shown in the Appendix. The numerical values of J and the chemical shifts are shown in Table III.

Calculations were performed for the cases of $\Delta\sigma=0.0$, 0.25, 0.50, 0.75, and 1.00 cps, and each result of calculation was compared with the recorded spectrum shown in Fig. 2. The results of calculation for the case of $\Delta\sigma=0.0$ are shown in Fig. 3. The absorption lines calculated apparently form two main peaks separated by about 6 cps. The zero point on the abscissa of Fig. 3 refers to the resonance point for $\gamma_A H_A\hbar$. This result is consistent with the feature of the observed spectrum shown in Fig. 2. This feature is retained for all cases examined, but in the cases of $\Delta\sigma$ larger than 0.5 cps many absorption lines appear in the range intermediate between the two main peaks. This is inconsistent with the feature of the observed spectrum. In the case of $\Delta\sigma=0.0$, the absorption lines contributing to the peak in the lower field show a trend toward exhibition of a doublet structure, which is consistent with the observed spectrum of Fig. 2, whereas they do not show such a trend in the case of $\Delta\sigma=0.25$ cps. Hence, we took the smaller value for $\Delta\sigma$(0.0 cps) and tried to make a more precise comparison of the calculated results with the observed spectrum by integrating the intensities of those lines in Fig. 3 having a suitable line shape and width. Rigorously speaking, calculations should be performed for both signs of the para shift relative to the ortho-meta shift, but we did not make the calculation for negative $\Delta\sigma$ during the course of this experiment. Since the $\Delta\sigma$ value of 0.0 cps gave the best fit among the cases examined, the present result seems to suggest, at least, that the chemical shift does not change monotonically, but is similar for ortho and para protons, and differs for the meta.

Though the results of calculation, shown in Fig. 3, present a feature of the doublet structure of the spectrum (the dotted lines refer to the system for $m_x=-\frac{1}{2}$ and the solid lines to $m_x=\frac{1}{2}$), they are due to the analyses of nonequal proton system, and disprove the postulate[14] about equal couplings to each proton.

Monofluorobenzene is a typical sample of nuclear magnetic resonance because the differences among the magnetic shieldings of the nuclei, $\Delta\sigma$, are small enough to fulfill the condition of $J>\Delta\sigma$, and the absorption lines are assembled in a region of the order of the (absolute) largest value of J. In such a case, especially in a many-spin system as this one, two or more lines are often superimposed or closely located to each other, and the procedure of integrating the intensities of the lines is believed to be useful. The shape of each line is determined by the field inhomogeneity, the balancing

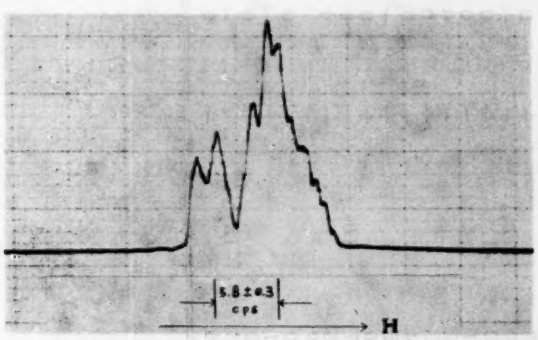

FIG. 2. The proton magnetic resonance spectrum in monofluorobenzene. The resonance frequency is 27.030 Mc.

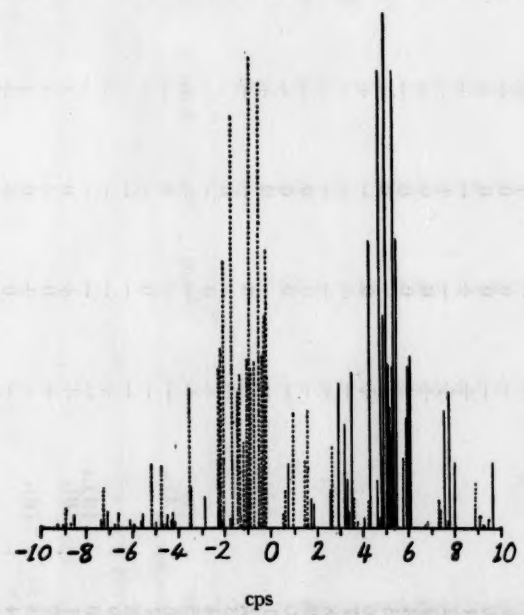

FIG. 3. The absorption lines calculated for the six-spin system of monofluorobenzene.

of the bridge system, the effect of the response of the measuring system, the slow passage condition,[22] the saturation effect, the quadrupole effect, etc. Since none of these factors is considered in detail, any of the Lorenzian, Gaussian, or even triangular shapes may be adopted as the model of the line shape for the preliminary examination. Hence we adopted a Gaussian line shape as the model and calculated the absorption spectrum with the help of the parametron digital computer, PC-1. In Fig. 4, curves *A*, *B*, and *C* refer to the cases where the half maximum line width of each component is taken as 0.5, 1.0, and 2.0 cps, respectively. Curve *C* is a doublet with components of almost equal intensity and seems to be close to the spectrum reported by Gutowsky *et al.*[15] The spectrum observed in this laboratory (Fig. 2) seems fitted to *A*, especially in the ratio of the height of the two components; the component in the lower field is about one-half of the one in the higher, and in the doublet structure of the component in the lower field. As to the further understanding of the details of the observed spectrum, more detailed investigations would be necessary. It is noted here only that this procedure of construction of the absorption spectrum seems very useful for the discussion of the power of resolution of the apparatus and the type of line shape.

As to the magnitude of J_{HF^p}, Gutowsky reported a value of -2.0 cps as the general value for the fluorinated benzenes,[23] and Bak *et al.*[18] obtained a value of 0.0 for monofluorobenzene. As we calculated the absorption spectra for both cases of -2.0 and 0.0 cps, the result for $J_{HF^p}=0.0$ is more fitted to the observed spectrum.

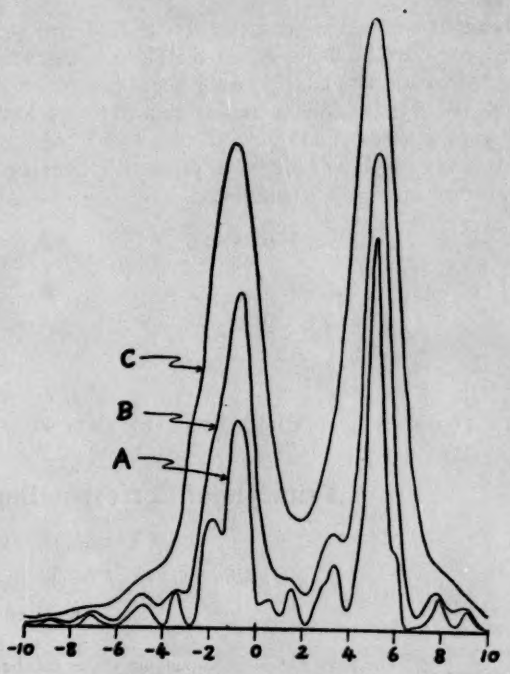

FIG. 4. The absorption spectrum of the proton magnetic resonance in monofluorobenzene as the result of the integration of all the absorption lines having Gaussian line shapes with the half maximum line widths of (*A*) 0.5, (*B*) 1.0, and (*C*) 2.0 cps, respectively.

ACKNOWLEDGMENTS

The authors are very grateful to Dr. Yonezo Morino of the University of Tokyo, and to Dr. Kenjiro Kambe and Dr. Mikio Katayama of the University of Electro-Communications for valuable discussions. Many thanks are also due to Dr. Toshio Uno of the Tokyo Metropolitan University and to Mr. Takao Iijima of the University of Tokyo for their help in the calculations by the digital computers.

APPENDIX

If the magnitude of the variation of the parameter $\mathbf{H}'$ is small enough in comparison with the differences between the zero-order energy levels, $\omega_{ij}(0)=E_i(0)-E_j(0)$, the perturbed states and energies are evaluated by employing the perturbation theory. However, as the magnitude of $\mathbf{H}'$ becomes large, contributions from the higher-order terms can not be neglected. The calculation of the higher-order perturbation is not always easy, and so an alternative method, shown here, will be adopted.

From Hamiltonian $\mathbf{H}=\mathbf{H}(0)+\mathbf{H}'$ and the orthogonal matrix $\mathbf{U}$ which diagonalizes zero-order Hamiltonian, $\mathbf{H}(0)$, we have a secular equation

$$|\,\mathbf{U}^*\mathbf{H}\mathbf{U}-\mathbf{E}\,|=0.$$

As a good approximation, we may be able to neglect the off-diagonal terms, $(\mathbf{U}^*\mathbf{H}\mathbf{U})_{ij}$ which satisfy the condition: $(\mathbf{U}^*\mathbf{H}\mathbf{U})_{ii}-(\mathbf{U}^*\mathbf{H}\mathbf{U})_{jj}\gg(\mathbf{U}^*\mathbf{H}\mathbf{U})_{ij}$. Thus, for example, we often obtain the approximate equation in which only the diagonal and the semidiagonal terms are retained as

$$\begin{vmatrix} a_{11}-E & a_{12} & & & & \\ a_{21} & a_{22}-E & a_{23} & & & \\ & a_{32} & a_{33}-E & & 0 & \\ & & & \cdot & & \\ & & 0 & & \cdot & \\ & & & & \cdot & \\ & & & & a_{nn-1} & a_{nn}-E \end{vmatrix}=0,$$

where, we replace the matrix elements of $\mathbf{U}^*\mathbf{H}\mathbf{U}$ with a conventional notation of a. The solutions of this equation are easily evaluated by using a further approximation; for example, the calculation of E_i is made as follows: We replace E's other than ith diagonal terms with a_{ii}, and calculate an approximate solution, E_i^I, by

[22] F. Bloch, Phys. Rev. 79, 471 (1956).
[23] G. A. Williams and H. S. Gutowsky, J. Chem. Phys. 30, 717 (1959).

solving the equation with respect to E. If we repeat this procedure by using E_i^I in the place of a_{ii}, we can generally expect to have a better approximate solution, E_i^{II}. We will be able to repeat this until we have a self-consistent solution.

Actually, we may be able to proceed by solving the following approximate equations:

$$\begin{vmatrix} a_{i-1,i-1}-E & a_{i-1,i} \\ a_{i-1,i} & a_{ii}-E \end{vmatrix}=0$$

and

$$\begin{vmatrix} a_{ii}-E & a_{i,i+1} \\ a_{i,i+1} & a_{i+1,i+1}-E \end{vmatrix}=0.$$

From the solution of these equations which correspond to E_i, say E_i' and E_i'', an approximate E_i will be evaluated by the equation

$$E_i^I=(|a_{i-1,i}|+|a_{i,i+1}|)^{-1} \times(|a_{i-1,i}|E_i'+|a_{i,i+1}|E_i'').$$

THE JOURNAL OF CHEMICAL PHYSICS VOLUME 32, NUMBER 6 JUNE, 1960

Principle of Corresponding States for Transport Properties

EUGENE HELFAND AND STUART A. RICE*†

Bell Telephone Laboratories, Incorporated, Murray Hill, New Jersey

(Received November 18, 1959)

The principle of corresponding states can be demonstrated by use of the autocorrelation function expressions for the transport properties and the assumption that the intermolecular potential has the form $u=\epsilon u^*(r/\sigma)$. The result follows from the fact that both the canonical ensemble distribution function and the solution of the mechanical equations of motion may be written in reduced variables. One finds that $\eta^*=\eta\sigma^2/m^{\frac{1}{2}}\epsilon^{\frac{1}{2}}$, $\kappa^*=\kappa k\epsilon^{\frac{1}{2}}/m^{\frac{1}{2}}\sigma^2$, and $D^*=Dm^{\frac{1}{2}}/\epsilon^{\frac{1}{2}}\sigma$ are universal functions of $T^*=Tk/\epsilon$, $P^*=P\sigma^3/\epsilon$, and in the quantum mechanical case $\hbar^*=\hbar/\sigma m^{\frac{1}{2}}\epsilon^{\frac{1}{2}}$.

PRINCIPLES of corresponding states have long been known and applied to both equilibrium and transport properties of pure materials.[1] One means of derivation proceeds by dimensional analysis with either the critical constants or appropriate combinations of molecular parameters commonly used for the reduction of variables.

Pitzer[2] has detailed a set of assumptions which allows the partition function to be cast into a reduced variable form, thus providing a statistical mechanical proof of the law of corresponding states for thermostatic properties. In essence, it is required that the intermolecular pair potential of all molecules be of the form $u=\epsilon u^*(r/\sigma)$, where ϵ and σ are characteristic energy and distance constants and u^* is a universal function of the one variable r/σ. Thus, the simple law of corresponding states may be expected to hold for spherical nonpolar molecules if, for instance, the potential is of the Lennard-Jones 6–12 type. Introduction of additional parameters, such as a reduced dipole moment, into the equation of state extends the validity of the principle of corresponding states, although this sometimes limits its utility.

Pitzer originally limited consideration to systems whose translational degrees of freedom are classical and internal degrees of freedom are unexcited. The translational restriction may be removed[3] by introduction of a reduced Planck constant as a parameter, leading to a mass dependence of the thermodynamic properties.

Aside from providing the basis for extension of the law of corresponding states to nonspherical potentials and quantum systems, the Pitzer technique of reducing the partition function has also been useful in deriving conformal solution theory.

The purpose of this brief paper is to show that with the intermolecular potential of the form suggested by Pitzer a law of corresponding states can be derived for the transport coefficients. The demonstration will be based on the use of expressions for the transport coefficients in terms of time integrals of appropriate autocorrelation functions.[4] Such equations have been

* Alfred P. Sloan Fellow.

† Permanent address: Department of Chemistry and Institute for Study of Metals, University of Chicago, Chicago 37, Illinois.

[1] J. O. Hirschfelder, C. F. Curtiss, and R. B. Bird, *Molecular Theory of Gases and Liquids* (John Wiley & Sons, Inc., New York, 1954), Chaps. 4 and 9.

[2] K. S. Pitzer, J. Chem. Phys. 7, 583 (1939).

[3] J. de Boer, Physica 14, 139 (1948).

[4] The principle of corresponding states may also be established by consideration of other formulations of the transport coefficients. A particularly transparent form is given by Rice and Kirkwood, [J. Chem. Phys. 31, 901 (1959)] where the classical thermal conductivity and viscosities are expressed in terms of the self-diffusion coefficient. In this case, only reduced temperature and pressure are required to obtain the correspondence.

derived by Kubo *et al.*[5] by consideration of the regression of fluctuations, which are assumed to follow the macroscopic laws; and by Mori,[6] who assumes that a local equilibrium distribution will relax rapidly to the stationary state. The rigorous demonstration of the theorem of corresponding states presented herein validates the dimensional analysis ordinarily used.

The important point in our proof of the law of corresponding states will be that in addition to the distribution function, the solution of the mechanical equation of motion may be written in reduced variables. The principles are demonstrated for the shear viscosity in the quantum mechanical case. The classical results, of course, follow in the limit $\hbar\to 0$. The bulk viscosity, thermal conductivity, and self-diffusion constant will be briefly discussed and the results stated.

The shear viscosity is given by the formula

$$\eta=V^{-1}\int_0^\infty dt\int_0^{1/kT}d\lambda\ \mathrm{tr}\{J_{xy}{}^{(v)}\cdot\exp[i(t+i\hbar\lambda)H/\hbar]J_{xy}{}^{(v)}\exp[-i(t+i\hbar\lambda)H/\hbar]\cdot\exp[-H/kT]\}/\mathrm{tr}\{\exp[-H/kT]\}. \quad (1)$$

Consider the reduced variables

distance $r^*=r/\sigma$, (2)

mass $m^*=m/m=1$, (3)

pair potential $u^*(r^*)=u/\epsilon$. (4)

From this basic set we find the reduced quantities

temperature $T^*=Tk/\epsilon$, $(k^*=1)$ (5)

time $t^*=t\epsilon^{\frac{1}{2}}/m^{\frac{1}{2}}\sigma$, (6)

momentum $\mathbf{p}_i{}^*=\mathbf{p}_i/m^{\frac{1}{2}}\epsilon^{\frac{1}{2}}$, (7)

volume $V^*=V/\sigma^3$, (8)

pressure $P^*=P\sigma^3/\epsilon$, (9)

Planck constant $\hbar^*=\hbar/\sigma m^{\frac{1}{2}}\epsilon^{\frac{1}{2}}$, (10)

$\mathbf{J}^{(v)}$ tensor $\mathbf{J}^{(v)*}=\mathbf{J}^{(v)}/\epsilon$,

$$=\sum_i(\mathbf{p}_i{}^*\mathbf{p}_i{}^*+\mathbf{r}_i{}^*\mathbf{F}_i{}^*)-P^*V^*\mathbf{1}$$

(where $\mathbf{F}_i$ is the force on i), (11)

and Hamiltonian $H^*=H/\epsilon$,

$$=\sum_i[(p_i{}^*)^2/2+\sum_j{}'u^*(r_{ij}{}^*)]. \quad (12)$$

The reduced Hamiltonian is a universal function of the momentum and position operators so that for any particular reduced volume (which enters through the boundary conditions) there is a universal set of reduced eigenfunctions and energy levels.

The use of Eqs. (2) to (12) in Eq. (1) results in the reduction

$$\eta^*=\eta\sigma^2/m^{\frac{1}{2}}\epsilon^{\frac{1}{2}}, \quad (13)$$

where η^* is given by Eq. (1) with a reduced variable replacing each unreduced variable. It is easily seen that, for instance, in an energy diagonal representation the reduced viscosity is a universal function of reduced temperature, pressure, and Planck's constant; i.e.,

$$\eta^*=\eta^*(T^*, P^*, \hbar^*), \quad (14)$$

where use of the correspondence equation of state, $V^*=V^*(T^*, P^*, \hbar^*)$ has been made.

It is pertinent to reiterate that (1) the density matrix has the reduced form $\exp[-H^*/T^*]/\mathrm{tr}\{\exp[-H^*/T^*]\}$, and (2) the similarity transform with reduced unitary operator $\exp[-i(t^*+i\hbar^*\lambda^*)H^*/\hbar^*]$ formally represents a reduced solution of the equations of motion, albeit in complex time.

The bulk viscosity differs from Eq. (1) only in that diagonal elements of the $\mathbf{J}^{(v)}$ tensor are involved. The correct reduction therefore is also

$$\phi^*=\phi\sigma^2/m^{\frac{1}{2}}\epsilon^{\frac{1}{2}}. \quad (15)$$

The demonstration of corresponding states for thermal conductivity follows in a manner completely paralleling the above from the formula given, for instance, by Mori.[6] We find the appropriate reduction to be

$$\kappa^*(T^*, P^*, \hbar^*)=\kappa k\epsilon^{\frac{1}{2}}/m^{\frac{1}{2}}\sigma^2. \quad (16)$$

Strictly speaking, self-diffusion is defined only in a classical system. One may, however, regard it as mutual diffusion of a tagged species in which case a quantum mechanical formula similar to Eq. (1) may be used. Alternatively one may, from the start, use for self-diffusion the Einstein equation written in terms of a time integral of the autocorrelation of momenta. The operator which replaces the similarity transform, as a formal solution of the equations of mechanics is $\exp(it\mathfrak{L})$, where $\mathfrak{L}$ is the self-adjoint Liouville operator.[7] Using the previous reduction scheme one can easily show that the reduced classical coefficient of self-diffusion is

$$D^*(T^*, P^*)=Dm^{\frac{1}{2}}/\epsilon^{\frac{1}{2}}\sigma. \quad (17)$$

In conclusion we wish to direct attention to notes by Gini-Castagnoli *et al.*[8] and Keyes.[9] These investigations deal with dimensional analysis reduction of data for liquid and solid systems, respectively. For liquids which by the previous considerations may be expected to have transport properties obeying the simple law of corresponding states, data are available only for argon,

[5] Kubo, Yokota, and Nakajima, J. Phys. Soc. Japan **12**, 1203 (1957).

[6] H. Mori, Phys. Rev. **112**, 1829 (1958).

[7] J. G. Kirkwood, J. Chem. Phys. **14**, 180 (1946).

[8] Gini-Castagnoli, Pizzella, and Ricci, Nuovo cimento **11**, 466 (1959).

[9] R. W. Keyes, J. Chem. Phys. **31**, 452 (1959).

methane, nitrogen, oxygen, and carbon monoxide. It is found that deviations from corresponding states are larger than in the case of most equilibrium properties. This may be an expression of the sensitivity of interaction cross sections to the details of the potential form which certainty differ significantly among monatomic, diatomic, and polyatomic molecules. Similarly, the principle of corresponding states is only approximately satisfied by the thermal conductivity of rare gas solids, presumably because of imperfection scattering and other extraneous effects. For dilute gases the Chapman-Enskog theory, which obeys corresponding states, closely predicts the transport properties. Data in the dense gas region are not sufficient for a quantitative test.

ACKNOWLEDGMENT

We should like to express our appreciation to Dr. Howard Reiss for a stimulating discussion which lead to this research.

THE JOURNAL OF CHEMICAL PHYSICS VOLUME 32, NUMBER 6 JUNE, 1960

Thermodynamic Inequalities for Elastic Solids

JAMES C. M. LI

Edgar C. Bain Laboratory for Fundamental Research, United States Steel Corporation, Monroeville, Pennsylvania

AND

HSIAO S. KIANG

Department of Chemistry, Indiana University, Bloomington, Indiana

(Received November 23, 1959)

A table of all the positive quantities among measurable coefficients is given for anisotropic elastic solids under the variation of only temperature and stress. Examples of inequality formulation are presented. Upper or lower limits containing only the Grüneisen's parameter and heat capacities are derived for adiabatic and isothermal compressibilities, thermal expansion, and thermal stress.

INTRODUCTION

IN a previous communication[1] a condensed collection of all the thermodynamic formulas involving first derivatives is given for elastic solids under the outside variations of only temperature and stress. It is sometimes helpful, especially when the available data are limited, to obtain an upper or lower limit of a quantity through the use of thermodynamic inequalities.[2] These inequalities, required by the second law of thermodynamics, are valid in the sense that systems which violate them cannot exist in nature or have more variables than those considered in deriving the inequalities; such variables may be due to impurities or imperfections which may not have been considered in the inequality formulation. Therefore these inequalities will be useful in establishing boundary values for a quantity or in detecting uncontrolled variables. The purpose of this report is to introduce a collection of all thermodynamic inequalities involving first derivatives for elastic solids under the variations of only temperature and stress.

[1] T. W. Ting and J. C. M. Li, Phys. Rev. **106**, 1165 (1957).

[2] L. Landau and E. Lifshitz, *Statistical Physics*, translated by D. Shoenberg (Clarendon Press, Oxford, 1938), p. 98; see also V. P. Silin, Soviet Phys. J.E.T.P. (English translation) **3**, 123 (1956).

TABLE OF POSITIVE QUANTITIES

The table of positive quantities (Table I) lists all the simple inequalities among coefficients. To obtain an inequality among first derivatives, the first step is to transform these first derivatives into coefficients through the use of the tables presented earlier.[1] Then by use of the table of positive quantities, it is possible to find inequalities among first derivatives. This will be illustrated later with examples.

The present table was prepared from a combination of a set of basic inequalities and a set of basic equalities given in the previous communication.[1] The basic inequalities are obtained by considering that for an isolated system at equilibrium the entropy is a maximum at constant energy and volume (or strain)[3] or when the temperature is uniform, the energy is a minimum at constant entropy and volume.[4] Let a small piece of elastic solid of energy U, entropy S, volume V_0 at the reference state, and strain ϵ be in contact with another identical piece. Consider the two pieces of elastic solids as an isolated system. Evidently the system is at equilibrium. To keep the energy and the

[3] *The Collected Works of J. Willard Gibbs* (Yale University Press, New Haven, 1948), Vol. I, p. 56.

[4] Reference 3 and for a recent discussion, see J. C. M. Li, J. Chem. Phys. **29**, 747 (1958).

volume constant, let the increase of energy dU of the first piece be compensated by the decrease of energy of the second piece and let any change of strain $d\epsilon_1$, $d\epsilon_2$, $\cdots$, $d\epsilon_6$ of the first piece be compensated by an opposite change in the second piece. It is seen therefore that the first order change of entropy is zero because the change of the entropy of the first piece is exactly compensated by the change of the second piece. Now since the entropy is a maximum, it is necessary and sufficient that the second order change of entropy be negative. For the second order change, the first piece has the same sign as the second piece and therefore only one piece needs to be considered:

$$(\partial^2 S/\partial U^2)(dU)^2+2\sum_i(\partial^2 S/\partial U\partial\epsilon_i)(dU)(d\epsilon_i)+2\sum_i\sum_{j\neq i}(\partial^2 S/\partial\epsilon_i\partial\epsilon_j)(d\epsilon_i)(d\epsilon_j)+\sum_i(\partial^2 S/\partial\epsilon_i^2)(d\epsilon_i)^2<0. \quad (1)$$

After identifying the following relations from the previous tables:

$$(\partial S/\partial U)_\epsilon=1/T \quad (2)$$

$$(\partial S/\partial\epsilon_i)_{U,\epsilon'}=-V_0(\tau_i/T) \quad (3)$$

where τ_i ($i=1, 2, \cdots, 6$) are the components of stress, in order that Eq. (1) can hold for any values of dU and $d\epsilon$, we deduce that it is necessary and sufficient that the following Jacobian matrix:

$$\frac{\partial(1/T, -V_0\tau_1/T, -V_0\tau_2/T, \cdots, -V_0\tau_6/T)}{\partial(U, \epsilon_1, \epsilon_2, \cdots, \epsilon_6)} \quad (4)$$

be negative definite. On the other hand, since the energy is a minimum at constant entropy and volume, a similar argument gives that the following Jacobian matrix:

$$\frac{\partial(T, V_0\tau_1, V_0\tau_2, \cdots, V_0\tau_6)}{\partial(S, \epsilon_1, \epsilon_2, \cdots, \epsilon_6)} \quad (5)$$

be positive definite. It can be shown that the conditions evaluated from the two Jacobian matrices are identical and each gives the basic set of inequalities. In order to use the previous tables,[1] the latter set has more practical variables and is therefore used. For other variables, transformation of Jacobian (5) gives the following Jacobian matrices:

$$\frac{\partial(S, V_0\tau_1, V_0\tau_2, \cdots, V_0\tau_6)}{\partial(T, \epsilon_1, \epsilon_2, \cdots, \epsilon_6)} \quad (6)$$

$$\frac{\partial(S, V_0\epsilon_1, V_0\epsilon_2, \cdots, V_0\epsilon_6)}{\partial(T, \tau_1, \tau_2, \cdots, \tau_6)} \quad (7)$$

$$\frac{\partial(T, V_0\epsilon_1, V_0\epsilon_2, \cdots, V_0\epsilon_6)}{\partial(S, \tau_1, \tau_2, \cdots \tau_6)} \quad (8)$$

TABLE I. Table of positive quantities. All the summations and products are from 1 to 6.

a_{ii}	$a_{ii}-c_{ii}$	$\alpha_i\alpha_j(k_{ij}-q_{ij})$	$\Sigma_i\Sigma_j a_{ij}\alpha_i\alpha_j$
c_{ii}	$k_{ii}-q_{ii}$	$\beta_i\beta_j(a_{ij}-c_{ij})$	$\Sigma_i\Sigma_j a_{ij}\beta_i\beta_j$
k_{ii}	$\lvert(a_{ij})\rvert-\lvert(c_{ij})\rvert$	$\Pi_i a_{ii}-\lvert(a_{ij})\rvert$	$\Sigma_i\Sigma_j a_{ij}\epsilon_i\epsilon_j$
q_{ii}	$\lvert(k_{ij})\rvert-\lvert(q_{ij})\rvert$	$\Pi_i c_{ii}-\lvert(c_{ij})\rvert$	$\Sigma_i\Sigma_j a_{ij}\mu_i\mu_j$
$\lvert(a_{ij})\rvert$	$-\Sigma_{ijk}\alpha_i\beta_i$	$\Pi_i k_{ii}-\lvert(k_{ij})\rvert$	$\Sigma_i\Sigma_j a_{ij}\xi_i\xi_j$
$\lvert(c_{ij})\rvert$	$\Sigma_{ijk}\epsilon_i\mu_i$	$\Pi_i q_{ii}-\lvert(q_{ij})\rvert$	$\Sigma_i\Sigma_j a_{ij}\sigma_i\sigma_j$
$\lvert(k_{ij})\rvert$	$\Sigma_{ijk}\epsilon_i\tau_i$	$a_{ii}a_{jj}-a_{ij}^2$	$\Sigma_i\Sigma_j a_{ij}\tau_i\tau_j$
$\lvert(q_{ij})\rvert$	$\Sigma_{ijk}\tau_i\xi_i$	$c_{ii}c_{jj}-c_{ij}^2$	$\Sigma_i\Sigma_j a_{ij}\epsilon_i\epsilon_j$
C_τ	$\Sigma_{ijk}\tau_i\epsilon_i$	$k_{ii}k_{jj}-k_{ij}^2$	The above expressions by replacing a_{ij} with c_{ij}, k_{ij}, or q_{ij}.
C_ϵ	$C_\tau-C_\epsilon$	$q_{ii}q_{jj}-q_{ij}^2$	
		$a_{ii}C_\epsilon-TV_0\beta_i^2$	
		$k_{ii}C_\tau-TV_0\alpha_i^2$	

to be all positive definite. These Jacobian matrices can be readily obtained from the previous tables. For example the Jacobian (7) is

$$\begin{vmatrix} C_\tau/T & V_0\alpha_1 & V_0\alpha_2 & \cdots & V_0\alpha_6 \\ V_0\alpha_1 & V_0k_{11} & V_0k_{12} & \cdots & V_0k_{16} \\ V_0\alpha_2 & V_0k_{21} & V_0k_{22} & \cdots & V_0k_{26} \\ \vdots & \vdots & \vdots & \vdots & \vdots \\ V_0\alpha_6 & V_0k_{61} & V_0k_{62} & \cdots & V_0k_{66} \end{vmatrix} \quad (9)$$

where $k_{ij}(i, j=1, 2, \cdots, 6)$ are the isothermal compliance defined[1] by $k_{ij}=(\partial\epsilon_i/\partial\tau_j)_{T,\tau'}$. Since it is positive definite, we have

$$C_\tau/T>0 \quad (10)$$

$$k_{ii}>0 \quad (11)$$

$$k_{ii}k_{jj}>k_{ij}^2 \quad (12)$$

$$C_\tau k_{ii}>TV_0\alpha_i^2 \quad (13)$$

and that all higher-order diagonal minor determinants be positive. Together with the equalities mentioned previously,[1] it is thus possible to prepare the table of positive quantities among coefficients.

EXAMPLES OF APPLICATION

To illustrate the use of the table of positive quantities, let us try to compare the work required to increase a definite amount of a component of stress at constant other components of strain under (1) isothermal conditions and (2) adiabatic conditions. The first case is equivalent to calculating $(\partial A/\partial\tau_i)_{\epsilon',T}$ and the second case, $(\partial U/\partial\tau_i)_{\epsilon',S}$. These two partial deriva-

tives can be evaluated readily using the Jacobians described previously[1] with the result:

$$(\partial A/\partial\tau_i)_{\epsilon',T}=V_0\tau_i/c_{ii} \quad (14)$$

$$(\partial U/\partial\tau_i)_{\epsilon',S}=V_0\tau_i/a_{ii}. \quad (15)$$

From the table of positive quantities, it is seen that $a_{ii}>c_{ii}$. Therefore, the work required in the first case is larger if τ_i is positive and smaller if τ_i is negative. But when τ_i is negative the work required is also negative, and hence the absolute magnitude of the work is always larger in the first case. It is noticed here that this condition is required by the second law of thermodynamics, will not depend at all on the sign of the coefficients of thermal expansion, thermal stress, etc., and can be altered only by introducing other external variables than the stress and temperature, which may not be kept constant in the two cases.

For the sake of demonstration let us compare the heat required to produce a definite increment of temperature under the condition (1) that all components of strain are kept constant, (2) first component of stress and other components of strain are kept constant, (3) first and second components of stress and other components of strain are kept constant, etc., and (7) all components of stress are kept constant. Let us designate these heats by Q_0, Q_1, Q_2, $\cdots$, Q_6. They are equivalent to $T(\partial S/\partial T)_{\epsilon}$, $T(\partial S/\partial T)_{\tau_1,\epsilon_2,\epsilon_3,\cdots,\epsilon_6}$, etc. From the previous tables,[1] it is readily found that

$$Q_1-Q_0=TV_0\beta_1^2/c_{11}. \quad (16)$$

Since, from the table of positive quantities, $c_{11}>0$, it is seen $Q_1>Q_0$. It can easily be shown that

$$Q_6>Q_5>Q_4>Q_3>Q_2>Q_1>Q_0. \quad (17)$$

Again this is a requirement of the second law of thermodynamics and cannot be violated if the external variables contain only temperature and stress.

The following statements are always true from the table of positive quantities and are believed to be useful in examining elastic data:

If α_i has the same sign as α_j, then $k_{ij}>q_{ij}$.

If α_i has a different sign from α_j, then $q_{ij}>k_{ij}$.

If β_i has the same sign as β_j, then $a_{ij}>c_{ij}$.

If β_i has a different sign from β_j, then $c_{ij}>a_{ij}$.

The determinant of any kind of elastic coefficients is less than the product of all the conjugate principal minor determinants.

If the six coefficients of thermal expansion are all positive (negative), then the six coefficients of thermal stress cannot be all positive (negative).

If the six components of stress are all positive (negative), then the six components of Hooke's law strain (abiabatic or isothermal) cannot all be negative (positive).

If the six components of strain are all positive (negative), then the six components of Hooke's law stress (adiabatic or isothermal) cannot be all negative (positive).

To illustrate the variety of possible applications, we shall derive some inequalities in which the concept of Grüneisen's parameter[5] is utilized. One of the thermodynamic definitions of the Grüneisen's parameter is[6] as follows:

$$\gamma=(V/C_V)(\partial P/\partial T)_V=-(V/T)(\partial T/\partial V)_S. \quad (18)$$

From the table of positive quantities, it can easily be shown that, for elastic solids under hydrostatic pressure, there is an upper limit for adiabatic compesssibility,

$$-(1/V)(\partial V/\partial P)_S<(V/TC\gamma^2). \quad (19)$$

An upper limit for isothermal compressibility,

$$-(1/V)(\partial V/\partial P)_T<(V/TC_V\gamma^2)\cdot(C_P/C_V). \quad (20)$$

An upper limit for the coefficient of thermal expansion,

$$(\gamma/V)(\partial V/\partial T)_P<(C_P/TC_V). \quad (21)$$

and a lower limit for the adiabatic thermal pressure,

$$\gamma(\partial P/\partial T)_S>(C_V\gamma^2/V). \quad (22)$$

Equations (19) through (22) are believed to be useful for systems with very limited elastic data. For anisotropic elastic solid, if the Grüneisen's parameter can be separated into six components,

$$\gamma_i=-(V_0/C_\epsilon)\beta_i=-(1/T)(\partial T/\partial\epsilon_i)_{S,\epsilon'}, \quad (23)$$

corresponding equations similar to Eqs. (19) through (22) can be obtained for each component. Furthermore, since the sign of γ_i is just opposite of that of β_i, all the statements mentioned before in connection with the sign of β_i can be valid by replacing β_i with γ_i with the proper change of sign.

It is believed that this condensed collection of all the thermodynamic inequalities will be useful in analyzing correlating, comparing, and estimating elastic data, and in testing microscopic theories which can predict macroscopic variations.

ACKNOWLEDGMENTS

The authors wish to thank Dr. L. S. Darken and Dr. R. A. Oriani for some discussions and comments.

[5] E. Grüneisen in *Handbuch der Physik* (Springer-Verlag, Berlin, 1926), Vol. 10, p. 1; J. C. Slater, *Introduction to Chemical Physics* (McGraw-Hill Book Company, Inc., New York, 1939), p. 219; L. S. Darken and R. W. Gurry, *Physical Chemistry of Metals* (McGraw-Hill Book Company, Inc., New York, 1953), p. 158.

[6] M. H. Rice, R. G. McQueen, and J. M. Walsh, Solid State Physics 6, 42 (1958).

Perturbation Treatment of the Characteristic Vibrations of Polypeptide Chains in Various Configurations*

TATSUO MIYAZAWA†

The Children's Cancer Research Foundation and the Department of Pathology, The Children's Medical Center, Boston, Massachusetts

(Received May 14, 1959)

A perturbation treatment has been made of localized group vibrations of helical polymer chains. The amide I and II frequencies were derived in terms of adjacent group interactions as well as interchain and intrachain hydrogen bonding interactions. Frequency shifts caused by these interactions depend upon the configuration of polypeptide chains and also upon the chain packing in the crystalline region. Each characteristic vibration of the amide group gives rise to parallel and perpendicular bands. The parallel bands of the α helix of poly-γ-benzyl-L-glutamate were observed at 1650 cm^{-1} (amide I) and 1516 cm^{-1} (amide II) whereas the perpendicular bands were observed at 1652 cm^{-1} (amide I) and 1546 cm^{-1} (amide II). Both the parallel-chain and antiparallel-chain pleated sheets exhibit the perpendicular amide I band at ca 1630 cm^{-1}. A characteristic band of β configurations at ca 1690 cm^{-1} was assigned to the parallel amide I band of the antiparallel-chain pleated sheet.

IT has been well established that the *trans*-CONH group exhibits the characteristic bands at ca 1650 cm^{-1} (amide I), 1550 cm^{-1} (amide II), and 1300–1250 cm^{-1} (amide III).[1,2] The nature of these vibrations have been elucidated by a normal coordinate treatment made of the *trans* isomer of N-methylacetamide and its deuterated compound.[3] In the case of the amide I vibration ca 80% of the potential energy is associated with the CO stretching, 10% with the CN stretching, and 10% with the NH in-plane bending displacement. In the case of the amide II vibration, 40% of the potential energy is associated with the CN stretching and 60% with the NH in-plane bending displacement. The potential energy distributions calculated for these simple molecules provide useful information in treating the similar characteristic vibrations of polypeptide chains.

The amide I and II bands have been widely used for the elucidation of the configurations of polypeptide chains since Elliott and Ambrose pointed out certain frequency-configuration correlations.[4] These correlations, however, do not appear to be reliable when applied to proteins.[5] In view of these findings, it was worth while to carry out a perturbation treatment of the amide I and II vibrations of polypeptide chains in various configurations and to study the causes for the changes of those frequencies.

A normal coordinate treatment has been made before by Higgs, and some approximate relations have been derived between infrared frequencies and the number of residues per turn of helical polymers.[6] In his treatment, however, neither interchain nor intrachain hydrogen bonding interactions were taken into account. The equations thus derived may well apply to nonhydrogen-bonded helical polymers, but not to polypeptide chains. In the present treatment general equations will be derived for the amide I or II frequencies taking into account the intrachain and interchain hydrogen bonding interactions.

AMIDE I AND II VIBRATIONS OF POLYPEPTIDE CHAINS

Prior to the perturbation treatment of polypeptide chains the amide I and II vibrations will be discussed referring to the normal modes expressed in terms of Cartesian displacements. Such atomic displacements of N-methylacetamide[3]

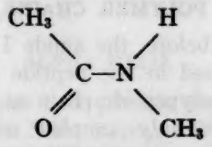

have been calculated by the method of Crawford and Fletcher.[7] It was learned from this calculation that the Cartesian displacements of the methyl groups associated with the amide I or II vibrations were negligible as compared with those of the C, O, N, and H atoms of the peptide group (see Fig. 1 of reference 3), that is, the vibrational motions are localized in the peptide CONH group. In a polypeptide chain successive peptide groups have one α carbon atom between them, —CONH—C_α—CONH—C_α—CONH—; however, since the amide I or II vibrations do not involve large displacements of those α carbon atoms the amide I (or II) vibration of a peptide group will interact only slightly with the same vibration of adjacent groups. In the present study such

* This investigation was supported in part by a grant from the National Institutes of Health.

† Present address: Institute for Protein Research, Osaka University, Osaka, Japan.

[1] G. B. B. M. Sutherland, *Advances in Protein Chemistry* (Academic Press, Inc., New York, 1952), Vol. 7; L. S. Bellamy, *The Infrared Spectra of Complex Molecules* (Methuen and Company, Ltd., London, England, 1954), Chap. 12.

[2] T. Miyazawa, T. Shimanuchi, and S. Mizushima, J. Chem. Phys. **24**, 408 (1956); T. Miyazawa, J. Chem. Soc. Japan **76**, 341, 1018 (1955); **77**, 171 (1956).

[3] T. Miyazawa, T. Shimanouchi, and S. Mizushima, J. Chem. Phys. **29**, 611 (1958).

[4] A. Elliott and E. J. Ambrose, Nature **165**, 921 (1950); A. Elliott, Proc. Roy. Soc. (London) **A221**, 104 (1953).

[5] Beer, Sutherland, Tanner, and Wood, Proc. Roy. Soc. (London) **A249**, 147 (1959).

[6] P. Higgs, Proc. Roy. Soc. (London) **A220**, 472 (1953).

[7] B. L. Crawford, Jr. and W. H. Fletcher, J. Chem. Phys. **19**, 141 (1951).

adjacent group interactions will be treated by the first order perturbation theory in order to analyze the amide I and II frequencies of polypeptide chains in various configurations. It may be mentioned that the interaction between the amide I vibration of a peptide group and the amide II (or any other localized) vibration of any other group will cause only second-order frequency shifts, whereas the interaction between the same vibrations of adjacent groups may cause first order frequency shifts.

We have just discussed the vibrational interaction between successive peptide groups in the chain. Peptide groups of a polypeptide chain, however, form either intrachain or interchain hydrogen bonds with other peptide groups, and the interactions between the amide I or II vibrations of adjacent peptide groups *across hydrogen bonds* may also cause first order frequency shifts. Such vibrational interactions naturally depend upon the relative configuration of successive peptide groups across hydrogen bonds and also upon the Cartesian displacements of the amide hydrogen atom and the carbonyl oxygen atom. The normal coordinate treatment of N-methylacetamide[5] has shown that in the case of the amide I vibration the displacement of the carbonyl oxygen atom is parallel to the CO bond while the displacement of the amide hydrogen atom is perpendicular to the NH bond. In the case of the amide II vibration the displacement of the amide hydrogen atom is perpendicular to the NH bond whereas the displacement of the oxygen atom is almost negligible. Detailed discussions of the vibrational interactions across hydrogen bonds, however, will be presented in the subsequent paper.

PERTURBATION TREATMENT OF LOCALIZED VIBRATIONS OF HELICAL POLYMER CHAINS

As mentioned before, the amide I or II vibrations are highly localized in the peptide group and these vibrations of a polypeptide chain as a whole may be treated using "weakly coupled oscillator model." The perturbation treatment will be made of this model using the amide I (or II) normal coordinates of the peptide groups incorporated in the polypeptide chain. The normal coordinate of the kth group (q_k) is the coordinate such that the kinetic energy (T_k) and the potential energy (V_k) of this group are expressed as $T_k=\frac{1}{2}\dot{q}_k^2$ and $V_k=\frac{1}{2}\lambda_0 q_k^2$, respectively, where λ_0 is equal to $4\pi^2\nu_0^2$ and ν_0 is the vibrational frequency. In terms of such normal coordinates of the peptide group the vibrational kinetic energy (T) and the potential energy (V) of the whole polypeptide chain may be expressed as shown below:

$$T=\tfrac{1}{2}\sum_k \dot{q}_k^2+\sum_{k<l} A_{kl}\dot{q}_k\dot{q}_l \qquad (1a)$$

and

$$V=\tfrac{1}{2}\lambda_0\sum_k q_k^2+\lambda_0\sum_{k<l} B_{kl}q_k q_l. \qquad (1b)$$

In each of these equations the first term is the sum of the energy of the unperturbed vibrations[8] and the second term arises from vibrational interactions among various peptide groups in the chain, where $A_{kl}\dot{q}_k\dot{q}_l$ and $B_{kl}q_k q_l$ are the kinetic energy interaction term and the potential energy interaction term, respectively, between the kth and lth groups.

With a finite helical polypeptide chain peptide groups are not quite equivalent; especially the peptide groups in terminal helical turns are in quite different environment from those lying in the middle part of the helical chain. However, if the helical polypeptide chain is sufficiently long such a chain may be approximated with an infinite helical chain having equivalent peptide groups at least in treating the localized vibrations such as the amide I or II vibrations. Then the interaction coefficients A_{kl} and B_{kl} of Eqs. (1a) and (1b) will depend only upon the separation $s(\equiv l-k)$ of the two groups l and k. Accordingly A_{kl} and B_{kl} will be replaced with A_s and B_s in the following discussions.

Wilson's GF matrix method may be used for the frequency calculation.[9] The elements of the kinetic energy matrix G^{-1} derived from Eq. (1a) are

$$G^{-1}_{k,k}=1 \quad \text{and} \quad G^{-1}_{k,k\pm s}=A_s, \qquad (2a)$$

and the elements of the potential energy matrix F derived from Eq. (1b) are

$$F_{k,k}/\lambda_0=1 \quad \text{and} \quad F_{k,k\pm s}/\lambda_0=B_s. \qquad (2b)$$

Before treating the problem of an infinite polymer chain it may be appropriate to discuss a system consisting of N equivalent oscillators. For this system both the G^{-1} and F/λ_0 matrices are of the following form:

$$X\equiv\begin{vmatrix} 1 & X_1 & X_2 & \cdot & \cdot & \cdot & X_2 & X_1 \\ & 1 & X_1 & X_2 & \cdot & \cdot & \cdot & X_2 \\ & & 1 & X_1 & X_2 & \cdot & \cdot & \cdot \\ & & & & \cdot & \cdot & \cdot & \cdot \\ & & & & 1 & X_1 & X_2 & \cdot \\ & \text{symmetric} & & & & 1 & X_1 & X_2 \\ & & & & & & 1 & X_1 \\ & & & & & & & 1 \end{vmatrix}$$

[8] Suppose only one group carries out the vibrational motion while all the others stay rigid. Then the vibrational interactions do not take place and the frequency is then equal to ν_0. Thus in the present treatment ν_0 is the frequency of the vibration unperturbed by vibrational interactions. ν_0 should not be taken as the frequency of a peptide group in the vapor phase.

[9] E. B. Wilson, Jr., J. Chem. Phys. 7, 1047 (1939); 9, 76 (1941).

and this matrix X may be diagonalized by the following transformation,

$$U^{+}XU=Y \tag{3}$$

where

$$U_{ab}=\exp[(a-1)(b-1)i\theta]/N^{\frac{1}{2}} \tag{4}$$

$$a \text{ or } b=1,2,\cdots,N$$

and

$$\theta=2\pi/N. \tag{5}$$

For even number of $N(=2n)$ the elements of the diagonal matrix Y are

$$Y_{aa}=1+\sum_{s=1}^{n-1}X_s[\exp\{s(a-1)i\theta\}+\exp\{-s(a-1)i\theta\}]+X_n\exp\{n(a-1)i\theta\}$$

$$=1+2\sum_{s=1}^{n-1}X_s\cos s\delta+(-1)^{a-1}X_n \tag{6}$$

where $\delta=(a-1)\theta$ is the phase angle between the motions of adjacent oscillators. Similarly for odd number of $N(=2n+1)$ the elements of the Y matrix are

$$Y_{aa}=1+\sum_{s=1}^{n}X_s[\exp\{s(a-1)i\theta\}+\exp\{-s(a-1)i\theta\}]$$

$$=1+2\sum_{s=1}^{n}X_s\cos s\delta. \tag{7}$$

For both cases the element of the characteristic vector associated with the kth oscillator (L_k) may be expressed in terms of the phase angle δ as shown below:

$$L_k(\delta)=\exp(ki\delta)/N^{\frac{1}{2}} \quad \text{or} \quad \exp(-ki\delta)/N^{\frac{1}{2}}. \tag{8}$$

Now for a system consisting of infinite number of equivalent oscillators the phase angle may have any value between 0 and 2π. The last term in Eq. (6) is due to the interaction between nth neighbors, that is, the interaction across one half the length of the whole system. If such long-range interactions may be neglected the matrix element depends only upon the phase angle δ as shown below:

$$Y(\delta)=1+2\sum_{s}X_s\cos s\delta. \tag{9}$$

We may now apply Eq. (9) to infinite helical polypeptide chains where end effects may be neglected and all the peptide groups are equivalent. In the present treatment only short-range interactions will be taken into account such as the adjacent group interactions in the chain or across hydrogen bonds. The elements of the G^{-1} and F matrices are

$$G^{-1}(\delta)=1+2\sum_{s}A_s\cos s\delta \tag{10}$$

and

$$F(\delta)=(1+2\sum_{s}B_s\cos s\delta)\lambda_0 \tag{11}$$

and the corresponding component of the characteristic vector $L(\delta)$ associated with the kth group is given in Eq. (8). Then the amplitude ratio of the kth and lth groups is

$$q_k:q_l=\cos k\delta:\cos l\delta$$

or

$$=\sin k\delta:\sin l\delta.$$

From Eqs. (10) and (11) the characteristic value for the phase angle δ is derived to be (if $A_s \ll 1$)

$$\lambda(\delta)=F(\delta)/G^{-1}(\delta)=1+2\sum_{s}(B_s-A_s)\cos s\delta. \tag{12}$$

The vibrational frequency ν is then found to be

$$\nu(\delta)=\lambda^{\frac{1}{2}}/2\pi=\nu_0+\sum_{s}D_s\cos s\delta \tag{13}$$

where

$$D_s=(B_s-A_s)\nu_0. \tag{14}$$

Thus the frequency shift due to intergroup vibrational interactions is proportional to $\cos s\delta$ and to the difference between the potential energy (B_s) and the kinetic energy (A_s) interaction coefficients. As long as the vibrational motions are localized in repeating groups Eqs. (13) and (14) apply to any helical polymer, hydrogen-bonded or not.

A group theoretical treatment on the infrared selection rule was made by Higgs.[6] For an infinite helical chain the phase angle δ may have any value; however, only two values of δ give rise to infrared active vibrations. For one of them the angle is equal to zero and the transition moment is parallel to the helix axis (parallel band). For the other degenerate pair of vibrations the phase angle is equal to χ(the angle relative to the helix axis which separates successive groups of the helix) and the transition moment is perpendicular to the axis (perpendicular band).

ALPHA HELIX

Eq. (13) may now be applied to the α helix of polypeptides.[10] In the α helix there are 3.6 peptide groups per turn and intrachain hydrogen bonds are formed between each pair of every third neighbors, and the interaction term D_3 will be as important as the interaction term D_1 (for adjacent groups in the chain). Then the frequency of the parallel band is found to be

$$\nu(0)=\nu_0+D_1+D_3 \tag{15a}$$

and the frequency of the perpendicular band is

$$\nu(\chi)=\nu_0+D_1\cos\chi+D_3\cos 3\chi \tag{15b}$$

where χ is equal to $2\pi/3.6$. The frequency difference of these bands depends on the values of D_1 and D_3.

The polarized infrared spectra of an oriented film of high molecular weight poly-γ-benzyl-L-glutamate were

[10] L. Pauling, R. B. Corey, and H. R. Branson, Proc. Natl. Acad. Sci. U. S. 37, 205 (1951).

measured in the region 1800–1500 cm^{-1} by the use of Perkin-Elmer Model 21 spectrometer and a silver chloride polarizer. The parallel amide I band (strong) and the perpendicular amide I band (medium) were observed at 1650 and 1652 cm^{-1}, respectively. On the other hand, the parallel amide II band (weak) and the perpendicular amide II band (strong) were observed at 1516 and 1546 cm^{-1}, respectively. When the sample is almost completely deuterated a CONH group is surrounded by COND groups and interactions among CONH groups do not take place. Then its amide II frequency, being equal to ν_0 in Eq. (13), will be different from those of the normal species. In fact, the two bands, 1546 and 1516 cm^{-1}, disappear on deuteration[11] and a band appears at 1535 cm^{-1} as expected theoretically. Numerical calculations of the interaction terms from these observed frequencies will be presented elsewhere.[12]

Assuming the additivity of the transition moments of repeating groups, the intensity ratio of the perpendicular band and the parallel band has been shown[6] to be $\frac{1}{2}\tan^2\theta$ where θ is the angle between the helix axis and the transition moment of each group. The intensity comparison of the amide II bands at 1546 and 1516 cm^{-1} allows the estimation of the angle θ even when the orientation is not high. The apparent dichroic ratio of the 1546 cm^{-1} band serves as a useful measure of the orientation of the sample, since this band is due to the transition moment exactly parallel to the helix axis. Referring to this apparent dichroic ratio, the angle θ for the amide I vibration may be determined even though the observed band is a composite of the parallel band and the perpendicular band. These applications will be published in the following paper.[12]

EXTENDED CONFIGURATIONS

In the fully extended configurations of polypeptides[13] the backbone chain and all the peptide groups are coplanar. On the other hand in the pleated sheet[14] the plane of each peptide groups makes an angle (ϕ) with the fiber axis. The fully extended configuration may be regarded to be a special case of the pleated sheet for which the angle ϕ is equal to zero.

The pleated sheet configuration has a twofold screw axis and each repeating unit contains two peptide groups. There are two infrared active vibrations; in one of them adjacent peptide groups move in phase ($\delta=0$), giving rise to a parallel band whereas in the other vibration adjacent groups move out-of-phase ($\delta=\pi$), giving rise to a perpendicular band. In the pleated sheet peptide groups do not form intrachain hydrogen bonds, and among various intrachain interactions only those between adjacent groups will be appreciable. As seen from Eq. (13) such intrachain interactions will shift the parallel band ($\delta=0$) by $+D_1$ and the perpendicular band ($\delta=\pi$) by $-D_1$. On the other hand, the interchain hydrogen bonds are formed between peptide groups in the parallel-chain pleated sheet or in the antiparallel-chain pleated sheet equally well,[14] and these hydrogen bonds may shift the amide I and II bands appreciably. The calculation of such frequency shifts proceeds just as in the case of intrachain vibrational interactions. Only the interactions between adjacent groups across hydrogen bonds may be taken into account and the frequency shift is found to be

$$\Delta\nu(\delta') = D_1' \cos\delta' \tag{16}$$

where δ' is the phase angle between adjacent group motions across interchain hydrogen bonds and the coefficient D_1' corresponds to D_1 in Eq. (13).

The direction of the transition moment of each peptide group in the pleated sheet may be specified now. Suppose the line joining the successive α carbon atoms of a chain is parallel to the z axis, the intersection of two adjacent peptide planes is parallel to the y axis, and x axis is perpendicular to both the z and y axes (Fig. 1). If the transition moment of the in-plane vibration in question is inclined from the y axis by an angle ψ, then, the x, y, and z components are proportional to $\sin\psi\sin\phi$, $\cos\psi$, and $\sin\psi\cos\phi$, respectively.

Infrared absorption bands of the crystalline region arise from in-phase motions of corresponding groups in various unit cells. With the parallel-chain pleated sheet, a unit cell contains two adjacent groups from one chain; therefore, adjacent chains move in phase in infrared active vibrations. In Fig. 1 are shown schematic drawings of these vibrations. It will be seen that adjacent groups across interchain hydrogen bonds move in phase ($\delta'=0$). Taking into account the intrachain interactions as well as the interchain interactions, the frequency of the parallel band is found to be

$$\nu(0, 0) = \nu_0 + D_1 + D_1' \tag{17a}$$

and the frequency of the perpendicular band is

$$\nu(\pi, 0) = \nu_0 - D_1 + D_1', \tag{17b}$$

where the first number in the parentheses is the phase angle δ and the second one is the phase angle δ'. The transition moment of the $\nu(0, 0)$ vibration is parallel to the fiber axis (z axis) and is proportional to $\sin\psi\cos\phi$, whereas the transition moment of the $\nu(\pi, 0)$ vibration is perpendicular to the fiber axis and its x and y components are proportional to $\sin\psi\sin\phi$ and $\cos\psi$, respectively.

With the antiparallel-chain pleated sheet, a unit cell contains four peptide groups; two groups from one chain and the other two from an adjacent chain. In this case adjacent chains may move in phase or out of

[11] Deuteration studies were made by Mr. Kenneth Norland of our laboratory.
[12] T. Miyazawa and E. R. Blout (to be published).
[13] W. T. Astbury and F. O. Bell, Nature **147**, 696 (1941).
[14] L. Pauling and R. B. Corey, Proc. Natl. Acad. Sci. U. S. **37**, 729 (1951).

phase and both the parallel band ($\delta=0$) and the perpendicular band ($\delta=\pi$) are split into two components. Schematic drawings of these vibrations are shown in Fig. 2. The phase angles δ and δ' as well as the direction of the over-all transition moments will be easily seen in this figure. The $\nu(0,0)$ vibration is infrared inactive since the transition moments of adjacent chains cancel each other. By using Eqs. (13) and (16) the frequencies of the three other vibrations are derived to be

$$\nu(0,\pi)=\nu_0+D_1-D_1' \tag{18a}$$

$$\nu(\pi,0)=\nu_0-D_1+D_1' \tag{18b}$$

and

$$\nu(\pi,\pi)=\nu_0-D_1-D_1'. \tag{18c}$$

The transition moments (and directions) of these three vibrations are proportional to $\sin\psi\cos\phi$ (along the z axis), $\cos\psi$ (along the y axis), and $\sin\psi\sin\phi$ (along the x axis), respectively. The applications of these equations to polypeptides and proteins will be presented in a subsequent paper.[12]

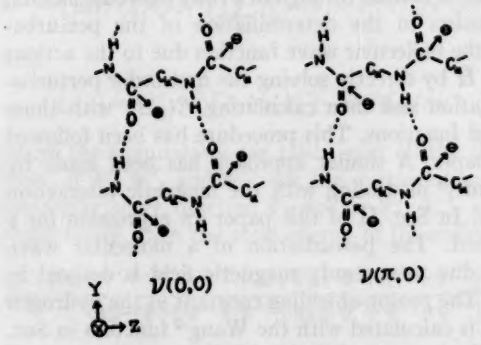

FIG. 1. A schematic representation of the vibrational modes of the parallel-chain pleated sheet; the arrows represent the components of the transition moments of peptide groups in the plane of the paper. The plus or minus signs represent the x components of the transition moments; the former those pointing upward, and the latter those pointing downward.

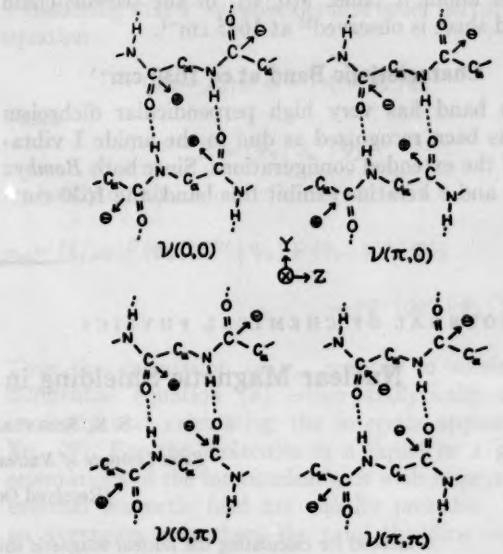

FIG. 2. A schematic representation of the vibrational modes of the antiparallel-chain pleated sheet.

Characteristic Band at ca 1690 cm^{-1}

It has been recognized that some polypeptides and proteins in extended configurations exhibit a weak band at ca 1690 cm^{-1} together with the well-defined strong band at ca 1630 cm^{-1}. This weak band was once considered to be due to some impurity (i.e., short chain peptides or some folded form), however, studies on the reversible configurational changes of polyglycine,[15] poly-L-lysine hydrochloride,[16] and sodium poly-α, L-glutamate[17] have confirmed that this band is a characteristic band of the extended configuration. These studies strongly indicate that this band is due to peptide groups and also that its origin is somehow related to the chain configuration.

Elliott and Malcolm have suggested that the 1690-cm^{-1} band is a combination band.[15] If this is the case, the band in question should be explained as some combination of the characteristic amide frequencies. The characteristic amide bands of polyglycine I have been observed at 1632 cm^{-1} (amide I), 1521 cm^{-1} (amide II), 1236 cm^{-1} (amide III), and 720 cm^{-1} (amide V) in the rocksalt region[2,15,18] at 628 cm^{-1} (amide IV) and 607 cm^{-1} (amide VI) in the potassium bromide region,[2] and at 217 cm^{-1} (amide VII[19]) in the cesium iodide region.[20] It will be seen that any binary combination of the amide I–VII bands does not account for the presence of the band of polyglycine I at ca 1690 cm^{-1}.

The 1690 cm^{-1} band is observed for *Bombyx* fibroin[21] which has been established to be in the antiparallel-chain pleated sheet,[22] but is not observed for β keratine[23] which has been suggested to be in the parallel-chain pleated sheet.[14] This band has very high parallel dichroism, and its frequency change[17] on deuteration is nearly the same as that of the amide I band at 1630 cm^{-1}. Accordingly, the 1690 cm^{-1} band is most reasonably assigned to the amide I vibration, $\nu(0,\pi)$, of the antiparallel-chain pleated sheet in which adjacent groups in the chain move in phase. The corresponding

[15] A. Elliott and B. R. Malcolm, Trans. Faraday Soc. **52**, 528 (1956).
[16] E. R. Blout and H. Lenormant, Nature **179**, 960 (1957).
[17] H. Lenormant, A. Baudras, and E. R. Blout, J. Am. Chem. Soc. **80**, 6191 (1958).
[18] E. R. Blout and S. G. Linsley, J. Am. Chem. Soc. **74**, 1946 (1952).
[19] The amide VII band is due to the torsional vibration about the CO—NH bond.
[20] T. Miyazawa (to be published).
[21] E. J. Ambrose and A. Elliott, Proc. Roy. Soc. (London) **A206**, 206 (1951).
[22] R. E. Marsh, R. B. Corey, and L. Pauling, Biochim. Biophys. Acta **16**, 1 (1955).
[23] K. D. Parker, quoted by Bamford *et al* in *Synthetic Polypeptides* (Academic Press, Inc., New York, 1956), p. 405.

parallel amide I band, $\nu(0, 0)$, of the parallel-chain pleated sheet is observed[23] at 1645 cm^{-1}.

Characteristic Band at ca 1630 cm^{-1}

This band has very high perpendicular dichroism and has been recognized as due to the amide I vibration of the extended configurations. Since both *Bombyx* fibroin and β keratine exhibit this band, the 1630 cm^{-1} band is assigned to the amide I vibration, $\nu(\pi, 0)$, of the antiparallel-chain and parallel-chain pleated sheets in which adjacent groups in the chain move out of phase.

ACKNOWLEDGMENT

The author wishes to express his sincere thanks to Dr. Elkan R. Blout for helpful discussions.

THE JOURNAL OF CHEMICAL PHYSICS VOLUME 32, NUMBER 6 JUNE, 1960

Nuclear Magnetic Shielding in Molecules: Hydrogen Molecule

S. K. SINHA* AND A. MUKHERJI

Saha Institute of Nuclear Physics, Calcutta, India

(Received October 2, 1959)

A method for calculating the nuclear magnetic shielding in molecules has been developed using valence-bond or LCAO type molecular orbitals. The perturbation of the molecular wave function due to a steady magnetic field is derived by solving the first-order perturbation equation. The method has been applied to the calculation of proton shielding in hydrogen molecule with the Wang function. The value of $\sigma^p = -0.55 \times 10^{-5}$ is in good agreement with the value of -0.56×10^{-5} derived by Ramsey from the experimental value of the spin-rotational coupling constant in hydrogen molecule.

I. INTRODUCTION

THEORETICAL estimation of the shift observed in the nuclear magnetic resonance line of a particular nucleus under different chemical environments has been of interest for some time. Quite a number of papers[1–5] have been published on this subject during the last few years.

The principle underlying all these calculations has been to evaluate the electronic energy of a molecule in the presence of an external magnetic field $\mathbf{H}$ and the magnetic moment $\boldsymbol{\mu}$ of the nucleus concerned. If $E(\mu H)$ is the part of the energy expression proportional to the product μH, then the shielding constant σ is given by

$$\sigma = E(\mu H)/\mu H. \tag{1}$$

For this purpose both the perturbation method and the variation method have been used.

The calculation by the perturbation method[1,6] requires a knowledge of the excited molecular wave functions and also the energies of the corresponding states. Since these wave functions and the energies consistent with them are not well known for many molecules, such a procedure is highly limited in its field of application. For tackling such problems the variational method of approach has proved on many occasions to be quite successful.[2,3,7,8] But in order to carry out this procedure efficiently one has to make a guess of the variation function.

There is another approach which yields results to the same order of accuracy as either of the foregoing two procedures if carried through in a fully rigorous manner. This consists in the determination of the perturbations of the molecular wave function due to the actions of $\boldsymbol{\mu}$ and $\boldsymbol{H}$ by directly solving the first-order perturbation equation and then calculating $E(\mu H)$ with those perturbed functions. This procedure has been followed in this paper. A similar approach has been made by Sternheimer[9] in dealing with the magnetic interaction in atoms. In Sec. II of this paper an expression for σ is obtained. The perturbation of a molecular wave function due to a steady magnetic field is derived in Sec. III. The proton-shielding constant in the hydrogen molecule is calculated with the Wang[10] function in Sec. IV. Earlier investigations in this line are discussed in the light of the present work in Sec. V.

II. EVALUATION OF σ

Let us consider a diamagnetic molecule where the nucleus under consideration has a magnetic moment $\boldsymbol{\mu}$

* Holder of a Department of Atomic Energy Fellowship, Government of India.

[1] N. F. Ramsey, Phys. Rev. **78**, 699 (1950).
[2] J. F. Hornig and J. O. Hirschfelder, J. Chem. Phys. **23**, 474 (1955).
[3] T. P. Das and R. Bersohn, Phys. Rev. **104**, 849 (1956).
[4] H. F. Hameka, Mol. Phys. **1**, 203 (1958).
[5] J. A. Pople, Proc. Roy. Soc. (London) **A239**, 541 (1957).
[6] A. Saika and C. P. Slichter, J. Chem. Phys. **22**, 26 (1954).
[7] B. R. McGarvey, J. Chem. Phys. **27**, 68 (1957).
[8] M. J. Stephen, Proc. Roy. Soc. (London) **A243**, 264 (1958).
[9] R. Sternheimer, Phys. Rev. **86**, 316 (1952).
[10] S. C. Wang, Phys. Rev. **31**, 579 (1928).

and all other nuclei have zero moments. We consider the case where the externally applied magnetic field **H** and the magnetic moment $\boldsymbol{\mu}$ are both oriented in the Y direction of a cartesian system of coordinates with the origin at the nucleus whose magnetic shielding we are interested in. The total Hamiltonian of the electronic system of the molecule in Hartree atomic units[11] is

$$\mathcal{H}=\tfrac{1}{2}\sum_k[i^{-1}\nabla(k)+\tfrac{1}{137}\{\mathbf{A}_H(k)+\mathbf{A}_\mu(k)\}]^2+V, \quad (2)$$

where $\mathbf{A}_H(k)$ and $\mathbf{A}_\mu(k)$ are the vector potentials describing, respectively, the uniform magnetic field **H** and the field produced by the nuclear magnetic moment $\boldsymbol{\mu}$ at the position of the kth electron. These are given by

$$\mathbf{A}_H(k)=\tfrac{1}{2}[\mathbf{H}\times\mathbf{r}(k)]$$

and

$$\mathbf{A}_\mu(k)=[1/r^3(k)][\boldsymbol{\mu}\times\mathbf{r}(k)]. \quad (3)$$

The potential V is defined by the equation

$$[-\tfrac{1}{2}\sum_k\nabla^2(k)+V]\Psi_0=E_0\Psi_0, \quad (4)$$

where Ψ_0 is the normalized unperturbed molecular wave function. Thus

$$\mathcal{H}=\mathcal{H}_0+\mathcal{H}'+\mathcal{H}''+\mathcal{H}''', \quad (5)$$

where

$$\left.\begin{aligned}
\mathcal{H}_0&=-\tfrac{1}{2}\sum_k\nabla^2(k)+V\\
\mathcal{H}'&=[H/(2\times137)]\sum_k l_y(k)\\
\mathcal{H}''&=(\mu/137)\sum_k[l_y(k)/r^3(k)]\\
\mathcal{H}'''&=[\mu H/(2\times137^2)]\sum_k\{[x^2(k)+z^2(k)]/r^3(k)\}
\end{aligned}\right\} \quad (6)$$

with

$$l_y(k)=i^{-1}\{z(k)[\partial/\partial x(k)]-x(k)[\partial/\partial z(k)]\},$$

where the summations are taken over all the electrons. Now, if Ψ', Ψ'', and Ψ''' are the perturbations of the molecular wave function Ψ_0 due to $\mathcal{H}'$, $\mathcal{H}''$, and $\mathcal{H}'''$, respectively, then the total energy of the molecule is

$$E=\frac{\langle\Psi_0+\Psi'+\Psi''+\Psi'''\,|\,\mathcal{H}\,|\,\Psi_0+\Psi'+\Psi''+\Psi'''\rangle}{\langle\Psi_0+\Psi'+\Psi''+\Psi'''\,|\,\Psi_0+\Psi'+\Psi''+\Psi'''\rangle}. \quad (7)$$

From the natures of $\mathcal{H}'$ and $\mathcal{H}''$, it can be easily shown that Ψ' and Ψ'' would involve the factors i in their radial parts. Hence one obtains

$$\begin{aligned}
E(\mu H)=\langle\Psi_0\,|\,\mathcal{H}'''\,|\,\Psi_0\rangle&+\langle\Psi_0\,|\,\mathcal{H}''\,|\,\Psi'\rangle+\langle\Psi'\,|\,\mathcal{H}''\,|\,\Psi_0\rangle\\
&+\langle\Psi_0\,|\,\mathcal{H}'\,|\,\Psi''\rangle+\langle\Psi''\,|\,\mathcal{H}'\,|\,\Psi_0\rangle\\
&+\langle\Psi'\,|\,\mathcal{H}_0-E_0\,|\,\Psi''\rangle+\langle\Psi''\,|\,\mathcal{H}_0-E_0\,|\,\Psi'\rangle.
\end{aligned}$$

[11] D. R. Hartree, *The Calculation of Atomic Structures* (John Wiley & Sons, Inc., New York, 1957), p. 5.

Assuming that Ψ' satisfies the first order perturbation equation

$$(\mathcal{H}_0-E_0)\Psi'=-(\mathcal{H}'-E')\Psi_0 \quad (8)$$

where

$$E'=\langle\Psi_0\,|\,\mathcal{H}'\,|\,\Psi_0\rangle$$

we finally obtain

$$\begin{aligned}
\sigma_{yy}=(1/\mu_H)[&\langle\Psi_0\,|\,\mathcal{H}'''\,|\,\Psi_0\rangle+\langle\Psi_0\,|\,\mathcal{H}''\,|\,\Psi'\rangle\\
&+\langle\Psi'\,|\,\mathcal{H}''\,|\,\Psi_0\rangle]. \quad (9)
\end{aligned}$$

Thus the calculation of σ_{yy} reduces to solving the differential equation (8) either analytically or numerically and calculating the integrals appearing in Eq. (9). For the molecules in a liquid or a gas, all orientations of the internuclear axis with respect to the external magnetic field are equally probable. Hence, on averaging over them the total shielding constant becomes

$$\sigma=\tfrac{1}{3}(\sigma_{xx}+\sigma_{yy}+\sigma_{zz}). \quad (10)$$

For a molecular system having more than two electrons, the solution of Eq. (8) becomes extremely difficult to tackle if Ψ_0 is taken to be the proper antisymmetrized combination of all the electronic orbitals. For a two-electron system, Ψ_0 is simply the bond wave function, which can be well approximated by a MO or a valence-bond type function and the solution can be easily obtained. In order to deal with a system having more electrons each bond has to be considered separately and the contributions of the electrons which do not take part in bond formation have also to be taken into account. With these approximations the magnetic shielding calculation in any molecule becomes quite simple.

III. PERTURBATION OF BOND WAVE FUNCTION DUE TO $\mathcal{H}'$

A. Valence Bond Function

Let the bond wave function be

$$\Psi_0(1,2)=c[\psi_a(1)\psi_b(2)+\psi_a(2)\psi_b(1)] \quad (11)$$

where ψ_a and ψ_b are two atomic orbitals forming the bond and centered around the nuclei A and B, respectively, and c is the normalization constant. In order to calculate the magnetic shielding of the nucleus A the origin of the vector potential $\mathbf{A}_H(k)$ as also the origin of the coordinate system is taken at A. The internuclear axis **AB** is chosen as the Z axis.

The following notation convention is adopted here: All variables and functions expressed with respect to the coordinate system with origin at A are designated by the symbol a, and those expressed with respect to a parallel coordinate system with origin at B are desig-

nated by the symbol b. Hartree atomic units[11] are used throughout. We can write

$$\psi_a(k)=\phi_a(k)Y_{l_1}^{m_1}(ak)$$
$$\psi_b(k)=\phi_b(k)Y_{l_2}^{m_2}(bk) \quad (12)$$

where ϕ_a and ϕ_b are functions of r_a and r_b, only, and $Y(a)$ and $Y(b)$ are spherical harmonics centered around the origins A and B, respectively.

The perturbing Hamiltonian in this case becomes

$$\mathcal{H}'_{a(1,2)}=[H/(2\times137)][l_{ya(1)}+l_{ya(2)}]. \quad (13)$$

If the internuclear distance AB be denoted by R then

$$l_{ya}=l_{yb}+(R/i)(\partial/\partial x_b). \quad (14)$$

Hence

$$\mathcal{H}'_{a(1,2)}\psi_{a(1)}\psi_{b(2)}$$
$$=[H/(12\times137)][\phi_{a(1)}\phi_{b(2)}\{Y_{l_2}^{m_2}(b2)l_{ya(1)}Y_{l_1}^{m_1}(a1)$$
$$+Y_{l_1}^{m_1}(a1)l_{yb(2)}Y_{l_2}^{m_2}(b2)\}$$
$$+(R/i)\phi_{a(1)}Y_{l_1}^{m_1}(a1)(\partial/\partial x_{b(2)})\phi_{b(2)}Y_{l_2}^{m_2}(b2)]. \quad (15)$$

Similar expressions would be obtained for the other term in $\Psi_0(1,2)$. The right side of Eq. (15) shows that the effect of the magnetic field can be classified under the following groups:

(i) The perturbation caused to the orbital centered around the nucleus whose magnetic shielding is being calculated, consists of the excitation to different m states only without any change in l value.

(ii) Perturbation similar to (*i*) takes place also to the orbital centered around the other nucleus.

(iii) The latter orbital is also excited to l states differing from it by $\Delta l=\pm1$.

It is evident that the effects (*i*) and (*ii*) are zero when the orbital under consideration is an s orbit.

Following Eq. (15) we can write

$$\mathcal{H}'_{a(1,2)}\Psi_{0(1,2)}=[H/(2\times137)]\{\psi_{a(1)}\eta_{b(2)}+\xi_{a(1)}\psi_{b(2)}$$
$$+\psi_{a(2)}\eta_{b(1)}+\xi_{a(2)}\psi_{b(1)}\} \quad (16)$$

Since the molecule is diamagnetic, E' in Eq. (10) should be taken to be zero.

Equation (15) also suggests that the perturbations to the two terms in expression (11) can, to a good approximation, be determined separately. The perturbation to the first term in expression (11) is chosen in the form

$$c[\psi_{a(1)}\psi'_{b(2)}+\psi'_{a(1)}\psi_{b(2)}] \quad (17)$$

and the first-order perturbation equation to determine ψ'_a and ψ'_b becomes

$$\{\mathcal{H}_{0a}(1,2)-\epsilon_0\}\{\psi_{a(1)}\psi'_{b(2)}+\psi'_{a(1)}\psi_{b(2)}\}$$
$$=-\mathcal{H}'_{a(1,2)}\psi_{a(1)}\psi_{b(2)} \quad (18)$$

where $\mathcal{H}_{0a(1,2)}$ satisfies the equation

$$\{\mathcal{H}_{0a}(1,2)-\epsilon_0\}\psi_{a(1)}\psi_{b(2)}=0. \quad (19)$$

We can replace $V_{a(1,2)}-\epsilon_0$ by

$$V_{a(1,2)}-\epsilon_0=\tfrac{1}{2}\frac{\{\nabla_{a(1)}^2+\nabla_{a(2)}^2\}\psi_{a(1)}\psi_{b(2)}}{\psi_{a(1)}\psi_{b(2)}}. \quad (20)$$

If we equate terms in Eq. (18) having different angular dependences around the two centers, it can be separated into single particle equations, which can be solved analytically or by the numerical integration method to obtain the perturbation functions $\psi'_{a(1)}$ and $\psi'_{b(2)}$. Similar expressions would be arrived at for the perturbation to the second term in expression (11).

B. Molecular Orbital Function

Let the wave function be

$$\Psi_{0(1,2)}=c\{\psi_{a(1)}+\beta\psi_{b(1)}\}\{\psi_{a(2)}+\beta\psi_{b(2)}\}. \quad (21)$$

Then

$$\mathcal{H}'_{a(1,2)}\{\psi_{a(1)}+\beta\psi_{b(1)}\}$$
$$=[H/(2\times137)]\{\phi_{a(1)}l_{ya(1)}Y_{l_1}^{m_1}(a1)$$
$$+\beta\phi_{b(1)}l_{yb(1)}Y_{l_2}^{m_2}(b1)$$
$$+\beta(R/i)[\partial/\partial x_{b(1)}]\phi_{b(1)}Y_{l_2}^{m_2}(b1)\}. \quad (22)$$

This expression shows, in addition to the considerations (*i*), (*ii*), and (*iii*) in subsection A, that for a σ orbital, the only angular excitation produced to the function centered around the nucleus B is from $l\rightarrow l+1$, while for a non-σ orbital this excitation consists of both $l\rightarrow l+1$ and $l\rightarrow l-1$. Thus

$$\mathcal{H}'_{a(1,2)}\Psi_{0(1,2)}$$
$$=[Hc/(2\times137)][\{\gamma_{a(1)}+\beta\nu_{b(1)}\}\{\psi_{a(2)}+\beta\psi_{b(2)}\}$$
$$+\{\psi_{a(1)}+\beta\psi_{b(1)}\}\{\gamma_{a(2)}+\beta\nu_{b(2)}\}] \quad (23)$$

and following the procedure laid down in subsection A, the perturbation to the first factor in expression (21) may be taken in the form

$$[\psi'_{a(1)}+\beta\psi'_{b(1)}]$$

where ψ'_a and ψ'_b are determined from the equation

$$\{\mathcal{H}_{0a}(1)-\epsilon_0\}\{\psi'_{a(1)}+\beta\psi'_{b(1)}\}$$
$$=-[H/(2\times137)]\{\gamma_{a(1)}+\beta\nu_{b(1)}\}, \quad (24)$$

where $\mathcal{H}_{0a(1)}$ satisfies the relation

$$\{\mathcal{H}_{0a}(1)-\epsilon_0\}\{\psi_{a(1)}+\beta\psi_{b(1)}\}=0. \quad (25)$$

IV. HYDROGEN MOLECULE

A wave function for hydrogen molecule in the ground state and of the form given in expression (11)

has been calculated by Wang.[10] It gives

$$\phi_a=\exp(-Zr_a) \quad \text{and} \quad \phi_b=\exp(-Zr_b) \tag{26}$$

and $l_1=m_1=l_2=m_2=0$ with $Z=1.166$ and $R=1.406$.

Here we take $\psi'_a=0$ and

$$\psi'_b=i(x_b/r_b^2)\exp(-Zr_b)\lambda(r_b) \tag{27}$$

Equation (18) then becomes

$$(d^2\lambda/dr_b^2)-K_2(d\lambda/dr_b)+[(K_2/r_b)-(2/r_b^2)]\lambda = K_1r_b \tag{28}$$

where $K_1=(\frac{2}{3})^{\frac{1}{2}}[ZHR/(2\times137)]$ and $K_2=2Z$.

Its solution, subject to the boundary conditions, $\lambda(r_b)\exp(-Zr_b)=0$ at $r=0$ and at $r=\infty$ is

$$\lambda(r_b)=-(K_1/K_2)r_b^2.$$

Thus the total perturbation to the wave function is

$$\Psi'_{(1,2)}=-i(K_1c/K_2)[\psi_{a(1)}x_{b(2)}\exp(-Zr_{b(2)}) +\psi_{a(2)}x_{b(1)}\exp(-Zr_{b(1)})]. \tag{29}$$

The magnetic shielding constant for the proton in a hydrogen molecule is therefore given by

$$\sigma_{yy}=\sigma_{yy}^d+\sigma_{yy}^p \tag{30}$$

where

$$\sigma_{yy}^d=(2\times137^2)^{-1}\left\langle\Psi_0\left|\frac{x_{a(1)}^2+z_{a(1)}^2}{r_{a(1)}^3}+\frac{x_{a(2)}^2+z_{a(2)}^2}{r_{a(2)}^3}\right|\Psi_0\right\rangle \tag{31}$$

is the so-called diamagnetic part, and

$$\sigma_{yy}^p=\tfrac{1}{137}[\langle\Psi_0\mid(l_{ya(1)}/r_{a(1)}^3)+(l_{ya(2)}/r_{a(2)}^3)\mid H^{-1}\Psi'\rangle +\langle H^{-1}\Psi'\mid(l_{ya(1)}/r_{a(1)}^3)+(l_{ya(2)}/r_{a(2)}^3)\mid\Psi_0\rangle] \tag{32}$$

is the second order paramagnetic part.

Determination of the explicit expressions for σ^d and σ^p require evaluation of integrals which are similar to those arising in Hameka's treatment of hydrogen molecule.[4]

Finally we obtain

$$\sigma^d=[c^2/(24Z^5\times137^2)][(1+ZR)/ZR] \times[1-\exp(-2ZR)(1-2ZR-2Z^2R^2-\tfrac{2}{3}Z^3R^3)] \tag{33}$$

and

$$\sigma^p=-[c^2/(24Z^5\times137^2)](1/ZR) \times[1-\exp(-2ZR)(1+2ZR+2Z^2R^2)], \tag{34}$$

where

$$c^2=8Z^6[1-\exp(-2ZR)(1+ZR+\tfrac{1}{3}Z^2R^2)^2]^{-1}. \tag{35}$$

This expression for σ^p is identical with that obtained by Aleksandrov.[12]

[12] I. V. Aleksandrov, Soviet Phys.-Doklady (English translation) 3, 325 (1958).

TABLE I. Values of magnetic shielding constant σ for H_2, calculated by different methods.

	$\sigma^p\times10^5$	$\sigma^d\times10^5$	$\sigma\times10^5$
Ramsey	−0.56[a]	+3.24[b]	2.68
Das and Bersohn	−0.49	...	...
McGarvey	−0.17	+2.91	2.74
Hameka	−0.780	+3.225	2.445
Aleksandrov[c]	−0.55	...	...
Ishiguro and Koide[d]	...	...	2.756
Present authors	−0.55	+3.17	2.62

[a] Determined from the experimental value of spin-rotational magnetic interaction constant for hydrogen molecule.

[b] Calculated by H. L. Anderson [Phys. Rev. 76, 1460 (1949)] with Nordsieck wave function.

[c] Footnote 13.

[d] Footnote 14.

The result of this calculation is given in Table I[13,14] together with those obtained by other investigators.

It may be noted that in the cases where one wants to calculate σ for a nucleus of an atom X bonded to a hydrogen atom, the perturbation to the wave function due to a uniform magnetic field would consist of two parts. As in expression (17) the two parts would correspond to excitations of the orbitals centered around X and around the hydrogen nucleus respectively. The latter would always be determined by a differential equation identical with Eq. (28) except for the value of the constants K_1 and K_2. And hence the solution will differ from expression (29) by a numerical factor only.

DISCUSSION

In the light of the present work, it appears that in a variational procedure the perturbed function (due to the uniform magnetic field) should be chosen as a combination of functions centered around the nuclei of the atoms whose bonding we are considering, and the origin of the vector-potential describing the uniform magnetic field can be taken at the nucleus whose shielding we want to calculate. The form of the function to be chosen will be suggested by the considerations (*i*), (*ii*), and (*iii*) in Sec. III. In cases where the perturbed function is chosen as the product of the ground-state function and a single centered function of the space-coordinates, the latter should consist of at least a sufficient number of terms to ensure the convergence of energy. In these cases the origin to describe the single-centered function can be kept variable so that with these limited number of terms the origin would adjust itself in order to represent the actual form of the perturbed function as close as possible.[8] We find that the form of the variation function chosen by McGarvey[7] is identical with the perturbed function we have obtained for hydrogen molecule. He uses similar variation functions with only two parameters for other molecules also. However, in the case of molecules, where

[13] I. V. Aleksandrov, Soviet Phys.-Doklady (English translation) 3, 799 (1958).

[14] E. Ishiguro and S. Koide, Phys. Rev. 94, 350 (1954).

the radial part of the orbitals constituting the bond cannot be well represented by a single exponential, the variation function would need more flexibility than can be given to it by only two variation parameters in order to represent the perturbed wave function properly. Also, there appears to be some numerical error in McGarvey's paper[7] so that even the value of σ^d calculated by him with Wang function does not agree with the value obtained by us.[14a]

The recent work by Hameka[4] considers the effect of arbitrary choice of the origin of the vector-potential describing the uniform magnetic field, and it is well-known that when the origin of the vector potential is different from the origin to describe the other terms in the Hamiltonian, an extra phase factor is to be incorporated in the wave function in order to ensure the gauge invariance of the Schrödinger equation. In the calculation of the magnetic shielding of nuclei, this effect introduces extra complications which have been avoided in the present calculations by taking the two origins at the same point.

We also note that the expression (34) is identical as has been already mentioned, with the expression for σ^p, as derived by Aleksandrov.[12] However, this identity is true for the case of hydrogen molecule only. For more complicated molecules, particularly where the atom in whose nuclear shielding we are interested has an orbital other than s-type taking part in the bond formation, the perturbation to the molecular wave function by the magnetic field as will be obtained with the present method will contain some terms in addition to those which will be obtained in the treatment of Aleksandrov.

ACKNOWLEDGMENT

We are very thankful to Professor A. K. Saha and to Mr. S. K. Ghosh for their interest in this work. We also appreciate some interesting discussions with Dr. D. K. Roy and Mrs. T. Roy. We are specially indebted to Dr. T. P. Das, who stimulated our interest in this line.

[14a] *Note added in proof.* After correction of this numerical error Dr. McGarvey obtains $\sigma^d=3.09\times10^{-5}$ and $\sigma^p=-0.16\times10^{-5}$ for protons in hydrogen molecule (private communication). This value of σ^d still differs from that obtained by us ($\sigma^d=3.17\times10^{-5}$) because he used $R=1.401$ a.u. while we took $R=1.406$ a.u., the value used by Wang in determining the valence bond function for the hydrogen molecule (reference 10).

THE JOURNAL OF CHEMICAL PHYSICS VOLUME 32, NUMBER 6 JUNE, 1960

Theory of Electronic Excitation and Reorganization in the Formaldehyde Molecule*

JOE M. PARKS† AND ROBERT G. PARR

Department of Chemistry, Carnegie Institute of Technology, Pittsburgh, Pennsylvania

(Received May 19, 1959)

The use of a previously described iterative method of separated electron pairs is demonstrated by calculations on the formaldehyde molecule. Investigation is made, for example, of detailed changes in the polarity of sigma bonding electron wave functions in this molecule when a pi or lone-pair electron is excited or ionized. The molecule is treated as a six-electron problem (four electrons in the C=O bond plus two lone-pair electrons on O); matrix elements involving the "core" are obtained by fitting experimental data. The use of Pariser-type one-center repulsion integrals is tested in conjunction with various sets of two-center repulsion integrals. Although one combination gives reasonable results, none of the combinations is found to be entirely satisfactory, and a procedure is outlined from which could be obtained one-center integrals approximately incorporating Arai-Hurley type corrections. It is demonstrated (with reservations) that the constant sigma structure assumption, usually made in calculations of pi electron excitations and ionizations, is not always good with regard to wave functions, but that it may lead to only small errors in calculated energies.

I. INTRODUCTION

As chemists we are interested in the effect on one set of electrons of changes in the electronic structure of another set of electrons. It was with the hope of achieving a quantitative description of such effects that the iterative method previously outlined was developed.[1] This method facilitates dealing with the reorganization of electrons in one part of the molecule, caused by electronic upheaval in another part.

This method will here be applied to the ground state of the formaldehyde molecule ($H_2C=O$), and to the ground states of those ions, and to those lower excited states of the molecule, which result from excitation or ionization of an electron from the oxygen lone-pair orbital (n) or the carbonyl pi bonding orbital (π) or the carbonyl sigma bonding orbital (σ) of the ground state (Ω_N), to the carbonyl pi antibonding orbital (π^*) or to the carbonyl sigma antibonding orbital (σ^*) (for the excited states), or to infinity (for the ionic states). These states are listed in Table I, with their experimental energies.

The following illustrates the principles of the method: The electronic structure and energy problem for the excited state $\Omega(n\to\pi^*)$ (obtained from the ground state Ω_N by transfer of an electron from a lone-pair orbital to the pi antibonding orbital) is separated into a $(\Pi N)^*$ part which includes the pi and lone-pair electrons, and a $(\Sigma)'$ part for the sigma electrons. On excitation of the pi–lone-pair system the sigma electrons experience an environment different from that in Ω_N. The sigma wave function must therefore adjust accordingly. The first step in the sigma adjustment creates a changed environment for the excited pi and lone-pair electrons. Readjustment of the pi–lone-pair wave function results, causing further readjustment of the sigma wave function, and so on until the $(\Sigma)'$ and $(\Pi N)^*$ system are mutually consistent. One can see how much charge transfer has resulted from sigma–pi interaction by comparing the initial wave function which has $n\to\pi^*$ excitation but no sigma reorganization with the wave functions finally obtained by iteration.

If the required atomic and molecular parameters are at hand one obtains a theoretical value for the $n\to\pi^*$ excitation energy, $\Delta E(n\to\pi^*)$, from such an iterative treatment. Conversely, and as is done in the present paper, one may impose the experimental $\Delta E(n\to\pi^*)$ datum and obtain thereby a semi-empirical value for β_σ^λ, one of the molecular parameters. Figure 1 of Sec. II

TABLE I. Experimental data and assignments for formaldehyde.

State	Energy (ev)[a]	Reference
Ω_N	0[b]	[b]
$^3\Omega(n\to\pi^*)$	3.02	[c]
$^1\Omega(n\to\pi^*)$	4.26	[d]
$^1\Omega(n\to\sigma^*)$	7.1	[d]
$^1\Omega(\pi\to\pi^*)$	8.0	[d]
$^2\Omega(n^+)$	10.83	[e]
$^2\Omega(\pi^+)$	11.8	[f]
$^2\Omega(\sigma^+)$	13.1	[f]

[a] Excitation and ionization energies are vertical.
[b] The dipole moment in the ground state is 2.34 D. J. M. Shoolery and A. H. Sharbaugh, Phys. Rev. **82**, 95 (1951).
[c] A. D. Cohen and C. Reid, J. Chem. Phys. **24**, 85 (1956).
[d] H. Sponer and E. Teller, Revs. Modern Phys. **13**, 75 (1941).
[e] W. C. Price, Phys. Rev. **46**, 529 (1934).
[f] T. M. Sugden and W. C. Price, Trans. Faraday Soc. **44**, 116 (1948).

* Supported in part by research grants from the National Science Foundation and the Office of Ordnance Research, U. S. Army. Based on a thesis submitted by Joe M. Parks in partial fulfillment of the requirements for the degree of Doctor of Philosophy at the Carnegie Institute of Technology (1956).

† National Science Foundation Predoctoral Fellow, 1954–1955. Present address: Department of Chemistry, University of Illinois, Urbana, Illinois.

[1] J. M. Parks and R. G. Parr, J. Chem. Phys. **28**, 335 (1958). See also the final paragraphs of reference 2(a).

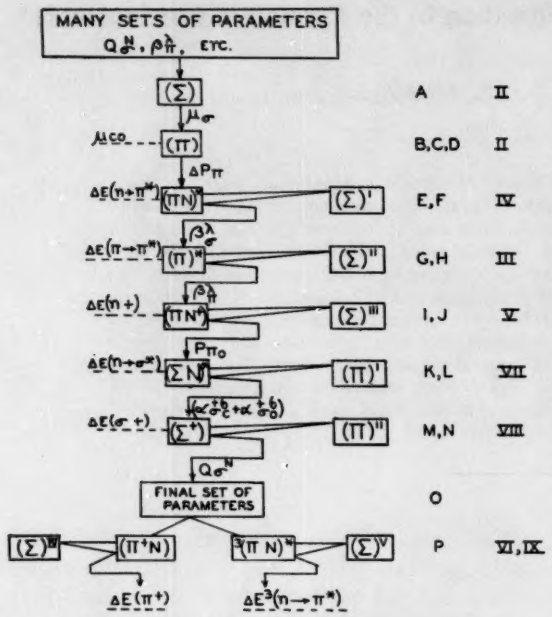

FIG. 1. Schematic form of the parameter evaluation process. Tables II–IX and Sec. III provide explanation of symbols. The steps in this process are: (A) A series of Q_σ^N values are picked and the corresponding μ_σ values determined. (B) A series of β_π^λ values are picked, and μ_π is calculated for each β_π^λ as a function of $(H_{12}^N)^\pi$. (C) For each Q_σ^N, β_π^λ pair, the value of $(H_{12}^{N\pi})$ giving $\mu_\sigma+\mu_\pi$ equal to the experimental dipole moment of $H_2C=O$ is determined. (D) For each Q_σ^N, β_π^λ pair, the value of ΔP_π is determined from the appropriate $(H_{12}^N)^\pi$ value. (E) For each Q_σ^N, β_π^λ pair, a predicted value of $\Delta E(n\to\pi^*)$ is calculated as a function of β_π^λ. (F) for each Q_σ^N, β_π^λ pair, the value of β_σ^λ which gives the experimental $\Delta E(n\to\pi^*)$ value is determined. (G) For each Q_σ^N, a predicted value of $\Delta E(\pi\to\pi^*)$ is calculated as a function of β_π^λ. (H) For each Q_σ^N, the value of β_π^λ which gives the experimental $\Delta E(\pi\to\pi^*)$ value is determined. (I) For each Q_σ^N, a predicted value of $\Delta E(n^+)$ is calculated as a function of P_{π_0}. (J) For each Q_σ^N, the value P_{π_0} which gives the experimental $\Delta E(n^+)$ value is determined. (K) For each Q_σ^N, a predicted value of $\Delta E(n\to\sigma^*)$ is calculated as a function of $(\alpha s_c+\alpha\sigma_o^{+6})$. (L) For each Q_σ^N, the value of $(\alpha\sigma_c+\alpha\sigma_o^{+6})$ which gives the experimental $\Delta E(n\to\sigma^*)$ value is determined. (M) For each Q_σ^N, a predicted value of $\Delta E(\sigma^+)$ is calculated. (N) The Q_σ^N value which gives the experimental $\Delta E(\sigma^+)$ value is determined. (O) For this final Q_σ^N value, the parameter values are determined. (P) For this Q_σ^N value, $\Delta E(\pi^+)$ and $\Delta E^3(n\to\pi^*)$ are predicted.

schematizes a full procedure by which six of the experimental quantities listed in Table I can in fact be used to determine values for six molecular parameters, and then the other two experimental quantities predicted. Predictions made this way of the pi ionization potential [energy of $\Omega(\pi^+)$] and the $n\to\pi^*$ triplet excitation energy [energy of $^3\Omega(n\to\pi^*)$] are given in Table XII of Sec. IV.

The molecular parameters employed are defined in the discussion in Sec. II of Tables II–IX. These tables contain formulas for the energies of the various states.

II. METHOD OF CALCULATION

This calculation is an MO–CI (molecular orbital with configuration interaction) type of calculation, differing from the usual calculations on unsaturated molecules[2] in that we do *not* assume an average sigma electron structure, the same for the ground, excited, and ionized states of the pi electron system. Inferences as to the degree of validity of the assumption of constant sigma structure may in fact be drawn from the results of the present calculations,[3] since the iterative problems for different states of the pi-lone-pair system will in general converge to different sigma structures.

Individual stages in the iterations follow methods which have been described.[1,4] All the electrons except the C=O sigma and pi bonding electrons and the least tightly bound lone-pair electrons of oxygen are relegated to a "core" of charge +6 which is assumed to be unchanged during all the excitations and ionizations listed in Table I. To illustrate with the example of the calculation on $\Omega(n\to\pi^*)$ mentioned in Sec. I, this involves iteration between $(\Pi N)^*$ and $(\Sigma)'$. The (+4) core for the $(\Pi N)^*$ problem contains, in addition to the unchanging (+6) core, two electrons with a wave function $(\Sigma)'$, different at each stage in the iteration. To begin one guesses a $(\Sigma)'$, fixing the (+4) core for the $(\Pi N)^*$ problem, which one then solves by the standard MO–CI method. This gives a wave function $(\Pi N)^*$ for four electrons, which makes up part of the +2 core for the $(\Sigma)'$ problem. An improved $(\Sigma)'$ can thus be found, and the whole process repeated.

In carrying out the calculations approximations are made which are related to those introduced by Pariser and Parr,[5,6] and similar methods are employed for determining certain integrals from atomic data.[7] Instead of using zero differential overlap everywhere,[8] Mulliken-type approximations[9] are employed systematically. (However, one should note that the general method being employed is valid regardless of what particular simplifications are used.)

Figure 1 outlines the calculations schematically, and Tables II–IX contain most of the theoretical formulas required. The formulas have been obtained by appropriate modifications and extensions of the methods that have already been described[1]; explanation of notation, new features, and fine points in the argument are given in the following.

Remarks on Tables II–IX

Table II contains the starting functions and matrix elements for an iterative linear variational treatment of the two electron (Π) problem and the two electron (Σ) problem for the [(Σ)(Π)] separation of the

[2] (a) R. G. Parr and P. G. Lykos, J. Chem. Phys. **24**, 1166; **25**, 1301 (1956); (b) R. McWeeny, Proc. Roy. Soc. (London) **A223**, 306 (1954).

[3] For example, compare the Q_σ values in the first and third columns in Tables XIV–XX.

[4] Parr, Ellison, and Lykos, J. Chem. Phys. **24**, 1106 (1956).

[5] R. Pariser and R. G. Parr, J. Chem. Phys. **21**, 466, 767 (1953); F. G. Fumi and R. G. Parr, *ibid.* **21**, 1864 (1953).

[6] R. G. Parr and R. Pariser, J. Chem. Phys. **23**, 711 (1955).

[7] R. Pariser, J. Chem. Phys. **21**, 568 (1953).

[8] R. G. Parr, J. Chem. Phys. **20**, 1499 (1952).

[9] R. S. Mulliken, J. chim. phys. **46**, 497 (1951).

TABLE II. Formulas for the $[(\Sigma)(\Pi)]$ separation of the state Ω_N.

(Π) Structure

Starting functions and matrix elements leading to $(\delta_1^N)^\pi$ and B_k^N:

$$\Pi_1 = |1\bar{1}| \qquad H_{11}=0 \qquad H_{12}=(H_{12}^N)^\pi$$
$$\Pi_2 = (1/2)^{\frac{1}{2}}[|1\bar{2}| + |2\bar{1}|] \qquad H_{22}=-2\beta_\pi^\lambda+K_{12}^\pi \qquad H_{13}=K_{12}^\pi$$
$$\Pi_3 = |2\bar{2}| \qquad H_{33}=-4\beta_\pi^\lambda \qquad H_{23}=H_{12}$$

$$(H_{12}^N)^\pi = 1/[2(1-S_\pi^2)]^{\frac{1}{2}}[(\omega_{\pi_c}{}^{+1}-\omega_{\pi_o}{}^{+1})+(P_{\pi_c}-P_{\pi_o})+\tfrac{1}{2}(\gamma_{\pi_c}-\gamma_{n_o})+Q_\sigma^N(g_{\sigma_c\pi_c}-g_{\sigma_o\pi_c}-g_{\sigma_c\pi_o}+g_{\sigma\pi_o})]$$
$$(H_{11}^N)^\pi = E_{\text{core}}{}^{+2}+(\alpha_{\pi_c}{}^{+2}+\alpha_{\pi_o}{}^{+2})^N+2(1-S_\pi)\beta_\pi^\lambda+\tfrac{1}{4}[\gamma_{\pi_c}+\gamma_{\pi_o}+2\gamma_{\pi_c\pi_o}]$$

(Σ) Structure

Starting functions and matrix elements leading to $(\delta_1^N)^\sigma$ and A_k^N:

$$\Sigma_1 = |1\bar{1}| \qquad H_{11}=0 \qquad H_{12}=(H_{12}^N)^\sigma$$
$$\Sigma_2 = (1/2)^{\frac{1}{2}}[|1\bar{2}| + |2\bar{1}|] \qquad H_{22}=-2\beta_\sigma^\lambda+K_{12}^\sigma \qquad H_{13}=K_{12}^\sigma$$
$$\Sigma_3 = |2\bar{2}| \qquad H_{33}=-4\beta_\sigma^\lambda \qquad H_{23}=H_{12}$$

$$(H_{12}^N)^\sigma = 1/[2(1-S_\sigma^2)]^{\frac{1}{2}}[(\omega_{\sigma_c}{}^{+1}-\omega_{\sigma_o}{}^{+1})+(P_{\sigma_c}-P_{\sigma_o})+\tfrac{1}{2}(\gamma_{\sigma_c}-\gamma_{\sigma_o})+Q_\pi^N(g_{\pi_c\sigma_c}-g_{\pi_o\sigma_c}-g_{\pi_c\sigma_o}+g_{\pi_o\sigma_o})]$$
$$(H_{11}^N)^\sigma = E'_{\text{core}}{}^{+2}+(\alpha_{\sigma_c}{}^{+2}+\alpha_{\sigma_o}{}^{+2})^N+2(1-S_\sigma)\beta_\sigma^\lambda+\tfrac{1}{4}[\gamma_{\sigma_c}+\gamma_{\sigma_o}+2\gamma_{\sigma_c\sigma_o}]$$

Sigma-pi interaction operators

$$(G_\pi^N(1)\,|\,=[g_{\pi_c}(1)+g_{\pi_o}(1)]+Q_\pi^N[g_{\pi_c}(1)-g_{\pi_o}(1)]$$
$$(G_\sigma^N(1)\,|\,=[g_{\sigma_c}(1)+g_{\sigma_o}(1)]+Q_\sigma^N[g_{\sigma_c}(1)-g_{\sigma_o}(1)]$$

$$Q_\pi^N=[2/(1-S_\pi^2)]^{\frac{1}{2}}B_2^N(B_1^N+B_3^N)$$
$$Q_\sigma^N=[2/(1-S_\sigma^2)]^{\frac{1}{2}}A_2^N(A_1^N+A_3^N)$$

Energy of Ω_N

$$E[\Omega_N]=E_{\text{core}}{}^{+4}+[(\alpha_{\pi_c}{}^{+4}+\alpha_{\pi_o}{}^{+4})+(G_\sigma^N\,|\,\pi_c^2)+(G_\sigma^N\,|\,\pi_o^2)$$
$$+2(1-S_\pi)\beta_\pi^\lambda+J_{11}^\pi-(\delta_1^N)^\pi]+[(\alpha_{\sigma_c}{}^{+4}+\alpha_{\sigma_o}{}^{+4})+2(1-S_\sigma)\beta_\sigma^\lambda+J_{11}^\sigma+2A_1^NA_3^NK_{12}^\sigma$$
$$+Q_\sigma^N\{(\alpha_{\sigma_c}{}^{+4}-\alpha_{\sigma_o}{}^{+4})+\tfrac{1}{2}(\gamma_{\sigma_c}-\gamma_{\sigma_o})\}+(A_2^N)^2(-2\beta_\sigma^\lambda+K_{12}^\sigma)+(A_3^N)^2(-4\beta_\sigma^\lambda)]$$

ground state Ω_N. $(\delta_1^N)^\pi$ and $(\delta_1^N)^\sigma$ are, respectively, the energies [referred to $(H_{11}^N)^\pi$ and $(H_{11}^N)^\sigma$] of $(\Pi)=\Sigma_k B_k^N\Pi_k$ and $(\Sigma)=\Sigma_k A_k^N\Sigma_k$, to be found (along with the B_k^N and A_k^N) by solution of the secular equations involving, at one stage of the iteration, matrix elements over the Π_k, and at another stage, matrix elements over the Σ_k. In $\Sigma_1 = |1\bar{1}|$ for example, which is an abbreviation for the ground state configurational Slater determinant of reference 1, Eq. (35), 1 stands for the bonding MO, ϕ_1 of Eq. (34), and the χ_a, χ_b of Eq. (34) are the sigma atomic orbitals σ_c (an sp^2 hybrid) and σ_0 (unhybridized). In $\Pi_1 = |1\bar{1}|$, χ_a and χ_b of ϕ_1 are the pi atomic orbitals π_c and π_o. In the matrix elements for the configuration interaction problem among the (Π) starting functions, K_{12}^π is the exchange repulsion integral over MO's, which gives the interaction energy of two electrons, each in the overlap region of the bonding and antibonding pi MO's, ϕ_1^π and ϕ_2^π. Written in terms of integrals over atomic orbitals, the MO exchange integral is

$$K_{12}^\pi=[\gamma_{\pi_c}+\gamma_{\pi_o}-2\gamma_{\pi_c\pi_o}]/[4(1-S_\pi^2)],$$

where γ_{π_c} (one subscript) is the one-center coulomb repulsion integral between two electrons which are both in the π_c atomic orbital. $\gamma_{\pi_c\pi_o}$ is the two-center coulomb repulsion integral between one electron in π_c and one in π_o. The quantity β_π^λ is a Löwdin β over π_c and π_o,[5]

$$\beta_\pi^\lambda=[\beta_{\pi_c\pi_o}{}^{+2}-S_\pi(\alpha_{\pi_c}{}^{+2}+\alpha_{\pi_o}{}^{+2})]/[1-S_\pi^2],$$

TABLE III. Formulas for the $[(\Sigma)''(\Pi)]$ separation of the state $\Omega(\pi\rightarrow\pi^*)$.

(Π)* Structure

Starting functions and matrix elements leading to E_2 and $B_k{}^V$:

$$\Pi_1=|1\bar{1}| \qquad H_{11}=0 \qquad H_{12}=(H_{12}{}^V)^\pi$$

$$\Pi_2=(1/2)^{\frac{1}{2}}[|1\bar{2}|+|2\bar{1}|] \qquad H_{22}=-2\beta_\pi{}^\lambda+K_{12}{}^\pi \qquad H_{13}=K_{12}{}^\pi$$

$$\Pi_3=|2\bar{2}| \qquad H_{33}=-4\beta_\pi{}^\lambda \qquad H_{23}=H_{12}$$

$$(H_{12}{}^V)^\pi=1/[2(1-S_\pi{}^2)]^{\frac{1}{2}}[(\omega_{\pi_c}{}^{+1}-\omega_{\pi_o}{}^{+1})+(P_{\pi_c}-P_{\pi_o})+\tfrac{1}{2}(\gamma_{\pi_c}-\gamma_{\pi_o})+Q_\sigma{}^V(g_{\sigma_c\pi_c}-g_{\sigma_o\pi_c}-g_{\sigma_c\pi_o}+g_{\sigma_o\pi_o})]$$

Secular equations:

$$0=[H_{12}-(b_3/b_1)(H_{11}+\eta_1)]B_1+[(H_{22}+\eta_1)-(b_2/b_1)H_{12}]B_2+[H_{23}-(b_2/b_1)H_{13}]B_3$$

$$0=[H_{13}-(b_2/b_1)(H_{11}+\eta_1)]B_1+[H_{22}-(b_3/b_1)H_{12}]B_2+[(H_{33}+\eta_1)-(b_3/b_1)H_{13}]B_3$$

$$0=[\quad b_1 \quad]B_1+[\quad b_2 \quad]B_2+[\quad b_3 \quad]B_3$$

(Σ)'' Structure

Starting functions and matrix elements leading to $A_k{}^V$:

$$\Sigma_1=|1\bar{1}| \qquad H_{11}=0 \qquad H_{12}=(H_{12}{}^V)^\sigma$$

$$\Sigma_2=(1/2)^{\frac{1}{2}}[|1\bar{2}|+|2\bar{1}|] \qquad H_{22}=-2\beta_\sigma{}^\lambda+K_{12}{}^\sigma \qquad H_{13}=K_{12}{}^\sigma$$

$$\Sigma_3=|2\bar{2}| \qquad H_{33}=-4\beta_\sigma{}^\lambda \qquad H_{23}=H_{12}$$

$$(H_{12}{}^V)^\sigma=1/[2(1-S_\sigma{}^2)]^{\frac{1}{2}}[(\omega_{\sigma_c}{}^{+1}-\omega_{\sigma_o}{}^{+1})+(P_{\sigma_c}-P_{\sigma_o})+\tfrac{1}{2}(\gamma_{\sigma_c}-\gamma_{\sigma_o})+Q_\pi{}^V(g_{\pi_c\sigma_c}-g_{\pi_o\sigma_c}-g_{\pi_c\sigma_o}+g_{\pi_o\sigma_o})$$

Sigma-pi interaction operators

$$\langle G_\pi{}^V(1)|=[g_{\pi_c}(1)+g_{\pi_o}(1)]+Q_\pi{}^V[g_{\pi_c}(1)-g_{\pi_o}(1)]$$

$$\langle G_0{}^V(1)|=[g_{\sigma_c}(1)+g_{\sigma_o}(1)]+Q_\sigma{}^V[g_{\sigma_c}(1)-g_{\sigma_o}(1)]$$

$$Q_\pi{}^V=[2/(1-S_\pi{}^2)]^{\frac{1}{2}}B_2{}^V(B_1{}^V+B_3{}^V)$$

$$Q_\sigma{}^V=[2/(1-S_\sigma{}^2)]^{\frac{1}{2}}A_2{}^V(A_1{}^V+A_3{}^V)$$

$\pi\rightarrow\pi^*$ Transition energy

$$E[\Omega(\pi\rightarrow\pi^*)]-E[\Omega_N]=E_2+(\delta_1{}^N)^\pi+2(A_1{}^VA_3{}^V-A_1{}^NA_3{}^N)[K_{12}{}^\sigma]$$
$$+[(A_2{}^V)^2-(A_2{}^N)^2][-2\beta\sigma^\lambda+K_{12}{}^\sigma]+[(A_3{}^V)^2-(A_3{}^N)^2][-4\beta_\sigma{}^\lambda]$$
$$+(Q_\sigma{}^V-Q_\sigma{}^N)[(\omega_{\sigma_c}{}^{+1}-\omega_{\sigma_o}{}^{+1})+(P_{\sigma_c}-P_{\sigma_o})+\tfrac{1}{2}(\gamma_{\sigma_c}-\gamma_{\sigma_o})-2(g_{x_o\sigma_c}-g_{x_o\sigma_o})$$
$$-(g_{\pi_c\sigma_c}-g_{\pi_c\sigma_o}+g_{\pi_o\sigma_c}-g_{\pi_o\sigma_o})]$$

where $\beta_{\pi_c\pi_o}{}^{+2}$ gives the energy of an electron in the overlap region of π_c and π_o moving in the field of a +2 core. Here $\alpha_{\pi_c}{}^{+2}$ is the energy of an electron in π_c moving similarly. As discussed in reference 1, Sec. VI, sigma bond polarity affects both $\beta_{\pi_c\pi_o}$ and the α, but cancels out of $\beta_\pi{}^\lambda$, under the generalized Mulliken approximation of reference 1, Eq. (56).

In $(H_{12}{}^N)^\pi$, the superscripts N, π signify the (Π) part of the calculation. A more familiar form is

$$(H_{12}{}^N)^\pi=[(\alpha_{\pi_c}{}^{+2}-\alpha_{\pi_o}{}^{+2})+\tfrac{1}{2}(\gamma_{\pi_c}-\gamma_{\pi_o})]/[2(1-S_\pi{}^2)]^{\frac{1}{2}}$$

which may be written as in Table II by noting that from reference 1, Eqs. (65) and (68),

$$\alpha_{\pi_c}{}^{+2}=\alpha_{\pi_c}{}^{+4}+(G_\sigma|\pi_c{}^2),$$

where $(G_\sigma|\pi_c{}^2)=(g_{\sigma_c\pi_c}+g_{\sigma_o\pi_c})+Q_\sigma(g_{\sigma_c\pi_c}-g_{\sigma_o\pi_c})$. Here Q_σ, the sigma bond polarity parameter, is defined in reference 1, Eq. (59), and $g_{\sigma_o\pi_c}=\gamma_{\sigma_o\pi_c}-\frac{1}{2}K_{\sigma_o\pi_c}$, where $K_{\sigma_o\pi_c}$ is an exchange repulsion integral over AO's, the interaction of two electrons in the overlap region of

TABLE IV. Formulas for the $[(\Sigma)'(\Pi N)^*]$ separation of the state $\Omega(n\rightarrow\pi^*)$

$(\Pi N)^*$ Structure

Starting functions and matrix elements leading to $\delta_5^{n\pi}$ and $B_k^{n\pi}$:

$$(\Pi N)_5=(1/2)^{\frac{1}{2}}[\,|\,1\bar{1}2\bar{n}\,|+|\,1\bar{1}n\bar{2}\,|\,] \qquad H_{55}=0$$

$$(\Pi N)_6=(1/2)^{\frac{1}{2}}[\,|\,2\bar{2}1\bar{n}\,|+|\,2\bar{2}n\bar{1}\,|\,] \qquad H_{66}=-2\beta_\pi^\lambda$$

$$(H_{56}^{n\pi})^\pi=-[1/2(1-S_\pi^2)^{\frac{1}{2}}][(\omega_{\pi_c}{}^{+1}-\omega_{\pi_o}{}^{+1})+(P_{\pi_c}-P_{\pi_o})+(\gamma_{\pi_c}-\gamma_{\pi_o})-g_{x_o\pi_c}+g_{x_o\pi_o}$$
$$-\tfrac{3}{2}K_{\pi_c x_o}+\tfrac{3}{2}K_{\pi_o x_o}+Q_\sigma^{n\pi}(g_{\sigma_c\pi_c}-g_{\sigma_o\pi_c}-g_{\sigma_c\pi_o}+g_{\sigma_o\pi_o})]$$

$(\Sigma)'$ Structure

Starting functions and matrix elements leading to $A_k^{n\pi}$:

$$\Sigma_1=|\,1\bar{1}\,| \qquad H_{11}=0 \qquad H_{12}=(H_{12}^{n\pi})^\sigma$$

$$\Sigma_2=(1/2)^{\frac{1}{2}}[\,|\,1\bar{2}\,|+|\,2\bar{1}\,|\,] \qquad H_{22}=-2\beta_\pi^\lambda+K_{12}^\sigma \qquad H_{13}=K_{12}^\sigma$$

$$\Sigma_3=|\,2\bar{2}\,| \qquad H_{33}=-4\beta_\sigma^\lambda \qquad H_{23}=H_{12}$$

$$(H_{12}^{n\pi})^\sigma=[1/2(1-S_\sigma^2)]^{\frac{1}{2}}[(\omega_{\sigma_c}{}^{+1}-\omega_{\sigma_o}{}^{+1})+(P_{\sigma_c}-P_{\sigma_o})+\tfrac{1}{2}(\gamma_{\sigma_c}-\gamma_{\sigma_o})$$
$$+\tfrac{1}{2}(g_{\pi_c\sigma_c}+g_{\pi_o\sigma_c}-g_{\pi_c\sigma_o}-g_{\pi_o\sigma_c})-(g_{x_o\sigma_c}-g_{x_o\sigma_o})+Q_\pi^{n\pi}(g_{\pi_c\sigma_c}-g_{\pi_o\sigma_c}-g_{\pi_c\sigma_o}+g_{\pi_o\sigma_o})]$$

Sigma-pi interaction operators

$$(G_{\pi z}^{n\pi}(1)\,|=(3/2)[g_{\pi_c}(1)+g_{\pi_o}(1)]+Q_\pi^{n\pi}[g_{\pi_c}(1)-g_{\pi_o}(1)]+g_{x_o}(1)$$

$$(G_\sigma^{n\pi}(1)\,|=[g_{\sigma_c}(1)+g_{\sigma_o}(1)]+Q_\sigma^{n\pi}[g_{\sigma_c}(1)-g_{\sigma_o}(1)]$$

$$Q_\pi^{n\pi}=-[1/(1-S_\pi^2)]^{\frac{1}{2}}B_5^{n\pi}B_6^{n\pi}$$

$$Q_\sigma^{n\pi}=[2/(1-S_\sigma^2)]^{\frac{1}{2}}A_2^{n\pi}(A_1^{n\pi}+A_3^{n\pi})$$

$n\rightarrow\pi^*$ Transition energy

$$E[\Omega(n\rightarrow\pi^*)]-E[\Omega_N]=(\delta_1^N)^\pi-(\delta_5)^{n\pi}+\tfrac{1}{2}(\omega_{\pi_c}{}^{+1}+\omega_{\pi_o}{}^{+1})+\tfrac{1}{2}(P_{\pi_c}+P_{\pi_o})$$
$$-\omega_{x_o}{}^{+1}-P_{x_o}-(1+S_\pi)\beta_\pi^\lambda+\tfrac{1}{2}K_{\pi_c\pi_o}+\tfrac{1}{2}\gamma_{\pi_c}+\tfrac{1}{2}\gamma_{\pi_o}-K_{12}^\pi$$
$$-\tfrac{1}{2}g_{\pi_c x_o}-\tfrac{1}{2}g_{\pi_o x_o}+\tfrac{3}{4}K_{\pi_c x_o}+\tfrac{3}{4}K_{\pi_o x_o}+2(A_1^{n\pi}A_3^{n\pi}-A_1^NA_3^N)[K_{12}^\sigma]$$
$$+[(A_2^{n\pi})^2-(A_2^N)^2][-2\beta_\sigma^\lambda+K_{12}^\sigma]+[(A_3^{n\pi})^2-(A_3^N)^2][-4\beta_\sigma^\lambda]$$
$$+Q_\sigma^{n\pi}[(\omega_{\sigma_c}{}^{+1}-\omega_{\sigma_o}{}^{+1})+(P_{\sigma_c}-P_{\sigma_o})+\tfrac{1}{2}(\gamma_{\sigma_c}-\gamma_{\sigma_o})-(g_{\sigma_c x_o}-g_{\sigma_o x_o})+\tfrac{1}{2}(g_{\sigma_c\pi_c}-g_{\sigma_o\pi_c}+g_{\sigma_c\pi_o}-g_{\sigma_o\pi_o})]$$
$$-Q_\sigma^N[(\omega_{\sigma_c}{}^{+1}-\omega_{\sigma_o}{}^{+1})+(P_{\sigma_c}-P_{\sigma_o})+\tfrac{1}{2}(\gamma_{\sigma_c}-\gamma_{\sigma_o})]$$

AO's σ_o and π_c. $\alpha_{\pi_c}{}^{+4}$ is defined by Eq. (66), reference 1, with

$$H_{\text{core}}{}^{+4}(1)=T(1)+C^{+2}(1)+O^{+2}(1)+2H^0(1),$$

where, for example, (through it is not used in this form)

$$C^{+2}(1)=-6e^2/r_{c1}+2g_{1_c}(1)+2g_{1_{s_c}}(1)$$

represents the valence state potential due to the carbon nucleus with two 1s electrons and two electrons in trigonally hybridized orbitals. For use in $\alpha_{\pi_c}{}^{+4}$, one writes

$$C^{+2}(1)=C^{\pi+}(1)-g_{\sigma_c}(1),$$

where $g_{\sigma_c}(1)=j_{\sigma_c}(1)-\tfrac{1}{2}k_{\sigma_c}(1)$ is defined by

$$\int\chi_a(1)j_{\sigma_c}(1)\chi_a(1)d\tau_1=\gamma_{a\sigma_c}$$

and

$$\int\chi_a(1)[k_{\sigma_c}(1)\chi_c(1)]d\tau_1=K_{a\sigma_c}.$$

TABLE V. Formulas for the $[(\Sigma)'''(\Pi N^+)]$ separation of the state $\Omega(n^+)$

(ΠN^+) Structure

Starting functions and matrix elements leading to $(\delta_1{}^{n+})^\pi$ and $B_k{}^{n+}$:

$$(\Pi N)_1 = |1\bar{1}n| \qquad H_{11}=0$$

$$(\Pi N)_2 = (1/2)^{\frac{1}{2}}[|2\bar{1}n| + |1\bar{2}n|] \qquad H_{22}=-2\beta_\pi{}^\lambda+K_{12}{}^\pi$$

$$(\Pi N)_3 = (1/6)^{\frac{1}{2}}[|2\bar{1}n| - |1\bar{2}n| - 2|1\bar{n}2|] \qquad H_{33}=-2\beta_\pi{}^\lambda-K_{12}{}^\pi+K_{\pi_c x_o}+K_{\pi_o x_o}$$

$$(\Pi N)_4 = |2\bar{2}n| \qquad H_{44}=-4\beta_\pi{}^\lambda$$

$$(H_{12}{}^{n+})^\pi=[1/2(1-S_\pi{}^2)]^{\frac{1}{2}}[(\omega_{\pi_c}{}^{+1}-\omega_{\pi_o}{}^{+1})+(P_{\pi_c}-P_{\pi_o})+\tfrac{1}{2}(\gamma_{\pi_c}-\gamma_{\pi_o})$$
$$-(g_{x_o\pi_c}-g_{x_o\pi_o})+Q_\sigma{}^{n+}(g_{\sigma_c\pi_c}-g_{\sigma_o\pi_c}-g_{\sigma_c\pi_o}+g_{\sigma_o\pi_o})]$$

$$H_{13}=-[3/8(1-S_\pi{}^2)]^{\frac{1}{2}}[K_{\pi_c x_o}-K_{\pi_o x_o}] \qquad H_{14}=K_{12}{}^\pi \qquad H_{23}=0$$
$$H_{24}=H_{12} \qquad H_{34}=-H_{13}$$

$(\Sigma)'''$ Structure

Starting functions and matrix elements leading to $A_k{}^{n+}$:

$$\Sigma_1 = |1\bar{1}| \qquad H_{11}=0 \qquad H_{12}=(H_{12}{}^{n+})^\sigma$$

$$\Sigma_2 = (1/2)^{\frac{1}{2}}[|1\bar{2}| + |2\bar{1}|] \qquad H_{22}=-2\beta_\sigma{}^\lambda+K_{12}{}^\sigma \qquad H_{13}=K_{12}{}^\sigma$$

$$\Sigma_3 = |2\bar{2}| \qquad H_{33}=-4\beta_\sigma{}^\lambda \qquad H_{23}=H_{12}$$

$$(H_{12}{}^{n+})^\sigma=[1/2(1-S_\sigma{}^2)]^{\frac{1}{2}}[(\omega_{\sigma_c}{}^{+1}-\omega_{\sigma_o}{}^{+1})+(P_{\sigma_c}-P_{\sigma_o})+\tfrac{1}{2}(\gamma_{\sigma_c}-\gamma_{\sigma_o})$$
$$-(g_{x_o\sigma_c}-g_{x_o\sigma_o})+Q_\pi{}^{n+}(g_{\pi_c\sigma_c}-g_{\pi_o\sigma_c}-g_{\pi_c\sigma_o}+g_{\pi_o\sigma_o})]$$

Sigma-pi interaction operators

$$(G_{\pi z}{}^{n+}(1)\,|\,=[g_{\pi_c}(1)+g_{\pi_o}(1)]+Q_\pi{}^{n+}[g_{\pi_c}(1)-g_{\pi_o}(1)]+g_{x_o}(1)$$

$$(G_\sigma{}^{n+}(1)\,|\,=[g_{\sigma_c}(1)+g_{\sigma_\sigma}(1)]+Q_\sigma{}^{n+}[g_{\sigma_c}(1)-g_{\sigma_o}(1)]$$

$$Q_\pi{}^{n+}=[2/(1-S_\pi{}^2)]^{\frac{1}{2}}B_2{}^{n+}(B_1{}^{n+}+B_3{}^{n+})$$

$$Q_\sigma{}^{n+}=[2/(1-S_\sigma{}^2)]^{\frac{1}{2}}A_2{}^{n+}(A_1{}^{n+}+A_3{}^{n+})$$

Lone-pair ionization potential

$$E[\Omega(n^+)]-E(\Omega_N]=(\delta_1{}^N)^\pi-(\delta_1{}^{n+})^\pi-\omega_{x_o}{}^{+1}-P_{x_o}$$
$$+2(A_1{}^{n+}A_3{}^{n+}-A_1{}^NA_3{}^N)[K_{12}{}^\sigma]+[(A_2{}^{n+})^2-(A_2{}^N)^2][-2\beta_\sigma{}^\lambda+K_{12}{}^\sigma]$$
$$+[(A_3{}^{n+})^2-(A_3{}^N)^2][-4\beta_\sigma{}^\lambda]+(A_4{}^{n+})^2[-2\beta_\sigma{}^\lambda-K_{12}{}^\sigma]$$
$$+Q_0{}^{n+}[(\omega_{\sigma_c}{}^{+1}-\omega_{\sigma_o}{}^{+1})+(P_{\sigma_c}-P_{\sigma_o})+\tfrac{1}{2}(\gamma_{\sigma_c}-\gamma_{\sigma_o})-(g_{\sigma_c x_o}-g_{\sigma_o x_o})]$$
$$-Q_\sigma{}^N[(\omega_{\sigma_c}{}^{+1}-\omega_{\sigma_o}{}^{+1})+(P_{\sigma_c}-P_{\sigma_o})+\tfrac{1}{2}(\gamma_{\sigma_c}-\gamma_{\sigma_o})]$$
$$+[1/(1-S_\sigma{}^2)]^{\frac{1}{2}}A_7{}^{n+}(A_1{}^{n+}-A_3{}^{n+})\{[1-\tfrac{4}{3}(B_3{}^{n+})^2][K_{x_o\sigma_c}-K_{x_o\sigma_o}]$$
$$+\tfrac{2}{3}(B_3{}^{n+})^2[K_{\pi_c\sigma_c}+K_{\pi_o\sigma_c}-K_{\pi_c\sigma_o}-K_{\pi_o\sigma_o}]\}$$

TABLE VI. Formulas for the $[(\Sigma)^{IV}(\Pi^+N)]$ separation of the state $\Omega(\Pi^+)$.

(Π^+N) Structure

Starting functions and matrix elements leading to $(\delta_1{}^{\pi+})$ and $B_k{}^{\pi+}$:

$$(\Pi^+N)_1 = |\, n\bar{n}1\,| \qquad H_{11}=0 \qquad H_{12}=-[1/4(1-S_\pi{}^2)]^{\frac{1}{2}}[K_{\pi_c x_o}-K_{\pi_o x_o}]$$

$$(\Pi^+N)_2 = |\, 1\bar{1}2\,| \qquad H_{33}=-2\beta_\pi{}^\lambda \qquad H_{14}=(1/2)[K_{\pi_c x_o}+K_{\pi_o x_o}]$$

$$(\Pi^+N)_3 = |\, n\bar{n}2\,| \qquad H_{44}=H_{22}-2\beta_\pi{}^\lambda \qquad H_{23}=H_{14}$$

$$(\Pi^+N)_4 = |\, 2\bar{2}1\,| \qquad H_{34}=H_{12}$$

$$H_{22}=(\omega_{\pi_c}{}^{+1}+\omega_{\pi_o}{}^{+1})+(P_{\pi_c}+P_{\pi_o})-2\omega_{x_o}{}^{+1}-2P_{x_o}-2S_\pi\beta_\pi{}^\lambda$$
$$-\tfrac{1}{2}\gamma_{\pi_c\pi_o}-2K_{\pi_c\pi_o}+\tfrac{3}{4}\gamma_{\pi_c}+\tfrac{3}{4}\gamma_{\pi_o}-K_{12}{}^\pi+\gamma_{x_o}-g_{\pi_c x_o}-g_{\pi_o x_o}$$
$$+Q_\sigma{}^{\pi+}[(g_{\sigma_c\pi_c}-g_{\sigma_o\pi_c}+g_{\sigma_c\pi_o}-g_{\sigma_o\pi_o})-2(g_{\sigma_c x_o}-g_{\sigma_o x_o})]$$

$$H_{24}=-[1/4(1-S_\pi{}^2)]^{\frac{1}{2}}[(\omega_{\pi_c}{}^{+1}-\omega_{\pi_o}{}^{+1})+(P_{\pi_c}-P_{\pi_o})+(\gamma_{\pi_c}-\gamma_{\pi_o})$$
$$+Q_\sigma{}^{\pi+}(g_{\sigma_c\pi_c}-g_{\sigma_o\pi_c}-g_{\sigma_c\pi_o}+g_{\sigma_o\pi_o})-2g_{x_o\pi_c}+2g_{x_o\pi_o}]$$

$$H_{13}=[1/4(1-S_\pi{}^2)]^{\frac{1}{2}}[(\omega_{\pi_c}{}^{+1}-\omega_{\pi_o}{}^{+1})+(P_{\pi_c}-P_{\pi_o})+Q_\sigma{}^{\pi+}(g_{\sigma_c\pi_c}-g_{\sigma_o\pi_c}-g_{\sigma_c\pi_o}+g_{\sigma_o\pi_o})]$$

$(\Sigma)^{IV}$ Structure

Starting functions and matrix elements leading to $A_k{}^{\pi+}$:

$$\Sigma_1 = |\, 1\bar{1}\,| \qquad H_{11}=0 \qquad H_{12}=(H_{12}{}^{\pi+})^\sigma$$

$$\Sigma_2 = (1/2)^{\frac{1}{2}}[|\, 1\bar{2}\,| + |\, 2\bar{1}\,|] \qquad H_{22}=-2\beta_\sigma{}^\lambda+K_{12}{}^\sigma \qquad H_{13}=K_{12}{}^\sigma$$

$$\Sigma_3 = |\, 2\bar{2}\,| \qquad H_{33}=-4\beta_\sigma{}^\lambda \qquad H_{23}=H_{12}$$

$$(H_{12}{}^{\pi+})^\sigma=[1/2(1-S_\sigma{}^2)]^{\frac{1}{2}}[(\omega_{\sigma_c}{}^{+1}-\omega_{\sigma_o}{}^{+1})+(P_{\sigma_c}-P_{\sigma_o})+\tfrac{1}{2}(\gamma_{\sigma_c}-\gamma_{\sigma_o})$$
$$-\tfrac{1}{2}g_{\pi_c\sigma_c}-\tfrac{1}{2}g_{\pi_o\sigma_c}+\tfrac{1}{2}g_{\pi_c\sigma_o}+\tfrac{1}{2}g_{\pi_o\sigma_o}+Q_t(\tfrac{1}{2}g_{\pi_c\sigma_c}+\tfrac{1}{2}g_{\pi_o\sigma_c}-\tfrac{1}{2}g_{\pi_c\sigma_o}-\tfrac{1}{2}g_{\pi_o\sigma_o}-g_{x_o\sigma_c}+g_{x_o\sigma_o})$$
$$+Q_\pi{}^{\pi+}(\tfrac{1}{2}g_{\pi_c\sigma_c}-\tfrac{1}{2}g_{\pi_o\sigma_c}-\tfrac{1}{2}g_{\pi_c\sigma_o}+\tfrac{1}{2}g_{\pi_o\sigma_o})]$$

Sigma-pi interaction operators

$$(G_{\pi x}{}^{\pi+}(1)\,|\,=(1+Q_t)[\tfrac{1}{2}g_{\pi_c}(1)+\tfrac{1}{2}g_{\pi_o}(1)]+(2-Q_t)[g_{x_o}(1)]+Q_\pi{}^{\pi+}[\tfrac{1}{2}g_{\pi_c}(1)-\tfrac{1}{2}g_{\pi_o}(1)]$$

$$(G_\sigma{}^{\pi+}(1)\,|\,= \quad [g_{\sigma_c}(1)+g_{\sigma_o}(1)]+Q_\sigma{}^{\pi+}[g_{\sigma_c}(1)-g_{\sigma_o}(1)]$$

$$Q_t=2[(B_2{}^{\pi+})^2+(B_4{}^{\pi+})^2]$$

$$Q_\pi{}^{\pi+}=[4/(1-S_\pi{}^2)]^{\frac{1}{2}}(B_1{}^{\pi+}B_3{}^{\pi+}-B_2{}^{\pi+}B_4{}^{\pi+})$$

$$Q_\sigma{}^{\pi+}=[2/(1-S_\sigma{}^2)]^{\frac{1}{2}}A_2{}^{\pi+}(A_1{}^{\pi+}+A_3{}^{\pi+})$$

Pi ionization potential

$$E[\Omega(\pi^+)]-E[\Omega_N]=(\delta_1{}^N)^\pi-(\delta_1{}^{\pi+})^\pi-\tfrac{1}{2}(\omega_{\pi_c}{}^{+1}+\omega_{\pi_o}{}^{+1})-\tfrac{1}{2}(P_{\pi_c}+P_{\pi_o})$$
$$-(1-S_\pi)\beta_\pi{}^\lambda-\tfrac{1}{4}\gamma_{\pi_c}-\tfrac{1}{4}\gamma_{\pi_o}+\tfrac{1}{2}\gamma_{\pi_c\pi_o}-\tfrac{1}{2}K_{\pi_c\pi_o}+[(A_3{}^{\pi+})^2-(A_3{}^N)^2][-4\beta_\sigma{}^\lambda]$$
$$+2(A_1{}^{\pi+}A_3{}^{\pi+}-A_1{}^NA_3{}^N)[K_{12}{}^\sigma]+[(A_2{}^{\pi+})^2-(A_2{}^N)^2][-2\beta_\sigma{}^\lambda+K_{12}{}^\sigma]$$
$$+(A_4{}^{\pi+})^2[-2\beta_\sigma{}^\lambda-K_{12}{}^\sigma]+Q_\sigma{}^{\pi+}[(\omega_{\sigma_c}{}^{+1}-\omega_{\sigma_o}{}^{+1})+(P_{\sigma_c}-P_{\sigma_o})+\tfrac{1}{2}(\gamma_{\sigma_c}-\gamma_{\sigma_o})$$
$$-\tfrac{1}{2}(g_{\sigma_c\pi_c}-g_{\sigma_o\pi_c}+g_{\sigma_c\pi_o}-g_{\sigma_o\pi_o})]-Q_\sigma{}^N[(\omega_{\sigma_c}{}^{+1}-\omega_{\sigma_o}{}^{+1})+(P_{\sigma_c}-P_{\sigma_o})+\tfrac{1}{2}(\gamma_{\sigma_c}-\gamma_{\sigma_o})]$$
$$+[1/(1-S_\sigma{}^2)]^{\frac{1}{2}}A_T{}^{\pi+}(A_1{}^{\pi+}-A_3{}^{\pi+})\{\tfrac{1}{2}[K_{\pi_c\sigma_c}+K_{\pi_o\sigma_c}-K_{\pi_c\sigma_o}-K_{\pi_o\sigma_o}]$$
$$-[1/(1-S_\pi{}^2)]^{\frac{1}{2}}B_1{}^{\pi+}B_3{}^{\pi+}[K_{\pi_c\sigma_c}-K_{\pi_o\sigma_c}-K_{\pi_c\sigma_o}+K_{\pi_o\sigma_o}]\}$$

TABLE VII. Formulas for the $[(\Sigma N)^{V}\Pi')]$ separation of the state $\Omega(n\rightarrow\sigma^*)$.

$(\Sigma N)^{V}$ Structure

Starting functions and matrix elements leading to $\delta_5{}^{n\sigma}$ and $A_k{}^{n\sigma}$:

$$\Sigma_5=(1/2)^{\frac{1}{2}}[|\,1\bar{1}2\bar{n}\,|+|\,1\bar{1}n\bar{2}\,|] \qquad H_{55}=0$$

$$\Sigma_6=(1/2)^{\frac{1}{2}}[|\,2\bar{2}1\bar{n}\,|+|\,2\bar{2}n\bar{1}\,|] \qquad H_{66}=-2\beta_\sigma{}^{\lambda}$$

$$H_{56}=-[1/4(1-S_\sigma{}^2)]^{\frac{1}{2}}[(\omega_{\sigma_c}{}^{+1}-\omega_{\sigma_o}{}^{+1})+(P_{\sigma_c}-P_{\sigma_o})+(\gamma_{\sigma_c}-\gamma_{\sigma_o})$$
$$-g_{x_o\sigma_c}+g_{x_o\sigma_o}-\tfrac{3}{2}K_{\sigma_cx_o}+\tfrac{3}{2}K_{\sigma_ox_o}+Q_\pi{}^{n\sigma}(g_{\pi_c\sigma_c}-g_{\pi_o\sigma_c}-g_{\pi_c\sigma_o}+g_{\pi_o\sigma_o})]$$

$(\Pi)'$ Structure

Starting functions and matrix elements leading to $B_k{}^{n\sigma}$:

$$\Pi_1=|\,1\bar{1}\,| \qquad H_{11}=0 \qquad H_{12}=(H_{12}{}^{n\sigma})^{\pi}$$

$$\Pi_2=(1/2)^{\frac{1}{2}}[|\,1\bar{2}\,|+|\,2\bar{1}\,|] \qquad H_{22}=-2\beta_\pi{}^{\lambda}+K_{12}{}^{\pi} \qquad H_{13}=K_{12}{}^{\pi}$$

$$\Pi_3=|\,2\bar{2}\,| \qquad H_{33}=-4\beta_\pi{}^{\lambda} \qquad H_{23}=H_{12}$$

$$(H_{12}{}^{n\sigma})^{\pi}=[1/2(1-S_\pi{}^2)]^{\frac{1}{2}}[(\omega_{\pi_c}{}^{+1}-\omega_{\pi_o}{}^{+1})+(P_{\pi_c}-P_{\pi_o})+\tfrac{1}{2}(\gamma_{\pi_c}-\gamma_{\pi_o})$$
$$+\tfrac{1}{2}(g_{\sigma_c\pi_c}+g_{\sigma_o\pi_c}-g_{\sigma_c\pi_o}-g_{\sigma_o\pi_o})-(g_{x_o\pi_c}-g_{x_o\pi_o})+Q_\sigma{}^{n\sigma}(g_{\sigma_c\pi_c}-g_{\sigma_o\pi_c}-g_{\sigma_c\pi_o}+g_{\sigma_o\pi_o})]$$

Sigma-pi interaction operators

$$(G_{\sigma x}{}^{n\sigma}(1)\,|=\tfrac{3}{2}[g_{\sigma_c}(1)+g_{\sigma_o}(1)]+Q_\sigma{}^{n\sigma}[g_{\sigma_c}(1)-g_{\sigma_o}(1)]+g_{x_o}(1)$$

$$(G_\pi{}^{n\sigma}(1)\,|=[g_{\pi_c}(1)+g_{\pi_o}(1)]+Q_\pi{}^{n\sigma}[g_{\pi_c}(1)-g_{\pi_o}(1)]$$

$$Q_\sigma{}^{n\sigma}=-[1/(1-S_\sigma{}^2)]^{\frac{1}{2}}A_5{}^{n\sigma}A_6{}^{n\sigma}$$

$$Q_\pi{}^{n\sigma}=[2/(1-S_\pi{}^2)]^{\frac{1}{2}}B_2{}^{n\sigma}(B_1{}^{n\sigma}+B_3{}^{n\sigma})$$

$n\rightarrow\sigma^*$ Transition energy

$$E[\Omega(n\rightarrow\sigma^*)]-E[\Omega_N]=(\delta_1{}^N)^{\sigma}-(\delta_5)^{n\sigma}+\tfrac{1}{2}(\omega_{\sigma_c}{}^{+1}+\omega_{\sigma_o}{}^{+1})+\tfrac{1}{2}(P_{\sigma_c}+P_{\sigma_o})-\omega_{x_o}{}^{+1}-P_{x_\sigma}-(1+S_\sigma)\beta_\sigma{}^{\lambda}+\tfrac{1}{2}K_{\sigma_c\sigma_o}$$
$$+\tfrac{1}{2}\gamma_{\sigma_c}+\tfrac{1}{2}\gamma_{\sigma_o}-K_{12}{}^{\sigma}-\tfrac{1}{2}g_{\sigma_cx_o}-\tfrac{1}{2}g_{\sigma_ox_o}+\tfrac{3}{4}K_{\sigma_cx_o}+\tfrac{3}{4}K_{\sigma_ox_o}+[(B_2{}^{n\sigma})^2-(B_2{}^N)^2][-2\beta_\pi{}^{\lambda}+K_{12}{}^{\pi}]$$
$$+[(B_3{}^{n\sigma})^2-(B_3{}^N)^2][-4\beta_\pi{}^{\lambda}]+2(B_1{}^{n\sigma}B_3{}^{n\sigma}-B_1{}^NB_3{}^N)[K_{12}{}^{\pi}]-Q_\pi{}^N[(\omega_{\pi_c}{}^{+1}-\omega_{\pi_o}{}^{+})+(P_{\pi_c}-P_{\pi_o})$$
$$+\tfrac{1}{2}(\gamma_{\pi_c}-\gamma_{\pi_o})+Q_\pi{}^{n\sigma}[(\omega_{\pi_c}{}^{+1}-\omega_{\pi_o}{}^{+1})+(P_{\pi_c}-P_{\pi_o})+\tfrac{1}{2}(\gamma_{\pi_c}-\gamma_{\pi_o})-(g_{\pi_cx_o}-g_{\pi_ox_o})]$$
$$+\tfrac{1}{2}(g_{\pi_c\sigma_c}-g_{\pi_o\sigma_c}-g_{\pi_c\sigma_o}+g_{\pi_o\sigma_o})]$$

Then

$$\int\pi_c(1)[T(1)+C^{+2}(1)]\pi_c(1)\,dv_1=\omega_{\pi_c}{}^{+1}-g_{\pi_c\sigma_c},$$

which *defines* $\omega_{\pi_c}{}^{+1}$, a valence-state orbital energy. For use in $\alpha_{\pi_o}{}^{+4}$, however, one writes instead

$$C^{+2}(1)=C^0(1)-g_{\sigma_c}(1)-g_{\pi_c}(1),$$

and then

$$\int\pi_o(1)[C^{+2}(1)+2H^0(1)]\pi_0(1)\,dv_1=P_{\pi_o}-g_{\sigma_c\pi_o}-g_{\pi_c\pi_o},$$

which defines P_{π_o}, a "penetration" integral. Combination of these with similar quantities obtained from $O^{+2}(1)$ gives $(H_{12}{}^N)^{\pi}$ of Table II. The polarity of the (Π) function is proportional to $B_2{}^N$, which depends on $(H_{12}{}^N)^{\pi}$, the effect of the (Σ) polarity on the (Π) polarity is manifest in the appearance of $Q_\sigma{}^N$ in $(H_{12}{}^N)^{\pi}$.

The matrix elements for the (Σ) calculation, which leads to a $Q_\sigma{}^N$ value, involve considerations similar to the foregoing. In $(H_{12}{}^N)^{\sigma}$, the effect of the (Π) polarity on the (Σ) polarity is manifest in the appearance of the quantity $Q_\pi{}^N$. The sigma-pi interaction operators are $G_\pi{}^N(1)$ and $G_\sigma{}^N(1)$ [the $G_I(1)$ of Eqs. (49) and (58) of reference 1]; $G_\pi{}^N(1)$ expresses the effect of pi electrons as part of the core, in the (Σ) problem; and $G_\sigma{}^N(1)$ similarly enters the (Π) problem.

TABLE VIII. Formulas for the $[(\Sigma^+)(\Pi)'']$ separation of the state $\Omega(\sigma^+)$.

(Σ^+) Structure[a]

Starting functions and matrix elements leading to $(\delta_1{}^{\sigma+})^\sigma$ and $A_k{}^{\sigma+}$:

$$\Sigma_1 = |\, n\bar{n}1\,| \qquad H_{11}=0$$

$$\Sigma_2 = |\, n\bar{n}2\,| \qquad H_{22}=-2\beta_\sigma{}^\lambda$$

$$(H_{12}{}^{\sigma+})^\sigma=[1/4(1-S_\sigma{}^2)]^{\frac{1}{2}}[(\omega_{\sigma_c}{}^{+1}-\omega_{\sigma_o}{}^{+1})+(P_{\sigma_c}-P_{\sigma_o})+Q_\pi{}^{\sigma+}(g_{\pi_c\sigma_c}-g_{\pi_o\sigma_c}-g_{\pi_c\sigma_o}+g_{\pi_o\sigma_o})]$$

$(\Pi)''$ Structure

Starting functions and matrix elements leading to $B_k{}^{\sigma+}$:

$$\Pi_1 = |\, 1\bar{1}\,| \qquad H_{11}=0 \qquad H_{12}=(H_{12}{}^{\sigma+})^\pi$$

$$\Pi_2 = (1/2)^{\frac{1}{2}}[|\, 1\bar{2}\,| + |\, 2\bar{1}\,|] \qquad H_{22}=-2\beta_\pi{}^\lambda+K_{12}{}^\pi \qquad H_{13}=K_{12}{}^\pi$$

$$\Pi_3 = |\, 2\bar{2}\,| \qquad H_{33}=-4\beta_\pi{}^\lambda \qquad H_{23}=H_{12}$$

$$(H_{12}{}^{\sigma+})^\pi=[1/2(1-S_\pi{}^2)]^{\frac{1}{2}}[(\omega_{\pi_c}{}^{+1}-\omega_{\pi_o}{}^{+1})+(P_{\pi_c}-P_{\pi_o})+\tfrac{1}{2}(\gamma_{\pi_c}-\gamma_{\pi_o})-\tfrac{1}{2}g_{\sigma_c\pi_c}-\tfrac{1}{2}g_{\sigma_o\pi_c}$$
$$+\tfrac{1}{2}g_{\sigma_c\pi_o}+\tfrac{1}{2}g_{\sigma_o\pi_o}+Q_\sigma{}^{\sigma+}(\tfrac{1}{2}g_{\sigma_c\pi_c}-\tfrac{1}{2}g_{\sigma_o\pi_c}-\tfrac{1}{2}g_{\sigma_c\pi_o}+\tfrac{1}{2}g_{\sigma_o\pi_o})]$$

Sigma-pi interaction operators

$$(G_{\sigma z}{}^{\sigma+}(1)\,| = \tfrac{1}{2}\{[g_{\sigma_c}(1)+g_{\sigma_o}(1)]+Q_\sigma{}^{\sigma+}[g_{\sigma_c}(1)-g_{\sigma_o}(1)]\}+2g_{z_o}(1)$$

$$(G_z{}^{\sigma+}(1)\,| = [g_{\pi_c}(1)+g_{\pi_o}(1)]+Q_\pi{}^{\sigma+}[g_{\pi_c}(1)-g_{\pi_o}(1)]$$

$$Q_\sigma{}^{\sigma+}=[4/(1-S_\sigma{}^2)]^{\frac{1}{2}}A_1{}^{\sigma+}A_3{}^{\sigma+}$$

$$Q_\pi{}^{\sigma+}=[2/(1-S_\pi{}^2)]^{\frac{1}{2}}B_2{}^{\sigma+}(B_1{}^{\sigma+}+B_3{}^{\sigma+})$$

Sigma ionization potential

$$E[\Omega(\sigma^+)]-E[\Omega_N]=(\delta_1{}^N)^\sigma-(\delta_1{}^{\sigma+})^\sigma-(1-S_\sigma)\beta_\sigma{}^\lambda-\tfrac{1}{2}(\omega_{\sigma_c}{}^{+1}+\omega_{\sigma_o}{}^{+1})$$
$$-\tfrac{1}{2}(P_{\sigma_c}+P_{\sigma_o})-\tfrac{1}{4}\gamma_{\sigma_c}-\tfrac{1}{4}\gamma_{\sigma_o}+\tfrac{1}{2}\gamma_{\sigma_c\sigma_o}-\tfrac{1}{2}K_{\sigma_c\sigma_o}+Q_\pi{}^{\sigma+}[(\omega_{\pi_c}{}^{+1}-\omega_{\pi_o}{}^{+1})$$
$$+(P_{\pi_c}-P_{\pi_o})+\tfrac{1}{2}(\gamma_{\pi_c}-\gamma_{\pi_o})-\tfrac{1}{2}(g_{\pi_c\sigma_c}-g_{\pi_o\sigma_c}+g_{\pi_c\sigma_o}-g_{\pi_o\sigma_o})]$$
$$-Q_\pi{}^N[(\omega_{\pi_c}{}^{+1}-\omega_{\pi_o}{}^{+1})+(P_{\pi_c}-P_{\pi_o})+\tfrac{1}{2}(\gamma_{\pi_c}-\gamma_{\pi_o})]+[(B_2{}^{\sigma+})^2-(B_2{}^N)^2][-2\beta_\pi{}^\lambda+K_{12}{}^\pi]$$
$$+[(B_3{}^{\sigma+})^2-(B_3{}^N)^2][-4\beta_\pi{}^\lambda]+2(B_1{}^{\sigma+}B_3{}^{\sigma+}-B_1{}^NB_3{}^N)[K_{12}{}^\pi]+(B_4{}^{\sigma+})^2[-2\beta_\pi{}^\lambda-K_{12}{}^\pi]$$
$$+[1/(1-S_\pi{}^2)]^{\frac{1}{2}}B_1{}^{\sigma+}(B_1{}^{\sigma+}-B_3{}^{\sigma+})\{\tfrac{1}{2}[K_{\sigma_c\pi_c}+K_{\sigma_o\pi_c}-K_{\sigma_c\pi_o}-K_{\sigma_o\pi_o}]$$
$$-[1/(1-S_\sigma{}^2)]^{\frac{1}{2}}A_1{}^{\sigma+}A_3{}^{\sigma+}[K_{\sigma_c\pi_c}-K_{\sigma_o\pi_c}-K_{\sigma_c\pi_o}+K_{\sigma_o\pi_o}]\}$$

[a] Neglect of interaction with configurations differing from Σ_1 and Σ_2 by a double orbital interchange makes the (apparently) $[(\Sigma^+N)(\Pi)]$ treatment equivalent to a $[(\Sigma^+)(N)(\Pi)]$ treatment.

The lone-pair electrons do not appear explicitly in Table II, because they have been included in the core for the Ω_N calculation. This differs from a four-electron (ΠN) problem involving interaction among $(\Pi N)_1 = |\, 1\bar{1}n\bar{n}\,|$, $(\Pi N)_2 = 2^{-\frac{1}{2}}[|\, 1\bar{2}n\bar{n}\,| + |\, 2\bar{1}n\bar{n}|]$, $(\Pi N)_3 = |\, 2\bar{2}n\bar{n}\,|$, $(\Pi N)_4 = |\, 1\bar{1}2\bar{2}\,|$, through neglect of the doubly excited configuration $(\Pi N)_4$, which has no electrons in the lone-pair MO, n.

The total energy of Ω_N is decomposed as

$$E[\Omega_N]=E_{\text{core}}{}^{+4}+[E_{\pi-\text{core}}{}^{+4}+E_{\pi\pi}+E_{\sigma\pi}]$$
$$+[E_{\sigma-\text{core}}{}^{+4}+E_{\sigma\sigma}],$$

or

$$E[\Omega_N]=E_{\text{core}}{}^{+4}+\Sigma_k\Sigma_l B_k{}^NB_l{}^N(H_{kl}{}^N)_{+2}{}^\pi$$
$$+\Sigma_k\Sigma_l A_k{}^NA_l{}^N(H_{kl})_{+4}{}^\sigma.$$

TABLE IX. Formulas for the $[(\Sigma)^V\,{}^3(\Pi N^*)]$ separation of the state ${}^3\Omega(n\rightarrow\pi^*)$.

${}^3(\Pi N)^*$ Structure

Starting functions and matrix elements leading to ${}^3\delta_5{}^{n\pi}$ and ${}^3B_k{}^{n\pi}$:

$${}^3(\Pi N)_5=(1/2)^{\frac{1}{2}}[\,|\,1\bar{1}2\bar{n}\,|\,-\,|\,1\bar{1}n\bar{2}\,|\,] \qquad H_{55}=0$$

$${}^3(\Pi N)_6=(1/2)^{\frac{1}{2}}[\,|\,2\bar{2}1\bar{n}\,|\,-\,|\,2\bar{2}n\bar{1}\,|\,] \qquad H_{66}=-2\beta_\pi{}^\lambda$$

$${}^3(H_{56}{}^{n\pi})=-[1/4(1-S_\pi{}^2)]^{\frac{1}{2}}[(\omega_{\pi_c}{}^{+1}-\omega_{\pi_o}{}^{+1})+(P_{\pi_c}-P_{\pi_o})+(\gamma_{\pi_c}-\gamma_{\pi_o})-g_{x_o\pi_c}+g_{x_o\pi_o}+\tfrac{1}{2}K_{\pi_c x_o}-\tfrac{1}{2}K_{\pi_o x_o}$$
$$+{}^3Q_\sigma{}^{n\pi}(g_{\sigma_c\pi_c}-g_{\sigma_o\pi_c}-g_{\sigma_c\pi_o}+g_{\sigma_o\pi_o})]$$

$(\Sigma)^V$ Structure

Starting functions and matrix elements leading to ${}^3A_k{}^{n\pi}$:

$$\Sigma_1=|\,1\bar{1}\,| \qquad H_{11}=0 \qquad H_{12}={}^3(H_{12}{}^{n\pi})^\sigma$$

$$\Sigma_2=(1/2)^{\frac{1}{2}}[\,|\,1\bar{2}\,|\,+\,|\,2\bar{1}\,|\,] \qquad H_{22}=-2\beta\sigma^\lambda+K_{12}{}^\sigma \qquad H_{13}=K_{12}{}^\sigma$$

$$\Sigma_3=|\,2\bar{2}\,| \qquad H_{33}=-4\beta_\sigma{}^\lambda \qquad H_{23}=H_{12}$$

$${}^3(H_{12}{}^{n\pi})^\sigma=[1/2(1-S_\sigma{}^2)]^{\frac{1}{2}}[(\omega_{\sigma_c}{}^{+1}-\omega_{\sigma_o}{}^{+1})+(P_{\sigma_c}-P_{\sigma_o})+\tfrac{1}{2}(\gamma_{\sigma_c}-\gamma_{\sigma_o})$$
$$+\tfrac{1}{2}(g_{\pi_c\sigma_c}+g_{\pi_o\sigma_c}-g_{\pi_c\sigma_o}-g_{\pi_o\sigma_o})-(g_{x_o\sigma_c}-g_{x_o\sigma_o})+{}^3Q_\pi{}^{n\pi}(g_{\pi_c\sigma_c}-g_{\pi_o\sigma_c}-g_{\pi_c\sigma_o}+g_{\pi_o\sigma_o})]$$

Sigma-pi interaction operators

$${}^3(G_{\pi x}{}^{n\pi}(1)\,|\,=\tfrac{3}{2}[g_{\pi_c}(1)+g_{\pi_o}(1)]+{}^3Q_\pi{}^{n\pi}[g_{\pi_c}(1)-g_{\pi_o}(1)]+g_{x_o}(1)$$

$${}^3(G_\sigma{}^{n\pi}(1)\,|\,=[g_{\sigma_c}(1)+g_{\sigma_o}(1)]+{}^3Q_\sigma{}^{n\pi}[g_{\sigma_c}(1)-g_{\sigma_o}(1)]$$

$${}^3Q_\pi{}^{n\pi}=-[1/(1-S_\pi{}^2)]^{\frac{1}{2}}{}^3B_5{}^{n\pi}\,{}^3B_6{}^{n\pi}$$

$${}^3Q_\sigma{}^{n\pi}=[2/(1-S_\sigma{}^2)]^{\frac{1}{2}}\,{}^3A_2{}^{n\pi}({}^3A_1{}^{n\pi}+{}^3A_3{}^{n\pi})$$

Triplet $n\rightarrow\pi^*$ transition energy

$$E[{}^3\Omega(n\rightarrow\pi^*)]-E[\Omega_N]=(\delta_1{}^N)^\pi-{}^3(\delta_5)^{n\pi}-(1+S_\pi)\beta_\pi{}^\lambda+\tfrac{1}{2}(\omega_{\pi_c}{}^{+1}+\omega_{\pi_o}{}^{+1})$$
$$+\tfrac{1}{2}(P_{\pi_c}+P_{\pi_o})-\omega_{x_o}{}^{+1}-P_{x_o}+\tfrac{1}{2}K_{\pi_c\pi_o}+\tfrac{1}{2}\gamma_{\pi_c}+\tfrac{1}{2}\gamma_{\pi_o}-K_{12}{}^\pi-\tfrac{1}{2}\gamma_{\pi_c x_o}-\tfrac{1}{2}\gamma_{\pi_o x_o}$$
$$+{}^3Q_\sigma{}^{n\pi}[(\omega_{\sigma_c}{}^{+1}-\omega_{\sigma_o}{}^{+1})+(P_{\sigma_c}-P_{\sigma_o})+\tfrac{1}{2}(\gamma_{\sigma_c}-\gamma_{\sigma_o})+\tfrac{1}{2}(g_{\sigma_c\pi_c}-g_{\sigma_o\pi_c}+g_{\sigma_c\pi_o}-g_{\sigma_o\pi_o})-(g_{\sigma_c x_o}-g_{\sigma_o x_o})]$$
$$-Q_\sigma{}^N[(\omega_{\sigma_c}{}^{+1}-\omega_{\sigma_o}{}^{+1})+(P_{\sigma_c}-P_{\sigma_o})+\tfrac{1}{2}(\gamma_{\sigma_c}-\gamma_{\sigma_o})]+[{}^3(A_2{}^{n\pi})^2-(A_2{}^N)^2][-2\beta\sigma^\lambda+K_{12}{}^\sigma]$$
$$+[{}^3(A_3{}^{n\pi})^2-(A_3{}^N)^2][-4\beta\sigma^\lambda]+2({}^3A_1{}^{n\pi}\,{}^3A_3{}^{n\pi}-A_1{}^NA_3{}^N)[K_{12}{}^\sigma]$$

The $A_k{}^N$ and $B_k{}^N$ are found in problems involving $(H_{kl}{}^N)_{+2}{}^\pi$ and $(H_{kl}{}^N)_{+2}{}^\sigma$. In the $E[\Omega_N]$ expression, $(H_{kl}{}^N)_{+2}{}^\pi$ and $(H_{kl})_{+4}{}^\sigma$ are referred to $E_{\text{core}}{}^{+4}$, and in addition to the possible energy zero difference, $(H_{kl})_{+4}{}^\sigma$ differs from $(H_{kl}{}^N)_{+2}{}^\sigma$ in not containing the sigma-pi repulsion. In the expression given in Table II the sigma-pi repulsion is included through, e.g., $(\alpha_{\pi_c}{}^{+2})^N=\alpha_{\pi_c}{}^{+4}+(G_\sigma{}^N\,|\,\pi_c{}^2)$ of $(H_{11}{}^N)^\pi$, where

$$(G_\sigma{}^N\,|\,\pi_c{}^2)=\int\pi_c(1)G_\sigma{}^N(1)\pi_c(1)\,dv_1.$$

$J_{11}{}^\pi$ is $\frac{1}{4}[\gamma_{\pi_c}+\gamma_{\pi_o}+2\gamma_{\pi_o\pi_o}]$ of $(H_{11}{}^N)^\pi$, and $A_1{}^NA_2{}^N$, $A_2{}^NA_3{}^N$ are combined in the sigma bond polarity parameter $Q_\sigma{}^N$.

The formulas for the $[(\Sigma)^N(\Pi)^*]$ separation of $\Omega(\pi\rightarrow\pi^*)$ in Table III are very similar to those for Ω_N, except that the secular equations show the effect of constraining the $(\Pi)^*$ structure to be orthogonal to the (Π) structure of Ω_N. This orthogonality is not automatic because the core Hamiltonians are not the same, the one for $(\Pi)^*$ containing $Q_\sigma{}^V$ while the one for (Π) contains $Q_\sigma{}^N$. The Lagrange multiplier η, involved in the constraint, turns out to be E_2, the energy of the $(\Pi)^*$ structure relative to $(H_{11}{}^V)^\pi$. The $(\Pi)^*-(\Pi)$ energy difference is given in the $\pi\rightarrow\pi^*$ transition energy expression; it is $E_2+(\delta_1{}^N)^\pi$ plus a number of terms expressing the sigma-pi repulsion energy difference.

In Table IV the $(\Pi N)^*$ part of the state $\Omega(n\rightarrow\pi^*)$ must of course be treated as a four electron problem. A point of interest is the form of the operator $G_{\pi\pi}{}^{n\pi}(1)$ used in the $(\Sigma)'$ problem; it reflects the fact that there are three electrons in the (Π) system and one in the lone-pair system to interact with the sigma electrons. The MO n is the lone-pair AO x_0.

Formulas in Table V have been obtained taking into account the sigma-bond *spin-polarization* due to odd-electron sigma-pi interaction in $\Omega(n^+)$. The usual *lack* of mixing of the $s_z=0$ component of the triplet (Σ) structure, $\Sigma_T=2^{-\frac{1}{2}}[|\,12\,|-|\,2\bar{1}\,|]$, with the singlet configurations is due to the fact that for, e.g., $\Sigma_1=|\,1\bar{1}\,|$ with $H_{1T}=2^{-\frac{1}{2}}[\bar{I}_{12}-I_{12}]$, it is often true that $\bar{I}_{12}=I_{12}$, where $\bar{I}_{ij}$ is a core matrix element—see reference (1), Eq. (51)—over molecular spin orbitals with β spin, I_{ij}, the same over MSOs with α spin. In the $\Omega(n^+)$ case, however, the odd electron character of the (ΠN^+) structure causes the α electron in the Σ bond to experience a different amount of exchange repulsion than the β electron, with the result that in

$$H_{1T}=2^{-\frac{1}{2}}\int\phi_1(1)[G_{\pi\pi}{}^{n+}(1)^{\alpha}-G_{\pi\pi}{}^{n+}(1)^{\beta}]\phi_2(1)\,dv_1$$

the *spin-free* operator giving the difference of the effect of (ΠN^+) electrons on α and β electrons is

$$G_{\pi\pi}{}^{n+}(1)^{\alpha}-G_{\pi\pi}{}^{n+}(1)^{\beta}=[\tfrac{1}{3}(B_3{}^{n+})^2-1]K_n(1),$$

where

$$\int\chi_a(1)K_n(1)\chi_c(1)\,dv_1=K_{an}$$

and $B_3{}^{n+}$ is a coefficient appearing in

$$(\Pi N^+)=B_1\,|\,1\bar{1}n\,|+(2^{-\frac{1}{2}}B_2+6^{-\frac{1}{2}}B_3)\,|\,2\bar{1}n\,|$$
$$+(2^{-\frac{1}{2}}B_2-6^{-\frac{1}{2}}B_3)\,|\,1\bar{2}n\,|-(\tfrac{2}{3})^{\frac{1}{2}}B_3\,|\,1\bar{n}2\,|+B_4\,|\,2\bar{2}n\,|.$$

The source of the α, β nonequivalence can be demonstrated by considering the diagonal contribution of the first term $B_1\,|\,1\bar{1}n\,|$ to the *spin-containing* operator corresponding to $G_I(1)$ of Eq. (44) of reference 1. This is $B_1{}^2[2J_1(1)+J_n(1)-(K_1(1)+K_n(1))-\bar{K}_1(1)]$. The coulomb operators $J_i(1)$ are indifferent to the spin of the orbital they act upon, but not so the exchange operators $K_i(1)$ and $\bar{K}_i(1)$. Of the latter, only $K_1(1)$ and $K_n(1)$ survive integration over spin coordinates in I_{ij}, while in $\bar{I}_{ij}$ only $\bar{K}_1(1)$ survives. The spin-free operators $G_{\pi\pi}{}^{n+}(1)^{\alpha}$ and $G_{\pi\pi}{}^{n+}(1)^{\beta}$ are obtained from the spin-containing operators by striking out terms which will not survive spin integration in, respectively, I_{ij} and $\bar{I}_{ij}$.

The formulas given in Table V ignore the fact that the nonsinglet character of the sigma structure caused by the singlet-triplet mixing will tend to mix a quartet (ΠN^+) structure (not given in Table V) with the doublet (ΠN^+) structure. Also, the iteration is supposed carried out using only the singlet (Σ) configuration, with the spin-polarization appended after the iteration is completed. Under the generalized Mulliken approximation of Eq. (56) of reference 1, the contribution of the spin-polarization energy-lowering to the lone-pair ionization potential is the term involving $A_4{}^{n+}(=A_T)$, the coefficient of Σ_T in $(\Sigma)'''$.

The formulas in Table VI for the $(\Sigma)^{IV}(\Pi^+N)$ separation of $\Omega(\pi^+)$ involve considerations similar to those in Table V, and there appear therein a quantity Q_t which is the charge transferred from the lone-pair to the pi system. The formulas of Table VII for $(\Sigma N)^*$ of $\Omega(n\rightarrow\sigma^*)$ may be obtained from those for $(\Pi N)^*$ of Table IV by the transformation $\pi\leftrightarrow\sigma$; the formulas of Table VIII for (Σ^+) of $\Omega(\sigma^+)$ can be obtained similarly from those for (Π^+N) of Table VI—with neglect, however, of interaction with $(\Pi^+N)_2$ and $(\Pi^+N)_4$, thus the lone-pair electrons being treated as part of the core. Comparison of ${}^T(H_{56}{}^{n\pi})$ in Table IX for ${}^3\Omega(n\rightarrow\pi^*)$, with $H_{56}{}^{n\pi}$ of Table VI for ${}^1\Omega(n\rightarrow\pi^*)$ shows that

$${}^T(H_{56}{}^{n\pi})-(H_{56}{}^{n\pi})=-[K_{\pi_c x_0}-K_{\pi_0 x_0}]/(1-S_\pi{}^2)^{\frac{1}{2}}.$$

This difference leads to different $Q_\pi{}^{n\pi}$ values for the singlet and triplet cases, with consequent differences in the *sigma structure* even though the form of ${}^3G_{\pi\pi}{}^{n\pi}(1)$ is the same as that of ${}^1G_{\pi\pi}{}^{n\pi}(1)$. There will, however, be no sigma spin polarization.

III. CHARACTERIZATION OF ACTUAL CALCULATIONS: QUESTION OF REPULSION INTEGRALS

Figure 1 gives the steps (discussed in Appendix A) which lead to the empirical parameter values of Table XIII (Sec. IV) and the energy predictions in Table XII (Sec. IV), under several alternative sets of subsidiary assumptions, each set of which characterizes an individual calculation. Circumstances leading to these subsidiary assumptions will now be discussed.

In the tables there are results for three values of the quantity $I_{\sigma\pi}$, which is the following combination of the one and two-center coulomb repulsion integrals between sigma and pi atomic orbitals:

$$I_{\sigma\pi}=(g_{\pi_c\sigma_c}-g_{\pi_0\sigma_c}-g_{\pi_c\sigma_0}+g_{\pi_0\sigma_0}).$$

The sign and magnitude of $I_{\sigma\pi}$ controls the direction and magnitude of the reorganization effects following excitation, as will be discussed in some detail in Sec. V. The question of what values actually should be chosen for these sigma-pi one- and two-center integrals (and for the pi–pi and sigma–sigma one- and two-center integrals) is not easily settled.

Let us first consider the one-center integrals. At the outset of these calculations it was thought that the best procedure for them would be to follow Pariser,[7] and obtain empirical values from ionic and atomic spectroscopic data. Such values for one-center integrals were used in all calculations reported here. Formulas involved in obtaining these integrals are given in Appendix B. The effects of ambiguities in the process of obtaining empirical values of one-center quantities

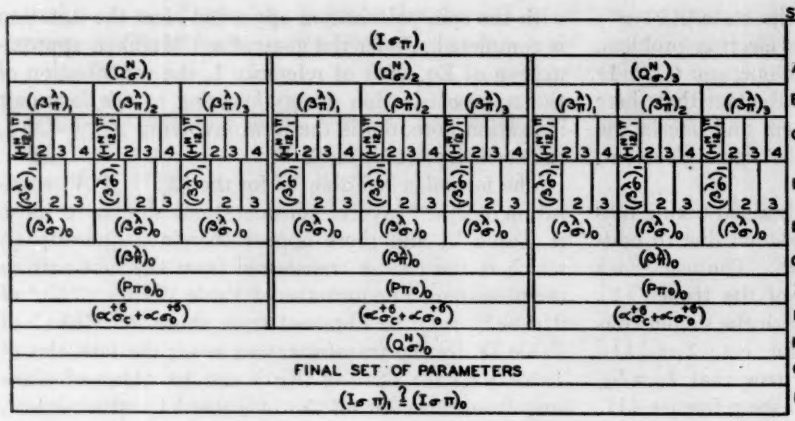

FIG. 2. Evolution of a set of compatible parameters.

TABLE X. Values of one-center parameters for the six-electron $H_2C=O$ problem.[a]

Carbon		Oxygen	
Parameter	Value (ev)	Parameter	Value (ev)
ω_{π_C}	-11.42	$\omega_{\pi_O}=\omega_{\sigma_O}$	-17.32
ω_{σ_C}	-14.68 ± 0.1	ω_{x_O}	-15.06
γ_{π_C}	10.842	$\gamma_{\pi_O}=\gamma_{\sigma_O}=\gamma_{x_O}$	14.671
γ_{σ_C}	11.217 ± 0.1	$\gamma_{\pi_O\sigma_O}=\gamma_{\pi_Ox_O}=\gamma_{\sigma_Ox_O}$	12.865
$\gamma_{\sigma_C\pi_C}$	10.164	$K_{\pi_O\sigma_O}=K_{\pi_Ox_O}=K_{\sigma_Ox_O}$	0.903
$K_{\sigma_C\pi_C}$	1.231		

[a] See Section II for definition of parameters.

from atomic spectroscopic data, emphasized by Mulliken,[10] were minimized by choosing integral values which reproduced closely the energies of the appropriate valence states, such energies being determined by Moffitt's procedure.[11] Hybridized valence state energies did not always fall into the simple class considered by Moffitt, and procedures similar to those given by Companion and Ellison[12] were worked out for these.[13] The resulting one-center parameter values are given in Table X.

Three different sets of two-center integrals were used in the calculations, as given in Table XI. (This is what leads to the three $I_{\sigma\pi}$ values mentioned in the foregoing). The "theoretical" values of Table XI were tried because use of them makes our method correspond in a certain sense[13] to Moffitt's atoms in molecules procedure—the variant in which $\frac{1}{2}(\bar{V}+\bar{V}\dagger)$ is *not* approximated by $[\langle H\rangle-\frac{1}{2}(\bar{M}\bar{W}+\bar{W}\bar{M})]$ but is calculated correctly by means of the "interaction operator."[14] However, the "theoretical" values are not the obviously correct choice to use with Pariser-type one-center integrals. This can be inferred from the fact that a two-center repulsion integral which is lower by 2 ev than the "theoretical" value appears in the set of integrals which Pariser and Parr[5] used to account for the benzene spectrum, and with which Pariser[15] successfully predicted a large number of transition energies for the polyacenes. Also, it has been found in the present work [calculation (1) of Table XII] that use of the "theoretical" integrals lead to extremely anomalous "charge-following" during the sigma-pi iterative process.

It was accordingly surmised that some sort of "correlation correction"[16] leading to lower values of two-center repulsions, was needed, and this correction was arbitrarily, but reasonably, taken to be an overlap integral times the mean of the empirical corrections to the corresponding "theoretical" *one*-center repulsion integrals. The set of integrals so obtained is the "cor-

[10] R. S. Mulliken, J. Chem. Phys. **2**, 782 (1934).
[11] W. Moffitt, Repts. Progr. Phys. **17**, 173 (1954).
[12] A. Companion and F. O. Ellison, J. Chem. Phys. **28**, 1 (1958).
[13] J. M. Parks (Ph.D. thesis, Carnegie Institute of Technology, 1956).
[14] W. Moffitt, Proc. Roy. Soc. (London) **A210**, 224 (1954).
[15] R. Pariser, J. Chem. Phys. **25**, 1112 (1956).
[16] The term "correlation" is only loosely applied here, since the "theoretical" integrals are not calculated with Hartree-Fock orbitals. The correction thus attempts to compensate both for the use of nonoptimum Z's in the molecular calculation, and for correlation effects.

related" set of Table XI; with this set the "charge-following" anomaly disappeared in most instances and good agreement was obtained for the pi ionization potential [calculation (2) of Table XII]. But, contrary to expectation, the "correlated" integrals led to a repulsive (positive) value for the empirical "penetration" integral, P_{π_0}. (P_{π_0} is the interaction of an electron in the oxygen π orbital with the carbon atom in a neutral valence state.) The "super-correlated" set of integrals in Table XI represents an attempt to remedy this situation by changing the value of what was thought to be the most crucial two-center integral by an amount sufficient to give $I_{\sigma\pi}$ the same magnitude as in the "theoretical" case, but the opposite sign. Although this final change was not successful in producing a negative value for the penetration integral, it will be seen in Sec. V that it did provide insight into the charge-following process.

In Appendix *D* are discussed possibilities for further modifications of the repulsion integrals.

IV. RESULTS

Table XII contains predictions of the pi bond ionization potential, $\Delta E(\pi^+)$; and the excitation energy to the $n\rightarrow\pi^*$ triplet state, $\Delta E^3(n\rightarrow\pi^*)$; also the corresponding experimental values. Table XIII contains sets of core parameters (See Sec. II and Appendix A) obtained by fitting the other experimental quantities in Table I. These core parameter values were used to obtain the predictions in Table XII, and were used also to determine the extent of the reorganization effects following excitation and ionization. The reorganization effects are displayed in Tables XIV–XX.

Besides the calculations (1), (2), (3) involving, respectively, the "theoretical," "correlated," and "super-correlated" repulsion integrals, and in which reorganization was included, there are contained in these tables results for simplified calculations (1′), (2′), (3′) which used the same repulsion integrals as above and the core parameters that were determined in calculations (1), (2), (3). However, in calculations (1′), (2′), (3′) no reorganization was considered.

Calculations (4) and (5) in the tables represent yet another set of simplified calculations in which reorganization is neglected. Both used "correlated" integrals. In calculation (4), squares of overlap integrals were neglected, and in calculation (5), first powers of overlaps were neglected, in comparison with unity. Further, in calculation (5) there was used a simplified formula for dipole moments, which neglects both overlaps and homopolar moments.

For both the complete and simplified calculations one can trace in Tables XIV–XX the changes in energy; the changes in pi bond polarity parameter Q_π;[17] and the changes in sigma bond polarity parameter Q_σ; which occur upon excitation, but before reorganization takes

[17] A negative Q_π value indicates more than one electron in π_0; see reference 1, discussion of Eq. (59), and similarly for Q_σ and σ_0.

TABLE XI. Sets of two-center repulsion integrals used in the present calculations.[a]

	$I_{\sigma\pi}=-3.937$ "theoretical" (1)	$I_{\sigma\pi}=1.5846$ "correlated" (2)	$I_{\sigma\pi}=3.937$ "super-correlated" (3)
$\gamma_{\pi_c\pi_o}$[b]	10.378	8.6356	0.6356
$\gamma_{\sigma_c\sigma_o}$	16.425	12.8317	12.8317
$\gamma_{\pi_c\sigma_o}$	11.039	8.2782	8.2782
$\gamma_{\pi_o\sigma_c}$	14.979	12.2182	9.8658
$\gamma_{\pi_o\sigma_c}$	10.135	8.6438	8.6348
$K_{\pi_c\sigma_o}$[c]	0.129	0.129	0.129
$K_{\pi_o\sigma_c}$	0.109	0.109	0.109
$K_{\pi_o\pi_c}$	0.038	0.038	0.038

[a] See text, Sec. III, for sources of these integrals. All values in ev.
[b] For example, $\gamma_{\pi_c\pi_o}=(\pi_c^2\mid\pi_o^2)$; $K_{\pi_c\pi_o}=(\pi_c\pi_o\mid\pi_o\pi_o)$.
[c] Mulliken and generalized Mulliken expansions were used to obtain exchange repulsions. See reference 1.

TABLE XII. Predictions and comparison with experiment.

Calculation[a]	$\Delta E(\pi^+)$	$\Delta E^3(n\rightarrow\pi^*)$
(1)	13.2034	3.4094
(2)	12.0385	3.9195
(3)	12.1778	3.9025
(4)	12.0659	3.8762
(5)	12.5100	3.9406
Experimental[b]	11.8	3.02

[a] See text, Sec. III and Sec. IV, for characterization of each calculation. All values are in ev.
[b] Table I contains the source of the data.

TABLE XIII. Core parameter sets.[a,b]

Calculation[c]	$\alpha_{\pi_c}{}^{+6}$	$\alpha_{\pi_o}{}^{+6}$	$\beta_\pi{}^\lambda$
(1)	−61.47689	−76.565322	−3.318754
(2)	−53.158804	−72.519707	−2.97545
(3)	−53.114674	−70.426222	−3.021432
(4)	−53.344795	−72.310570	−2.978389
(5)	−52.587839	−72.731943	−3.057806
Calculation	$\alpha_{\sigma_c}{}^{+6}$	$\alpha_{\sigma_o}{}^{+6}$	$\beta_\sigma{}^\lambda$
(1)	−81.360022	−76.34703	−3.192637
(2)	−70.010749	−71.562111	−4.03720
(3)	−62.624724	−71.723812	−3.252181
(4)	−69.081116	−70.548646	−3.32869
(5)	−67.961218	−68.905910	−2.848553

[a] The core parameters are discussed in Sec. II. All values are in ev.
[b] Results for $I_{\sigma\pi}=-3.937$ are given also in Table XXI, Appendix A. There it is noted that P_{π_o} has a positive value. This is also found to be true for $I_{\sigma\pi}=+1.5846$ and $I_{\sigma\pi}=+3.937$—see text for discussion.
[c] See text, Sections III and IV, for characterization of each calculation.

TABLE XIV. Reorganization effects following $n\rightarrow\pi^*$ excitation.[a,b]

Calculation[c]		Ω_N	$\{\Omega(n\rightarrow\pi^*)\}$[d]	$\Omega(n\rightarrow\pi^*)$[e]
(1),[f] (1′)	Energy	0 ev	4.8144 ev	4.2771 ev
	Q_π	−0.2099	−0.2524	−0.1218
	Q_σ	−0.0542	−0.0542	0.4729
(2), (2′)	Energy	0	4.2827	4.2560
	Q_π	−0.2545	−0.3754	−0.3712
	Q_σ	−0.0022	−0.0022	−0.0904
(3), (3′)	Energy	0	4.5464	4.29165
	Q_π	−0.2965	−0.3856	−0.3504
	Q_σ	0.0489	0.0489	−0.2579
(4)	Energy	0	4.2650	
	Q_π	−0.2181	−0.3499	
	Q_σ	0.0032	0.0032	
(5)	Energy	0	4.2599	
	Q_π	−0.3240	−0.3815	
	Q_σ	−0.1335	0.1335	

[a] Details of the iteration leading to the figures in the final column are described in Appendix A, step E.
[b] Negative Q_σ means excess (more than one) sigma electrons on oxygen. Negative Q_π means excess pi electrons on oxygen. See reference 1, Eq. (59).
[c] See text, Secs. III and IV, for characterization of calculations.
[d] Results in this column are obtained using the same (Σ) structure as in Ω_N. They constitute "no-reorganization" values.
[e] Results in this column are those for mutual consistency of (Σ) and (ΠN)* structure, i.e., after reorganization.
[f] Iteration for this part of calculation (1) is illustrated in detail in Table XXI.

place. (Compare the second column with the first column.) For the complete calculations one can trace the further change in energy, pi polarity, and sigma polarity, which occurs when reorganization is considered. (Compare the third column with the second.)

TABLE XV. Reorganization effects following $\pi\rightarrow\pi^*$ excitation.[a,b]

Calculation[c]		Ω_N	$\{\Omega(\pi\rightarrow\pi^*)\}$[d]	$\Omega(\pi\rightarrow\pi^*)$[e]
(1), (1′)	Energy	0 ev	8.0037 ev	8.00 ev
	Q_π	−0.2099	−0.1931	−0.1180
	Q_σ	−0.0542	−0.0542	0.0836
(2), (2′)	Energy	0	8.0056	8.00
	Q_π	−0.2545	−0.4393	−0.4459
	Q_σ	−0.0022	−0.0022	0.0425
(3), (3′)	Energy	0	8.0264	8.00
	Q_π	−0.2965	−0.4360	−0.4717
	Q_σ	0.0489	0.0489	0.1724
(4)	Energy	0	8.000	
	Q_π	−0.2181	−0.3959	
	Q_σ	0.0032	0.0032	
(5)	Energy	0	8.0000	
	Q_π	−0.3240	−0.4014	
	Q_σ	0.1335	0.1335	

[a] Details of the iteration leading to the figures in the final column are described in Appendix A, step G.
[b] Negative Q_σ means excess (more than one) sigma electrons on oxygen. Negative Q_π means excess pi electrons on oxygen.
[c] See text, Secs. III and IV, for characterization of calculations.
[d] Results in this column are obtained using the same (Σ) structures as in Ω_N. They constitute "no-reorganization" values.
[e] Results in this column are those for mutal consistency of (Σ) and (Π) structures; i.e., after reorganization.

TABLE XVI. Reorganization effects following lone-pair ionization.[a,b]

Calculation[c]		Ω_N	$\{\Omega(n^+)\}$[d]	$\Omega(n^+)$[e]
(1), (1′)	Energy	0 ev	11.3995 ev	10.83 ev
	Q_π	−0.2099	−0.4435	−0.2310
	Q_σ	−0.0542	−0.0542	0.4871
(2), (2′)	Energy	0	10.8657	10.83
	Q_π	−0.2545	−0.5570	−0.5582
	Q_σ	−0.0022	−0.0022	0.0219
(3), (3′)	Energy	0	11.1139	10.83
	Q_π	−0.2965	−0.5661	−0.5213
	Q_σ	0.0489	0.0489	−0.2743
(4)	Energy	0	10.83	
	Q_π	−0.2181	−0.5306	
	Q_σ	0.0032	0.0032	
(5)	Energy	0	10.83	
	Q_π	−0.3240	−0.5532	
	Q_σ	0.1335	0.1335	

[a] Details of the iteration leading to the figures in the final column are described in Appendix A, step I.
[b] Negative Q_σ means excess (more than one) sigma electrons on oxygen. Negative Q_π means excess pi electrons on oxygen.
[c] See text, Secs. III and IV, for characterization of calculations.
[d] Results in this column are obtained using the same (Σ) structure as in Ω_N. They constitute "no-reorganization" values.
[e] Results in this column are those for mutual consistence of the (Σ) and (ΠN^+) structures; i.e., after reorganization.

Some of these polarity changes will be discussed in the next section.

V. DISCUSSION OF RESULTS: CRITERION OF REASONABLE CHARGE-FOLLOWING

The calculations imply that appreciable reorganization effects may accompany electron excitation or

TABLE XVII. Reorganization effects following $n\rightarrow\sigma^*$ excitation.[a]

Calculation[c]		Ω_N	$\{\Omega(n\rightarrow\sigma^*)\}$[d]	$\Omega(n\rightarrow\sigma^*)$[e]
(1), (1′)	Energy	0 ev	7.4077 ev	7.10 ev
	Q_π	−0.2099	−0.2099	0.0593
	Q_σ	−0.0542	0.2417	0.3069
(2), (2′)	Energy	0	7.2377	7.10
	Q_π	−0.2545	−0.2545	−0.2906
	Q_σ	−0.0022	0.0209	0.0157
(3), (3′)	Energy	0	7.1457	7.10
	Q_π	−0.2965	−0.2965	−0.3618
	Q_σ	0.0489	−0.1595	−0.1537
(4)	Energy	0	7.10	
	Q_π	−0.2181	−0.2181	
	Q_σ	0.0032	0.0250	
(5)	Energy	0	7.10	
	Q_π	−0.3240	−0.3240	
	Q_σ	0.1335	0.0946	

[a] Details of the iteration leading to the figures in the final column are described in Appendix A, step K.
[b] Negative Q_σ means excess (more than one) sigma electrons on oxygen. Negative Q_π means excess pi electrons on oxygen.
[c] See text, Secs. III and IV, for characterization of calculations.
[d] Results in this column are obtained using the same (II) structure as in Ω_N. They constitute "no-reorganization" values.
[e] Results in this column are those for mutual consistency of the (II) and (ΣN) structures; i.e., after reorganization.

ionization. Columns one and three of Tables XIV–XX show small reorganization effects on energies, but non-negligible effects on the sigma bond polarity parameters Q_σ.

In considering the results, we need to find out which set of two-center repulsion integrals (when used in conjunction with Pariser-type one-center repulsion integrals) leads to behavior which is physically the most reasonable. We shall see that it is safe to reject the "theoretical" integrals, but that to choose the better of the "correlated" and "super-correlated" integral sets is more difficult.

Table XII shows that the "theoretical" integrals give a very poor prediction of $\Delta E(\pi^+)$ and only a fair

TABLE XVIII. Reorganization effects following sigma ionization.[a,b]

Calculation[c]		Ω_N	$\{\Omega(\sigma^+)\}$[d]	$\Omega(\sigma^+)$[e]
	Energy	0 ev	13.8966 ev	13.10 ev
(1), (1′)	Q_π	−0.2099	−0.2099	−0.6010
	Q_σ	−0.0542	−0.3442	−0.2836
	Energy	0	13.5457	13.10
(2), (2′)	Q_π	−0.2545	−0.2545	−0.5372
	Q_σ	−0.0022	−0.2418	−0.0724
	Energy	0	13.2264	13.10
(3), (3′)	Q_π	−0.2965	−0.2965	−0.4405
	Q_σ	0.0489	−0.2616	−0.0947
	Energy	0	13.10	
(4)	Q_π	−0.2181	−0.2181	
	Q_σ	0.0032	−0.2459	
	Energy	0	13.10	
(5)	Q_π	−0.3240	−0.3240	
	Q_σ	0.1335	−0.1928	

[a] Details of the iteration leading to the figures in the final column are described in Appendix A, step M.
[b] Negative Q_σ means excess (more than one) sigma electrons on oxygen. Negative Q_π means excess pi electrons on oxygen.
[c] See text, Secs. III and IV, for characterization of calculations.
[d] Results in this column are obtained using the same (Π) structure as in Ω_N. They constitute "no-reorganization" values.
[e] Results in this column are those for mutual consistency of (Π) and (Σ^+) structures; i.e., after reorganization.

prediction of $\Delta E\ ^3(n\rightarrow\pi^*)$. The "correlated" integrals give quite a good $\Delta E(\pi^+)$ prediction, and the "super-correlated" prediction is almost as good. The prediction for $\Delta E\ ^3(n\rightarrow\pi^*)$ of these last two integral sets is poor, however. We see that one cannot decide among the three sets on the basis of these predictions alone.

An additional, rather stringent criterion for a suitable set of integrals is that its use be accompanied by reasonable "charge-following" behavior. Consider for example the calculation of the lone-pair ionization potential carried out with "super-correlated" integrals: calculation (3) of Table XVI. After the initial ionization has removed a lone-pair electron, the resulting positive hole in the atomic orbital x_0 attracts more pi electronic charge to oxygen than was there in the ground state (Q_π of $\{\Omega(n^+)\}$[18] is a larger negative

[18] Braces { } indicate a state for which reorganization has not yet occurred—only excitation or ionization.

TABLE XIX. Reorganization effects following pi ionization.[a,b]

Calculation[c]		Ω_N	$\{\Omega(\pi^+)\}$[d]	$\Omega(\pi^+)$[e]
	Energy	0 ev	13.3372 ev	13.2034 ev
(1), (1′)	Q_π	−0.2099	−0.2504	−0.2117
	Q_σ	−0.0542	−0.0542	0.1089
	Energy	0	12.0517	12.0385
(2), (2′)	Q_π	−0.2545	−0.3246	−0.3311
	Q_σ	−0.0022	−0.0022	0.0975
	Energy	0	12.2034	12.1778
(3), (3′)	Q_π	−0.2965	−0.3415	−0.3276
	Q_σ	0.0489	0.0489	−0.0423
	Energy	0	12.0659	
(4)	Q_π	−0.2181	−0.5898	
	Q_σ	0.0032	0.0032	
	Energy	0	12.5101	
(5)	Q_π	−0.3240	−0.6830	
	Q_σ	0.1335	0.1335	

[a] Details of the iteration leading to the figures in the final column are described in Appendix A, step P.
[b] Negative Q_σ means excess (more than one) sigma electrons on oxygen. Negative Q_π means excess pi electrons on oxygen.
[c] See text, Secs. III and IV, for characterization of calculations.
[d] Results in this column are obtained using the same (Σ) structure as in Ω_N. They constitute "no-reorganization" values.
[e] Results in this column are those for mutual consistency of (Σ) and (Π^+N) structures; i.e., after reorganization.

quantity than Q_π of Ω_N). When the sigma electrons are allowed to adjust to the new situation, it is seen that the hole also attracts them, and that this attraction overcomes the repulsion on the sigma electrons due to the increased pi negative charge on oxygen [Q_σ of $\Omega(n^+)$ is a larger negative quantity than Q_σ of Ω_N).

TABLE XX. Reorganization effects following $^3(n\rightarrow\pi^*)$ excitation.[a,b]

Calculation[c]		Ω_N	$\{^3\Omega(n\rightarrow\pi^*)\}$[d]	$^3\Omega(n\rightarrow\pi^*)$[e]
	Energy	0 ev	4.2268 ev	3.4094 ev
(1), (1′)	Q_π	−0.2099	−0.1433	0.0385
	Q_σ	−0.0542	−0.0542	0.5480
	Energy	0	3.9521	3.9196
(2), (2′)	Q_π	−0.2545	−0.3121	−0.3047
	Q_σ	−0.0022	−0.0022	−0.1056
	Energy	0	4.2438	3.9025
(3), (3′)	Q_π	−0.2965	−0.3297	−0.2640
	Q_σ	0.0489	0.0489	0.3082
	Energy	0	3.8762	
(4)	Q_π	0.2181	−0.3115	
	Q_σ	0.0032	0.0032	
	Energy	0	3.9406	
(5)	Q_π	−0.3240	−0.3667	
	Q_σ	0.1335	0.1335	

[a] Details of the iteration leading to the figures in the final column are described in Appendix A, step P.
[b] Negative Q_σ means excess (more than one) sigma electrons on oxygen. Negative Q_π means excess pi electrons on oxygen.
[c] See text, Secs. III and IV, for characterization of calculations.
[d] Results in this column are obtained using the same (Σ) structure as in Ω_N. They constitute "no-reorganization values."
[e] Results in this column are those for mutual consistency of (Σ) and (ΠN)* structures; i.e., after reorganization.

Finally, the resulting increase in sigma negative charge on oxygen forces some of the pi negative charge to leave oxygen [Q_π of $\Omega(n^+)$ is a smaller negative quantity than Q_π of $\{\Omega(n^+)\}$].

This reasonable behavior is to be contrasted with that displayed by the "theoretical" integrals in the calculation of the lone-pair ionization potential: calculation (1) of Table XVI. Here again the positive hole in the x_0 orbital created by the initial ionization attracts pi electronic charge to oxygen. But in this case it appears that the repulsion on the sigma electrons due to the increased pi electronic charge on oxygen has forced sigma electrons away in spite of the attraction of the positive hole for the sigma electrons. Such behavior is suspect, but might perhaps not be unreasonable. However, the subsequent behavior of the pi electrons is undoubtedly spurious. Instead of being repelled by the sigma electrons which have left oxygen, the pi electrons go right along with the sigma electrons and also leave oxygen! In every excitation and ionization of Tables XIV–XX, this anomalous charge-following effect appeared when "theoretical" integrals were used. This certainly signifies that the "theoretical" integrals should not be used in conjunction with the present empirical one-center integrals. A more detailed discussion of the cause of the spurious behavior will be given in the following.

The "super-correlated" integrals do not definitely exhibit the anomalous charge-following, but in one case, the $\Delta E(n\rightarrow\sigma^*)$ calculation, we do find it for the "correlated" integrals: calculation (2) of Table XVII. The anomaly here is in the behavior of the sigma electrons only. After the initial excitation has transferred a lone-pair electron to the sigma system, the resulting hole in the x_0 orbital appears not to attract sigma electrons to oxygen, but rather to repel them. However, the pi electrons adjust to this in a reasonable manner, giving increased pi charge on oxygen. But then the anomaly appears—sigma electrons follow the pi electrons in moving to oxygen.

The "correlated" integrals lead to dubious results in two other instances. In the $\Delta E(n^+)$ calculation—calculation (2) of Table XVI—the increased pi charge on oxygen caused by hole attraction repels the sigma electrons in spite of the hole attraction for them. In the $\Delta E(\sigma^+)$ calculation—calculation (2) of Table XVIII—after the initial ionization has removed one sigma electron, the other moves toward oxygen. But the pi charge also moves toward oxygen. This behavior is not obviously incorrect but neither is it obviously correct. On balance then, the "super-correlated" integral set leads to less doubtful behavior than do the other integral sets.

VI. DISCUSSION OF RESULTS: EFFECTS OF SIGMA-PI INTERACTION

To see in more detail the way sigma-pi interaction acts to affect the reorganization process, we shall now consider such questions as (a) why there is a greater reorganization effect in the $\Delta E(n\rightarrow\pi^*)$ calculation than in the $\Delta E(\pi\rightarrow\pi^*)$ case, for $I_{\sigma\pi}=+3.937$ ("super-correlated" integrals) [calculation (3) of Table XIV *vs* calculation (3) of Table XV;] and (b) why the reorganization effect is larger for $I_{\sigma\pi}=+3.937$ ("super-correlated") than for $I_{\sigma\pi}=+1.5846$ ("correlated") in the $\Delta E(n\rightarrow\pi^*)$ case [calculation (3) *vs* calculation (2) of Table XIV].

It is clear that the extent of *sigma* electron reorganization will be greater, the greater the change in pi, lone-pair structure from one type of excitation to another. For a given type of excitation, the extent of sigma electron reorganization will be greater, the greater the facility with which the change in pi, lone-pair structure is manifested upon the sigma electrons. The manner in which these reorganization-determining factors appear in the configuration interaction matrix elements for the examples cited will now be examined. It will also become evident how the incorrect choice of two-center repulsion values leads to anomalies.

It is noted in Appendix A that the polarity of the Σ structure in the present treatment depends on the ratio $(H_{12})^\sigma/[\beta_\sigma{}^\lambda-\frac{1}{2}K_{12}{}^\sigma]$.[19] In the previous paper[1] it was shown that the effect of a change in the pi, lone-pair structure disappears from $\beta_\sigma{}^\lambda$ under a generalized Mulliken approximation and that Q_π appears in

$$(H_{12}{}^x)^\sigma=[(\alpha_{\sigma_c}{}^{+2})^x-(\alpha_{\sigma_o}{}^{+2})^x+\tfrac{1}{2}(\gamma_{\sigma_c}-\gamma_{\sigma_o})]/(1-S_\sigma{}^2)^{\frac{1}{2}};\qquad x=N,\ V,\ n\pi,\ \cdots$$

only through $(\alpha_{\sigma_c}{}^{+2})^x$ and $(\alpha_{\sigma_o}{}^{+2})^x$.[20] In fact,

$$(\alpha_{\sigma_c}{}^{+2})^N=\alpha_{\sigma_c}{}^{+6}+2g_{x_0\sigma_c}+g_{\pi_c\sigma_c}+g_{\pi_o\sigma_c}+Q_\pi{}^N(g_{\pi_c\sigma_c}-g_{\pi_o\sigma_c}),$$

$$(\alpha_{\sigma_c}{}^{+2})^V=\alpha_{\sigma_c}{}^{+6}+2g_{x_0\sigma_c}+g_{\pi_c\sigma_c}+g_{\pi_o\sigma_c}+Q_\pi{}^V(g_{\pi_c\sigma_c}-g_{\pi_o\sigma_c}).$$

The state $\{\Omega(\pi\rightarrow\pi^*)\}$[18] differs from Ω_N only in its different value of Q_π. By contrast, for $\{\Omega(n\rightarrow\pi^*)\}$, where a more radical change in structure has occurred, one finds

$$(\alpha_{\sigma_c}{}^{+2})^{n\pi}=\alpha_{\sigma_c}{}^{+6}+g_{x_0\sigma_c}+\tfrac{3}{2}(g_{\pi_c\sigma_c}+g_{\pi_o\sigma_c})+Q_\pi{}^{n\pi}(g_{\pi_c\sigma_c}-g_{\pi_o\sigma_c}).$$

With similar expressions for $(\alpha_{\sigma_o}{}^{+2})^x$, one finds

$$(H_{12}{}^V)^\sigma=(H_{12}{}^N)^\sigma+[(Q_\pi{}^V-Q_\pi{}^N)I_{\sigma\pi}]/[2(1-S_\sigma{}^2)]^{\frac{1}{2}},$$

and one finds also that

$$(H_{12}{}^{n\pi})^\sigma=(H_{12}{}^N)^\sigma+[(Q_\pi{}^{n\pi}-Q_\pi{}^N+\tfrac{1}{2})I_{\sigma\pi}]/[2(1-S_\sigma{}^2)]^{\frac{1}{2}},$$

where

$$I_{\sigma\pi}=(g_{\pi_c\sigma_c}-g_{\pi_o\sigma_c}-g_{\pi_c\sigma_o}+g_{\pi_o\sigma_o}).$$

To consider now the magnitude of the sigma reorganizations following $\pi\rightarrow\pi^*$ excitation—calculation

[19] For a given change in pi polarity, the change in sigma polarity is smaller, the larger $[\beta\sigma^\lambda-\frac{1}{2}K_{12}{}^\sigma]$ is. In this respect the quantity $1/[\beta\sigma^\lambda-\frac{1}{2}K_{12}{}^\sigma]$ behaves like a longitudinal bond polarizability.

[20] For explanation of notation see Sec. II.

(3) of Table XV; at $I_{\sigma\pi}=+3.937$ it is found that $Q_\pi^N=-0.2965$, $\{Q_\pi^V\}=-0.4360$, the latter being the value before reorganization. These two values do not differ greatly, which means that there is only a small "driving-force" for sigma reorganization, the potential field in which the sigma electrons move not being greatly changed by $\pi\rightarrow\pi^*$ excitation.[21] As for the direction of the sigma electron shift, Table XV shows $Q_\sigma^N=0.04893$, the sign of which is found to correspond to a negative value for $(H_{12}^N)^\sigma$.[22] In $(H_{12}^V)^\sigma$, $[Q_\pi^V-Q_\pi^N)I_{\sigma\pi}]$ term makes $(H_{12}^V)^\sigma$ more negative still than $(H_{12}^N)^\sigma$, and there is found a larger positive value for Q_σ^V than for Q_σ^N. Reorganization following $\pi\rightarrow\pi^*$ excitation has driven sigma electrons away from oxygen.

To consider the magnitude of the sigma reorganization following $n\rightarrow\pi^*$ excitation—calculation (3) of Table XIV—at $I_{\sigma\pi}=+3.937$ it is seen that the driving force for sigma reorganization, due to change in pi polarity following $n\rightarrow\pi^*$ excitation, is smaller than that following $\pi\rightarrow\pi^*$ excitation: $\{Q_\pi^{n\pi}\}=-0.3856$ *vs* $Q_\pi^V=-0.4360$, with $Q_\pi^N=-0.2965$. However, the term $(Q_\pi^{n\pi}-Q_\pi^N)I_{\sigma\pi}$ in $(H_{12}^{n\pi})^\sigma$, though smaller than in the $\pi\rightarrow\pi^*$ case is still of a sign to drive sigma electrons away from oxygen. The complete sigma-pi interaction term in $(H_{12}^{n\pi})^\sigma$ is $[(Q_\pi^{n\pi}-Q_\pi^N+\frac{1}{2})I_{\sigma\pi}]$, in which the attraction of the sigma electrons by the positive hole in x_0 is embodied in the quantity $\frac{1}{2}$. This positive term dominates the negative $(Q_\pi^{n\pi}-Q_\pi^N)$ term in $(H_{12}^{n\pi})^\sigma$, and we find, therefore, a large negative value for $Q_\sigma^{n\pi}$: sigma electrons have been brought *to* oxygen by reorganization following $n\rightarrow\pi^*$ excitation.

To consider how the magnitude of $I_{\sigma\pi}$ affects the degree of sigma reorganization, we see that in $(H_{12}^{n\pi})^\sigma$, the responsible term $[(Q_\pi^{n\pi}-Q_\pi^N+\frac{1}{2})I_{\sigma\pi}]$ is smaller for $I_{\sigma\pi}=1.5846$ than for $I_{\sigma\pi}=3.937$, so that $(H_{12}^{n\pi})^\sigma$ will differ less from $(H_{12}^N)^\sigma$ in the former case and so give less difference in Q_σ^N and $Q_\sigma^{n\pi}$. Another factor is that $|\beta_\sigma^\lambda|$ in calculation (2) ($I_{\sigma\pi}=1.5846$) is found to be larger than in calculation (3) ($I_{\sigma\pi}=3.937$), which further reduces the sigma reorganization effect in the former calculation.[19]

As for the anomalous charge-following, one sees with the expression

$$(H_{12}^{n\pi})^\sigma=(H_{12}^N)^\sigma+\{1/[2(1-S_\sigma^2)]^{\frac{1}{2}}\}\times[(Q_\pi^{n\pi}-Q_\pi^N+\tfrac{1}{2})I_{\sigma\pi}],$$

that if $I_{\sigma\pi}$ were negative (as it is with the "theoretical" set of repulsion integrals) one would find $(H_{12}^{n\pi})^\sigma$ to be a larger negative quantity than $(H_{12}^N)^\sigma$, which would make it *appear* that the small increase in pi electronic charge on oxygen, following $n\rightarrow\pi^*$ excitation, had overcome the influence of the positive hole in x_0, and had itself forced the sigma electrons away from oxygen. Actually, however, in this (incorrect) sort of calculation, the hole would be spuriously repelling, and the excess pi electrons spuriously (but not as effectively) attracting sigma electrons.

VII. RESUME

The iterative method employed here has made possible a detailed tracing of reorganization effects in the formaldehyde molecule, both through formulas and numerical results. Factors influencing the direction and extent of bond polarity changes following excitation and ionization have been examined.

The empirical treatment of the (+6) core of the molecule has yielded a set of (+6) core parameters, which may be combined with coulomb repulsion integrals, as in Sec. IV, to give parameters for a core containing all of the sigma electrons. These parameters may be used, with discretion, in a four-electron pi, lone-pair calculation for a carbonyl group. Sidman has in fact already used some of the parameters with the present one-center and two-center repulsions in Pariser-Parr-type calculations on carbonyl groups in various molecules.[23] References to other calculations on formaldehyde may be found in his paper.

The extent to which, according to the present calculations, the sigma bond polarity changes during reorganization should make one wary in interpreting results of calculations in which the assumption of constant sigma structure during excitation is made. But it should be noted that the present calculations may not be entirely accurate, so that this conclusion may be wrong.

We have shown how the criterion of reasonable charge-following behavior may be used as a necessary condition on the two-center repulsion integral values one uses with a particular set of one-center values. It has been pointed out, however, that Pariser-type one-center integrals may in fact not be the proper ones to use in such calculations.

All in all, then, reorganization effects on the sigma bond polarity seem to be by no means small, but reorganization effects on the energies do not appear to be particularly significant. The energy effects probably are less than the errors in the best present day semi-empirical spectra predictions, although they are definitely of a magnitude which must be considered when, some day, calculation of changes in electronic structure during reaction is attempted.

---

[21] The fact that $\{Q_\pi^V\}$ differs from Q_π^N by only a small amount is at variance with the popular conception which associates a large oscillating dipole with the $N\rightarrow V$ transition. Only if one neglects the mixing of Π_3, will $\Omega(\pi\rightarrow\pi^*)$ appear to have a large dipole moment of opposite sign to that in Ω_N, as the following typical figures show when substituted in the Q_π formula: $B_1^N=0.9690$, $B_2^N=-0.2103$, $B_3^N=-0.1287$; $B_1^V=0.1263$, $B_2^V=0.8713$, $B_3^V=-0.4741$. It is because of $|B_3^V|>|B_1^V|$ and the opposite signs that causes Q_π^V to have the same sign as Q_π^N

$$[Q_\pi=2^{+\frac{1}{2}}(1-S_\pi^2)^{-\frac{1}{2}}B_2(B_1+B_3)].$$

[22] The relation of the sign of Q_σ to the sign of (H_{12}^σ) can be understood when (H_{12}^σ) is expressed in a form involving electronegativities. See reference 1, Eq. (87).

[23] J. W. Sidman, J. Chem. Phys. **27**, 429 (1957).

TABLE XXI. Numerical illustration of the parameter evaluation process.[a,b]

		Part 1		*Step*
Q_σ^N		−0.045		A
μ_σ		0.829218		
β_π^λ	−3.30	−3.325	−3.35	
$(H_{12}^N)^\pi$	μ_π	μ_π	μ_π	
0.0	0.253266	0.253351	0.253435	
0.5	0.682315	0.680475	0.678646	B
1.0	1.107530	1.103685	1.109942	
1.5	1.525797	1.520105	1.514453	
2.0	1.933694	1.926105	1.918613	
$(H_{12}^N)_\sigma^\pi$	1.481874	1.488693	1.495526	C
ΔP_π	−2.119620	−2.110219	−2.100798	D
	−2.50	−2.25	−2.00	
	4.354792	4.337919	4.309208	
β_σ^{0} [c]	−2.00	−2.00	−1.75	
$\Delta E(n\rightarrow\pi^*)$	4.238019	4.273605	4.234215	E
	−2.25	−1.75	−1.85	
	4.302313	4.197479	4.264862	
$(\beta_\sigma^0)_0$	−2.055531	−1.951667	−1.833936	F
$\Delta E(\pi\rightarrow\pi^*)$	7.962374	8.012169	8.058972	G
(β_π^λ)		−3.318738		H
ΔP_π		−2.112575		
$(\beta_\sigma^0)_{0'}$		−1.979086		
$(P_{\pi_0})_0$		2.939930[d]		I, J
$-\frac{1}{2}(\alpha\sigma_c^{+6}+\alpha\sigma_o^{+6})$		78.666137		K, L
$\Delta E(\sigma^+)$		12.774583		M

[a] The two-center repulsion integrals used here are the "theoretical" set, with $I_{\sigma\pi}=-3.937$ (see Sec. III).
[b] See Fig. 2 and Appendix A for a discussion paralleling this Table.
[c] $\beta_\sigma^0\equiv[\beta_\sigma^\lambda-\frac{1}{2}K_{12}^\sigma]$.
[d] The P_{π_0} value calculated without including sigma bond spin-polarization is 2.96428.

APPENDIX A
Parameter Evaluation

If the necessary integrals were all known, molecular calculations could be straightforwardly carried out with the formulas of Tables II–IX. But with core parameters not known, and any particular set of two-center repulsions having uncertain *a priori* worth, one is forced to proceed in a somewhat devious manner. When one has by some means obtained a set of two-center repulsion integrals (characterized by an $I_{\sigma\pi}$ value, see Sec. III) and has determined one-center quantities from atomic data (see Appendix B) one can proceed to the evaluation of core parameters from molecular data. This appendix contains a description of the scheme used for this purpose, essentially an inversion of the formulas of Tables II–IX.

TABLE XXI. (Continued)

		Part 2		*Step*
Q_σ^N		−0.145		A
μ_π		1.307673		
β_π^λ	−3.30	−3.325	−3.35	
$(H_{12}^N)^\pi$	μ_π	μ_π	μ_π[a]	B
$(H_{12}^N)_0{}^\pi$	0.911185	0.915249	0.919325	C
ΔP_π	−3.300123	−3.294520	−3.288901	D
	−5.00	−4.50	−4.00	
	4.284617	4.294359	4.2964843	
β_σ^0	−4.00	−4.00	−3.50	
$\Delta E(n\rightarrow\pi^*)$	4.229792	4.263310	4.255480	E
	−4.50	−3.50	−3.00	
	4.260768	4.222022	4.198113	
$(\beta_\sigma^0)_0$	−4.485562	−3.952975	−3.548950	F
$\Delta E(\pi\rightarrow\pi^*)$	7.962035	8.012442	8.062847	G
$(\beta_\pi^\lambda)_0$		−3.318829		
$(\Delta P_\pi)_0$		−3.295904		H
$(\beta_\sigma^0)_0$		−4.072485		
$(P_{\pi_0})_0$		3.707385[b]		I, J
$-\frac{1}{2}(\alpha_{\sigma_C}{}^{+6}+\alpha_{\sigma_O}{}^{+6})$		81.144782		K, L
$\Delta E(\sigma^+)$		16.93952		M

[a] μ_π vs $(H_{12}^N)^\pi$ values are the same as in Part 1.
[b] The P_{π_0} value calculated without including sigma bond spin-polarization is 3.72867.

The core parameters are $\alpha_{\pi_C}{}^{+6}$, $\alpha_{\pi_O}{}^{+6}$, β_π^λ, $\alpha_{\sigma_C}{}^{+6}$, $\alpha_{\sigma_O}{}^{+6}$, β_σ^λ. The molecular data used in their evaluation are: the dipole moment, $\mu(H_2CO)$; the $n\rightarrow\pi^*$ transition energy, $\Delta E(n\rightarrow\pi^*)$; the $\pi\rightarrow\pi^*$ transition energy, $\Delta E(\pi\rightarrow\pi^*)$; the lone-pair ionization potential, $\Delta E(n^+)$; the $n\rightarrow\sigma^*$ transition energy, $\Delta E(n\rightarrow\sigma^*)$; and the sigma ionization potential, $\Delta E(\sigma^+)$.

Figure 1 indicates the procedure. It is a flow sheet of the parameter evaluation process, showing the sequence of calculations, the introduction of the empirical data cited, and the core parameters (or quantities related to them) determined at each step. A brief statement of what was done at each step is given in the caption.

These statements serve to explain Fig. 2, which shows how at each step there are built up subsets of parameters compatible with each other in that their use leads to the reproduction of the empirical data introduced prior to that step. As is seen in Fig. 2, for a particular $I_{\sigma\pi}$ value there are chosen a trial series of Q_σ^N values and a trial series of β_π^λ values. For each Q_σ^N, β_π^λ pair, an $(H_{12}^N)_0{}^\pi$ value is found. (The subscripts 0, 0′ outside parentheses denote a quantity picked to fit an experimental datum.) Then, for each Q_σ^N, $(H_{12}^N)_0{}^\pi$, β_π^λ set a $(\beta_\sigma^\lambda)_0$ value is found. The same Q_σ^N value appears in several Q_σ^N, $(H_{12}^N)_0{}^\pi$, $(\beta_\sigma^\lambda)_0$, (β_π^λ) sets; for each Q_σ^N value a $(\beta_\pi^\lambda)_0$ value is found, with accompanying $(H_{12}^N)_{0'}{}^\pi$, $(\beta_\sigma^\lambda)_{0'}$ values. For each Q_σ^N, $(H_{12}^N)_{0'}{}^\pi$, $(\beta_\sigma^\lambda)_{0'}$, $(\beta_\pi^\lambda)_0$ set a $(P_{\pi_0})_0$ value and then an $(\alpha_{\sigma_C}{}^{+6}+\alpha_{\sigma_O}{}^{+6})$ value are determined. Finally,

TABLE XXI. (Continued)

		Part 3		*Step*
Q_σ^N		−0.195		A
μ_σ		1.549515		
β_π^λ	−3.30	−3.325	−3.35	
$(H_{12}^N)^\pi$	μ_π	μ_π	μ_π[a]	
				B
$(H_{12}^N)_0^\pi$	0.626622	0.629364	0.632115	C
ΔP_π	−3.889297	−3.885517	−3.881724	D
	−10.00	−10.00	−9.00	
	4.231574	4.264300	4.287803	
β_σ^0	−15.00	−11.00	−7.00	
$\Delta E(n\rightarrow\pi^*)$	4.257922	4.27154	4.260273	E
	−16.00	−9.00	−5.00	
	4.261107	4.254967	4.206665	
$(\beta_\sigma^0)_0$	−15.596655	−9.504453	−6.983473	F
$\Delta E(\pi\rightarrow\pi^*)$	7.964694	8.014659	8.064621	G
$(\beta_\pi^\lambda)_0$		−3.317665		
$(\Delta P_\pi)_0$		−3.3886627		H
$(\beta_\sigma^0)_0$		−10.921643		
$(P_{\pi_o})_0$		4.098143[b]		I, J
$-\frac{1}{2}(\alpha_{\sigma_c}{}^{+6}+\alpha_{\sigma_o}{}^{+6})$		90.873201		K, L
$\Delta E(\sigma^+)$		31.04757		M

[a] μ_π vs (H_{12}^N) values are the same as in Part 1.
[b] The P_{π_o} value calculated without including sigma bond spin-polarization is 4.10849.

Part 4

Q_σ^N		−0.054210		
β_π^λ		−3.318754		
β_σ^λ		−3.196237		
P_{π_o}	3.010578[a]		$\alpha_{\pi_c}{}^{+6}$	−61.479689[b]
ΔP_π	−2.221564		$\alpha_{\pi_o}{}^{+6}$	−76.565322
$-\frac{1}{2}(\alpha_{\sigma_c}{}^{+6}+\alpha_{\sigma_o}{}^{+6})$	78.853528		$\alpha_{\sigma_c}{}^{+6}$	−81.360022
$(H_{12}^N)_\sigma$	0.150145		$\alpha_{\sigma_o}{}^{+6}$	−76.347030
Q_π^N	−0.209911			
	$\Delta E(\pi^+)$	13.20345[c,d]		
	$\Delta E^s(n\rightarrow\pi^*)$	3.40940[c]		

[a] Note that P_{π_o} has a positive value—see Sec. III for discussion.
[b] Values in the second column are derived from those in the first. See step O.
[c] This value is predicted with the above parameters.
[d] Q_t in this calculation (see Table VI) was 0.02522.

it is decided which Q_σ^N value is $(Q_\sigma^N)_0$, and the accompanying $(H_{12}^N)_{0'',\pi}$, $(\beta_\sigma^\lambda)_{0''}$, $(\beta_\pi^\lambda)_{0'}$, $(P_{\pi_o})_{0'}$, $(\alpha_{\sigma_c}{}^{+6}+\alpha_{\sigma_0}{}^{+6})_{0'}$ values are determined.

The logic in the process depicted in Fig. 1 will now be established. Once it is understood just what restrictions are implied by the specification of a Q_σ^N value in step A and a β_π^λ value in step B, the remaining steps follow naturally. The quantity

$$Q_\sigma^N = 2^{\frac{1}{2}} A_2^N (A_1^N + A_3^N)/(1-S^2)^{\frac{1}{2}}$$

is one result of the (Σ) problem for Ω_N (Table II), when one has a known (II) structure and known core parameters. Conversely, when it is specified that the Q_σ^N from a $2\times2(\Sigma)$ problem[24] have a particular value, there is imposed on the relevant core parameters, β_σ^λ and $(\alpha_{\sigma_c}{}^{+6}-\alpha_{\sigma_o}{}^{+6})$, a certain restriction, which involves Q_π^N [hence, the (II) structure]. The restriction is the following: The ratio of the quantity $(H_{12}^N)^\sigma$ to the quantity $[\beta_\sigma^\lambda - \frac{1}{2}K_{12}^\sigma]$ must be a number k, where k is fixed by Q_σ^N according to[25]

$$Q_\sigma^N = -2^{\frac{1}{2}}(1-S^2)^{-\frac{1}{2}} k[1-(1+k^2)^{\frac{1}{2}}]/\{[1-(1+k^2)^{\frac{1}{2}}]^2+k^2\}.$$

This becomes a useful restriction only after β_π^λ has been specified and the consequences of this further specification made operative. The (Σ) structure has a certain dipole moment μ_σ, which is fixed by specification of Q_σ^N. The (II) structure has a moment μ_π, and the sum $\mu_\sigma+\mu_\pi$ must be equal to μ_{CO}, the experimental CO bond moment in H_2CO.[26] When μ_σ is fixed by specification of Q_σ^N, so also is μ_π, through the relation $\mu_\pi=\mu_{CO}-\mu_\sigma$. Then upon specification of β_π^λ, only one $(H_{12}^N)^\pi$ value can produce the required value of μ_π. This second restriction is used to determine $(H_{12}^N)_0{}^\pi$ for a given Q_σ^N, β_π^λ pair (in step C). The first restriction can now become effective, because β_π^λ and $(H_{12}^N)_0{}^\pi$ fix a Q_π^N value. With Q_π^N established, if one now specified any β_σ^λ value, the first restriction would fix an $(\alpha_{\sigma_c}{}^{+6}-\alpha_{\sigma_o}{}^{+6})$ value automatically. Since $(H_{12}^N)_0{}^\pi$ involves $(\alpha_{\pi_c}{}^{+6}-\alpha_{\pi_0}{}^{+6})$ (and also Q_σ^N) one could now write down values for a set of parameters $(\alpha_{\pi_c}{}^{+6}-\alpha_{\pi_0}{}^{+6})$, β_π^λ, $(\alpha_{\sigma_c}{}^{+6}-\alpha_{\sigma_o}{}^{+6})\beta_\sigma^\lambda$ which would reproduce μ_{CO} when used in iterative calculations on (Σ) and (II) of Ω_N. These are the four unknown theoretical quantities involved in the μ_{CO} calculation. Imposition of the experimental μ_{CO} value puts one condition on them, leaving three degrees of freedom, represented by Q_σ^N, β_π^λ, β_σ^λ. Two more experimental conditions actually are imposed in the next few steps, leaving only Q_σ^N unrestricted. These are the $\Delta E(n\to\pi^*)$ and $\Delta E(\pi\to\pi^*)$ experimental values, introduced through steps E, F, G, H.[27] P_{π_o} and $(\alpha_{\sigma_c}{}^{+6}+\alpha_{\sigma_o}{}^{+6})$ are next determined for each Q_σ^N value, allowing implicit separation to $\alpha_{\pi_c}{}^{+6}$, $\alpha_{\pi_o}{}^{+6}$, $\alpha_{\sigma_c}{}^{+6}$, $\alpha_{\sigma_o}{}^{+6}$ as needed. Steps I, J, K, L, accomplish this determination, using the experimental $\Delta E(n^+)$ and $\Delta E(n\to\sigma^*)$ values. Finally, the remaining degree of freedom Q_σ^N is fixed by the experimental value of $\Delta E(\sigma^+)$. For the final Q_σ^N value one obtains explicitly $\alpha_{\pi_c}{}^{+6}$, $\alpha_{\pi_o}{}^{+6}$, $\alpha_{\sigma_c}{}^{+6}$, $\alpha_{\sigma_o}{}^{+6}$, from ΔP_π, P_{π_o}, $(\alpha_{\sigma_c}{}^{+6}+\alpha_{\sigma_o}{}^{+6})$ and Q_σ^N; the pi ionization potential and the $n\to\pi^*$ triplet transition energy are then obtained.

Table XXI, paralleling Fig. 2, illustrates the parameter evaluation process numerically for the case $I_{\sigma\pi}=+3.937$, which characterizes the "theoretical" two-center repulsion integrals.

It may be noted in this table that the forced orthogonalization in the $\Omega(\pi\to\pi^*)$ treatment, the sigma bond spin-polarization in the $\Omega(n^+)$ treatment, and the charges transferred from n to π in the $\Omega(\pi^+)$ treatment, all are of insignificant magnitude.

TABLE XXII. Oxygen: valence state energies and their formulation in terms of spectroscopic energies.

Valence state	Formulation[a]	Energy (ev)
1. O^{+2}, s^2s^2; V_0	$\frac{3}{4}E[^1D]+\frac{1}{4}E[^1S]$	52.114
2. O^{+2}, s^2yz; V_2	$\frac{3}{4}E[^3P]+\frac{1}{4}E[^1D]$	49.388
3. O^{+1}, s^2xyz; V_3	$\frac{1}{2}E[^4S]+\frac{1}{2}E[^2D]$	15.28
4. O^{+1}, s^2y^2z; V_1	$\frac{1}{2}E[^2D]+\frac{1}{2}E[^2P]$	17.77
5. O^0, s^2x^2yz; V_2	$\frac{3}{4}E[^3P]+\frac{1}{4}E[^1D]$	0.49
6. O^{-1}, $s^2x^2yz^2$; V_1	$E[^2P]$	-2.2[b]
7. O^{-2}, $s^2x^2y^2z^2$; V_0	$E[^1S]$	(4.46)[c]
8. O^0, $s^2x^2y^2$; V_0	$\frac{3}{4}E[^1D]+\frac{1}{4}E[^1S]$	2.707
9. O^0, s^2p^4; ^3P	$E[^3P]$	0

[a] Terms in each case arise from the configuration appropriate to the valence state.

[b] Though several types of measurement have yielded values near -2.2 ev for the electron affinity of oxygen (H. O. Pritchard, Chem. Revs. **52**, 529 (1953), a recent photo-detachment experiment gives -1.48 ev (Branscomb and Smith, Phys. Rev. **98**, 1127 (1955), and a new extrapolation method gives -1.13 ev, [T. Y. Wu, Phys. Rev. **100**, 1195 (1955)]. If these are correct, our calculations may be upset to some extent.

[c] This value is quite uncertain, there having been used in its estimation an electron affinity derived from a lattice cycle [see Branscomb and Smith, Phys. Rev. **98**, 1127 (1955)].

[24] We are not interested in the unobserved state $\Omega(\sigma\to\sigma^*)$ to which $\Sigma_3=|2\bar{2}|$ makes a significant contribution. There is only a slight mixing of Σ_3 in the lowest state of the (Σ) problem, which we ignore, thus giving the secular determinant 2×2 dimensions.

[25] $Q_\sigma{}^N$ is related to $(A_2{}^N)^2$; the solutions of the 2×2 secular equations can be conveniently expressed in terms of k and

$$[\beta_\sigma^\lambda - \tfrac{1}{2}K_{12}^\sigma],$$

the latter being one half the difference of the diagonal elements.

[26] As an approximation we have used $\mu_{CO}=\mu(H_2CO)$ in the calculation. I. Hisatsune and D. F. Eggers [J. Chem. Phys. **23**, 487 (1955)] have shown that infrared intensity data lead to μ_{CH} equal to either 0.1 D (from all three symmetry species) or 0.5 D (from two species, forcing a value 1.0 D for the third, the unsymmetric in-plane vibration). Some uncertainty exists in their rationale of the 1.0 D value, however, so for simplicity we have ignored μ_{CH} entirely.

[27] The $\Delta E(n\to\pi^*)$ expression in Table IV contains

$$\tfrac{1}{2}(P_{\pi_c}+P_{\pi_o})-P_{z_o}.$$

π_o and x_o have the same interaction with electrons on C if $Q_{CH}\approx0$ (as we are assuming in taking $\mu_{CH}\approx0$) and the difference in their interaction with electrons on H is ≈0.1 ev which we have neglected, and thereby set $P_{z_o}=P_{\pi_o}$.

TABLE XXIII. Carbon: nonhybridized valence state energies and their formulation in terms of spectroscopic energies.

Valence State[a]	Formulation	Energy (ev)
1. C^0, s^2xz; V_2	$\frac{3}{4}E[^3P]+\frac{1}{4}E[^1D]$	0.316
1. C^0, sxz^2; V_2	$\frac{3}{8}E[^3D]+\frac{1}{8}E[^1D]+\frac{3}{8}E[^3P]+\frac{1}{8}E[^1P]$	9.8505
2. C^{-1}, s^2xyz; V_3	$\frac{1}{2}E[^4S]+\frac{1}{2}E[^2D]$	−0.97
6, 2. C^{-1}, $sxyz^2$; V_3	$\frac{1}{2}E[^4P]+\frac{1}{4}E[^2P]+\frac{1}{4}E[^2D]$	7.68[b]
3. C^{-2}, s^2xy^2z; V_2	$\frac{3}{4}E[^3P]+\frac{1}{4}E[^1D]$	9.92
3. C^{-2}, sxy^2z^2; V_2	$\frac{3}{4}E[^3P]+\frac{1}{4}E[^1P]$	20.70
4. C^{+1}, sxz; V_3	$\frac{1}{2}E[^4P]+\frac{1}{4}E[^2P]+\frac{1}{4}E[^2D]$	19.68
5. C^0, $sxyz$; V_4	$\frac{5}{16}E[^5S]+\frac{3}{16}E[^3S]+\frac{3}{8}E[^3D]+\frac{1}{8}E[^1D]$	8.2605
7. C^{+2}, $^1(sz)$; V_0	$E[^1P]$	48.326
7. C^{+2}, $^3(sz)$; V_0	$E[^3P]$	42.124
7. C^{+2}, $^3(zx)$; V_0	$E[^3P]$	52.667
7. $\phi_s{}^0(s^2)$	$E[^1S; s^2]$	35.640
7. $\phi_{2z}{}^0(p^2)$	$[1/(N^4+1)]\{\frac{2}{3}(1-N^2+N^4)E[^1D; p^2]+\frac{1}{3}(1+2N+N^4)E[^1S; p^2]\}$	56.143
8. C^{+1}, $^1(sz)y$; V_1	$\frac{3}{4}E[^2P]+\frac{1}{4}E[^2D]$	23.869
8. C^{+1}, $^3(sx)y$; V_1	$\frac{1}{12}E[^2P]+\frac{1}{4}E[^2D]+\frac{2}{3}E[^4P]$	18.288
8. C^{+1}, $^3(zx)y$; V_1	$\frac{1}{3}E[^2D]+\frac{2}{3}E[^4S]$	29.217
8. $\phi_s{}^0(s^2p)$	$E[^2P; s^2p]$	11.264
8. $\phi_{2z}{}^0(p^3)$	$[1/2(N^4+1)]\{(1+N^2)^2E[^2P; p^3]+(N^2-1)^2E[^2D; p^3]\}$	31.725
9. C^0, $^1(sz)y^2$; V_0	$\frac{1}{2}E[^1D]+\frac{1}{2}E[^1P]$	13.495
9. C^0, $^3(sx)y^2$; V_0	$\frac{1}{2}E[^3P]+\frac{1}{2}E[^3D]$	8.635
9. C^0, $^3(zx)y^2$; V_0	$E[^3P]$	19.45
9. $\phi_s{}^0(s^2p^2)$	$\frac{2}{3}E[^1D, s^2p^2]+\frac{1}{3}E[^1S, s^2p^2]$	1.736
9. $\phi_{2z}{}^0(p^4)$	$[1/(N^4+1)]\{\frac{2}{3}(1-N^2+N^4)E[^1D; p^4]+\frac{1}{3}(N^2+1)^2E[^1S, p^4]\}$	21.425[c]

[a] The numbering here indicates in which hybridized valence state energy (Table XXIV) each energy is to be used.

[b] In (2) and (6) the necessary excited states of C^-, sp^4 are not known experimentally. For $E[\Omega(C^-, sxyz^2; V_3]$ we therefore use the value given by Pritchard and Skinner [Trans. Faraday Soc. **49**, 1254 (1953)], and similarly for C^-, s^2p^3 in (2).

[c] The states of C^0, p^4 (near 20 ev) needed in (9) are not observed experimentally. We have estimated them by the following method; the error thus introduced might be as high as 2 ev. We find empirical values for $\omega_0(\equiv I_p-I_s-J_{ss}-J_{sp}+2F_0)$, F_2 and K_{sp} from C^0, sp^3 data. We also calculate a theoretical value for ω_0 from the values of the Slater-Condon parameters given by Moffitt [Proc. Roy. Soc. (London) **A202**, 534 (1950)] obtained from analytic orbitals with the Coulson-Duncanson Z values [W. E. Duncanson and C. A. Coulson, Proc. Roy. Soc. (Edinburgh) **A62**, 37 (1943)]. The ratio of the empirical ω_0 to the calculated ω_0 we use as a factor by which to reduce the individual theoretical values of I_p, I_s etc. to "empirical" size. With the "empirical" parameters so obtained we calculate $E[\Omega(C^0, p^4: {}^2P)]=19.45$ ev; $E[\Omega(C^0, p^4: {}^1D)]=20.30$ ev; $E[\Omega(C^0, p^4: {}^1S)]=22.41$ ev. all relative to $E[\Omega(C^0, s^2p^2; {}^3P)]$. We may infer the degree of error in this procedure by calculating energies of observed states; the C^0, s^2p^2 energies calculated with these parameters are in error by 0.5 ev, the C^0 sp^3 energies by up to 1.0 ev. The ±2-ev uncertainty we assign to the C^0, p^4 energies is probably pessimistic.

APPENDIX B

One-Center Quantities

Table X of Sec. III contains one-center parameter values obtained by expressing valence state energy differences first in terms of spectroscopic state energy differences (Tables XXII–XXIV), then in terms of Slater one-center parameters (Tables XXV, XXVI), equating the results and solving for the one-center parameters. Since fewer one-center parameters occur in the valence state energy differences than there are valence state energy differences entering the molecular problem, a choice of the most important differences to be reproduced must be made. This is discussed in the notes to Tables XXIII and XXV. The procedure of reproducing valence state energy differences in preference to spectroscopic state differences minimizes the Mulliken ambiguity effect[6] in diagonal terms of the molecular problem, but not in off-diagonal terms, where in effect, spectroscopic state energies can occur not combined into valence state energies.

TABLE XXIV. Valence state energies of hybridized carbon in terms of nonhybridized valence state energies.

Valence State[a]	Formulation[b]	Energy (ev)
1. C^0, $t_1t_2\sigma_c^2$; V_2	$N^2\{E[\Omega(C^0, s^2xz; V_2)]\}+N^2\lambda^2\{E[\Omega(C^0, sxz^2; V_2)]\}$	6.672
2. C^{-1}, $t_1t_2\sigma_c^2\pi_c$; V_3	$N^2\{E[\Omega(C^-, s^2xyz; V_3)]\}+N^2\lambda^2\{E[\Omega(C^-, sxyz^2; V_3)]\}$	4.797
3. C^{-2}, $t_1t_2\sigma_c^2\pi_c^2$; V_2	$N^2\{E[\Omega(C^{-2}, s^2xy^2z; V_2)]\}+N^2\lambda^2\{E[\Omega(C^{-2}, sxy^2z^2; V_2)]\}$	17.106
4. C^{+1}, $t_1t_2\sigma_c$; V_3	$E[\Omega(C^+, sxz; V_3)]$	19.684
5. C^0, $t_1t_2\sigma_c\pi_c$; V_4	$E[\Omega(C^0, sxyz; V_4)]$	8.2605
6. C^{-1}, $t_1t_2\sigma_c\pi_c^2$; V_3	$E[\Omega(C^-, sxy^2z; V_3)]$	7.68
7. C^{+2}, t_1t_2; V_3	$(N^4\lambda^2/4)\{E[\Omega(C^{+2}, {}^1(sz); V_0)]\}+\frac{3}{4}N^2\lambda^2\{E[\Omega(C^{+2}, {}^3(sx); V_0)]\}$ $+\frac{3}{4}N^2\{E[\Omega(C^{+2}, {}^3(zx); V_0)]\}+(N^4\lambda^4/8)\{1-[K_{xz}/(E_{zz}-E_s)]\}E_s^0(s^2)$ $+(N^4\lambda^4/8)\{[(N^4+1)/(N^4\lambda^4)]+[K_{xz}/(E_{zz}-E_s)]\}E_{zz}^0(p^2)$	46.825
8. C^{+1}, $t_1t_2\pi_c$; V_3	$\frac{1}{4}N^4\lambda^2\{E[\Omega(C^{+1}, {}^1(sz)y; V_1)]\}+\frac{3}{4}N^2\lambda^2\{E[\Omega(C^{+1}, {}^3(sx)y; V_1)]\}$ $+\frac{3}{4}N^2\{E[\Omega(C^{+1}, {}^3(zx)y; V_1)]\}+\frac{1}{8}N^4\lambda^4\{1-[K_{xz}/(E_{zz}-E_s)]\}E_s^0(s^2p)$ $+\frac{1}{8}N^4\lambda^4\{[(N^4+1)/(N^4\lambda^4)]+(K_{xz}/(E_{zz}-E_s)]\}E_{zz}^0(p^3)$	22.942
9. C^0, $t_1t_2\pi_c^2$; V_2	$\frac{1}{4}N^4\lambda^2\{E[\Omega(C^0, {}^1(sz)y^2; V_0)]\}+\frac{3}{4}N^2\lambda^2\{E[\Omega(C^0, {}^3(sx)y^2; V_0)]\}$ $+\frac{3}{4}N^2\{E[\Omega(C^0, {}^3(zx)y^2; V_0)]\}+\frac{1}{8}N^4\lambda^4\{1-[K_{xz}/(E_{zz}-E_s)]\}E_s^0(s^2p^2)$ $+\frac{1}{8}N^4\lambda^4\{(N^4+1)/(N^4\lambda^4)]+[K_{xz}/(E_{zz}-E_s)]\}E_{zz}^0(p^4)$	13.136±0.8[c]

[a] The carbon orbitals are: $\sigma_c=N(s_c+\lambda z_c)$, $\pi_c=y_c$, and t_1, $t_2=Ns_c-(N/\lambda)z_c\pm(1/\lambda)x_c$, with $\lambda^2=2$ and $N^2=\frac{1}{3}$.

[b] Some observed atomic spectroscopic states involve effects of configuration interaction. Corrections were applied to provide the pre-CI energies which enter the formulas.

[c] The energy (9) may contain an error due to estimation of the C^0, p^4 energy levels (see footnote, Table XXIII) and another error due to the use of K_{zz} in $E_{zz}^0(p^4)$. A 2-ev variation in the C^0, p^4 levels changes (9) by 0.8 ev; a 1-ev variation in K_{zz} changes (9) by only 0.08 ev. The energies of (7) and (8) contain only the K_{zz} error.

APPENDIX C

Two-Center Repulsion Integrals

"Theoretical" repulsion integrals given in Table XI, Sec. III are those calculated with Slater-type orbitals. They were obtained from $Z_c=3.18$, $Z_o=4.55$ and $R_{co}=1.21$ A, from Roothaan's formulas[28] and tables.[29] "Correlated" integrals given in Table XI were obtained from the "theoretical" integrals by subtracting from each a quantity which was an overlap integral times the mean of the empirical corrections to the corresponding one-center integrals. For example, from the "theoretical" $\gamma_{\pi_c\pi_o}$ value was subtracted

$$\tfrac{1}{2}S_\pi[(\gamma_{\pi_c}{}^t-\gamma_{\pi_c}{}^e)+(\gamma_{\pi_o}{}^t-\gamma_{\pi_o}{}^e)]$$

where $\gamma_{\pi_c\pi_o}$, $\gamma_{\pi_c}{}^t$ and $\gamma_{\pi_o}{}^t$ were calculated with the Slater orbitals, and $\gamma_{\pi_c}{}^e$, $\gamma_{\pi_o}{}^e$, were obtained from atomic spectra (Appendix B). The sigma-pi overlap integrals are zero, so for $\gamma_{\sigma_c\pi_o}$ and $\gamma_{\sigma_o\pi_c}$ the sigma overlap integral was used, and for $\gamma_{\pi_c\pi_o}$, there was used the pi overlap integral times the appropriate mean of one-center corrections. "Super-correlated" integrals were obtained from the "correlated" set by changing $\gamma_{\sigma_c\pi_o}$. This integral was reduced by an amount sufficient to make $I_{\sigma\pi}=3.937$ for this set of integrals, as mentioned in Sec. III.

[28] C. C. J. Roothaan, J. Chem. Phys. **19**, 1445 (1951).

[29] C. C. J. Roothaan, *Tables of Two-Center Coulomb Integrals between 1s, 2s, and 2p Orbitals* (University of Chicago, Physics Department, ONR Report, 1955).

APPENDIX D

Supplementary Remarks on Integral Values[30]

Concerning further possible changes in two-center repulsion integral values, recent works of Arai,[31] and of Hurley,[32] indicate that attempts to improve the present calculations through different choices of *two*-center repulsion integrals would be fruitless. It appears that the proper procedure actually lies in the use of "theoretical" two-center repulsions, but considerably different values for the *one*-center integrals than Pariser (and Moffitt, in essence) would prescribe.

Dr. Peter Lykos has pointed out to the authors that under the Pariser-Parr treatment, polyacene spectra formulas[15] involve values only for the *differences* between one-center and two-center repulsions, and that therefore other sets of integrals than that based on Pariser's value for the one-center repulsion will be just as effective for spectra prediction. In particular, a set using one-center integrals based on the Arai-Hurley method should be effective for calculation of binding and ionization energies, and also for excitation energies.

As Hurley points out, Moffitt's method amounts to correcting the "theoretical" *one*-center quantities for the facts (1) that at infinite distance the effective

[30] Written by JMP while at the Experimental Station, E. I. du Pont de Nemours and Company, Wilmington, Delaware, 1956–1958.

[31] T. Arai, J. Chem. Phys. **24**, 435 (1956) and later papers.

[32] A. C. Hurley, Proc. Phys. Soc. (London) **A68**, 149 (1955); **A69**, 49, 301 (1956) and later papers.

TABLE XXV. Results of formulating oxygen valence state energies in terms of one-center quantities.[a]

Valence state	Formulation	Energy (ev)
1. O^{+2}, s^2z^2; V_0	$E_{core}+2I_p+J_{zz}$	47.506
2. O^{+2}, s^2yz; V_2	$E_{core}+2I_p+J_{zy}-\frac{1}{2}K_{zy}$	45.249
3. O^{+1}, s^2xyz; V_3	$E_{core}+3I_p+3J_{zy}-\frac{3}{2}K_{zy}$	15.514
4. O^{+1}, s^2y^2z; V_1	$E_{core}+3I_p+J_{zz}+2J_{zy}-K_{zy}$	(17.77)
5. O^0, s^2x^2yz; V_2	$E_{core}+4I_p+J_{zz}+5J_{zy}-\frac{5}{2}K_{zy}$	0.451
6. O^{-1}, $s^2x^2yz^2$; V_1	$E_{core}+5I_p+2J_{zz}+8J_{zy}-4K_{zy}$	(−2.2)
7. O^{-2}, $s^2x^2y^2z^2$; V_0	$E_{core}+6I_p+3J_{zz}+12J_{zy}-6K_{zy}$	5.518
8. O^0, $s^2x^2y^2$; V_0	$E_{core}+4I_p+2J_{zz}+4J_{zy}-2K_{zy}$	(2.707)
9. O^0, s^2p^4; ^3P	$E_{core}+4I_p+3J_{\pi\pi'}-K_{\pi\pi'}+3J_{\sigma\pi'}-2K_{\sigma\pi'}$	(0)

[a] With values for the valence-state energies from Table XXII and the formulas for Slater-Condon parameters [E. U. Condon and G. H. Shortly, *Theory of Atomic Spectra* (Cambridge University Press, New York, 1935)] we find using the above formulas, $F_2=0.301$ ev from (9)−(8), then $F_0=13.467$ ev and $I_p=-54.561$ ev from (8)−(4) and (6)−(8), and finally $E_{core}=141.9577$ ev$+E[O^0, {}^3P]$ from (9). These values give the oxygen one-center parameters listed in Table X. As emphasized in the text this set cannot reproduce the remaining valence-state energies exactly. The 4- to 5-ev errors in the high-energy states (1) and (2) are of little consequence to the molecular calculation, but we are forced to tolerate the 0.3-ev error in (3) and the 0.04-ev error in (5). [The values these parameters give for (7) is probably as nearly correct as the value in Table XXII.] It might be noted that if (5) were used instead of (8) to evaluate F_2, the new set of parameters would put (8) at 2.934 ev instead of 2.707 ev. This we feel to be too large an error to tolerate in such a low-energy state, and we prefer rather to accept (5) at 0.451 ev instead of the true 0.49 ev. An ordinary least-squares treatment to obtain a set of parameters giving a "best fit" to all or some of these states would not be satisfactory, since it would tend to minimize the error in the less important states at the expense of the more important states.

TABLE XXVI. Results of formulating hybridized carbon valence state energies in terms of one-center parameters.

Valence state	Formulation	Energy (ev)[a]
1. C^0, $t_1t_2\sigma_c^2$; V_2	$E_{core}+2I_{\sigma_c}+J_{\sigma_c\sigma_c}$	(6.672)
2. C^{-1}, $t_1t_2\sigma_c^2\pi_c$; V_3	$E_{core}+2I_{\sigma_c}+J_{\sigma_c\sigma_c}+I_{\pi_c}+2J_{\sigma_c\pi_c}-K_{\sigma_c\pi_c}$	(4.797)
3. C^{-2}, $t_1t_2\sigma_c^2\pi_c^2$; V_2	$E_{core}+2I_{\sigma_c}+J_{\sigma_c\sigma_c}+2I_{\pi_c}+J_{\pi_c\pi_c}+4J_{\sigma_c\pi_c}-2K_{\pi_c\sigma_c}$	13.764
4. C^{+1}, $t_1t_2\sigma_c$; V_3	$E_{core}+I_{\sigma_c}$	(19.684)
5. C^0, $t_1t_2\sigma_c\pi_c$; V_4	$E_{core}+I_{\sigma_c}+I_{\pi_c}+J_{\sigma_c\pi_c}-\frac{1}{2}K_{\sigma_c\pi_c}$	(8.2605)
6. C^{-1}, $t_1t_2\sigma_c\pi_c^2$; V_3	$E_{core}+I_{\sigma_c}+2I_{\pi_c}+J_{\pi_c\pi_c}+2J_{\sigma_c\pi_c}-K_{\sigma_c\pi_c}$	(7.68)
7. C^{+2}, t_1t_2; V_2	E_{core}	43.913
8. C^{+1}, $t_1t_2\pi_c$; V_3	$E_{core}+I_{\pi_c}$	(22.942)
9. C^0, $t_1t_2\pi_c^2$; V_2	$E_{core}+2I_{\pi_c}+J_{\pi_c\pi_c}$	12.813

[a] With values of the valence state energies from Table XXIV we find $G_{\sigma_c\pi_c}(\equiv J_{\sigma\pi}-\frac{1}{2}K_{\sigma\pi})=9.548$ ev and $I_{\pi_c}=-20.972$ ev from (5)−(4) and (2)−(1). Then (6)−(5) gives $J_{\pi_c\pi_c}=10.842$ ev, (8) gives $E_{core}=43.913\pm0.1$ ev$+E[\Omega(C^0, {}^3P)]$, and (4) gives $I_{\sigma_c}=-24.229\pm0.1$ ev. Finally, (1) gives $J_{\sigma_c\sigma_c}=11.217\pm0.1$ ev. With these parameters the remaining state energies are in error by 3 ev for the unimportant (7), and by 0.32 ev for (9). [The value for (3) given by these parameters is probably as good as any other value for (3).] It might appear reasonable to use (7) instead of (8) for evaluating E_{core}, but the new set of parameters so obtained would put (9) at 15.721 ev. This is considerably less acceptable as an approximation to the true 13.136 ± 0.8 than is the 12.813 ev value we use.

The possible error in the energy of (8) (see Table XXIV) causes uncertainty in some of the parameters above. Fortunately for the molecular calculation, the uncertainties *exactly* cancel in giving the energies of states (1)−(6), which means that these energies will be incorporated into the molecular calculation without error. Only in the less important states (7)−(9) will there remain any error.

We note that the valence state data give $G_{\sigma_c\pi_c}$, but do not separate this into $J_{\sigma_c\pi_c}$ and $K_{\sigma_c\pi_c}$. A separation is necessary for the MO formulation, and for consistency with a nonhybridized treatment we use $K_{sz}=2.429$ ev (derived from C^0, sp^3 data) and $K_{zy}=0.632$ ev (from C^0, s^2p^2 data). Then $K_{\sigma_c\pi_c}=N^2[K_{sz}+\lambda^2K_{zz}]=1.231\pm0.1$ ev and $J_{\sigma_c\pi_c}=10.164\pm0.05$ ev.

charge Z for neutral atoms cannot be used for an orbital calculation of the energies of the energies of positive and negative ions, and (2) that in an orbital calculation using even the proper Z's for each neutral and ionic species (or better, Hartree-Fock functions) there remains a true correlation correction due to the fact that these wave functions do not contain inter-electronic terms. The work of Hurley suggests that it is necessary to make only the correlation correction (at the equilibrium internuclear separations occurring in molecules). This implies that in the present calculations we should be using one-center quantities which reproduce certain *modified* valence state energies. These modified energies are to be obtained as follows: Calculate (1) the energies of all valence states, whether neutral or ionic, using the same value Z^0 for the effective charge. Calculate (2) the energies of these valence states using the appropriate one of Z^+, Z^-, Z^0, for each state. Obtain (3) empirical values for the energies of these valence states. Then, [(2)−(3)] is the correlation correction to be subtracted from (1) to give the modified valence state energies which the one-center parameters should be chosen to reproduce. [Z^0 in (1), but not in (2), may be used as a variational parameter in the entire molecular calculation, but, as implied above, Hurley's work shows that the usual Slater value is often close to what would be found variationally.]

In spite of the fact that a satisfactory *a priori* prescription was not used in obtaining repulsion integrals for the present calculations, the possibility exists that the stringency of the proper charge-following requirement (see Sec. V) has resulted in a set of integrals which has *differences* of one-center and two-center values in the neighborhood of the differences which would be found by following an Arai-Hurley motivated prescription.

Photolysis of Ammonia in a Solid Matrix at Low Temperatures*

O. SCHNEPP† AND K. DRESSLER‡

National Bureau of Standards, Washington 25, D. C.

(Received December 2, 1959)

Solid deposits of argon containing 0.3 mole % ammonia were irradiated at 4.2°K with light of wavelengths shorter than 2000 A. The emission of a hydrogen discharge with a LiF window and of a thin-walled quartz mercury arc were used. The production of the unstable species NH and NH_2 was observed by means of electronic absorption spectroscopy. Experiments using filters led to the conclusion that NH is produced by irradiation with light of wavelengths shorter than 1550 A. NH_2 is produced by radiation above 1700 A and below 1550 A with comparable quantum efficiency. Warmup experiments show that NH_2 disappears close to 20°K whereas NH is stable up to at least 36°K. Photolysis at 20°K is approximately five times less efficient than at 4.2°K. On certain assumptions a molar absorption coefficient of 40 000 is estimated for both NH and NH_2 and the f values of the observed transitions of these molecules are estimated to be of the order of 10^{-3}.

I. INTRODUCTION

IN the course of an investigation which was aimed at studying the vacuum ultraviolet absorption spectrum of a dilute solid solution of ammonia in argon, it was discovered that the known[1] absorption spectrum of the NH radical at 3380 A appeared on the plates. It was therefore decided to investigate the formation of NH and NH_2 radicals during photolysis with light of wavelengths shorter than 2000 A.

Photolysis of ammonia is expected to occur in wavelength regions where its absorption spectrum is diffuse or continuous. The longest wavelength region of absorption of ammonia has been reported[2] to consist of diffuse bands extending from 2260 A to shorter wavelengths, superimposed on continuous absorption whose intensity reaches a maximum near 1900 A and then decreases to reach a minimum at about 1550 A. Beyond this wavelength a second region of absorption is characterized by a continuous background whose intensity increases steeply with wavelength. Sharp bands are superimposed on this continuum.

Photolysis of ammonia gas has been reported to yield the NH_2 radical[3] and this unstable species has been extensively studied spectroscopically.[4] However the NH radical has not been previously reported as a product of the photolysis of ammonia although it has been observed as a product of explosive reactions in hydrazine, initiated by a photolyzing flash.[5] The absorption spectra of trapped NH and NH_2 radicals in solid argon have been identified by Robinson and McCarty[1] in the products from electric discharges condensed at low temperature. The same spectra have been observed here and have been used to monitor the formation of the radicals in the photolysis experiments.

II. EXPERIMENTAL

Ammonia gas was condensed in a liquid nitrogen trap from a storage cylinder and allowed to warm up after volatile impurities had been pumped off. The middle fraction was distilled off and mixed with argon gas in the ratio 1:300. This mixture was admitted into the vacuum space of a stainless-steel double Dewar and deposited on a sapphire window at 4.2°K. The rate of deposition was such that a layer of 2 μ thickness was produced in the 10 min during which the gas was admitted at a constant rate. The layer thickness of the deposit was determined on the basis of the observation that first-order yellow interference color in reflected light appeared in the center of the window after one minute of deposition. The interference colors could be clearly observed to fourth order and indicated constant increase of the layer thickness with time for the first five minutes of deposition. We assumed an index of refraction of 1.25 for the solid argon deposit containing 0.3% ammonia. This value is obtained by correcting the molar refractivity of gaseous argon for the change in density on solidification and is believed to be accurate to at least 10% for our condensed gas mixture. The layer thickness previously quoted is thus also correct within these limits but holds only for the center of the cold window which was round and about 1 cm in diameter. The range of interference colors which ap-

* This research was performed under the National Bureau of Standards Free Radicals Research Program, supported by the Department of the Army. This work was supported in part by the Office of Ordnance Research.

† On leave from the Department of Chemistry, Israel Institute of Technology, Haifa, Israel.

‡ Guest Scientist from the Department of Chemistry, the Catholic University of America, Washington 17, D.C. Present address: Princeton University Observatory, Princeton, New Jersey.

[1] G. W. Robinson and M. McCarty, Jr., J. Chem. Phys. **28**, 349, 350 (1958); **30**, 999 (1959); M. McCarty, Jr., and G. W. Robinson, J. Am. Chem. Soc. **81**, 4472 (1959); for a reproduction of spectra, see Can. J. Phys. **36**, 1590 (1958).

[2] K. Watanabe, J. Chem. Phys. **22**, 1564 (1954), earlier references are given in this paper.

[3] G. Herzberg and D. A. Ramsay, J. Chem. Phys. **20**, 347 (1952); D. A. Ramsay, *ibid.* **21**, 165 (1953).

[4] K. Dressler and D. A. Ramsay, Phil. Trans. Royal Soc. (London) **A251**, 553 (1959).

[5] D. A. Ramsay, J. Phys. Chem. **57**, 415 (1953).

peared at different parts of the window indicated that the thickness of the deposit varied uniformly from one extreme edge to the other, from 50 to 150% of the thickness measured at the center.

The source of the photolyzing radiation was in most cases a conventional hydrogen source, operated at about 200 v-a and at a hydrogen pressure of 45 mm. This source was provided with a lithium-fluoride window and bolted directly to the Dewar. Some experiments were performed using a low-pressure mercury arc which was certified by the manufacturer to emit about 50% of its output energy at 1849 A. The mercury arc was also mounted so that no air separated the thin-walled quartz lamp from the deposit, and was operated at about 300 v-a. Both lamps were at a distance of 12 cm from the cold window, and the radiation was incident on that side of the window which held the deposit.

The unstable molecules NH and NH_2 were detected by their absorption spectra in the near ultraviolet and visible spectral region, respectively. A 150-w high-pressure xenon arc was used as a source for both spectra but these were photographed on two different spectrographs. The absorption due to NH at 3380 A was recorded on Eastman-Kodak 103a-0 plates by means of a quartz Hilger F-4 spectrograph. The absorption due to NH_2 was photographed on 103a-F plates with a medium Hilger spectrograph with glass optics. When the hydrogen source was used as photolysis lamp the spectra could be photographed through the source tube but in the case of the mercury lamp this had to be removed for the observation of the absorption spectra. A simple mirror arrangement permitted spectra to be taken on one or the other of the two spectrographs. It was thus possible to record the spectra of the two unstable species in short succession. Slit widths of 10 μ were used throughout and the exposure times were of the order of seconds, ranging from less than a second to 10 sec.

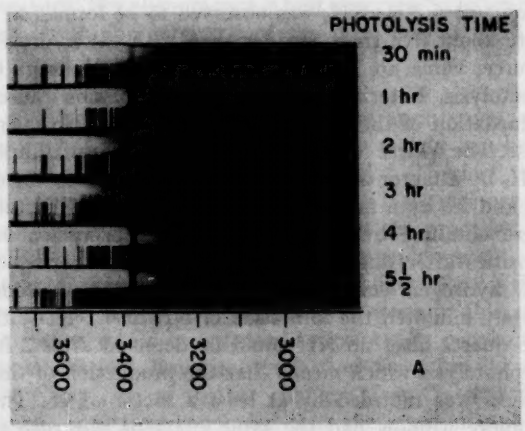

FIG. 1. Reproduction of plate showing the formation of NH radicals during the photolysis of a deposit of solid argon containing 0.3 mole % ammonia at 4.2°K. The photolyzing radiation was the emission of a hydrogen discharge. The light source for the absorption spectra was a high-pressure xenon lamp.

TABLE I. Summary of the effect of experimental conditions on the rate of formation of NH and of NH_2. The rates of formation of these species on photolysis of 0.3% ammonia in argon at 4.2°K with a hydrogen discharge source were taken to be unity for each of the two radicals. The rates listed represent rounded-off relative values within each column.

Source	Filter	Temp.	Relative rate of production NH	Relative rate of production NH_2
H_2 source	(LiF)	4.2°K	1.0	1.0
	quartz		<0.1	0.1
			Not detected	
	Sapphire		0.1	0.1
	Ice		<0.1	<0.1
			Not detected	
	(LiF)	20°K	0.2	0.2
Hg arc	...	4.2°K	<0.1	0.2
			Not detected	

The cold window was clamped to a copper block with the aid of indium wire gaskets to insure the best possible thermal contact. The copper block was screwed into the bottom of the helium container. Temperatures were measured by means of a thermocouple soldered to the copper block. The window temperature is likely to be a few degrees higher than that of the copper mount due to imperfect thermal contact. After all the coolant (liquid helium or liquid hydrogen) had evaporated from the Dewar, the temperature of the window rose slowly enough to allow spectra to be recorded as a function of temperature between 4.2°K and about 40°K. Above this temperature, the vapor pressure of the solid argon on the window was high enough to break the insulation and allow conductivity from the liquid nitrogen compartment so that 77°K was quickly reached. Therefore no observations could be made above 40°K.

Experiments were performed in which the photolyzing radiation was filtered before reaching the deposit. The filters used were quartz and sapphire windows which were tested on a vacuum spectrograph for transmission properties. The quartz window transmitted about 50% of the light out to 1570 A, where its absorption began rising steeply, allowing only 1% transmission at 1540 A. The sapphire window's transmission was 50% at 1800 A, 10% at 1700 A and 1% at 1500 A. These transmission data represent visual estimates directly from photographic plates. In another experiment, a layer of ice was deposited on top of the ammonia argon layer. The layer thickness of ice was chosen as 3μ, which produces a very steep cutoff at 1630 A.[6]

III. RESULTS

In Figs. 1 and 2 the results of a typical photolysis experiment at 4.2°K are shown. The photolyzing radi-

[6] K. Dressler and O. Schnepp, J. Chem. Phys. (to be published).

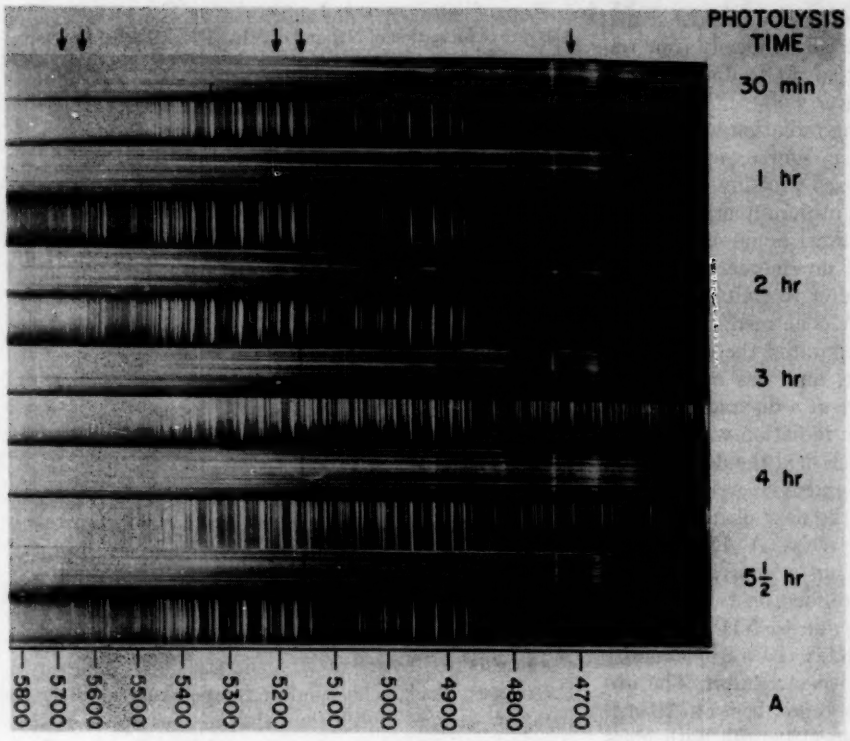

FIG. 2. Reproduction of plate showing the formation of NH_2 radicals during the photolysis of a deposit of solid argon containing 0.3 mole % ammonia at 4.2°K. The photolyzing radiation was the emission of a hydrogen discharge. The light source for the absorption spectra was a high-pressure xenon lamp.

ation was the emission of a hydrogen discharge through a lithium fluoride window. The known absorption spectra[1] of NH and NH_2 in solid argon at 4.2°K are seen to be clearly distinguishable after a half hour of photolysis. The absorption intensities clearly increase during the first two hours and then level off. It is possible that the NH_2 concentration levels off somewhat sooner but this cannot be said with certainty due to the error involved in the visual comparison of intensities. The building-up process of NH_2 is best followed by comparing the intensities of the lines at 5150 A and 5195 A at different stages of photolysis in Fig. 2. The figure shows in addition the lines at 4711 A, 5625 A, and 5684 A. Other NH_2 absorption lines were also observed, but due to the variation in plate sensitivity and source intensity with wavelength it was not convenient to include a wider spectral range in the figures. The NH concentration is indicated by the absorption intensity of the complex feature at 3380 A in Fig. 1.

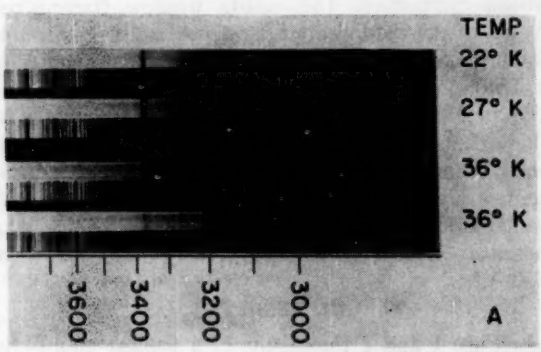

FIG. 3. Reproduction of plate illustrating the stability of the NH radical during warm up of a deposit of 0.3 mole % ammonia in argon which had been photolyzed at 4.2°K.

Table I summarizes the effect of experimental conditions on the rate of production of NH and NH_2. When the mercury source was used for photolysis of ammonia at 4.2°K, NH_2 was observed to be formed at a rate about five times smaller than with the hydrogen source, while no NH was detected after 2½ hours of photolysis. Filtering of the hydrogen emission caused retardation of the NH_2 production at 4.2°K in every case. The quartz filter reduced the rate of formation of NH_2 by a factor of 8, the sapphire filter by a factor of 10 and ice by a factor of more than 12. These factors were obtained by visual matching of absorption intensities after different photolysis times. Filtering of the hydrogen emission variously retarded or completely inhibited the formation of NH at 4.2°K. With the quartz filter no NH could be detected after 2 hr of photolysis which means that the production of this radical was retarded by at least a factor of 15. The sapphire window had the same effect on the rate of production of NH as on that of NH_2, i.e., it retarded its formation by a factor of 10. No NH could be detected with the ice filter which means a retardation by at least a factor of 15. An experiment was performed in

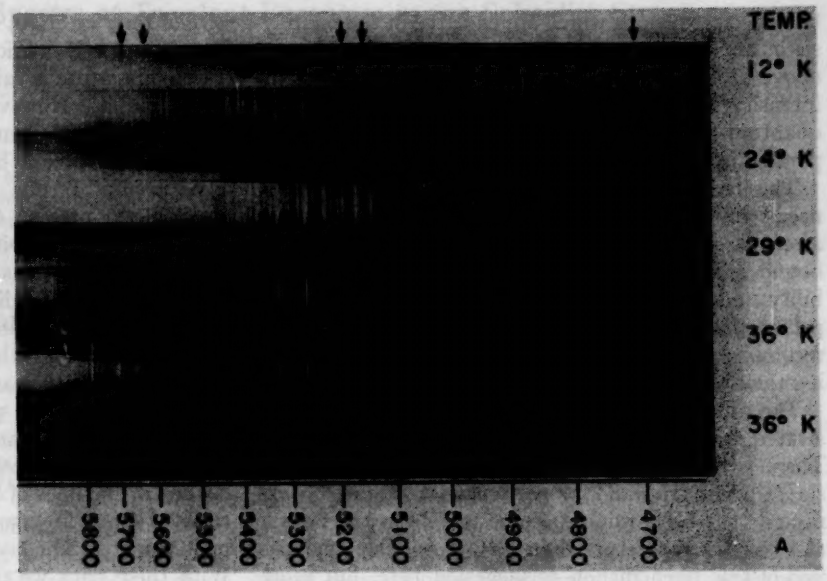

FIG. 4. Reproduction of plate illustrating the change of concentration of the NH_2 radical during warm up of a deposit of 0.3 mole % ammonia in argon which had been photolyzed at 4.2°K.

which ammonia in argon, in the same concentration as before, was photolyzed with the hydrogen source at 20°K. In this case the formation of both NH and NH_2 was retarded by a factor of about 5.

The relative stability of each radical as a function of temperature was studied by following their characteristic absorptions during warmup after photolysis at 4.2°K. The results of such a study are shown in Figs. 3 and 4. It is to be noted that the NH and NH_2 spectra were taken alternately so that the stabilities of these radicals can be compared without reference to the absolute temperature measurements. NH is seen to be stable up to the highest temperature investigated (36°K). NH_2 on the other hand, seems to be quite stable at 12°K but rapidly disappears above this temperature. The phenomenon is best observed by following the absorption intensity of the NH_2 line at 5684 A in Fig. 4.

IV. DISCUSSION

The buildup of the radical concentrations produced by photolysis of ammonia in argon matrix has been described with the aid of Figs. 1 and 2. The fact that the concentrations of both NH and NH_2 increase at first and then level off indicates that the processes by which these species are formed are independent. In other words, it is not thought to be likely that NH is formed from the photolysis of NH_2 since in this case the latter would be expected to eventually decrease in concentration. Experiments lasting for 6 hr did not show any sign of further changes after the first two hours. It is thus concluded that the experimental results indicate that both NH and NH_2 are primary products of photolysis. The leveling off of the radical concentrations with photolysis time is believed to indicate approach to complete decomposition of the ammonia sample. Absorption of the light by the radicals formed is not believed to protect some of the ammonia sample from photolysis since an estimate based on molar absorption coefficients of 50 000 in the vacuum ultraviolet and assuming total conversion shows that 20% of the light is still transmitted by the deposit even at the wavelengths of such intense absorption. As a result, it seems likely that the radical concentration in the matrix after photolysis is of the order of the ammonia concentration before photolysis.

As has been described, experiments were performed in which the rate of production of radicals was studied as the experimental conditions were varied. The results are summarized in Table I. These indicate that NH is not formed on photolysis with light of wavelength longer than 1550 A. The sapphire filter does not eliminate the formation of NH completely, probably due to its low transmission region which extends to comparatively short wavelengths. NH_2, on the other hand, is produced with reasonable efficiency by 1850 A radiation. The quartz filter experiment with the hydrogen source demonstrates that this source is about 10 times more effective in producing NH_2 below 1550 A than above this wavelength. The sapphire filter experiment similarly shows that the hydrogen source is about 10 times more effective below 1700 A than above this wavelength. The region between 1550 A and 1700 A therefore is concluded to be comparatively ineffective in producing photolysis. This conclusion is the more valid since the hydrogen emission is five times more intense in the region 1550 to 1650 A than in the region 1300 to 1550 A and fifty times more intense than in the region above 1700 A. This observation is consistent with the fact that the absorption spectrum of gaseous ammonia has a minimum near 1550 A. There are then

two spectral regions which are effective in the photolysis of ammonia in argon matrix to produce NH_2, one above 1700 and the other below 1550 A. In view of the intensity distribution in the hydrogen emission the quantum efficiencies may be concluded to be comparable in these two regions.

The reduced rate of radical production at 20°K needs some comment. It is known that hydrogen atoms are unstable at that temperature in weakly bound solid matrices,[7] presumably due to their mobility under these conditions. It is therefore to be expected that hydrogen atoms formed during photolysis recombine with the NH and NH_2 radicals, thus reducing their rate of formation.

The difference in stability of NH and NH_2 demonstrated by the warm up experiments is unexpected. There is no obvious reason why NH should be more stable than NH_2, and in particular it cannot be expected that NH_2 would become mobile in the matrix at a lower temperature than NH. A possible explanation of this phenomenon is suggested here, but more experimental work is necessary to test it. It was argued that both radicals are formed during primary photolysis processes. In this case, formation of NH will be accompanied by the splitting off of two hydrogen atoms or, more probably, a hydrogen molecule, while formation of NH_2 will be accompanied by the formation of a single hydrogen atom. If now during photolysis at 4.2°K the hydrogen atoms do not move far from the site of their creation, recombination between hydrogen atoms and NH_2 radicals will occur very efficiently as the temperature is raised and the hydrogen atoms become mobile. However, recombination between NH radicals and hydrogen molecules is improbable since it may well involve a high potential barrier. No direct experimental results supporting this hypothesis are available at present. Some recent results reported by Cochran[8] dealing with the production of NH_2 by photolysis of various substances using paramagnetic resonance as the radical detection technique are not consistent with the proposed mechanism.

Assuming that the radical concentration after photolysis is of the same order as the concentration of the ammonia before photolysis, we can estimate absorption coefficients and f values. We estimate visually from the plates that 90% of the light is absorbed in the centers of the lines of both NH and NH_2. The dilution ratio of 1:300 in argon gives a concentration of 0.14 mole per liter. The layer thickness is known to be 2 μ. With these data we calculate a molar absorption coefficient of 40 000. An order of magnitude estimate of the f value was made assuming the spectral width over which the quoted absorption coefficient is to be integrated to be 10 cm^{-1}. This gives f values of 10^{-3} for both NH and NH_2. Since the highest possible radical concentration and a rather narrow spectral band has been assumed here, this value has to be taken as a lower limit.

[7] C. K. Jen, S. N. Foner, E. L. Cochran, and V. A. Bowers, Phys. Rev. **104**, 846 (1956); **112**, 1169 (1958); L. A. Wall, D. W. Brown, and R. E. Florin, J. Chem. Phys. (to be published).

[8] E. L. Cochran, paper delivered at the Fourth International Symposium on Free Radical Stabilization, held at the National Bureau of Standards, Washington, D.C. (September, 1959).

Multiple Emission Spectra of Trivalent Europium in the Scheelite Structure

L. G. VAN UITERT AND R. R. SODEN

Bell Telephone Laboratories, Inc., Murray Hill. New Jersey

(Received November 25, 1959)

Spectra resulting from emission from four electronic levels are observed for members of the series $Ca_{1-2x}Na_xEu_xWO_4$. Their relative intensities are concentration dependent. Successively lower lying emission levels are quenched by what appear to be exchange interactions resulting from coupling between two or more neighboring Eu^{3+} ions.

INTRODUCTION

THE absorption and emission spectra of trivalent europium have been examined by a number of investigators.[1–5] This ion is of particular interest because of its known multiple emission states[2,3] and the rather marked dependence of the intensities of its spectral lines upon the nature of its host lattice.[4] Synthetic scheelite ($CaWO_4$) containing europium was studied by de Rohden[5] as early as 1915. He reported the more intense lines of the visible part of the spectrum, but not much of the weaker structure including many of the lines found by Gobrecht[2] in the rare earth octahydrosulfate.

The principal studies of the emission of trivalent europium have been carried out employing its hydrated sulfates, bromates, and chlorides; metal organic compounds; and anhydrous fluorides. As has been found in the case of trivalent terbium,[6] such environments quench emission from certain electronic levels. The examination of the fluorescent spectra of crystals of the isomorphous series $CaWO_4$-$Na_{0.5}Eu_{0.5}WO_4$ herein shows that emission from four electronic levels contributes to the spectra shown by Eu^{3+} in the scheelite structure.

MATERIALS

Members of the series $Ca_{1-2x}Na_xEu_xWO_4$, where $x=3\times10^{-5}$, 10^{-4}, 5×10^{-4}, 10^{-2}, 0.1, and 0.50, were prepared by crystallization from a sodium ditungstate flux, as described previously.[7] The luminescent efficiencies of the tungstates are quite dependent upon lattice perfection. The flux method of preparation provides for a uniform lattice in the several samples so that emission intensities can be readily compared.

MEASUREMENTS

Measurements were carried out employing a Gaertner spectrometer adapted with an AMINCO photomultiplier microphotometer employing a 1P22 tube. The several compositions were measured in the amounts required to fill a holder slot which was 1 in. long$\times\frac{1}{2}$ in. wide by $\frac{1}{4}$ in. deep. The samples were excited by a 3660 A rich H4 spotlight through a Corning 5874 filter. Long-wave uv radiation was employed to avoid strong broad-band emission which results when employing higher frequency sources. Mercury lines have been deducted from the plotted spectra, and the intensities of emission have been corrected for the sensitivity variations of the system. All measurements are compared to a common standard—the intensity of the 545 A peak in $Na_{0.5}Tb_{0.5}WO_4$[6] which is given the value of 100.

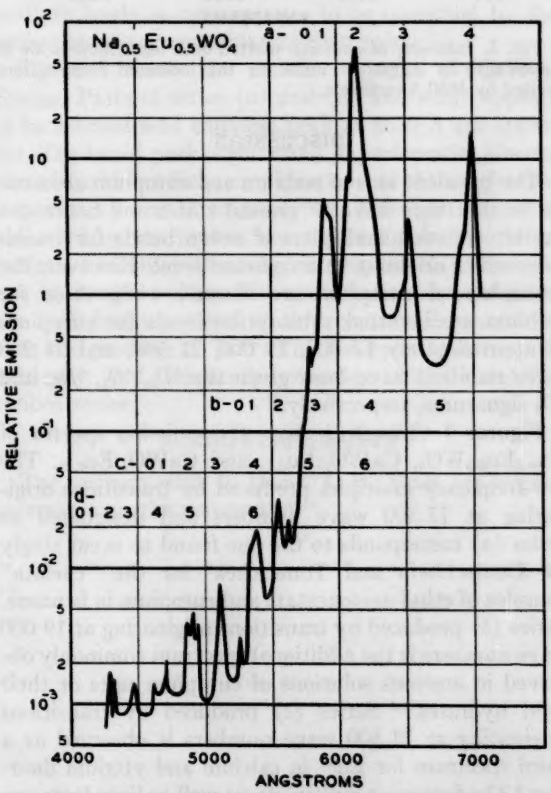

FIG. 1. Intensity of emission plotted on a logarithmic scale vs wavelength in Angstrom units for the indicated compositions excited by 3660 A radiation.

[1] See references in P. Pringsheim, *Fluorescence and Phosphorescense* (Interscience Publishers, New York, 1949).
[2] H. Gobrecht, Ann. Phys. (5) **28.S**, 673–700 (1937).
[3] O. Deutschbein and R. Tomaschek, Ann. Phys. (5) **29.S**, 311 (1937).
[4] Reference 1, Chap. 6.
[5] M. Ch. de Rohden, Ann. Chim. **3**, 338 (1915).
[6] L. G. Van Uitert and R. R. Soden, J. Chem. Phys. (to be published).
[7] L. G. Van Uitert and R. R. Soden, J. Chem. Phys. (to be published).

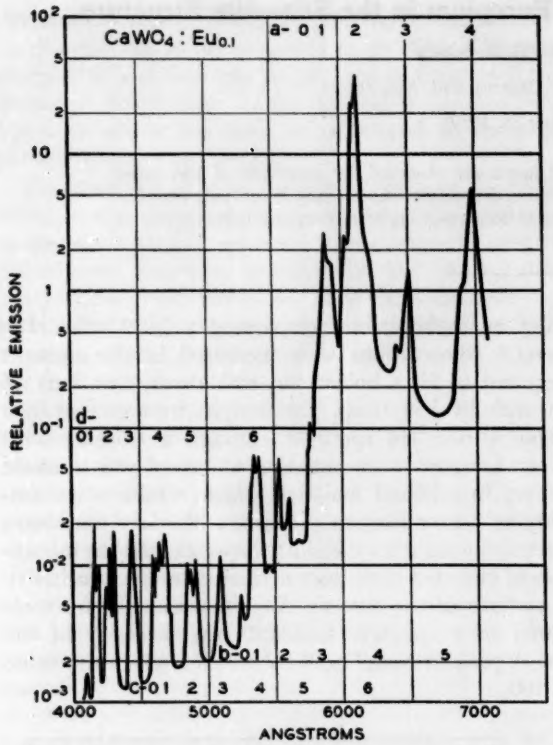

FIG. 2. Intensity of emission plotted on a logarithmic scale vs wavelength in Angstrom units for the indicated compositions excited by 3660 A radiation.

DISCUSSION

The trivalent ions of terbium and europium are similar in that they have ^7F ground states and hence can exhibit emission multiplets of seven bands for transitions which originate at a common level. However, the multiplets of europium are normal, while those for terbium are inverted. Absorption levels for europium at approximately 17 300, 19 000, 21 500, and 24 200 wave numbers have been given the $^5D_0$, $^5D_1$, $^5D_2$, and $^5D_3$ signatures, respectively.[8]

Figures 1 through 3 show the emission spectra of $Na_{0.5}Eu_{0.5}WO_4$, $CaWO_4$:$Eu_{0.1}$, and $CaWO_4$:$Eu_{0.01}$. The low-frequency multiplet produced by transitions originating at 17 300 wave numbers and designated as series (*a*) corresponds to the one found to occur singly by Deutschbein and Tomaschek[3] for the "chelate" complex of ethyl-acetoacetate and europium in benzene. Series (*b*) produced by transitions originating at 19 000 wave numbers is the additional spectrum commonly observed in aqueous solutions of europium salts or their solid hydrates.[2,3] Series (*c*) produced by transitions originating at 21 500 wave numbers is observed as a third spectrum for Eu^{3+} in calcium and yttrium fluorides.[9] The foregoing multiplets, as well as lines from one originating at 23 900 wave numbers [series (*d*) in these figures], have been observed in calcium oxide.[3,10] The lines of the (*d*) series in particular are observed in much greater detail in the scheelite structure than in the environment previously reported. The foregoing relationships suggest that the extent to which the *f* electrons of the rare earths are perturbed by their surroundings decreases in the order: oxygen chelates > hydrates > fluorides > oxides.

As shown in Fig. 1, the intensities of the several spectra decrease rapidly as the wave numbers of the emitting electronic levels increase in $Na_{0.5}Eu_{0.5}WO_4$. In comparison, the intensity of series (*a*) is decreased in $CaWO_4$:$Eu_{0.1}$, as shown in Fig. 2, while there is a marked increase in that for (*d*) and somewhat smaller increases for (*b*) and (*c*). In $CaWO_4$:$Eu_{0.01}$, the intensity of series (*a*) is further decreased, as seen in Fig. 3, while that for series (*d*) has again increased. At lower europium contents, there is a steady decrease in intensity for each of the spectra with concentration.

The dependencies of intensity upon concentration for the several spectra are shown in Fig. 4. The wavelengths indicated correspond to a strong line for each of the spectra. The data follow a pattern similar to that reported for trivalent terbium in the scheelite structure.[6] It was indicated in the former work that exchange

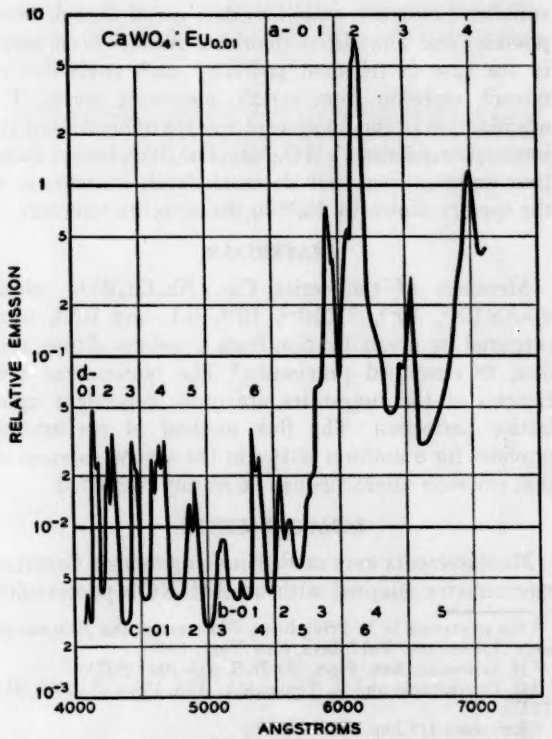

FIG. 3. Intensity of emission plotted on a logarithmic scale vs wavelength in Angstrom units for the indicated compositions excited by 3660 A radiation.

[8] G. H. Dieke and L. A. Hall, J. Chem. Phys. **27**, 465 (1957).
[9] N. Chatterjee, Z. physik **113**, 96–114 (1939).
[10] S. Fagerberg, Nov Acta Regia Soc. Sci. Upsaliensis **7**, 6 (1931).

coupling between the paramagnetic rare earth ions could account for the quenching of high-wave-number emission states.

The high-frequency spectrum (d) of Eu^{3+}, while much less intense than the comparable spectrum of Tb^{3+}, has a concentration dependence similar to the latter. Both show maximum intensities when 1 to 3% of the calcium sites are occupied by the rare earth ions. The high-frequency spectra are probably associated with the isolated paramagnetic ions in this structure; that is, with Tb^{3+} or Eu^{3+} ions which do not have like ions in any of their four nearest neighbor calcium sites. The maxima may then occur for the compositions having the greatest concentrations of such isolated rare earth ions. On a statistical basis, they would be expected at concentrations greater than those observed. The difference is attributable to the attractive energy associated with exchange coupling.

The spectra originating at intermediate electronic levels show similar maxima when about 20% of the calcium sites are occupied by Eu^{3+}. This may correspond to the concentration at which the sum of the isolated and paired Eu^{3+} ions is greatest. Emission from the intermediate levels in turn appears to be quenched by the formation of aggregates larger than pairs.

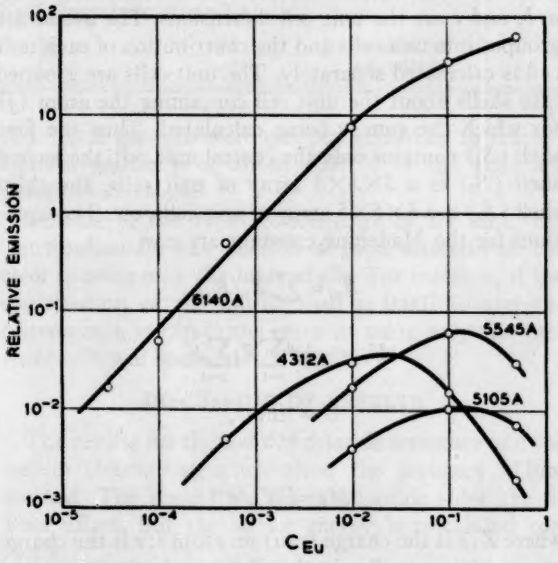

FIG. 4. Intensity of emission vs Eu^{3+} concentration for strong lines of the several spectra of europium: a=6140 A, b=5545 A, c=5105 A, d=4312 A; C_{Eu}=Eu^{3+} ions per formula volume of $CaWO_4$.

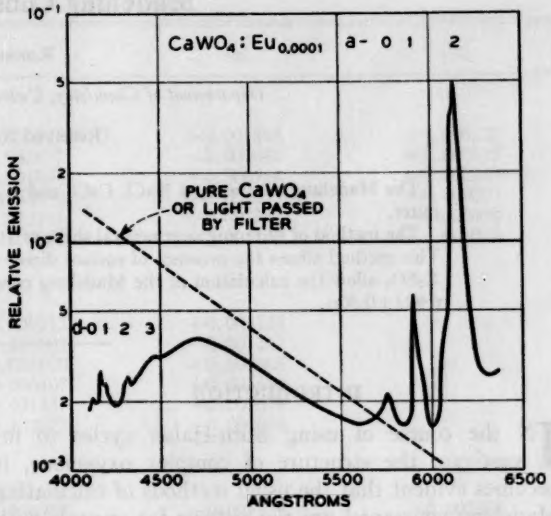

FIG. 5. Intensity of emission plotted on a logarithmic scale vs wavelength in Angstrom units for the indicated compositions excited by 3660 A radiation.

Figure 5 shows the emission spectra of $CaWO_4$: $Eu_{0.0001}$. Parts of series (a) and (d) and what appears to be a broadband emission peak at 4650 A are apparent. The broad peak is the result of preferential absorption of the higher-frequency components of the light that is passed by the filter employed. The light passed is indicated by the broken line in the figure. The latter pattern was observed using either pure $CaWO_4$ or an empty sample holder. The preferential absorption at the high frequency end of the spectrum is associated with the presence of Eu^{3+}. The absorption increases in efficiency and frequency coverage with increasing concentration.

ACKNOWLEDGMENTS

The authors wish to thank J. H. Scaff for helpful comments on the manuscript.

Madelung Constant for K_2SO_4(II)

ROBERT H. WOOD

Department of Chemistry, University of Delaware, Newark, Delaware

(Received November 30, 1959)

The Madelung constants of NaCl, CsCl, and K_2SO_4 have been calculated with the aid of a digital computer.

The method of summing over neutral shells of atoms with each shell being composed of unit cells is used. This method allows the presence of surface dipole moments (de Boer effect) to be ignored. The results for K_2SO_4 allow the calculation of the Madelung constant as a function of the charge on the oxygen ($M_\delta = 6.922+0.36\epsilon$).

INTRODUCTION

IN the course of using Born-Haber cycles to investigate the structure of complex oxyanions, it becomes evident that the usual methods of calculating Madelung constants[1] are too tedious for crystals with little symmetry.

In order to reduce the labor involved a method was developed which converged rapidly even for crystals of low symmetry, and in which the calculations could be easily performed by a digital computer.

CALCULATIONS

Evjen[2] calculates the Madelung constant by dividing the crystal into a series of neutral, concentric shells and calculating the contribution of each shell to the energy of an ion in the center of the shells. Accuracy is easily achieved because the contribution of each shell falls off rapidly with increasing size of the shell. However, de Boer[3] has shown that a correction for surface dipole moments is necessary. The effect of a surface dipole moment on the energy of an ion is given by the following formula:

$$E=(Z_j)eV=(Z_j)e\mu d\Omega$$

where V is the potential due to the surface dipole; Z_j is the charge on the atom, μ is the dipole moment per unit area; $d\Omega$ is the solid angle intercepted by the surface dipole with respect to the atom; and e is the charge on an electron. Because a "molecule" is neutral it is easily seen that a correction for the de Boer effect is not necessary if the same surface dipole moment is present in the calculation of all of the atoms in a molecule. In order to exclude the necessity for a correction for the de Boer effect, the lattice energy has been calculated as the following sum:

$$U=-\tfrac{1}{2}\sum_{j=1}^{n}e_j\sum_m\sum_l\sum_k\sum_i e_i[(x_j-x_i-ka)^2+(y_j-y_i-lb)^2+(z_j-z_i-mc)^2]^{-\frac{1}{2}}$$

where n is the number of atoms in a "molecule," and a, b, and c are the unit cell dimensions. The atoms are grouped into unit cells and the contribution of each unit cell is calculated separately. The unit cells are grouped into shells about the unit cell containing the atom (j) for which the sum is being calculated. Thus the first shell (S_1) contains only the central unit cell, the second shell (S_2) is a $3\times3\times3$ array of unit cells, the third shell (S_3) is a $5\times5\times5$ array of unit cells, etc. The equations for the Madelung constant are now

$$S_{pj}=\sum_i Z_i/R_{ij}$$

$$U_r=-\tfrac{1}{2}e^2\sum_{j=1}^{n}Z_j\sum_{p=1}^{r}S_{pj}$$

$$U=\lim_{r\to\infty}U_r$$

and

$$M_\delta=UV_m^{\frac{1}{3}}e^{-2}$$

where $Z_i e$ is the charge (esu) on atom i; e is the charge on an electron; R_{ij} is the distance between atom i and atom j; the sum over $j=1$ to n includes all atoms in a "molecule"; the sum over i includes all atoms in shell p; U is the lattice energy; V_m is the volume of a "molecule" and M_δ is the Madelung constant using $(V_m)^{\frac{1}{3}}$ as the characteristic distance. The results of several calculations as given in Tables I and II show the rapid convergence of this method of grouping unit cells.

This rapid convergence is not attained with some methods of grouping unit cells. For instance, if the cells are grouped according to their contribution to the energy and all cells whose contribution is less than a certain amount are discarded, then the convergence is very poor. An 8-hr calculation for potassium sulfate (using a Bendix G-15D computer) gave an accuracy

[1] For a review of methods see J. R. Partington, *Advanced Treatise on Physical Chemistry* (Longmans-Green, London, 1952), Vol. 3, p. 373; T. C. Waddington, Advances in Inorganic and Radiochemistry **1**, 157 (1959).

[2] H. M. Evjen, Phys. Rev. **39**, 675 (1932).

[3] F. de Boer, Rec. trav. chim. **67**, 697 (1948); also E. J. W. Verwey, F. de Boer, and J. H. Van Santen, J. Chem. Phys. **16**, 1091 (1948).

TABLE I. S_{pj} for K_2SO_4(II), CsCl, and NaCl.

Atom	Charge z_j	S_{1j}	S_{2j}	S_{3j}	S_{4j}
K_2SO_4					
K_1	+1	−0.481749	−0.050845	+0.001816	+0.000229
K_2	+1	−0.525151	−0.055177	−0.002049	+0.000127
S	+2	−1.893520	+0.091894	+0.000764	−0.000185
O_1	−1	+0.824810	+0.124959	+0.001813	−0.000057
O_2	−1	+0.945990	+0.013283	−0.002747	−0.000490
O_3	−1	+1.048173	−0.106033	−0.001162	−0.000050
K_2SO_4					
K_1	+1	−0.580237	−0.009217	+0.004154	
K_2	+1	−0.337196	−0.151602	−0.007242	
S	−2	+0.824617	+0.083990	+0.000805	
O_1	0	−0.536659	+0.080407	+0.001654	
O_2	0	−0.459494	+0.031337	−0.001673	
O_3	0	−0.577641	+0.134872	+0.004974	
CsCl (Hypothetical) a_0=1 A					
Cs	+1	−1.154703	+0.646980	+0.027728	+0.007386
Cl	−1	+0.442366	+3.131296	+0.016945	+0.007475
NaCl (hypothetical) a_0=2 A					
Na	+1	−1.456034	−0.290975	−0.000386	+0.000067
Cl	−1	+0.802683	+0.945788	−0.000713	+0.000071

of 1.3% if the cells were grouped according to energy, and an accuracy of about 0.001% if the cells are grouped into shells.

Because of the rapid convergence of the sum, the contribution on any shell is a good estimate of the error in using only the inner shells. For instance, if the contribution of the fourth shell is 0.007%, and the convergence is rapid, the error in using only the first three cells will be about 0.007%.

DISCUSSION OF RESULTS

The results for the sodium chloride structure and the cesium chloride structure show the accuracy of the method. The results for cesium chloride show the de Boer effect, but the lattice energy is calculated correctly.

The calculations for K_2SO_4 are for the atomic positions given by Wycoff[4] with the unit cell lengths given by Swanson *et al.*[5]

The results for K_2SO_4 can be used to derive electrostatic energies and Madelung constants as a function of the charge on the oxygen atoms (ϵ).

(1) For

$$K_2S^{(-2-4\epsilon)}O_{4c}=2K_g^{+}+S_g^{(-2-4\epsilon)}+4O_g,$$

$$U=(1.4501+5.3936\epsilon+8.1956\epsilon^2)e^2 \text{ esu}^2/\text{A},$$

$$M_3=6.922+25.745\epsilon+3.912\epsilon^2.$$

(2) For

$$K_2SO_{4(c)}=2K_g^{+}+SO_{4g}^{=}(D_{S-O}=1.504 \text{ A},$$

$$U=(1.4501+0.074\epsilon)e^2 \text{ esu}^2/\text{A},$$

$$M_3=6.922+0.36\epsilon,$$

where e is the charge on the electron in esu. These results were derived using the fact that for any atom $\Sigma_p S_{pj}=A+B(\epsilon)$ where A and B are constants and ϵ is the charge on the oxygen with the total charge on the sulfate remaining constant. This is easily proved if $\Sigma_p S_{pj}$ is broken down into a sum over all oxygen atoms, a sum over all sulfur atoms, and a sum over all potassium atoms.

The difference between Eqs. (1) and (2) is just the electrostatic energy of the gaseous sulfate ion. This energy was calculated assuming a tetrahedral configura-

TABLE II. Lattice energies U_r/e^2.

Crystal	U_1/e^2	U_2/e^2	U_3/e^2	U_4/e^2
K_2SO_4 $\epsilon=-1$	+4.330543	4.254748	4.252471	4.252155
K_2SO_4 $\epsilon=0$	1.283333	1.447733	1.450082	
CsCl type a_0=1A	0.798534	2.040692	2.035301	2.035345 U_∞=2.035356
NaCl type a_0=2A	1.129359	1.747740	1.747577	1.747579 U_∞=1.747558

[4] R. W. G. Wycoff, *Crystal Structures* (Interscience Publishers, Inc., New York, 1948), Sec. VIII, p. 5.

[5] H. E. Swanson, R. K. Fuyat, and G. M. Ugrinic, Natl. Bur. Standards Circ. No. 539, Vol. III, p. 62.

tion with the sulfur to oxygen distance equal to 1.504 A. This distance is the average of the sulfur-oxygen distances in the K_2SO_4(II) crystal.

The Madelung constant for K_2SO_4 with the charge on the oxygen equal to zero can be estimated by the methods of Templeton[6] and Kapustinskii[7–9] The results are: For Templeton's method $M_3=6.42$, and for Kapustinskii's method (using thermochemical radii) $M_3=6.83$. The errors in these estimates are 7 and 1.4%, respectively.

ACKNOWLEDGMENTS

The author is indebted to Professor Robert F. Jackson for help in programing this problem, and to the University of Delaware Computing Center for machine time.

[6] D. H. Templeton, J. Chem. Phys. **21**, 2097 (1953); **23**, 1826 (1955).
[7] A. F. Kapustinskii and K. B. Yatsimirskii, J. Gen. Chem. U.S.S.R. (Eng. Transl. **19**, A665 (1949).
[8] A. F. Kapustinskii, Acta Physicochim. U.R.S.S. **18**, 370 (1943).
[9] For a summary of Kapustinskii's work, see A. F. Kapustinskii, Quart. Revs. (London) **10**, 283 (1956).

THE JOURNAL OF CHEMICAL PHYSICS VOLUME 32, NUMBER 6 JUNE, 1960

Relaxation of an Isolated Ensemble of Harmonic Oscillators

KURT E. SHULER

National Bureau of Standards, Washington 25, D. C.

(Received December 14, 1959)

The collisional relaxation of an isolated ensemble of harmonic oscillators (at constant volume and energy) from initial nonequilibrium distributions is discussed in this paper. The "transport equation" for the relaxation process is derived and it is shown that it can be linearized even though the relaxation takes place via binary oscillator collisions. The final, stationary distribution is found to be a Boltzmann one with a temperature uniquely defined by the mean energy of the ensemble. The Boltzmann H function is obtained for this system of relaxing oscillators and it is shown that $dH/dt<0$ for all t. The time rate of change of the mean-square deviation of the energy during the relaxation process is computed and is shown to be closely related to the time variation of the mean *energy* in the relaxation of an ensemble of harmonic oscillators in contact with a thermal reservoir.

I. INTRODUCTION

IN some previous papers[1] we have discussed the relaxation of an ensemble of harmonic oscillators from initial vibrational nonequilibrium distributions through collisional interactions with a thermal reservoir (heat bath). In this paper we extend this treatment to consider the relaxation of an ensemble of harmonic oscillators from initial nonequilibrium distributions through collisional interactions with each other *in the absence of a thermal reservoir*. This ensemble of harmonic oscillators forms a closed, isolated system of constant volume and constant energy. The transport equation for such a system of relaxing oscillators has been derived and a general solution has been obtained analogous to that presented previously.[1(a)–(c)] It is shown that the equilibrium, stationary vibrational distribution is always a Boltzmann one irrespective of the initial nonequilibrium distribution. The Boltzmann H function for this system of relaxing oscillators has also been computed, and it is shown that $dH/dt<0$ for all times t. Finally a discussion is presented of the time variation of the mean-square deviation of the energy during the relaxation process.

[1] (a) R. J. Rubin and K. E. Shuler, J. Chem. Phys. **25**, 59 (1956); (b) E. W. Montroll and K. E. Shuler, *ibid.* **26**, 454 (1957); (c) E. W. Montroll and K. E. Shuler, Advances in Chem. Phys. **1**, 361 (1958).

II. RELAXATION PROCESS

We consider a closed, isolated ensemble of harmonic oscillators. The dimensions of the container are taken to be sufficiently large and the concentration of oscillators sufficiently high that the influence of the container walls can be neglected. The interaction of the oscillators and the consequent energy transfer is through binary collisions. We now assume that the transfer of *vibrational* energy between two colliding oscillators is much more efficient than the vibrational-translational energy transfer. It is clear that in such a system the translational degrees of freedom of the oscillators do not act as a heat bath for the relaxation process. In order to have conservation of energy in such a relaxation process which does not involve the translational degrees of freedom, it is necessary to restrict oneself to *systems of identical oscillators*, i.e., all oscillators must have the same vibrational frequency.

Vibrational equilibration will be established much more rapidly in such an ensemble than the equilibration between the translational and vibrational degrees of

freedom. Herzfeld[2] cites experimental evidence for the case of Cl_2, for instance, where only 400 collisions are required to establish a vibrational Boltzmann distribution whereas 34 000 collisions are required to establish equilibrium between translation and vibration. There do not appear to be sufficient experimental data nor adequate calculations, however, to make any definite statements as to the importance or prevalence of this type of energy transfer. The treatment presented here should, however, be of some interest as an example of the relaxation of an isolated system of constant energy which can be worked out analytically and in explicit detail.

We now make the further assumption that only one quantum per oscillator can be exchanged in a collision. For two oscillators which are, respectively, in quantum states r and s this "selection rule" $\Delta n=\pm 1$ results in a transition of the type of $r\rightarrow r\pm 1$ as $s\mp 1$. These selection rules are characteristic of interactions which can be treated as small perturbations linear in the interaction coordinate.[3] The transition probabilities per collision P_{mn} for such collisional interactions are

$$P_{mn}=[(m+1)\delta_{n-1,m}+m\delta_{n+1,m}]P_{10}=P_{nm} \quad (2.1)$$

where P_{10} is the transition probability per collision for the transition $1\rightarrow 0$. For joint transitions between two oscillators one then finds

$$\begin{aligned} P_{n,n+1;m,m-1}&=(n+1)mP_{10}\\ P_{n,n-1;m,m+1}&=n(m+1)P_{10}, \end{aligned} \quad (2.2)$$

etc. If we let $x_n(t)$ = fraction of oscillators (= average occupation number) in state n; $P_{n,n+1;m,m-1}$ = probability per collision for the energy transfer $n\rightarrow n+1$ as $m\rightarrow m-1$ for two interacting oscillators; Z = number of collisions suffered by an oscillator per unit time, the relaxation equation ("master equation") can be written as [1(a)]

$$\begin{aligned} Z^{-1}[dx_n(t)/dt]&=\sum_{m=0}^{\infty}[-x_nx_m(P_{n,n+1;m,m-1}+P_{n,n-1;m,m+1})\\ &\quad +x_{n+1}x_mP_{n+1;m,m+1}+x_{n-1}x_mP_{n-1,n;m,m-1}]\\ &\quad n=0, 1, \cdots, \infty. \end{aligned} \quad (2.3)$$

Since all the subsequent summations also extend from zero to infinity, the limits will be omitted in the equations to follow. Substitution of the transition probabilities (2.2) yields

$$\begin{aligned} (P_{10}Z)^{-1}[dx_n(t)/dt]&=[(n+1)x_{n+1}-(2n+1)x_n+nx_{n-1}]\sum_m mx_m\\ &\quad +[(n+1)x_{n+1}-nx_n]\sum_m x_m. \end{aligned} \quad (2.4)$$

The mean dimensionless vibrational energy, $\epsilon=E/h\nu$, of a system of harmonic oscillators is given by

$$\epsilon=E/h\nu=\sum_m mx_m. \quad (2.5)$$

Substitution of this relation and the normalization condition

$$\sum_m x_m(t)=1 \quad (2.6)$$

into (2.4) yields

$$\begin{aligned} (P_{10}Z)^{-1}[dx_n(t)/dt]&=\epsilon[(n+1)x_{n+1}-(2n+1)x_n+nx_{n-1}]\\ &\quad +[(n+1)x_{n+1}-nx_n] \qquad n=0, 1, \cdots, \infty. \end{aligned} \quad (2.7)$$

If we now introduce the parameter α where

$$\epsilon=\alpha/(1-\alpha) \quad (2.8)$$

with $0<\alpha<1$ such that $\epsilon>0$ and call $k_{10}\equiv PZ_{10}$ the collisional transition probability per unit time for transitions $1\rightarrow 0$ we obtain finally

$$\begin{aligned} dx_n(t)/dt&=k_{10}(1-\alpha)^{-1}\{(n+1)x_{n+1}\\ &\quad -[n+(n+1)\alpha]x_n+\alpha nx_{n-1}\} \qquad n=0, 1, \cdots, \infty. \end{aligned} \quad (2.9)$$

Before discussing the implication of this equation we will first show that the mean vibrational energy of this system of oscillators is indeed constant throughout the relaxation process and that ϵ is thus not a function of time. Using the energy relation (2.5) and the normalization condition (2.6) one obtains, from (2.4)

$$\begin{aligned} \frac{1}{k_{10}}\sum_n n\frac{dx_n(t)}{dt}&=\frac{1}{k_{10}}\frac{d\epsilon(t)}{dt}=\sum_n n[(n+1)x_{n+1}-nx_n]\\ &\quad +\sum_n\sum_m nmx_m[(n+1)x_{n+1}-(2n+1)x_n+nx_{n-1}]. \end{aligned} \quad (2.10)$$

This reduces, after performing the indicated summations, to

$$\frac{1}{k_{10}}\frac{d\epsilon}{dt}=\sum_m mx_m-\sum_n nx_n=\epsilon-\epsilon=0 \quad (2.11)$$

since in summing the oscillators over all their quantum states the designation of the summation index is immaterial. We are thus justified in treating ϵ as the constant mean vibrational energy of the system of oscillators and in using (2.8) with $\alpha\neq\alpha(t)$ in the subsequent development.[4]

[2] K. F. Herzfeld in *Temperature, Its Measurement and Control in Science and Industry* (Reinhold Publishing Corporation, New York, 1955), Chap. 15.

[3] L. Landau and E. Teller, Physik. Z. Sowjetunion **10**, 34 (1936).

[4] Equation (2.9) has been obtained previously by Herzfeld (see footnote 2). The derivation presented here is more detailed and explicit particularly as regards the linearization of the initial Boltzmann-type transport equation and the importance of the constancy of ϵ during the relaxation process in an isolated system.

It should be noted that the relaxation equation (2.9) is of the identical form as the relaxation equation (1.6) of Montroll and Shuler[1(b)] except for the appearance of α in place of $\exp(-\theta)$ for the heat-bath relaxation, where $\theta=h\nu/kT$ and T was the temperature of the heat bath. Since both α and θ are constants, i.e., do not depend either on the quantum states n or the time t, *the solution of the relaxation Eq.* (2.9) *proceeds identically with that of the heat-bath relaxation equation* (1.6) *of Montroll and Shuler*[1(b)] *with* α *substituted in place of* $\exp(-\theta)$.

As discussed earlier, the energy transfer takes place by binary collisions. This is reflected in the form of Eq. (2.3) which is nonlinear in the (fractional) concentration of the oscillators. The linearization in going from (2.3) to (2.7) is made possible by the energy equation (2.5). This is a unique property of harmonic oscillators. As is well known, transport equations of the type (2.3) involving binary encounters can in general not be linearized in such a simple fashion—a famous example in point being the Boltzmann transport equation.

We will now show that the stationary solution of the relaxation equation (2.9) is the Boltzmann distribution whose "modulus" is uniquely determined by the mean energy ϵ of the system. The stationary (equilibrium) solution of Eq. (2.9), i.e., the solution for $dx_n(t)/dt=0$ is given by

$$x_{n+1}^{eq}/x_n^{eq}=\alpha. \tag{2.12}$$

In general,

$$x_n^{eq}/x_{n-r}^{eq}=\alpha^r. \tag{2.13}$$

The use of (2.6) then leads to

$$x_n^{eq}=\alpha^n/\sum_i \alpha^i. \tag{2.14}$$

Equation (2.14) is clearly of the form of the Boltzmann distribution. It now remains to be shown that $\alpha=\exp(-h\nu/kT)$ at equilibrium. We will just sketch this demonstration here since it involves a well-known procedure.[5] It follows from Eq. (2.14) that x_n^{eq} is a function of the quantum number n. Equation (2.14) can be rewritten as

$$x_{n+r}^{eq}x_{n-r}^{eq}=x_n^{eq}x_n^{eq}. \tag{2.15}$$

From the conservation of vibrational energy during the collision one obtains

$$\mathcal{E}_{n+r}^{(a)}+\mathcal{E}_{n-r}^{(b)}=\mathcal{E}_n^{(a)}+\mathcal{E}_n^{(b)} \tag{2.16}$$

where $\mathcal{E}_{n+r}^{(a)}$ represents the vibrational energy of oscillator (a) in the quantum state $n+r$, etc. For harmonic oscillators, (2.16) can be written as

$$(n+r)h\nu+(n-r)h\nu=nh\nu+nh\nu. \tag{2.17}$$

A comparison of Eqs. (2.15) and (2.17) shows that x_n^{eq} must be of the form

$$x_n^{eq}=A\exp(-\beta nh\nu)=\exp(-\beta nh\nu)\sum_n \exp(-\beta nh\nu) \tag{2.18}$$

where the last expression follows from the normalization (2.6). One then finds on comparing (2.14) with (2.18) that $\alpha=\exp(-\beta h\nu)$ at equilibrium. To identify β with $1/kT$ one now divides the total ensemble of oscillators into subsystems in contact with one another and shows that they will have the same mean energy at equilibrium and are therefore in thermal equilibrium. From this one can then show via the perfect gas law, for instance, that $\beta=1/kT$. The identification

$$\alpha^{eq}=\exp(-h\nu/kT)=\exp(-\theta) \tag{2.19}$$

in conjunction with (2.8) gives the correct equilibrium value

$$\epsilon^{eq}=e^{-\theta}/(1-e^{-\theta}) \tag{2.20}$$

for the dimensionless mean energy of the ensemble of oscillators. The temperature T of the equilibrium distribution at $t\to\infty$ is thus determined uniquely by the (constant) mean energy of the system of oscillators.[6]‡

III. H THEOREM FOR HARMONIC OSCILLATORS

It is well known[7] that the time derivative of the Boltzmann H function, i.e., dH/dt, can readily be obtained as a function of the transition probabilities P_{mn} and the average occupation numbers x_n via the "master equation." We will now investigate the behavior of the H function for our ensemble of harmonic oscillators using the "master equation" (2.9).

The Boltzmann H function is defined for our system by

$$H(t)=\sum_n x_n(t)\ \ln x_n(t)+\text{const.} \tag{3.1}$$

At equilibrium when

$$x_n^{eq}=(1-e^{-\theta})e^{-n\theta} \tag{3.2}$$

one finds

$$H^{eq}=\ln(1-e^{-\theta})-[\theta e^{-\theta}/(1-e^{-\theta})]+\text{const}$$
$$=-S^{eq}/k+\text{const} \tag{3.3}$$

[5] See, for example, P. Jordan, *Statistische Mechanik auf Quantentheoretischer Grundlage* (Vieweg and Son, Braunschweig, 1933), Chap. 1.

[6] P. M. Mathews, I. I. Shapiro, and D. L. Falkoff (to be published) have shown that a subsystem of harmonic oscillators in thermal contact with a heat bath in an arbitrary stationary distribution will relax to a canonical distribution with a temperature uniquely determined by the mean energy of the particles of the reservoir. Our findings above constitute an extension of this result to isolated ensembles.

‡ Note added in proof: The relaxation of an isolated ensemble of harmonic oscillators has also been considered recently by A. I. Osipov, Doklady Akad. Nauk SSSR **130**, 523 (1960), whose work appeared in print while this paper was in proof. Osipov's results are in complete agreement with the results presented in section II of this paper.

[7] See, for example, W. Pauli, *Probleme der Modernen Physik* (S. Hirzel, Leipzig, 1928), p. 30; C. Kittel, *Elementary Statistical Physics* (John Wiley & Sons, New York, 1958), Sec. 36.

where S is the entropy of a system of harmonic oscillators and k is the Boltzmann constant. Differentiation of (3.1) leads to

$$dH(t)/dt=\sum_n[\ln x_n(t)+1][dx_n(t)/dt] \tag{3.4}$$

which reduces to

$$dH(t)/dt=\sum_n \ln x_n(t)[dx_n(t)/dt] \tag{3.5}$$

since $\sum_n dx_n(t)/dt=0$ from (2.6). Physically speaking, this last equality is just a consequence of the conservation of mass during the relaxation process. Substitution of dx_n/dt from Eq. (2.9) into (3.5) yields, after some algebraic manipulation

$$[(1-\alpha)/k_{10}](dH/dt) =\sum_n (n+1)(x_{n+1}-\alpha x_n)\ln(x_n/x_{n+1}). \tag{3.6}$$

Equation (3.6) does not yet exhibit the usual symmetrical form for dH/dt. This symmetrization is usually carried out by using the summational invariants (mass, momentum, energy) for a collision.[8] We shall carry out the symmetrization in an analogous manner suitably modified for this problem. The invariants for our relaxation process are the mean energy $\epsilon=\alpha/(1-\alpha)$ and the "density" (total population) $\sum_n x_n$. From Eqs. (2.5) and (2.6) it can readily be verified that for all times t

$$\sum_n (n+1)(x_{n+1}-\alpha x_n)=0. \tag{3.7}$$

We can now add $\ln\alpha\sum_n(n+1)(x_{n+1}-\alpha x_n)=0$ to both sides of equation (3.6) to obtain the final expression

$$dH/dt=k_{10}(1-\alpha)^{-1}\sum_n (n+1)(x_{n+1}-\alpha x_n)\ln(\alpha x_n/x_{n+1}). \tag{3.8}$$

One will note from Eq. (3.8) that $dH/dt\leq 0$ since $(x_{n+1}-\alpha x_n)$ and $\ln(\alpha x_n/x_{n+1})$ are of opposite signs for all values of x_{n+1} and αx_n. At equilibrium, when $dH/dt=0$, one obtains $x_{n+1}^{eq}/x_n^{eq}=\alpha$ which agrees with Eq. (2.12).

For the relaxation of an ensemble of oscillators in contact with a thermal reservoir, an equation analogous to (3.8) can be derived for the time rate of change of the Helmholtz free energy $A=E-TS$. As is well known from thermodynamics, for closed systems at constant volume and *constant temperature* (i.e., in contact with a heat bath), the Helmholtz free energy A replaces the Boltzmann H function as the "indicator" of irreversible changes in the system. The derivation of the time rate of change of the Helmholtz free energy A is presented in the Appendix.

[8] See, for example, J. O. Hirschfelder, C. F. Curtiss, and R. B. Bird *Molecular Theory of Gases and Liquids* (John Wiley & Sons, New York, 1954), Chap. 7.

It will be instructive to work out a specific example for the relaxation of our isolated system of oscillators and for the concomitant time variation of the H function. We will investigate the relaxation of an initial δ-function distribution with all the oscillators initially in level $m=1$, i.e.,

$$\left.\begin{aligned} x_1(0)&=1\\ x_{m\neq 1}(0)&=0\end{aligned}\right\}. \tag{3.9}$$

Equations (2.5) and (2.8) and (3.9) now fix the value of α as $\alpha=0.5$. The time-dependent fractional population $x_n(t)$ for the relaxation of an initial δ-function distribution for our system of harmonic oscillators is given by

$$x_n(\tau)=\frac{(\alpha-1)(B/\alpha)^n}{(\alpha e^{-\tau}-1)}\sum_{i=0}^{\min(n,m)}\frac{m!n!}{(m-i)!(n-i)!(i!)^2}\times B^{n-i}(B-A)^i \tag{3.10}$$

where τ is the dimensionless time[9]

$$\tau=k_{10}t \tag{3.11}$$

and

$$A=(e^{-\tau}-\alpha)/(e^{-\tau}-1);$$
$$B=[\alpha(e^{-\tau}-1)/(\alpha e^{-\tau}-1)]. \tag{3.12}$$

Equation (3.10) is the general solution of the relaxation equation (2.9) for an initial δ-function distribution. It is analogous to the δ-function relaxation equation for a system of harmonic oscillators in contact with a heat bath[10] except for the substitution of α for $\exp(-\theta)$.

Equation (3.10) has been evaluated numerically for the initial distribution (3.9). The Boltzmann H function as a function of the dimensionless time τ has been evaluated from Eq. (3.1) using the values of $x_n(\tau)$ obtained from (3.10). The results of these calculations are shown in Fig. 1.

The equilibrium values of H and x_n as $\tau\rightarrow\infty$ correspond to the equilibrium solution (3.2) with $\theta=0.6931$ corresponding to $\alpha^{eq}=\exp(-\theta)=0.5$. This is in agreement with the results contained in equations (2.18) and (2.19). The H function shown in Fig. 1 for the relaxation of an initial δ-function distribution of harmonic oscillators may be compared with the H function calculated by Alder and Wainwright[11] for the relaxation of an initial δ-function distribution of velocities for hard-sphere atoms.

[9] Equation (3.11) correctly defines τ for *vibrational-vibrational* energy transfer, as may be noted from Eq. (1.7a) and the general definition of τ below Eq. (1.8) in Montroll and Shuler.[1(b)] In Eq. (1.7a) the symbol on the left-hand side of the equation should be κ instead of k.

[10] K. E. Shuler, J. Phys. Chem. **61**, 849 (1957). The upper limit of summation in Eq. (10) of this reference should be min (n, m) as in Eq. (3.10) above.

[11] J. Alder and T. Wainwright in *Proceedings of the International Symposium on Transport Processes in Statistical Mechanics, Brussels, 1956* (Interscience Publishers, Inc., New York, 1958), p. 127, Fig. 17.

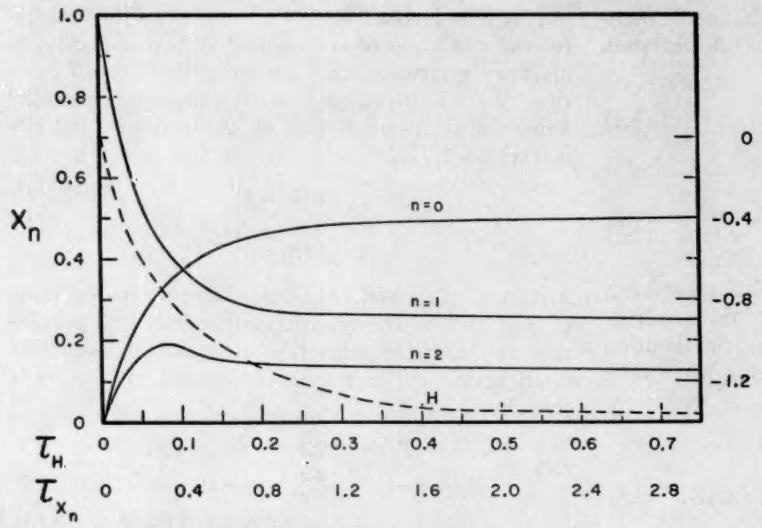

FIG. 1. The relaxation of the (fractional) population x_n and of the Boltzmann H function in an isolated system of harmonic oscillators from an initial δ-function distribution with $x_1(0)=1$.

IV. TIME VARIATION OF MEAN-SQUARE DEVIATION OF ENERGY DURING RELAXATION PROCESS

We now wish to discuss the time rate of change of the mean-square deviation of the energy of the ensemble of oscillators during the relaxation process. The mean-square deviation of the energy, $\langle(\delta\epsilon)^2\rangle_{Av}$, from the average energy is given by

$$\langle(\delta\epsilon)^2\rangle_{Av}=\langle\epsilon^2\rangle_{Av}-\langle\epsilon\rangle_{Av}^2. \tag{4.1}$$

From (2.5) it follows that

$$\langle(\delta\epsilon)_\tau^2\rangle_{Av}=\sum_n n^2x_n(\tau)-[\sum_n nx_n(\tau)]^2. \tag{4.2}$$

The moments in Eq. (4.2) can be evaluated from the general moment equation derived by Montroll and Shuler[1(b)] where we again substitute α for $\exp(-\theta)$. The factorial moment defined by

$$f_m(\tau)=\sum_n n(n-1)\cdots(n-m+1)x_n(\tau)$$

$$m=1, 2, \cdots, \tag{4.3}$$

$$f_0(\tau)=\sum_n x_n(\tau)=1$$

can be shown to be the solution of the equation

$$[(1-\alpha)/k_{10}](df_m/dt)+m(1-\alpha)f_m=m^2\alpha f_{m-1}. \tag{4.4}$$

Dividing through by $(1-\alpha)$ one obtains

$$(df_m/d\tau)+mf_m=\langle\epsilon\rangle_{Av}m^2f_{m-1} \tag{4.5}$$

where Eqs. (2.5) and (3.12) have been used for $\langle\epsilon\rangle_{Av}$ and τ, respectively. For our isolated system of oscillators, $\langle\epsilon\rangle_{Av}$ is a constant. From Eq. (4.5) one finds

$$f_1=\sum_n nx_n(\tau)=\langle\epsilon\rangle_{Av} \tag{4.6}$$

and

$$f_2(\tau)=\sum_n n(n-1)x_n(\tau)$$

$$=2\langle\epsilon\rangle_{Av}^2(1-e^{-2\tau})+f_2(0)e^{-2\tau} \tag{4.7}$$

From (4.6) and (4.7) it follows that

$$\sum_n n^2x_n(\tau)=f_2(\tau)+f_1=(\langle\epsilon\rangle_{Av}+2\langle\epsilon\rangle_{Av}^2)(1-e^{-2\tau})$$

$$+e^{-2\tau}\sum_n n^2x_n(0). \tag{4.8}$$

Combining (4.2), (4.6), and (4.8) we obtain, using the time in variance of $\langle\epsilon\rangle_{Av}$,

$$\langle(\delta\epsilon)_\tau^2\rangle_{Av}=\langle\epsilon\rangle_{Av}(1+\langle\epsilon\rangle_{Av})(1-e^{-2\tau})+\langle(\delta\epsilon)_0^2\rangle_{Av}e^{-2\tau}. \tag{4.9}$$

From Eq. (4.9) it follows that as $\tau\to\infty$, i.e., at equilibrium,

$$\langle(\delta\epsilon)_{eq}^2\rangle_{Av}=\langle\epsilon\rangle_{Av}(1+\langle\epsilon\rangle_{Av}) \tag{4.10}$$

where $\langle(\delta\epsilon)_{eq}^2\rangle_{Av}$ is to be identified with the equilibrium energy fluctuation. Substitution of Eq. (2.20) and use of the definition $\epsilon=E/h\nu$ yields

$$\langle(\delta E)_{eq}^2\rangle_{Av}=(h\nu)^2e^\theta/(e^\theta-1)^2=kT^2C_v \tag{4.11}$$

where $C_v=k\theta^2e^\theta(e^\theta-1)^2$ is the heat capacity (at constant volume) of a canonical ensemble of harmonic oscillators. The energy fluctuations at equilibrium thus reduce to the predicted value for a canonical ensemble.[12] It should be noted that Eq. (4.10) is of the same form as that derived by Einstein for the energy fluctuation of an equilibrium Bose gas of photons, i.e., for blackbody radiation.[13] This is of course not too surprising since thermal radiation, in quantum theory, is equivalent to a collection of harmonic oscillators. Or, put in another way, one could rephrase the above relaxation problem as being one in which quanta $h\nu$ are transferred between harmonic oscillators. The energy fluctuations at equilibrium, Eq. (4.10), then would be those for a thermal radiation field.

[12] See, for example, Kittel (footnote 7), pp. 118–119.

[13] See, for example, L. D. Landau and E. M. Lifshitz, *Statistical Physics* (Addison-Wesley Publishing Company, Reading, Massachusetts, 1958), Chap. XII.

Combining Eqs. (4.9) and (4.10) one can finally write

$$[\langle(\delta\epsilon)_\tau^2\rangle_{Av}-\langle(\delta\epsilon)_{eq}^2\rangle_{Av}]/[\langle(\delta\epsilon)_0^2\rangle_{Av}-\langle(\delta\epsilon)_{eq}^2\rangle_{Av}]=e^{-2\tau} \tag{4.12}$$

for the time variation of the mean-square deviation of the energy during the relaxation.[14] It is of interest to compare this result with that obtained by Montroll and Shuler[1(b)] for the relaxation of the mean energy $\langle\epsilon\rangle_{Av}$,

$$(\langle\epsilon\rangle_{Av\tau}-\langle\epsilon\rangle_{Aveq})/(\langle\epsilon\rangle_{Av0}-\langle\epsilon\rangle_{Aveq})=e^{-\tau} \tag{4.13}$$

for a system of harmonic oscillators in contact with a thermal reservoir. It will be noted that the time variation of $\langle(\delta\epsilon)^2\rangle_{Av}$ in our isolated system of relaxing oscillators is essentially the same as the time variation of the mean energy $\langle\epsilon\rangle_{Av}$ for a system of relaxing oscillators in contact with a thermal reservoir and that it is independent of the form of the initial distribution $\{x_n(0)\}$.

V. ACKNOWLEDGMENT

The author wishes to thank Dr. M. S. Green and Dr. J. Rubin for their helpful comments on this paper.

APPENDIX

"Relaxation" of Helmholtz Free-Energy Function A for System of Harmonic Oscillators in Contact with Thermal Reservoir

We consider a system of harmonic oscillators in an arbitrary initial distribution in contact with a thermal reservoir with a stationary temperature T. We now define a function $\mathfrak{A}(t)$ as

$$\mathfrak{A}(t)=\sum_n[nx_n(t)+\theta^{-1}x_n(t)\ \ln x_n(t)]. \tag{A.1}$$

At equilibrium one finds, using Eqs. (2.5) and (3.1-3.3),

$$\mathfrak{A}^{eq}=\epsilon^{eq}-\theta^{-1}(S^{eq}/k) \tag{A.2}$$

where k is the Boltzmann constant. Equation (A.2) can be rewritten as

$$A^{eq}=h\nu\mathfrak{A}^{eq}=E^{eq}-TS^{eq} \tag{A.3}$$

where A^{eq} is the Helmholtz free-energy function at equilibrium. Differentiation of (A.1) with respect to time leads to

$$d\mathfrak{A}(t)/dt=\sum_n(dx_n/dt)\,(n+\theta^{-1}\ln x_n) \tag{A.4}$$

since $\sum_n dx_n/dt=0$ from (2.6). For a system of harmonic oscillators in contact with a heat bath, dx_n/dt is given by Eq. (1.7) of Montroll and Shuler.[1(b)] This equation is identical with Eq. (2.9) of this paper if α in Eq. (2.9) is replaced by $\exp(-\theta)$. Equation (A.4) then becomes

$$d\mathfrak{A}/d\tau=\sum_n\{(n+1)x_{n+1}-[n+(n+1)e^{-\theta}]x_n+ne^{-\theta}x_{n-1}\}\times(n+\theta^{-1}\ln x_n) \tag{A.5}$$

with[1(b)]

$$\tau=\kappa(1-e^{-\theta})t. \tag{A.6}$$

If one notes that $\sum_n nx_n\ \ln x_n=\sum_n(n+1)x_{n+1}\ \ln x_{n+1}$, $\sum_n nx_{n-1}\ \ln x_n=\sum_n(n+1)x_n\ \ln x_{n+1}$, etc., and that $-\theta=\ln[\exp(-\theta)]$ Eq. (A.5) reduces to

$$d\mathfrak{A}/d\tau=\theta^{-1}[\sum_n(n+1)\,(x_{n+1}-e^{-\theta}x_n)\ \ln(e^{-\theta}x_n/x_{n+1})]. \tag{A.7}$$

Since $(x_{n+1}-e^{-\theta}x_n)$ and $\ln(e^{-\theta}x_n/x_{n+1})$ are of opposite signs for all values of x_{n+1} and x_n, one has $d\mathfrak{A}/d\tau<0$ for all times τ. At equilibrium $d\mathfrak{A}/d\tau=0$, from which it follows that

$$x_{n+1}^{eq}/x_n^{eq}=\exp(-\theta) \tag{A.8}$$

which is the correct expression for a stationary canonical ensemble of harmonic oscillators of the temperature T. Substitution of the equilibrium oscillator distribution (3.2) into (A.1) leads to the equilibrium expression

$$A^{eq}=-kT\ln(1-e^{-\theta})^{-1}=-kT\ln Q \tag{A.9}$$

where Q is the vibrational partition function for harmonic oscillators. The function $\mathfrak{A}(\tau)=A(\tau)/h\nu$ can thus serve as the analog of the Boltzmann H function in studying the approach to equilibrium of a closed system in contact with a thermal reservoir.

[14] For an initial δ-function distribution $\langle(\delta\epsilon_0)^2\rangle_{Av}=0$ and Eq. (4.12) reduces to $\langle(\delta\epsilon)_\tau^2\rangle_{Av}=\langle(\delta\epsilon^2)_{eq}\rangle_{Av}(1-e^{-2\tau})$ corresponding to an exponential increase in the mean-square deviation from zero to the equilibrium value (4.10).

Heterogeneous Nature of Reaction in Radiation-Induced Solid-State Polymerization of Acrylamide*

GEORGE ADLER AND WALTER REAMS

Brookhaven National Laboratory, Upton, Long Island, New York

(Received December 28, 1959)

It has been suggested that the radiation-induced solid-state polymerization of acrylamide is a heterogeneous reaction, that is, it goes by a two-phase mechanism [G. Adler, J. Chem. Phys. **31**, 848 (1959) and B. Baysal, G. Adler, D. Ballantine, and P. Colombo, J. Polymer Sci. (to be published)]. According to this concept, the reaction procedes at definite sites within the crystal. After the first few reaction steps, it forms regions of pure or nearly pure polymer imbedded in pure monomer. Further reaction would take place at the interface between the two. The polymer and monomer regions would remain segregated until the crystal is completely polymerized. It has been shown previously that the reaction can take place without the crystal breaking up. The alternative to this scheme seems to be that the reaction takes place within the crystal lattice and is directed by it. This requires a more homogeneous reaction mechanism. It seems feasible, in principle to distinguish between the two mechanisms by x-ray diffraction. A single crystal technique that allows us to look at all the reflections simultaneously appeared to be most promising. It was therefore decided to run a series of rotation diagrams on a crystal in various stages of polymerization.

EXPERIMENTAL

A CRYSTAL of acrylamide was grown by slow evaporation from solution in acetone. A 0.4- × 0.4- × 4-mm section was cut from this and oriented on a goniometer head. It was then mounted in a rotation camera with the long axis of the crystal parallel to the rotation axis. A rotation diagram was taken using nickel-filtered copper radiation. The crystal, still mounted on the goniometer head, was then irradiated in a Co^{60} source at 410 000 rad/hr to a dose 250 000 rad. Another rotational diagram was then taken. The crystal was returned to the same cobalt source for more radiation and another rotation diagram taken. In all, eight rotation diagrams were made, the crystal being returned to the Co^{60} source for radiation seven times. The first two x-ray diagrams were taken without a beam stop. All work, including the irradiations, was done at 24°C.

RESULTS

The rotation diagrams are shown in Fig. 1(a)–(h). For comparison, the conversion to monomer corresponding to this radiation dose is also listed. This conversion is estimated from data taken from bulk acrylamide irradiated under the same conditions. It should be emphasized that this conversion figure is somewhat too low because polymerization will take place slowly in the x-ray beam as well as in the cobalt source and because the reaction continues even if the material is removed from the radiation field.[1,2] This error should be most serious at conversions between 15 and 80%.

DISCUSSION

If the reaction procedes by a two-phase mechanism, the diffraction pattern should be a superposition of that of both phases throughout the course of the reaction. Since the polymer in completely polymerized crystals is amorphous,[1] the diffraction pattern should show a diffuse amorphous ring due to polymer superimposed on the characteristic crystalline pattern. As the percent conversion increases, the diffuse ring should grow more intense while the crystalline reflections grow correspondingly weaker.

There should be no systematic retention or weakening of any class of reflections. All should fade more or less uniformly. Except for loss of intensity and the effect of some strain and misalignment of the mosaic blocks due to shrinkage of the polymer, the crystalline reflections should persist unchanged until the reaction is essentially complete.

On the other hand, if the reaction procedes by the more homogeneous mechanism, the diffraction effects can be expected to be different. Since the reaction would take place within the crystal lattice, the polymer would be oriented, at least in the early stages. Because of the difference in dimensions between the polymer molecule and the sum of the monomer molecules from which it was made, there would be large buildup of strain within the lattice, and this strain would probably be anisotropic. Because it is probable that the reaction would go in preferred crystallographic directions within the lattice, there should be a systematic weakening or retention of certain classes of reflections. Above all, there should be no evidence of phase separation. At low conversions, the x-ray diagrams should show the monomer pattern distorted by strain. At high conversions, where the polymer is dominant, no monomer pattern should be seen. Since the system would be analogous to a solution of the monomer in the polymer, the x-ray diagram would show only diffuse rings or arcs if the polymer is oriented.

The diffraction diagrams demonstrate that during the entire course of the reaction, both the crystalline

* Work done under the auspices of the U. S. Atomic Energy Commission.

[1] G. Adler, J. Chem. Phys. **31**, 848 (1959).

[2] B. Baysal, G. Adler, D. Ballantine, and P. Colombo, J. Polymer Sci. (to be published).

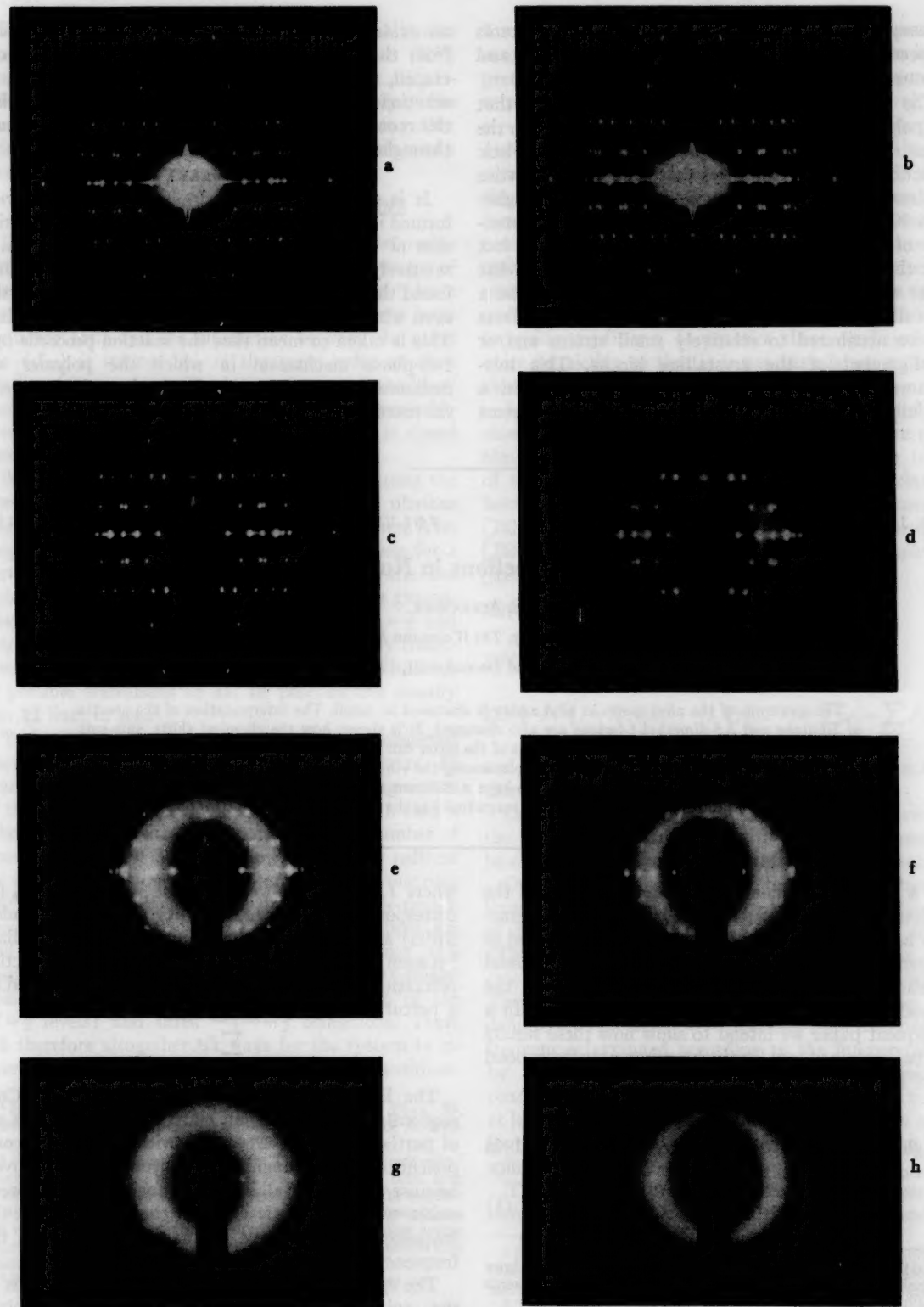

FIG. 1. Rotation diagram of acrylamide crystal irradiated in a Co^{60} source, copper radiation, nickel filter. (a) unirradiated crystal, percent polymer = 0; (b) radiation dose 0.25×10^6 rad, percent polymer approximately 1%; (c) radiation dose 0.5 rad, percent polymer greater than 3.5%; (d) radiation dose 1.0×10^6 rad, percent polymer greater than 11%; (e) radiation dose 1.5×10^6 rad, percent polymer greater than 38%; (f) radiation dose 2.0×10^6 rad, percent polymer greater than 71%; (g) radiation dose 2.5×10^6 rad, percent polymer greater than 90%; (h) radiation dose 3×10^6 rad, percent polymer greater than 98% (the spot on the lower right is due to light leak).

monomer and the polymer are present. The diagrams all seem to be a superposition of the monomer and polymer patterns.

The faint symmetrical ring in Fig. 1(c) shows that the polymer is amorphous even at low coversions in the order of 4% or less. The presence of characteristic reflections in Fig. 1(g) shows that the monomer lattice persists essentially unchanged at conversions higher than 90%. There is no systematic weakening or retention of any class of reflections. Aside from the fact that the high-angle reflections seem to fade somewhat faster than low-angle ones. There also seems to be a very slight broadening of the reflections. These effects can be attributed to relatively small strains and/or misalignment of the crystalline blocks. This misalignment can be seen under the microscope in a partially polymerized crystal. At any rate, there seems no evidence of the large anisotropic strains expected from the homogeneous mechanism. It must be concluded, therefore, that except for the initial steps, the reaction procedes by a two-phase mechanism in which the monomer and polymer remain as separate phases throughout the course of the reaction.

SUMMARY

It is shown by x-ray diffraction that the polymer formed in the radiation-induced solid-state polymerization of crystalline acrylamide is amorphous even at relatively low conversions. On the other hand, it is found that the crystal lattice of the acrylamide persists even when the crystal is more than 90% polymerized. This is taken to mean that the reaction proceeds by a two-phase mechanism in which the polymer and monomer exist as separate phases throughout most of the reaction.

THE JOURNAL OF CHEMICAL PHYSICS VOLUME 32, NUMBER 6 JUNE, 1960

Relative Signs of Spin-Spin Interactions in Nuclear Magnetic Resonance.* II

S. ALEXANDER

Nuclear Magnetic Resonance Laboratory, The Weizmann Institute of Science, Rehovot, Israel

(Received December 21, 1959)

The spectrum of the allyl group in allyl amine is discussed in detail. The interpretation of the spectra of 1-butene and 3,3-dimethyl-1-butene are also discussed. It is shown how the chemical shifts, spin-spin interactions, and in particular the relative signs of the latter can be determined by numerical methods.

In all three molecules all spin-spin interactions among the vinyl protons have the same sign. One of the three vinyl-methylene interactions is found to have a different sign than the other two. This interaction has the same sign (and approximately the same magnitude) as the methyl-methylene interaction in 1-butene.

IN a previous communication[1] we have reported the determination of relative signs of spin-spin interactions between protons in 3,3-dimethyl-1-butene and in 1-butene. We now intend to give some additional experimental data and to discuss in more detail the methods used in interpreting the NMR spectra. In a subsequent paper we intend to show how these results can be explained qualitatively using a valence-bond model for the electronic wave functions.

I. THE HAMILTONIAN

High-resolution NMR spectra are interpreted in terms of a spin Hamiltonian[2]:

$$\mathcal{H}=\sum_i \omega_i I_i^z+\sum_{i<j} J_{ij}(I_i I_j), \qquad (1)$$

where I_i is the spin vector of the ith nucleus, ω_i the corresponding resonance frequency (including chemical shifts) and the J_{ij} are the indirect spin-spin couplings between the nuclear spins in the molecule. Neglecting relaxation effects, the line intensities are determined by a perturbation proportional to

$$\sum_i I_i^x. \qquad (2)$$

The Hamiltonian (1) commutes with $\Sigma_i I_i^z$. Consequently the Hamiltonian matrix separates into a set of partial matrices ($\mathcal{H}^M$), each with a definite z component of the total angular momentum (M). Moreover, because of Eq. (2), all allowed transitions are between states with $\Delta M=\pm 1$. One can therefore measure the frequencies (ω_i) relative to an arbitrary zero on the frequency scale.

The spectrum depends only on the relative signs of the spin-spin interactions, not on their absolute signs.[3]

* Part of a dissertation submitted by S. Alexander to Hebrew University, Jerusalem, in partial fulfillment of the requirements for a Ph.D. degree (May, 1958).

[1] S. Alexander, J. Chem. Phys. **28**, 358 (1958).

[2] H. S. Gutowsky, D. W. McCall, and C. P. Slichter, Phys. Rev. **84**, 589 (1951); E. L. Hahn and D. E. Maxwell, *ibid.* **84**, 1246 (1951).

[3] W. A. Anderson, Phys. Rev. **102**, 151 (1956).

For the interpretation of NMR spectra one is also interested in the traces of the partial matrices ($\mathcal{H}^M$) into which the Hamiltonian separates. When all particles have the same spin these traces depend only on the sum of all ω_i and the sum of all J_{ij}. This puts rather stringent conditions on the possible interpretations of a spectrum.

2. THE SPECTRUM OF THREE PROTONS

The simplest system in which one can determine relative signs of spin-spin interactions is a system of three nonequivalent nuclei. Gutowsky *et al.*[4] have treated the case where one nucleus has a very large frequency shift and the interaction between the other two (J_{ij}) is strong, i.e., of the same order as their relative shift ($\omega_i-\omega_j$). The interactions with the "far" nucleus can then be treated as a first-order perturbation, and the rest of the problem can be solved in closed form.

When all three spin-spin interactions are strong the interpretation of the spectrum is no longer obvious (see, for example, Fig. 1 of reference 1), and there is no simple approximation which can serve as a basis for a perturbation calculation. For three protons one has eight energy levels which break down into four groups. There is one level with $M=\frac{3}{2}$, one with $M=-\frac{3}{2}$ and two groups of three levels with $M=\pm\frac{1}{2}$. As only transitions with $\Delta M=\pm 1$ are allowed this limits the number of possible transitions to 15. In practice one usually sees 12 lines or less.[5]

To interpret a spectrum one has to fit the observed lines into an eight-level scheme of this structure. In practice there were always many different arrangements of the observed line frequencies consistent with such a scheme within experimental accuracy. The number of "possible" interpretations is, however, greatly reduced by the conditions on the traces of the partial matrices ($\mathcal{H}^M$).[6] We always had 10–12 lines in a three-proton spectrum. It was therefore assumed that these are still essentially single-spin transitions. Under this assumption one has three $\frac{3}{2}\rightarrow\frac{1}{2}$ transitions, six single-spin $\frac{1}{2}\rightarrow-\frac{1}{2}$ transitions (i.e., two from each of the $M=\frac{1}{2}$ levels) and three $-\frac{1}{2}\rightarrow-\frac{3}{2}$ transitions. There are therefore altogether six ways for the system to go from $+\frac{3}{2}$ to $-\frac{3}{2}$, each consisting of three transitions. To interpret the spectrum we calculated all possible sums of three line frequencies. For any possible interpretation one must then find six such sums to have the same value.[7] Each sum must consist of one $\frac{3}{2}\rightarrow\frac{1}{2}$, one $\frac{1}{2}\rightarrow-\frac{1}{2}$, and one $-\frac{1}{2}\rightarrow-\frac{3}{2}$ transition. Each of the three $\frac{3}{2}\rightarrow\frac{1}{2}$ and $-\frac{1}{2}\rightarrow-\frac{3}{2}$ transitions has to appear in two sums (because there are only three of each kind) while the six $\frac{1}{2}\rightarrow-\frac{1}{2}$ transitions appear only once.[8] Using these facts the determination of all the interpretations consistent with a given set of six coinciding sums is quite straightforward. One can assign the three frequencies in one of the sums at random and then try to assign the other sums in a way consistent with the foregoing conditions. In practice these conditions are quite restrictive so that it is not very laborious to do this in an exhaustive manner.

As mentioned previously the assignment of the observed frequencies to the energy level scheme must also be consistent with the conditions on the traces of the $\mathcal{H}^M$.[6] These conditions amount to relations between the sum of the three $(\frac{3}{2}\rightarrow\frac{1}{2})$ transitions $[\Sigma\Omega(\frac{3}{2}\rightarrow\frac{1}{2})]$, the sum of the six $\frac{1}{2}\rightarrow-\frac{1}{2}$ transitions $[\Sigma\Omega(\frac{1}{2}\rightarrow-\frac{1}{2})]$, and the sum of the $-\frac{1}{2}\rightarrow-\frac{3}{2}$ transitions $[\Sigma\Omega(-\frac{1}{2}\rightarrow-\frac{3}{2})]$. One has

$$\Sigma\Omega(\tfrac{3}{2}\rightarrow\tfrac{1}{2})=3\,\mathrm{Tr}(\mathcal{H}^{\frac{1}{2}})-\mathrm{Tr}(\mathcal{H}^{\frac{3}{2}})=\sum_i\omega_i+\sum_{i<j}J_{ij}, \qquad (3)$$

$$\Sigma\Omega(\tfrac{1}{2}\rightarrow-\tfrac{1}{2})=2\,\mathrm{Tr}(\mathcal{H}^{\frac{1}{2}})-2\,\mathrm{Tr}(\mathcal{H}^{-\frac{1}{2}})=2\sum_i\omega_i,$$

$$\Sigma\Omega(\tfrac{1}{2}\rightarrow-\tfrac{3}{2})=\mathrm{Tr}(\mathcal{H}^{-\frac{1}{2}})-3\,\mathrm{Tr}(\mathcal{H}^{-\frac{3}{2}})=\sum_i\omega_i-\sum_{i<j}J_{ij},$$

and in addition the value of each of the six coinciding three-frequency sums is $\Sigma\omega_i$.

Only arrangements of the observed frequencies on the level scheme consistent with these conditions can be considered possible interpretations of the spectrum.

Once all the possible interpretations of the observed lines are determined, one can find the numerical values of the corresponding "experimental" energy levels. (The transitions between these levels should in each case give the frequencies of the observed spectrum.) The "experimental" energy levels corresponding to a definite interpretation were obtained from the observed frequencies (arranged according to the interpretation) by a least-squares calculation with the subsidiary conditions on the traces. It was always possible to find at least one set of "experimental" levels for each of the four possible combinations of relative signs of the spin-spin interactions.

The second step in the calculation was the determination of the best values of the parameters ω_i and J_{ij}

[4] H. S. Gutowsky and G. A. Williams, J. Chem. Phys. **25**, 1288 (1956); H. S. Gutowsky, A. Holm, A. Saika, and G. A. Williams, J. Am. Chem. Soc. **79**, 4596 (1957).

[5] For weak interactions there are 12 allowed "single-spin" transitions. When one interaction is very strong, the total spin of two nuclei is approximately conserved, which limits the number of allowed transitions to eight. When two or three interactions are very strong this is further reduced to five. It therefore seems improbable that all 15 transitions should have a considerable intensity.

[6] For a system of three nuclei of spin $\frac{1}{2}$ these conditions are

$$\mathrm{Tr}(\mathcal{H}^{\frac{1}{2}})=(\tfrac{1}{4})\sum_i\omega_i+(\tfrac{1}{4})\sum_{i<j}J_{ij}=-\mathrm{Tr}(\mathcal{H}^{-\frac{1}{2}}),$$

$$\mathrm{Tr}(\mathcal{H}^{\frac{3}{2}})=(\tfrac{1}{4})\sum_i\omega_i-(\tfrac{1}{4})\sum_{i<j}J_{ij}=-\mathrm{Tr}(\mathcal{H}^{-\frac{3}{2}}).$$

[7] Because of the special structure of the spin Hamiltonian this procedure is more convenient than the standard spectroscopic method of calculating the differences between the line frequencies.

[8] The distinction between the set of levels $+\frac{3}{2}$; $+\frac{1}{2}$, and the set $-\frac{3}{2}$; $-\frac{1}{2}$ is quite arbitrary. One can always change the sign of all M's without changing the spectrum. Consequently it is immaterial which frequency is chosen as $\frac{3}{2}\rightarrow\frac{1}{2}$ and which as $-\frac{1}{2}\rightarrow-\frac{3}{2}$.

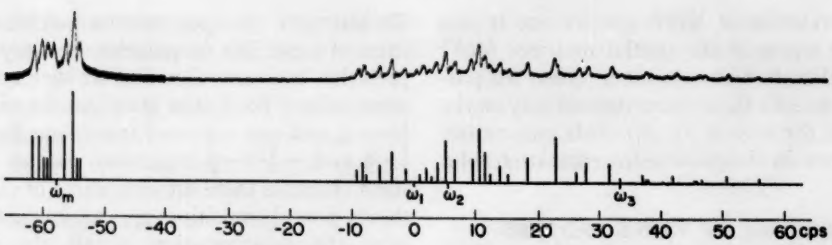

FIG. 1. Experimental and calculated spectrum of allyl amine. The field decreases from left to right at a rate of 4.2 milligauss/min. The experimental lines appearing are from left to right: the group of lines of the methylene protons and the vinyl lines. The calculated spectrum displayed corresponds to interpretation 4 in Fig. 3. The measurement was made at a constant frequency of 31.6 Mc.

corresponding to each set of levels. As a starting point we used the representation where all the I_i^z are diagonal. The first-order parameters were determined by a least-squares fit of the diagonal elements of the formal Hamiltonian (in this representation), with our experimental levels. (These elements are linear expressions in the ω_i and J_{ij}.) The values of the parameters obtained were then substituted in the formal Hamiltonian (Eq. (1)]. The matrix obtained in this way was diagonalized. The eigenvalues of this numerical matrix may be quite different from the experimental levels. The representation in which the numerical matrix is diagonal is, however, a better approximation of the "true" representation than the one used initially. One can therefore calculate a new, better set of parameters from the diagonal elements of the formal Hamiltonian in this representation, and proceed by substituting these parameters in Eq. (1).

Four successive iterations of this type were carried out. Usually a very good fit of the calculated and "experimental" energy levels was obtained for all interpretations. To determine the right interpretation we compared the experimental line intensities with those calculated from Eq. (2) in the final representation. All numerical calculations were carried out with an electronic computor.

TABLE I. The experimental line frequencies in cps (ν) and intensities (I) as compared with those calculated for three different interpretations of the spectrum of 3,3 dimethyl-1-butene. The intensities are all normalized to the same total intensity. The corresponding chemical shift and spin-spin parameters are shown in Table II. All measurements were made at a constant frequency of 31.6 Mc.

	Exptl		I		II		III	
No.	ν	I	ν	I	ν	I	ν	I
1	0.0	70	0.0	48	0.0	26	0.0	13
2	2.8	40	2.6	8	2.6	32	2.7	45
			2.8	13	2.8	31	2.8	39
3	5.4	80	5.4	78	5.3	56	5.3	54
4	11.9	45	11.9	33	11.9	71	11.9	107
5	14.3	100	14.4	126	14.4	91	14.4	50
6	18.0	110	18.1	156	18.1	122	18.2	91
7	20.6	50	20.7	38	20.7	71	20.7	100
8	31.0	100	31.2	126	31.2	127	31.1	120
9	40.2	80	40.2	67	40.2	64	40.2	67
10	49.4	45	49.3	32	49.3	34	49.3	33
11	58.4	25	58.3	24	58.3	23	58.3	22

We give in Table I the experimental and calculated results for three different interpretations of the spectrum of 3,3-dimethyl-1-butene.[1] (The experimental intensities cited were determined from the heights of the maxima of the individual lines.) It will be seen that the frequencies fit well in all three cases.[9] However, only interpretation I, which corresponds to equal signs of all J's, reproduces the pattern of the intensities in the experimental spectrum. In particular line No. 2, which is found to be a superposition of two different transitions, is weaker than both its neighbors, as observed.[10] The error in the determination of the experimental intensities is rather large so one cannot really expect a more accurate fit in the intensities.

3. THE ALLYL GROUP (—CH_2—CH=CH_2)

Figure 1 shows the observed and calculated spectrum of allyl amine. Our interpretation is based on the frequencies of the transitions of the vinyl protons only. We treated the interactions of these protons with the methylene protons as a first-order perturbation. The lines in the vinyl spectrum were divided into three subspectra corresponding to the three possible z components ($M_m=0, \pm1$) of the spin of the methylene

TABLE II. Relative frequency shifts (ω_i) at 31.6 Mc and spin-spin interactions (J_{ij}) of the vinyl protons in 3,3-dimethyl-1-butene. All parameters are given in cps. The ω_i are measured relative to the same zero as the line frequencies in Table I.

	I	II	III
ω_1	9.6	9.9	8.8
ω_2	12.7	12.8	13.2
ω_3	41.4	41.5	41.5
J_{12}	1.4	2.6	3.5
J_{13}	10.8	−9.1	9.3
J_{23}	17.5	18.2	−17.4

[9] Only three interpretations are given. In the fourth case (i.e., when J_{12} has a different sign than J_{13} and J_{23}) it was also possible to fit the "experimental" levels very nicely. However it turned out that the representation in which this was possible gave zero intensity to some of the lines observed while some other transitions were very strong. The spectrum obtained in this way was so different from the one observed that it can be rejected offhand. In this connection see Fig. 2 of this paper where the very bad fit of the similar interpretation is obvious. The reason for the large influence of the signs of J_{12} is not clear to us.

[10] See Fig. 1 of reference 1.

protons, and each of these was treated as a separate three-proton spectrum.

In the choice of the subspectra we used the methods described previously for the interpretation of the three-proton spectrum. Practically all combinations of lines were considered as possible subspectra at the start. However the separation of the "three-frequency sums" for the three subspectra should, at the most, be of the order of the sum of the three methylene-vinyl interactions. The order of the latter is known from the methylene spectrum. Because of this condition all three subspectra have to be distributed more or less evenly across the observed spectrum. Except for some ambiguity in the assignment of the first six lines on the left (Fig. 1) and some very weak lines on the right it is then possible to determine the $M_m=0$ subspectrum uniquely. Only a limited number of possibilities, (corresponding to the different relative signs of the methylene-vinyl interactions) are left for the other two subspectra. Whenever the general conditions on the spectrum were not sufficient to decide the assignment of a certain line within experimental error, we carried out separate calculations for each possible assignment. Because of the conditions imposed by the form of the Hamiltonian, the calculated spectra (and parameters) are not very sensitive to slight changes in the initial choice, so that the calculated spectra were always very similar. The results given in this paper are based on the choice of subspectra which gave the best fit for each assignment.

The relative signs of the interactions between the vinyl protons were determined from the calculation on the subspectrum corresponding to $M_m=0$ (Fig. 2). The two weak lines in the experimental spectrum (No. 5) were not taken into account in the calculation. It can

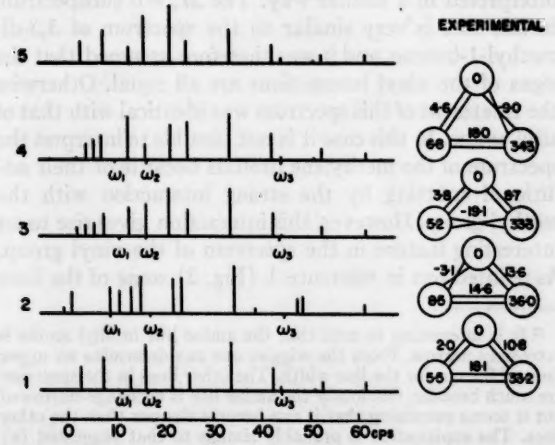

FIG. 2. The subspectrum of the spectrum of the vinyl protons in allyl amine corresponding to $M_m=0$. No. 5 is a schematic representation of the experimental lines. Nos. 1–4 are calculated spectra for different interpretations of this spectrum. On the right the relative frequency shifts in cps are given in the circles and the interaction constants in cps are shown on the corresponding bonds. The interaction which has a different sign than the other two is written negative. (All frequency shifts are at a measuring frequency of 31.6 Mc.)

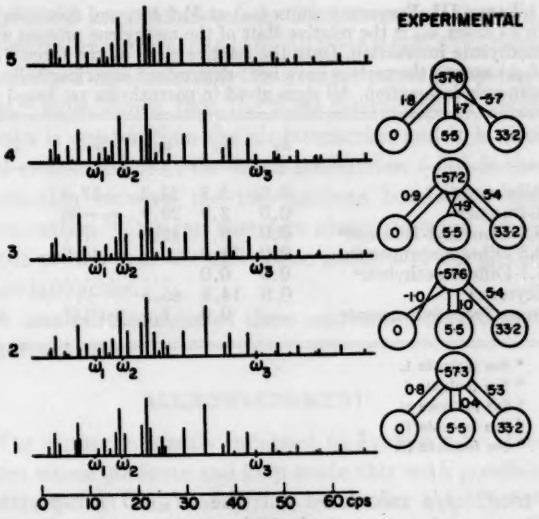

FIG. 3. Experimental and calculated spectra of the vinyl protons in allyl amine. Spectra corresponding to different relative signs of the interactions between the methylene and vinyl protons are shown. All calculated spectra are based on No. 1 in Fig. 2. The experimental spectrum (No. 5) is shown schematically. The frequency shifts (ω_i) of the vinyl protons are given in the lower circles and the methylene shift in the circle above them. The vinyl methylene interactions are given (in cps) on the corresponding bonds.

be seen from the figure that transitions near the frequencies of the strong lines appear in the calculated spectra Nos. 1, 3, and 4. However only No. 1 fits the observed intensities. In particular the first two lines from the left are reproduced in this calculation. It should also be noted that the 9th and 10th lines from the left, which were disregarded in the interpretation, appear in the calculated spectrum. The signs of the three interactions are therefore equal.[11]

There are four essentially different ways of choosing the pair of subspectra corresponding to $M_m=\pm 1$. Each choice corresponds to a different set of relative signs of the interactions with the methylene protons. Each of the groups of lines chosen in this way was treated as a separate three-proton spectrum (according to Sec. 2). In interpreting these subspectra equal signs were assumed for all the interactions among the vinyl protons. From each subspectrum we obtained three "effective" frequency shifts and three spin-spin interactions. If the first-order perturbation treatment of the interactions with the methyl protons (J_{im}) is justified, the interaction constants obtained in this way should be equal to those obtained from the vinyl protons with the $M_m=0$ subspectrum. The effective ω_i's for a pair of subspectra, corresponding to a definite set of relative signs of the J_{im}, should be symmetric around the

[11] The experimental $M_m=0$ subspectrum shown in Fig. 2 is the one which gave the best fit for the interpretation with equal signs. However, this interpretation was better than the other three for all the possible choices of the subspectrum $M_m=0$ which were consistent with a reasonable division of the observed vinyl spectrum into three subspectra.

TABLE III. Frequency shifts (ω_i) at 31.6 Mc, and spin-spin interactions (J_{ij}) in several molecules. ω_1 is arbitrarily set equal to zero in all cases. ω_m is the relative shift of the methylene protons and J_{im} are their interactions with the vinyl protons. J_{mm} is the methyl-methylene interaction. Only the relative signs of the three J_{ij} among themselves and those of the methylene interactions (J_{im} and J_{mm}) among themselves have been determined experimentally. The absolute signs are those given by a valence-bond calculation of the spin-spin interaction. All signs given in parentheses are based on theoretical considerations only.

	ω_1	ω_2	ω_3	ω_m	J_{12}	J_{13}	J_{23}	J_{1m}	J_{2m}	J_{3m}	J_{mm}
Allyl amine	0.0	5.5	33.2	−57.8	+2.0	+10.8	+18.1	−1.7	−1.8	+5.6	...
1-Butene[a]	0.0	2.9	29.9	∼−80	+1.9	+10.4	+17.4	−1.3	−1.9	+6.3	+6
3,3-Dimethyl-1-butene[a]	0.0	3.1	31.8	...	+1.4	+10.8	+17.5	...	...	...	...
2.3 Dibromo-propene[b]	0.0	13.0	...	−43.0	(+)2.2	...	...	(−)1.0	<0.3	...	...
1,1-Difluoro-ethylene[c]	0.0	0.0	...	...	(+)4.0	...	...	...	...	...	...
Styrene[d]	0.0	14.8	46.5	...	(+)1.5	(+)9.6	(+)16.2	...	...	...	...
trans-Propenylbenzene[e]	...	0.0	7.5	+137	...	...	(+)15.6	...	−1.8	+6.6	...

[a] See footnote 1.
[b] See footnote 3.
[c] See footnote 13.
[d] See footnote 14.
[e] See footnote 15.

"true" ω_i's calculated for the $M_m=0$ subspectrum (i.e., equal to $\omega_i \pm J_{im}$). This was never exactly true. The deviations could, however, be attributed to experimental errors in determining the frequencies.

As the $M_m=0$ lines are about twice as strong as the other lines, the ω_i and J_{ij} for the vinyl protons, obtained with this group can be considered more reliable. In calculating the final spectra we therefore used these parameters. The J_{im} were taken to be half the difference of the "effective" ω_i's obtained from the pair of sub-spectra for each sign assignment of the J_{im}. Each of the final calculated spectra (Fig. 3) is a superposition of three calculated subspectra. The $M_m=0$ subspectrum is No. 1 of Fig. 2 in all cases. To get the other two, we substituted effective ω_i's (i.e., ω_i plus or minus the corresponding J_{im}) and the J_{ij}'s of the subspectrum $M_m=0$ in the Hamiltonian [Eq. (1)] and calculated the resulting spectrum. (This is equivalent to treating the methylene-vinyl interactions as a first-order perturbation.) Comparison of the different spectra in Fig. 3 shows that No. 4 fits the experimental results even in the finest details. In this case both the frequencies and the line intensities can be fitted only with this interpretation. It can therefore be concluded that the large interaction has a different sign from the other two.

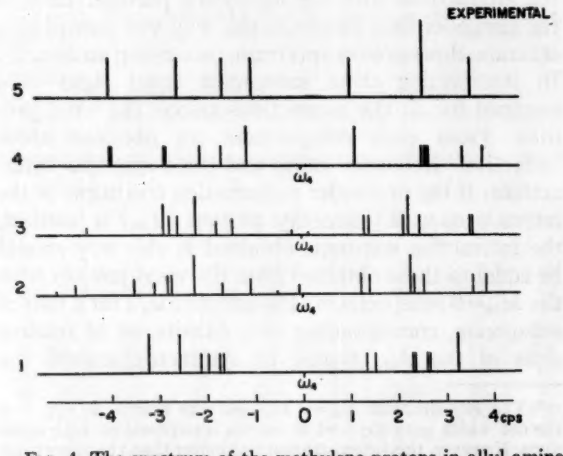

FIG. 4. The spectrum of the methylene protons in allyl amine. The calculated spectra (Nos. 1–4) are calculated with the same parameters as the corresponding spectra in Fig. 3.

The energy-level scheme obtained from the calculation on the vinyl group can be used to calculate the spectrum of the methylene protons (except for an additive constant). The results of this calculation are shown in Fig. 4. In this case also No. 4 gives the best fit. Some of the finer features of the calculated spectrum could certainly not be observed because of the finite line widths (see Fig. 1). Nevertheless, a part of the discrepancy could probably be removed only by taking into account higher-order terms in the vinyl-methylene interactions.[12]

The spectrum of the vinyl protons of 1-butene[1] was interpreted in a similar way. The $M_m=0$ subspectrum in this case is very similar to the spectrum of 3,3-dimethyl-1-butene, and it was therefore assumed that the signs of the vinyl interactions are all equal. Otherwise the treatment of this spectrum was identical with that of allyl amine. In this case it is not possible to interpret the spectrum of the methylene protons because of their additional splitting by the strong interaction with the methyl group. However, this interaction gives rise to an interesting feature in the spectrum of the vinyl group. As pointed out in reference 1 (Fig. 2) some of the lines

[12] It is interesting to note that the amine line in allyl amine is extremely narrow. From the wiggles one can determine an upper limit of 0.2 cps for the line width. The other lines in the spectrum are much broader. Obviously the amine line is exchange-narrowed but it seems surprising that it can become sharper than the other lines. The explanation is probably similar to that suggested (a) by J. T. Arnold [Phys. Rev. **102**, 136 (1956)] for ethanol and discussed in detail (b) by F. Bloch [Phys. Rev. **102**, 104 (1956)]. The width of a line in a spin-spin multiplet is determined by the T_1's of the "coupled" nuclei in addition to the true T_2 of the transition. This T_1 contribution can be considered as a slow exchange between certain components of the multiplet. With this picture one can see why a fast chemical exchange will give a line which converges to the "true" T_2 and not to the width of the multiplet components.

in this spectrum show a doublet structure which cannot be explained from the interactions with the methylene group alone. A perturbation calculation shows that these splittings can be explained as a higher-order effect of the interactions between the methyl and methylene protons through the interaction of the latter with the vinyl protons. The fact that these splittings are observed in certain lines but not in others enables one to determine the sign of the methyl-methylene interaction relative to the methylene-vinyl interactions. The calculation shows that the largest of the latter and the methyl-methlene interaction have the same sign.

4. RESULTS

In Table III we give our results on the chemical shifts and spin-spin interactions in the three molecules analyzed. In addition the data on some related molecules[13–15] are given. Only the relative signs of the three vinyl-vinyl interactions among themselves and those of the methylene interactions among themselves have been determined experimentally. In a recent paper Gutowsky *et al.*[16] have shown that the *trans* interaction in vinyl groups is greater than the *cis* interaction and it is also well established that the small interaction (J_{12}) is the interaction between the two protons bonded to the same carbon.[16] One can therefore identify proton No. 3 as the proton near the methylene group and J_{23} as the trans interaction.

A detailed discussion of these results is deferred to a subsequent paper.

ACKNOWLEDGMENT

The author is greatly indebted to Professor S. Meiboom whose guidance and help made this work possible and to Dr. D. Gill and Mr. A. Szoke for helpful discussions.

[13] H. M. McConnell, A. D. McLean, and C. A. Reilly, J. Chem. Phys. **23**, 1152 (1955).
[14] Varian Bulletin, Vol. 2., Spectrum 38 (1958).
[15] R. W. Fessenden and J. S. Waugh, J. Chem. Phys. **30**, 944 (1959).
[16] H. S. Gutowsky, M. Karplus, and D. M. Grant, J. Chem. Phys. **31**, 1278 (1959).

Electronic Structure and Spectrum of Acetanilide

HIROAKI BABA AND SATOSHI SUZUKI
Research Institute of Applied Electricity, Hokkaido University, Sapporo, Japan

(Received January 18, 1960)

A molecular orbital calculation has been made for the π electronic structure of acetanilide and related compounds. The simple LCAO procedure, on which the calculation is based, was somewhat modified to allow for electron repulsion. The electronic behaviors of the acetanilide molecule are examined from the viewpoint of the interaction of the phenyl and acetyl groups through the nitrogen atom. From the calculated excitation energies, oscillator strengths, and charge distributions, the features of the observed ultraviolet absorption and other electronic phenomena can be satisfactorily explained. It is shown that the changes of the longer-wavelength bands in passing from aniline to acetanilide may be interpreted in terms of two electronic effects: (1) a decrease in the tendency of the nonbonding electrons at the nitrogen atom to migrate into the benzene ring; (2) an extension of conjugation. The electronic properties in the ground state are shown to be explicable by taking account of the former effect.

I. INTRODUCTION

IN connection with the nature of peptide linkage much attention has been devoted to the molecular structure of acetanilide. A variety of physical techniques, including x-ray diffraction,[1] dipole moment[2] and vapor pressure[3] measurements, and infrared[4,5] and ultraviolet[6–9] spectroscopy, have been applied to the study of the structure of this substance. In contrast with these experimental studies, there has been scarcely any theoretical consideration of its electronic structure.

Acetanilide is a derivative of acetamide, and is related to a peptide link. It is also regarded as an acetyl derivative of aniline (see Fig. 1). From the latter point of view, it is of interest to see what sort of electronic effect will be produced on the aniline molecule when a carbonyl, a well-known electron-attracting group, is directly attached to its nitrogen atom.

In this study, a molecular-orbital calculation has been made for the π-electronic structure of acetanilide with a view to understanding its absorption spectrum as well as its electronic properties in the ground state. Reference is made, for the sake of comparison, to the structure and the spectra of aniline and acetamide.

II. ULTRAVIOLET ABSORPTION SPECTRA

The ultraviolet absorption spectra of acetanilide, aniline, and benzene are shown in Fig. 2.[10,11] The spectrum of acetanilide was measured by the present authors with a Hitachi quartz spectrophotometer of type EPU-2A.[12] The solvent, isooctane, being carefully purified, an absorption maximum was detected in the vicinity of 2000 A.

The absorption bands (or transitions) of each substance are designated as I, II, and III in the sequence of increasing wave number. It is to be noted that, by the acetylation of aniline, band I is displaced to the blue with a reduction in intensity, whereas band II is displaced to the red with an increase in intensity.

III. METHOD OF CALCULATION

It is generally accepted that the Hückel LCAO molecular-orbital (MO) theory is not adequate for explaining the electronic spectra of conjugated molecules, since it does not take electron interaction into account.[13] For dealing with the problem of electronic transition, one should in principle resort to a more rigorous theoretical method which is based on the correct many-electron Hamiltonian and includes configuration interaction or the self-consistent field procedure. Although the rigorous theory has been ingeniously simplified by Pariser and Parr,[14] Pople,[15] and others, it is still cumbersome to apply the theory to such a complicated molecule as acetanilide which contains two hetero atoms, nitrogen and oxygen.

In view of these circumstances, a more practical method was adopted in the present calculation. The simplicity of the Hückel theory, particularly in determining molecular orbitals, is retained; and at the same time this simple theory is subjected to some modifications by reference to the rigorous one. Account is taken of the interaction of electrons by including, to some extent, configuration interaction.

[1] C. J. Brown and D. E. C. Corbridge, Acta Cryst. **7**, 711 (1954).
[2] S. B. Kulkarni, J. Indian Chem. Soc. **26**, 207 (1949); S. Nagakura and A. Kuboyama, Rept. Inst. Sci. Technol., University of Tokyo **5**, 27 (1951).
[3] A. Aihara, J. Chem. Soc. Japan **76**, 492 (1955).
[4] K. Kuratani, J. Chem. Soc. Japan **70**, 453 (1949); J. Mann and H. W. Thompson, Proc. Roy. Soc. (London) **A211**, 168 (1952); N. B. Abbott and A. Elliott, Proc. Roy. Soc. (London) **A234**, 247 (1956).
[5] A. Gierer, Z. Naturforsch. **8b**, 654 (1953).
[6] F. W. Klingstedt, Z. physik. Chem. **B1**, 74 (1928); G. A. Anslow and S. C. Nassar, J. Opt. Soc. Am. **31**, 118 (1941).
[7] H. E. Ungnade, J. Am. Chem. Soc. **75**, 432 (1953).
[8] H. E. Ungnade, J. Am. Chem. Soc. **76**, 5133 (1954).
[9] W. F. Forbes and M. B. Sheratte, Can. J. Chem. **33**, 1829 (1955).
[10] (a) Am. Petrol. Inst. Research Project 44, *Ultraviolet Spectral Data*, Serial No. 171; (b) Serial No. 40; (c) Serial No. 172.
[11] H. B. Klevens and J. R. Platt, Tech. Rept., Laboratory of Molecular Structure and Spectra, University of Chicago, Part 1, p. 145 (1953–1954).
[12] A deviation from Beer's law occurred in the spectrum of acetanilide in isooctane solution. A similar phenomenon has been reported by Ungnade.[7] The details of our measurement are found in J. Chem. Soc. Japan **81**, 366 (1960).
[13] See, for example, H. C. Longuet-Higgins, *Advances in Chemical Physics*, Vol. 1, edited by I. Prigogine (Interscience Publishers, Inc., New York, 1958), pp. 239–265.
[14] R. Pariser and R. G. Parr, J. Chem. Phys. **21**, 466, 767 (1953).
[15] J. A. Pople, Trans. Faraday Soc. **49**, 1375 (1953); Proc. Phys. Soc. (London) **A68**, 81 (1955).

FIG. 1.

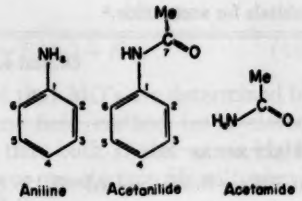

The structure of crystalline acetanilide has been determined by Brown and Corbridge.[1] In this calculation a somewhat simplified molecular model was employed. It is assumed that all the bond angles are 120°, and all the bond lengths except for the C=O length are 1.39 A, the latter length being taken as 1.23 A. Further, the molecule is assumed to be planar.[16] As to the spatial arrangement of the phenyl and methyl groups, the experimental result of Brown and Corbridge is followed, viz., the two groups are situated at the *trans* positions with respect to the C_7—N bond (see Fig. 1).

In this paper we are solely concerned with the singlet transitions.

IV. MOLECULAR ORBITALS

The MO's of acetanilide and related compounds have been obtained by the simple LCAO-MO method with neglect of overlap integrals. The first problem to be settled in this sort of calculation is to assign appropriate values to parameters for hetero atoms.

The Coulomb integrals α_N and α_O and the resonance integral β_{CO} are expressed as

$$\left.\begin{aligned}\alpha_N&=\alpha+\delta_N\beta,\\ \alpha_O&=\alpha+\delta_O\beta,\\ \beta_{CO}&=\rho_{CO}\beta,\end{aligned}\right\} \tag{1}$$

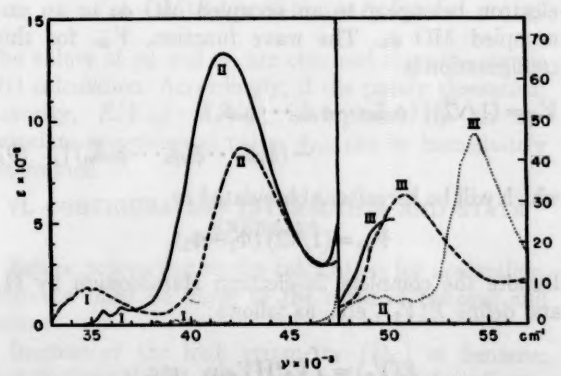

FIG. 2. Ultraviolet absorption spectra of acetanilide and related compounds. Solid line: acetanilide in isooctane; broken line: aniline in isooctane (<47 500 cm^{-1})[10a] and in heptane (>47 500 cm^{-1})[11]; dotted line: benzene in isooctane (<45 000 cm^{-1})[10b] and in heptane (>45 000 cm^{-1}).[10c]

[16] According to Brown and Corbridge, in crystalline state a single molecule of acetanilide lies approximately in two planes, one containing the aniline portion, and the other the acetyl group.

where $\alpha\equiv\alpha_C$ and $\beta\equiv\beta_{CC}$. For a reason described later it is assumed, throughout the present calculation, that

$$\delta_N=1.2. \tag{2}$$

As to the parameters δ_O and ρ_{CO}, calculations are made for several sets of values:

$$\delta_O=1.5,\quad \rho_{CO}=1; \tag{3a}$$

$$\delta_O=1.5,\quad \rho_{CO}=\sqrt{2}; \tag{3b}$$

$$\delta_O=2,\quad \rho_{CO}=1; \tag{3c}$$

$$\delta_O=2,\quad \rho_{CO}=\sqrt{2}. \tag{3d}$$

Of these sets of parameter values, (3b) is finally chosen as the most appropriate one, as will be shown later.

Coulomb and resonance integrals other than those in Eqs. (1) were assumed to be equal to α and β, respectively. No allowance was made for the effect (such as hyperconjugation) of the methyl group in acetanilide.

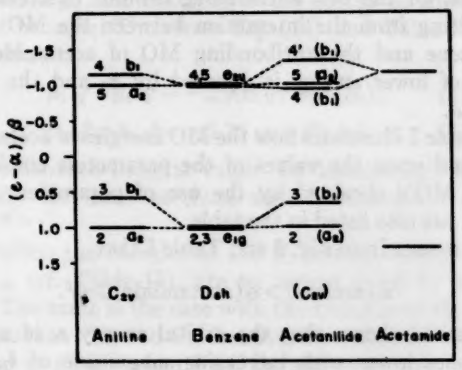

FIG. 3. Orbital energy levels ($\delta_N=1.2$, $\delta_O=1.5$, $\rho_{CO}=\sqrt{2}$).

It is well known that, in benzene, among the six MO's the following two pairs of degenerate orbitals are responsible for the lower electronic transitions:

$$\left.\begin{aligned}\phi_2^0&=\tfrac{1}{2}(\chi_2+\chi_3-\chi_5-\chi_6), & e_2^0&=\alpha+\beta;\\ \phi_3^0&=[1/(12)^{\frac{1}{2}}](2\chi_1+\chi_2-\chi_3-2\chi_4-\chi_5+\chi_6), & e_3^0&=\alpha+\beta;\\ \phi_4^0&=[1/(12)^{\frac{1}{2}}](2\chi_1-\chi_2-\chi_3+2\chi_4-\chi_5-\chi_6), & e_4^0&=\alpha-\beta;\\ \phi_5^0&=\tfrac{1}{2}(-\chi_2+\chi_3-\chi_5+\chi_6), & e_5^0&=\alpha-\beta.\end{aligned}\right\} \tag{4}$$

In these expressions ϕ_i^0 is the ith MO, χ_p the pth carbon $2p\pi$ atomic orbital, and e_i^0 the energy of MO ϕ_i^0; the superscript zeros refer to benzene.

In Fig. 3 are shown the calculated energies of MO's and their symmetry types for acetanilide and the related molecules. Actually acetanilide has no symmetry, but the orbitals obtained in the present approximation are identical with those which would be found if C_1—N—C_7=O were linear (cf. Fig. 1). Thus

TABLE I. Orbital energies and orbitals for acetanilide.[a]

i	Symmetry	Orbital energy $(\epsilon_i-\alpha)/\beta$ (a)	(b)	(c)	(d)	Orbital ϕ_i (b)
2	(a_2)	1.000	1.000	1.000	1.000	$\frac{1}{2}(\chi_2+\chi_3-\chi_5-\chi_6)$
3	(b_1)	0.706	0.666	0.733	0.693	$0.399\,\chi_1+0.365\,(\chi_2+\chi_6)-0.156\,(\chi_3+\chi_5)-0.469\,\chi_4$ $-0.464\,\chi_N-0.152\,\chi_7+0.257\,\chi_O$
4	(b_1)	−0.756	−0.944	−0.710	−0.890	$0.422\,\chi_1-0.235\,(\chi_2+\chi_6)-0.200\,(\chi_3+\chi_5)+0.424\,\chi_4$ $+0.072\,\chi_N-0.577\,\chi_7+0.334\,\chi_O$
5	(a_2)	−1.000	−1.000	−1.000	−1.000	$\frac{1}{2}(-\chi_2+\chi_3-\chi_5+\chi_6)$
4′	(b_1)	−1.249	−1.334	−1.240	−1.301	$0.341\,\chi_1-0.046\,(\chi_2+\chi_6)-0.279\,(\chi_3+\chi_5)+0.419\,\chi_4$ $-0.362\,\chi_N+0.577\,\chi_7-0.288\,\chi_O$

[a] Cases (a), (b), (c), and (d) correspond, respectively, to parameters (3a), (3b), (3c), and (3d) in the text.

the MO's of acetanilide belong apparently to the symmetry group C_{2v}.[17] The group-theoretical notation is the same as that used in Eyring *et al.*[18]; the x axis is chosen perpendicular to the benzene ring for aniline or acetanilide. Of the two antibonding orbitals of acetanilide resulting from the interaction between the MO ϕ_4^0 of benzene and the antibonding MO of acetamide, the one of lower energy is denoted by ϕ_4 and the other by $\phi_{4'}$.

Table I illustrates how the MO energies of acetanilide depend upon the values of the parameters employed. The MO's obtained by the use of parameter values (3b) are also listed in the table.

It is seen from Fig. 3 and Table I that

$$e_3(\text{aniline})>e_3(\text{acetanilide})>e_3^0. \tag{5}$$

It can be shown that the orbital energy e_3 of aniline becomes lower with increasing magnitude of δ_N.[19] It might therefore be said that the acetylation of aniline exerts on the orbital energy e_3 such an effect as would be produced if the electronegativity of the nitrogen atom were raised.

As for the energy of MO ϕ_4, one has

$$e_4(\text{aniline})>e_4^0>e_4(\text{acetanilide}). \tag{6}$$

It is to be noted that the relations (5) and (6) hold, irrespective of which set of parameter values is used among (3a)–(3d).

V. METHOD FOR EVALUATING RESONANCE INTEGRAL

Several methods have been proposed for evaluating the resonance integral β that appears in the simple MO theory. Among them the one used by Goodman and Shull[20] in the treatment of the substituted benzene spectra seems most reasonable. In studies of the spectra of mono-substituted benzenes and naphthalenes, we have taken, after the scheme of Goodman and Shull, different values for β corresponding to different electron configurations.[21] The same method was adopted in the present calculation. The foundation of the method for evaluating the resonance integral will be described below.

According to the simple MO theory, the energy required for exciting an electron from an occupied orbital, ϕ_i, to an unoccupied orbital, ϕ_k, is given by

$$e_k-e_i=(m_k-m_i)\beta, \tag{7}$$

where $e_i=\alpha+m_i\beta$.

In the rigorous theory, a configurational wave function is obtained as an antisymmetrized product of molecular spin-orbitals. In the case of a $2n$-electron system, the lowest energy configurational wave function, V_0, may be expressed as

$$V_0=(\phi_1\bar{\phi}_1\cdots\phi_n\bar{\phi}_n), \tag{8}$$

where $\phi_1, \cdots\phi_n$ are the n lowest energy MO's. An excited configuration arises from the excitation of an electron belonging to an occupied MO ϕ_i to an unoccupied MO ϕ_k. The wave function, V_{ik}, for this configuration is

$$V_{ik}=(1/\sqrt{2})\{(\phi_1\bar{\phi}_1\cdots\phi_i\bar{\phi}_k\cdots\phi_n\bar{\phi}_n) - (\phi_1\bar{\phi}_1\cdots\bar{\phi}_i\phi_k\cdots\phi_n\bar{\phi}_n)\}, \tag{9}$$

which will be hereafter abbreviated to

$$V_{ik}=(1/\sqrt{2})(\Phi_1-\Phi_2).$$

Denote the complete $2n$-electron Hamiltonian by $\mathbf{H}$, and define $E(V_0)$, etc., as follows:

$$E(V_0)=\int V_0^*\mathbf{H}V_0 d\nu, \quad \text{etc.}$$

Let the usual Coulomb and exchange electron repulsion integrals be denoted by J_{ik} and K_{ik}.[22] Then it can be

[17] Symbols of symmetry types for apparent symmetry are given in parentheses.

[18] H. Eyring, J. Walter, and G. E. Kimball, *Quantum Chemistry* (John Wiley & Sons, Inc., New York, 1944), p. 376.

[19] F. A. Matsen, J. Am. Chem. Soc. **72**, 5243 (1950).

[20] L. Goodman and H. Shull, J. Chem. Phys. **27**, 1388 (1957).

[21] H. Baba and S. Suzuki, Bull. Chem. Soc. Japan (to be published).

[22] C. C. J. Roothaan, Revs. Modern Phys. **23**, 69 (1951).

shown that

$$E(V_{ik})=E(\Phi_1)+K_{ik}. \quad (10)$$

Now, let it be assumed that MO's are determined by Roothaan's self-consistent field method for a closed-shell ground state, and that both ϵ_i and ϵ_k are eigenvalues of the self-consistent one-electron Hamiltonian.[22] Then it follows that

$$E(\Phi_1)-E(V_0)=(\epsilon_k-J_{ik}+K_{ik})-\epsilon_i=\epsilon_k^{(i)}-\epsilon_i. \quad (11)$$

$\epsilon_k^{(i)}$ is identical with the energy quantity which was considered by Mulliken[23] to be acceptable as the orbital energy of the excited MO ϕ_k. It would be plausible to relate e_k-e_i to $\epsilon_k^{(i)}-\epsilon_i$, if it were not for the following difficulty: namely, $\epsilon_k^{(i)}$ is dependent not only upon MO ϕ_k, but also upon MO ϕ_i from which the excitation occurs, whereas e_k does not depend on ϕ_i. Hence it is not reasonable to equate e_k-e_i directly with $\epsilon_k^{(i)}-\epsilon_i$. In view of this situation, the resonance integral is regarded as a quantity depending upon both i and k, and is denoted by $\beta_{i\to k}$ instead of β. Then it follows that

$$(m_k-m_i)\beta_{i\to k}=E(\Phi_1)-E(V_0). \quad (12)$$

$E(\Phi_1)$ corresponds to the mean of the energies for singlet and triplet configurations. From Eqs. (10) and (11) the energy of the singlet configuration V_{ik}, with which we are concerned here, is obtained as

$$E(V_{ik})-E(V_0)=(\epsilon_k^{(i)}+K_{ik})-\epsilon_i. \quad (13)$$

In the simple MO theory, where no consideration is given to electron spin, no term corresponding to K_{ik} of the preceding equation is to be found. However, allowance may be made for this discrepancy by the procedure in which $\beta_{i\to k}$ is determined empirically. Thus, instead of Eq. (12), the following relation is assumed:

$$(m_k-m_i)\beta_{i\to k}=E(V_{ik})-E(V_0). \quad (14)$$

The values of m_k and m_i are obtained from the simple MO calculation. Accordingly, if the purely theoretical quantity, $E(V_{ik})-E(V_0)$, is replaced by an appropriate experimental value, $\beta_{i\to k}$ can be immediately determined.

VI. CONFIGURATION INTERACTION AND STATE ENERGIES

Before proceeding to the calculation for acetanilide, reference must be made to the cases of benzene and aniline.

Because of the high symmetry (D_{6h}) of benzene, V_{24}^0, V_{35}^0 and V_{25}^0, V_{34}^0 are degenerate pairs of configurations, and the interaction of the configurations of each pair is automatically introduced.[14] The characteristics of the states resulting from the configuration interaction are summarized in Table II.

[23] R. S. Mulliken, J. Chim. Phys. **46**, 497 (1949); R. G. Parr and R. S. Mulliken, J. Chem. Phys. **18**, 1338 (1950).

TABLE II. Lower excited states of benzene.

Symmetry D_{6h}	Symmetry C_{2v}[a]	State wave function	Observed excitation energy (ev)[b]	Band assignment
B_{2u}	B_2^-	$(1/\sqrt{2})(V_{24}^0-V_{35}^0)$	4.88	I
B_{1u}	A_1^+	$(1/\sqrt{2})(V_{25}^0+V_{34}^0)$	6.14	II
E_{1u}	B_2^+	$(1/\sqrt{2})(V_{24}^0+V_{35}^0)$	6.74	III
	A_1^-	$(1/\sqrt{2})(V_{25}^0-V_{34}^0)$		

[a] See text for values in parentheses. Parameters: $\delta_N=1.2$, $\delta_O=1.5$, $\rho_{CO}=1.5$.
[b] See footnote reference 11.

From Eqs. (4)

$$m_2^0=m_3^0=1, \qquad m_4^0=m_5^0=-1.$$

One may reasonably consider that

$$E(V_{24}^0)=E(V_{35}^0)=\tfrac{1}{2}\{W^0(B_{2u})+W^0(E_{1u})\},$$
$$E(V_{25}^0)=E(V_{34}^0)=\tfrac{1}{2}\{W^0(B_{1u})+W^0(E_{1u})\},$$

where $W^0(B_{2u})$, for example, is the energy of the B_{2u} state of benzene. Thus from Eq. (14) and Table II it follows that

$$\beta_{2\to 4}^0=\beta_{3\to 5}^0=-2.905 \text{ ev}=\beta^0(B_2), \quad (15a)$$
$$\beta_{2\to 5}^0=\beta_{3\to 4}^0=-3.22 \text{ ev}=\beta^0(A_1). \quad (15b)$$

These resonance integral values for benzene are substantially the same as those used by Goodman and others.[20,24]

In aniline the energies of the B_2 configurations, V_{24} and V_{35} (cf. Table II), are no longer equal to each other. The same is the case with the energies of the A_1 configurations, V_{25} and V_{34}. Let $\beta_{i\to k}$ for aniline be taken as equal to $\beta^0(B_2)$ when $V_{ik}\subset B_2$, and to $\beta^0(A_1)$ when $V_{ik}\subset A_1$. Then the configuration energies $E(V_{ik})$'s may be obtained from Eq. (14).

The next step of the calculation is concerned with the interaction between the configurations of the same symmetry. The matrix element of the total Hamiltonian $\mathbf{H}$ between V_{ik} and V_{jl} is given by

$$\int V_{ik}^*\mathbf{H}V_{jl}dv=2[ki\,|\,jl]-[kl\,|\,ji] \quad (i\neq j,\ k\neq l), \quad (16)$$

where

$$[ij\,|\,kl]=\int\phi_i^*(1)\phi_k^*(2)(e^2/r_{12})\phi_j(1)\phi_l(2)dv. \quad (17)$$

As the MO's ϕ_i, etc., appearing in Eq. (16), use is made of the orthonormal MO's which are obtained by the simple LCAO procedure. Neglecting differential overlap, the integral $[ij\,|\,kl]$ may be expressed in terms of Coulomb repulsion integrals over atomic orbitals such as

$$(pp\,|\,qq)=\int\chi_p^*(1)\chi_q^*(2)(e^2/r_{12})\chi_p(1)\chi_q(2)dv. \quad (18)$$

[24] E. G. McRae and L. Goodman, J. Mol. Spectroscopy **2**, 464 (1958).

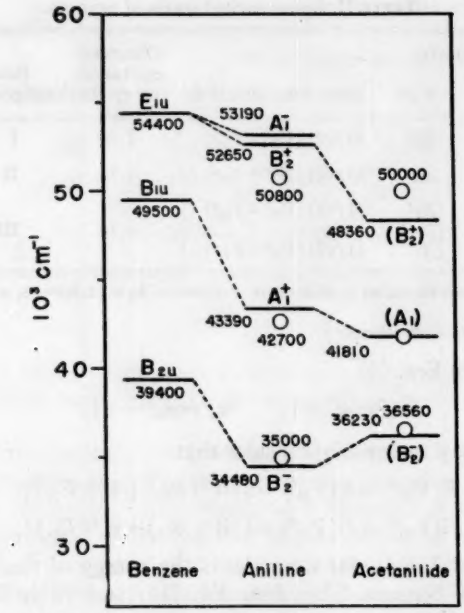

FIG. 4. Calculated and observed lower excited states. Observed states are represented by circles.

The integrals of this type were evaluated by the method of Pariser and Parr.[14] Necessary values of the ionization potentials and electron affinities in valence states were taken from the table of Pritchard and Skinner.[25] The values of the integrals $(11 \mid 11)_{CC}$ and $(11 \mid 22)_{CC}$ were slightly modified in such a way that the energies of the B_2^+ and A_1^- states of benzene, calculated in the present approximation, might be equal to each other and to the observed value, 6.74 ev (cf. Table II). The results are

$$(11 \mid 11)_{CC}=11.21 \text{ ev}, \qquad (11 \mid 22)_{CC}=6.70 \text{ ev}.$$

The state energies of aniline were thus calculated for various values of the parameter δ_N. As a result it was found that the calculated energies are in best agreement with the observed ones when $\delta_N=1.2$.[21] The calculated energies for this value of δ_N are shown in Fig. 4 together with the observed ones. The assignment of the transitions presented in the figure is the same as Goodman and Shull's.[20] It should be noted that an alternative assignment has been proposed by Nagakura and Tanaka[26] and Murrell.[27]

Let us now proceed to the case of acetanilide. In this molecule there appears an extra excited MO of type b_1, as shown in Fig. 3 and Table I. Furthermore, since acetanilide has in reality no symmetry, interaction may occur between those configurations which belong apparently to different symmetry types. Consequently, the problem of configuration interaction is much more complicated in acetanilide than in aniline. To avoid this difficulty, only the interaction is here considered between configurations of apparently the same symmetry type and of nearly equal energy. Accordingly, the interaction of V_{24} and V_{35} is to be taken into account. On the other hand, V_{34} may be regarded as representing approximately an excited state without mixing with any other configurations.

The configuration energies and also the state energies have been calculated in the same manner as in the case of aniline. The resonance integral β_{i-k} was taken as equal to $\beta^0(B_2)$ for V_{24} and V_{35}, and to $\beta^0(A_1)$ for V_{34}. The values of the matrix element

$$\int V_{24}^* H V_{35} d\nu$$

were calculated to be 0.498, 0.635, 0.491, and 0.600 ev, respectively, for the parameters (3a), (3b), (3c), and (3d). These values are somewhat smaller than the corresponding value, 0.766 ev, for aniline. The calculated energies for the lower excited states are listed in Table III together with the state wave functions for the parameter values of (3b). Inspection of Table III reveals that the best agreement is found between the calculated and the observed excitation energies when the parameters (3b) are adopted. It is to be noted here that, so far as the lowest excited state of acetanilide is concerned, the value of the calculated energy is almost independent of the magnitudes of the parameters δ_O and ρ_{CO}.

Both the calculated and the observed excitation energies for benzene, aniline, and acetanilide are summarized in Fig. 4, in which the calculation for acetanilide is based on the parameter values of (3b). From Table III and Fig. 4, it may be pointed out that the calculated excitation energies are in the following orders:

$$\left.\begin{array}{ll} \text{Band I,} & \text{aniline}<\text{acetanilide}<\text{benzene;} \\ \text{Band II,} & \text{acetanilide}<\text{aniline}<\text{benzene.} \end{array}\right\} \quad (19)$$

These relations hold for each set of parameter values.

In this section, it has been found that the following parameter values are most suitable for the calculation of the excitation energies:

$$\delta_N=1.2, \qquad \delta_O=1.5, \qquad \rho_{CO}=\sqrt{2}.$$

The calculations described in the succeeding sections are therefore made exclusively by the use of these values. It should be noted in this connection that a variety of values have been hitherto assumed for the parameters in question, viz., $\delta_N=1\sim2$, $\delta_O=1.2\sim2$, $\rho_{CO}=1.4\sim2$.[19,28]

[25] H. O. Pritchard and H. A. Skinner, Chem. Revs. **55**, 745 (1955).
[26] S. Nagakura and J. Tanaka, J. Chem. Soc. Japan **75**, 331 (1954).
[27] J. N. Murrell, Proc. Phys. Soc. (London) **A68**, 969 (1955).
[28] H. C. Longuet-Higgins and C. A. Coulson, Trans. Faraday Soc. **43**, 87 (1947); L. E. Orgel, T. L. Cottrell, W. Dick, and L. E. Sutton, Trans. Faraday Soc. **47**, 113 (1951); R. D. Brown, Quart. Revs. **6**, 63 (1952); B. Pullman and A. Pullman, *La chimiothérapie des cancers et des leucémies* (C.N.R.S. International Symposium, Paris, 1958), pp. 201–214.

TABLE III. Energies and wave functions for lower excited states of acetanilide.[a]

Symmetry	Excitation energy (ev) (a)	(b)	(c)	(d)	observed	Wave function (b)	Band assignment
(B_2^-)	4.524	4.491	4.509	4.540	4.532	$0.481V_{24}-0.876V_{35}$	I
(A_1)	4.705	5.183	4.645	5.099	5.183	V_{24}	II
(B_2^+)	5.530	5.995	5.492	5.870	6.200	$0.876V_{24}+0.481V_{35}$	III

[a] Cases (a), (b), (c), and (d) correspond, respectively, to parameters (3a), (3b), (3c), and (3d) in the text.

TABLE IV. Calculated and observed intensities for the first and second absorption bands.

Band	Aniline f_{calc}[a]	Aniline f_{obs}	Acetanilide f_{calc}[a]	Acetanilide f_{obs}	Benzene f_{calc}	Benzene f_{obs}[b]
I	0.091 (0.027)	0.026	0.070 (0.021)	0.01	0	0.0014
II	0.289 (0.087)	0.17	0.669 (0.20)	0.28	0	0.10

[a] See text for values in parentheses. Parameters: $\delta_N=1.2$, $\delta_O=1.5$, $\rho_{CO}=\sqrt{2}$.
[b] Taken from Klevens and Platt (footnote 11).

VII. INTENSITIES

Using the state wave functions determined in the preceding calculation, the oscillator strengths, f, were calculated on the basis of the well-known relation[29]:

$$f=1.085\times10^{11}\nu\mathbf{Q}^2.$$

The results are shown in Table IV. The values of f_{calc} for the transitions to B_2^+ states in aniline, acetanilide, and benzene are 0.773, 0.609, and 1.14, respectively. It is seen from Table IV that the f_{calc} values are in the following orders:

$$\left.\begin{array}{ll}\text{Band I,} & \text{aniline}>\text{acetanilide}>\text{benzene;}\\ \text{Band II,} & \text{acetanilide}>\text{aniline}>\text{benzene.}\end{array}\right\} \quad (20)$$

These are in complete agreement with the orders of the observed f values, given in Table IV. However, as is often the case,[29] the absolute values of the calculated oscillator strengths are too high. A correction factor of 0.30 was introduced, which is the ratio between f_{obs} and f_{calc} for the $A_{1g}\rightarrow E_{1u}$ transition of benzene. The corrected values, given in parentheses in Table IV, roughly accord with the observed ones.

From the present calculation information on the direction of the transition moments can be obtained. In the case of aniline, the direction of the transition moments is immediately known from the symmetry types of the excited states concerned. Thus the moments of transitions I and III lie along the direction perpendicular to the C—N axis, while the moment of transition II lies along the direction of the C—N axis itself. In acetanilide, the moments of both transitions I and III are perpendicular to the C_1—N axis. The moment of transition II makes an angle of 20.5° with the C_1—N axis, being inclined towards the acetyl group.[30]

[29] R. S. Mulliken and C. A. Rieke, Repts. Progr. in Phys. 8, 231 (1941).

VIII. ELECTRONIC PROPERTIES IN THE GROUND STATE

The π-electron densities and π-bond orders in the ground state were calculated in the usual way[31] for acetanilide and related substances.[32] The results are summarized in the molecular diagrams of Fig. 5. Discussion on the diagrams will be given in the next section.

IX. DISCUSSION

It may be inferred by intuition that the acetylation of aniline produces electronic effects of the following types[8]:

(a) a decrease in the tendency of the nonbonding electrons at the nitrogen atom to migrate into the benzene ring;
(b) an extension of conjugation.

With these two effects in mind, let us first consider the difference between the spectra of aniline and acetanilide. The most noticeable spectral changes caused by the acetylation of aniline are on the one

[30] By the use of polarized ultraviolet radiation, Tanaka has recently determined the direction of the transition moments for the absorption bands of acetanilide. His experimental result is nearly in accord with the expectation from the present calculation (J. Tanaka, preliminary report, presented at the Symposium on Electronic States in Molecules, held by the Chem. Soc. Japan, September, 1959).
[31] C. A. Coulson, *Valence* (Oxford University Press, New York, 1952), Chap. IX.
[32] Since the present treatment does not allow for the effect of methyl group, the results of the calculations made for acetanilide, acetamide, and acetaldehyde might be applied to formanilide formamide, and formaldehyde, respectively.

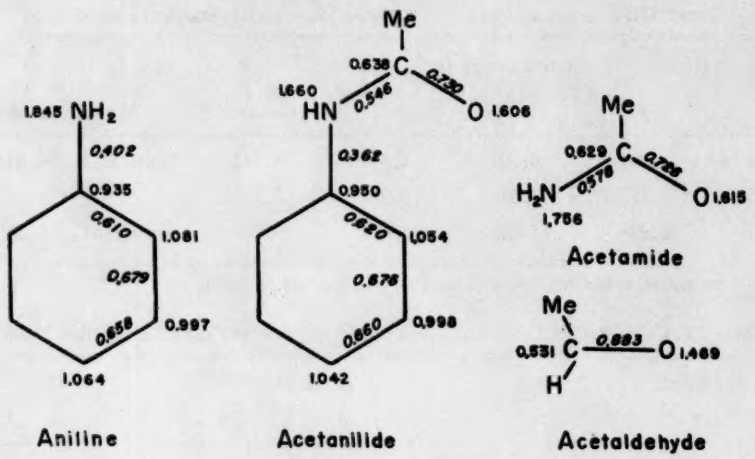

FIG. 5. π Electron densities and π-bond orders ($\delta_N = 1.2$, $\delta_O = 1.5$, $\rho_{CO} = \sqrt{2}$).

hand the blue shift and the decrease in the intensity of band I, and on the other hand the red shift and the increase in the intensity of band II. As has been already shown in relations (19) and (20), these observations are in satisfactory agreement with the results of the present calculation.

By reference to the result of a semiquantitative treatment, given by one of the authors[33] on the basis of the theory of electron migration,[34] it is found that the behavior of band I can be interpreted in terms of the above effect (a). On the contrary, the effect (b) has been presumed to be important for understanding the behavior of band II.[8,35] These rather intuitive interpretations are substantiated in a refined manner by the present theoretical investigation. It is seen from Fig. 3 and Table III that configuration V_{35} makes the greatest contribution to the excited state associated with transition I both in aniline and in acetanilide. As to the MO energy e_3, one has the relation (5). Moreover, since MO ϕ_5^0 is of a_2 type, its energy remains unaltered when a substituent group is introduced into benzene; consequently the MO energy e_5 of acetanilide coincides with that of aniline. These arguments naturally lead to the conclusion that the blue shift of band I in passing from aniline to acetanilide is largely due to the effect of type (a). The excited state corresponding to absorption band II of acetanilide is approximately represented by the configuration V_{34}. Then, taking into account the nature of the excited MO ϕ_4 of acetanilide [cf. Table I and relation (6)], it will be easily understood that the effect (b) is primarily responsible for the behavior of band II.

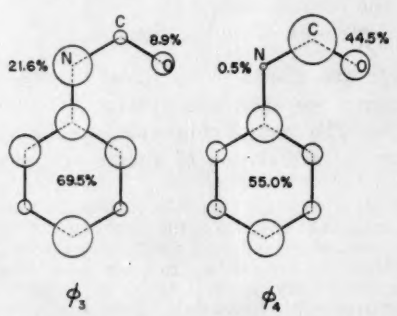

FIG. 6. Distribution of an electron in MO ϕ_3 or in MO ϕ_4.

Mention should be made here of the electron distribution associated with ϕ_3 and ϕ_4 of acetanilide. Figure 6 shows the distribution of an electron occupying the MO ϕ_3 or ϕ_4, in which the magnitudes of the squares of the coefficients of the atomic orbitals in ϕ_3 and ϕ_4 (see Table I) are indicated by the sizes of the circles. In the figure are also shown the probabilities in percent of finding the electron in the ring, the nitrogen atom and the carbonyl group. It is seen that the excitation of an electron from ϕ_3 to ϕ_4 is accompanied by a large amount of electron transfer from the ring and the nitrogen atom to the carbonyl group. It is worth noting that the first $\pi \rightarrow \pi^*$ absorption band in amides (at 1717 A in formamide)[36] has been attributed to the intramolecular electron transfer from the nitrogen atom to the carbonyl group.[37–39] The charge-transfer absorption band of acetamide will be displaced to the longer wavelengths by the attachment of a phenyl group to the nitrogen, on account of the extension of conjugation. From this point of view, it might be said that band II of acetanilide is originally analogous to the charge-transfer band of acetamide. On the other hand,

[33] H. Baba, J. Chem. Soc. Japan **72**, 411 (1951).
[34] A. L. Sklar, J. Chem. Phys. **7**, 984 (1939); K. F. Herzfeld, Chem. Revs. **41**, 233 (1947).
[35] J. P. Picard and A. F. McKay, Can. J. Chem. **31**, 896 (1953).
[36] H. D. Hunt and W. T. Simpson, J. Am. Chem. Soc. **75**, 4540 (1953).
[37] S. Nagakura, J. Chem. Phys. **23**, 1441 (1955); Tech. Rept., Laboratory of Molecular Structure and Spectra, University of Chicago, Part 1, p. 61 (1957–1958).
[38] J. Tanaka, J. Chem. Soc. Japan **78**, 1636 (1957).
[39] D. L. Peterson and W. T. Simpson, J. Am. Chem. Soc. **79**, 2375 (1957).

it can be shown from the data in Tables I and III that the transition corresponding to band I of acetanilide causes partial electron transfer from the nitrogen atom to the ring.

Let us now turn to discussion of the diagrams given in Fig. 5. In benzene, the π-electron density is unity at every carbon atom, and the π-bond order of every C—C bond is 0.667. Inspection of the diagrams for aniline and acetanilide reveals that the acetamino group has less of a tendency to release electrons towards the ring than does the amino group. For instance, the acetylation of aniline diminishes the electron densities at *ortho* and *para* positions, and gives rise to a reduction of the double bond character of the C—N bond. Further it alters the π-bond order of each C—C bond in aniline, in the direction of the order of a C—C bond in benzene. Thus the conclusion follows that the effect of the acetylation on the electronic properties in the ground state is of the type (a) stated before.

Next let a comparison be made of the diagrams for acetanilide, acetamide, and acetaldehyde. It will then be found that the phenylation of the amide causes a decrease in the double bond character of the C—N bond. It also causes such changes in the values of both the electron density at the oxygen atom and the order of the C=O bond that they approach to the corresponding values in the aldehyde. All these facts mean that the magnitude of the migration of the nonbonding nitrogen electrons into the carbonyl group is diminished by the phenylation of the amide. It should be noticed here that the nitrogen atom of acetanilide has a smaller π-electron charge than do the nitrogen atoms of aniline and acetamide.

The information drawn from the diagrams in Fig. 5 may thus be summarized as follows:—When two electron-accepting groups, phenyl and carbonyl, are attached to a nitrogen atom, the total migration of the nonbonding electrons from the nitrogen atom is increased, as compared with the case in which only one of them is attached; whereas the migration of the nonbonding electrons into each group is diminished because of the competition of the two groups for the migrating electrons.

This conclusion is supported by several experimental facts. The reaction of aniline with an electrophilic agent, such as bromine, proceeds so rapidly as to afford exclusively the trisubstituted product. The reactivity is considerably reduced by the acetylation of aniline, so that in the case of acetanilide the reaction is limited to the stage of monosubstitution.[40] This chemically well-known fact accords with what will be expected from the comparison of the electron density values for the two substances.

The infrared C=O stretching frequency of acetamide is raised by the introduction of aromatic substituents into the nitrogen atom. An explanation for this observation was given by Gierer[5] under the view that the aromatic substituents localize the C=O bond, and favor the keto structure. In connection with an investigation on hindered internal rotation, by means of NMR spectroscopy, it was suggested by Gutowsky and Holm[41] that in N-methylformanilide or in N-methylacetanilide the competition of the phenyl group with the oxygen for the nonbonding pair of electrons on the nitrogen would tend to decrease the double bond character of the C—N bond. These views are in agreement with the expectation from the present calculation.

X. ACKNOWLEDGMENTS

The authors wish to express their thanks to Professor K. Higasi for his valuable advice and encouragement. They are also indebted to Professor S. Nagakura and Dr. J. Tanaka for helpful discussions.

[40] L. F. Fieser and M. Fieser, *Textbook of Organic Chemistry* (D. C. Heath and Company, Boston, Massachusetts, 1950), p. 482.

[41] H. S. Gutowsky and C. H. Holm, J. Chem. Phys. **25**, 1228 (1956).

Thermal Diffusion of Ternary Mixtures

A. E. DE VRIES AND M. F. LARANJEIRA*

F.O.M.—Laboratorium voor Massaspectrografie, Hoogte Kadijk 202, Amsterdam

(Received December 17, 1959)

Experiments have been performed on ternary mixtures, consisting of two isotopes and a nonisotopic compound. It is found that the influence of the third compound on the separation of the isotopes cannot always be foreseen, the hardness (R_T value) being of extreme importance.

INTRODUCTION

SOME time ago a series of column experiments was done at our laboratory in which the separation of two isotopes was measured with different concentrations of a third component.[1]

While in the case of nitrogen added to CO the separation between $^{12}C^{16}O$ and $^{14}C^{16}O$ did not change within the experimental error, a decrease was observed by the addition of ethylene and ethane. Although in general it is not allowed to compare separations in a column, it was reasoned that in this case the change had to be attributed to the elementary effect.

Theoretical predictions of the influence of a third component on the separation of isotopes can only be made in a semiquantitative way,[2,3] but no experiments had been made to test the theory. We, therefore, did some experiments by means of a convection-free apparatus, the "swing separator," ("Trennschaukel").[4] These experiments were done with rare-gas mixtures because expected effects would be rather large.

EXPERIMENTS

a. Trennschaukel Experiments

Procedure

These experiments were done in a "swing separator," consisting of nine stainless steel tubes with an i.d. of 15 mm connected in series by stainless steel capillary tubes with an inner diameter of 0.8 mm. The upper part of the tubes was held at a temperature of about 660°K heated by means of a copper block, the lower part was at about 285°K by cooling water. About 1 cm^3 of the gas mixture was pumped to and fro periodically by means of a glass U tube which was partially filled with mercury. The U tube was swung by an electromotor and an eccentric wheel. Theoretically the stationary state should be reached within 1 hr for neon. Experimentally it was found that a constant separation was reached after 4 hr. During this 4-hr run samples were drawn every 15 min. For the actual measurements each experiment was run for 24 hr in order to secure equilibrium. Analyses were made by the gas mass spectrometer of our laboratory.

Chemicals

The gases used were from Loos & Company, Amsterdam, 99.9% pure and used without any further purification.

b. Column Experiments

Procedure

The experiments were done in a 1.5-m hot-wire column with a top reservoir of 2000 ml and a bottom reservoir of 150 ml provided with a Geiger counter. The temperature of the wire was about 600°K, that of the cooling water about 300°K. The Geiger counter indicated the stationary state and in the case of CO alone the separation could be found by the activity measurements before and after separation. In the case of added N_2 the CO:N_2 ratio was determined by oxidation of the CO with excess O_2. Both the pressure decrease during the reaction and the partial pressure of the CO_2 which could be condensed in liquid air gave the CO:N_2 ratio. In the case of ethylene and ethane as added compounds the CO could be determined by freezing out the organic compounds in liquid air and measuring their pressure after pumping away the CO. It was experimentally proven that no exchange between CO and C_2H_4 or C_2H_6 occurred.

Chemicals

CO was made by mixing $CaCO_3$ which contained some $Ca^{14}CO_3$ with zinc, and heating the mixture to 950°C. The CO formed was freed from some CO_2 by leading the gas through a liquid air trap.

N_2 was prepared by heating crystallized NaN_3.

Ethylene was made by the addition of alcohol to a mixture of P_2O_5 and H_3PO_4 heated to 200°C. The gas was led through traps with KOH and concentrated H_2SO_4, condensed in liquid air and fractionated.

* On leave from Comissão de Estudos de Energia Nuclear do Instituto de Alta Cultura, Lisboa, Portugal.

[1] A. E. de Vries, "The enrichment of radioactive isotopes by thermal diffusion," thesis, Amsterdam, 1956.

[2] E. J. Hellund, Phys. Rev. **57**, 328 (1940).

[3] E. Whalley and E. R. S. Winter, Trans. Faraday Soc. **46**, 517 (1950).

[4] M. F. Laranjeira, "Experimental and theoretical thermal diffusion factors in binary and ternary mixtures," thesis, Amsterdam, 1959.

TABLE I.

Mixture	α_b (isotopic mixture)	α_t (conc. added component 100%)	α_t/α_b exptl	α_t/α_b calc for r.e.s. model
1. ^{36}Ar–^{40}Ar—He	0.0146	0.0247	1.7	2.9
2. ^{36}Ar–^{40}Ar—Ne	0.0146	0.037	2.5	1.6
3. ^{20}Ne–^{22}Ne—H_2	0.027	0.010	0.37	1.7
4. ^{20}Ne–^{22}Ne—He	0.027	0.015	0.56	1.8
5. ^{14}CO–^{12}CO—N_2			1.0	1.0
6. ^{14}CO–^{12}CO—C_2H_4			<0.7	~1.0
7. ^{14}CO–^{12}CO—C_2H_6			<0.6	~1.0

Ethane was obtained by the reaction of ethylcyanide with sodium at room temperature. The gas was led through traps with KOH and H_2SO_4, condensed in liquid air and fractionated. The purity of CO and N_2 was confirmed by the mass spectrometer, that of ethylene and ethane by a vapor-pressure graph.

RESULTS

The separations obtained in the column are given in the figure, in which

$$q(^{14}CO, ^{12}CO) = (^{14}CO/^{12}CO)_{bottom}/(^{14}CO/^{12}CO)_{top}.$$

The separation factor is strongly dependent on the pressure and shows the expected behavior.[6] Ratios of thermal diffusion factors for the ternary and binary mixture were obtained by comparing the q values at the optimal pressures for which we have

$$\alpha'/\alpha = \ln q'/\ln q. \quad (1)$$

For the "swing separator" experiments it was found that the inverse of the thermal diffusion factor is linearly dependent on the concentration of the added component. We, therefore, only give the results for the binary isotopic mixture and for the limiting case of 100% added third gas. These results are put down in the table. In the same table are put down the ratios of the thermal diffusion factors for binary and ternary mixtures. Also are given the calculated ratios for rigid elastic spheres. In the case of the column the ratios were obtained directly, but the α values themselves could not be determined.

DISCUSSION

It is clear from the experimental results that the actual values of α_t/α_b are not predictable by a calculation with the elementary theory if one assumes rigid elastic spheres. This is, of course, not surprising. An important point is, however, that even the answer to the question if the added compound will decrease or increase the separation between the isotopes cannot be given in general.

In all cases the difference between observed and calculated values is in agreement with the following rule: if the added compound is harder (has a larger R_T value) than the isotopes the separation is larger than calculated; if the compound is softer the separation is less than calculated. The R_T value of a substance is as usual defined as the ratio of the experimentally determined α and α calculated for rigid elastic spheres, both for an isotopic mixture. The R_T values of the noble gases have been taken from the recent measurements by Moran and Watson.[5] For the average temperature of our Trennschaukel experiments, 470°K, they find the following values:

	He	Ne	Ar
R_T	0.33	0.56	0.42

The low value of He at higher temperatures is explained by the low number of electrons: "at temperatures where the helium clouds begin to overlap to any extent, repulsion decreases since there are no inner electron shells to provide the repulsion." It seems reasonable to assume that the R_T value of H_2 will be lower than that of Ne.

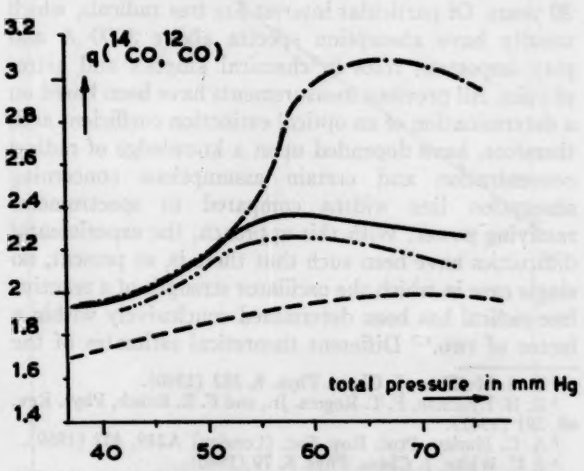

FIG. 1. Separations obtained in fractionating column: —·—·— ^{14}CO–^{12}CO, ^{14}CO–^{12}CO–95% N_2; ——— ^{14}CO–^{12}CO–50% C_2H_4; —··—··— ^{14}CO–^{12}CO–95% C_2H_4; ------- ^{14}CO–^{12}CO–50% C_2H_6.

[5] T. I. Moran and W. W. Watson, Phys. Rev. **109**, (1958), 1184.

CO and N_2 are remarkably alike.[6] Another argument for this is the fact that the thermal diffusion factor between $^{12}C^{16}O$ and $^{14}N_2$ is only of the order of 10^{-3}.[1]

Ethane and ethylene are certainly softer than CO.[6] Although they have the masses 28 and 30 they behaved in the column as gases with masses of, respectively, 30 and 32.[1] In the case of CO and N_2 no influence is observed as is theoretically predicted.

The influence of the hardness appears to be very pronounced in ternary mixtures. This may be of importance for the study of molecular interactions and of practical interest for column separations because enrichments of isotopes of soft compounds like gases with Cl and S may be carried out with the addition of a suitable added compound. In a case like $H^{35}Cl$ and $H^{37}Cl$ one would expect the separation to increase by the addition of Ar due to the hardness effect because the separation for ^{36}Ar-^{40}Ar decreased by the addition of HCl.[7]

Part of the work with the Trennschaukel experiments will be described more extensively in *Physica*.

ACKNOWLEDGMENTS

This work has been performed as part of the research program of the "Stichting voor Fundamenteel Onderzoek der Materie (F.O.M.) "with the support of the "Nederlandse Organisatie voor Zuiver Wetenschappelijk Onderzoek (Z.W.O.)."

[6] R. C. Jones and W. H. Furry, Revs. Modern Physics **18**, 159 (1946).

[7] E. Schuhmacher, "Quantitatieve trennung polynärer gasgemische durch thermodiffusion," thesis, Zürich, 1951.

THE JOURNAL OF CHEMICAL PHYSICS VOLUME 32, NUMBER 6 JUNE, 1960

Experimental Oscillator Strengths of CH and NH

R. G. BENNETT AND F. W. DALBY

Radiation Physics Laboratory, Engineering Department, E. I. du Pont de Nemours & Company, Inc., Wilmington, Delaware

(Received December 28, 1959)

The radiative lifetimes of the $A\,^3\Delta$ and $B\,^2\Sigma$ states of CH and the $A\,^3\Pi$ state of NH have been measured to be $(5.6\pm0.6)10^{-7}$, $(1.0\pm0.4)10^{-6}$, and $(4.25\pm0.6)10^{-7}$ sec, respectively. The oscillator strengths of the respective ground-state transitions were then calculated to be $(4.9\pm0.5)10^{-3}$, $(1.2\pm0.4)10^{-3}$, and $(8.0\pm1.1)10^{-3}$.

I. INTRODUCTION

THE importance of the oscillator strengths of simple molecules has stimulated a large number of theoretical[1–3] and experimental[4–6] investigations in the past 20 years. Of particular interest are free radicals, which usually have absorption spectra above 3000 A and play important roles in chemical kinetics and astrophysics. All previous measurements have been based on a determination of an optical extinction coefficient and, therefore, have depended upon a knowledge of radical concentration and certain assumptions concerning absorption line widths compared to spectrometer resolving power. With this approach, the experimental difficulties have been such that there is, at present, no single case in which the oscillator strength of a reactive free radical has been determined conclusively within a factor of two.[6,7] Different theoretical estimates of the same quantity may vary by an even larger factor.[2,3] It has, therefore, seemed desirable to determine oscillator strengths by a method which does not depend on the uncertain parameters which made earlier experiments so difficult.

In this work the radiative lifetimes of excited states of a free molecule are measured directly and the oscillator strengths (f values) of the transition are calculated using the theory due to Einstein.[8] The excited state of interest is produced by bombarding a suitably chosen parent gas, at a few microns pressure, with low-energy electrons. The electron source is then turned off and the light output measured as a function of time to yield the radiative lifetime for spontaneous emission from the upper state. The lifetime τ is related to the oscillator strength f of the electronic transition by the relation[9]

$$f=(mc\lambda^2/8\pi^2e^2)\,(d_m/d_n)\,(1/\tau),$$

where d_m and d_n are the degeneracy of the upper and lower electronic states, respectively, and λ is the wavelength of the transition.

[1] R. S. Mulliken, J. Chem. Phys. **8**, 382 (1940).
[2] R. H. Lyddane, F. T. Rogers, Jr., and F. E. Roach, Phys. Rev. **60**, 281 (1941).
[3] A. C. Hurley, Proc. Roy. Soc. (London) **A249**, 402 (1959).
[4] J. U. White, J. Chem. Phys. **8**, 79 (1940).
[5] O. Oldenberg and F. F. Rieke, J. Chem. Phys. **6**, 439, 779 (1938).
[6] R. J. Dwyer and O. Oldenberg, J. Chem. Phys. **12**, 351 (1944).
[7] P. J. Dyne, J. Chem. Phys. **28**, 999 (1958); W. E. Kaskan, *ibid.* **29**, 1420 (1958).
[8] A. Einstein, Physik. Z. **18**, 121 (1917).
[9] Compare, for example, G. Herzberg, *Molecular Spectra and Molecular Structure: Diatomic Molecules* (D. Van Nostrand Company, Princeton, New Jersey, 1950).

Here we report experimental values for the radiative lifetimes of the upper states of the $A \rightarrow X$ and $B \rightarrow X$ systems of CH, and the $A \rightarrow X$ system of NH. The experimental technique and the relevant theory have been described in an earlier paper on the f value of the N_2^+ first negative system.[10]

II. RESULTS

A. Oscillator Strength of the $A\ ^2\Delta \rightarrow X\ ^2\Pi$ System of CH

The emission spectrum observed when CH_4, at a pressure of 2 μ, was bombarded with 100-ev electrons is shown in Figs. 1 and 2. The dominant feature is the (0, 0) transition of the $A\ ^2\Delta \rightarrow X\ ^2\Pi$ system of CH at 4312 A. The smaller peak near 3900 A is the transition of the $B\ ^2\Sigma \rightarrow X\ ^2\Pi$ system of CH. Atomic hydrogen transitions are observed at 4861, 4340, 4101, and 3970 A.

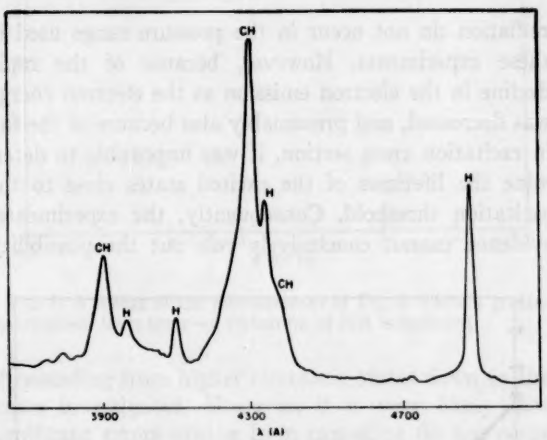

FIG. 1. Emission spectrum observed when CH_4 was bombarded with 100-ev electrons. A small Bausch and Lomb grating monochromator was used.

An interference filter was used to isolate a spectral region of interest. For the lifetime measurements a filter was chosen with peak transmission at 4230 A to avoid overlap with the atomic hydrogen line. The full width at half-maximum transmission is 100 A. The electron-beam pulse widths used were initially $(2.4)10^{-7}$ sec and later $(15)10^{-7}$ sec. The lifetime of the $A\ ^2\Delta$ level was determined to be $(5.6\pm0.6)10^{-7}$ sec from a series of 22 measurements (cf. Fig. 3). The error quoted includes statistical error only. The measured lifetime was independent of pressure in the range 5 to 0.2 μ, and of the energy of the bombarding electrons in the range 185 to 80 ev. By taking 4270 A as the weighted mean wavelength of the light included in the observation, the oscillator strength f for the transition is calculated to be $(4.9\pm0.5)10^{-3}$.

Preliminary measurements on the 3900 A system yield a lifetime of $(1.0\pm0.4)10^{-6}$ sec for the $B\ ^2\Sigma$ level.

[10] K. G. Bennett and F. W. Dalby, J. Chem. Phys. **31**, 434–441 (1959).

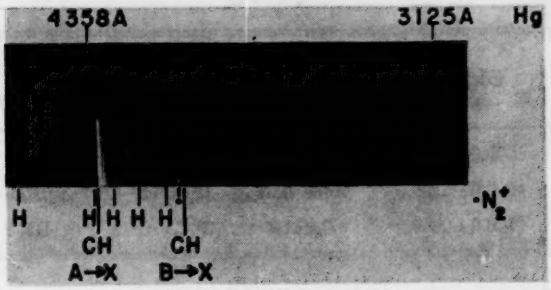

FIG. 2. The spectrum of Fig. 1 taken with a Hilger medium quartz spectrograph.

This corresponds to an oscillator strength of $(1.2\pm0.4)10^{-3}$ when the degeneracy difference of the B and X levels is taken into account.

B. Oscillator Strength of the $A\ ^2\Pi \rightarrow X\ ^2\Sigma$ System of NH

The emission spectrum obtained when NH_3, at 1 μ, was bombarded with 100-ev electrons is shown in Figs. 4 and 5. The interesting features are the two band heads at 3360 and 3250 A which may be identified, respectively, with the $A\ ^3\Pi \rightarrow X\ ^3\Sigma$ and $c\ ^1\Pi \rightarrow a\ ^1\Delta$ transitions of NH. The other lines are due to atomic hydrogen.

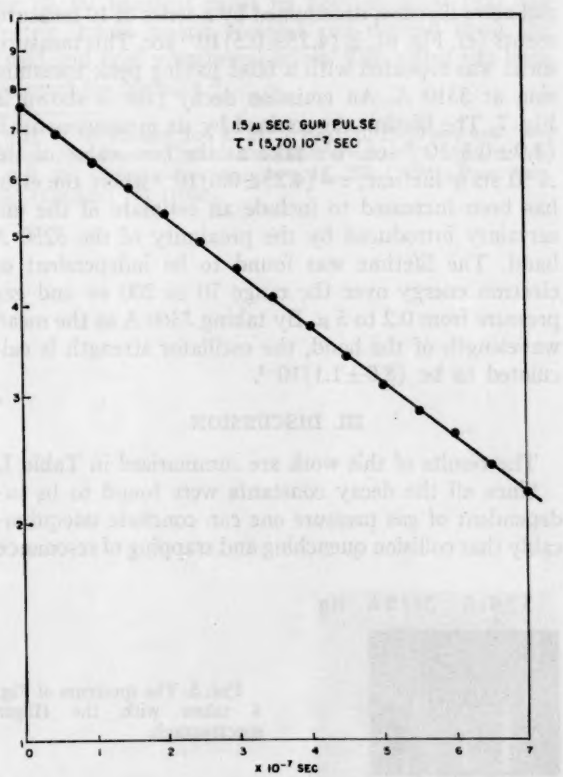

FIG. 3. Semilogarithmic plot of the free decay of light associated with the (0, 0) $A \rightarrow X$ transition of CH.

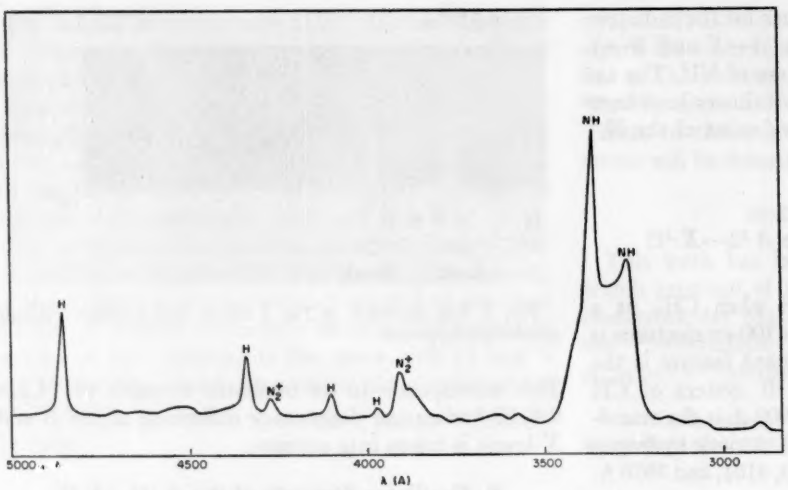

FIG. 4. Emission spectrum observed when NH_3 was bombarded with 100-ev electrons.

The interference filter used for the lifetime measurements has peak transmission at 3375 A. The transmission is reduced by a factor of 0.27 at 3250 A. It is estimated that at least 85% of the light included in the measurement is due to the 3360 A band. Since this band includes the (0, 0) and (1, 1) vibrational transitions, the transition probability determined is an average of the two individual probabilities. Electron pulse durations of $(2.4)10^{-7}$ and $(15)10^{-7}$ sec were used. The mean radiative lifetime, determined by a series of 10 measurements (cf. Fig. 6), is $(4.25\pm0.5)10^{-7}$ sec. This measurement was repeated with a filter having peak transmission at 3310 A. An emission decay plot is shown in Fig. 7. The lifetime determined by six measurements is $(4.9\pm0.5)10^{-7}$ sec. We take as the best value of the $A\ ^2\Pi$ state lifetime, $\tau=(4.25\pm0.6)10^{-7}$ where the error has been increased to include an estimate of the uncertainty introduced by the proximity of the 3250 A band. The lifetime was found to be independent of electron energy over the range 70 to 200 ev and gas pressure from 0.2 to 5 μ. By taking 3360 A as the mean wavelength of the band, the oscillator strength is calculated to be $(8.0\pm1.1)10^{-3}$.

III. DISCUSSION

The results of this work are summarized in Table I. Since all the decay constants were found to be independent of gas pressure one can conclude unequivocably that collision quenching and trapping of resonance radiation do not occur in the pressure range used in these experiments. However, because of the rapid decline in the electron emission as the electron energy was decreased, and presumably also because of the fall in excitation cross section, it was impossible to determine the lifetimes of the excited states close to the excitation threshold. Consequently, the experimental evidence cannot conclusively rule out the possibility

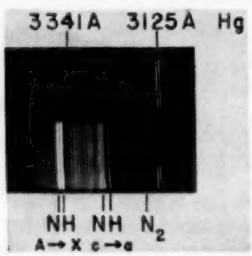

FIG. 5. The spectrum of Fig. 4 taken with the Hilger spectrograph.

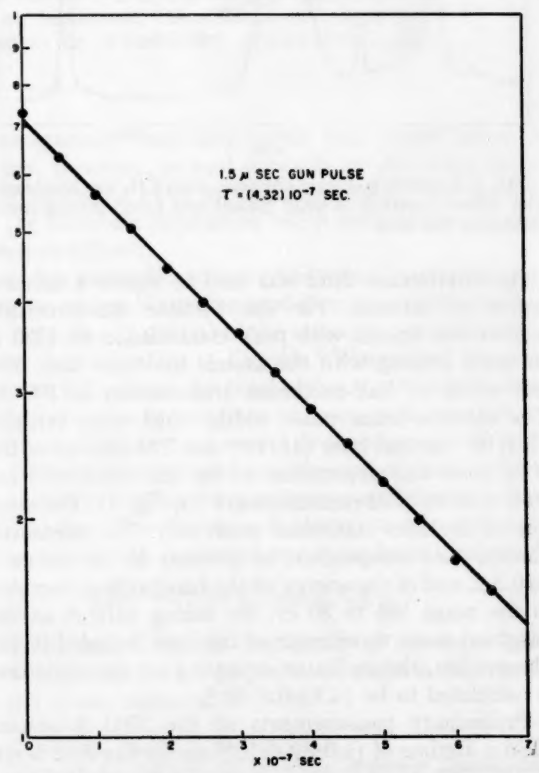

FIG. 6. Semilogarithmic plot of the free decay of light associated with (0, 0) $A\rightarrow X$ transition of NH.

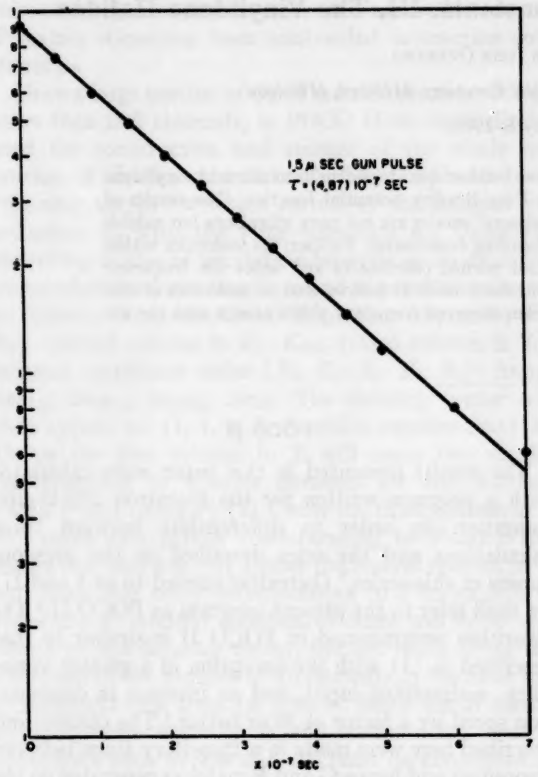

FIG. 7. A repeat of the measurement of Fig. 6 where a greater contribution from the $c \rightarrow a$ transition of NH is included.

of cascading from higher electronic states down to the states investigated. However, it is very likely that significant errors arising from cascading do not occur for the transitions studied here. There are no known higher electronic states which combine with the A states of the CH and NH molecules. For atoms, both experimental and theoretical investigations have shown that the excitation probability under electron bombardment decreases markedly for the higher excited states.[11] Although few such investigations have been made for molecules, a similar result seems to be indicated.

TABLE I.

Molecule	Transition	Mean/radiative lifetime, τ (10^{-7} sec)	Oscillator strength
CH	$A\ ^2\Delta \rightarrow X\ ^2\Pi$	5.6 ±0.6	0.0049±0.0005
CH	$B\ ^2\Sigma \rightarrow X\ ^2\Pi$	10.0 ±4.0	0.0012±0.0004
NH	$A\ ^3\Pi \rightarrow X\ ^3\Sigma$	4.25±0.6	0.0080±0.0011

The absolute extinction coefficients for a particular rotational line of the CH and NH transitions studied here can now be deduced by using the expressions given in an earlier paper.[10] The required rotational line strengths[9] and vibrational transition probabilities are well known. [For CH and NH the Franck-Condon factors for the (0, 0) band can be taken to be unity to a good approximation.]

In calculating transition probabilities for other than the (0, 0) band, it must be kept in mind that the electric dipole matrix element can depend upon the initial and final vibrational levels. This effect has been reviewed by Nicholls.[12]

[11] H. S. W. Massey and E. H. S. Burhop, *Electronic and Ionic Impact Phenomena* (Oxford University Press, New York, 1956).
[12] R. W. Nicholls, Ann. Geophys. **14**, 208 (1958); Proc. Roy. Soc. (London) 741 (1956).

Transferability of Urey-Bradley Force Constants. III. The Vinylidene Halides

JAMES R. SCHERER AND JOHN OVEREND

Spectroscopy Laboratory, The Dow Chemical Company, Midland, Michigan

(Received January 8, 1960)

Force constants have been calculated by a least-squares method for vinylidene bromide and vinylidene fluoride using complete deuterium isotopic data and a Urey-Bradley potential function. The results of this work show that the "C=C stretching" and "CH_2 scissors" modes are not pure vibrations but exhibit appreciable coupling between C=C stretching and CH_2 bending coordinates. Further, the molecules within the vinylidene-halide series do not seem to have constant normal coordinates and hence the frequency differences are not entirely associated with changes in the force field. It follows that in molecules of this type, it is dangerous to infer changes in bond strength from observed frequency shifts except with the aid of a complete normal-coordinate analysis.

INTRODUCTION

PERHAPS the most appealing feature of the Urey-Bradley Force Field (UBFF) from the point of view of a chemical spectroscopist is the simplicity resulting from a replacement of general quadratic cross terms by nonbonded interactions. While this feature facilitates normal-coordinate calculations for relatively large molecules when the frequency data are insufficient to fix all the terms in a general quadratic potential function, there is, nevertheless a real danger that this simplified model may not correspond to physical reality. For this reason it is important to investigate the general validity of the UBFF in cases where the isotopic frequency data are sufficiently plentiful to allow determination of the potential function by a least-squares refinement. Curtis[1] has shown by a study of isotopic ethylenes that the UBFF gives normal coordinates comparable with those of the general quadratic force field. Moreover, he has emphasized the desirability of not only finding a refined set of force constants but of establishing their reliability as well. If we temporarily accept that Urey-Bradley force constants (UBFC's) obtained by least-squares methods give reasonable descriptions of the normal coordinates we are left with the task of determining sets of these refined force constants which will transfer to larger molecules where the frequency data are insufficient to determine all the potential constants.

With a view to obtaining reliable UBFC's, a study was undertaken of a series of bromoethylenes where isotopic frequency data have been made available. In this work, which will be published at a later date, the preliminary calculations on vinylidene bromide brought to light some very interesting facts concerning the nature of the group-frequency and nongroup-frequency modes of this molecule. These calculations were extended to vinylidene fluoride and the results, we feel, are sufficiently important to warrant their presentation in advance of our work on the bromoethylenes.

[1] E. C. Curtis, dissertation, University of Minnesota, 1959.

POCO II

The results presented in this paper were calculated with a program written for the Datatron 220 digital computer. In order to differentiate between these calculations and the ones described in the previous papers of this series,[2] (hereafter refered to as I and II) we shall refer to the present program as POCO II.[3] The algorithm programmed in POCO II is similar to that described in (I) with the exception of a greater versatility, a simplified input, and an increase in computation speed by a factor of 30 or better.[4] The calculations described here were made in a transitory stage between computers and hence **G** and **F** matrices generated on the Datatron 204 were used as input (with a modification in **Z**) to POCO II. Another input option to POCO II has now been completed, which generates these matrices from input Cartesian coordinates and an internal-coordinate code and stores them on magnetic tape prior to their use in the calculations.

A new space-saving feature of POCO II is the construction and use of only that part of the **Z** matrix which arises from the nonbonded repulsions, the diagonal terms of the UBFF being compressed into a "defining vector" **v**. This is illustrated in Fig. 1, which shows a pictorial representation of the **Z** matrix described in (I). If the F-index vector (row index of **Z**) is arranged so that all the n' diagonal elements are in ascending order, i.e., 1-1, 2-2, 3-3, $\cdots$ n'-n', and are followed by the off-diagonal F indices in arbitrary order, the **Z** matrix assumes the represented simple form. It is noted that the lower left submatrix in **Z** is a null matrix and also that, in the case of a completely unsymmetrical potential function, the submatrix $\mathbf{Z}_d$ is an identity matrix. With symmetry, $\mathbf{Z}_d$ becomes nondiagonal, there being the possibility of having more than one internal coordinate corresponding to a single type of UBFC, ϕ_d. It follows that the remaining

[2] J. Overend and J. R. Scherer, J. Chem. Phys. **32**, 1289, 1296 (1960).

[3] POCO II stands for *po*tential *co*nstants.

[4] This may be broken down into a factor of ~15 resulting from increase in machine speed and a factor of ~2 resulting from more efficient programming techniques.

submatrix $\mathbf{Z}_0$ contains the various contributions to the **F** matrix stemming from nonbonded interaction constants ϕ_0.

Since a large portion of the **Z** matrix contains nothing more than null elements, in POCO II we have eliminated the construction and storage of the whole left portion of **Z**, the submatrix $\mathbf{Z}_d$ being replaced by a "defining vector" $\boldsymbol{\nu}$ which correlates the internal coordinates R_i with the force constants ϕ_d. Using the stretching modes of vinylidene bromide as an example, we number the force constants and internal coordinates as follows: Force constants: K_{CH} (first column in **Z**), K_{CC} (second column in **Z**), K_{CBr} (third column in **Z**); internal coordinate order (R_1, R_2, R_3, R_4, R_5): Δr_{CH_1}, Δr_{CH_2}, Δr_{CBr_1}, Δr_{CBr_2}, Δr_{CC}. The defining vector will then appear as: (1, 1, 3, 3, 2) which signifies that: (1) Under the first column in **Z** will come two entries corresponding to *F*-index elements 1-1 and 2-2; i.e., $(\Delta r_{CH}')^2$ and $(\Delta r_{CH_2})^2$. (2) Under the third column in **Z** will come two entries corresponding to *F*-index elements 3-3, and 4-4. (3) Under the second column in **Z** will come one entry corresponding to *F*-index 5-5. If there are n' internal coordinates there will be n' elements in this defining vector, the net result being the reduction of the number of $\mathbf{Z}_d$ elements in the most unsymmetrical case from $(n')^2$ to n'. Since the **Z** matrix never appears formally in the computation, matrix operations such as **ZΦ** and **JZ** must be accomplished by more subtle (although not difficult) programming techniques.

As an additional refinement on the **Z**-matrix technique, the vector of *F* indices, which defines the internal-coordinate potential- energy interactions stemming from the UBFF, is generated by the program from the internal-coordinate input code and stored as the first column of **Z**.[5] Similarly, each column of the **Z** matrix has an index number k which signifies that it corresponds to the kth element in the UBFC vector, **Φ**, and these indices are stored as the first row of **Z**. Provision has also been made to enter manually additional rows and columns into the **Z** matrix to take care of special types of intramolecular tensions or other interactions which are not peculiar to the UBFF.

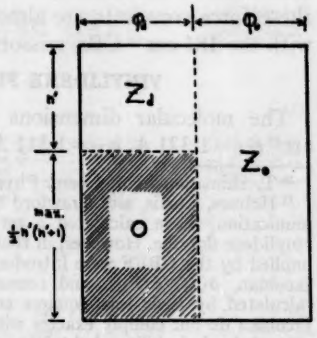

FIG. 1. Schematic representation of the *Z* matrix.

[5] In practice it is more convenient to store and use Z'.

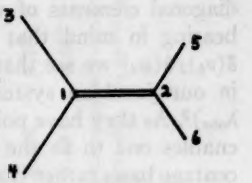

FIG. 2. Atom numbering adopted for the vinylidene halides.

INTERNAL COORDINATES

The internal coordinates were defined as follows, the notation being that of Fig. 2:

CC stretch	$R' = \Delta r_{12}$
CBr stretch	$R_2 = \Delta r_{13}$
	$R_3 = \Delta r_{14}$
CH stretch	$R_4 = \Delta r_{25}$
	$R_5 = \Delta r_{26}$
CCX bend	$R_6 = r_{CX}\Delta\alpha_{312}$
	$R^7 = r_{CX}\Delta\alpha_{412}$
XCX bend	$R_8 = r_{CX}\Delta\alpha_{314}$
CCH bend	$R_9 = r_{CH}\Delta\alpha_{521}$
	$R_{10} = r_{CH}\Delta\alpha_{621}$
HCH bend	$R_{11} = r_{CH}\Delta\alpha_{526}$.

The symmetry coordinates used in the calculations are defined by the **U** matrix given in the Appendix. Because of their use in other phases of molecular dynamics and because of their importance in specifying the exact nature of the normal coordinates, the $\mathfrak{L}'$ matrices are also reproduced in the Appendix. Since inclusion of the machine-generated **G** and **Z** matrices would involve an undue amount of space, they will not be included here. The reader may, if he so wishes, check many of the calculations by use of the given $\mathfrak{L}'$ matrices and the calculated frequencies.

THE WEIGHT MATRIX

As we have summarized in (I), the least-squares refinement process requires the construction of a Jacobian of the frequency parameters λ with respect to the UBFC's.

$$\Delta\boldsymbol{\Lambda} \approx \mathbf{JZ}\Delta\boldsymbol{\Phi}.$$

We wish to minimize the weighted-square residual of the λ's:

$$\Delta\boldsymbol{\Lambda}'\mathbf{P}\Delta\boldsymbol{\Lambda} = \Delta\boldsymbol{\Phi}'(\mathbf{JZ})'\mathbf{P}(\mathbf{JZ})\Delta\boldsymbol{\Phi}$$

where **P** is an arbitrary diagonal weight matrix. It follows from this expression that the final converged force constants, as well as the subsequent error analysis, are strongly dependent on the nature of the weight matrix. Mann *et al.*[6] have used a weight matrix, the

[6] D. E. Mann, T. Shimanouchi, J. H. Meal, and L. Fano, J. Chem. Phys. **27**, 43 (1957).

diagonal elements of which are $1/\nu^2$ or $\propto 1/\lambda_{obs}$, but bearing in mind that their Jacobian was defined as $\delta(\nu_k)/\delta(\phi_i)$ we see that a corresponding weight matrix in our Jacobian system should have elements $\propto(1/\lambda_{obs})^2$. As they have pointed out, this type of weighting enables one to fit the observed frequencies on a percentage basis rather than on an absolute basis.

With the use of older frequency data where the error in measurement may have been roughly proportional to the magnitude of the frequency, a percentage fitting seems proper. However, modern spectrometers allow present-day measurements to be made with a more or less constant accuracy across the whole spectrum. It would seem reasonable in these cases to determine a potential function which would reflect this constancy in the differences between observed and calculated frequencies. Consequently we have preferred to fit the observed frequencies on an absolute basis ($\mathbf{P} \propto 1/\lambda_{obs}$; $\mathbf{JZ} \propto \partial\lambda/\partial\phi$).[7]

It may be argued that we ought to leave room for more error in the higher frequency modes, such as carbon-hydrogen stretching vibrations, because of anharmonicity effects which have not been taken into account. On the contrary, the least-squares refinement can deal only with random effects, and hence, if we are to ignore anharmonicity we must use the same weight matrix which would have been used had we access to harmonic frequencies. Indeed, we should find, and in fact do, that many of the calculated CH stretching frequencies have deviations a few times their calculated uncertainties, indicating that we have not eliminated the problem of anharmonicity, but have statistically ignored it.

In cases where the location of a fundamental is unknown or where liquid-phase data are used along with gas-phase data, it might seem reasonable to introduce our relative confidence by varying the elements of **P**. However, such cases are quite personal and one is free to make his own decisions. Outside these special cases, we have preferred to assume equal weights across the whole vibrational spectrum.

VINYLIDENE BROMIDE

Manneback and Rahman[8] have previously calculated the planar vibrational frequencies using a general quadratic force field with certain interactions set to zero, but they did not extend their treatment to an analysis of the implied normal coordinates.

The geometrical parameters used in the present study are $r_{CBr}=1.90$ A, $r_{CH}=1.07$ A, $r_{CC}=1.31$ A, $<$HCH$=117°$, $<$BrCBr$=114°$ and the observed-frequency data are taken from Raman work by de Hemptinne, Velghe and van Riet.[9]

At the start of this investigation it was thought that flexibility of the C=C bond[10] ought to be included as an additional parameter in the potential function. Accordingly, an extra column was included in the **Z** matrix having ± 1 entries in the appropriate *cis* and *trans* interaction terms. Since, in the process of refining, this term converged to a small value which the error analysis showed to be indeterminate; it was set to zero and eliminated in the final refinement. Also, since the repulsive constant F_{HH} was found to be small and indeterminate, it too was set to zero and eliminated in the final refinement. Table I lists the observed and calculated frequencies, the potential-energy distributions, and the final converged force constants along with their uncertainties determined from the error matrix of the UBFC's.[1] Two features of this table deserve immediate comment. It is noted that the uncertainty in the *cis* repulsive constant C_{HBr} is of the same order of magnitude as the force constant. We have retained it, however, since its contribution to the potential energy is of the order of 10% in one mode of each of the three isotopes, freely admitting the utility of its inclusion may be marginal. The other notable feature is that the uncertainties in the H_{BrBr} bending constant and the F_{BrBr} repulsive constants are much larger than their refined magnitudes. Examination of the potential-energy distributions reveals that in each of these three isotopes there is a mode at approximately 184 cm^{-1} which contains significant contributions only from these two force constants. On the other hand there are no other frequencies which are strong functions of these two force constants. Indeed, in the refinement process we were attempting to determine two force constants from effectively one vibrational frequency. The fact that we did not succeed too well is reflected in the uncertainties for these force constants. The implication is that even with complete (deuterium) isotope data it is impossible to determine all the UBFC's of this molecule. Should we wish to obtain a set of force constants with lower over-all uncertainties we must supply values for one or both of these force constants from other molecules where they are known with more certainty, i.e., C_2Br_4, or possibly use ^3H isotopic data. As a final comment, this indeterminancy will not hinder our discussion of the remainder of the normal modes since these force constants are almost completely associated with the 184 cm^{-1} CBr_2 scissors mode.

VINYLIDENE FLUORIDE[11]

The molecular dimensions used for this molecule are[12] $r_{CF}=1.321$ A, $r_{CC}=1.311$ A, $r_{CH}=1.07$ A, $<$FCF=

[7] Curtis, see footnote 1, used a weight matrix of $1/\lambda_{obs}$ and the University of Minnesota group are presently using a similar weight matrix.

[8] C. Manneback and A. Rahman, Ann. Soc. Sci. Bruxells Ser. 1, **67**, 140–76 (1953).

[9] M. de Hemptinne, C. Velghe, and R. van Riet, Bull. Class. Sci. Acad. Roy. Belg. **30**, 40 (1944).

[10] T. Shimanouchi, J. Chem. Phys. **26**, 594 (1957).

[11] Holmes, Curtis, and Crawford (R. R. Holmes, private communication) have calculated a set of UB force constants for vinylidene fluoride. However, in their calculation, the constraints mplied by the UBFF were introduced as additional rows of the Jacobian, $\partial(\lambda_k)/\partial(F_{ij})$, and consequently the force constants calculated by their least-squares treatment with this extended Jacobian do not comply exactly with the UBFF constraints. In view of the desirability of obtaining consistent sets of transferable force constants, we have chosen to recalculate the vinylidene-fluoride force constants using the present technique.

[12] I. L. Karl and J. Karl, J. Chem. Phys. **18**, 963 (1950).

TABLE I. Potential energy distribution CBr_2CH_2 (entries rounded to nearest %).

		obs ν	(cm^{-1}) calc ν	$\Delta\nu$	K_{CC}	K_{CBr}	K_{CH}	H_{CBr}[a]	H_{BrBr}[a]	H_{CH}[a]	H_{HH}[a]	F_{CBr}	F_{BrBr}	F_{CH}	C_{HBr}
CBr_2CH_2	A_1	3023	3028	−5	1	...	94	...	...	...	...	...	...	5	...
		1593	1601	−8	66	2	...	...	...	7	18	2	...	2	...
		1379	1372	7	20	2	1	...	...	16	42	...	...	16	2
		467	467	0	1	58	...	1	−8	...	...	33	13	...	2
		184	184	0	...	...	...	9	−48	...	...	19	117	...	2
	B_1	3108	3120	−12	...	...	95	...	...	...	...	...	...	4	...
		1065	1067	−2	...	11	...	4	...	49	...	4	...	29	3
		696	700	−4	...	72	...	6	...	9	...	6	−2	5	3
		322	320	2	...	7	...	20	...	1	...	64	...	...	8
CBr_2CD_2	A_1	2230	2213	17	5	...	90	...	...	...	1	...	...	4	...
		1545	1539	6	79	4	4	...	−1	1	4	2	1	6	...
		1019	1020	−1	3	2	2	...	...	21	56	...	...	14	2
		453	453	0	1	56	...	1	−7	...	1	32	13	...	2
		183	183	0	...	...	...	9	−48	...	...	20	117	...	2
	B_1	2339	2324	15	...	...	95	...	...	...	...	...	...	4	...
		932	930	2	...	33	...	8	...	33	...	7	...	20	1
		625	620	5	...	54	...	2	...	24	...	6	−1	14	3
		283	284	−1	...	4	...	20	...	3	...	62	...	1	10
CBr_2CHD	A'	3061	3077	−16	...	...	95	...	...	...	...	...	...	5	...
		2282	2266	16	2	...	92	...	...	...	...	...	...	4	...
		1563	1565	−2	76	3	2	...	−1	3	8	2	1	4	...
		1258	1260	2	7	2	1	...	...	25	44	...	...	18	2
		949	949	0	...	25	...	6	...	34	6	6	...	20	1
		655	654	1	...	60	...	3	...	18	1	6	−1	10	3
		458	459	−1	1	57	...	1	−7	...	...	32	13	...	2
		300	300	0	...	5	...	20	...	2	...	63	...	1	9
		184	183	1	...	...	...	8	−48	...	...	20	117	...	2
	UBFC		(md/A)		7.546	2.224	4.906	0.056	−0.154	0.260	0.342	0.672	0.997	0.409	0.031
	Uncertainty				0.25	0.24	0.070	0.031	0.88	0.035	0.018	0.20	2.4	0.12	0.037

[a] The bending coordinates have been scaled with the r_{CX} and r_{CH} bond distances according to Eq. (1) in Paper I. Because of an inconsistency between the potential functions given on pp. 44 [Eq. (1)] and 47 in reference 6, the H_{CX} force constant in that reference must be multiplied by r_{CC}/r_{CX} to be compared with the H_{CX} force constant reported here.

TABLE II. Refinements of CH_2CF_2.

			I			II			III		
	Mode	ν_{obs} (cm^{-1})	$p_i\lambda_{obs}$	ν_{calc}	$\Delta\nu$	$p_i\lambda_{obs}$	ν_{calc}	$\Delta\nu$	$p_i\lambda_{obs}$	ν_{calc}	$\Delta\nu$
CH_2CF_2	1	3060	1	3088	−28	1	3087	−27	1	3082	−22
	2	1734[a]	1	1742	−8	1	1745	−11	1	1746	−12
	3	?	0.2[b]	1362	18	0.2[d]	1369	45	1[f]	1357	−2
	4	926	1	928	−2	1	926	0	1	927	−1
	5	550	1	551	−1	1	551	−1	1	551	−1
	6	3103	1	3130	−27	1	3131	−28	1	3134	−31
	7	1302	1	1306	−4	1	1305	−3	1	1306	−4
	8	955	1	954	1	1	956	−1	1	955	0
	9	438	1	431	7	1	430	8	1	431	7
CD_2CF_2	1	2274	1	2267	7	1	2267	7	1	2266	8
	2	1705	1	1690	15	1	1693	12	1	1691	14
	3	?	0.2[c]	1085	−25	1[e]	1085	−9	1[e]	1083	−7
	4	858	1	852	6	1	855	3	1	852	6
	5	543	1	538	5	1	537	6	1	537	6
	6	2354	1	2337	17	1	2338	16	1	2341	13
	7	1284	1	1273	11	1	1272	12	1	1273	11
	8	807	1	802	5	1	801	6	1	802	5
	9	374	1	375	−1	1	376	−2	1	376	−2
$CHDCF_2$	1	3133	1	3110	23	1	3110	23	1	3109	24
	2	2325	1	2301	24	1	2301	24	1	2302	23
	3	1715	1	1715	0	1	1717	−2	1	1717	−2
	4	1298	1	1312	−14	1	1313	−15	1	1311	13
	5	1224	1	1219	5	1	1222	2	1	1217	7
	6	929	1	933	−4	1	932	−3	1	933	−4
	7	829	1	824	5	1	825	4	1	824	5
	8	542	1	545	−3	1	545	−3	1	545	−3
	9	392	1	398	−6	1	399	−7	1	398	−6

[a] Corrected for Fermi resonance.
[b] ν obs=1380 cm^{-1}.
[c] ν obs=1060 cm^{-1}.
[d] ν obs=1414 cm^{-1}.
[e] ν obs=1076 cm^{-1}.
[f] ν obs=1359 cm^{-1}.

110°, <HCH=117°. The force constants obtained by Morino *et al.*[13] were used as starting approximations in the least-squares refinement and the observed-frequency data were taken from Edgell and Ultee[14] and Smith *et al.*[15] Because Edgell and Ultee's assignments did not seem, in our estimation, to fix convincingly the position of the symmetric CH_2 and CD_2 scissors, we felt that it might be rewarding to set the corresponding weight matrix elements P_i to small values thereby allowing the least-squares process to seek out the most probable positions for these doubtful modes. Under column I in Table II are the converged frequencies for the three isotopes of CF_2CH_2 using the Edgell and Ultee assignment of the observed frequencies. The calculated value for ν_3 of CD_2CF_2 turns out to be 25 cm^{-1} higher than the 1060 cm^{-1} value adopted by Edgell and Ultee[14] and accordingly we have taken the observed band center at 1076 cm^{-1} as the position of ν_3 in this molecule.

In an attempt to shed some light on the question of the assignment of ν_3 in CH_2CF_2, which Smith *et al.* took as the band at 1414 cm^{-1}, and which Edgell and Ultee, on the basis of product rule arguments, postulated to be ca 1380 cm^{-1} a further refinement was made in which this particular frequency (1414 cm^{-1}) was given a weight of $0.2/\lambda$. The difference between the calculated frequency ν_3 and that adopted by Edgell and Ultee, i.e., 11 cm^{-1}, is clearly within the limits to be expected for a calculation of this type, whereas the difference between the calculated frequency and that which Smith *et al.* assigned to this mode, i.e., 45 cm^{-1} appears extraordinarily large. Edgell and Byrd[16] have observed a medium intensity Raman peak in liquid CF_2CH_2 at 1359 cm^{-1} which they assign to the CH_2 scissors mode. Using this assignment the refined frequencies are given in column III. It is notable that the fit is reasonably good and does not seem to require any consideration of appreciable Fermi resonance between the overtone of the twisting mode (ca 1400 in CH_2CF_2 and 1030 in CD_2CF_2) and the respective CH_2 scissors modes. The potential-energy distribution and finally converged force constants are presented in Table III.

Holmes *et al.*[11] found that their refined force constants gave calculated frequencies of 1407 and 1073 cm^{-1} for the scissors modes of the light and heavy compounds, even though they gave normal weights ($1/\nu^2$) to the input values of 1380 and 1060 cm^{-1}, and concluded that the correct assignment of the CH_2 scissors mode is to the band at 1414 cm^{-1}. We find it

[13] Y. Morino, K. Kuchitsu, and T. Shimanouchi, J. Chem. Phys. **20**, 726 (1952).
[14] F. Edgell and C. J. Ultee, J. Chem. Phys. **22**, 1983–92 (1954).
[15] D. C. Smith, J. R. Nielsen, and H. H. Claassen, J. Chem. Phys. **18**, 326–31 (1950).
[16] W. F. Edgell and W. E. Byrd, J. Chem. Phys. **17**, 740–1 (1949).

TABLE III. Potential energy distribution CH_2CF_2 (entries rounded to nearest %).

		obs ν	calc ν (cm^{-1})	$\Delta\nu$	K_{CC}	K_{CF}	K_{CH}	H_{CF}[a]	H_{FF}[a]	H_{CH}[a]	H_{HH}[a]	F_{CF}	F_{FF}	F_{CH}	F_{HH}	C_{HF}
CH_2CF_2	A_1	3060	3082	−22	1	...	94	...	...	...	...	...	...	3	3	...
		1734	1746	−12	71	9	...	1	1	5	6	3	2	2	1	...
		1359	1357	2	5	8	...	...	...	33	41	1	1	10	6	−6
		926	927	−1	7	50	...	...	...	2	3	20	18	2	...	−4
		550	551	−1	1	...	...	11	14	1	1	19	59	...	...	−6
	B_1	3103	3134	−31	...	...	97	...	...	...	...	...	...	3	...	...
		1302	1306	−4	...	60	...	9	...	24	...	5	−1	5	...	−2
		955	955	0	...	30	...	...	...	59	...	6	−1	13	...	−9
		438	431	7	...	1	...	43	...	19	...	64	...	4	...	−32
CD_2CF_2	A_1	2274	2266	8	7	...	87	...	...	...	...	1	...	2	2	...
		1705	1691	14	69	11	6	1	1	1	2	2	2	3	1	...
		1076	1083	−7	...	27	1	1	1	22	27	10	6	4	4	−2
		858	852	6	7	28	...	...	...	15	19	10	18	6	3	−6
		543	537	6	2	...	...	10	13	2	3	20	55	1	...	−7
	B_1	2354	2341	13	...	...	97	...	...	1	...	...	...	2	...	...
		1284	1273	11	...	74	...	9	...	11	...	6	−2	2	...	−1
		807	802	5	...	18	...	3	...	57	...	13	...	13	...	−5
		374	376	−2	...	...	...	39	...	32	...	57	...	7	...	−36
$CHDCF_2$	A'	3133	3109	22	...	...	96	...	...	...	...	...	...	3	1	...
		2325	2302	23	4	...	91	...	...	1	...	1	...	2	1	...
		1715	1717	−2	71	10	4	1	1	3	3	2	2	2	1	...
		1298	1311	−13	1	46	...	7	...	28	10	4	−1	7	2	−3
		1224	1217	7	1	36	...	3	...	22	27	4	1	5	4	−3
		929	933	−4	5	46	...	...	...	16	2	18	14	4	...	−4
		829	824	5	2	20	...	2	...	46	6	11	5	11	1	−6
		542	545	−3	1	...	...	11	13	1	1	20	57	...	...	−6
		392	398	−6	...	...	...	40	...	27	...	60	...	6	...	−34
	UBFC		(md/A)		8.548	4.660	5.058	0.228	0.146	0.421	0.258	1.073	1.700	0.245	0.109	−0.101
	Uncertainty				0.28	0.30	0.10	0.11	0.23	0.086	0.026	0.30	0.63	0.20	0.055	0.062

[a] See footnote to Table I.

TABLE IV. Potential energy distribution for CH_2CF_2. Alternate assignment (entries rounded to nearest %).

		obs ν	calc ν	$\Delta\nu$	K_{CC}	K_{CF}	K_{CH}	H_{CF}[a]	H_{FF}[a]	H_{CH}[a]	H_{HH}[a]	F_{CF}	F_{FF}	F_{CH}	F_{HH}	C_{HF}
CH_2CF_2	A_1	3060	3084	−24	1	...	92	...	...	...	...	...	...	4	2	...
		1734	1743	−10	71	9	...	1	1	4	6	2	2	2	1	...
		1414	1393	21	4	6	...	...	...	28	44	...	...	13	6	−4
		926	923	3	7	52	...	...	...	1	2	20	18	2	...	−2
		550	550	0	1	...	...	10	16	...	...	17	58	...	...	−4
	B_1	3103	3137	−34	...	...	96	...	...	...	...	...	...	4	...	...
		1302	1302	0	...	60	...	9	...	21	...	5	−1	8	...	−2
		955	956	−1	...	31	...	...	...	52	...	6	...	19	...	−7
		438	430	8	...	1	...	42	...	13	...	62	...	5	...	−24
CD_2CF_2	A_1	2274	2261	13	6	...	87	...	...	...	...	1	...	3	2	...
		1705	1696	9	69	11	5	1	1	1	2	2	2	5	1	...
		1076	1090	−14	...	22	1	...	1	21	32	8	4	7	5	−2
		858	859	−1	7	33	...	...	...	10	16	12	18	7	2	−4
		543	538	−5	2	...	...	10	16	1	2	18	54	1	...	−5
	B_1	2354	2339	15	...	...	96	...	...	1	...	...	...	3	...	...
		1284	1269	15	...	74	...	9	...	10	...	5	−2	4	...	−1
		807	800	7	...	18	...	3	...	52	...	12	...	20	...	−4
		374	377	−3	...	...	...	39	...	24	...	55	...	9	...	−28
$CHDCF_2$	A'	3133	3112	21	...	...	94	...	...	...	...	...	...	4	1	...
		2325	2299	26	3	...	91	...	...	1	...	...	...	3	1	...
		1715	1718	−3	71	10	3	1	1	2	3	2	2	4	1	...
		1298	1319	−21	1	35	...	5	...	28	17	3	...	11	2	−3
		1224	1230	−6	...	44	...	4	...	16	23	4	...	6	3	−2
		929	929	0	5	48	...	...	...	12	1	17	14	6	...	−3
		829	825	4	2	21	...	2	...	41	6	10	5	17	1	−5
		542	545	−3	1	...	...	10	16	1	1	18	56	1	...	−5
		392	399	−7	...	1	...	40	...	19	...	58	...	7	...	−26
	UBFC (md/A)				8.430	4.650	4.977	0.219	0.175	0.368	0.284	1.000	1.624	0.370	0.102	−0.082
	Uncertainty				0.36	0.34	0.13	0.13	0.29	0.10	0.031	0.36	0.79	0.25	0.065	0.077

[a] See footnote to Table I.

TABLE V. Origin of the frequency differences between CH_2CBr_2 and CH_2CF_2 in the "C=C stretching" and "CH_2 scissors" modes.[a]

	$\Delta\nu_{C=C}^{(F-Br)}$	ΔK_{CC}	ΔK_{CX}	ΔK_{CH}	ΔH_{CX}	ΔH_{XX}	ΔH_{CH}	ΔH_{HH}	ΔF_{CX}	ΔF_{XX}	ΔF_{CH}	ΔF_{HH}	ΔC_{HX}
$\Delta\nu_i(cm^{-1})$	145	140	59	−1	5	2	−8	−84	7	9	−3	10	−4
	$\Delta\nu_{CH_2}^{(Br-F)}$												
$\Delta\nu_i(cm^{-1})$	15	102	−38	6	−2	−9	−113	19	−4	−5	48	−41	53
$\Delta\nu_i(cm^{-1})$[b]	−21	103	−29	4	−2	−9	−88	−16	−3	−3	17	−41	46

[a] Because of the approximations involved in converting $\Delta\lambda$ to $\Delta\nu$ the sum of the above contributions only approximates the actual frequency difference between ν_{calc} values.
[b] Alternate assignments corresponding to Table IV.

disturbing that two independent normal-coordinate analyses, based on such similar potential functions, should stand in conflict on the point of the assignment of this particular mode. The most significant difference between the two treatments is that we have at all times considered the equations of the UBFF as rigid constraints, whereas Holmes *et al.* merely required that their calculated force constants give a least-squares fit to these equations of constraint in addition to the observed frequencies. Consequently, while our potential function contains only 12 UBFC's as adjustable parameters, the method used by Holmes *et al.* is tantamount to fitting 17 independently-adjustable force constants. In view of the fact that the more flexible potential function points to the 1414 cm^{-1} band as the CH_2 scissors mode, it may be argued that the rigid constraints of the UBFF are too severe for the present analysis to yield an unbiased decision on this question.

With this in mind we have calculated a second set of force constants fitted to the alternative (1414 cm^{-1}) assignment, giving a weight of $(1/\lambda_{obs})$ to each fundamental. It may be noted from the frequencies and potential-energy distributions given in Table IV that even though the frequency fit is not quite as good as in Table III (weighted-square residuals, 0.0118 and 0.0088, respectively), the potential-energy distributions and final force constants do not differ significantly. Since the Edgell-Byrd assignment seems more compatible with the UBFF, we have used the normal coordinates based on that assignment in the following discussion.

As in the case of vinylidene bromide, it was not found necessary to include a flexibility parameter. It is again interesting that because of an increased mixing in the normal modes of this molecule the gross indeterminancy of the F_{XX} force constant has been somewhat decreased. Although, as in the case of vinylidene bromide, the uncertainties could be decreased by a transfer of force constants, our conclusions about modes other than the CF_2 scissors mode near 543 cm^{-1} will not be affected seriously. The uncertainties in the calculated frequencies as revealed by the moment matrix of the λ's[1] are approximately constant, varying from 10 to 17 cm^{-1} over the whole spectrum.

DISCUSSION

Comparison of the potential energy distributions given in Tables I and III show that the CX_2 scissors modes (Br$\sim$184 cm^{-1}, F$\sim$543 cm^{-1}) are relatively pure. The CF_2 rocking mode at 438 cm^{-1}, on the other hand, shows a large contribution from the CH_2 rocking coordinate, the amount of H_{CH} contribution going from 19% in CH_2CF_2 to 32% in the 374 cm^{-1} band of CD_2CF_2. Although this type of coupling is important in CH_2CF_2, it seems less important in the corresponding CH_2CBr_2 modes.

It may also be seen that the antisymmetric CBr_2 stretch at 696 cm^{-1} in CH_2CBr_2 is a relatively pure vibration with only a slight contribution from the CH_2 rocking coordinate. In CD_2CBr_2 however, it mixes quite strongly with the CD_2 rocking coordinate; on the other hand, this same type of mixing which is found in the 1302 cm^{-1} and 955 cm^{-1} CH_2CF_2 modes occurs to a *lesser extent* in CD_2CF_2, the 1284 cm^{-1} mode being a reasonably pure antisymmetric CF_2 stretch.

As will become apparent later in the discussion, any explanation of shifts in "C=C stretching" and "CH_2 scissors" modes from molecule to molecule must, in this case, be accompanied by considerations of the individual normal coordinates: This may be seen by inspection of the $\mathfrak{L}'$ matrices and the potential energy distributions. In CH_2CBr_2, the 1593 cm^{-1} mode is only 66% C=C stretch with a significant contribution from the H_{HH} bending constant arising from interaction with the CH_2 scissors. In CD_2CBr_2, however, the CH_2 scissors mode drops to 1019 cm^{-1}, the CC stretching mode then becoming reasonably pure. It is also noted that in going from CH_2CBr_2 to CD_2CBr_2 the CH_2 scissors mode at 1379 cm^{-1}, which contains a 20% contribution from stretch of the C=C bond, becomes a respectable scissors vibration containing only 3% C=C stretch. This over-all behavior is to be contrasted with the corresponding modes of CH_2CF_2 and CD_2CF_2. In the former case it is seen that the C=C stretching mode (1734 cm^{-1}) is relatively pure with a 9% contribution from the C—F stretch. In CD_2CF_2 the C=C stretching mode is only slightly less pure than in CH_2CF_2: however, the 1076 cm^{-1} and 858 cm^{-1} CD_2CF_2 modes involve such intimate mixing between the CH_2 scissors and the CF_2 sym stretch that from a potential-energy point of view it is difficult to determine the nature of these two vibrations. A more readily visualized representation of these modes in Cartesian space may be seen in Fig. 3.

It is instructive to consider the differences between the "C=C stretching" and "CH_2 scissors" modes from another point of view. The potential-energy distributions were derived from an equation of the form:

$$\lambda_{calc}=a_1\phi_1+a_2\phi_2+a_3\phi_3+\cdots=\sum a_i\phi_i$$

where the coefficients a_i determine the dependence of λ on each force constant in the molecule. If the normal coordinate is reasonably constant between molecules (i.e., the deformations and masses are approximately the same) the coefficients a_i are constant and the frequency shifts may be determined from a consideration of the force-constant differences, the equations of the "C=C stretching" modes of CH_2CF_2 and CH_2CBr_2 are

$$\begin{aligned}\lambda_{C=C}(CH_2CF_2)=&\,0.1500K_{CC}+0.0335K_{CF}+0.0017K_{CH}\\&+0.0572H_{CF}+0.1144H_{FF}+0.2124H_{CH}\\&+0.4249H_{HH}+0.0447F_{CF}+0.0164F_{FF}\\&+0.1140F_{CH}+0.1797F_{HH}+0.0385C_{HF}\end{aligned}$$

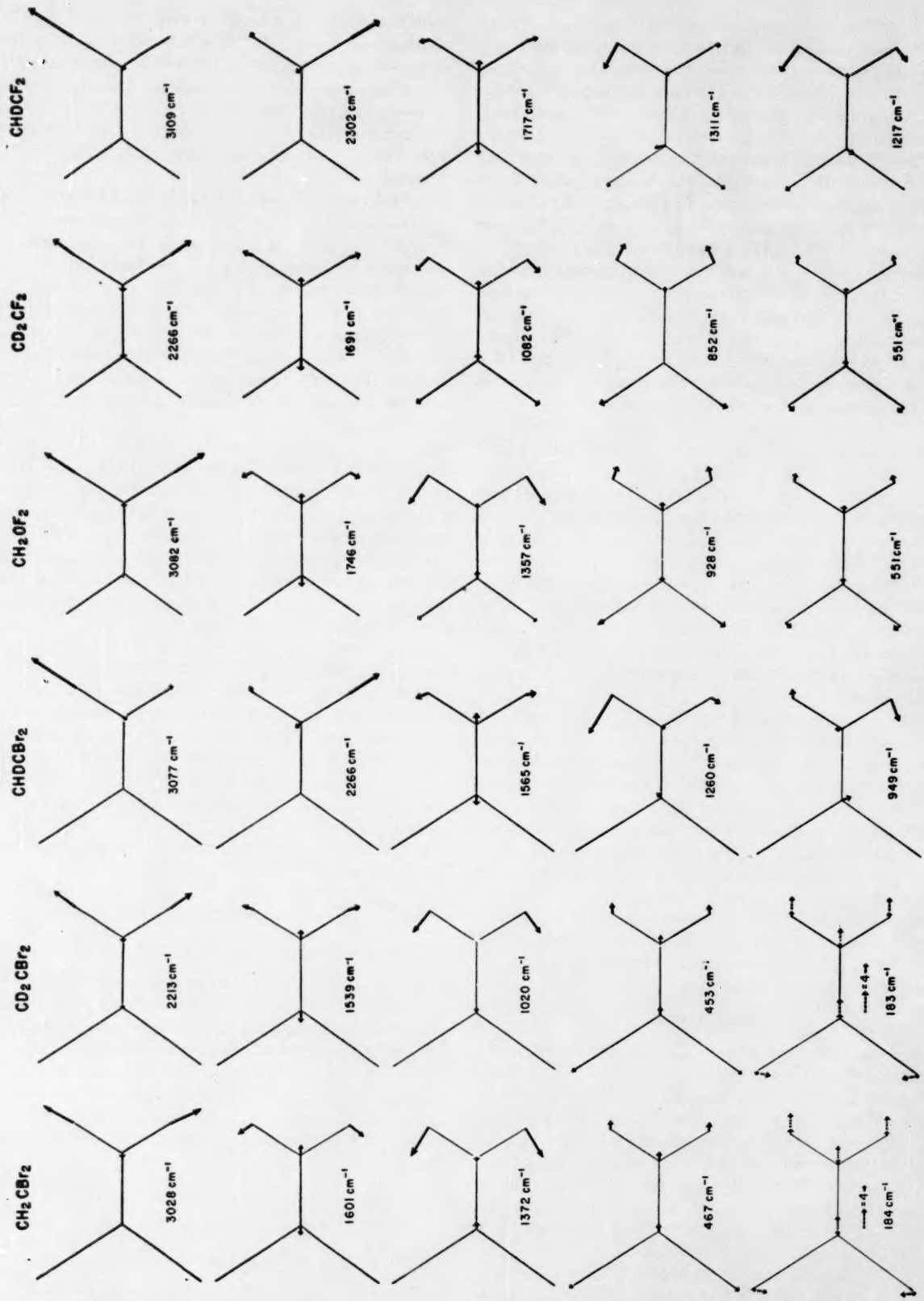
CHDCF2
3109 cm-1
2302 cm-1
1717 cm-1
1311 cm-1
1217 cm-1
CD2CF2
2266 cm-1
1691 cm-1
1082 cm-1
852 cm-1
551 cm-1
CH2OF2
3082 cm-1
1746 cm-1
1357 cm-1
928 cm-1
551 cm-1
CHDCBr2
3077 cm-1
2266 cm-1
1565 cm-1
1260 cm-1
949 cm-1
CD2CBr2
2213 cm-1
1539 cm-1
1020 cm-1
453 cm-1
183 cm-1
CH2CBr2
3028 cm-1
1601 cm-1
1372 cm-1
467 cm-1
184 cm-1

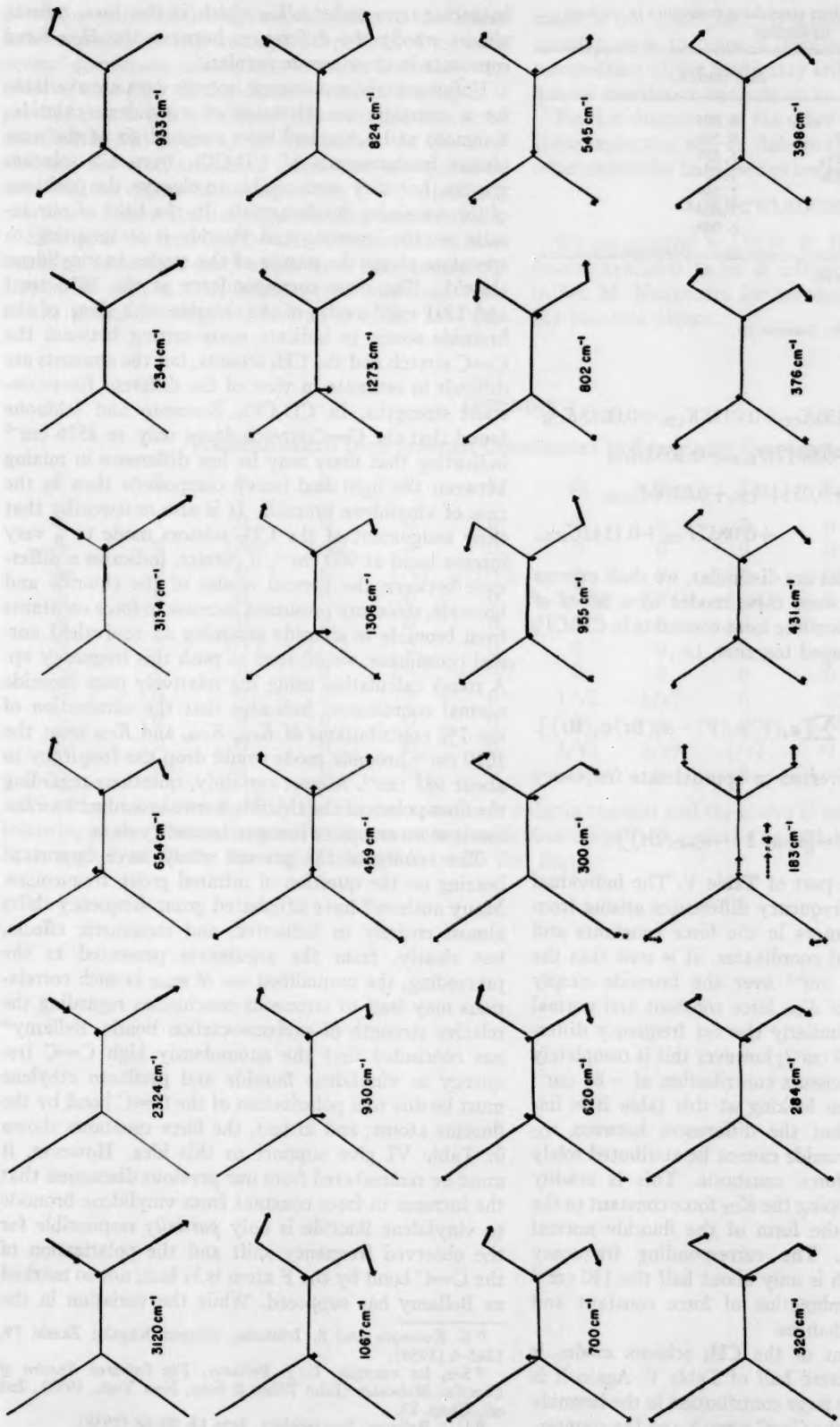

FIG. 3. Planar Cartesian displacements for vinylidene bromide and fluoride. (A/unit change in normal coordinate).

TABLE VI. Carbon-carbon stretching constants in various molecules.

	K_{CC} (md/A)
C_2F_4	8.89[a]
CH_2CF_2	8.55[b]
CH_2CBr_2	7.55[b]
CH_2CCl_2	7.67[d]
C_2H_4	7.39[c]
C_2Br_4	7.01[a]
C_2Cl_4	6.98[a]

[a] From Mann *et al.* (footnote 6).
[b] This work.
[c] From Curtis (footnote 1).
[d] From Enomoto and Ichinohe (footnote 17).

and

$$\lambda_{C=C}(CH_2CBr_2) = 0.1330K_{CC} + 0.0175K_{CBr} + 0.0018K_{CH} + .0405H_{CBr} + 0.0811H_{BrBr} + 0.4055H_{CH} + 0.8111H_{HH} + 0.0514F_{CBr} + 0.0106F_{BrBr} + 0.0857F_{CH} + 0.1142C_{HBr}.$$

Since the normal modes are dissimilar, we shall express the difference $\Delta\lambda$ between these modes by a series of terms in which corresponding force constants in CH_2CF_2 and CH_2CBr_2 are grouped together, i.e.,

$$\lambda_{C=C}(F) - \lambda_{C=C}(Br) = \sum_i [a_i(F)\phi_i(F) - a_i(Br)\phi_i(Br)].$$

These quantities, converted to approximate frequency differences

$$(\Delta\nu_{C=C})^{F-Br} \approx [\nu_{C=C}(F) - \nu_{C=C}(Br)]$$

are given in the first part of Table V. The individual terms represent the frequency differences arising from a combination of changes in the force constants and changes in the normal coordinates. It is seen that the fluoride gains $\sim$140 cm^{-1} over the bromide simply from a combination of K_{CC} force constant and normal coordinate change. Similarly the net frequency difference under ΔK_{CF} is 59 cm^{-1}; however this is completely nullified by a large scissors contribution of -84 cm^{-1} in the bromide. When looking at this table it is important to realize that the differences between ν_{CC} in the fluoride and bromide cannot be attributed solely to changes in the force constants. This is readily demonstrated by dropping the K_{CF} force constant to the K_{CBr} value keeping the form of the fluoride normal coordinate invariant. The corresponding frequency drop is 75 cm^{-1} which is only about half the 140 cm^{-1} shift due to the combination of force constant and normal coordinate changes.

A similar treatment of the CH_2 scissors modes is carried out in the second half of Table V. Again it is worthwhile noting the large contribution in the bromide due to coupling with the C=C stretch and the counter-balancing term under ΔH_{CH} which, in this case, reflects almost wholly the differences between the H_{CH} force constants in these two molecules.

Unfortunately, not enough isotopic data are available for a complete consideration of vinylidene chloride. Enomoto and Ichinohe[17] have assigned six of the nine planar fundamentals of CD_2CCl_2 from CS_2-solution spectra, but they were unable to observe the positions of the remaining fundamentals. In the light of our results on the bromide and fluoride it is tempting to speculate about the nature of the modes in vinylidene chloride. The close correspondence of the 1616 cm^{-1} and 1391 cm^{-1} modes of the chloride with those of the bromide seems to indicate some mixing between the C=C stretch and the CH_2 scissors, but the amounts are difficult to estimate in view of the different force-constant strengths. In CD_2CCl_2 Enomoto and Ichinohe found that the C=C stretch drops only to 1576 cm^{-1} indicating that there may be less difference in mixing between the light and heavy compounds than in the case of vinylidene bromide. It is also noteworthy that their assignment of the CD_2 scissors mode to a very intense band at 980 cm^{-1}, if correct, indicates a difference between the normal modes of the chloride and bromide, since any presumed increase in force constants from bromide to chloride assuming an equivalent normal coordinate, would tend to push this frequency up. A rough calculation using the relatively pure bromide normal coordinates, indicates that the elimination of the 7% contributions of K_{CC}, K_{CBr} and K_{CH} from the 1019 cm^{-1} bromide mode would drop the frequency to about 985 cm^{-1}. Almost certainly, questions regarding the finer points of the chloride normal coordinates must await more complete isotopic frequency data.

The results of the present study have important bearing on the question of infrared group frequencies. Many authors[18] have attributed group-frequency shifts almost entirely to inductive, and mesomeric effects, but clearly, from the arguments presented in the preceeding, the unqualified use of $\nu_{C=C}$ in such correlations may lead to erroneous conclusions regarding the relative strength of carbon=carbon bonds. Bellamy[19] has concluded that the anomolously high C=C frequency in vinylidene fluoride and perfluoro ethylene must be due to a polarization of the C=C bond by the fluorine atoms; and in fact, the force constants shown in Table VI give support to this idea. However, it must be remembered from our previous discussion that the increase in force constant from vinylidene bromide to vinylidene fluoride is only *partially* responsible for the observed frequency shift and the polarization of the C=C bond by the F atom is in fact, not so marked as Bellamy has supposed. While the variation in the

[17] S. Enomoto and S. Ichinohe, Nippon Kagaku Zasshi **79**, 1343–6 (1958).
[18] See, for example, L. J. Bellamy, *The Infrared Spectra of Complex Molecules* (John Wiley & Sons, New York, 1958), 2nd ed., Chap. 23.
[19] L. J. Bellamy, Spectrochim. Acta **13**, 60–68 (1958).

normal coordinates throughout this series of vinylidene halides precludes any attempt other than a rigorous normal-coordinate calculation, to assess accurately the relative strengths of the carbon=carbon bonds, it is possible that in related alkenes this variation in normal coordinates will prove to be less severe. In the final analysis, however, a detailed calculation is required to establish the degree of mixing of the C=C stretching coordinate before qualitative predictions may be made.

Alkenes of the type RR'C=CH_2 are observed to have bands at 1410–1420 cm^{-1} which have been commonly associated with a CH_2 scissors-type vibration. The results of this investigation lead us to expect that this mode is not a simple CH_2 scissors motion and consequently, as in the case of the C=C stretch, the actual composition of the mode may only be determined by a normal coordinate analysis on an alkene-type molecule.

Further discussion of the other UB force constants of these molecules will be deferred until the data on the other molecules in the series become available.

ACKNOWLEDGMENTS

We are grateful to Dr. R. R. Holmes for making his results available to us in advance of publication and to Dr. M. Nakamura for his assistance in interpreting the Japanese papers.

APPENDIX I

Transformation from Internal Coordinates to Symmetry Coordinates

U	R_1	R_2	R_3	R_4	R_5	R_6	R_7	R_8	R_9	R_{10}	R_{11}
S_1	1	0	0	0	0	0	0	0	0	0	0
S_2	0	$1/\sqrt{2}$	$1/\sqrt{2}$	0	0	0	0	0	0	0	0
S_3	0	0	0	$1/\sqrt{2}$	$1/\sqrt{2}$	0	0	0	0	0	0
S_4	0	0	0	0	0	$-1/(6)^{\frac{1}{2}}$	$-1/(6)^{\frac{1}{2}}$	$2/(6)^{\frac{1}{2}}$	0	0	0
S_5	0	0	0	0	0	0	0	0	$-1/(6)^{\frac{1}{2}}$	$-1/(6)^{\frac{1}{2}}$	$2/(6)^{\frac{1}{2}}$
S_6	0	$1/\sqrt{2}$	$-1/\sqrt{2}$	0	0	0	0	0	0	0	0
S_7	0	0	0	$1/\sqrt{2}$	$-1/\sqrt{2}$	0	0	0	0	0	0
S_8	0	0	0	0	0	$1/\sqrt{2}$	$-1/\sqrt{2}$	0	0	0	0
S_9	0	0	0	0	0	0	0	0	$1/\sqrt{2}$	$-1/\sqrt{2}$	0
S_{10}	0	0	0	0	0	$1/\sqrt{3}$	$1/\sqrt{3}$	$1/\sqrt{3}$	0	0	0
S_{11}	0	0	0	0	0	0	0	0	$1/\sqrt{3}$	$1/\sqrt{3}$	$1/\sqrt{3}$

The $\mathfrak{L}'$ matrices as defined by the internal coordinate order in the text and the above U matrix are given on the following pages. These matrices are represented here with dimensions 9×9, each row being folded into 2 lines having S_1 through S_5 on the 1st line and S_6 through S_9 on the 2nd line.

L' MATRIX - CH_2CBr_2

-00.06829204	.00069377	1.01665970	-00.00204472	-00.23582874
.00000000	.00000000	.00000000	.00000000	
.36468244	-00.13236160	.04242544	.34872529	1.10300590
.00000000	.00000000	.00000000	.00000000	
-00.16980729	.10488973	.04481966	-00.27319537	1.43745210
.00000000	.00000000	.00000000	.00000000	
.01070744	.18278327	.00114769	-00.31531056	-00.02523299
.00000000	.00000000	.00000000	.00000000	
-00.00264988	-00.00206577	.00035862	-00.30568112	.00124051
.00000000	.00000000	.00000000	.00000000	
.00000000	.00000000	.00000000	.00000000	.00000000
.00133009	1.05481080	.18943032	-00.15808103	
.00000000	.00000000	.00000000	.00000000	.00000000
-00.18560793	.01860424	.67508322	-01.12921380	
.00000000	.00000000	.00000000	.00000000	.00000000
.30569979	.00735536	-00.56691187	-00.31683067	
.00000000	.00000000	.00000000	.00000000	.00000000
-00.04241673	.00467832	-00.46166072	-00.03790679	

L' MATRIX - CD_2CBr_2

-00.13589279	.01687522	.72734389	-00.04528051	-00.32424394
.00000000	.00000000	.00000000	.00000000	
.38147487	-00.15751220	.10357336	.41389568	.50177993
.00000000	.00000000	.00000000	.00000000	
-00.04970914	.07859633	.04543115	-00.19805664	1.22114440
.00000000	.00000000	.00000000	.00000000	
.01209815	.17510650	.00268335	-00.28925198	-00.06551079
.00000000	.00000000	.00000000	.00000000	
-00.00245526	-00.00117308	.00052496	-00.30472593	-00.00177108
.00000000	.00000000	.00000000	.00000000	
.00000000	.00000000	.00000000	.00000000	.00000000
-00.00129156	.78575751	.26879882	-00.24212718	
.00000000	.00000000	.00000000	.00000000	.00000000
.27236742	.00209392	-00.84567811	.79882923	
.00000000	.00000000	.00000000	.00000000	.00000000
.23378131	.00271846	-00.25788635	-00.45253299	
.00000000	.00000000	.00000000	.00000000	.00000000
-00.02939826	.00649648	-00.41498332	-00.06937694	

L' MATRIX - $CHDCBr_2$

-00.04371487	.00027795	.68264513	-00.00086389	-00.14038655
.00101155	.78129949	.14432206	-00.11534516	
.09670846	-00.01083236	-00.56199239	.02911098	.27568158
-00.00153984	.50326419	.18396265	-00.18700001	
-00.38193893	.14969283	-00.07202112	-00.39378368	-00.72391046
.00266668	.03800054	.01754053	.05868867	
-00.09513881	.07743405	.05055043	-00.20015385	1.34551510
-00.04601151	.00113915	.17523553	-00.52973151	
.01660102	-00.03233154	-00.00507734	.08053332	-00.38783443
-00.24161167	.00600939	.78138498	-00.80574245	
.00276359	-00.02608995	-00.00133995	.05847929	-00.11274971
.26044570	.00616197	-00.37316552	-00.40997388	
-00.01144665	-00.17796737	-00.00222949	.30017460	.04614170
-00.01268784	.00117253	-00.01620849	.03540459	
.00056535	.00368004	-00.00161092	.00157654	-00.01875220
-00.03474084	.00582427	-00.43630404	-00.05701024	
.00254908	.00160301	-00.00043892	.30516066	.00034545
-00.00007584	.00003599	.00392822	.00246873	

L' MATRIX - CH_2CF_2

-00.07599893	.00390444	1.01760130	-00.01128382	-00.17143095
.00000000	.00000000	.00000000	.00000000	
.38739982	-00.18303901	.04109485	.41431330	.79838869
.00000000	.00000000	.00000000	.00000000	
-00.07929794	.13590789	.01014592	-00.25415511	1.60356430
.00000000	.00000000	.00000000	.00000000	
.06517034	.23245107	.00920723	-00.08941348	-00.30316370
.00000000	.00000000	.00000000	.00000000	
.01494982	.00696286	.00425843	-00.50295986	-00.09489789
.00000000	.00000000	.00000000	.00000000	
.00000000	.00000000	.00000000	.00000000	.00000000
-00.00159269	1.05498320	.14102731	-00.18630609	
.00000000	.00000000	.00000000	.00000000	.00000000
.36098610	.00625538	-00.63801484	.75125978	
.00000000	.00000000	.00000000	.00000000	.00000000
-00.18767779	.00279726	-00.03899003	.86789441	
.00000000	.00000000	.00000000	.00000000	.00000000
-00.01561762	.00338458	-00.45399392	-00.22168191	

L' MATRIX - CD_2CF_2

-00.16224853	.03017249	.72038611	-00.07595834	-00.30381455
.00000000	.00000000	.00000000	.00000000	
.36922936	-00.19855787	.14757605	.44173015	.43271752
.00000000	.00000000	.00000000	.00000000	
.00851010	.19967744	.03150367	-00.24370502	1.03689810
.00000000	.00000000	.00000000	.00000000	
.05960869	.16037395	.00745166	.06093283	-00.68563813
.00000000	.00000000	.00000000	.00000000	
.01824199	.01204077	.00671956	-00.48305385	-00.16613669
.00000000	.00000000	.00000000	.00000000	
.00000000	.00000000	.00000000	.00000000	.00000000
-00.00754875	.78528180	.20640265	-00.27131330	
.00000000	.00000000	.00000000	.00000000	.00000000
.38867018	.02107672	-00.62976031	.50171164	
.00000000	.00000000	.00000000	.00000000	.00000000
-00.12084601	.01849560	-00.22655394	.71874633	
.00000000	.00000000	.00000000	.00000000	.00000000
-00.00742404	.00388865	-00.37954644	-00.25295062	

L' MATRIX - $CHDCF_2$

.05049643	-00.00247758	-00.69454367	.00720608	.10826666
-00.00119802	.77096485	.10476116	-00.13570595	
-00.11502163	.02013771	.54526034	-00.05099394	-00.24876581
-00.00594845	.51709745	.14309889	-00.20373032	
.38049586	-00.19237591	.09550320	.43158505	.58364267
.00026430	.05478204	.02324160	.01698714	
-00.02794984	.06207534	.01942207	-00.11146199	.77218927
.30968500	.01862243	-00.54216929	.68894726	
-00.02883911	.12598235	.01507990	-00.20284385	1.16891460
-00.22544214	.00230471	.32733988	.01188527	
-00.05655358	-00.20688832	-00.00884159	.08810572	.22305398
-00.08563647	.00110786	-00.03626455	.41646620	
.03117553	.07767749	.00880099	.05987884	-00.38948380
-00.10745352	.01038767	-00.17623521	.62140704	
.01637801	.00919562	.00598865	-00.49291830	-00.12241693
-00.00527227	.00222170	-00.05209956	.01179590	
-00.00222911	-00.00228287	.00085405	.02317564	.04955124
-00.01034436	.00383159	-00.40792523	-00.24282861	

Effect of Pressure on Color Centers in Ag^+-Doped Alkali Halides*

R. A. EPPLER AND H. G. DRICKAMER

Department of Chemistry and Chemical Engineering, University of Illinois, Urbana, Illinois

(Received December 21, 1959)

The effect of pressure on various color centers in silver-doped alkali halides has been studied. The crystals include NaCl (two concentrations), KCl, and KBr. The resulting shifts are used to confirm the assignments of some peaks, and, in certain cases, to decide among conflicting interpretations.

INTRODUCTION

IF alkali-halide crystals containing small amounts (from 0.05 to 2%) of silver halide impurities are subjected to x-rays, five bands appear in addition to the *F* band. This was discovered independently by Kats[1] and by the group at the Naval Research Laboratory,[2–4] who named these bands *A* through *E*. Etzel and Schulman[4] made an extensive investigation of the properties of these bands. More recently, Maenhout-van der Vorst and Dekeyser[5] and Ishiguro[6,7] have made further studies on these bands. Although it is true that the nature of these centers is not yet certain, models have been proposed for them which will be described in the next section.

THEORY

a. *A* Center

The *A* center is almost certainly a hole phenomenon. Etzel and Schulman[4] propose that the center is a substitutional silver ion which has been trapped by a hole, while Maenhout-van der Vorst and Dekeyser[5] propose that it is a substitutional silver ion adjoining a *V* center (hole trapped in a positive ion vacancy).

b. *B* Center

It is generally agreed[4–6,8] that this center is a substitutional silver ion adjoining an *F* center (electron trapped at a negative ion vacancy).

c. *C* Center

The fact that the strength of the *C* band is strongly dependent on concentration has led both Etzel and Schulman[4] and Maenhout-van der Vorst and Dekeyser[5] to postulate that there are two silver ions in the center. The latter adds to this two *F* centers, while the former only one.

d. *D* Center

The greatest amount of controversy concerns this band; Kats[1] attributed this band to the *B* center. Etzel and Schulman's[4] bleaching experiments led them to the conclusion that no unbound electrons were involved in the center, and they proposed a center consisting of a substitutional silver atom adjoining a *V* center. Maenhout-van der Vorst and Dekeyser,[5] however, found the band in additively colored crystals where only electron centers are to be found. They attribute the band to a substitutional silver ion adjoining an *M* center (electron trapped at a negative ion vacancy plus a vacancy pair).

e. *E* Center

Maenhout-van der Vorst and Dekeyser[5] attributed this band to an interstitial silver ion adjoining an *F* center. Ishiguro,[6,7] however, has found that while bleaching in the *F* center at room temperature enhances the *B* band, bleaching at liquid nitrogen temperature enhances the *E* band. Moreover, the *E* center is thermally unstable at only slightly above room temperature.[8] From all this Ishiguro concludes that the *E* center is an electron trapped in the field of a substitutional silver ion, or, in other words, a *B* center which has lost its associated vacancy.

EXPERIMENTAL

The crystals used in this study were single crystals of NaCl (0.1% and 1.0% AgCl), KCl (1.0% AgCl), and KBr (0.1% AgBr). (All concentrations are in the melt.) The doped crystals were obtained from J. H. Schulman of the Naval Research Laboratory. They were cleaved to 0.5 ×0.5- ×2-mm and irradiated 1 in. from an x-ray tube with tungsten target and beryllium windows for 1 to 20 hr. All irradiation and handling was done in the dark or in a very dim red light.

The high-pressure equipment and techniques used have been previously described.[9,10]

The effect of pressure on these bands has been studied in sodium chloride with two impurity-concentration

* This work was supported in part by the U. S. Atomic Energy Commission under contract, Chemical Engineering Project 5.

[1] M. L. Kats, Doklady Akad. Nauk. U.S.S.R. **85**, 539 (1952); Zhur. Eksp. Teoret. Fiz. **23**, 720 (1952).

[2] E. Burstein, J. J. Oberly, B. W. Henvis, and M. White, Phys. Rev. **86**, 255 (1952).

[3] H. W. Etzel, J. H. Schulman, R. J. Gintler, and E. W. Claffy, Phys. Rev. **85**, 1063 (1952).

[4] H. W. Etzel and J. H. Schulman, J. Chem. Phys. **22**, 1549 (1954).

[5] W. Maenhout-van der Vorst and W. Dekeyser, Physica **23**, 903 (1957).

[6] M. Ishiguro, T. Okuno, and Veda, Mem. Inst. Sci. Ind. Research, Osaka Univ. **13**, 69 (1956).

[7] M. Ishiguro, T. Okuno, and Kojima, Mem. Inst. Sci. Ind. Research, Osaka Univ. **15**, 1 (1958).

[8] H. N. Hersh, J. Chem. Phys. **30**, 790 (1959).

[9] R. A. Fitch, T. E. Slykhouse, and H. G. Drickamer, J. Opt. Soc. Am. **47**, 1015 (1957).

[10] R. A. Eppler and H. G. Drickamer, J. Chem. Phys. (submitted for publication).

levels, in potassium chloride and in potassium bromide [see Figs. 1(a) through 4(b)]. Figure 5–7 show typical spectra.

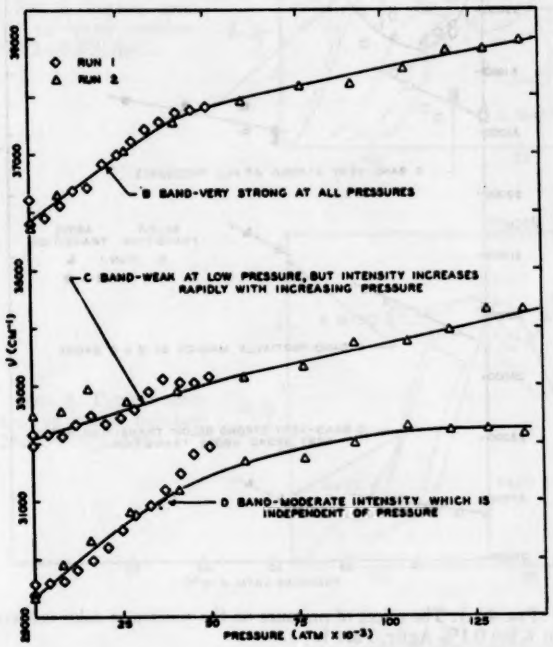
RUN 1
RUN 2
B BAND-VERY STRONG AT ALL PRESSURES
C BAND-WEAK AT LOW PRESSURE, BUT INTENSITY INCREASES RAPIDLY WITH INCREASING PRESSURE
D BAND-MODERATE INTENSITY WHICH IS INDEPENDENT OF PRESSURE
PRESSURE (ATM X 10⁻³)

FIG. 1(a). The effect of pressure on the spectra of color centers in NaCl: 0.1% AgCl, Part 1.

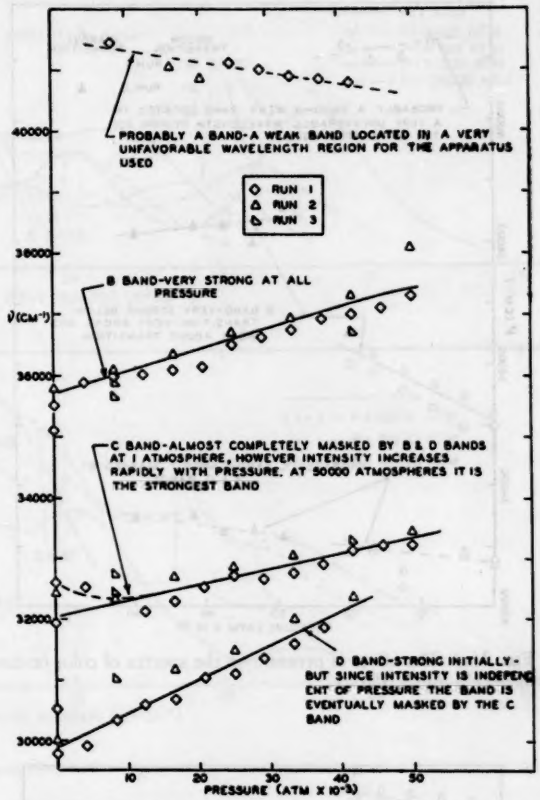
PROBABLY A BAND-A WEAK BAND LOCATED IN A VERY UNFAVORABLE WAVELENGTH REGION FOR THE APPARATUS USED
RUN 1
RUN 2
RUN 3
B BAND-VERY STRONG AT ALL PRESSURE
C BAND-ALMOST COMPLETELY MASKED BY B & D BANDS AT 1 ATMOSPHERE, HOWEVER INTENSITY INCREASES RAPIDLY WITH PRESSURE. AT 50000 ATMOSPHERES IT IS THE STRONGEST BAND
D BAND-STRONG INITIALLY-BUT SINCE INTENSITY IS INDEPENDENT OF PRESSURE THE BAND IS EVENTUALLY MASKED BY THE C BAND
PRESSURE (ATM X 10⁻³)

FIG. 2(a). The effect of pressure on the spectra of color centers in NaCl: 1.0% AgCl, Part 1.

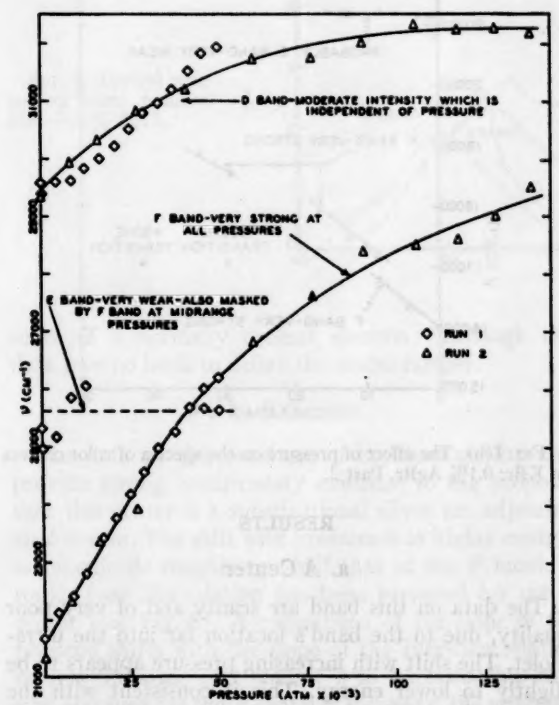
D BAND-MODERATE INTENSITY WHICH IS INDEPENDENT OF PRESSURE
F BAND-VERY STRONG AT ALL PRESSURES
E BAND-VERY WEAK-ALSO MASKED BY F BAND AT MIDRANGE PRESSURES
RUN 1
RUN 2
PRESSURE (ATM X 10⁻³)

FIG. 1(b). The effect of pressure on the spectra of color centers in NaCl: 0.1% AgCl, Part 2.

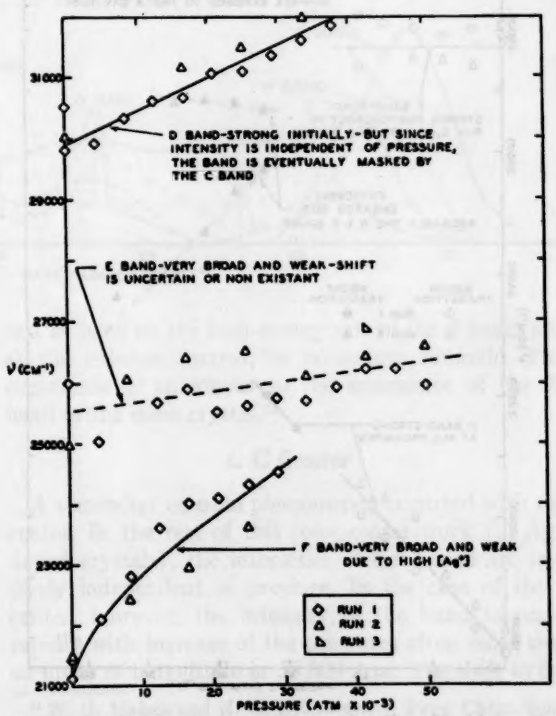
D BAND-STRONG INITIALLY-BUT SINCE INTENSITY IS INDEPENDENT OF PRESSURE, THE BAND IS EVENTUALLY MASKED BY THE C BAND
E BAND-VERY BROAD AND WEAK-SHIFT IS UNCERTAIN OR NON EXISTANT
F BAND-VERY BROAD AND WEAK DUE TO HIGH [Ag⁺]
RUN 1
RUN 2
RUN 3
PRESSURE (ATM X 10⁻³)

FIG. 2(b). The effect of pressure on the spectra of color centers in NaCl: 1.0% in AgCl, Part 2.

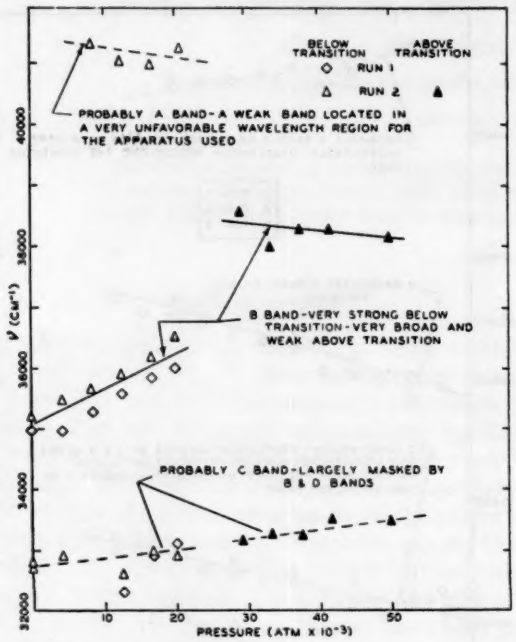
BELOW TRANSITION
ABOVE TRANSITION
RUN 1
RUN 2
PROBABLY A BAND-A WEAK BAND LOCATED IN A VERY UNFAVORABLE WAVELENGTH REGION FOR THE APPARATUS USED
B BAND-VERY STRONG BELOW TRANSITION-VERY BROAD AND WEAK ABOVE TRANSITION
PROBABLY C BAND-LARGELY MASKED BY B & D BANDS
ν (CM⁻¹)
PRESSURE (ATM X 10⁻³)

FIG. 3(a). The effect of pressure on the spectra of color centers in KCl: 1% AgCl, Part 1.

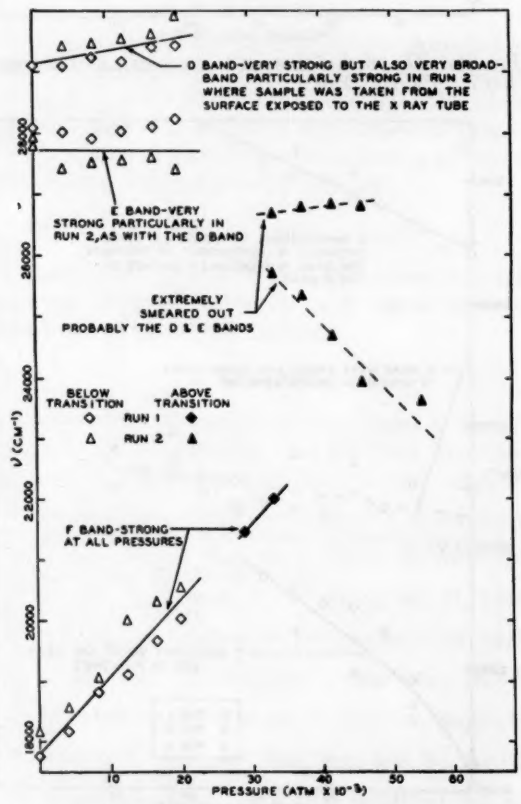
D BAND-VERY STRONG BUT ALSO VERY BROAD-BAND PARTICULARLY STRONG IN RUN 2 WHERE SAMPLE WAS TAKEN FROM THE SURFACE EXPOSED TO THE X RAY TUBE
E BAND-VERY STRONG PARTICULARLY IN RUN 2, AS WITH THE D BAND
EXTREMELY SMEARED OUT PROBABLY THE D & E BANDS
BELOW TRANSITION
ABOVE TRANSITION
RUN 1
RUN 2
F BAND-STRONG AT ALL PRESSURES
ν (CM⁻¹)
PRESSURE (ATM X 10⁻³)

FIG. 3(b). The effect of pressure on the spectra of color centers in KCl: 1% AgCl, Part 2.

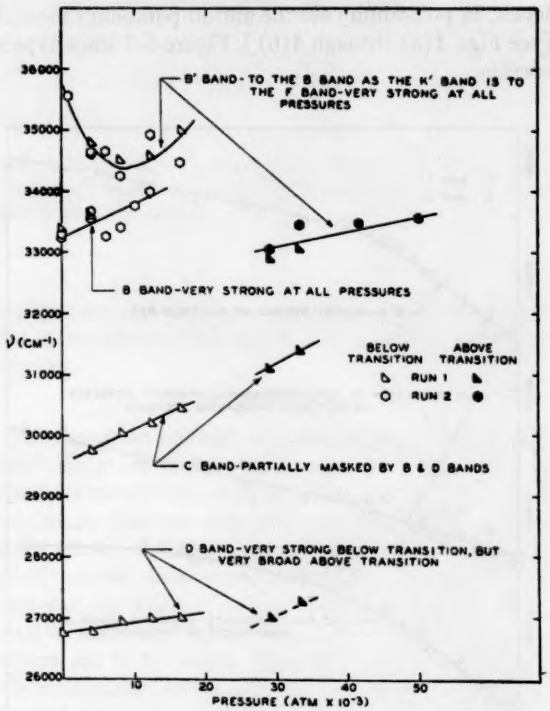
B' BAND-TO THE B BAND AS THE K' BAND IS TO THE F BAND-VERY STRONG AT ALL PRESSURES
B BAND-VERY STRONG AT ALL PRESSURES
BELOW TRANSITION
ABOVE TRANSITION
RUN 1
RUN 2
C BAND-PARTIALLY MASKED BY B & D BANDS
D BAND-VERY STRONG BELOW TRANSITION, BUT VERY BROAD ABOVE TRANSITION
ν (CM⁻¹)
PRESSURE (ATM X 10⁻³)

FIG. 4(a). The effect of pressure on the spectra of color centers in KBr: 0.1% AgBr, Part 1.

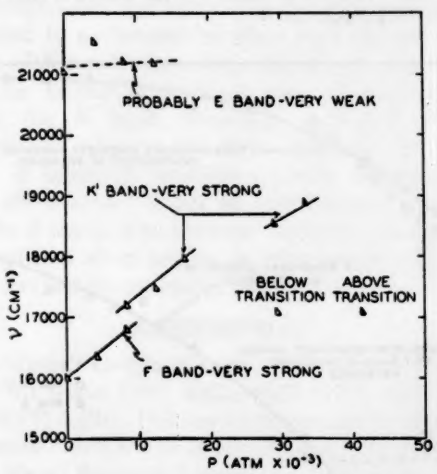

FIG. 4(b). The effect of pressure on the spectra of color centers in KBr: 0.1% AgBr, Part 2.

RESULTS

a. *A* Center

The data on this band are scanty and of very poor quality, due to the band's location far into the ultraviolet. The shift with increasing pressure appears to be slightly to lower energy. This is consistent with the generally held conclusion that this is a hole phenomenon, (that is, a phenomenon associated with the ab-

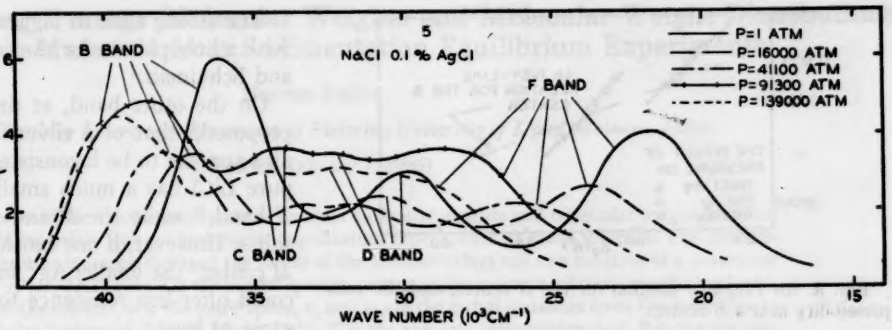

FIG. 5. Typical spectra vs wave number: NaCl—0.1% AgCl.

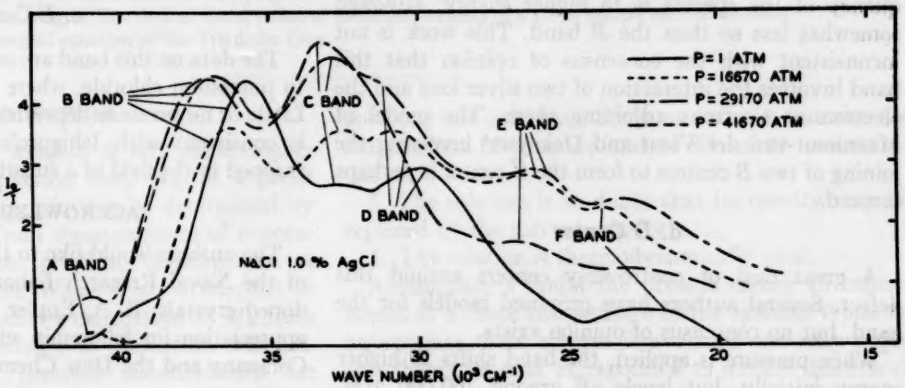

FIG. 6. Typical spectra vs wave number: NaCl—1.0% AgCl.

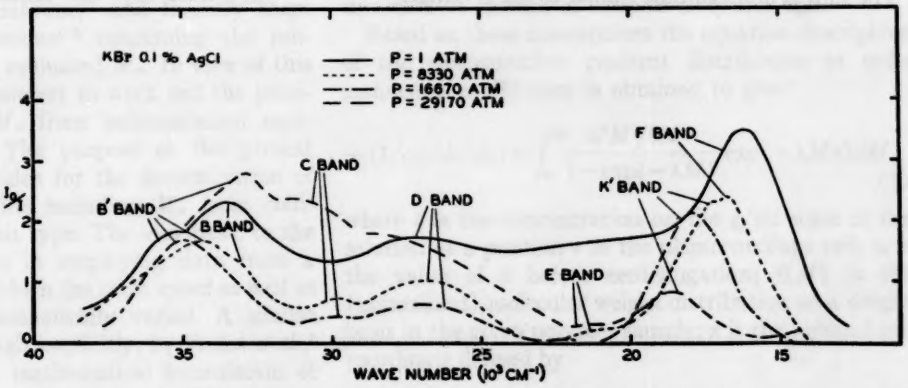

FIG. 7. Typical spectra vs wave number: KBr—0.1% AgCl.

sence of a normally present electron) although the data give no basis to define the model further.

b. *B* Center

The data on this band are of excellent quality and provide strong confirmatory evidence to the proposal that this center is a substitutional silver ion adjoining an *F* center. The shift with pressure is to higher energy, in magnitude roughly one-half that of the *F* band. A rough Ivey-like relation has been prepared for the *B* center (see Fig. 8). A comparison of the slope of the pressure shifts with the slope of the Ivey-like relation reveals the same approximate 2 to 1 relationship that was observed for the *F* center.[10] However, the strongest evidence for this model of the center is the emergence of a *B'* band on the high-energy side of the *B* band, and at the expense thereof, in potassium bromide. This occurrence is analogous to the emergence of the *K'* band in the same crystal.[11]

c. *C* Center

A somewhat unusual phenomenon occurred with this center. In the rest of this color-center work (in Ag^+-doped crystals), the intensities of the bands are relatively independent of pressure. In the case of the *C* center, however, the intensity of the band increases rapidly with increase of the pressure; often more than an order of magnitude in 50 000 atm. The shift in fre-

[11] W. G. Maisch and H. G. Drickamer, J. Phys. Chem. Solids 5, 328 (1958).

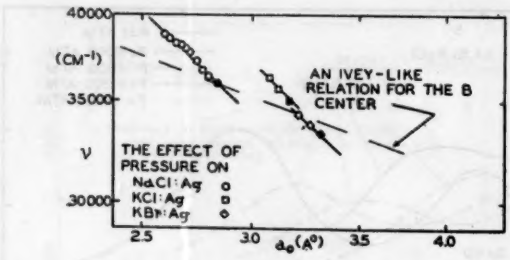

FIG. 8. An Ivey-like relation for the B center, and the compressibility near a B center.

quency of the spectra is to higher energy, although somewhat less so than the B band. This work is not inconsistent with the consensus of opinion that this band involves the interaction of two silver ions and the electron or electrons adjoining them. The model of Maenhout-van der Vorst and Dekeyser[5] involving the joining of two B centers to form the C center is perhaps favored.

d. D Center

A great deal of controversy centers around this defect. Several authors have proposed models for the band, but no consensus of opinion exists.

When pressure is applied, the band shifts to higher energy initially, but levels off around 100 000 atm. The shift is in magnitude similar to the B center.

The strong shift to higher energy seems inconsistent with a hole picture for the center, as proposed by Etzel and Schulman.[4]

On the other band, at first glance the other model proposed,[5] that of a silver ion adjoining an M center also appears to be inconsistent, because the M band in pure LiCl has a much smaller pressure shift than the F band,[10] while the D and B bands have comparable shifts. However, if one considers the Knox model of the M center[12] the smaller Ag^+ ion in the center of the cavity could offer less resistance to compression at low pressures, at least.

e. E Center

The data on this band are confined almost exclusively to potassium chloride, where the band is quite strong. Little or no pressure dependence of ν_m is detected. This is consistent with Ishiguro's model[6,7] of an electron trapped in the field of a substitutional silver ion.

ACKNOWLEDGMENTS

The authors would like to thank Dr. J. H. Schulman of the Naval Research Laboratory for furnishing the doped crystals. R. A. Eppler would like to express his appreciation for fellowship support from the Shell Oil Company and the Dow Chemical Company.

[12] R. S. Knox, Phys. Rev. Letters 2, 87 (1959).

Method for Calculating Average Molecular Weights and Molecular Weight Distributions of Polymeric Materials from Sedimentation Equilibrium Experiments

HIROSHI FUJITA

Physical Chemistry Laboratory, Department of Fisheries, University of Kyoto, Maisuru, Japan

(Received January 7, 1960)

A method is proposed for the determination of average molecular weights and molecular weight distributions of polymeric materials from sedimentation equilibrium experiments in theta solvents. The data required are the refractive index gradients at the center of the ultracentrifuge cell as a function of a parameter $\lambda=(1-\bar{v}\rho_0)(r_2^2-r_1^2)\omega^2/2RT$; here $\bar{v}$ is the partial specific volume of the polymer solute in the given solvent, ρ_0 is the density of the solvent, ω is the rotor speed, r_1 and r_2 are the radial distances from the rotor axis to the meniscus and the bottom of the cell, respectively, T is the absolute temperature, and R is the gas constant. The most important feature of the proposed method is that it allows calculation of the number-average molecular weight. The desired distribution of molecular weights of a given sample can be obtained by solving an integral equation of the Fredholm type.

INTRODUCTION

AVERAGE molecular weights of any order higher than the number-average one, M_n, of a given polymeric material can in principle be determined by the existing methods[1,2] from measurements of concentration or concentration gradient distributions at sedimentation equilibrium. Wales *et al.*[3] attempted to devise a method which allows calculation of M_n from such data, but no unambiguous procedure was obtained. Usual osmotic pressure measurements for the determination of M_n are complicated by the choice of an "ideal membrane," and recently there have been many discussions[4–6] concerning the reliability of an osmotically evaluated M_n. In view of this situation it is of great interest to work out the possibility of determining M_n from sedimentation equilibrium measurements. The purpose of the present paper is to propose an idea for the determination of average molecular weights including M_n from colligative experiments of this type. The idea basic to the present method consists in employing data from a series of experiments in which the rotor speed as well as the cell length are systematically varied. A similar idea was expressed, though implicitly, by Wales *et al.*,[3] but it appears that no mathematical formulation of such an idea has yet been presented in the literature.

THEORY

We consider a sedimentation equilibrium experiment on a polydisperse polymeric material dissolved in a solvent. It is assumed that:

1. The partial specific volumes of all solutes (different in molecular length but uniform in chemical composition) not only have the same value, $\bar{v}$, but also are independent of pressure and of all solute concentrations.

2. The solution is so dilute that its density may be replaced by the solvent density ρ_0.

3. The solution is thermodynamically ideal.

Assumption 3 limits the present theory to experiments at a theta temperature of the system. When no appropriate theta solvent is available one may apply this theory to data extrapolated to infinite dilution of the solution, but then the entire process requires a considerable amount of labor to carry through.

Based on these assumptions the equation descriptive of the concentration gradient distribution at sedimentation equilibrium is obtained to give[7]

$$-(1/c_0)(dc/dx)=\int_0^\infty \frac{\lambda^2M^2f(M)}{1-\exp(-\lambda M)}\exp(-\lambda Mx)dM \tag{1}$$

where c is the concentration on the g/ml scale of the solution at a position r in the ultracentrifuge cell; c_0 is the value of c before centrifugation; $f(M)$ is the (normalized) molecular weight distribution on a weight basis in the given polymer sample; x is the reduced cell coordinate defined by

$$x=(r_2^2-r^2)/(r_2^2-r_1^2); \tag{2}$$

and λ is a parameter (constant for an experiment) given by

$$\lambda=(1-\bar{v}\rho_0)(r_2^2-r_1^2)\omega^2/2RT. \tag{3}$$

The symbols appearing in Eqs. (2) and (3) have the following meanings: T=absolute temperature of the system, R=universal gas constant, ω=angular speed of the rotor, r_1=radial distance from the rotor axis to the cell meniscus, r_2=radial distance from the rotor axis to the cell bottom.

[1] W. D. Lansing and E. O. Kraemer, J. Am. Chem. Soc. **57**, 1369 (1935).
[2] M. Wales, J. Phys. & Colloid Chem. **52**, 235 (1948).
[3] M. Wales, F. T. Adler, and K. E. Van Holde, J. Phys. & Colloid Chem. **55**, 145 (1951).
[4] H. P. Frank and H. Mark, J. Polymer Sci. **10**, 129 (1953); **17**, 1 (1955).
[5] D. T. F. Pals and A. J. Staverman, J. Polymer Sci. **28**, 69 (1957).
[6] J. B. Donnet, R. Roth, and G. Meyerhoff, J. Polymer Sci. **27**, 591 (1958).

[7] For example, Williams, Van Holde, Baldwin, and Fujita, Chem. Revs. **58**, 715 (1958). The quantity usually measured is the refractive index gradient. In order to convert this quantity to the concentration gradient it is necessary to assume that the specific refractive index increment is the same for all solutes.

Evaluation of Eq. (1) at $x=\frac{1}{2}$ gives

$$-(1/c_0)(dc/dx)_{x=\frac{1}{2}} = \int_0^\infty \frac{\lambda^2 M^2 f(M)}{\exp(\lambda M/2)-\exp(-\lambda M/2)}dM. \quad (4)$$

This indicates that the value of $-(1/c_0)(dc/dx)_{x=\frac{1}{2}}$ varies with λ. So we may write Eq. (4) in the form:

$$q(\lambda) = \int_0^\infty K(\lambda M) f_1(M)\, dM, \quad (5)$$

where

$$q(\lambda) = -(1/c_0)(dc/dx)_{x=\frac{1}{2}}/\lambda, \quad (6)$$

$$f_1(M) = Mf(M), \quad (7)$$

$$K(\lambda M) = (\lambda M/2)/\sinh(\lambda M/2). \quad (8)$$

Equation (5) is an integral equation of the Fredholm type in which $q(\lambda)$ is a given function and $K(\lambda M)$ is a kernel. The desired distribution of molecular weights, $f(M)$, could be determined by solving this integral equation when the form of $q(\lambda)$ is known over the entire range of positive λ, $0<\lambda<\infty$. The experimental determination of $q(\lambda)$ will be discussed later. First we show, assuming $q(\lambda)$ to have been given over the entire range of λ, how Eq. (5) can be used to evaluate average molecular weights.

Average Molecular Weights

Since

$$\lim_{y\to 0} K(y) = 1,$$

it follows from Eq. (5) that

$$\int_0^\infty f_1(M)\, dM = q(0)$$

which may be written

$$M_w = q(0) \quad (9)$$

where M_w is the weight-average molecular weight of the sample. We see that M_w can be obtained by extrapolating the curve for $q(\lambda)$ back to $\lambda=0$. The kernel function $K(\lambda M)$ is an even function of λ and so is $q(\lambda)$. Hence it is convenient to plot $q(\lambda)$ against λ^2, rather than λ, which will facilitate this extrapolation.

Next, integration of Eq. (5) with respect to λ^2 over the range $0<\lambda^2<\infty$ and rearrangement yields

$$\int_0^\infty q(\lambda)\, d(\lambda^2) = 33.66 \int_0^\infty [f(M)/M]\, dM \quad (10)$$

where the numerical constant 33.66 is the value of

$$8\int_0^\infty [\xi^2/\sinh\xi]\, d\xi.$$

In terms of the number-average molecular weight, M_n, Eq. (10) may be written

$$M_n = 33.66 \Big/ \int_0^\infty q(\lambda)\, d(\lambda^2). \quad (11)$$

Thus the value of M_n can be determined by evaluating the area enclosed by the curve for $q(\lambda)$ plotted against λ^2.

Differentiating Eq. (5) with respect to λ^2 and then integrating the resulting equation with respect to λ over the range $0<\lambda<\infty$, we obtain

$$\int_0^\infty [dq(\lambda)/d(\lambda^2)]\, d\lambda = -0.1732 \int_0^\infty M^2 f(M)\, dM \quad (12)$$

where the numerical constant 0.1732 is the value of the integral

$$(1/4)\int_0^\infty [(\xi\cosh\xi - \sinh\xi)/(\xi \sinh^2\xi)]\, d\xi.$$

Equation (12) may be expressed in terms of the z-average molecular weight M_z, giving

$$M_z = -(57.74/M_w)\int_0^\infty [dq(\lambda)/d(\lambda^2)]\, d\lambda. \quad (13)$$

In an analogous manner, equations for the higher average molecular weights, M_{z+1}, M_{z+2}, etc., in terms of $q(\lambda)$ can be derived. For example,

$$M_{z+1} = -(24/M_z M_w)[dq(\lambda)/d(\lambda^2)]_{\lambda=0}. \quad (14)$$

Since the derivative $dq(\lambda)/d(\lambda^2)$ may not be evaluated very accurately from an experimentally derived $q(\lambda)$ vs λ^2 curve (generally we have to resort to graphical differentiation), not much reliance may be placed upon the values of M_z and M_{z+1} computed by the preceding formulas. The expressions for the higher average molecular weights involve derivatives of higher orders, so that the results to be obtained for these molecular weights are less accurate. In actual cases, M_{z+1} will be the highest of average molecular weights for which fairly accurate values may be acquired by the procedure described before. The most important feature of this procedure is that it allows determination of the number-average molecular weight.

Molecular Weight Distribution

In order to obtain the complete picture of the molecular weight distribution curve, Eq. (5) has to be solved directly. Unfortunately, this integral equation has a form for which no inversion formula is yet available. Then we have to resort to an appropriate numerical method of solution, but there must be no essential difficulty in carrying this through because the kernel function $K(\lambda M)$ has no singular point on the real axis. Figure 1 shows the kernel function graphically. The necessary numerical solution of Eq. (5) will be done easily on a high-speed computor.

Remarks

In the foregoing development it was assumed that the concentration gradient at $x=\frac{1}{2}$ can be obtained experimentally. This condition is suited for the use of the schlieren optical system. It should be remarked, however, that interference optics is coming into use, especially for sedimentation equilibrium experiments, so that the concentration itself, rather than the concentration gradient, is of increasing importance as the directly measurable quantity. Accordingly, it is desirable to develop a theory similar to that in the foregoing on the basis of the equation which describes the concentration distribution along the cell. It is a very simple matter to derive the necessary equations for this case, but they will be presented elsewhere.

DETERMINATION OF THE FUNCTION $q(\lambda)$

Values of $q(\lambda)$ may be obtained by measuring dc/dx at $x=\frac{1}{2}$ from sedimentation equilibrium curves determined at various values of λ. It should be noted that, in general, refractive index gradients can be measured most accurately in the central region of the cell. This point is one of the advantages of the present method over the previous ones in which accurate measurements of refractive index gradients near the cell ends are required. The value of λ can be changed by varying either the rotor speed or the cell length r_2-r_1 (more rigorously, the difference $r_2^2-r_1^2$) or both.

It is essential for the present method that the data can be obtained experimentally up to the region of λ where $q(\lambda)$ may be regarded as effectively zero. Since the cell length is of the order of 1 cm or less, the maximum range of λ which can be covered is limited by the maximum operational speed of the rotor. It is the general observation in ultracentrifugal studies that when a solution of a macromolecular solute is centrifuged at the speed generally employed in sedimentation velocity experiments almost all the solutes are eventually sedimented down to the cell bottom and the main part of the cell is left in the solvent alone (provided the buoyancy term is not close to unity). This fact suggests that except in special circumstances the behavior of $q(\lambda)$ in its tail portion may be studied with rotor speeds available at present. As will be illustrated later, if the sample does not contain extremely low-molecular-weight fractions the low speeds obtainable in the current equilibrium centrifuge are sufficient for this purpose.

The theory has been developed on the basis of the assumption that the solution is thermodynamically ideal. In actual cases, this condition is not obtained with solutions of polymer solutes, but we have to be satisfied with doing experiments at a theta temperature of the system. When $q(\lambda)$ approaches the zero base line, high concentrations are necessarily set up in the region near the cell bottom. In this region the solution should deviate from thermodynamic ideality even at a theta temperature of the system. This deviation is due to the contributions from the third and higher virial coefficients which are generally nonvanishing at the theta temperature. Thus we must expect that the tail portion of the curve for $q(\lambda)$ will contain some effect from thermodynamic nonideality. Since this effect is reduced as the concentration decreases it is highly desirable to perform a series of experimental runs at as low initial concentrations as possible. The magnitude of the error produced upon final results by this kind of effect will be investigated in a future communication.

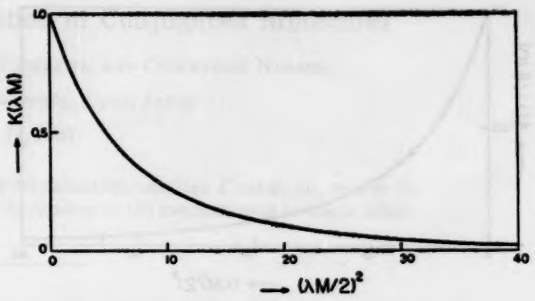

FIG. 1. The form of the kernel function $K(\lambda M)$.

The behavior of $q(\lambda)$ in the vicinity of $\lambda=0$ must also be determined accurately. This is particularly important when evaluating M_w and M_{z+1}, because these molecular weights are, according to the present theory, determined by the intercept and the tangent of the $q(\lambda)$ vs λ^2 curve at $\lambda=0$. Experimentally, not too low speeds of rotation may be used, since, as the rotor speed is decreased, the resolving power of the centrifuge is lost and the effect of fluctuations in speed may become appreciable. However, the desired small values of λ can be obtained by shortening cell length. By using cells 1–2 mm long, as contrasted to the 7–10 mm commonly used, it is possible to have fairly small λ. It is of importance to note that λ^2 is proportional to ω^4 and $(r_2^2-r_1^2)^2$. This indicates that by choosing ω and r_2-r_1 properly a very wide range of λ^2 can be covered.

As an example, we consider sedimentation equilibrium experiments with a monodisperse sample of molecular weight M'. We use a four-cell equilibrium centrifuge in which one cell acts as a balancing weight and provides an index for the optical measurements. For this sample Eq. (5) reduces to

$$q(\lambda)=(\lambda M'/2)M'/\sinh(\lambda M'/2). \tag{15}$$

Hence

$$q(0)=M' \tag{16}$$

which is obviously a special case of Eq. (9). Combining these two relations gives

$$q(\lambda)=(\lambda M'/2)q(0)/\sinh(\lambda M'/2). \tag{17}$$

Thus we see that the q vs λ^2 plot for a monodisperse sample follows a curve similar to that shown in Fig. 1.

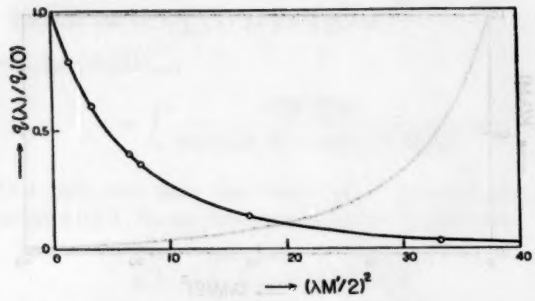

FIG. 2. The $q(\lambda)$ vs λ^2 curve for a monodisperse sample of molecular weight M'. The open circles represent the values of $q(\lambda)$ expected from the hypothetical experiments considered in the text.

We adjust the $r_2^2-r_1^2$ values for the three solution cells, A, B, C, as follows:

Cell A:

$$r_2^2-r_1^2=(r_2-r_1)(r_2+r_1)=0.5\times13.5=6.75\ \text{cm}^2;$$

Cell B:

$$r_2^2-r_1^2=0.4\times12.0=4.80\ \text{cm}^2;$$

Cell C:

$$r_2^2-r_1^2=0.3\times10.7=3.21\ \text{cm}^2.$$

Assume that $T=300°\text{K}$, $M'=5\times10^5$, and $1-\bar{v}\rho_0=0.3$. We perform two experiments at the following rotor speeds:

Expt. I: $\omega=80$ rps;

Expt. II: $\omega=120$ rps.

These are typical of the speeds usually employed in sedimentation equilibrium studies on high polymeric materials.

The values of λ^2 computed for these six combinations of ω and $r_2^2-r_1^2$ range from 1.5 to 33.3 when expressed in terms of the dimensionless variable $(\lambda M'/2)^2$. In Fig. 2 the open circles indicate the locations of $q(\lambda)$ calculated from Eq. (17) for these six λ^2, while the solid line is the complete q vs λ^2 curve for this sample. It is seen that with only these six points a fairly accurate outline of the whole q curve can be estimated. One more experimental run at a suitably chosen speed and with cells of different lengths will provide data which, together with the earlier six points, enable us to draw an almost complete q curve.

It is apparent that more accurate and more complete pictures of the desired q curve can be obtained by increasing number of experiments with suitably chosen speeds and cell lengths and that those will lead to more precise knowledge of average molecular weights as well as the molecular weight distribution of the given sample. However, since the time required for attaining sedimentation equilibrium is generally considerable the method proposed in the preceding is unlikely to be employed for routine work. Perhaps in cases when a not too detailed knowledge of the molecular weight distribution is required, two or three experiments under suitably chosen conditions will suffice to obtain information necessary for the application of this method.

ACKNOWLEDGMENTS

I wish to thank Professor J. W. Williams, Department of Chemistry, University of Wisconsin, for his interest in this investigation. I am particularly indebted to Dr. M. Wales, Shell Development Company, who provided me both with valuable comments and advice on this manuscript. This work was supported by a grant from the National Science Foundation (G-3599) for which grateful acknowledgment is made here.

Charge Transfer Mechanism of Reaction of Conjugated Molecules

KENICHI FUKUI, KEIJI MOROKUMA, TEIJIRO YONEZAWA, AND CHIKAYOSHI NAGATA

Faculty of Engineering, Kyoto University, Kyoto, Japan

(Received January 22, 1960)

Mathematical interrelations are found between the superdelocalizability and the Z value, i.e., two of the reactivity indexes of conjugated molecules. MO theoretical discussions on the mechanism of aromatic substitution are also made.

FOR all the MO (molecular-orbital) theoretical contributions which have been made on the chemical reactivity of conjugated molecules, there remains much to be revealed on the essential feature of aromatic substitution or of other reactions of conjugated molecules.

A theory of chemical reactivity of conjugated molecules, called the "frontier electron theory," has been presented by the present authors.[1] In that theory the highest occupied and the lowest unoccupied MO's in the ground state played a dominant role. In other words, the intramolecular orientation could well be predicted by the density distribution of the electrons occupying these particular orbitals. The discovery of the peculiar behavior of these electrons (frontier electrons) may thus be said to have afforded materials which might be a clue to elucidating the mechanism of aromatic substitution. Nagakura and Tanaka[2] concluded from experimental data that an electrophilic substitution takes place only when the lowest unoccupied level of the attacking reagent is of lower energy than the highest occupied one of the substrate and that a nucleophilic reaction occurs only when the lowest unoccupied level of the substrate lies energetically lower than the highest occupied level of the nucleophilic reagent. (This condition will hereafter be called condition A.) On the other hand the present authors proposed a mechanism of aromatic substitution which involves a charge transfer through a hyperconjugation between the substrate and the reagent. In this mechanism the approaching reagent and the leaving atom were treated as the constituents of a pseudoatom having a π-type orbital (quasi-π orbital). By adopting this mechanism the characteristic behavior of frontier electrons was successfully explained, and a reactivity index, superdelocalizability, which is applicable to predicting the intermolecular relative reactivity, was simultaneously derived.[3] Further, in the latest paper,[4] the mechanism of charge transfer, as previously mentioned, was investigated more minutely. The theoretical conclusions are summarized as follows:

1. In order that an electrophilic, or a nucleophilic, substitution can occur, the energy of reagents must satisfy condition A. But it is to be noted that the meaning of the orbital energies is somewhat different from that of Nagakura and Tanaka. They settled condition A on the basis of the ionization potential and the electron affinity, in principle, of the reagent having been submitted to the transfer of one electron, whereas we meant the Coulomb integral of the orbital, which will participate in the bond formation, of the reagent without charge transfer.

2. The energy of the quasi-π orbital in an electrophilic, or a nucleophilic, substitution rises or falls swiftly to the height of a frontier orbital instantaneously with hyperconjugation and then increases or decreases continuously with increasing extent of hyperconjugation to the transition state, where it will be near the Coulomb integral of a carbon atom.

3. Frontier electron density, superdelocalizability, and a generalized index are derived as reactivity indexes from the hyperconjugation energy at the transition state.

Recently, another theoretical contribution to the mechanism of electrophilic substitution has been presented by Brown.[5] At the transition state of the rate-determining step in some electrophilic substitutions of aromatic hydrocarbons, he thought, a complex is formed between the substrate and the reagent because of a charge transfer through the position of substitution, and that thus the stabilization energy of the complex is the most important factor affecting the reactivity. After condition A concerning energy levels of the substrate and the reagent, he treated this complex quantum-chemically as an intermediate between the configuration without charge transfer and the configurations corresponding to the transfer of one electron from occupied orbitals of the substrate to the unoccupied orbital of the electrophile, that is, in a simple form of configuration interaction treatment of the charge-transfer complex discussed by Mulliken.[6] Thus he concluded that a quantity, what he called the "Z

[1] K. Fukui, T. Yonezawa, and H. Shingu, J. Chem. Phys. **20**, 722 (1952); K. Fukui, T. Yonezawa, C. Nagata, and H. Shingu, J. Chem. Phys. **22**, 1433 (1954).

[2] S. Nagakura, and J. Tanaka, J. Chem. Phys. **22**, 563 (1954); J. Chem. Soc. Japan, Pure Chem. Sec. **75**, 933 (1954); Bull. Chem. Soc. Japan **32**, 734 (1959).

[3] K. Fukui, T. Yonezawa, and C. Nagata, Bull. Chem. Soc. Japan **27**, 423 (1954).

[4] (a) K. Fukui, T. Yonezawa, and C. Nagata, J. Chem. Phys. **27**, 1247 (1957); (b) *ibid.*, Eq. (24).

[5] R. D. Brown, J. Chem. Soc. **1959**, 2224, 2232.

[6] R. S. Mulliken, J. Am. Chem. Soc. **74**, 811 (1952); J. Phys. Chem. **56**, 801 (1952).

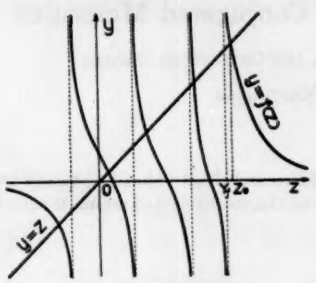

FIG. 1. Functional relations $y=Z$ and $y=f(Z)$ for $Y_f>0$.

value," which refers only to the frontier orbital of the substrate would be an index of reactivity.

In this paper, mathematical interrelations between the superdelocalizability and the Z value are pointed out both in heterolytic and homolytic reactions. A few comparative discussions on the theories of the mechanism of aromatic substitution are also made.

MATHEMATICAL INTERRELATIONS BETWEEN SUPERDELOCALIZABILITY AND Z VALUE

1. Heterolytic Reaction

First of all the electrophilic reaction will be considered. Suppose $\epsilon_E(=\alpha+h\beta)$ and $\epsilon_f(=\alpha+\lambda_f\beta)$ are the energy of the unoccupied orbital of the electrophile and that of the frontier orbital for an electrophilic attack (the highest occupied orbital) of the substrate, respectively, where α and β are the Coulomb integral of a carbon atom and the resonance integral of a benzene bond, then condition A is written as

$$\epsilon_f-\epsilon_E=(-\beta)(h-\lambda_f)=(-\beta)Y_f>0. \tag{1}$$

Since $(-\beta)$ is positive, Y_f must be positive.

It would now be desirable to summarize the procedures and results given by Brown.[5] It was proved that the stabilization energy due to the contribution of all possible charge-transfer configurations is expressed in units of $(-\beta)$ by the largest root (Z_0) of the following equation:

$$F(Z)=Z-\sum_i^{occ}[2(C_r^i)^2\gamma^2/(Z-Y_i)]=0, \tag{2}$$

where C_r^i is the coefficient of the rth atomic orbital (χ_r) in the ith MO whose energy is $\alpha+\lambda_i\beta$, Y_i is equal to $(h-\lambda_i)$, γ is a positive quantity which represents the extent of interaction between the rth atomic orbital and the electrophile at the transition state, and $\sum_{occ}$ should cover all occupied MO's. For small γ, after utilizing a perturbation theory and neglecting higher orders of γ, Z_0 is directly obtained from Eq. (2), as follows:

$$Z_0=Y_f+[2(C_r^f)^2\gamma^2/Y_f]. \tag{3}$$

(the larger its magnitude, the more reactive that position).

Brown adopted Z_0, calling it the Z value, as a reactivity index for the electrophilic substitution, and by adjusting the values of h and γ succeeded in interpreting the rate of nitration of conjugated hydrocarbons. It is very interesting that in his theory the frontier orbital plays an exclusive role in deciding not only the intramolecular orientation but the intermolecular relative reactivity. In this sense his theory may serve as an alternate physical basis of the frontier electron theory. But on this point some discussions are to be given in the last section.

We might add a few remarks on his procedure with respect to the following points:

1. Figure 1 illustrates two relations $y=f(Z)$ and $y=Z$, where

$$f(Z)=\sum_i^{occ}[2(C_r^i)^2\gamma^2/(Z-Y_i)]. \tag{4}$$

Of the values of Z at intersecting points of the two relations the largest one corresponds to Z_0. This figure will be useful later for comparing with the case where Y_f is negative.

2. In Brown's paper[5] it seems as if Eq. (3) resulted from deliberately taking only two configurations (one without charge transfer and one with charge transfer from the frontier orbital to the electrophile) into account from all possible configurations and then regarding γ small. It is of importance to notice that the more general Eq. (2), which includes all configurations, leads directly to Eq. (3), provided γ is small enough.

Now from the point of view of the quasi-π orbitals used in our previous theoretical studies, the configuration interaction treatment of the mechanism of an electrophilic substitution will be given.

According to our theory the energy of the quasi-π orbital gets and stays higher than that of the highest occupied orbital of the substrate at the transition state. If we again put the energy of the quasi-π orbital $\alpha+h\beta$, Y_f is negative in this case. These mathematical circumstances are essentially different from Brown's theory. Equation (2) is valid also in this case; but, as illustrated in Fig. 2, the largest root is never given by Eq. (3). It is easily expanded with respect to γ and, neglecting higher terms of γ, is written:

$$Z_0=\sum_i^{occ}[2(C_r^i)^2/(-Y_i)]\gamma^2=\sum_i^{occ}[2(C_r^i)^2/(\lambda_i-h)]\gamma^2. \tag{5}$$

This is the same as that previously obtained by the present authors,[4(b)] a generalized form of the superdelocalizability. As an extreme case, when the adjustable parameter h is taken as zero, Eq. (5) becomes simply

$$Z_0=\sum_i^{occ}[2(C_r^i)^2/\lambda_i]\gamma^2\equiv S_r^{(E)}\gamma^2, \tag{6}$$

where $S_r^{(E)}$ is the superdelocalizability for an electrophilic attack.

Thus the superdelocalizability, which was theoretically derived in the hyperconjugation consideration,[3,4] is now acquired also in this configuration interaction treatment. Apart from the difference of the models of substitution mechanism, especially of the meanings of h involved in this interrelation, the superdelocalizability and the Z value were both proved to be given as the largest positive root of Eq. (2) corresponding to the positive and the negative values of Y_f, respectively.

If λ_f is equal to h, i.e., Y_f is equal to zero, Z_0 is written in a modified form as follows:

$$Z_0=\sqrt{2}\,|\,C_r^f\,|\,\gamma+\sum_i^{\text{occ}-f}[2(C_r^i)^2/Y_i]\gamma^2. \qquad (7)$$

Here the frontier electron density comes to determine a greater part of the reactivity.

For a nucleophilic reaction, though Brown did not treat this case, if one similarly defines the Z value according to condition A, one will easily find that the Z value is mathematically related to the superdelocalizability in the same way as for an electrophilic reaction.

2. Homolytic Reaction

In order to clarify the interrelations between the indexes derived in various methods, an analogous treatment would be significant also for a radical reaction. Possible doublet configurations are classified into three classes: the configuration without charge transfer (R· ··· ArH, wave function Ψ_0), those corresponding to one-electron transfer from the ith occupied orbital of the attacked molecule to the half-occupied one of the attacking radical ($R^-\cdots ArH^+$, wave function Ψ_i), and those from the half-occupied orbital of the radical to the jth unoccupied one of the molecule ($R^+\cdots ArH^-$, wave function Ψ_j). Interconfigurational integrals have the following values:

$$\left.\begin{aligned}&\int\Psi_0\mathbf{H}\Psi_k d\tau=(C_r^k)\int\chi_R H\chi_r d\tau=C_r^k\gamma\beta,\\&\qquad\qquad(k\text{: every MO}),\\&\int\Psi_k\mathbf{H}\Psi_l d\tau=0,\\&\qquad\qquad(k,l\text{: every MO};\ k\neq l),\end{aligned}\right\} \qquad (8)$$

where $\mathbf{H}$ is as usual the total Hamiltonian, expressed by the sum of effective one-electron Hamiltonians H, and χ_R is the half-occupied orbital of the attacking radical or the half-occupied quasi-π orbital at the transition state, which has the energy of $\alpha+h\beta$. Thus $F(Z)$ function is represented by

$$F(Z)=Z-\sum_i^{\text{occ}}[(C_r^i)^2\gamma^2/(Z-Y_i)]-\sum_j^{\text{unocc}}[(C_r^j)^2\gamma^2/(Z+Y_j)]. \qquad (9)$$

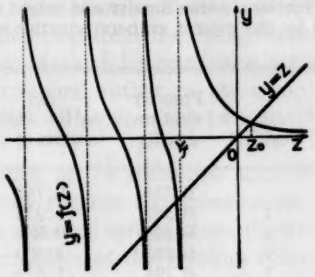

FIG. 2. Functional relations $y=Z$ and $y=f(Z)$ for $Y_f<0$.

According to our theory the half-occupied quasi-π orbital lies between the highest occupied and the lowest unoccupied orbitals.[4] Then the stabilization energy in units of $(-\beta)$ at the transition state is

$$Z_0=\{\sum_i^{\text{occ}}[(C_r^i)^2/(\lambda_i-h)]+\sum_j^{\text{unocc}}[(C_r^j)^2/(h-\lambda_j)]\}\gamma^2. \qquad (10)$$

If we put h equal to zero, this reduces to

$$Z_0=\{\sum_i^{\text{occ}}[(C_r^i)^2/\lambda_i]+\sum_j^{\text{unocc}}[(C_r^j)^2/-\lambda_j]\}\gamma^2, \qquad (11)$$

which is, namely, the superdelocalizability for a radical attack, also acquired in our hyperconjugation treatment of this problem.[4,7] In this connection Nagakura and Tanaka[2] state that the energy of the half-occupied level of most radicals is lower than that of the lowest unoccupied level of the attacked molecule and higher than that of the highest occupied level. Then in the configuration interaction treatment, it follows that the stabilization energy at the transition state, that is, the reactivity index, is expressed by Eq. (10).

Thus, in a radical reaction, although not in heterolytic reactions, the configuration interaction treatment, no matter to which of the quasi-π orbital or the half-occupied orbital of the radical our attention may be paid, may be said to present the identical index to the hyperconjugation treatment.

DISCUSSION

In the preceding section we derived some mathematical correlations between the Z value and the superdelocalizability. As to heterolytic reactions the former corresponds to the most positive root of the equation $F(Z)$ for a negative value of Y_f, while the latter does so for its positive value.

[7] In more scarce cases, when the half-occupied level lies lower than the highest occupied one of the molecule, that is, $Y_f>0$, Z_0 is obtained as

$$Z_0=Y_f+(C_r^f)^2\gamma^2/Y_f.$$

And when the half-occupied level stands higher than the lowest unoccupied one, a similar equation would be given. To these representations, only one or the other of the frontier orbitals is contributing, rather resembling the case of the Z value for heterolytic reaction.

TABLE I. Frontier electron density and extent of charge transfer calculated by the present authors' equation and by Brown's equation.

Compound	Position	Frontier electron density	Δq_h by Eq. (13) in units of γ^2	Δq_E by Eq. (12)[a]
Benzene		0.333	0.750	0.760[b]
Naphthalene	1	0.362	1.222	0.932
	2	0.138	0.889	0.974
Anthracene	9	0.387	2.500	0.945
	1	0.193	1.625	0.972
	2	0.097	1.125	0.986
Naphthacene	5	0.295	3.800	0.964
	1	0.112	2.000	0.986
	2	0.067	1.400	0.992
Phenanthrene	9	0.344	1.240	0.936
	1	0.231	1.160	0.957
	3	0.198	1.140	0.963
	4	0.110	0.960	0.979
	2	0.004	0.840	0.999

[a] Following values of parameters are assumed in accord with Brown: $h_E=2.0$ and $\gamma=0.6$.

[b] For the system which has doubly degenerate frontier levels Eq. (12) should be modified as follows:

$$\Delta q_E=1-2[(c_r^f)^2+(c_r^{f-1})^2]\gamma^2/(h_E-\lambda_f)^2.$$

This value was calculated with this equation.

In spite of the mathematical interrelations and the similar viewpoints of two theories, both of which attach great importance to the frontier orbital, Brown's theory[5] of aromatic substitution seems very different from the present authors' theory.[1,3,4] In this section we will make a comparative discussion of the two theories and point out some problems in the mechanism of aromatic substitution.

1. Extent of Charge Transfer

First, the discussion will be confined for simplicity to electrophilic substitution. According to Brown's theory the extent of the charge transfer, Δq_E, from the substrate to the electrophile at the transition state, is given, regarding γ small, as

$$\Delta q_E=1-[2(C_r^f)^2\gamma^2/(h_E-\lambda_f)^2], \qquad (12)$$

where h_E is the coefficient in the energy of the lowest unoccupied orbital of the electrophile at the transition state, which is expressed as $\alpha+h_E\beta$. Inspection of the third and the fifth columns of Table I and comparison of Eq. (12) with the corresponding reactivity index, Eq. (3), make it obvious that the larger the frontier electron density, which is the intramolecular reactivity index as seen in Eq. (3), on an atom is, the smaller the quantity of charge transferred through the atom. That is to say, a molecule suffers substitution reaction at the position through which the least amount of charge is transferred to the electrophile. This prediction would seem to conflict with chemical intuition.

On the contrary, the extent of charge transfer in the present authors' theory is expressed for a small conjugation by

$$\Delta q_h=\sum_j^{occ}[2(C_r^j)^2\gamma^2/(\lambda_j-h_\pi)^2], \qquad (13)$$

where h_π is the Coulomb integral of the quasi-π orbital, being variable depending on Δq_h. With the progress of reaction, that is, with the increase of γ, the charge transfers continuously to the quasi-π orbital oozing out of the substrate according to Eq. (13). This situation was explained in detail with the $(\Delta q_h-h,\ \gamma)$ diagram (see footnote 4). At the transition state, where h_π was taken to be zero, as clearly seen in the third and the fourth columns of Table I, the extent of charge transfer is completely parallel in a molecule to the frontier electron density, that is, the most reactive position is also the one through which the largest amount of charge transfers.

For a nucleophilic reaction the circumstances are quite the same.

Thus we have encountered two mutually contradictory conclusions as to the relation of transferred charge and reactivity of one position. Further experiments will unravel this entanglement.

2. Energy Levels of Reagents

Condition *A* was set up by Nagakura and Tanaka in regard to the energy level of reagents in their isolated state, which has almost no concern with the transition state.[2] Brown, however, applied this rule also to the transition state. Indeed he formally distinguished the transition state by marking ‡ from the separated state; however, by adopting condition *A*, Y_f for the transition state was made a positive value. It might be dangerous to discuss the relative height of the unoccupied level of the electrophile at the transition state to the height of the highest occupied one of the substrate on the basis of the values in the separate state.

According to our theory, as it was stated in the earlier part of this paper, in order for an electrophilic substitution to take place, the highest occupied level of the substrate must be higher than the quasi-π orbital energy which corresponds to the unoccupied level of the reagent. And, since the Coulomb integral of the quasi-π orbital is decided by its charge density in order to satisfy self-consistency, it is natural that it lies lower than the highest occupied level of the substrate at the stage where no charge is yet transferred.

3. Variation of Level Energy during Reaction

It is well expected that the energy of the reagent may vary considerably as the reaction proceeds. By introducing the self-consistent relation between the energy of the quasi-π orbital and its electron density that the former gets higher with the increase of the latter, the present authors indicated without difficulty that the energy of the quasi-π orbital rises during the progress of reaction in an electrophilic substitution and it falls in a nucleophilic substitution, and consequently

that it approaches the Coulomb energy of a carbon atom. Since mathematical expressions were given to these relations, one can easily trace the proceedings of the substitution reaction. (See also footnote 4.)

On the other hand, Brown did not take into account such a change in the energy level due to the transference of charge but rather that due to the solvation of the electrophile. But his discussion on the effects of solvation seems to be too complicated to formulate, and to make it difficult to follow after the completion of the reaction, including the feature of the activated complex, according to his theory.

4. Transition State

It does not seem clear in Brown's model what the activated complex, or the transition state, of the first step of his mechanism is. The first step is

$$\mathrm{Ar{-}H+E^{+}\rightleftharpoons \overset{\mathrm{E}}{\underset{{}^{+}\mathrm{Ar{-}H}}{\vdots}}} \quad \text{(II)}.$$

Though in his formalism he distinguished the activated complex of this step from the charge-transfer complex (II), the state to which his conclusion actually pertains seems to correspond rather to the complex (II). To make a distinction between the two complexes may be difficult.

The definition of the transition state is clear in our theory.[3] If one regards the three-center system consisting of the attacked carbon atom, the hydrogen atom, and the electrophile as the reaction center, the lowest occupied orbital of the system will be found to be a σ orbital in nature. The transition state was defined as the state at which this orbital has the maximum energy during the course of the reaction. Near the state the next orbital was proved to have a π character, and the stabilization energy due to the conjugation of this quasi-π orbital with the substrate was calculated as reactivity index. The superdelocalizability is a scale of this stabilization energy. This treatment would be rational in an aromatic substitution which implies dissociation and formation of a σ bond.

THE JOURNAL OF CHEMICAL PHYSICS VOLUME 32, NUMBER 6 JUNE, 1960

Calculation of Delocalization Contribution to Infrared Intensity*

WALTER D. JONES† AND WILLIAM T. SIMPSON

Department of Chemistry, University of Washington, Seattle, Washington

(Received December 21, 1959)

Infrared intensity may be related to energies and intensities of electronic transitions by using the theory of the vibrational perturbation of electronic transitions and holding the electronic state quantum number fixed. This suggests in particular relating the infrared intensity of an appropriate normal mode to the strong ultraviolet absorption in dye-like molecules having conjugated π-electron systems. The perturbation theory is tested by applying it to a displaced hydrogen atom and the hydrogen molecule ion. The results suggest the need for modifying the theory to employ floating orbitals. A floating orbital theory of infrared intensity which still brings in ultraviolet transition energies and moments is then constructed. This theory is next applied to the model compounds H_3^+, H_5^+ and H_7^+ and there is predicted an extraordinarily high delocalization contribution to the intensity for the anti-symmetric stretch. Values for the dipole derivatives are calculated ranging up to 65 debyes/A.

INTRODUCTION

IT has been observed[1] that conjugation of π-electron systems has a pronounced effect on the infrared intensities of certain stretching frequencies. Calculations[2] based on the assumption of fixed charges on the moving nuclei show that this mechanism is inadequate to account for the high intensities. It can be assumed then, that an important contribution to the derivative of the electric dipole with respect to the appropriate vibrational coordinate is a redistribution of the delocalized electrons as the molecule is distorted by vibration. In this paper there is developed a theory of infrared intensities associated with delocalization. The theory is illustrated with some calculations for a simple representative molecular system.

Before considering the theory we shall discuss briefly the formamidinium ion, a system which would be expected to show the effect we are to study:

$$\underset{\langle c\rangle}{[\mathrm{H_2N{-}CH{=}\overset{+}{N}H_2}} \leftrightarrow \underset{\langle a\rangle}{\mathrm{H_2\overset{+}{N}{=}CH{-}NH_2}}].$$

* This research was supported in part by the U. S. Air Force through the Air Office of Scientific Research of the Air Research and Development Command.

† Present address: Department of Physics, Bowdoin College, Brunswick, Maine.

[1] G. M. Barrow, J. Chem. Phys. 21, 2008 (1953); R. E. Richards and W. R. Burton, Trans. Faraday Soc. 45, 874 (1949).

[2] C. A. Coulson and M. J. Steppen, Trans. Faraday Soc. 53, 272 (1957); H. Sponer and K. F. Herzfeld, Z. Physik 133, 41 (1953).

This ion can be described by the two structures $\langle c\rangle$ and $\langle a\rangle$ where the electronic wave functions are $|\,c\rangle$ and $|\,a\rangle$. Wave functions for the ground state and first excited state of this system, not normalized, can be approximated by

$$|\,N_0\rangle = |\,c\rangle + |\,a\rangle \qquad |\,V_0\rangle = |\,c\rangle - |\,a\rangle$$

calculated at the equilibrium positions of the nuclei.

Neglecting the motion of the hydrogen atoms, consider the antisymmetric vibration of the C, N skeleton which is essentially the shortening of r_2 and the lengthening of r_1.

$$\mathrm{N}^{r_1}\mathrm{C}^{r_2}\mathrm{N}.$$
$$\leftarrow\ \rightarrow\ \leftarrow$$

This motion has a tendency to increase the electron attraction in the r_2 region at the expense of that in the r_1 region, thus favoring structure $\langle c\rangle$. In consequence the perturbed wave function for the ground state can be represented as comprised of some $|\,V_0\rangle$.

$$|\,N\rangle = |\,N_0\rangle + a_{NV}Q\,|\,V_0\rangle$$
$$= (1+a_{NV}Q)\,|\,c\rangle + (1-a_{NV}Q)\,|\,a\rangle,$$

where Q is the normal coordinate for the antisymmetric stretch and the mixing coefficient $a_{NV}>0$.

The effect of adding some $|\,V_0\rangle$ is to induce the motion of some positive charge from the nitrogen on the left as in $\langle a\rangle$ to the nitrogen on the right as in $\langle c\rangle$, and back again as the vibration completes its cycle. This produces a large oscillating electric moment which, moreover, should increase markedly with the length of the molecule going out in the vinylogous series.[3]

One recognizes that a theory of infrared intensities is implicit in the theory of vibrational interactions with electronic states.[4] The electronic energy eigenstates of a molecule which has been distorted by vibration are found by treating the nuclear displacements as a perturbation and expanding the relevant wave functions in terms of the set of electronic wave functions referred to the equilibrium nuclear configuration. The formalism includes transitions for which the electronic quantum number is unchanged, a fact which leads to a theory giving vibrational intensities as related to intensities of electronic transitions.

Assuming the Born-Oppenheimer approximation, the wave function for the ground electronic state may be written

$$\chi_n{}^i(Q_i)\prod_{j\neq i}\chi_0{}^j(Q_j)\,|\,NQ\rangle.$$

Here $|\,NQ\rangle$ is the normal state electronic wave function, a function of both the electronic coordinates, r, and nuclear displacement coordinates, Q; and $\chi_n{}^i$ is the wave function for the ith normal mode, the one singled out for study. Accordingly, the vibrational quantum number n takes on the values 0 or 1.

The intensity is calculated by squaring the transition matrix element of the electric moment operator for electrons and nuclei. The nontrivial part of this matrix element is

$$\int \chi_0{}^i(Q_i)\,\langle NQ_i\,|\,\mathbf{M}\,|\,NQ_i\rangle\chi_1{}^i(Q_i)\,dQ_i,$$

where $\mathbf{M}$ is the electric moment operator for the electrons only. The units of Q_i need to be compatible throughout, but there is no need to include a Jacobian making a connection with the Cartesian coordinates in $d\tau$ provided that the χ's are normalized. The dependence of the electronic matrix element on the displacements includes the derivative term for the normal mode in question

$$\mathbf{M}'Q = \langle NQ\,|\,\mathbf{M}\,|\,NQ\rangle - \langle NO\,|\,\mathbf{M}\,|\,NO\rangle,$$

where the subscript i has been dropped (and $\mathbf{M}'$ is what is sometimes called $d\mu/dQ$, or the dipole derivative). Using the derivative form and taking Q to be a *normal coordinate* one finds for the electronic moment[5]

$$\mathbf{M}'\int \chi_0 Q\chi_1\,dQ = M'(\hbar/2\omega)^{\frac{1}{2}},$$

where now $\mathbf{M}'$ has to involve a normal coordinate. Thus we see that the intensity is directly proportional to the dipole derivative squared and inversely to the frequency. The frequency dependence may be understood as automatically bringing in the changes in amplitude squared which occur as the force constants vary, while the dipole derivative is in a rough way a measure of the charge associated with this amplitude.

In what follows we shall concentrate on the calculation of $\mathbf{M}'$ for a particular normal coordinate. This is accomplished by expanding the electronic wave function for a displaced configuration in terms of functions all calculated for $Q=0$

$$|\,NQ\rangle = |\,NO\rangle + \sum_V a_{NV}Q\,|\,VO\rangle,$$

where V is used for excited states (and later for a particular excited state in the so-called valence shell).

[3] Dr. L. G. S. Brooker (private communication) has found experimentally that for chain lengths so long as to give rise to a main electronic transition at 10 000 A or so, the spectrum becomes more like that of a polyene with an even number of carbon atoms, indicating that the conditions for resonance have become unfavorable. The potential curve for the antisymmetric stretch must then have two minima, and the theory in the present paper becomes inapplicable. The appearance of a double minimum is related to the Jahn-Teller theorem in that as the chain lengthens the energy difference between the N and V states approaches zero. Interaction of the N and V states through a nuclear displacement amounting to bond alternation apparently produces $|\,c\,\rangle$ (or $|\,a\,\rangle$) as the state lower in energy. See also Y. Ooshika, J. Phys. Soc. Japan **12**, 1246 (1957), H. Labhart, J. Chem. Phys. **27**, 957 (1957), and H. C. Longuet-Higgins and L. Salem, Proc. Roy. Soc. (London) **251A**, 172 (1959).

[4] G. Herzberg and E. Teller, Z. physik. Chem. **B21**, 410 (1933).

[5] E. B. Wilson, Jr., J. C. Decius, and P. C. Cross, *Molecular Vibrations* (McGraw-Hill Book Company, Inc., New York, 1955), pp. 14–22.

The coefficients in the expansion are given by

$$a_{NV}(E_N-E_V)=\langle NO\,|\,H^1\,|\,VO\rangle,$$

where the E's are the unperturbed energies and

$$H=H^0+H^1Q+\cdots.$$

The electric moment to the first order in Q is

$$\langle NO\,|\,\mathbf{M}\,|\,NO\rangle+2Q\sum_V a_{NV}\langle NO\,|\,\mathbf{M}\,|\,VO\rangle,$$

so that

$$\mathbf{M}'=2\sum_V a_{NV}\langle NO\,|\,\mathbf{M}\,|\,VO\rangle.$$

Note that the matrix elements in the sum are quantities which determine the integrated intensities of electronic transitions.

In order for an infrared transition to have intensity the V state species must be such as to give an ultraviolet intensity. To obtain a nonvanishing a_{NV} going with such an ultraviolet transition the electronic part of the perturbation, H^1, must then have the species of a translation. Since the full perturbation, H^1Q, is totally symmetric, Q must also have the species of a translation; all of which therefore reproduces the well-known vibrational selection rule.

The appearance in $\mathbf{M}'$ of the ultraviolet transition moments and (implicitly in the a_{NV}) transition energies makes one think of constructing an empirical theory of infrared intensity. However, such a plan has characteristic pitfalls just as, for example, in the case of the theory of the one-term dispersion formula.

In the next section we shall consider several examples which point to the necessity of modifying the theory described before, and subsequently we shall consider the modifications and some calculated results.

THE DISPLACED HYDROGEN ATOM[6] AND THE HYDROGEN MOLECULE ION

As an initial illustration of the theory the ground state of a perturbed single hydrogen atom will be calculated. The general nuclear displacement perturbation, in expanded form, is

$$-e^2\sum_{A,\nu}Z_A\mathbf{Q}_A\cdot\mathbf{r}_{A\nu}/|\,r_{A\nu}\,|^3+\cdots,$$

where Z_A is the nuclear charge of the Ath nucleus, $\mathbf{r}_{A\nu}$ is the vector leading from the equilibrium position of the nucleus to the νth electron, and Q_A is the displacement of the Ath nucleus. To find H^1Q where Q is a particular normal coordinate one introduces the transformation from the Q_A's to normal coordinates and collects terms referring to the particular normal coordinate. The perturbation in the present case is taken as a small displacement in the z direction, Q:

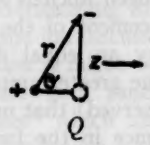

Q

It is recognized at once that the new ground state function is a $1s$ orbital centered on the displaced nucleus and that the true perturbed electric moment for the electron will be $-eQ$, where e is positive. The set of hydrogen wave functions based on the undisplaced center can be used in the expansion. The electronic part of the perturbation is found from the foregoing formula to be

$$H^1=-(e^2\cos\theta)/r^2.$$

The angular dependence of this term is that of p_z functions so that only these functions will be found to mix in. The general perturbation integral is found by the use of the generator function

$$\sum_{q=0}^{\infty}\frac{L_q^s(\rho)}{q!}u^q\equiv(-1)^s\frac{\exp[-\rho u/(1-u)]}{(1-u)^{s+1}}u^s,$$

where the radial dependence of p_z functions is given by

$$\mathfrak{N}_n\rho e^{-\rho/2}L_{n+1}^3(\rho),\quad \rho=2r/na_0.$$

In the same way the transition moments, $1s\rightarrow np_z$, can be found.[7] The difference in energy levels for the hydrogen atom functions is well known. The resulting series is

$$\mathbf{M}'Q=-eQ\frac{2^7}{3}\sum_{n=2}^{\infty}\frac{n^5}{(n^2-1)^4}\left(\frac{n-1}{n+1}\right)^{2n},$$

which converges to $-0.605\ eQ$, so that with $e=1$ (atomic units) $\mathbf{M}'=-0.605$.

If the functions used had constituted a complete set the results should have converged perfectly to $\mathbf{M}'=-1$. However, the hydrogen functions do not constitute a complete set without taking into consideration the continuum. The deficit of -0.395 represents a substantial error, or pseudoinfrared intensity.[8]

In the preceding calculation we had available the exact functions and energies of the excited states for the system studied. Calculations for molecules are subject to uncertainties both in the wave functions and in the energy levels, and the influence of these uncertainties must be sought. As a first step we consider the HD^+ molecule a simple system for which the oscillating electric moment is exactly known within the limitations of the Born-Oppenheimer approximation.

[6] The value reported here was first found by Dr. G. S. Levinson working in this laboratory.

[7] A. Kupper, Ann. Physik 86, 511 (1928).

[8] If the complete set of functions, the use of which is described by H. Shull and P. O. Löwdin, J. Chem. Phys. 23, 1362 (1955) is used the electric moment is found to converge correctly to $-eQ$, or $\mathbf{M}'=-1$.

It is sufficient in discussing the perturbation of this system by a vibrational displacement to consider the motion of the hydrogen nucleus alone. By symmetry, the effect of displacement of the deuteron is exactly compensated for by an equal displacement of the proton. It is only the greater amplitude of the proton (center of mass conserved) that makes a contribution, equal to the difference in the two motions. The net displacement of the proton will be taken as Q, while the deuteron is assumed stationary.

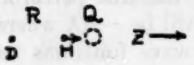

As in the Born-Oppenheimer approximation, the electron will be assumed to follow the nuclear motions perfectly. Then the true electronic contribution to the dipole derivative will be $-\frac{1}{2}$ since there is effectively half an electron on each positively charged center, regardless of whether it is a deuteron or a proton. From the example of the displaced hydrogen atom it might be expected that the result calculated will be some fraction of $-\frac{1}{2}$ depending on the efficiency of the approximate functions used; the nearer the result to $-\frac{1}{2}$ the better the approximation.

The approximate functions used in the calculation are the LCAO-MO functions

$$|NO\rangle=(2+2s)^{-\frac{1}{2}}(a_0+b_0),$$

$$|VO\rangle=(2-2s)^{-\frac{1}{2}}(a_0-b_0),$$

where a_0 and b_0 are $1s$ AO's centered on the initial positions of the deuteron and proton, respectively, and s is the overlap integral. The perturbation term for this system is the same as for the displaced hydrogen atom. In fact in both cases there is the displacement of a proton. Here, however, the displacement occurs in the presence of an adjacent deuteron. The perturbation integral in atomic units was found to be

$$\langle NO|H^1Q|VO\rangle$$

$$=-Q/2(1-s^2)^{\frac{1}{2}}(1/R^2)[1-\exp(-2R)(2R^2+2R+1)]$$

and the transition moment

$$\langle NO|\mathbf{M}|VO\rangle=R/2(1-s^2)^{\frac{1}{2}}.$$

The difference in energy levels is known to be[9]

$$E_V-E_N=2/(1-s^2)\{s[-1/R+\exp(-2R)(1+1/R)]+\exp(-R)(1+R)\}.$$

From these results the dipole derivatives at the hypothetical "equilibrium" distances $R=2.5$ and $R=5.0$ have been calculated as -0.812 and -1.181, respectively.

It is at once apparent that this simplified calculation overcompensates for the displacement instead of falling short as expected. Further, the result gets worse as the internuclear distance increases, even though the functions are getting better. To get a mathematical picture of what is happening we can see that for large R, $\langle NO|H^1Q|VO\rangle$ decreases as Q/R^2, $\langle NO|\mathbf{M}|VO\rangle$ increases as R, and ΔE decreases as $R\exp(-R)$. Thus the calculated moment, for large values of R, must behave as

$$(Q/R^2)R/R\exp(-R)=Q[\exp(R)/R^2]$$

Since $\exp(R)$ increases faster than R^2, the calculated moment, as does the mixing coefficient, becomes catastrophically large for large values of R. To employ degenerate perturbation theory is not clearly indicated because Q can be as small as desired. We are making the fundamental error, however, of not using the full first-order perturbed function.

To understand what is happening we must consider the nature of the functions being used. For large values of R, ΔE goes rapidly to zero in comparison to the perturbation, and the functions $|NO\rangle$ and $|VO\rangle$ become degenerate. In the absence of any perturbation, symmetry would predict equal sharing of the electron. When the proton is displaced, the symmetry of the perturbation is such that the integral over a b_0^2 distribution vanishes, giving no change in the energy of an electron on the proton. However, moving the proton away from the deuteron decreases the attraction of the hydrogen nucleus for the electron when it is on the deuteron and increases the energy of such an electron. Thus the degeneracy is removed in such a way that the electron prefers the proton when the proton moves away from the deuteron. Correspondingly the deuteron is preferred when the proton is closer than the equilibrium distance. The result is a catastrophically large oscillating moment, for very large nuclear separations. This tendency is partially overcome at finite bond distances by the chemical bonding effects. Thus at a distance of 2.5 au. we do not find a moment owing to the complete transfer of the electron from one center to another, but we do calculate a moment that is unexpectedly large. It should be pointed out that if the perturbation resulting from a displacement of the hydrogen had given a nonvanishing integral over the b_0^2 distribution, the complete catastrophe would not have occurred. So the restriction to linear combinations of $1s$ functions contributed to the breakdown of the calculation. In any case the difficulty illustrated by the foregoing is very likely so serious that it would not be enough just to keep it in mind in applications of the theory.

The procedure that will overcome this difficulty involves a simple expedient. If the atomic orbitals are allowed to move with the centers as they are displaced, spurious intensity of this type is not introduced into the calculation. It will be appreciated that allowing the AO to move with the center gives the exact solution for a single displaced proton in a trivial way.

[9] See for example L. Pauling and E. B. Wilson, Jr., *Introduction to Quantum Mechanics* (McGraw-Hill Book Company, Inc., New York, 1935), pp. 328–329.

Let us consider again the problem of moving the proton in HD^+. This time we use linear combinations of floating AO's

$$|N_0Q\rangle=(2+2s)^{-\frac{1}{2}}(a+b)$$
$$|V_0Q\rangle=(2-2s)^{-\frac{1}{2}}(a-b),$$

where now the a and b orbitals no longer have the zero subscript; but the N and V symbols have, signifying that the contributions of a and b are as obtained at the equilibrium configuration. It is still possible that the best wave function involves some mixing of $|N_0Q\rangle$ and $|V_0Q\rangle$, which we shall now investigate by making a variation calculation. In effect we are looking for a_{NV} in

$$|N\rangle=|N_0Q\rangle+a_{NV}Q\,|V_0Q\rangle$$
$$|V\rangle=|V_0Q\rangle+a_{VN}Q\,|N_0Q\rangle,$$

though now through the use of the secular equation technique for the full Hamiltonian instead of perturbation theory. The off-diagonal part is

$$\langle N_0Q\,|\,H\,|\,V_0Q\rangle-\langle N_0Q\,|\,V_0Q\rangle E.$$

It is inexpedient to separate H into a perturbed and unperturbed part at this point, because we can see by symmetry that the matrix elements are zero. To show this explicitly we examine, e.g.,

$$\langle N_0Q\,|\,V_0Q\rangle=(2+2s)^{-\frac{1}{2}}(2-2s)^{-\frac{1}{2}}\left[\int a^2d\tau-\int b^2d\tau\right]=0.$$

There is no mixing, and thus no delocalization contribution. (There is in a sense delocalization in HD^+ but no change in the amount of delocalization during the vibration). The wave function is therefore

$$|N\rangle=|N_0Q\rangle.$$

The calculation of the electronic contribution to the electric moment over $|N_0Q\rangle$ gives the result $\mathbf{M}'=-\frac{1}{2}$ for the simple reason that the orbital, b, follows the proton as it moves, and the electron is in the b floating orbital half the time.

To sum up, using floating orbitals does away with the spurious infrared intensity found both in the displaced hydrogen atom case and in the case of HD^+. It should be emphasized that there is nothing incorrect about the Herzberg-Teller approach, if it is carried out all the way. Floating orbitals are introduced to make up for the errors brought in by our attempts to make the theory simple and workable by not using a full set of basis functions. As might be expected, going over to floating orbitals is no cure-all, but it is believed that the improvement is sufficient to give the results physical meaning.

THEORY

For simplicity, the treatment will be restricted to the hypothetical molecules H_n^+ where n is an odd number. Even so it is not felt that there is a great sacrifice in applicability: in particular the results for H_3^+ are pertinent for the understanding of the π electrons in formamidinium ion, the ion discussed in the Introduction. In this connection it might be thought better to study H_3^-, but there is a fundamental similarity between the two cases[10] which makes it all right to work on the positive ion, which is the simpler.

The plan is to treat H_3^+ using a valence-bond and later an antisymmetrized molecular-orbital approach, and then using a form of Hückel theory. In addition H_5^+ is considered using the valence-bond and Hückel theory, and finally H_7^+ using just the Hückel theory. This way the results for H_5^+ and particularly H_7^+ are anchored to the simpler results which themselves are given credibility by their mutual consistency. The Hückel theory is certainly not universally satisfactory, but probably works as well for ions of the type $H_n^\pm$ (n odd) as for any system.

The perturbation for these molecules will be the high-energy antisymmetric stretch in which the bonds alternate. Using a model in which all bond force constants are equal and all interaction constants zero one finds the normal coordinates listed in Table I. It turns out that for this particular normal mode the contribution to the dipole derivative that comes from the motion of the protons is exactly zero, so that in what follows we shall be able to focus attention exclusively on the electronic contribution.

A theory giving electric dipole derivatives and based on electronic states and transition moments in which floating AO's are used may be extracted from the work of Liehr.[11] He derives expressions for intensities of electronic transitions including vibrational perturbation, and as with Herzberg-Teller theory one has only to hold the electronic quantum number constant to have a theory of infrared intensity. A discussion of infrared intensity as well as of the calculation of force constants along these lines has been given by Bratoz and Daudel.[12] The derivation presented here departs from that given by Liehr but basically the results are the same. The theory is presented in what we hope is a systematic fashion, permitting insight and discussion as it is developed.

The calculation could be made in a straightforward manner by displacing the nuclei and their associated AO's infinitesimally as in a vibration and calculating the wave function for the new configuration using the variational technique. This, together with the wave function calculated for the equilibrium configuration, would be used to determine the electric moment as a function of the displacement. However, it is intended in this paper to preserve the flavor of the Herzberg-

[10] A. D. McLachlan, Mol. Phys. **2**, 271 (1959).
[11] A. D. Liehr, Z. Naturforsch. **13A**, 311 (1958).
[12] R. Daudel and S. Bratoz, Cahier Phys. **75–76**, 39 (1956); S. Bratoz, Compt. rend. 243, 1493 (1956); and S. Bratoz, *ibid.* **244**, 2050 (1957).

TABLE I. Normal coordinates. The numbers give the proton displacements as fractions of $Qm^{-\frac{1}{2}}$.

Δz	a	b	c	d
H_3^+	−0.408	0.817	...	...
H_5^+	0.195	−0.512	0.633	...
H_7^+	−0.119	0.333	−0.482	0.535

Teller theory, so that one may relate high intensities in the infrared to associated high intensities in the electronic spectrum. The procedure just mentioned would not make this possible.

In the present approach there are two stages. The object of the first stage is using the variation method to obtain a set of basis functions having an AO makeup that reduce to the "correct" functions when the nuclei are at equilibrium. (Here we use the term "correct" in place of "true" because we do not contemplate making a thoroughly accurate variation calculation). The electron densities represented by these basis functions after the molecule has been perturbed are expected to exclude any delocalization effects introduced by the perturbation, even though the orbitals are allowed to float. This is accomplished by holding certain of the coefficients fixed at the values appropriate for the equilibrium configuration.

Stage two of the calculation is the mixing of these basis functions to give the delocalization effects. In this way the delocalization contribution is related to functions that correspond to electronic excited state functions of the molecule.

We shall consider the simplest case, H_3^+, according to the valence-bond method while building up the theory. The generalizations needed for going over to the orbital approaches and for the larger molecules are not difficult. The stationary-state functions for H_3^+ are based on products of AO's in which electrons are assigned, one to a center. Having the positive charge on center c leads to two orbital product functions

$$\sum_P (-1)^P Pa\alpha_1 b\beta_2$$

and

$$\mathfrak{R}_{ab}\sum_P (-1)^P Pa\alpha_1 b\beta_2 = \sum_P (-1)^P Pa\beta_1 b\alpha_2$$

where $a\alpha_1$ means electron one in the $a\alpha$ spinorbital, and $\mathfrak{R}_{ab}$ is the operator which interchanges spins going with orbitals a and b. The function with a bond between a and b corresponding to the structure $\langle c \rangle$

$$a\!-\!b\ \ c^+$$

is

$$|\, c\rangle = \mathfrak{N}_c(1-\mathfrak{R}_{ab})\sum_P (-1)^P Pa\alpha_1 b\beta_2$$

Similarly, we have the other functions implied by the spatial degeneracy

$$|\, a\rangle = \mathfrak{N}_a(1-\mathfrak{R}_{bc})\sum_P (-1)^P Pb\alpha_1 c\beta_2$$

and

$$|\, b\rangle = \mathfrak{N}_b(1-\mathfrak{R}_{ac})\sum_P (-1)^P Pa\alpha_1 c\beta_2.$$

Since $|\, b\rangle$ does not have a bond between adjacent centers it will be higher in energy and will not mix in as much. We therefore leave it out, thus effecting a simplification which is roughly analogous to the assumption of perfect pairing. This automatically leads to but a single V state. (The restriction to a single V state will be retained in the remainder of this paper, so that what is being calculated is the contribution to the infrared intensity from a single strong ultraviolet transition).

If the ab and bc distances are equal the structure functions $|\, a\rangle$ and $|\, c\rangle$ are strictly spatially degenerate, and mixing them with equal weights leads to two state functions which are "correct" for the equilibrium configuration

$$|\, N_0Q\rangle = \mathfrak{N}_{NQ}(|\, c\rangle + |\, a\rangle)$$
$$|\, V_0Q\rangle = \mathfrak{N}_{VQ}(|\, c\rangle - |\, a\rangle).$$

The inclusion of Q as a label implies that these functions are defined for configurations other than the equilibrium one, which is intended In general the functions "float" in the sense that the AO's which enter into their makeup float. The subscripts, 0, mean that the *weights are to remain the same* as when $Q=0$. The generalization to other kinds of N_0 and V_0 functions which have an orbital makeup and "float" in the present sense is straightforward, because the subsequent theory makes no more reference to the structure functions.

It would appear that stage one is complete, but it is not, owing to the fact that the N_0 and V_0 functions will not in general remain orthogonal when Q is varied from zero. Since we are going to carry out a unitary transformation as a part of stage two we need to define a new set of mutually orthogonal functions related to the ones above. These are

$$|\, N_0\rangle = |\, N_0Q\rangle + vQ\,|\, V_0Q\rangle$$
$$|\, V_0\rangle = |\, V_0Q\rangle + nQ\,|\, N_0Q\rangle.$$

The members of the new set are characterized by leaving out the Q label, even though the functions are defined for Q different from zero. The orthogonality (first-order)

$$\langle N_0\,|\, V_0\rangle = \langle N_0Q\,|\, V_0Q\rangle + (n+v)Q = 0$$

gives us a condition on $n+v$ which, on account of

$$\langle N_0Q\,|\, V_0Q\rangle = \langle N_0O\,|\, V_0O\rangle + \langle N_0Q\,|\, V_0Q\rangle' Q$$

and

$$\langle N_0O\,|\, V_0O\rangle = 0$$

becomes

$$n+v=-\langle N_0Q \mid V_0Q\rangle'.$$

This completes stage one.

In stage two we transform the Hamiltonian using $\mid N_0\rangle$ and $\mid V_0\rangle$ and find a 2×2 upper block which (as we have planned) is not perfectly diagonal unless $Q=0$. The off-diagonal element calculated to the first order in Q is

$$\begin{aligned}\langle N_0 \mid H \mid V_0\rangle &= \langle N_0Q \mid H^0+H^1Q \mid V_0Q\rangle \\ &\quad +v\langle V_0Q \mid H^0+H^1Q \mid V_0Q\rangle Q \\ &\quad +n\langle N_0Q \mid H^0+H^1Q \mid N_0Q\rangle Q \\ &= [vE_V+nE_N+\langle N_0Q \mid H^0 \mid V_0Q\rangle' \\ &\quad +\langle N_0O \mid H^1 \mid V_0O\rangle]Q.\end{aligned}$$

Here the E's are unperturbed energies, and the functions at $Q=0$ have been used to evaluate the matrix element over H^1Q, a procedure which is correct to the first order. Also, use has been made of the "correctness" of $\mid N_0O\rangle$ and $\mid V_0O\rangle$

$$\langle N_0O \mid H^0 \mid V_0O\rangle=0$$

in obtaining the term which is in the form of a derivative.

Applying matrix perturbation theory within the 2×2 block we have for the ground state wave function an expression involving the off-diagonal element

$$\mid N\rangle = \mid N_0\rangle - \langle N_0 \mid H \mid V_0\rangle(E_V-E_N)^{-1} \mid V_0\rangle.$$

We may now calculate the electric moment to the first order

$$\begin{aligned}\langle N \mid \mathbf{M} \mid N\rangle &= \langle N_0 \mid \mathbf{M} \mid N_0\rangle \\ &\quad -2\langle N_0 \mid H \mid V_0\rangle(E_V-E_N)^{-1}\langle N_0 \mid \mathbf{M} \mid V_0\rangle \\ &= \langle N_0O \mid \mathbf{M} \mid N_0O\rangle+\langle N_0Q \mid \mathbf{M} \mid N_0Q\rangle'Q \\ &\quad +2v\langle N_0O \mid \mathbf{M} \mid V_0O\rangle Q \\ &\quad -2(vE_V+nE_N+\langle N_0Q \mid H^0 \mid V_0Q\rangle' \\ &\quad +\langle N_0O \mid H^1 \mid V_0O\rangle)(E_V-E_N)^{-1}\langle N_0O \mid \mathbf{M} \mid V_0O\rangle Q.\end{aligned}$$

The first term is the permanent dipole moment, and does not contribute to the infrared intensity. The second term gives the changes in electric moment accompanying the displacements with Q for a wave function constrained as described in stage one. All the other terms have the ultraviolet transition moment as a factor

$$\begin{aligned}\mathbf{M}'Q &= [2v(E_V-E_N)-2(vE_V+nE_N+\langle N_0Q \mid H^0 \mid V_0Q\rangle' \\ &\quad +\langle N_0O \mid H^1 \mid V_0O\rangle)] \\ &\quad \times(E_V-E_N)^{-1}\langle N_0O \mid \mathbf{M} \mid V_0O\rangle Q.\end{aligned}$$

If we incorporate the condition on $n+v$ from stage one

$$n+v=-\langle N_0Q \mid V_0Q\rangle'$$

we obtain the main result: the contribution having to do with the V state (hence with the delocalization, for the V state we are considering)

$$\begin{aligned}\mathbf{M}' &= -2(\langle N_0Q \mid H^0-E_N \mid V_0Q\rangle'+\langle N_0O \mid H^1 \mid V_0O\rangle) \\ &\quad \times(E_V-E_N)^{-1}\langle N_0O \mid \mathbf{M} \mid V_0O\rangle.\end{aligned}$$

Returning to the final expression for $\mathbf{M}'$ given in the introduction,

$$\mathbf{M}'=2a_{NV}\langle NO \mid \mathbf{M}_\perp \mid VO\rangle,$$

we see that the mixing coefficient has now to be taken from

$$\begin{aligned}a_{NV}(E_N-E_V) &= \langle N_0Q \mid H^0-E_N \mid V_0Q\rangle' \\ &\quad +\langle N_0O \mid H^1 \mid V_0O\rangle\end{aligned}$$

or alternately the equivalent (to the first order) more compact

$$a_{NV}(E_N-E_V)=\langle N_0Q \mid H-E_N \mid V_0Q\rangle'.$$

The a_{NV} value vanishes by symmetry for HD^+, as can easily be seen using the compact form, because the $\mid N_0Q\rangle$ and $\mid V_0Q\rangle$ remain symmetric and antisymmetric under the displacement Q. That is, as we had already discovered, the delocalization contribution is zero when we go over to floating orbitals, so that all the intensity for HD^+ comes from the other term

$$\langle N_0Q \mid \mathbf{M} \mid N_0Q\rangle'=-\tfrac{1}{2},$$

which may be considered as giving the contribution from fixed charges.

To fix our attention on what is called $\mathbf{M}'$ here and disregard the contribution $\langle N_0Q \mid \mathbf{M} \mid N_0Q\rangle'$ is intuitively reasonable in that the separation into parts is independent of the orthogonalization parameters v and n and also because it works out for HD^+. Still there is some uncertainty, particularly with regard to the planned empirical aspect. If the observed electronic transition energy and intensity are to be used in place of E_V-E_N and $\langle N_0O \mid \mathbf{M} \mid V_0O\rangle$ one has to hope that the approximate functions obtained for $\mid N_0O\rangle$ and $\mid V_0O\rangle$ are at least based on a correct assignment; and granting this, that they reproduce reasonably well the changes in electron density occurring when Q varies, along with reproducing the $Q=O$ properties.

We return to the example of H_3^+ where now we are interested in what the theory predicts.

RESULTS

All calculations are based on an assumed proton-proton "equilibrium" interatomic distance of 2 au. The wave functions for H_3^+, normalized for $Q=0$, are

$$\begin{aligned}\mid N_0Q\rangle &= 0.598(\mid c\rangle+\mid a\rangle) \\ \mid V_0Q\rangle &= 0.910(\mid c\rangle-\mid a\rangle).\end{aligned}$$

The evaluation of matrix elements is discussed in the Appendix. The experimental transition energy and

TABLE II. Quantities occurring in the infrared intensity of H_3^+ and H_5^+. True Hamiltonian.

	E_V-E_N	$\langle N_0O\|\mathbf{M}\|V_0O\rangle$	$\langle N_0Q\|H-E_N\|V_0Q\rangle' m^{\frac{1}{2}}$	$\langle N_0Q\|\mathbf{M}\|N_0Q\rangle' m^{\frac{1}{2}}$	$\mathbf{M}' m^{\frac{1}{2}}$
			Valence bond		
H_3^+	0.268	−2.18	0.142	0.82	2.32
H_5^+	0.229	−3.35	−0.193	−1.47	−5.64
			Antisymmetrized MO		
H_3^+	0.339	−2.08	0.157	0.46	1.93

intensity are not known, so these quantities have been calculated along with the mixing parameters. The results are given in Table II. The various matrix elements which involve Q^{-1} are tabulated containing a factor $m^{\frac{1}{2}}$, where m is the proton mass. Thus $\mathbf{M}' m^{\frac{1}{2}} = -2\langle N_0Q\,|\,H-E_N\,|\,V_0Q\rangle' m^{\frac{1}{2}} \langle N_0O\,|\,\mathbf{M}\,|\,V_0O\rangle (E_V-E_N)^{-1}$ For H_3^+ this gives

$$\mathbf{M}' = 2.32 m^{-\frac{1}{2}}$$

or for the infrared transition moment, as described in the Introduction,

$$2.32(\hbar/2\omega m)^{\frac{1}{2}}$$

where $(\hbar/2\omega m)^{\frac{1}{2}}$ is a characteristic amplitude (of ca 10^{-2} A). The factor 2.32 in $\mathbf{M}'$ emerges as an effective charge in units of the charge of an electron and can be converted into debyes/A by multiplication by 4.80. $\mathbf{M}' m^{\frac{1}{2}} = 2.32$ is thus equivalent to 11.2 debyes/A, a very high charge factor compared with what is ordinarily found. For example Hisatsune and Eggers report values in the range of 1.2–3.6 debyes/A for the C—O stretch in formaldehyde (a substance which has a π bond but without any delocalization beyond what is found in the bond itself).[13]

The calculated contribution from the motion of the electrons when the wave function is constrained to $|\,N_0Q\rangle$ is 0.82 (to be compared with 2.32). This is a little high because for the H_n^+ system the proton moment vanishes, and one might expect the electronic contribution from "fixed charges" to do the same. The discrepancy gives a measure of what might be called the "noise level" of the theory as it is applied in a practical case. With this perspective we can still conclude that a large delocalization contribution to the infrared intensity should be found for molecules which are represented by the model substance H_3^+. It is tempting to subscribe to the generalization that $\mathbf{M}' m^{\frac{1}{2}}$ values greater than a unit electronic charge are almost a sure sign that there is a delocalization contribution to infrared intensity.

The calculation for H_5^+ using valence-bond functions is very similar to the H_3^+ calculation. The structure functions used are $|\,e\rangle$, $|\,c\rangle$, and $|\,a\rangle$ where for example, $|\,e\rangle$ is based on

$$|\,e\rangle = 0.584(1-\mathcal{R}_{ab})(1-\mathcal{R}_{cd}) \times \begin{vmatrix} a\alpha_1 & b\beta_1 & c\alpha_1 & d\beta_1 \\ a\alpha_2 & b\beta_2 & c\alpha_2 & d\beta_2 \\ a\alpha_3 & b\beta_3 & c\alpha_3 & d\beta_3 \\ a\alpha_4 & b\beta_4 & c\alpha_4 & d\beta_4 \end{vmatrix} \quad (a-b \quad c-d \quad e^+).$$

The normalization is slightly different for $|\,c\rangle$ and there is not perfect spatial degeneracy, but virtually so. The structures, e.g.,

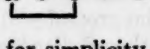

have been excluded for simplicity, and, as before, the distance between adjacent protons has been given the supposed equilibrium value of 2 au. The state functions, normalized for $Q=0$, turn out to be

$$|\,N_0Q\rangle = 0.448(|\,e\rangle + |\,a\rangle) + 0.444\,|\,c\rangle$$

and

$$|\,V_0Q\rangle = 0.773(|\,e\rangle - |\,a\rangle).$$

The various quantities having to do with the infrared intensity are listed in Table II underneath the corresponding quantities for H_3^+.

The N, V transition energy decreases (color deeper) and the transition moment is understandably greater for the longer molecule. The (effective) mixing coefficient is somewhat greater but because of the transition energy and intensity change the charge factor in the infrared intensity is considerably greater (-5.64 compared with 2.32). The sign change occurs because in the actual computation the motion of the center atom was used as a practical coordinate, together with having the a-atom displacements positive

$$a\rightarrow \quad \leftarrow b \qquad c\rightarrow$$
$$a\rightarrow \quad \leftarrow b \qquad c\rightarrow \quad \leftarrow d \qquad e\rightarrow .$$

The final value for $\mathbf{M}' m^{\frac{1}{2}} = 5.64$ is 27 debyes/A.

The characteristics of the valence bond functions that make them adaptable to the two-stage treatment outlined in the last section is their atomic orbital make-up and the possibility of defining constrained

[13] I. C. Hisatsune and D. F. Eggers, Jr., J. Chem. Phys. 23, 487 (1955).

functions $\cdots |N_0Q\rangle$ and $|V_0Q\rangle$. One can just as well use Slater determinants based on LCAO-MO's, where now the constraint consists in fixing the weights of the AO's in the molecular orbitals at the values found for the equilibrium configuration. It is a well-known checking device to compare valence-bond with molecular-orbital results, so the infrared intensity for H_3^+ has been calculated using the orbital theory. The coefficients which minimize the energy for a function

$$|N_0Q\rangle = 2^{-\frac{1}{2}} \begin{vmatrix} p\alpha_1 & p\beta_1 \\ p\alpha_2 & p\beta_2 \end{vmatrix}$$

were determined as

$$p = 0.285(a+c) + 0.624b.$$

The antisymmetric MO which occurs in $|V_0Q\rangle$ is determined by symmetry

$$q = 0.785(c-a),$$

and the function, not normalized, is

$$|V_0Q\rangle = (1-\mathcal{R}_{pq}) \begin{vmatrix} p\alpha_1 & q\beta_1 \\ p\alpha_2 & q\beta_2 \end{vmatrix},$$

where $\mathcal{R}_{pq}$ exchanges spins between p and q thereby creating a singlet.

The results are given in Table II and do not differ by very much from the valence bond results. The (effective) mixing coefficients which, in a semiempirical theory, would be the key quantities are 0.14 and 0.16 for the valence-bond and molecular-orbital functions respectively. The concordance is all that could be desired.

Calculations like the preceding ones become quite involved for more than two electrons, so we have attempted to treat the problem using a one-electron effective Hamiltonian which essentially gives Hückel Theory. This technique is used on H_3^+ and H_5^+, where a comparison with the many-electron results is possible, and then on H_7^+ as well.

The Hamiltonian used is[14]

$$H = \sum_\nu h_\nu$$

(summed over the electrons) where

$$h_\nu = T_\nu + \sum_i [Z_i - (1/r_{i\nu})]$$

(summed over the nuclei). The Z's in h_ν are

$$Z_a = \Omega_a[(n-2)/(n-1)] \int a \sum_{i \neq a} (1/r_i)\, a\, d\tau$$

where a is an AO on center a and the operator Ω_a has the property

$$\Omega_a b = \delta_{ab} b.$$

The factor $(n-2)/(n-1)$ is introduced to account for the loss of an electron in forming a positive ion. For a negative ion the factor $n/(n-1)$ would be used.

The *modus operandi* is analogous to the antisymmetrized molecular orbital calculation above in that Slater determinants must be used, but having the Hamiltonian, H, a sum of one-electron parts makes the calculation reduce to a one-electron calculation modified by an extra factor of $2^{\frac{1}{2}}$ in all matrix elements connecting the N and V states.

The wave functions derived for the equilibrium positions involve the following LCAO molecular orbitals with weights correct for $Q=0$

H_3^+

$$p = 0.279(a+c) + 0.633b$$

$$q = 0.785(a-c)$$

H_5^+

$$p = 0.262(a+e) + 0.299(b+d) + 0.358c$$

$$q = 0.483(a-e) + 0.336(b-d)$$

$$r = 0.670(a+e) - 0.118(b+d) - 0.647c$$

H_7^+

$$p = 0.052(a+g) + 0.146(b+f) + 0.330(c+e) + 0.413d$$

$$q = 0.182(a-g) + 0.362(b-f) + 0.349(c-e)$$

$$r = 0.387(a+g) + 0.393(b+f) - 0.099(c+e) - 0.451d$$

$$s = 0.601(a-g) + 0.026(b-f) - 0.573(c-e).$$

The results are given in Table III. Comparison with Table II shows that the mixing coefficients and ultraviolet intensities are about the same as calculated using the true Hamiltonian. The ultraviolet transition energies are somewhat smaller, which may make the $\mathbf{M}'m^{\frac{1}{2}}$ values calculated here a little too large. The fact that the magnitude of the mixing coefficients is 0.185 both for H_5^+ and H_7^+ is noteworthy. According to this result any change in the charge factor in the infrared intensity must be attributed to changes in the ultraviolet intensity divided by the ultraviolet frequency. In fact the theoretical $\mathbf{M}'m^{\frac{1}{2}}$ values go up very nearly as the square of the chain length, reflecting the dual dependence on $\langle N|\mathbf{M}|V\rangle$ and $(E_V - E_N)^{-1}$, which means that quite apart from the amplitude factor $(\hbar/2\omega m)^{\frac{1}{2}}$, the actual intensities should increase as the fourth power of the chain length. Attempts are cur-

[14] W. D. Jones, J. Chem. Phys. 31, 1317 (1959).

TABLE III. Quantities occurring in the infrared intensity of H_3^+, H_5^+, and H_7^+. Effective Hamiltonian.

	E_V-E_N	$\langle N_0O\vert\,\mathbf{M}\,\vert V_0O\rangle$	$\langle N_0Q\vert\,H-E_N\,\vert V_0Q\rangle' m^{\frac{1}{2}}$	$\langle N_0Q\vert\,\mathbf{M}\,\vert N_0Q\rangle' m^{\frac{1}{2}}$	$\mathbf{M}' m^{\frac{1}{2}}$ (debyes/A)
H_3^+	0.244	−2.063	0.154	1.14	2.62 (12.6)
H_5^+	0.150	−3.46	−0.185	−1.56	−8.54 (41.0)
H_7^+	0.138	−5.02	0.185	1.87	13.5 (64.8)

rently being made to measure the infrared intensity for actual substances resembling the model compounds studied here.

APPENDIX

EVALUATION OF MATRIX ELEMENTS

All one-electron elements such as overlap and nuclear attraction integrals were evaluated by use of well-known analytical expressions.[7] Their derivatives were obtained directly from these analytical functions of the bond distances.

Analytical expressions were available for two of the electron repulsion integrals,

$$\int a_\mu b_\nu (r_{\mu\nu})^{-1} a_\mu b_\nu d\tau$$

and

$$\int a_\mu b_\nu (r_{\mu\nu})^{-1} b_\mu a_\nu d\tau.$$

Values for the remaining integrals were obtained from tables prepared by Barker *et al.*[15] The derivatives for these latter integrals were obtained by differentiating the approximate expression[16]

$$\int a_\mu b_\nu (r_{\mu\nu})^{-1} c_\mu d_\nu d\tau \cong \tfrac{1}{4}\int ac\,d\tau \int bd\,d\tau \Big[\int a_\mu b_\nu (r_{\mu\nu})^{-1} a_\mu b_\nu d\tau + \int a_\mu d_\nu (r_{\mu\nu})^{-1} a_\mu d_\nu d\tau + \int c_\mu b_\nu (r_{\mu\nu})^{-1} c_\mu b_\nu d\tau + \int c_\mu d_\nu (r_{\mu\nu})^{-1} c_\mu d_\nu d\tau\Big]$$

with respect to the various bond distances.

The numerical values for these elements were evaluated at the assumed internuclear distance of 2 a.u. The values used are available on request.

[15] R. S. Barker, H. Eyring, C. J. Thorne, and D. A. Baker, *Use of Electron Repulsion Integral Approximations in Molecular Quantum Mechanics*, (Tech. Rept. No. 2 of the Institute of Rate Processes and Department of Mathematics, University of Utah, 1953).

[16] A discussion of this approximate expression is found in Barker *et al.* (see footnote 15).

Reactions Initiated by the β Decay of Tritium. III. The Tritium-Cyclopropane System

PRESTON L. GANT AND KANG YANG

Radiation Laboratory, Continental Oil Company, Ponca City, Oklahoma

(Received December 2, 1959)

The β decay of tritium in the gaseous tritium-cyclopropane system initiates reactions forming various tritiated compounds. Identified products are cyclopropane, propane, propylene, isobutane, ethane, ethylene, and acetylene. Dependence of the labeling yields on T_2 concentration clearly showed that energetic electrons as well as the decay species $(He^3T)^+$ initiated the labeling processes. Ionic and/or hot-atom reactions are assumed to occur to explain the effects of nitric oxide and temperature on the labeling yields.

I. INTRODUCTION

HIGH activation energy is required for reactions of the type

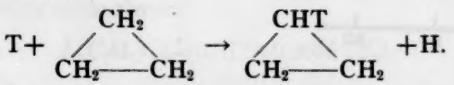

Recoil tritons with high kinetic energy thus replace hydrogen in cyclopropane,[1] but thermal deuterium atoms do not.[2]

We found that β decay of tritium initiates such high-energy processes. In addition, we confirmed the formation of the following tritiated compounds (in the gaseous tritium-cyclopropane system); propane, propylene, isobutane, ethane, ethylene, and acetylene. The kinetics of the formation of these compounds was investigated, and the results are reported here.

Use of an experimental parameter, $L(X)$, facilitates the understanding of labeling mechanisms.[3] This term, $L(X)$, was defined as the number of tritium atoms incorporated in a compound X, per tritium atom decayed. If $L(X)$ is independent of (T_2),[4] then labeling processes yielding tritiated compound X involved the decay species $(He^3T)^+$,[3] while dependence of $L(X)$ on (T_2) shows that energetic electrons play a role.[3]

Further details of the labeling mechanism are obtained by investigating the effects of nitric oxide and temperature on the $L(X)$ values.

II. EXPERIMENTAL

Matheson's cyclopropane (99.5%) and nitric oxide (99%) were degassed by repeated evacuation at liquid-nitrogen temperature, then subjected to trap-to-trap distillation on a high-vacuum line. Carrier-free tritium gas received from Oak Ridge National Laboratory was used without purification.

Reaction was started by introducing varying amounts of tritium (1 to 8 C) into cyclopropane (70 cm Hg, 25°C, 156 cc) contained in a cylindrical Pyrex vessel (5.1 cm in diam and 7.6 cm long). In some experiments, cyclopropane was premixed with nitric oxide (4.2 cm Hg, 25°C, 156 cc).

The product analyses were made using a gas chromatograph modified by the addition of a 10-cc ion chamber and a vibrating-reed electrometer.[5] Other details of the experimental methods were described previously.[3]

III. RESULTS

A. Labeled Products

Our results on the formation of labeled compounds are summarized in Figs. 1 to 7 and Table I.[6] The $L(X)$ values in Table I and Fig. 1 are extrapolations to zero time. They were calculated from the relation

$$L(X) = 1.55 \times 10^5 (d/dt)[X]/[T_2] \quad (t \text{ in hr}).$$

Here, $[X]/[T_2]$ is the area of the X peak over the area of T_2 peak in the chromatogram.

Cyclopropane

The $L[(CH_2)_3]$ is composed of two parts, one (T_2) dependent and the other (T_2) independent (Fig. 1). Here $(CH_2)_3$ denotes cyclopropane. The rate of formation of tritiated cyclopropane at 0°C is lower than at 25°C (Fig. 2 and Table I). Nitric oxide partly inhibits its formation (Fig. 2). The part of $L[(CH_2)_3]$ corresponding to the nitric-oxide-inhibited rate does not depend on (T_2) (Table I).

TABLE I. Labeling yields at various experimental conditions. $L(X)$ is defined as the number of tritium atoms incorporated in a compound X, per tritium decayed.

Exptl. conditions	$L[(CH_2)_3]$	$L(C_3H_8)$	$L(C_3H_6)$	$L(C_2H_4)$
4 C, 0°C, NO absent	0.104	0.245	0.180	0.046
4 C, room temp, NO absent	0.135	0.237	0.178	0.051
4 C, room temp, NO present	0.056	0	0.034	0.030
8 C, room temp, NO present	0.056	0	0.053	0.053

[1] J. K. Lee, B. Musgrave, and F. S. Rowland, J. Am. Chem. Soc. **81**, 3803 (1959).
[2] H. S. Shiff and E. W. R. Steacie, Can. J. Chem. **29**, 1 (1951).
[3] K. Yang and P. L. Gant, J. Chem. Phys. **31**, 1589 (1959).
[4] It has been convenient in much of the following discussion to express the concentration of tritium as (T_2), the number of curies present in the constant-volume reaction system.
[5] P. Riesz and K. E. Wilzbach, J. Phys. Chem. **62**, 6 (1958).
[6] Due to the presence of HT (0.06%) and tritiated methane (0.2%) in T_2 gas, the rates of formation of these compounds were not measurable.

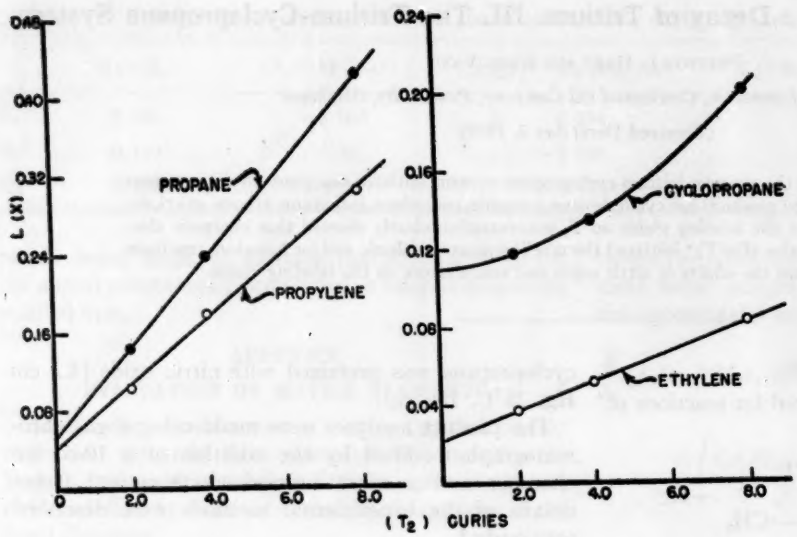

FIG. 1. Dependency of $L(X)$ values on (T_2).

Propane and Propylene

Yields of labeled propane and propylene are related to (T_2) as follows:

$$L(C_3H_8)=0.052+0.0462\ (T_2)$$

$$L(C_3H_6)=0.041+0.0376\ (T_2);\qquad (T_2)\text{ in C.}$$

Temperature has no effect on the initial rate of formation of either compound (Figs. 3 and 4). Nitric oxide completely inhibits the propane formation but only partly the propylene formation.

Isobutane

Due to tailing of the cyclopropane peak in the chromatograph, the isobutane analysis involved large uncertainties. The $L(iso\text{-}C_4H_{10})$ was approximately 0.06. Within experimental accuracy, $L(iso\text{-}C_4H_{10})$ did not depend on (T_2) or temperature; however, nitric oxide completely eliminated its formation.

Ethylene

When nitric oxide is absent, $L(C_2H_4)$ sharply decreases with increasing reaction time (Fig. 5). In the presence of nitric oxide, $L(C_2H_4)$ is constant over the reaction periods, i.e., the plot of $[C_2H_4]/[T_2]$ vs time is

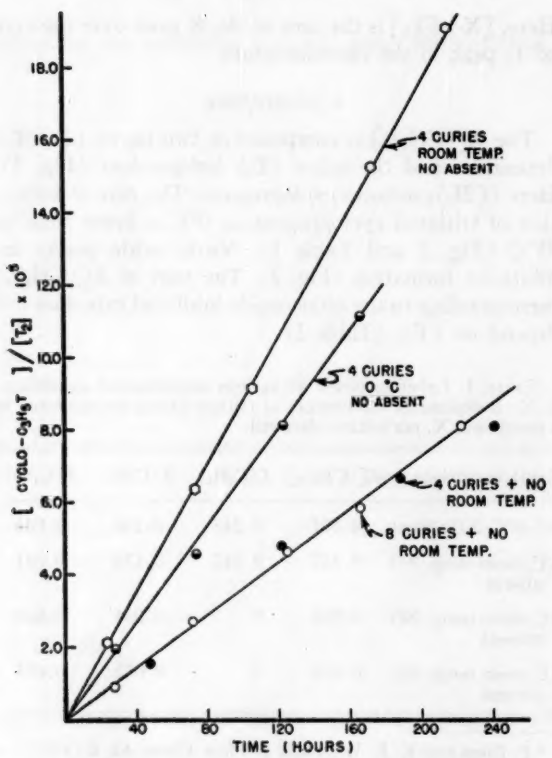

FIG. 2. Formation of labeled cyclopropane at various experimental conditions.

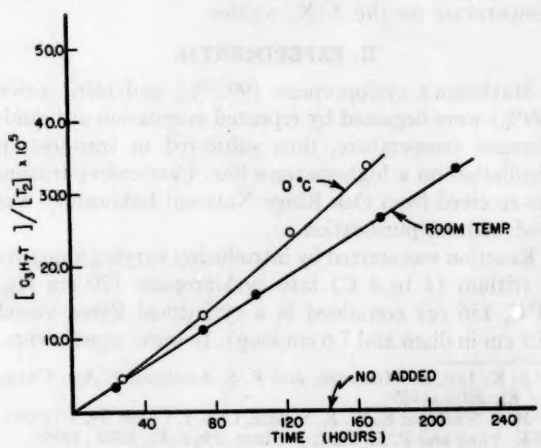

FIG. 3. Formation of labeled propane at various experimental conditions.

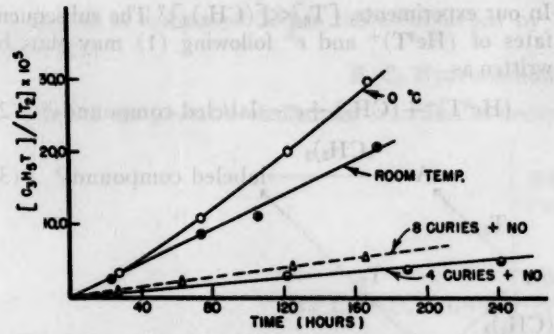

FIG. 4. Formation of labeled propylene at various experimental conditions.

linear (Fig. 5). Dependence of $L(C_2H_4)$ on (T_2) is

nitric oxide absent:

$$L(C_2H_4)_{t\to 0}=0.022+0.0076\ (T_2);$$

nitric oxide present:

$$L(C_2H_4)=0.005+0.0076\ (T_2).$$

Ethane and Acetylene

The rate of formation of labeled ethane increases with increasing (T_2) and is higher at the lower temperature (Fig. 6). Nitric oxide completely eliminates its formation. The formation of acetylene is only measurable at high (T_2) and in the presence of nitric oxide (Fig. 7). The plots of $[X]/[T_2]$ vs time for both ethane and acetylene are markedly concave. They are probably formed by the secondary processes involving a radiolysis product (most likely ethylene).

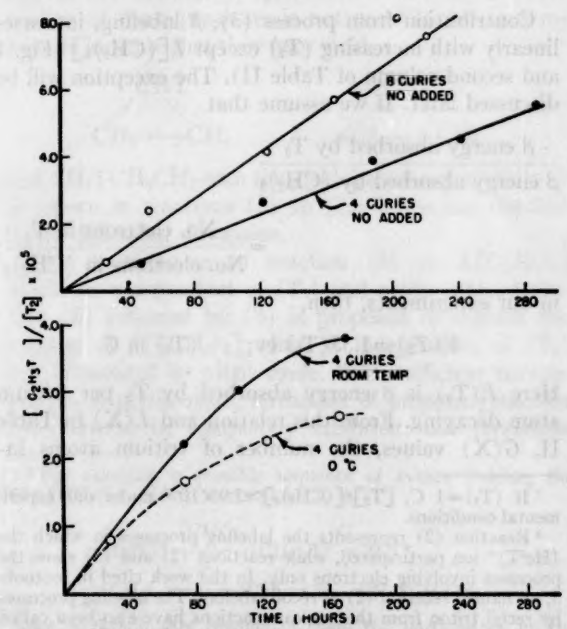

FIG. 5. Formation of labeled ethylene at various experimental conditions.

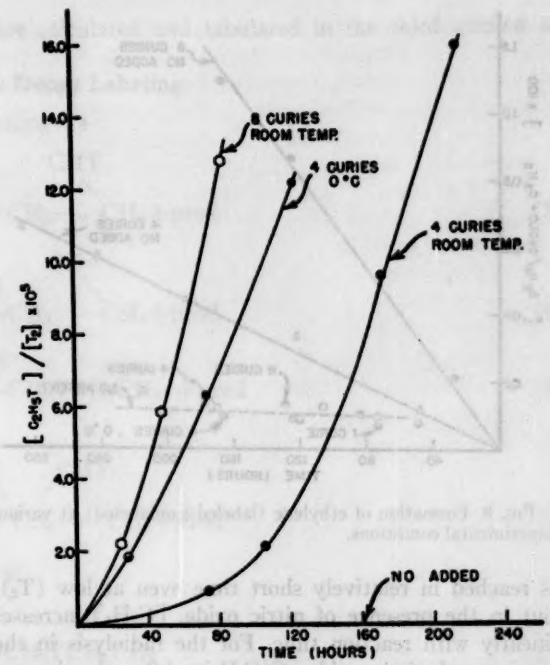

FIG. 6. Formation of labeled ethane at various experimental conditions.

B. Total (Labeled + Unlabeled) Products

The thermal conductivity cell on the chromatograph confirmed the formation of ethylene, ethane, propane, and propylene. The yield of propylene was too small for quantitative measurements. Figure 8 shows the formation of total ethylene at various experimental conditions. When nitric oxide is absent, $[C_2H_4]$ reaches a steady-state value. It is important in the subsequent discussion to observe that the steady state $[C_2H_4]$ is quite substantial—of the order of 0.1% of $[(CH_2)_3]$—and

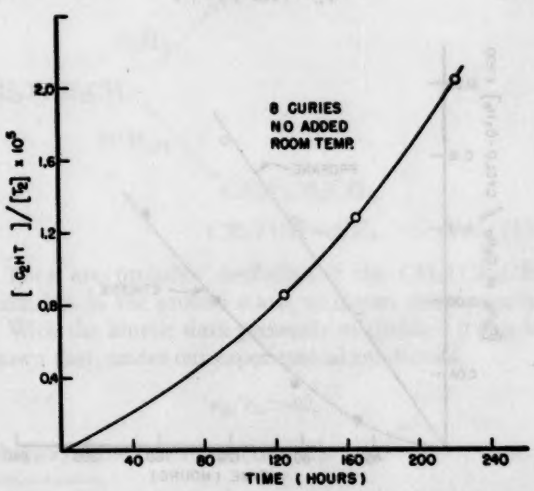

FIG. 7. Formation of labeled acetylene; $(T_2)=8$ C; NO added; room temperature.

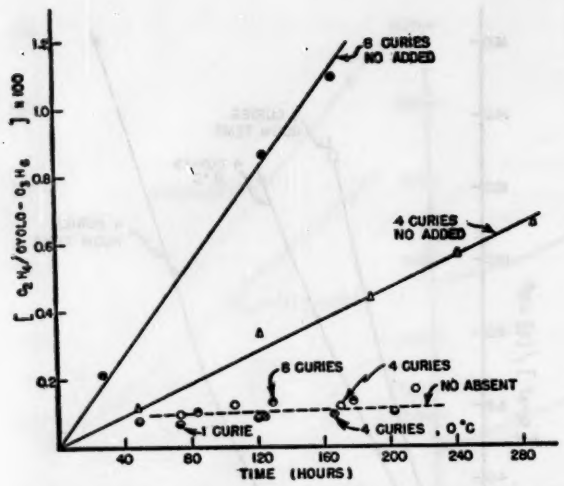

FIG. 8. Formation of ethylene (labeled+unlabeled) at various experimental conditions.

is reached in relatively short time even at low (T_2); but in the presence of nitric oxide, $[C_2H_4]$ increases linearly with reaction time. For the radiolysis in the presence of nitric oxide, $G(C_2H_4)\simeq 4.0$ molecules per 100 ev absorbed by cyclopropane.

Figure 9 shows the formation of total ethane and propane. Nitric oxide completely inhibits their formation. In the absence of the inhibitor, $G(C_3H_8)\simeq 0.8$ molecules per 100 ev absorbed by cyclopropane. The rate curve for ethane strongly suggests that secondary reactions involving radiolysis products play an important role in the formation of ethane.

IV. DISCUSSION

A. Decay and β Labeling

The initial reaction in this system is

$$T_2 \rightarrow (He^3T)^+ + e^- . \qquad (1)$$

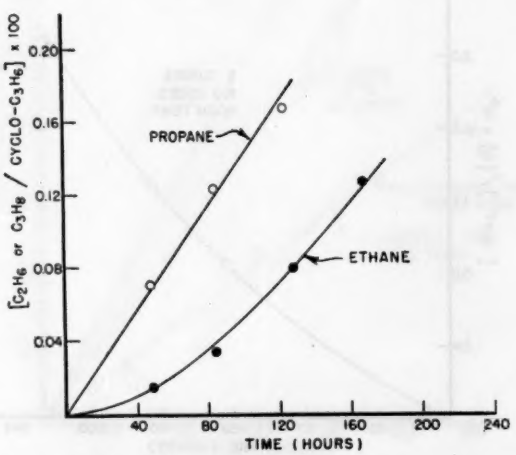

FIG. 9. Formation of propane and ethane (labeled+unlabeled); $(T_2)=8$ C, room temperature, NO absent.

In our experiments, $[T_2] \ll [(CH_2)_3]$.[7] The subsequent fates of $(He^3T)^+$ and e^- following (1) may thus be written as

$$(He^3T)^+ + (CH_2)_3 + e^- \rightarrow \text{labeled compounds}^8 \qquad (2)$$

$$A \xrightarrow{(CH_2)_3} \text{labeled compounds}^8 \qquad (3)$$

$$e^- \xrightarrow{T_2} A, \quad e^- \xrightarrow{(CH_2)_3} B, \quad A \xrightarrow{T_2} \text{labeled compounds}^8, \quad B \xrightarrow{(CH_2)_3} \text{unlabeled compounds.} \qquad (4)$$

Here, A and B represent excited species including ions and radicals. Process (2), to be called decay labeling,[8] makes a contribution, $L(X)_d$, to $L(X)$ that tends to be independent of (T_2). The $L(X)_d$ values estimated from the intercepts of lines in Fig. 1 are summarized in the first column of Table II. Tritiated cyclopropane is the main product of this process.

TABLE II. Labeling yields by decay and β labeling. $L(X)$ is defined as the number of tritium atoms incorporated in a compound X per tritium decayed. $G(X)$ is the number per 100 ev absorbed by tritium gas. Subscripts d and β distinguish decay and β labeling.

X	$L(X)_d$	$L(X)_\beta/T_2$	$G(X)$
Cyclopropane	0.109	?	?
Propane	0.052	0.0462	3.42
Propylene	0.041	0.0376	2.79
Ethylene	0.022	0.0076	0.56

Contribution from process (3), β labeling, increases linearly with increasing (T_2) except $L[(CH_2)_3]$ (Fig. 1 and second column of Table II). The exception will be discussed later. If we assume that

$$\frac{\beta \text{ energy absorbed by } T_2}{\beta \text{ energy absorbed by } (CH_2)_3} = \frac{\text{No. electrons in } T_2}{\text{No. electrons in } (CH_2)_3};$$

in our experiments, then,

$$E(T_2) = 1.35(T_2) \text{ ev}; \qquad (T_2) \text{ in C.}$$

Here $E(T_2)$ is β energy absorbed by T_2 per tritium atom decaying. From this relation and $L(X)$ in Table II, $G(X)$ values, the number of tritium atoms in-

[7] If $(T_2)=1$ C, $[T_2]/[(CH_2)_3]\simeq 2.9\times 10^{-3}$ under our experimental conditions.

[8] Reaction (2) represents the labeling processes in which the $(He^3T)^+$ ion participated, while reactions (2) and (3) show the processes involving electrons only. In the work cited in footnote 3, we named reaction (2) as recoil labeling. The labeling processes by recoil triton from the nuclear reactions have also been called recoil labeling (see footnote 1). In order to distinguish two phenomena, we shall hereafter call reaction (2) decay labeling.

corporated in compound X per 100 ev absorbed by T_2 are calculated and tabulated in the third column of Table II.

B. C_3 Hydrocarbons by Decay Labeling

Some of the probable elementary reactions in decay labeling are

$$(He^3T)^+ + (CH_2)_3 + e^- \begin{cases} \xrightarrow{0.056} \text{CHT}(CH_2)_2 + \text{prod} & (5) \\ \xrightarrow{<0.053} \text{CT}\cdot(CH_2)_2 + \text{prod} & (6) \\ \xrightarrow{<0.093} CH_2TCH_2CH_2\cdot + \text{prod} & (7) \end{cases}$$

$$\text{CT}\cdot(CH_2)_2 + R \begin{cases} \xrightarrow{0.053} \text{CHT}(CH_2)_2 + \text{prod} & (8) \\ \longrightarrow ? \end{cases}$$

$$CH_2TCH_2CH_2 + R \begin{cases} \xrightarrow{0.051} CH_2TCH_2CH_3 & (9) \\ \xrightarrow{0.041} CH_2TCH{=}CH_2 + \text{prod.} & (10) \\ \longrightarrow ? \end{cases}$$

Here R denotes free radicals resulting from the β radiolysis of cyclopropane. Reactions (5) to (7) probably involve various elementary steps with ions and/or hot radicals.[9] At present, an unambiguous discussion of these processes is not possible; but our results do indicate that they may yield

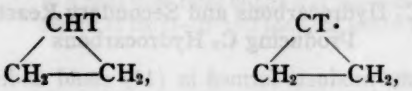

and $CH_2TCH_2CH_2$ with the yield (per decay of tritium) as shown in reactions (5) to (7). These are clarified in the following discussion.

The contribution of reaction (5) to $L[(CH_2)_3]$ would be independent of (T_2) and nitric oxide. Reaction (6) followed by (8) is proposed to explain the portion of $L[(CH_2)_3]$ which is independent of (T_2) but eliminated by nitric oxide. With sufficient concentration of nitric oxide, formation of propane [reaction (9)] should be completely inhibited; but propylene may still be formed by the reaction

$$CH_2TCH_2CH_2\cdot + NO \rightarrow HNO + CH_2TCH_2\cdot \quad (11)$$

Besides reaction with free radicals, reactions (8)–(10), tritiated propyl and cyclopropyl radicals could react with ethylene resulting from the β radiolysis of cyclorpropane and with cyclopropane itself:

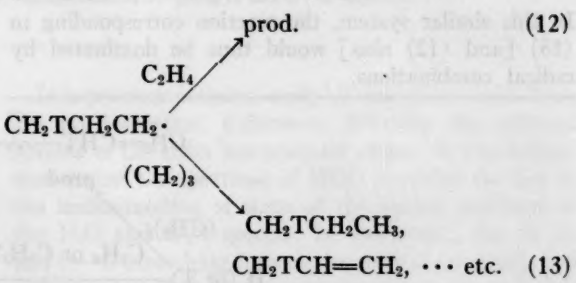

They are probably negligible if the $CH_2TCH_2CH_2$ radical is in the ground state, as shown subsequently.

With the kinetic data presently available,[10] it can be shown that, under our experimental conditions,

$$r_{13}/r_{12} \simeq 40,$$

where r_i is the rate of reaction (i).

[9] For example, a possible sequence of events yielding the $CH_2TCH_2CH_2$ radical in reaction (7) is

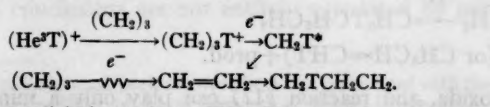

Since a β-radiolysis product, $CH_2{=}CH_2$, participates in the formation of $CH_2TCH_2CH_2$, these reactions may be responsible for the slight nonlinearity observed in Figs. 3 and 4.

[10] Recently published rate constant for methyl-ethylene reaction [R. K. Brinton, J. Chem. Phys. **29**, 781 (1958)] was taken to be k_{12}. For k_{13}, see work cited in footnote 11.

If reaction (13) is as important as reactions (9) and (10), then we expect the following: (a) The $L(C_3H_8)$ and $L(C_3H_6)$ deviate from the linear increase with increasing (T_2), and (b) the $L(C_3H_8)$ and $L(C_3H_6)$ depend on the temperature. Since none of these are observed in our experiments (Fig. 1 as well as Table I), it must be assumed that the extent of reaction (13) is negligible for the values of (T_2) at which these observations are made.

In order to show that this is a plausible assumption, we shall consider an analogous system (for which some rate information is available) in which methyl radicals are being generated at a rate r_i and are being removed by the following reactions:

$$CH_3\cdot + (CH_2)_3 \xrightarrow{k_p} \text{prod}$$

$$2CH_3\cdot \xrightarrow{k_t} \text{prod.}$$

At a steady state,

$$[R]=\frac{-k_p[(CH_2)_3]+(k_p^2[(CH_2)_3]^2+4k_tr_i)^{\frac{1}{2}}}{2k_t}.$$

For r_i we shall use an estimate of the rate at which H atoms are formed in the tritium-cyclopropane system. With 1 C of tritium present and assuming the formation of one radical per 30 ev, that rate would be 7.3×10^{-14} moles cc^{-1} sec^{-1}; taking $k_p=10^{11}\exp(-10\,300/RT)$ $mole^{-1}$ cc sec^{-1} [11] and $k_t=10^{13.6}\exp(-0\pm700/RT)$ $mole^{-1}$ cc sec^{-1} [12] gives

$$[CH_3\cdot]=4.2\times10^{-13}\text{ moles cc}^{-1}$$

and

$$k_p[CH_3][(CH_2)_3]/k_t[CH_3\cdot]^2\simeq7\times10^{-3}.$$

In this similar system, the reaction corresponding to (13) [and (12) also] would thus be dominated by radical combinations.

C. C_3 Hydrocarbons by β Labeling

Present experimental results are not sufficient to suggest elementary reactions leading to β labeling. A general picture of these processes might be given as follows:

$$T_2+(CH_2)_3 \xrightarrow{e^-} CH_2TCH_2CH_2\cdot, \quad (14)$$

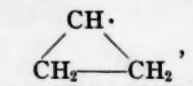

$$CH_2{=}CH_2, \text{ etc.}$$

$$+T \quad (15)$$

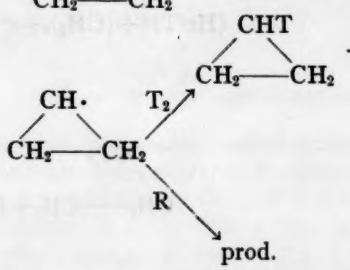

$$\text{prod.} \quad (16)$$

Tritiated propyl radicals formed in (14) react with free radicals to give propane and propylene [reactions (9) and (10)]. These contributions to $L(C_3H_8)$ and $L(C_3H_6)$ increase linearly with increasing (T_2). It is likely that the reactions yielding propyl radicals in (14) involve ionic and or hot-atom species. This would explain the fact that the rates of formation of propane and propylene are initially independent of temperature (Figs. 3 and 4 and Table I).

The contribution to $L[(CH_2)_3]$ from reaction (15) would be (T_2)-dependent and would increase with increasing temperature and be eliminated by nitric oxide. Because of competition with reaction (16), a linear increase of $L[(CH_2)_3]$ with (T_2) would not be expected (Fig. 7).

D. C_2 Hydrocarbons and Secondary Reactions Producing C_3 Hydrocarbons

Various products formed in (14) could undergo the following reactions:

$$CH_2{=}CHT \xrightarrow{e^-} CH{\equiv}CT^+ + \text{prod}, \quad (17)$$

$$H\ (\text{or T}) + (CH_2)_3 \xrightarrow{C_2H_4 \text{ or } C_2H_3T} \text{prod} + C_2H_4T \xrightarrow{R} CH_2TCH_3 \ (\text{or } CH_2{=}CHT) + \text{prod}, \quad (18)$$

$$CH_2T^* + (CH_2)_3 \xrightarrow{C_2H_4} \text{prod.} + CH_2TCH_2CH_2 \xrightarrow{R} CH_2TCH_2CH_2 \ (\text{or } CH_3CH{=}CHT) + \text{prod}. \quad (19)$$

Reactions (18) and (19) will be suppressed by nitric oxide, and reaction (17) can play only a minor role since acetylene yields are very small; thus the amount of ethylene formed, presumably by ionic or hot-atom

[11] A. F. Trotman-Dickenson and E. W. R. Steacie, J. Chem. Phys. **19**, 329 (1951).
[12] R. Gomer and G. B. Kistiakowsky, J. Chem. Phys. **19**, 85 (1951).

reactions, in (14) will increase with increasing time (Figs. 5 and 8). In the absence of nitric oxide, ethylene will be consumed by reaction with thermalized radicals; and $[C_2H_4]$ will approach a steady-state value. If the principal source of thermalized tritium atom is the decay species $(He^3T)^+$ (i.e. $(He^3T)^+ + e^- \rightarrow He^* + T$, etc.), then the part of $L(C_2H_4)$ due to (18) would be independent of (T_2) (Fig. 1).

Reaction (19) explains the increase in the rate of formation of tritiated propane and propylene at longer reaction time. The excited methyl radicals in (20) may come from the reactions

$$(CH_2)_3^+[\text{or } (CH_2)_3] + T_2 \text{ (or } T_2^+) \rightarrow (CH_2)_3T^+ \xrightarrow{e} CH_2T^* + CH_2{=}CH_2, \text{ etc.}$$

If the CH_2T^* radical had an excitation energy available for reaction in the order of 4–9 kcal, then we would expect a slight increase in the rate of formation of tritiated propane (or propylene) at lower temperature because of competing reactions in (19).

V. SUMMARY

Various tritiated products are formed when β decay of tritium occurs in gaseous cyclopropane. Both the decay species $(He^3T)^+$ and energetic electrons initiate labeling processes. Ionic and/or hot-atom reactions together with thermalized free radical processes explain our results.

VI. ACKNOWLEDGMENTS

Dr. L. O. Morgan and Dr. F. H. Dickey offered valuable discussions in the preparation of this manuscript.

THE JOURNAL OF CHEMICAL PHYSICS VOLUME 32, NUMBER 6 JUNE, 1960

Inter- and Intramolecular Potentials and the Spectrum of Ice*

C. HAAS† AND D. F. HORNIG

Frick Chemical Laboratory, Princeton University, Princeton, N. J.

(Received December 28, 1959)

Whereas the spectra of H_2O and D_2O ice cannot yet be explained unambiguously, the spectra of HDO in dilute solution in either H_2O or D_2O may be interpreted readily. In particular, since ν_{OH} occurs at 3275 cm^{-1} and $2\nu_{OH}$ at 6300 cm^{-1}, nearly the harmonic value, the barrier to proton transfer lies well above the latter level and must exceed 23 kcal/mole. The width of ν_{OD} at 2416 cm^{-1} is only 20 cm^{-1}, whereas that of ν_{OH} is about 80 cm^{-1} and $2\nu_{OH}$ about 600 cm^{-1}. These widths can be explained by proton tunneling if the barrier height is near 32 kcal, in which case the second minimum must lie below the level ν_{OH}. It must therefore be less than 14 kcal/mole above the primary minimum. A doubling of ν_{OD} from OD···OD pairs was also observed and the magnitude of the splitting is consistent with an effective charge of 0.6e on the protons. It is clear from these results that the usual width of hydrogen bonded OH lines is not an intrinsic characteristic of the O—H···O bond but results largely from intramolecular coupling of the O—H motions.

ICE has recently been the subject of extensive and critical reviews by a series of authors.[1] The main results of the structural studies by means of x rays, electron diffraction, and neutron diffraction have been (1) to confirm the Pauling disorder in hexagonal ice, (2) to establish the existence of a cubic phase between about −80°C and −140°C, and (3) to show that the solid deposited from the vapor below −140°C is probably a glass. The numerous infrared and Raman spectra which have been obtained are consistent but as yet there is no general agreement on their interpretation. This literature was extensively reviewed by Ockman,[2] but his conclusions are not entirely supported by our work.

In a previous infrared study[3] it was shown that there are no important differences between the infrared spectra of the three low-pressure phases. It was further shown that the spectrum of HDO provided the key to the understanding of some of the vexing problems of the H_2O and D_2O spectra. In particular, the O—H and O—D stretching frequencies were determined, and these must lie midway between the symmetric and antisymmetric frequencies in H_2O and D_2O. On this basis, it was concluded that the three frequencies in the 3300 cm^{-1} region should be assigned to the overtone of the bending frequency ($2\nu_2$, ca 3150 cm^{-1}), the asymmetric stretch (ν_3, ca 3250 cm^{-1}) and the symmetric stretch (ν_1, ca 3350 cm^{-1}). Ockman reversed the assignment of $2\nu_2$ and ν_1, and the fact that the highly polarized peak at 3150 cm^{-1} is the most intense peak in the Raman spectrum appears to support his position.

* The experimental work reported here was carried out with the support of the Office of Naval Research at Brown University.

† Present address: Philips Research Laboratory, Eindhoven, Netherlands.

[1] Advances in Phys. 7, No. 26 (1958).

[2] N. Ockman, Advances in Phys. 7, 199–200 (1958).

[3] D. F. Hornig, H. F. White, and F. P. Reding, Spectrochim. Acta, 12, 338 (1958).

There are still more complications. The HOD criterion does not support an assignment of the stretching region in D_2O corresponding to that in H_2O. Furthermore, a peak was located in the HDO spectrum at 1470 cm^{-1} which was assigned to the bending mode. However, we have since realized that this frequency is too high to agree with what are usually thought of as the bending frequencies in H_2O and D_2O: this again raises the question whether the bands at 1600 and 1200 cm^{-1} in H_2O and D_2O are really bending modes or overtones of the librations at 850 and 605 cm^{-1}. We have, unfortunately, no new information on this score.

The present investigation was undertaken because it was felt that, without regard to H_2O and D_2O, more information could be obtained from the infrared spectrum of HDO as to (1) the quantitative evaluation of the inter- and intramolecular potential function in ice and (2) the source of the broadening of the stretching frequencies in hydrogen-bonded systems.

EXPERIMENTAL TECHNIQUES

The samples of ice were studied in a low-temperature cell similar to those used previously.[3] In order to prepare the films, a flask with a mixture of H_2O and D_2O vapor of the desired composition and pressure was connected to the evacuated cell by a copper tube and stopcock; when the stopcock was opened, a small stream of the vapor was blown on the cooled AgCl window mounted in the cell, and a film of ice was slowly condensed on the window. The films showed very little scattering; the thin ones employed in regions of strong absorption scattered only a few percent, while the thick films used to study overtones showed a maximum scattering of 50% at 10 000 cm^{-1}. No attempt was made to measure the thickness of the films.

A number of films were made by condensing vapor on a window maintained at −80°C in order to be sure that hexagonal ice was obtained. To do this, the pressure in the cell had to be at least 10 μ Hg to avoid evaporation of the film. However, a careful comparison of the spectra of films prepared in this way with those of films condensed at −190°C showed no detectable differences. All of our spectra, though, show more structure and, in some cases, sharper bands than most of those reported in the literature, leading us to believe there was a high degree of crystallinity in our films. In that case, the broad structureless bands which have been reported may be characteristic of the glassy form of ice.

This observation appears to conflict with the x-ray and electron-diffraction studies. However, the thin (4-mm) AgCl window had a low heat capacity; ice has a large heat of sublimation, and the thermal contact between the window and cold-metal block was rather bad. In view of these facts, it is not impossible that during film formation the surface of the window was considerably warmer than the copper block to which our thermocouple was connected. This conclusion is supported by the observation that no ice condensation was observed during film formation for about 15 minutes after the thermocouple first read −190°C. It therefore seems quite likely that the films were crystalline and consisted of cubic ice. That the spectra were identical with those of hexagonal ice is not surprising since the nearest neighbor geometry is identical in the two phases.

The infrared spectra were studied from 660 cm^{-1} to 10 000 cm^{-1} on a double-beam spectrometer similar to that described previously,[4] using NaCl, CaF_2, and quartz prisms.

RESULTS

The infrared spectra of thin films of H_2O, HDO, and D_2O at −190°C are reproduced in Figs. 1 and 2. By comparing the spectra of films of different composition, it is usually possible to decide which molecule is responsible for each band. The spectra have been analyzed in this way and the various bands ascribed to the three molecules present. The results are shown in Table I and compared with those of footnotes 2 and 3.

The spectra agree well with those obtained previously, but a number of significant new features appear. Chief among them are (1) the overtone of the HOD bending vibration at 2875 cm^{-1} and (2) the combination $\nu_{OH}+\nu_{OD}$ at 5720 cm^{-1} as well as the overtone $2\nu_{OH}$ at 6300 cm^{-1} in HDO, which make it possible to evaluate the O—H potential in these molecules.

A special region of particular interest is shown in Fig. 3. For a 10% solution of HDO in H_2O, a sharp O—D stretching band (width only 20 cm^{-1}) appears at 2416 cm^{-1}. When the HDO concentration is increased to 18%, two side bands appear at 2393 cm^{-1} and 2442 cm^{-1}; if the D concentration is increased still further, the side bands spread out, and the appearance of the band approaches that in D_2O. These observations closely parallel those in HCl—DCl mixed crystals[5] and undoubtedly result from the coupling of the vibrations of hydrogen-bonded neighbors.

DISCUSSION

(a) Bending Vibration

The problem connected with the bending frequency is that in H_2O and D_2O the first overtone of the librational frequency is superimposed on the fundamental, while its own overtone is approximately coincident with the stretching frequencies. This is not the case with HOD, although overtones and combinations of librations may occur throughout the region from 1200 cm^{-1} to 1650 cm^{-1}, and the relatively sharp peak at 1490 cm^{-1} had previously been assigned to the HOD bend. We have now observed another HOD band at 2875 cm^{-1} whose corresponding assignment would be to the first overtone of the bend.

---

[4] D. F. Hornig, G. E. Hyde, and W. Adcock, J. Opt. Soc. Am. **40**, 497 (1950).

[5] D. F. Hornig and G. L. Hiebert, J. Chem. Phys. **27**, 752 (1957).

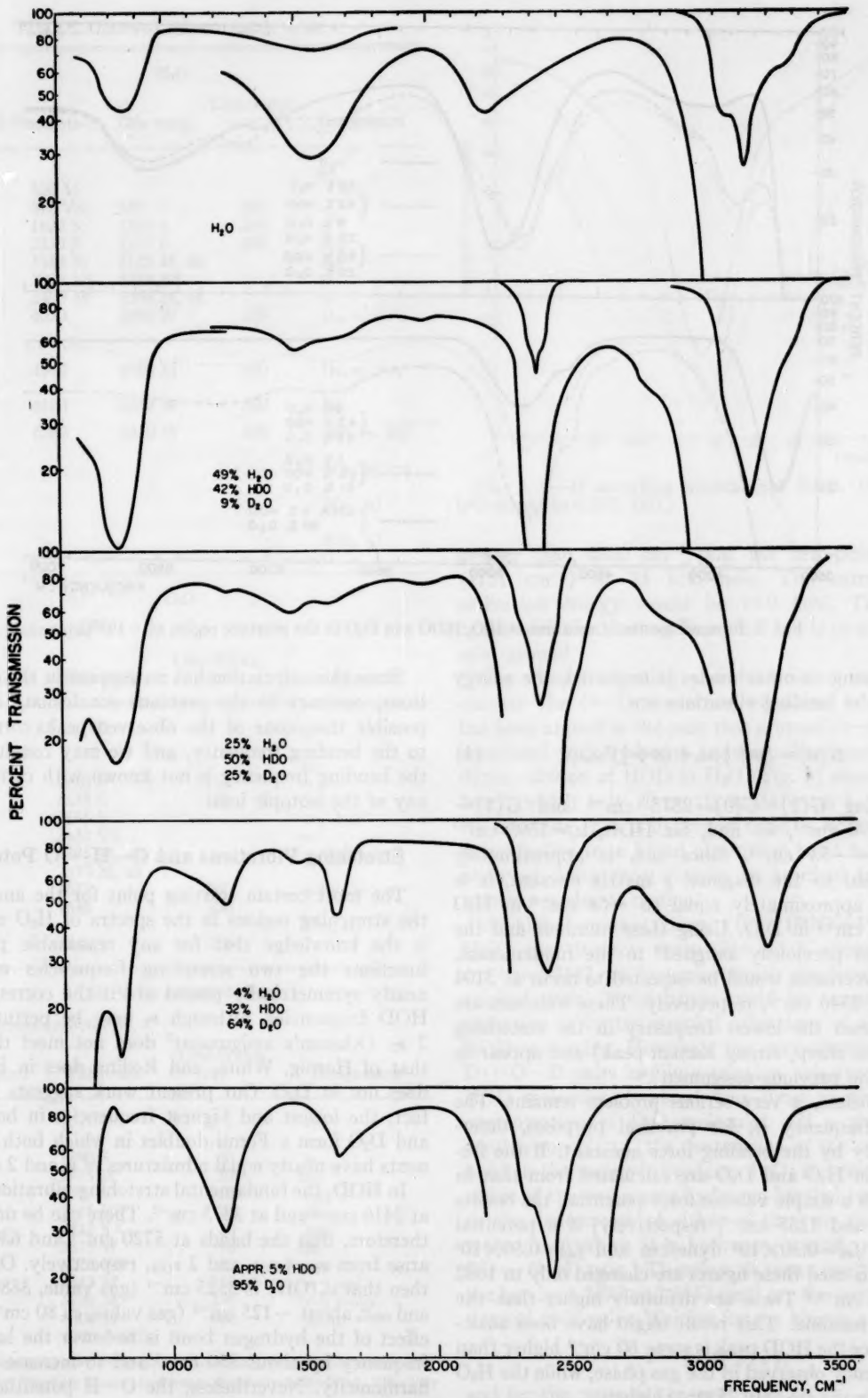

FIG. 1. Infrared spectra of mixtures of H_2O, HDO and D_2O at $-195°C$.

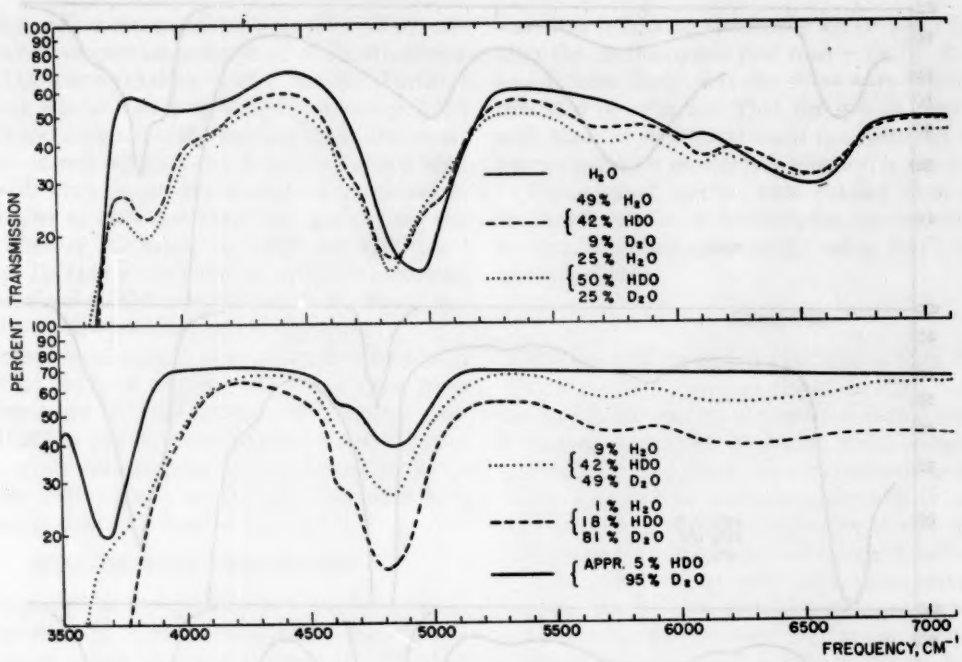

FIG. 2. Infrared spectra of mixtures of H_2O, HDO and D_2O in the overtone region at −195°C.

If coupling to other modes is neglected, the energy levels of the bending vibrations are

$$G(n)=(n+\tfrac{1}{2})\omega_e+(n+\tfrac{1}{2})^2\omega_e x_e. \qquad (1)$$

Substituting $G(2)-G(0)=2875$ cm^{-1} and $G(1)-G(0)=1490$ cm^{-1}, we find, for HDO, $\omega_e=1595$ cm^{-1} and $\omega_e x_e=-53$ cm^{-1}. Since $\omega_e x_e$ is approximately porportional to the diagonal g matrix element, it is therefore approximately equal to -68 cm^{-1} in H_2O and -37 cm^{-1} in D_2O. Using these numbers and the frequencies previously assigned[3] to the fundamental, the first overtones would be expected to occur at 3104 cm^{-1} and 2346 cm^{-1}, respectively. These numbers are not far from the lowest frequency in the stretching region (the sharp, strong Raman peak) and appear to confirm the previous assignment.[3]

Nevertheless, a very serious problem remains. The bending frequency is, for practical purposes, determined only by the bending force constant. If the frequencies in H_2O and D_2O are calculated from that in HOD with a simple valence force potential, the results are 1687 and 1255 cm^{-1}, respectively; if a potential including $f_{dd}=0.30\times10^5$ dyne/cm and $f_{ad}=0.50\times10^5$ dyne/cm is used these figures are changed only to 1682 and 1265 cm^{-1}.[6] These are definitely higher than the observed maxima. This result might have been anticipated since the HOD peak is some 80 cm^{-1} higher than the frequency observed in the gas phase, while the H_2O and D_2O peaks are only 25 cm^{-1} higher.

[6] H. F. White, thesis, Brown University, 1952.

Since this calculation has no support in the observations, contrary to the previous conclusion,[3] it seems possible that none of the observed peaks corresponds to the bending frequency, and we may conclude that the bending frequency is not known with certainty in any of the isotopic ices.

Stretching Vibrations and O—H···O Potential

The most certain starting point for the analysis of the stretching regions in the spectra of H_2O and D_2O is the knowledge that for any reasonable potential functions the two stretching frequencies must be nearly symmetrically placed about the corresponding HOD frequencies, although ν_1 may be perturbed by $2\,\nu_2$. Ockman's assignment[2] does not meet this test; that of Hornig, White, and Reding does in H_2O but does not in D_2O. Our present work suggests that, in fact, the lowest and highest frequencies in both H_2O and D_2O form a Fermi doublet in which both components have nearly equal admixtures of ν_1 and $2\,\nu_2$.

In HOD, the fundamental stretching vibrations occur at 2416 cm^{-1} and at 3275 cm^{-1}. There can be no doubt, therefore, that the bands at 5720 cm^{-1} and 6300 cm^{-1} arise from $\nu_{OH}+\nu_{OD}$ and $2\,\nu_{OH}$, respectively. One finds then that ω_e(OH) is 3525 cm^{-1} (gas value, 3880 cm^{-1}) and $\omega_e x_e$ about -125 cm^{-1} (gas value, ca 80 cm^{-1}). The effect of the hydrogen bond is to lower the harmonic frequency by about 350 cm^{-1} and to increase the anharmonicity. Nevertheless, the O—H potential is not greatly different from that in the gas, and the barrier for proton transfer to a neighbor must certainly be much

TABLE I. Observed infrared bands in ice.

H_2O				
Footnote 2	Footnote 3	This work	Line width (cm^{-1})	Assignment
160				ν_T
590	520 M			...
846	812 VS	850	200	ν_L
1580	1620 S	1585 S	250	ν_2
2235	2230 S	2225 S	200	$3\nu_L$
3140	3140 M	3125 M, sh		$2\nu_2$
3224	3220 VS	3210 VS		ν_3
3340	3400 M	3360 M, sh		ν_1
3975	4050	3990 W	250	$(\nu_1, \nu_3)+\nu_L$
4200 ?				...
4520 ?				...
4960	4940	4960 M	300	$(\nu_1, \nu_3)+\nu_2$
5600 ?				...
6062	6100	6050 W	300	$4\nu_2$
6400, 6672	6580	6550 W	400	$2(\nu_1, \nu_3, 2\nu_2)$
7685, 7856				$2(\nu_1, \nu_3)+\nu_2$
9000, 9520				$3(\nu_1, \nu_3)$
11 100, 12 500				$4(\nu_1, \nu_3)$

D_2O			
Frequency (cm^{-1})			
Footnote 3	This work	Line Width (cm^{-1})	Assignment
160	... W		ν_T
385 M	...		...
605 VS	...		ν_L
1212 S	1210 S	150	ν_2
1627	1635 S	180	$3\nu_L$
(2380)	2336 S		$(\nu_1, 2\nu_2)^-$
2440 VS	2432 VS		ν_3
(2520)	2495 M, sh		$(\nu_1, 2\nu_2)^+$
	2570 M, sh		
3720	3675	200	$\nu_1+\nu_2, \nu_3+\nu_2$
...	4640	100	$2(\nu_1, \nu_3)$
...	4840	250	

HOD (in dilute solution)			
Frequency (cm^{-1})			
Footnote 1	This work	Line Width (cm^{-1})	Assignment
600 VS	...	...	ν_{L1}
810 VS	...	...	ν_{L2}
1470 S	1490 S	50	ν_2
1925 W	1975 W	50	$3\nu_L$
...	2393 S[a]	20	ν_{OD}^+
2440 VS	2416 VS	20	ν_{OD}
...	2442 S[a]	20	ν_{OD}^-
...	2875 W	70	$2\nu_3$
3310 VS	3275 VS	80	ν_{OH}
...	3845 M	150	$\nu_3+\nu_{OD}$
...	5720 M	250	$\nu_{OH}+\nu_{OD}$
...	6300 M (6000–6600)	600	$2\nu_{OH}$

Intensity: VS=Very Strong; S=Strong; M=Medium; W=Weak; VW=Very Weak.
[a] 18% HOD solid solution in H_2O.
sh=shoulder.

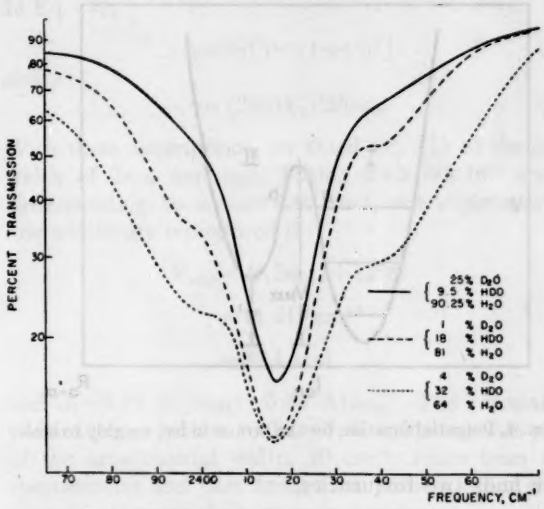

FIG. 3. O—D stretching vibration of HDO. (Note: 25% D^2O should be 0.25% D_2O.)

greater than 6300 cm^{-1} plus the zero-point energy (1731 cm^{-1}) or 23 kcal/mole. The corresponding activation energy would be 18.0 kcal. This finding agrees with that from ordinary ice[3] but is on much more solid ground.

The most interesting new features of our spectra concern the O—D stretching vibration in HOD. It has been argued in the past that a broad O—H band is associated with hydrogen bonding. The spectrum of a dilute solution of HOD in H_2O (Fig. 3) shows a sharp band (width only 20 cm^{-1}) at 2416 cm^{-1}. Therefore, we conclude that a hydrogen bond is not necessarily accompanied by a broad absorption band but that the observed width must usually be ascribed to coupling to other modes of motion.

At higher concentrations (18% HOD+1% D_2O in H_2O), two distinct, sharp side bands appear at 2393 cm^{-1} and 2442 cm^{-1}, symmetrically displaced from the original peak. These bands could be caused by D_2O molecules or by the coupled vibrations of neighboring HOD molecules. However, the concentration of O—D···O—D pairs in dilute solution, relative to that of HOD molecules, is about four times as great as the concentration of D_2O molecules. (If a given O—D bond is considered, the deuteration of the other O—D bond in the molecule produces D_2O; the deuteration of either of the two atoms hydrogen bonded to its oxygen or the deuteration of either of the two atoms in the molecule to which it is hydrogen bonded produces an OD···O—D pair.) Therefore, it seems most likely that the bands at 2393 and 2442 cm^{-1} are the coupled vibrations of such pairs. Writing for the kinetic energy,

$$T=\tfrac{1}{2}\mu(\dot{r}_1^2+\dot{r}_2^2),$$

and for the potential energy

$$V=\tfrac{1}{2}f_r(r_1^2+r_2^2)+f_{rr}r_1r_2,$$

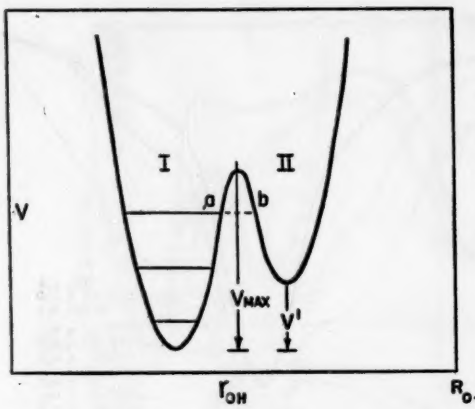

FIG. 4. Potential function for the proton in ice, roughly to scale.

one finds two frequencies,

$$\nu^+=\nu_0(1+f_{rr}/2f_r)$$

for $r_1=r_2$ and

$$\nu^-=\nu_0(1-f_{rr}/2f_r)$$

for $r_1=-r_2$, where

$$4\pi^2\nu_0^2=f_r/\mu.$$

The ratio of the intensities of the two vibrations is expected to be $I^+/I^-=(1-\cos\theta)/(1+\cos\theta)$. For $\theta=109°$ then, $I^+/I^-=2$.

In Fig. 3, the band at 2393 cm^{-1} is roughly twice the intensity of that at 2442 cm^{-1}, so we attribute the lower frequency to the in-phase vibration of the two OD groups (ν^+), the higher to the out-of-phase vibration (ν^-). Substituting these frequencies yields

$$f_{rr}=-0.123\times10^5 \text{ dynes/cm}$$

for the intermolecular OD···OD coupling constant. This may be compared with -0.099 for the corresponding constant in boric acid.[7]

It is interesting to compare this force constant with that calculated for electrostatic interaction between deuterium atoms which would be

$$f_{rr}=(e^2/r_{D\cdots D}{}^5)[3r_{O-D}r_{D\cdots O}+r_{O-D}r_{D\cdots O}\cos^2\theta - 2(r_{O-D}{}^2+r_{D\cdots O}{}^2)\cos\theta]e'^2,$$

where the r's are the distances, e is the electronic charge and e' is the effective charge in units of electronic charge. For $r_{O-D}=1.0$ A, $r_{D\cdots O}=1.76$ A and $\theta=109°$ 28′, $r_{D\cdots D}=2.30$ A, and we obtain $e'=0.63$.

At first sight, this value seems somewhat high, corresponding roughly to a $\partial\mu/\partial r$ of $3d$/A, whereas the value in the gas phase is only about half that. On the other hand, the present result would predict that the intensity of a hydrogen-bonded OH vibration is about four times the unbonded value. This conclusion is in good agreement with the experimental value, 3.2 d/A.[8,9] We therefore conclude that, while the "effective charge" picture is naive, it points to a considerable polarization of the O—H bond in ice. In this connection, it is interesting that, when the same calculation is made for crystalline boric acid, a value of $e'=0.56$ is obtained, in fair agreement with the present results. A similar conclusion has previously been reached for the crystalline hydrogen halides.[5]

At still higher D concentrations, the side bands gradually broaden and merge into the over-all band as longer chains of bonded deuterium atoms occur.

A similar behavior is expected for the OH stretching vibration in a dilute solution of HOD in D_2O. However, in this case, the spectrum shows a much broader peak (width 80 cm^{-1}) at 3275 cm^{-1}. Since we expect the splitting of OH pairs to be $\sqrt{2}$ times that of OD, or 70 cm^{-1}, the side bands cannot be resolved from the main peak. The fact that the uncoupled O—H peak is so much broader than the corresponding uncoupled O—D peak is hard to understand. In going from D to H, one might expect the line width to increase by a factor of $\sqrt{2}$ if the width depends on the amplitude of lattice vibrations. The experimental factor of about four cannot be explained in this way; an explanation will be suggested in the next section.

Proton Tunneling

A remarkable feature of the HOD spectrum is that in a dilute solution where one may expect intermolecular coupling to be virtually absent, the overtones are so broad, especially $2\nu_{OH}$ (width 600 cm^{-1}). Recalling that ν_{OH} itself is much broader than ν_{OD}, it appears as if the width is caused by a phenomenon which is sensitive to the mass.

A possible explanation of the anomaly is suggested by the following considerations. It is usually assumed that the potential energy of a hydrogen bond has two minima[10] for the position of the proton (see Fig. 4). In this case, the lifetime of states I will be limited by tunneling from states I to states II. Obviously this process is only important if the energy level E lies above the second minimum. The lifetime of the hydrogen in a vibrational state I of energy E is given approximately by

$$\tau=\nu^{-1}\exp\{2\int_a^b \hbar^{-1}[2m(V-E)]^{\frac{1}{2}}dx\}, \qquad (2)$$

where the integral depends on the form of the energy barrier, which in turn depends on the O···O distance R. Because of the O—O lattice vibrations, there will be a certain distribution of R; we may write for the distri-

[7] D. F. Hornig and R. C. Plumb, J. Chem. Phys. **26**, 637 (1956).

[8] G. M. Barrow, J. Phys. Chem. **59**, 1129 (1955).

[9] C. M. Huggins and G. C. Pimentel, J. Phys. Chem. **60**, 1615 (1956).

[10] See, for example, E. R. Lippincott and R. Schroeder, J. Chem. Phys. **23**, 1099 (1955).

bution function at low temperatures:

$$F(R)=(\beta/\pi)^{\frac{1}{2}}\exp[-\beta(R-R_0)^2],$$

where

$$\beta=4\pi^2\mu\nu_0/h,$$

ν_0 and μ being the frequency and effective mass for the O—O vibration. For the average line width $\Delta\nu$, we find:

$$\Delta\nu=\langle(1/\tau)\rangle_{Av}=\nu\int_0^\infty F(R)\times\exp\{-2\int_a^b\hbar^{-1}[2m(V-E)]^{\frac{1}{2}}dx\}dR. \quad (3)$$

We do not pretend to give an accurate calculation of this effect but merely want to indicate that by making reasonable assumptions about the various quantities involved one calculates band widths which are not far from those observed. For example, we chose for the shape of the potential energy barrier above E a symmetric angle with base width d_0 and height ΔV_0. To take account of the influence of the O···O vibrations, we assumed that the shape of the barrier did not change so that the height and width varied with the O···O distance R, as

$$V_{max}-E=(V_{max}-E)_{R=R_0}\times R/R_0, \quad (4)$$

$$d=d_0+R-R_0. \quad (5)$$

Equation (3) then takes the form

$$\Delta\nu/\nu=(\beta/\pi)^{\frac{1}{2}}\int_{-\infty}^{\infty}\exp\left[-\left\{\beta(R-R_0)^2+(4/3\hbar)(d_0+R-R_0)^2\left[2m\Delta V_0\left(1+\frac{R+R_0}{d_0}\right)\right]^{\frac{1}{2}}\right\}\right]dR. \quad (6)$$

In Eq. (6),

$$\Delta V_0=(V_{max}-E)_{R=R_0}.$$

For small amplitudes of vibration, the integrand of Eq. (6) can be expanded about its maximum point where $(R-R_0)/d_0=x_0$, yielding

$$\Delta\nu/\nu=\{1-[(\gamma^2/(1+\gamma^2)]^{\frac{1}{2}}\}^{\frac{1}{2}}\times\exp\{-\beta d_0^2x_0^2[1-(x_0/3\gamma^2)]\}. \quad (7)$$

In Eq. (7),

$$x_0=2\gamma[\gamma-(1+\gamma^2)^{\frac{1}{2}}] \quad (8)$$

and

$$\gamma=(2m\Delta V_0)^{\frac{1}{2}}2\hbar\beta d_0. \quad (9)$$

With these assumptions, we fitted Eq. (7) to the line width of $2\nu_{OH}$ and ν_{OH}. Taking $\beta=2.69\times10^{17}$ cm^{-2}, corresponding to $\nu_{O\cdots O}=200$ cm^{-1}, the experimental line widths are reproduced if

$$V_{max}=E(2\nu_{OH})+3288$$
$$=11\,319\text{ cm}^{-1}$$
$$=32.4\text{ kcal}$$

and $d_0=0.19$ A$(2\nu_{OH})$; 0.36 A(ν_{OH}). The calculated width for ν_{OD} is then 10.0 cm^{-1}. Considering that part of the experimental width, 20 cm^{-1}, arises from the spectrometer and part arises from sources other than tunneling through the barrier, the agreement is excellent indeed. We conclude, therefore, that tunneling is an important factor in the HOD line widths. A calculation with a more realistic barrier than the triangle is probably not worthwhile, but it will certainly result in a lower value for V_{max}. On the other hand, V_{max} is substantially above $2\nu_{OH}$, so that 32.4 kcal$>V_{max}>$23.1 kcal. The corresponding activation energy for proton transfer in ice, therefore, lies between 27.5 kcal/mole and 18 kcal/mole.

It seems worth while to note that apart from any other broadening effect, the influence of the O···O vibrations on the tunneling cannot be neglected; for a constant O···O distance, it is not possible to reproduce the observed line widths with any reasonable parameters for the barrier. Because of the O···O vibration there is a finite probability of small O···O distances for which the barrier is both lower and narrower. Thus, the O···O vibration is extremely effective in increasing the rate of proton tunneling.

If this explanation of the line widths in HOD is correct, we can also say, finally, that the second minimum must be lower than the energy corresponding to ν_{OH}, 5007 cm^{-1}. Consequently, $V'<14.4$ kcal/mole.

ACKNOWLEDGMENTS

We should like to acknowledge the support of The Office of Naval Research. The expansion leading to Eq. (7) was suggested by Mr. H. W. King.

Rotation-Vibration Interaction in Electronic Transitions. Application to Rotational "Temperature" Measurements

THOMAS C. JAMES*†

Department of Chemistry, Harvard University, Cambridge 38, Massachusetts

(Received November 19, 1959)

The effect of rotation-vibration interaction on line intensities in electronic transitions in diatomic molecules is discussed. It is shown that this effect is closely related to the variation in the electronic transition moment with internuclear distance. The relation of this to the determination of rotational temperatures is discussed, using the OH radical as an example. It is shown that a neglect of this interaction can lead to the observation of apparently abnormal temperatures.

IN the usual discussion of intensities of electronic transitions use is made of the Franck-Condon principle in order to predict the intensity of vibrational bands comprising the total electronic transition. It is customary to assume that the variation in the electronic transition moment with internuclear distance is sufficiently slow that it can be replaced by an average value. Furthermore, it is usually assumed that line intensities in these bands are not affected by rotation-vibration interaction. That is, one assumes that the vibrational wave functions are independent of the rotational quantum number. Since there exist a number of applications of intensity measurements where these two approximations might lead to the derivation of erroneous conclusions from intensity measurements, it is felt worthwhile to discuss these two approximations.

It has, of course, long been realized that for accurate intensity calculations one should consider the effect of the variation in the electronic transition moment with internuclear distance. There have been a number of papers[1,2] recently dealing with this subject and also giving methods for obtaining the rate of change of the transition moment with internuclear distance from a study of vibrational band intensities. The question of the effect of neglecting the rotation-vibration interaction in electronic transitions has received less attention, although in a recent note Learner and Gaydon[3] discuss this question and indicate that this neglect is not justified.

In this paper both of these topics will be discussed, although more attention will be given to the effect of rotation-vibration interaction. Since the measurement of rotational temperatures by studying rotational line intensities in electronic transitions is important in many kinetic and astrophysical applications where one is interested in the distribution of rotational energy for the system, it is important to know how these two factors can influence rotational line intensities and hence rotational temperature measurements. Further, it will be pointed out that it should be possible to gain information about the variation of the electronic transition moment with respect to internuclear distance from a study of rotational line intensities within a given band.

THEORY

The intensity of a given line in an electronic transition is determined by the square of the matrix element

$$\int \psi_{el}'\psi_{rib}'\psi_{rot}'\left(\sum_i e_i r_i\right)\psi_{el}''\psi_{rib}''\psi_{rot}''d\tau, \qquad (1)$$

where it is assumed that the Born-Oppenheimer separation of electronic, vibrational, and rotational wave functions is valid. In this case the above integral leads to

$$\int \psi_{rib}'\psi_{rot}' R(r) f(\theta,\phi)\psi_{rib}''\psi_{rot}''d\tau, \qquad (2)$$

where $R(r)$ is the electronic transition moment for the particular electronic transition. The integral over the rotational coordinates can now be carried out so that the intensity of a given rotational line is related to

$$\left[\int \psi_{rib}' R(r)\psi_{rib}''\right]^2 S_{J'J''}, \qquad (3)$$

where $S_{J'J''}$ is the rotational line strength. The intensity of a given vibrational band (v', v'') is, therefore, determined by the vibrational matrix element

$$\int \psi_{vib}' R(r)\psi_{vib}''dr. \qquad (4)$$

As mentioned previously, it is frequently assumed that the transition moment varies sufficiently slowly with the internuclear distance r that it may be replaced by an average value $\langle R(r)\rangle_{Av}$. In this case the intensity of the various bands in the electronic spectrum is proportional to the so-called overlap integrals or Franck-Condon factors

$$\int \psi_v'\psi_v''dr.$$

* Socony Mobile of New Jersey Fellow.

† Present address: Department of Chemistry, Northwestern University, Evanston, Illinois.

[1] P. A. Fraser, Can. J. Phys. **32**, 515 (1954).

[2] R. W. Nicholls, Proc. Phys. Soc. (London) **A69**, 741 (1956).

[3] R. C. M. Learner and A. G. Gaydon, Nature **183**, 242 (1959).

A more realistic approach would be to use some definite empirically or theoretically justifiable functional form for $R(r)$ and use this in Eq. (3) in order to calculate the intensities. Lacking such a function one could also expand the transition moment in a power series in the internuclear distance and consider the effect of successive terms. Since one can speak a little more generally by considering a power series expansion this is the approach that will be used. Only the first two terms will be considered, but this should be sufficient for answering the question as to how slow the variation in $R(r)$ should be in order that the overlap integrals should give a fair approximation to the intensities.

The other problem which needs to be considered is the fact that the foregoing expression [Eq. (4)] is really incomplete in that one should append subscripts to each of the wave functions to indicate the rotational level in the initial and final state. Therefore, one should really write in place of Eq. (4):

$$\int \psi_{v',J'} R(r) \psi''_{v'',J''} dr. \tag{5}$$

These vibrational wave functions, and therefore the foregoing integral, are J dependent due to rotational-vibration interaction. In other words, the effective potential energy curve depends on the rotational state of the molecule. This causes the vibrational wave functions to depend on rotational as well as vibrational quantum numbers. The question which has to be answered is: What is the magnitude of this J dependence and how drastically does it affect intensities? It will become apparent as a result of subsequent development that the answer to this question is closely related to the effect of the variation of $R(r)$ with r. In what follows, the essential features of the inclusion of rotation-vibration interaction and the variation of the transition moment will be given without giving the mathematical details involved. The quantitative results will be reserved for the Appendix in order that the essential features of the argument will be as clear as possible. For the sake of simplicity it will be assumed that both of the electronic states involved are $^1\Sigma$ and that the vibration can be approximated as harmonic.

For $^1\Sigma$ states the rotational energy can be written as $\hbar^2 J(J+1)/2\mu r^2$. If one then expands $1/r^2$ in a power series and neglects terms beyond the square term in $\xi=(r-r_e)/r_e$, the effective potential energy of nuclear motion is:

$$U_{eff}(r)=\tfrac{1}{2}kr_e^2\xi^2+[\hbar^2 J(J+1)/2\mu r_e^2](1-2\xi+3\xi^2). \tag{6}$$

Now, by a change of variable the first-power term in ξ can be eliminated leading to a harmonic oscillator form potential. In this approximation the solutions of the radial Schrödinger equation

$$(1/r^2)(d/dr)[r^2(d\psi/dr)] + \left\{\frac{-J(J+1)}{r^2}+\frac{2\mu}{\hbar^2}[E-U(r)]\right\}\psi=0 \tag{7}$$

have been obtained. These solutions $\Phi_{v,J}(\eta_J)=r\psi_{v,J}(r)$ depend on a new variable η_J which is a function of J, r_e, and ω_e. The quantities η_J differ in the two electronic states owing to the difference in the equilibrium internuclear distance r_e and the difference in vibration frequency ω_e. The intensity of the transition is then proportional to the square of the matrix element

$$R_{v',J',v'',J''}=\int \Phi_{v',J'}(\eta_{J'}) R(r) \Phi_{v'',J''}(\eta_{J''}) dr. \tag{8}$$

If $R(r)$ is approximated as $R(r)=R_0+(\partial R/\partial r)(r-r_e)$ this matrix element has the following form:

$$R_{v',J',v'',J''}=C_{J,J''}R_0[A_{v',J',v'',J''} + \gamma'^{\frac{1}{2}}\chi(B_{v',J',v'',J''}(1-3/4\gamma'^2 J'(J'+1)) + A_{v',J',v'',J''}\gamma'^{\frac{1}{2}}J'(J'+1)], \tag{9}$$

where $R_0=R(r_e')$ and $\chi=(\partial R/\partial r)_{r_e'}r_e'/R(r_e')$ and $\gamma'=2B_e'/w_e'$. The quantities $C_{J,J''}$, $A_{v',J',v'',J''}$, and $B_{v',J',v'',J''}$ vary with J' and J'' and therefore, in addition to causing a variation in the foregoing matrix element with J, they lead to a difference in this matrix element in the P, Q, and R branches of the spectrum. Explicit expressions for these quantities are given in the Appendix. Here an approximate expression for $R_{0,J',1,J''}$ will be given in which only the most important terms are included:

$$R_{0,J',1,J''} \propto R_0[G(r, J'')+\gamma''^{\frac{1}{2}}K(J', J'') + \gamma'^{\frac{1}{2}}\chi(1-\tfrac{1}{2}[G(r, J'')+\gamma''^{\frac{1}{2}}K(J', J'')]^2 + G(r, J'')J'(J'+1)\gamma'^{\frac{1}{2}})], \tag{10}$$

where

$$G(r, J'')=\gamma''^{-\frac{1}{2}}[(r_e'-r_e'')/r_e''] + [(r_e'-r_e'')/r_e'']3/4\gamma''^{\frac{1}{2}}J''(J''+1)$$

$$K(J', J'') = [r_e'(\gamma')^2/r_e''(\gamma'')^2]J'(J'+1)-J''(J''+1);$$

$$\gamma''=2B_e''/w_e''; \qquad \gamma'=2B_e'/w_e'.$$

In the preceding expression the doubly primed constants refer to the electronic state in the $v=1$ level and the singly primed constants refer to the electronic state corresponding to the $v=0$ level. Depending on which state one takes to be the doubly primed state, one is talking about the (0, 1) or the (1, 0) transition. From the form of the expression for $G(r, J'')$ it is evident that the relative signs of the terms in R_0 and $R_0\chi$ in Eq. (8) are different for the two transitions. This means that if the variation in the transition moment is

TABLE I.

$[(2)^{\frac{1}{2}}/R_0]\langle 0, K'|\, R\,|1, K''\rangle$

K'	$K''=K'+1$	$K''=K'-1$	$K''=K'$
5	$0.370+0.0922\chi$	$0.390+0.0910\chi$	$0.384+0.0912\chi$
10	$0.381+0.0950\chi$	$0.415+0.0930\chi$	$0.399+0.0931\chi$
15	$0.398+0.0989\chi$	$0.450+0.0961\chi$	$0.428+0.0968\chi$
20	$0.426+0.1029\chi$	$0.494+0.1002\chi$	$0.460+0.1015\chi$

$[(2)^{\frac{1}{2}}/R_0]\langle 1, K'|\, R\,|0, K''\rangle$

K'	$K''=K'+1$	$K''=K'-1$
5	$-0.429+0.1019\chi$	$-0.421+0.1025\chi$
10	$-0.411+0.1049\chi$	$-0.447+0.1065\chi$
15	$-0.430+0.1112\chi$	$-0.484+0.1153\chi$
20	$-0.461+0.1190\chi$	$-0.529+0.1240\chi$

$(R_0)^{-1}\langle 0, K'|\, R\,|0, K''\rangle$

K'	$K''=K'+1$	$K''=K'-1$
5	$0.958-0.0174\chi$	$0.954-0.0185\chi$
10	$0.956-0.00985\chi$	$0.947-0.0118\chi$
15	$0.952+0.00505\chi$	$0.938+0.00218\chi$
20	$0.944+0.0190\chi$	$0.926+0.0148\chi$

sufficiently large for the terms in R_0 and $R_0\chi$ to have approximately the same magnitude, then in the foregoing approximation one of the bands (0, 1) or (1, 0) would have approximately four times the intensity it would have if there were no variation ($\chi=0$), while the other would have a much reduced intensity. This means that practically speaking one would find much greater intensity differences between the (0, 1) and the (1, 0) bands than one would estimate from a consideration of overlap integrals and population differences. In bands for which the magnitude of the terms in R_0 and $R_0\chi$ is the same and for which they have opposite signs so as practically to cancel each other, it would be necessary to consider the effect of higher terms in the expansion of the transition moment. If the variation in the transition moment is actually linear in the region of interest, then such higher terms would not contribute to the intensity. In the limit of identical shapes (same internuclear distance and force constant) of the two electronic states comprising the transition, the intensity of the $\Delta v=0$ transitions is determined primarily by R_0, while that of the $\Delta v=\pm 1$ transitions is determined primarily by $R_0\chi$.

Usually one would not be able to make any definite statements about the distribution of vibrational intensities in molecules with large γ's unless an approximate value for χ were known. The method whereby the general functional form of $R(r)$ can be determined from vibrational intensity measurements has been given by Fraser[1] and applied to several molecules of interest by Nicholls.[2] It makes use of the approximate relationship [which is exact for a linear variation in $R(r)$ with respect to r]

$$\int \psi_{v'} R(r) \psi_{v''} dr = R(\bar{r}) \int \psi_{v'} \psi_{v''} dr, \tag{11}$$

where

$$\bar{r} = \int \psi_{v'} r \psi_{v''} dr \Big/ \int \psi_{v'} \psi_{v''} dr.$$

Making use of Eq. (11), one can obtain the form of $R(r)$ from intensity measurements and calculated values of the r centroids and Franck-Condon factors involved in each transition. When the data for a number of molecules is examined in this manner it is found by Nicholls that there are cases in which the neglect of the variation in $R(r)$ is not at all justified.

APPLICATION TO OH RADICAL

The effect of rotation-vibration interaction on intensities is most easily demonstrated in terms of a particular transition of a molecule, since the relative magnitudes of the $A_{v',J'}^{v'',J''}$, $B_{v',J'}^{v'',J''}$, and $C_{J'}^{J''}$ terms in Eq. (9) and their rate of change with J are strongly dependent on the particular molecule and electronic transition chosen. Effects which are large in one transition might be completely negligible in another. The example, the $^2\Sigma \rightarrow {}^2\Pi$ transition in the OH radical, is chosen because of its general interest and because it appears to be an ideal electronic transition to illustrate the effect of rotation-vibration interaction since the effect is not negligible for this molecule. As mentioned previously, the calculations have been made on the assumption that the electronic transition involved is a $^1\Sigma$—$^1\Sigma$ transition. These formulas will be used in treating the OH molecule rather than more complicated expressions which would be required if spin and electronic angular momentum were taken into account.[4] This will not introduce a significant error and will certainly not affect the qualitative conclusions since at the J's where rotation-vibration interaction terms become really important, OH can be considered as a Hund's Case b molecule so that the quantum number K (which is the total angular momentum apart from spin) can be used in place of J to give an account of the centrifugal distortion. The spin quantum numbers, being restricted to small values, are not significant factors in the centrifugal distortion at high values of K. In Table I values of the vibrational matrix elements for the (0, 0), (0, 1), and (1, 0) bands are given using formula (9) with K in place of J. These

[4] In treating the OH $^2\Sigma$—$^2\Pi$ transition as a $^1\Sigma$—$^1\Sigma$ transition this refers only to the evaluation of the vibrational matrix elements which are altered due to centrifugal distortion. The exact factors which would enter into the radial equation would depend on whether Hund's Case a or b were a good approximation. For the evaluation of the rotational line strengths one would have to use the formulas appropriate for the particular type of transition. In the above case they would be the rotational line strengths calculated for a $^2\Sigma$—$^2\Pi$ transition.

TABLE II.

	$(R_0^2)^{-1}\|\langle 0, K'\|R\|1, K''\rangle\|^2$			$(R_0^2)^{-1}\|\langle 1, K'\|R\|0, K''\rangle\|^2$		$(R_0^2)^{-1}\|\langle 0, K'\|R\|0, K''\rangle\|^2$	
a	0.00316			0.270		1.055	
K'	$K''=K'+1$	$K''=K'-1$	$K''=K'$	$K''=K'+1$	$K''=K'-1$	$K''=K'+1$	$K''=K'-1$
5	0.00238	0.00433	0.00379	0.289	0.284	1.030	1.028
10	0.00274	0.00625	0.00452	0.284	0.316	0.976	0.970
15	0.00289	0.00940	0.00625	0.315	0.370	0.874	0.867
20	0.00414	0.01395	0.00830	0.361	0.435	0.778	0.771

[a] Harmonic oscillator value neglecting rotation vibration interaction.

calculations were made from the values of the quantities $A_{v',J',v'',J''}$, $B_{v',J',v'',J''}$ and $C_{v',J''}$ given in the Appendix rather than the approximate expression (10). In these calculations R_0 and χ are the values of these quantities at the equilibrium internuclear distance in the upper state. The matrix elements were calculated at $K'=5$, 10, 15, and 20 for the P and R branches. Calculations for the Q branch of the (0, 1) band were also made. K' refers to the K value of the upper $^2\Sigma$ state and K'' to the K value in the lower $^2\Pi$ state.

These tables clearly indicate the effect of considering the variation of the transition moment with r. If this variation is very small, then the (1, 0) band has a slightly higher transition probability than the (0, 1) band, neglecting for the moment frequency and population differences. If χ is negative and has a magnitude such that the terms in R_0 and $R_0\chi$ are of comparable magnitude then the (1, 0) band will have a much greater transition probability than the (0, 1) band. On the other hand, if χ were positive, then the (0, 1) band would have a much higher transition probability. Similar comparisons can also be made between these bands and the (0, 0) band.

The effect of rotation-vibration interaction in altering the value of the transition moment matrix element is also clear from an inspection of Table I. Since the terms in R_0 and $R_0\chi$ change at different rates it is clear that line intensities in a given band could change in a somewhat irregular manner. This change would also be different in different branches of the spectrum. In order to see what the K dependence of these matrix elements is like, a value of χ is needed. From a consideration of vibrational intensities in the $^2\Sigma\rightarrow{}^2\Pi$ transition in OH Nicholls[2] found that the transition moment could be represented in the form:

$$R(r)=\text{const}(1-0.756r),$$

where r is in Angstroms. Using this result, the value of χ is $\chi=-3.26$. Making use of this value and the results in Table I, values for the R_e matrix element can be calculated. The squares of these matrix elements are the quantities of interest and are given in Table II.

An examination of this table shows that the K dependence of the (0, 1), (1, 0), and (0, 0) vibrational matrix elements is quite different in each case. In the (1, 0) band this matrix element has essentially the same value for the P and R branches. There is an increase in this matrix element with K, with the value in the R branch increasing a little more rapidly. In the (0, 0) band there is very little difference in the P and R branches, but the value of the vibrational matrix element decreases with increasing K, the ratio of the square of the matrix element at $K=20$ compared to the $K=1$ value being 0.73. On the other hand, the P and R branches of the (0, 1) band show appreciable differences in this quantity. There is very little change in the P branch except at the highest K values, whereas in the R branch the ratio of the square of the matrix element at $K=20$ compared to the $K=1$ value is 4.4. This result is in approximate agreement with the result obtained by Learner and Gaydon[3] who calculated the transition probability at $K=1$ and at $K=20$ using Morse functions and a transition moment proportional to $\exp(-3r)$. They found a ratio of 3 for the R-branch intensity at $K=20$ compared to the value at $K=1$. They obtained the result that there was no change in the P-branch value at $K=20$ compared to the $K=1$ value, whereas according to Table II the value at $K=20$ is somewhat higher than the value at $K=5$. These differences are not surprising in view of the sensitivity of the results to the value of χ and in view of the different method of calculation. The large intensity difference between the (0, 1) and (1, 0) bands is also clear from Table II. In this case the use of overlap integrals to estimate the relative intensity of these bands would have led to a large error.

EFFECT ON ROTATIONAL TEMPERATURES

Before concluding we want to consider the bearing that these considerations have on the determination of rotational temperatures. Figure 1 shows the variation of the vibrational matrix element calculated for harmonic potentials. This is a plot of the data listed in Table II. It is clear from this plot that if rotation-vibration interaction is neglected a large error could result in temperature determinations from rotational line intensities. According to Fig. 1, the Q and R branches would give temperatures much higher than the true temperature. The R branch, for example, would give an apparent temperature of approximately

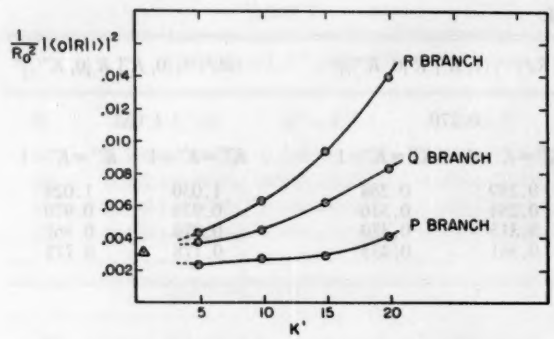

FIG. 1. Plot of the square of the (0, 1) matrix element against K'. Dotted circles represent calculated points; dotted triangle, the value calculated neglecting rotation-vibration interaction.

4800°K if the true temperature were 3000°K. This is the error which would result if the temperature was determined from a plot of the logarithm of the intensity divided by the product of the frequency and the rotational transition probability against $J(J+1)$. Looking at the (1, 0) matrix element, one sees that if rotation vibration interaction were not considered then a temperature determination from rotational intensities would give a value above the true temperature for systems in the $V=1$ state, whereas from the (0, 0) matrix element, one sees that the observed rotational temperature would appear to be lower in the $V=0$ state if the K dependence of the (0, 0) matrix element were neglected. The (0, 0) band would give about 2650°K if the true temperature were 3000°K.

It is apparent from a consideration of Table I that the behavior of the vibrational matrix element in the three branches is very sensitive to the value of χ. The results for the (0, 1) band are obtained as a small difference between two much larger quantities and are rather sensitive to the accuracy of these quantities. For this reason it would be necessary to carry out calculations to a higher order than the harmonic approximation in order to be certain of the behavior for any given value of χ. Since one can cause the behavior of the vibrational matrix elements to change rather drastically by changing the value of χ one should be able to get a fairly accurate value of χ if accurate rotational line intensity data were available and the calculation of the matrix elements was carried out to a high order.

If the vibrational matrix element possessed a maximum or minimum in its variation with J for experimentally accessible J values, then this could lead to what would at first glance seem to be a somewhat erratic distribution of rotational energy populations. If the curve for a particular branch possessed a minimum this could cause lower rotational levels to appear to be at lower temperatures and higher rotational levels to appear to be at higher rotational temperatures even in cases where thermal equilibrium was established.

An additional point which should be mentioned is that the J dependence of the vibrational matrix elements in the rotation-vibration spectrum would be expected to be different, and should lead to differences in rotational temperatures obtained from the infrared spectra as compared with those obtained from visible spectra. This is not meant to imply that such differences as have been found are entirely due to the neglect of rotation-vibration interaction, but rather to suggest that in the interpretation of these differences one should also consider the rotation-vibration interaction effects. This could either increase or decrease such discrepancies. Since the dipole moment function of OH is not known it is not possible to make estimates of errors which could be made in temperature measurements in the infrared spectra.

CONCLUSION

This work indicates the importance of rotation-vibration interaction in the analysis of intensity measurements on the rotational structure of band spectra. While it is true that in many systems the rotation-vibration interaction produces only slight corrections to rotational line intensities, there are a number of molecules where such considerations can be expected to be extremely important, namely, systems with relatively large values of $\gamma=2B_e/w_e$ such as obtains for most of the hydrides. The application in the field of chemical kinetics where, for example, one attempts to draw conclusions as to mechanisms of reactions and relaxation times in flames and shock tubes from a study of rotational and vibrational distributions, is apparent.

There is a considerable amount of data in the literature on rotational temperatures as obtained from intensity measurements. In some bands there seem to be large temperature differences obtained from P, Q, and R branches. There also seem to be cases in which rotational temperatures are consistently different in different vibrational levels. In many cases quite erratic temperature distributions have been observed and have been taken to indicate the lack of a Maxwell-Boltzman distribution of rotational energy. It should be clear that a number of these anomalies could be explained on the basis of the effect of rotation-vibration interaction on intensities and that a great deal of caution is needed in interpreting the meaning of such observations. The desirability of making rough calculations to see in which bands intensity anomalies are to be expected is obvious. Generally weak bands would have a greater chance of showing large effects, since it is in these bands that one is more likely to have a situation where the intensity is controlled by the small difference in large quantities and is quite sensitive to the values of these quantities.

An analysis of the intensity and temperature data which is available from several investigations would be worthwhile. Unfortunately, there is a considerable discrepancy in the results obtained by different observers. There are so many possible sources of error in intensity measurements, particularly in emission, that unless one

has an intimate knowledge of the experimental conditions the extraction of line strengths is beset with uncertainties. For this reason it would be worthwhile to make accurate intensity measurements in absorption whenever possible. Since it is possible to obtain a value of χ from a study of relative rotational line intensities, it would be of interest to compare the rotational value with the value from vibrational data. Since in many cases it is the weak bands which are desirable for temperature measurements because of self-absorption problems, the bands being observed will frequently be the ones in which rotation-vibration interaction is an urgent consideration and for which fairly reliable values of χ are necessary.

Finally, it should be stressed that the consideration of the rotation-vibration interaction will be most important in those cases where the variation of the transition moment with internuclear distance is important, since it is in these cases that the rotation-vibration interaction can produce the most drastic changes in the vibrational matrix elements with rotational quantum numbers.

ACKNOWLEDGMENT

The author wishes to thank Dr. William Klemperer for his interest in the problem and for numerous helpful suggestions and criticisms. The aid of the National Science Foundation is also gratefully acknowledged.

APPENDIX

In this appendix the explicit expressions for the quantities $A_{v',J'}{}^{v'',J''}$, $B_{v',J'}{}^{v'',J''}$, and $C_{J'}{}^{J''}$ which appear in the text will be given. The solution of the radial equation (7) is given in the paper by Herman and Wallis[5] on line intensities in diatomic molecules. The evaluation of the matrix element [Eq. (8)] can be carried out in the same manner as that described by Herman and Wallis for the calculation of dipole-moment matrix elements in the infrared spectrum of a diatomic molecule. The results are a little more complicated because of the difference in the internuclear distance and difference in the shape of the potential energy curve in the two different electronic states.

The quantities $A_{v',J'}{}^{v'',J''}$, $B_{v',J'}{}^{v'',J''}$, and $C_{J'}{}^{J''}$ are given by

$$C_{J'}{}^{J''}=(m)^{\frac{1}{2}}c^k$$

$$A_0'=\sqrt{2}^{-1}b; \qquad A_1{}^0=\sqrt{2}^{-1}d; \qquad A_0{}^0=1$$

$$B_0'=\sqrt{2}^{-1}(nb+m); \qquad B_1{}^0=\sqrt{2}^{-1}(nd+p);$$

$$B_0{}^0=n$$

$$b=2\delta/(1+\beta^2); \qquad n=-\beta\delta/(1+\beta^2);$$

$$m=2\beta/(1+\beta^2)$$

$$d=-2\beta\delta/(1+\beta^2); \qquad p=2/(1+\beta^2);$$

$$k=-\delta^2/2(1+\beta^2)$$

$$\beta=(w_e''/w_e')^{\frac{1}{2}}[1+3/4\gamma'^2F(J', J'')]$$

$$\delta\simeq(\gamma'')^{-\frac{1}{2}}[(r_e'-r_e'')/r_e'']$$

$$+[(r_e'-r_e'')/r_e'']3/4\gamma''J''(J''+1)+\gamma''^{\frac{1}{2}}K(J', J'')$$

$$K(J', J'')=r_e'(\gamma')^2/r_e''(\gamma'')^2J'(J'+1)-J''(J''+1)$$

$$F(J', J'')=(\gamma''/\gamma')^2J''(J''+1)-J'(J'+1).$$

In these expressions the doubly primed constants refer to the states appearing as the upper index on the quantities $A_{v',J'}{}^{v'',J''}$, $B_{v',J'}{}^{v'',J''}$, and $C_{J'}{}^{J''}$. R_0 and $R_0\chi$ of Eq. (9) in the text refer to the values of these quantities in the singly primed state. $R_{v',J'}{}^{v'',J''}$ would refer to the (v', v'') transition with R_0 and χ evaluated in the electronic state corresponding to the v' level.

[5] R. Herman and R. F. Wallis, J. Chem. Phys. 23, 637 (1955).

Application of Least-Squares Method to Gaseous Benzene in Electron Diffraction Investigation*

KATSUMA KIMURA† AND MASAJI KUBO

Chemical Department, Nagoya University, Nagoya, Japan

(Received December 18, 1959)

The intensity data of gaseous benzene obtained at 18°C by the sector-microphotometer technique in electron diffraction were analyzed by use of a least-squares method, D_{6h} symmetry being assumed for the molecule. A total of thirteen parameters comprising two bond distances, seven root-mean-square amplitudes, three background parameters, and one intensity scale factor were refined in the least-squares treatment. Uncertainties in these parameters were determined by computing standard errors due to the over-all errors involving systematic and random errors. Results for bond distances r and root-mean-square amplitudes l are as follows: $r(C—C)=1.396_9\pm0.003$ A; $r(C—H)=1.084_3\pm0.0020$ A; $l(C_1—C_2)=0.045_6\pm0.003$ A; $l(C_1\cdots C_3)=0.055_5\pm0.005$ A; $l(C_1\cdots C_4)=0.061_4\pm0.009$ A; $l(C_1—H_1)=0.074_8\pm0.010$ A; $l(C_1\cdots C_5)=0.097_5\pm0.008$ A; $l(C_1\cdots H_3)=0.092_6\pm0.016$ A; $l(C_1\cdots H_4)=0.096_0\pm0.0023$ A. These values were compared with data available in the literature. An empirical formula is proposed for experimental background scattering and the selection of weighting factors in least-squares refinement is discussed.

INTRODUCTION

A MAJORITY of the early electron diffraction data on gaseous molecules has recently been revised in the light of modern experimental and analytical technique, while considerable interest has been directed to the improvement of analysis of diffraction patterns. Recent studies with the sector-microphotometer method in electron diffraction afford accurate information about geometric configurations as well as the root-mean-square amplitudes of vibration, the latter permitting an independent check to be made on force models evaluated from spectroscopic data. One of the most important contributions to the recent diffraction analysis is the method of least squares first introduced by Jones *et al.*[1] and later extensively applied to sector-microphotometer data by Bastiansen *et al.*[2] In a previous paper,[3] we have proposed a new method of least squares for the density-intensity calibration in electron diffraction studies.

The molecular dimensions of a benzene molecule in the gaseous state have been determined by means of electron diffraction[4,5] and Raman spectroscopy.[6] Benzene is not amenable to microwave studies because of its vanishing dipole moment. In the earlier sector-electron diffraction studies on benzene,[4,5] the analysis of intensity data was carried out mainly through the ordinary radial distribution method, with which it was not feasible to take into account all possible combinations of small variations in a multi-parameter structure.

We have considered it worthwhile to pay some special effort to tne reinvestigation of benzene for the following reasons. First, we have undertaken to check earlier structural parameters by the extensive use of a least-squares method and to estimate the degree of accuracy by evaluating their standard errors, which have not been given for the molecule as yet. Secondly, we wanted to furnish a good illustration of the least-squares analysis with special emphasis on the subtraction of background scattering as well as on the selection of weighting factor in least-squares refinements. For this purpose, benzene is suitable as a test molecule. The present paper presents, along with our previous work,[3] an example of the least-squares analysis extensively applied to every step in the reduction of the observed optical densities of diffraction patterns to structural parameters.

EXPERIMENTAL

The electron diffraction photographs of benzene were taken at 18°C through an r^3 sector, using an apparatus already reported.[7,8] A camera distance of 12 cm was used, the s region covering 5.35—30.05 ($s=(4\pi/\lambda)\sin\theta$, where λ is the wavelength of the electron beam, and 2θ is the angle of scattering). Electron beams used had a wavelength of about 0.052 A. The intensities were calculated at intervals of $\Delta s=\pi/20$. Optical densities were converted into relative intensities by means of a least-squares procedure described in the previous paper.[3,8]

In electron diffraction experiments, the total scattered intensity per unit area of a photographic plate, $T(s)$, is directly observed rather than the scattered intensity per unit solid angle, $I_T(s)$. They are related to

* Presented at the Symposium on Molecular Structures held by the Chemical Society of Japan in Kyoto on October 12, 1958.

† Present address: The Institute for Solid State Physics, The University of Tokyo, Azabu-Shinryudo-cho, Minato-ku, Tokyo.

[1] M. E. Jones, K. Hedberg, and V. Schomaker, J. Am. Chem. Soc. **77**, 5278 (1955).

[2] O. Bastiansen, L. Hedberg, and K. Hedberg, J. Chem. Phys. **27**, 1311 (1957).

[3] K. Kimura and M. Kimura, J. Chem. Phys. **32**, 1398 (1960).

[4] The structural data of benzene obtained with the sector-microphotometer method was reported by I. L. Karle for the first time in J. Chem. Phys. **20**, 65 (1952).

[5] O. Bastiansen and S. J. Cyvin, Nature **180**, 980 (1957); A. Almenningen, O. Bastiansen, and L. Fernholt, Det. Kgl. Norske Vid. Selsk. Skr. **3** (1958).

[6] B. P. Stoicheff, Can. J. Phys. **32**, 339 (1954); B. P. Stoicheff and A. Langseth, *ibid.* **34**, 350 (1956).

[7] M. Iwasaki, Bull. Chem. Soc. Japan **32**, 205 (1959).

[8] K. Kimura and M. Kubo, J. Chem. Phys. **30**, 151 (1959).

each other by the following expression:

$$T(s)=\alpha(s)I_T(s), \tag{1}$$

where $\alpha(s)$ is the product of the sector function and $\cos^3\theta$. The latter takes into account the fact that a photographic plate was placed perpendicular to the incident beam. $I_T(s)$ is given by

$$I_T(s)=\text{const}\{I_M(s)+I_B(s)\}/s^4, \tag{2}$$

where

$$I_M(s)=\sum_{i,j}(Z_i-f_i)(Z_j-f_j)\exp(-a_{ij}s^2)\sin(sr_{ij})/sr_{ij},$$

$$I_B(s)=\sum_i\{(Z_i-f_i)^2+Z_iS_i(s)\},$$

$a_{ij}=l_{ij}^2/2$, Z denotes the atomic number, f and S the atomic form factor and the incoherent scattering factor for x-rays,[9] respectively, l_{ij} the root-mean-square amplitude, and r_{ij} the equilibrium distance between nuclei, i and j. In order to facilitate computation, the following function corresponding to $s^3I_T(s)$ was used as an intensity function for analysis:

$$J^{\text{obs}}=(s^3/\alpha)T. \tag{3}$$

EXPERIMENTAL BACKGROUND INTENSITY

Owing to various extraneous scatterings as well as effects due to the finite size of the scattering volume, it was found that the experimental background usually differed more or less from the theoretical background representing the sum of atomic coherent plus incoherent scatterings. This difference appeared to a considerable extent over the s range observed in the present investigation. Therefore, the theoretical background intensity should not be subtracted from the total observed intensity without appropriate corrections.

First, in order to find an analytic function which fits the experimental background curve, a smooth background curve was drawn through the total intensity curve in such a way as to give a fairly good molecular model.[10] A comparison between the theoretical and the experimental background indicated that the ratio of these intensities was not constant but could be expressed by a quadratic equation of s:

$$I_B^{\text{theoret}}/I_B^{\text{exptl}}=\lambda s^2+\mu s+\nu, \tag{4}$$

over the whole range of observations, where λ, μ, and ν are adjustable constants. From a preliminary least-squares fit for these parameters, it was found that $\lambda=0.01436$, $\mu=-0.1107$, and $\nu=0.9802$. These constants were further refined along with structure parameters by means of the least-squares method, as described in the following.

LEAST-SQUARES REFINEMENTS

The present analysis was made on the basis of the regular hexagon structure of a benzene molecule. Accordingly, independent distance parameters that were refined were C—H and C—C bond distances defining the geometry of the D_{6h} model. In order to determine the molecular terms completely, ten additional parameters are required for the root-mean-square amplitudes of all conceivable atom pairs. However, seven vibration parameters, $a(C_1—C_2)$, $a(C_1\cdots C_3)$, $a(C_1\cdots C_4)$, $a(C_1—H_1)$, $a(C_1\cdots H_2)$, $a(C_1\cdots H_3)$, and $a(C_1\cdots H_4)$, were taken for the present refinements. Three remaining ones, $a(H_1\cdots H_2)$, $a(H_1\cdots H_3)$, and $a(H_1\cdots H_4)$, were omitted, because of their negligibly small contributions to the molecular terms. In all, thirteen parameters were chosen for adjustment by the least-squares method. They comprise one scale factor, three background parameters, and nine structural parameters.

The first observation equations employed was

$$J(s)=\{kI_M(s)+(\lambda s^2+\mu s+\nu)^{-1}I_B(s)\}/s, \tag{5}$$

where k is an intensity scale factor. Since this observation equation is not suitable as a least-squares equation, it was modified as follows. If a set of good approximate values for all the parameters is known, the Taylor expansion of Eq. (5) followed by taking linear terms gives an approximate observation equation:

$$J_i^{\text{obs}}-J_i'=K'\Delta k+L'\Delta\lambda+M'\Delta\mu+N'\Delta\nu+[R_1'\Delta r_1+R_2'\Delta r_2+\sum_{i,j}A_{ij}'\Delta a_{ij}]. \tag{6}$$

The coefficients in Eq. (6) are the partial derivatives of $J(s)$ with respect to the corresponding parameters. Δ's are corrections to be sought. Primes indicate that the quantities have been evaluated for the trial values. The brackets in Eq. (6) enclose parameters associated with the molecular structure of benzene. As a criterion for determining the parameters, a residual function,

$$R=\sum_i p_i(J_i^{\text{obs}}-J_i')^2 \tag{7}$$

is required to be minimum with respect to variations in the parameters, where p_i is a weighting factor and the summation is taken over all the observed intensities that are mutually independent. The condition of minimum R's leads to the normal equations of least squares.

The method described in the preceding was applied to the present problem in two successive refinements. Differences, $J^{\text{obs}}-J'$, were computed at intervals of $\Delta s=\pi/20$, 161 intensity data being used for determining thirteen unknown parameters. Since observation equations have degrees of accuracy differing from one another, p's must be chosen so as to reduce the observa-

[9] The values given by H. Viervoll, Acta Cryst. 2, 277 (1949) were used, while $S(s)$ values were taken from Bewilogua. See, for example, A. H. Compton and S. K. Allison, *X-ray in Theory and Experiment* (D. Van Nostrand Company, Inc., Princeton, New Jersey, 1936), 2nd ed., p. 780.

[10] For C—C and C—H bond distances, the available data (references 4 and 5) were averaged, while theoretical values were used for root-mean-square amplitudes.

TABLE I. Results of two steps in least-squares refinement for benzene.

Least-squares parameter	Trial value in the first refinement	First refinement	Second refinement	Standard deviation due to random errors	Standard deviation given by Eq. (9)
r(C—C)	1.3950	1.3965	1.3969	0.0008	0.0027
r(C—H)	1.0800	1.0831	1.0845	0.0058	0.0201
$a(C_1—C_2)$	0.001020	0.001047	0.001038	0.000041	0.000140
$a(C_1\cdots C_3)$	0.001500	0.001538	0.001552	0.000074	0.000253
$a(C_1\cdots C_4)$	0.001750	0.001943	0.001890	0.000168	0.000579
$a(C_1—H_1)$	0.002970	0.002762	0.002798	0.000227	0.000784
$a(C_1\cdots H_2)$	0.004990	0.004694	0.004770	0.000240	0.000830
$a(C_1\cdots H_3)$	0.004190	0.004321	0.004277	0.000466	0.001618
$a(C_1\cdots H_4)$	0.004400	0.004580	0.004611	0.000701	0.002421
k	0.6903	0.6849	0.6863	0.0015	0.0049
λ	0.01436	0.014262	0.014259	0.000004	0.000013
μ	−0.1107	−0.11080	−0.11083	0.00006	0.00021
ν	0.9802	0.98016	0.98019	0.00005	0.00017

tion equations mentioned before to those having unit weights. The weighting function was taken inversely proportional to the square of the standard error of J^{obs} [11,12]:

$$p_i=\{\sigma(J)_{min}\}^2/\sigma(J_i)^2, \tag{8}$$

where $\sigma(J_i)$ is the standard error of J_i^{obs} and $\sigma(J)_{min}$ denotes the minimum value among the $\sigma(J_i)$. Trial values used in the first refinement were as follows: For distance parameters, r(C—C) = 1.395 A and r(C—H) = 1.080 A, i.e., the average values of the respective available data.[4,5] Theoretical values derived from spectroscopic data were used for vibration parameters, while preliminary values obtained in the preceding section were used for the background parameters. The values obtained in the first refinement were used as trial values in the next refinement.

The standard error of the ith parameter was evaluated by the expression:

$$\sigma_i^2=\{\sigma_o(J)^2+\sigma_s(J)^2\}(\mathbf{B}^{-1})_{ii}, \tag{9}$$

where $\sigma_o(J)$ given by $[R/(n-m)]^{\frac{1}{2}}$ represents the standard error of an observation and $\sigma_s(J)$ is the standard error due to systematic errors such as the uncertainty of wavelengths, uncertainties in reading the no-light line and the base line on the microphotometer trace, etc.[3] $\mathbf{B}$ in Eq. (9) is a square matrix having the coefficients in the normal equations as its elements.

[11] For convenience in computations, the values of p were rounded off to integers.

[12] The standard errors of observed J were calculated from those of the relative intensities of electron scattering reasonably evaluated by applying a least-squares method to the calibration of characteristics of photographic emulsions. A more detailed description is given in reference 3.

Results in the two least-squares calculations are summarized in Table I. Standard errors free from systematic errors are listed in the fifth column of Table I. They were evaluated from the first term in Eq. (9) alone. The standard errors listed in the last column were calculated with Eq. (9) and are over-all standard errors originating from the random and systematic errors.

DISCUSSION

It was observed in the two steps of refinement that the standard errors fall off fairly rapidly, as seen from Table I. Presumably, if further successive procedures were carried through, the standard errors could be reduced. However, this seems to be insignificant, because the standard errors resulting from the second refinement are considerably less than those due to systematic errors. In the present analysis, the following approximations were made on the theoretical side: incomplete refinement of the vibration parameters, the use of form factors for neutral atoms, the linear approximation form used in the least-squares calculations, and the harmonic oscillator approximations for atom pairs in the molecule. However, it is evident that these approximations are adequate for accuracies comparable with the magnitude of possible experimental errors.

The effects of multiple scatterings, the extended gas volume, and reflections from camera walls were not proportional to the atomic scattering, but related to it through a quadratic function of s in the present investigation. It was fortunate that the experimental background curve could be well reproduced with only three adjustable parameters. This makes it possible to carry out a complete least-squares treatment including the background and molecular parameters. The quad-

ratic function used here as a correction for the theoretical background is not generally applicable, because the correction depends upon various experimental conditions.

The final parameter values for a benzene molecule are presented in Table II, together with their standard errors. For comparison, values reported by Karle[4] and Bastiansen *et al.*[5] are listed in Table II. The structural data obtained in this work are in agreement with those observed by Karle within the limits of error, except those of $l(C_1\cdots H_2)$ and $l(C_1\cdots H_3)$. The agreement with those of Bastiansen *et al.* is also good. Karle has employed the radial distribution method for obtaining the probable values and employed the intensity correlation method for the estimation of the limits of error. On the other hand, Bastiansen *et al.* have analyzed a radial distribution curve alone, the zero line being determined by an experimental envelope which is somewhat uncertain in the innermost region of s. The present measures of uncertainties are standard errors, while those given by Karle are the limits of error. Bastiansen *et al.* have reported no values of standard errors for the molecular parameters, although they have shown the ratios of experimental internuclear distances to calculated ones. The three sets of data given in Table II involve different definitions of error. Accordingly, direct comparison between their accuracy is difficult. It is significant that the standard errors, given as measures of the uncertainties for all parameters refined in the present work, are based on the reasonable least-squares concept.

Table III shows that agreement is satisfactory between the observed and theoretical data for the root-mean-square amplitudes of benzene. The theoretical data were calculated on the basis of a set of force constants given by Miller and Crawford,[13] which are slightly different from those evaluated by Cyvin.[14]

TABLE II. Comparison of the structural parameters of benzene obtained in the present work with those from earlier electron diffraction studies (in A).

Structural parameter	Present work	Karle	Bastiansen *et al.*
$r(C-C)$	$1.396_9\pm0.003$	$1.393+a\pm0.005$ $1.393-a\pm0.005$	1.397 1.398
$r(C-H)$	$1.084_3\pm0.020$	1.08 ± 0.02	1.081
$l(C_1-C_2)$	$0.045_6\pm0.003$	$0.055-(1/3)a\pm0.007$	0.0454
$l(C_1\cdots C_3)$	$0.055_5\pm0.005$	$0.067-(1/3)b\pm0.007$	0.054
$l(C_1\cdots C_4)$	$0.061_4\pm0.009$	0.075 ± 0.01	0.062
$l(C_1-H_1)$	$0.074_8\pm0.010$	0.072 ± 0.015	0.073
$l(C_1\cdots H_2)$	$0.097_5\pm0.008$	0.092 ± 0.02	0.093
$l(C_1\cdots H_3)$	$0.092_8\pm0.016$	0.116 assumed	0.090
$l(C_1\cdots H_4)$	$0.096_0\pm0.023$	0.135 assumed	0.098
	D_{6h} symmetry assumed	where $0\leq a<0.03$ $0\leq b<0.05$	

TABLE III. Comparison between theoretical and experimental values of the root-mean-square amplitudes in benzene.

Atom pair	Theoretical value (at 25°C)	Experimental value (at 18°C)
$l(C_1-C_2)$	0.0452 A	$0.045_6\pm0.003$ A
$l(C_1\cdots C_3)$	0.0548	$0.055_5\pm0.005$
$l(C_1\cdots C_4)$	0.0592	$0.061_4\pm0.009$
$l(C_1-H_1)$	0.0771	$0.074_8\pm0.010$
$l(C_1\cdots H_2)$	0.1000	$0.097_5\pm0.008$
$l(C_1\cdots H_3)$	0.0916	$0.092_8\pm0.016$
$l(C_1\cdots H_4)$	0.0938	$0.096_0\pm0.023$
$l(H_1\cdots H_2)$	0.1597	
$l(H_1\cdots H_3)$	0.1388	
$l(H_1\cdots H_4)$	0.0966	

It is also of interest to compare the present values for the bond distances of benzene with those obtained from Raman spectroscopy and x-ray diffraction. From the measurements of the rotational Raman spectra of the vapor at 61°C, Stoicheff *et al.* have found that $r_0(C-C)=1.397_4\pm0.001$ A and $r_0(C-H)=1.084\pm0.005$ A.[15] Taking into account a correction for the anisotropic thermal motion in crystals, Cox *et al.*[16] have obtained an improved value of 1.39_2 A from the x-ray measurement for the C—C bond distance in the crystalline state at −3°C. Strictly speaking, the distances determined by electron diffraction study are different to some extent from the spectroscopic distances,[17] because of the anharmonicity of vibrations in the molecule. Presumably, the difference is of a comparable order of magnitude with the extent of errors given here. Therefore, it is concluded that no discrepancies exist between the results from different physical methods.

It is true that the radial distribution method and the intensity correlation method have advantages over the least-squares method in some respects. For instance, they are free from any preconceived assumptions on molecular structures. But, once some simplifying conditions such as those due to molecular symmetry are established or assumed as in the present case, the analysis by the least-squares method is straightforward and

[13] B. L. Crawford and F. A. Miller, J. Chem. Phys. **17**, 249 (1949).

[14] S. J. Cyvin, Acta Chem. Scand. **11**, 1499 (1957).

[15] The values for the distances were derived on the assumptions that isotopic substitution does not affect the distances and that a benzene molecule has a planar hexagonal structure.

[16] E. G. Cox, D. W. J. Cruickshank, and J. A. S. Smith, Nature **175**, 766 (1955).

[17] Bartell *et al.* have discussed the difference between the results of electron diffraction and those of spectroscopy in terms of arbitrariness arising from the different operational definitions of molecular parameters, L. S. Bartell and R. A. Bonham, J. Chem. Phys. **31**, 400 (1959).

can help in the proper evaluation of the standard errors for all parameters used. Whereas in computing the radial distribution curve all the experimental intensities are included with equal weights, even though some of them are less reliable because of certain reasons for which corrections often cannot easily be made, the intensities can be given appropriate weights in the least-squares treatment so that all the experimental data are amalgamated to yield a set of molecular data with specified errors.

ACKNOWLEDGMENT

The authors gratefully acknowledge many helpful discussions with Dr. M. Kimura.

THE JOURNAL OF CHEMICAL PHYSICS VOLUME 32, NUMBER 6 JUNE, 1960

Approximate Isotopic Frequency Rule and Its Application to the Spectra of Complex Molecules

S. KRIMM

Harrison M. Randall Laboratory of Physics, The University of Michigan, Ann Arbor, Michigan

(Received January 4, 1960)

An isotopic frequency rule is derived which is valid to a good approximation for individual modes of fully substituted hydrogen-containing groups in a complex molecule. It is given by $\lambda^i/\lambda=1-(\Sigma_j\Delta T_j/\rho T)$, where $\lambda=4\pi^2\nu^2$, $\rho=m^i/m$ = ratio of the isotopic to the normal mass, T = total kinetic energy associated with the vibration, and $\Sigma_j\Delta T_j$ = differential kinetic energy associated with the substituted atoms. When applied to H_2O and NH_3 this rule reproduces frequency ratios to better than 0.5%. The rule is used to predict the frequency ratios for the various modes of the CH_2 group, and with illustrations from the infrared spectra of high polymers it is shown how this rule can be of assistance in making assignments and in providing information on the separability of group vibrations.

INTRODUCTION

THE detailed analysis of the infrared and Raman spectra of a complex molecule (such as, for example, a high polymer) can provide significant information about the structure of the molecule and about the nature of its intramolecular and intermolecular forces. Such an analysis requires that a complete assignment be made of the observed bands in the spectrum to the predicted modes of vibration of the molecule. One of the techniques for identifying the origin of spectral bands, and thereby assisting in the assigning of these bands, is isotopic substitution. For example, when deuterium is substituted for hydrogen in a molecule, we can expect that the frequencies of those modes involving the motions of hydrogen atoms will be lowered. Thus, qualitatively, the shift of a band to lower frequencies upon such isotopic substitution serves to identify the band as originating to some extent in a hydrogen mode. In this article we are interested in investigating what can be said in greater detail about the normal mode from the quantitative magnitude of the frequency shift ratio.

From the theory of small vibrations it is possible to deduce an exact rule relating the frequencies of the normal and the substituted molecules, viz., the Teller-Redlich product rule.[1,2] The difficulty with using this rule in the analysis of complex molecules is that it relates the products of all frequencies belonging to the same symmetry species. Therefore, if a large molecule has low symmetry, as is usually the case, we only obtain a relationship between a large number of frequencies. Ideally, we would like a relation between only two frequencies, that of a given mode in the normal molecule and the frequency of the corresponding mode in the substituted molecule. Although such relations have been derived for small mass changes,[3] they are not very satisfactory when the mass alters by a factor of two, as when deuterium is substituted for hydrogen. Since the latter substitution is the most useful one in the study of complex molecules, we are concerned here with the derivation of a rule which, even if approximate, will be valid for such cases. Specifically, we wish to determine, for example, the frequency shift ratio for each of the modes of a CH_2 group when both hydrogen atoms are replaced by deuterium atoms.

THEORY

For a differential mass change in a molecule, the theory of small vibrations provides an exact expression for the differential frequency shift. It can be shown[4,5] that this is given by

$$d\lambda_k/\lambda_k=-\sum_j dT_j/T_k, \qquad (1)$$

[1] G. Herzberg, *Infrared and Raman Spectra* (D. Van Nostrand Company, Inc., Princeton, New Jersey, 1945), p. 231.

[2] E. B. Wilson, Jr., J. C. Decius, and P. C. Cross, *Molecular Vibrations* (McGraw-Hill Book Company, Inc., New York, 1955), p. 183.

[3] Work cited in footnote 2, p. 188.

[4] E. Teller, Hand- und Jahrb. Chem. Physik 9(II), 43 (1934).

[5] H. J. Bernstein, Can. J. Chem. 29, 284 (1951).

where

$$\lambda = 4\pi^2\nu^2. \quad (2)$$

In these equations, ν is the frequency, λ_k is the value of λ associated with the kth mode of the normal molecule, $T_k = \sum_i m_i \dot{q}_{ki}^2$ = total kinetic energy associated with the kth vibration in the normal molecule, and $\sum_j dT_j = \sum_j dm_j \dot{q}_{kj}^2$ = the differential kinetic energy in the kth mode associated with the substituted atoms j when a mass change dm_j is made. If we assume the substitution of all atoms of one kind in the group, viz., hydrogen in the present case, then Eq. (1) provides an exact expression for the derivative of λ_k with respect to m, the mass of the hydrogen atom:

$$d\lambda_k/dm = -\lambda_k\left(\sum_j \dot{q}_{kj}^2/T_k\right). \quad (3)$$

If these exists an expression for λ_k as a function of m, then Eq. (3) can be used to obtain the finite change in λ, $\Delta\lambda_k$, associated with a finite change in mass, Δm.

No exact expression exists for $\lambda_k(m)$ which is generally true for all molecules. However, for the kinds of small molecules or groups which concern us (e.g., OH, CH_2, CH_3), it can be shown (see Appendix) that to a good approximation

$$\lambda_k = a_1 + (a_2/m), \quad (4)$$

where a_1 and a_2 are constants. If we designate by a superscript i quantities relating to the isotopically substituted molecule, then Eq. (4) leads to

$$\Delta\lambda_k/\Delta m \equiv (\lambda_k{}^i - \lambda_k)/(m^i - m) = -(a_2/mm^i). \quad (5)$$

Since it also follows from Eq. (4) that

$$d\lambda_k/dm = -(a_2/m^2), \quad (6)$$

Eq. (5) can be written

$$\Delta\lambda_k/\Delta m = (\rho)^{-1}(d\lambda_k/dm), \quad 7)$$

where

$$\rho = m^i/m. \quad (8)$$

By substituting Eq. (3) into Eq. (7), we find that

$$(\lambda_k{}^i - \lambda_k)/\Delta m = -(\lambda_k/\rho)\cdot\left(\sum_j \dot{q}_{kj}^2/T_k\right). \quad (9)$$

From this it follows that

$$\lambda_k{}^i/\lambda_k = 1 - \left(\sum_j \Delta T_j/\rho T_k\right), \quad (10)$$

where $\sum_j \Delta T_j = \sum_j \Delta m \dot{q}_{kj}^2$. Equation (10) is the basic relation of the isotopic frequency rule.

RESULTS AND DISCUSSION

In order to test the validity of Eq. (10), we will consider its application to H_2O and NH_3. It becomes immediately apparent that in order to make use of this rule it is necessary to know the normal coordinates; only in this way can we know the relative amplitudes of motion of the atoms, and therefore the relative kinetic energies required in Eq. (10). Since such normal coordinates are not known in complex molecules, it would seem that the frequency rule would be of little use. However, it frequently happens that the true normal coordinate is very well approximated by a suitably chosen symmetry coordinate. For the preceding type of small molecule, the condition of conservation of momentum then uniquely defines the amplitudes of motion, and therefore permits the application of Eq. (10). The departures from the predicted frequency ratios can then serve as a measure of the departure of the true mode in the complex molecule from that represented by the simple symmetry coordinate. For H_2O and NH_3, symmetry coordinates were chosen in which the atoms move along and perpendicular to the bonds in the molecule, viz., valence coordinates. [See Figs. 55(b) and 58 of footnote 1 for descriptions of these symmetry coordinates.] The results of applying Eq. (10) are shown in Table I, and are compared with the ratios for the observed fundamentals and the zero-order frequencies[6] (in the latter case the observed frequencies are corrected for anharmonicities). For example, for ν_1 of H_2O the relative amplitudes of motion of the H and O atoms (and therefore the $\dot{q}$) are in the ratio of 1 to $\frac{1}{5}\cos 52.5°$, respectively. Therefore,

$$\lambda_k{}^i/\lambda_k = 1 - 2/[2(2+\tfrac{1}{4}\cos^2 52.5)] = 0.5222,$$

and $\nu_1/\nu_1{}^i = 1.384$.

TABLE I. Application of isotopic frequency rule to H_2O and NH_3.

	$(\nu/\nu^i)_{calc}$	$(\nu/\nu^i)_{obs}$	
		Fundamentals	Zero-order frequencies
H_2O, D_2O:			
$\nu_1(\nu_s)$[a]	1.384	1.369 (−1.1%)	1.387 (+0.2%)
$\nu_2(\delta)$	1.365	1.348 (−1.2%)	1.363 (−0.2%)
$\nu_3(\nu_a)$	1.365	1.353 (−0.9%)	1.368 (+0.2%)
NH_3, ND_3:			
$\nu_1(\nu_s)$	1.395	1.379 (−1.1%)	1.400 (+0.4%)
$\nu_2(\delta_s)$	1.317	1.270 (−3.6%)	1.313 (−0.3%)
$\nu_3(\nu_a)$	1.359	1.350 (−0.7%)	1.357 (−0.1%)
$\nu_4(\delta_a)$	1.403	1.367 (−2.6%)	1.380 (−1.6%)

[a] ν=stretching, δ=bending, s=symmetric, a=antisymmetric.

Several comments can be made on the results shown in Table I. First, as would be expected, the agreement is better for the zero-order frequencies than for the observed fundamentals. Second, in the cases of the ν_1, ν_2, and ν_3 modes of H_2O and the ν_1, ν_2, and ν_3 modes of NH_3 the chosen symmetry coordinate actually approximates closely the true normal coordinate, and it can be seen that the observed ratios are in quite good agreement with the calculated ones. For ν_4 of NH_3, the symmetry coordinate is, in fact, not a good approximation to the normal coordinate, and the observed ratio does deviate more significantly from the com-

[6] D. M. Dennison, Revs. Modern Phys. 12, 175 (1940).

TABLE II. Frequency shift ratios for CH_2 and CH_3 groups.

		$(\nu/\nu^i)_{calc}$
CH_2, CD_2:	ν_s[a]	1.379
	ν_a	1.349
	δ	1.349
	γ_w[b]	1.323
	γ_t	1.414
	γ_r	1.379
CH_3, CD_3:	ν_s	1.398
	ν_a	1.349
	δ_s	1.300
	δ_a	1.403
	γ_r	1.292

[a] See footnote to Table I.
[b] γ_w=wagging, γ_t=twisting, γ_r=rocking.

puted one. However, if the true normal coordinate for ν_4 is used in the calculation, the computed value of ν/ν^i is in much better agreement with the observed value. Third, even though the ratios for the fundamental frequencies deviate somewhat more from the calculated values than do those for the zero-order frequencies, the relative values are in the same order as predicted. From the foregoing observations it can be concluded that the isotopic frequency rule given by Eq. (10) is valid to a good approximation for such small groups, and that it should provide a satisfactory basis for identifying individual modes.

Similar calculations for CH_2 and CH_3 groups are shown in Table II. These are again based on symmetry coordinates of the kind used for H_2O and NH_3. In the γ_w, γ_t, and γ_r (wagging, twisting, and rocking) modes of CH_2, motions perpendicular to the bonds have been assumed, the amplitudes being determined by the conservation of momentum condition. That is, the calculation is based on the assumption of isolated groups. In neither case can satisfactory tests of the validity of these ratios be made from the examination of small molecules, since the normal modes in such cases depart significantly from those assumed. Nevertheless, the magnitudes observed are in the order predicted. (For example, the ratio of zero-order CH_3 frequencies for CH_3Cl, CD_3Cl is[7]: ν_s—1.388, ν_a—1.350, δ_s—1.325, δ_a—1.391, γ_r—1.320.)

The application of the isotopic frequency rule to the spectra of complex molecules helps to establish its validity and range of application. We will consider the use of this rule in connection with the assignments of the $\nu_s(CH_2)$, $\nu_a(CH_2)$, $\delta(CH_2)$, $\gamma_w(CH_2)$, and $\gamma_r(CH_2)$ modes of some high polymers for which satisfactory data are available (the $\gamma_t(CH_2)$ mode is usually hard to identify). The results for these polymers are collected in Table III. For the detailed arguments on the assignments, reference is made to a recent review article.[8]

As we noted in the foregoing the calculated frequency ratios are for isolated CH_2 groups. When a CH_2 group is part of a larger molecule, it will generally be be true that atoms in the rest of the molecule also move during modes which we usually associate with only the CH_2 group. To the extent that other atoms partake in the vibrational motion, we may expect the observed frequency ratios to deviate from the calculated ones given in Table III. This deviation should provide a measure of the separability of the group frequency involved. From considerations of the motions of the atoms in the infrared active modes of the polyethylene chain, we expect the relative amplitudes of motion of the atoms in the CH_2 groups to approximate most closely those of an isolated CH_2 group. It is therefore gratifying to find that the ratios for the CH_2 modes in polyethylene most closely agree with the predicted values. (We expect some deviation because fundamental frequencies, rather than zero-order frequencies, are being used.) The larger ratio for γ_r as compared to ν_s may indicate that in the former mode there is less carbon motion than in the latter mode, or it may be a result of different anharmonicities for the two vibrations. In polyvinyl chloride, on the other hand, the ratios as well as their relative magnitudes differ significantly from the predicted values. This may be taken to indicate that what we call a CH_2 mode in this molecule actually significantly involves motions of the other atoms. That is, this is a poor instance of a separable group frequency. This situation is confirmed by other data on polyvinyl chloride: upon full deuteration of the molecule, the C—Cl stretching frequencies shift from a mean value of 623 cm^{-1} to one of 581 cm^{-1}. This 42-cm^{-1} drop in the chlorine stretching frequencies when the hydrogen atoms are replaced by deuterium is a clear indication that the vibrational modes of this molecule significantly involve motions of all of the atoms. It would appear also that the more nearly isolated the group vibration is from motions in the remainder of the molecule the more nearly equal will be the ratios for ν_a and δ, for example, even though the actual values deviate from the predicted ratios. Polystyrene seems to offer an illustration of this situation.

The spectrum of polyvinylidene chloride provides an illustration of how the isotopic frequency rule can be used as an aid in making assignments. Assignments for the $\nu_s(CH_2)$, $\nu_a(CH_2)$, $\delta(CH_2)$, and $\gamma_w(CH_2)$ modes in polyvinylidene chloride can be made with little difficulty, both in the normal and in the deuterated molecules. There has been some question, however, about the $\gamma_r(CH_2)$ mode. One assignment would result in a frequency shift ratio of 1.240 on deuteration; an alternative assignment would give a ratio of 1.388. Upon examining the ratios for the other CH_2 modes, it is clear that the latter value is entirely reasonable, while the former is considerably out of line. Other arguments also favor the latter assignment, thus indicating that consistency with the results of the fre-

[7] W. T. King, I. M. Mills, and B. Crawford, J. Chem. Phys. 27, 455 (1957).
[8] S. Krimm, (to be published).

TABLE III. Application of isotopic frequency rule to some high polymers.

	ν_s (CH_2)	ν_a (CH_2)	δ(CH_2)	γ_w (CH_2)	γ_r (CH_2)
Predicted ratio	1.379	1.349	1.349	1.323	1.379
Observed ratio					
Polyethylene	1.372	1.342	1.341	...	1.384
Polyvinyl chloride	1.320	1.303	1.283	...	1.220
Polystyrene	1.358	1.330	1.334	...	...
Polyvinylidene chloride	1.378	1.340	1.340	1.322	1.388
Polyethylene terephthalate {C:	1.268	1.222	1.210	1.198(?)	1.271
{A:	1.365	1.356	1.352	1.302(?)	...

quency rule provides another criterion for judging whether or not an assignment is satisfactory. The results for polyethylene terephthalate are in agreement with observations made above, and indicate the possible difference between the vibrational modes of a group in the crystalline chain structure and in the amorphous chain structure.

In summary, we have been able to show that an isotopic frequency rule can be derived which is valid to a good approximation for single modes of groups within a complex molecule. Not only does the application of this rule provide information on the separability of group vibrations, but it also can be of assistence in making assignments.

ACKNOWLEDGMENT

The author is indebted to K. T. Hecht for many helpful discussions.

APPENDIX

The relation expressed by Eq. (4), while not generally true, is valid to a good approximation for some small molecules. For diatomic molecules this is obviously the case, since in this instance

$$\lambda = k/\mu = (k/m_1) + (k/m_2). \tag{A1}$$

For a nonlinear symmetric triatomic molecule, XY_2, the frequencies, on the assumption of a valence force field, are given by (see work cited in footnote 1, p. 168)

$$\lambda_3 = [1 + (2m_Y/m_X)\sin^2\alpha](k_1/m_Y) \tag{A2}$$

$$\lambda_1 + \lambda_2 = [1 + (2m_Y/m_X)\cos^2\alpha](k_1/m_Y) + (2/m_Y)[1 + (2m_Y/m_X)\sin^2\alpha](k_3/l^2) \tag{A3}$$

$$\lambda_1\lambda_2 = 2[1 + (2m_Y/m_X)](k_1/m_Y^2)\cdot(k_3/l^2). \tag{A4}$$

For the antisymmetric stretching frequency, given by Eq. (A2), it can be seen that a relation of the form of Eq. (4) is satisfied. From Eqs. (A3) and (A4) we find that

$$\lambda_1 = (A/m_X) + (B/m_Y) \pm [(B^2 - 4D)\cdot(1/m_Y^2) + (2AB - 4C)\cdot(1/m_Y^2)\cdot(m_Y/m_X) + (A^2/m_X^2)]^{\frac{1}{2}}, \tag{A5}$$

where A, B, C, and D are constants involving the force constants, k_1 and k_3/l^2, and A^2, B^2, AB, C, and D are of the same order of magnitude. Since for example for CH_2 $m_X = 12m_Y$, and $(B^2 - 4D) \sim A^2$, the last term in the brackets of Eq. (A5) can be neglected; the error introduced is about 0.7%. Expanding the bracket, and dropping terms in $(m_Y/m_X)^2$ and higher powers (since they will be negligible compared to 1), we find that

$$\lambda_1 \cong \left[\frac{A}{m_X} \pm \frac{(B^2 - 4D)^{-\frac{1}{2}}(2AB - 4C)}{m_X}\right] + [B \pm (B^2 - 4D)^{\frac{1}{2}}]\cdot m_Y^{-1}. \tag{A6}$$

Since m_X is kept constant upon isotopic substitution, this can be written as

$$\lambda_1 \cong a_1 + (a_2/m) \tag{A7}$$

which is of the form of Eq. (4). An analogous relationship holds for λ_2, and can also be shown to be similarly valid for the frequencies of a pyramidal XY_3 molecule.

Pyroelectric Effect in the Cubic ZnS Structure

ROLF LANDAUER

Research Laboratory, International Business Machines Corporation, Poughkeepsie, New York

(Received December 4, 1960)

The classical theory of pyroelectricity, which uses only the symmetry of the crystal class, is shown to be incorrect. The surface structure is also relevant. The case of cubic ZnS is discussed in detail.

THE classical theory of pyroelectricity[1] correlates the existence of a pyroelectric effect with the symmetry of the crystal class rather than with the symmetry of the actual crystal under consideration. The theory allows only those classes which possess a unique polar axis to be pyroelectric.[2] It is clear that this cannot be the complete answer. Consider a crystal which has sufficient symmetry to prevent it from having a dipole moment according to this theory, e.g., NaCl. Take a crystal of NaCl which satisfies the theorem and has no net dipole moment. Take some Na^+ ions from one of its surfaces and transfer them to the opposite surface. We have now given the crystal a net dipole moment. Pyroelectricity requires not only a dipole moment but a temperature-dependent one, and, in the case cited, there would not be such a temperature dependence.[3] If, however, we had taken an example which is less clearly ionic, one in which the effective charge associated with an ion is temperature dependent, then the dipole moment would also be temperature dependent. Furthermore, in the NaCl structure there would be no reason, in terms of thermal equilibrium, why one crystal surface should be rich in Na^+ ions and the opposite one rich in Cl^-, though such a situation could perhaps be brought about by exposing the opposing faces to different vapors.

Consider, instead, the case of ZnS which exists in two forms. Cubic ZnS, or sphalerite, has no polarization according to the usual theory, while hexagonal ZnS or wurtzite is permitted to have a pyroelectric effect. Consider the cubic case in detail. Cubic ZnS can be considered[4] as a sequence of layers perpendicular to its (1, 1, 1) axis, usually denoted in the fashion ABCABCABC···. Each layer can be taken to consist of a sublayer of Zn atoms near the $(\bar{1}, \bar{1}, \bar{1})$ face of the layer and a second sublayer of S atoms near the (1, 1, 1) face. The layers will consist of hexagons of the form shown in Fig. 1, and each Zn atom is bonded to three nearest neighbor S atoms in the same layer. Each S atom is also bonded to three nearest neighbor Zn atoms in the layer. Between the layers, as described, there are fewer bonds, each atom is bonded to one nearest neighbor atom in an adjacent layer, and all these interlayer bonds are parallel to the (1, 1, 1) axis. It is clear that each layer has a dipole moment and that all layers have the same moment. Hence the crystal, if it consists of an integral number of these layers has a net dipole moment. The dipole moment, however, depends critically on the fact that $(\bar{1}, \bar{1}, \bar{1})$ face of the crystal is a layer of Zn atoms and the (1, 1, 1) face is a layer of S atoms. This configuration, however, is not an unlikely one, since it corresponds to the minimum number of bonds broken at the surfaces, and this is relevant to the surface energy, to the extent that the crystal is covalent. Birman[5] estimates that ZnS is $\frac{1}{2}$ covalent. Other compounds, such as SiC or BN, are much more highly covalent and are much more likely to have surfaces of the type invoked. Note, however, that experimentally one measures the change in dipole moment with temperature (or, perhaps, hydrostatic pressure). A highly ionic or highly covalent system would be likely to have a smaller change in effective ionic charge with temperature than a borderline system such as ZnS.

The fact that ZnS has a phase transition at 1020°C and at higher temperatures favors the hexagonal form, as do the more highly ionic species such as CdS and ZnO, and at lower temperatures favors the cubic form, which is more characteristic of the covalent state, does make it plausible that the effective charge changes with temperature.

Even if the ZnS crystal is not terminated as its (1, 1, 1) and $(\bar{1}, \bar{1}, \bar{1})$ faces as it is here pictured, it is still likely to have a dipole moment. If, for example, the crystal is terminated so that it has the maximum number of broken surface bonds, then the dipole moment will be three times as large and in the opposite direction from the one we have considered. All intermediate cases are possible, and only a crystal which is terminated in a very particular way will have no dipole moment. In our case, a layer of S atoms on the (1, 1, 1) surface equal to $\frac{3}{4}$ the maximum number and a layer of S atoms on the $(\bar{1}, \bar{1}, \bar{1})$ surface equal to $\frac{1}{4}$ the

[1] W. Cady, *Piezoelectricity* (McGraw-Hill Book Company, Inc., New York, 1946), p. 699.

[2] J. F. Nye, *Physical Properties of Crystals* (Oxford University Press, New York, 1957), p. 79.

[3] Strictly speaking, thermal expansion does cause a change in both the total dipole moment and the polarization per unit volume. The experimentally relevant quantity, however, is the image charge induced on shorted circuited electrodes, and this quantity is unaffected by an effect such as uniform thermal expansion, in which the electrode separation and the dipole moments are scaled similarly.

[4] A detailed picture of the lattice is given, for example, in Seitz, *Modern Theory of Solids* (McGraw-Hill Book Company, Inc., New York, 1940), p. 50, Fig. 60.

[5] J. L. Birman, Phys. Rev. **109**, 810 (1958).

maximum number would case the dipole moment to vanish. More generally, the pyroelectric effect must be regarded as a surface effect, since adsorbed layers can affect the moment just as well as the transfer of ions comprising the crystal.

The experimental situation in pyroelectricity is confusing, since there are a numer of causes which can result in false observations of pyroelectricity. In particular a pyroelectric effect has been observed in cubic ZnS[6] and has been ascribed to nonuniform heating. It may be noted, however, that a change in effective ionic charge of the order of 10^{-6} electronic charges per °C would be adequate to account for the magnitude of the observed effect, if we assume that the surface composition was such as to minimize the number of broken bonds.

Hexagonal ZnS, which we have not considered explicitly, would presumably show a very similar polarization along the c axis. This would be a polarization in addition to the more usually expected polarization arising from the fact that the bond structure surrounding an atom has lost its perfect tetrahedral arrangement in the hexagonal structure. The latter would, in the case of ZnS with its almost ideal c/a ratio, be likely to be very small. The resultant similarity between the polarization of hexagonal and cubic phases may be connected with Lempicki's[7] recent pyroelectric observations on ZnS. Lempicki found that hexagonal crystals with little faulting had no pyroelectric effect, while crystals which were largely cubic or at least had appreciable faulting showed an effect. We do not have a detailed explanation of this observation. It is, however, reasonable to suppose that the crystals in which the layer structure we have described is relatively perfect as one goes over the area of a single layer are the ones in which faulting occurs readily. And it is these crystals to which our explanation would also apply most readily.

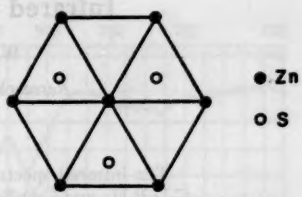

FIG. 1. The full circles represent a plane of Zn atoms which is near the $(\bar{1}, \bar{1}, \bar{1})$ end of the layer. The plane of S atoms is near the (1, 1, 1) end.

The difference in polarization between hexagonal and cubic ZnS has been involved a number of times in explanations of the anomalous photovoltage in ZnS.[8] Our present picture does not destroy these explanations, since it is not the net polarization that counts in generating internal fields, but its divergence, and a small difference in polarization between the two phases is likely to exist. It should, however, be noted that a single stacking fault, separating two perfectly hexagonal regions, is enough to produce a dipole layer. To a first approximation, one considers that the introduction of the stacking fault simply corresponds to a displacement of the crystal on one side with respect to the crystal on the other side. Since the displacement vector is perpendicular to the stacking fault, this introduces no dipole layer. If, however, one then admits that there will be changes in the wave functions for the atoms next to the fault, a dipole layer comes into existence.

[6] See footnote 1, p. 708.
[7] A. Lempicki, Phys. Rev. **113**, 1204 (1959).
[8] W. J. Merz, Helv. Phys. Acta **31**, 625 (1958), also footnote 7, and private communications from many people, particularly R. C. Casella and D. O. North.

Infrared Spectra of Alkyldiboranes. II. Monoethyldiboranes

WALTER J. LEHMANN,* CHARLES O. WILSON, JR.,† AND I. SHAPIRO*

Research Laboratory, Olin Mathieson Chemical Corporation, Pasadena, California

(Received January 18, 1960)

The infrared spectra of five isotopic variants of monoethyldiborane, $C_2H_5B_2{}^{10}H_5$, $C_2H_5B_2H_5$, $C_2H_5B_2D_5$, $C_2D_5B_2H_5$, and $C_2D_5B_2D_5$, are analyzed and frequency assignments are made. The frequencies and intensities of the various bands are compared with those in the corresponding monomethyldiboranes and the related terminally substituted B_2H_5D and B_2D_5H, as well as with triethylboranes. In addition, vapor-pressure data in the −58° to −110°C range for isotopically normal ethyldiborane are reported.

INTRODUCTION

THIS second in the series of papers dealing with the infrared spectra of alkyldiboranes analyzes the spectra of five isotopic variants of monoethyldiborane. The analysis is based primarily on the corresponding treatment of the monomethyldiboranes.[1] Since the internal vibrations of the ethyl group should be more or less independent of the rest of the molecule, at least to a first approximation, we can correlate ethyl group assignments with those of the triethylboranes.[2,3]

EXPERIMENTAL

The various monoethyldiboranes were prepared by the reaction of diborane with triethylborane, following the procedure described for the monomethyldiboranes.[1] Purification was accomplished by distillation through a trap at −112°C and condensation at −145°C. Mass spectrometric analyses indicated negligible impurities. In the ethyl-deuterated compounds the protium content of the ethyl group was ca 0.7%, resulting in ca 3.5% of the $-C_2D_4H$ species.

Vapor-pressure data for monoethyldiborane are listed in Table I. Above −58°C disproportionation proceeded too rapidly for the attainment of reliable results. The vapor pressure curve for the −110° to −58°C temperature range can be expressed by the equation:

$$\log P_{mm} = (-883.25/T°_K) + 0.011376 T°_K + 3.2343,$$

with an average standard deviation of 0.05 mm. The extrapolated boiling point is −9.53°C. Ethyldiborane forms a glass below −156°C.

TABLE I. Vapor pressure data for $C_2H_5B_2H_5$.

Temp °C	Pressure, mm	Calc pressure, mm	Deviation
−110.42	0.45	0.45	0.00
−99.10	1.40	1.38	+0.02
−92.60	2.45	2.49	−0.04
−89.08	3.35	3.39	−0.04
−86.78	4.15	4.12	+0.03
−84.86	4.95	4.85	+0.10
−83.40	5.50	5.47	+0.03
−80.63	6.85	6.86	−0.01
−71.92	13.55	13.63	−0.08
−58.49	36.50	36.46	+0.04

The infrared spectra were recorded on a Perkin-Elmer Model 21 spectrophotometer equipped with sodium chloride optics. These spectra were obtained before there was much evidence of the disproportionation products, viz, diborane and 1,2-diethyldiborane. The four spectra involving isotopically normal boron are reproduced in Fig. 1; their measured frequencies plus those of $C_2H_5B_2{}^{10}H_5$ are listed in Table II.

For the sake of brevity, the designations "A_1" to "E_1" (analogous to the monomethyldiboranes) will be used (see heading of Table II).

ASSIGNMENT OF FREQUENCIES

Comparison of spectra "A_1" through "E_1" quickly yields clues as to which fragment of each molecule ($-B_2H_5$, $-B_2D_5$, $-C_2H_5$, or $-C_2D_5$) is responsible for a particular absorption. Additional support for $-B_2H_5$ and $-B_2D_5$ assignments may be obtained by comparison with the spectra of the corresponding monomethyldiboranes[1] and partially deuterated diboranes,[4] B_2H_5D and B_2D_5H. The group assignments are indicated by numerals in Fig. 1.

The symmetry of the ethyldiborane molecule is not established. The methyl group may be located in the $HBBH_2$ plane, facing toward either the BH or the BH_2 group; in either case the molecule may possess a plane of symmetry—point group[5] C_s. On the other hand, if the ethyl group is rotated in any other way the molecule would have no symmetry element and would be classed as point group C_1. The infrared spectrum alone does not enable us to decide among these alternatives.

* Present address: Hughes Tool Company—Aircraft Division, Building 24, Culver City, California.

† Present address: National Engineering Science Company, Pasadena, California.

[1] W. J. Lehmann, C. O. Wilson, Jr., and I. Shapiro, J. Chem. Phys. **32**, 1087 (1960) (first paper of this series).

[2] W. J. Lehmann, C. O. Wilson, Jr., and I. Shapiro, J. Chem. Phys. **28**, 781 (1958).

[3] W. J. Lehmann, C. O. Wilson, Jr., and I. Shapiro, J. Chem. Phys. **31**, 1071 (1959).

[4] W. J. Lehmann, J. F. Ditter, and I. Shapiro, J. Chem. Phys. **29**, 1248 (1958); also see W. J. Lehmann and J. F. Ditter, J. Chem. Phys. **31**, 549 (1959).

[5] G. Herzberg, *Infrared and Raman Spectra of Polyatomic Molecules* (D. Van Nostrand Company, Princeton, New Jersey, 1945).

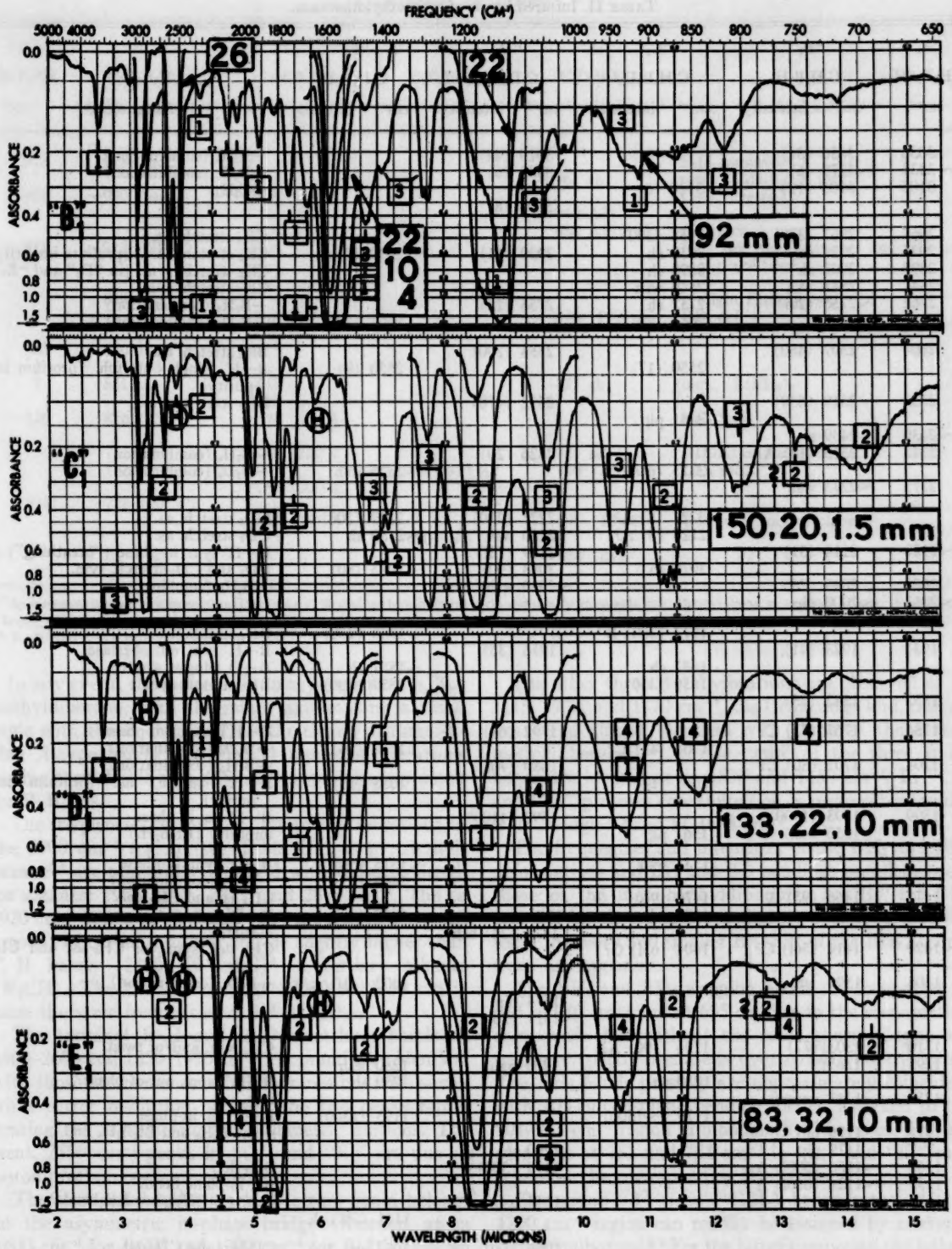

FIG. 1. Infrared spectra of gaseous monoethyldiboranes; pressures reported for 5-cm cells. "B_1": $C_2H_5B_2H_5$; "C_1": $C_2H_5B_2D_5$; "D_1": $C_2D_5B_2H_5$; "E_1": $C_2D_5B_2D_5$. Boxed numbers refer to bands as follows: 1: —B_2H_5 bands; 2: —B_2D_5 bands; 3: —C_2H_5 bands; 4: —C_2D_5 bands; circled H: Protium-impurity bands.

TABLE II. Infrared bands of monoethyldiboranes.

"A_1" $C_2H_5B_2{}^{10}H_5$ cm^{-1}	"B_1" $C_2H_5B_2H_5$ cm^{-1} intensity[a]	"C_1" $C_2H_5B_2D_5$ cm^{-1} intensity[a]	"D_1" $C_2D_5B_2H_5$ cm^{-1} intensity[a]	"E_1" $C_2D_5B_2D_5$ cm^{-1} intensity[a]	Assignment[b]
3636	3636 (31)		3610 (44)		$-B_2H_5$ (combination)
~3333	~3279 (6)		3333 (6)		$-B_2H_5$ (combination)
3105	3105 (12)	~3120 (6)			$-C_2H_5$
			3096 (8)		
2967	2967 (330)	2958 (300)			CH_3 stretch. as.
2924	2924 sh	2932 sh	2930 (11)	2910 (7)b	CH_2 stretch. as. } protium impurity
2898	2907 sh	2898 sh			CH_3 stretch. sym. } in "D_1" and "E_1"
2841	2841 wsh	2849 wsh			CH_2 stretch. sym.
2762	~2755 (20i)	2732 sh	2755 (12)		$-B_2H_5$ (combination)
		2681 (28)		2667 (19)	$-B_2D_5$ (combination)
2604	2597 (480)		2584 (290)		BH_2 stretch. as.
		2550 (17)		2550 (9)	B—H (single) stretch. (protium impurity)
2525	2519 (630)		2512 (470)		BH_2 stretch. sym.
		2481 pip			
~2439	~2439 sh				
2342	2315 (18) A?		2326 (20)		$-B_2H_5$ (combination)
		2315 (6) A?		~2326 wsh	$-B_2D_5$ (combination)
2273	~2273 wsh				
		2227 (8) A?	2227 (210)	2222 (200)	CD_3 stretch. as.
		2128 (8) A?	2150 wsh	~2150 sh	CD_2 stretch. as.
~2120	2114 (31)		2119 (72i)		B—H' sym. in-phase ("breathing")
		2070 sh	2083 (90)	2083 (80)	CD_3 and CD_2 stretch. sym.
2053	2049 (28)		~2030 wsh		$-B_2H_5$ (combination)
~2012	~2000 pip				
		1972 (280) B		1968 (250)	BD_2 stretch. as.
1934	1923 (41)		1916 (35)		B—H' sym. out-of-phase
		1887 sh		~1887 sh	B—D (single) stretch.
		1859 (350)		1859 (300)	BD_2 stretch. sym.
1852	1842 (25)				
1786	1767 (72) C?		1792 (63)		B—H' as. out-of-phase
		1764 (41) C?		1748 (26)	$-B_2D_5$ (combination)
1704	1701 (80) C?		1680 (70i)		$-B_2H_5$ (combination)
		1658 (14)		1658 (15)	B—H' (single) as. (protium impurity)
1599	1593 (1900)		1592 (1100)		B—H' as. in-phase
	1550 wsh	1567 pip			impurity ($Et_2B_2H_4$)
		1531 wsh		~1515 wbsh	B—D' sym. in-phase
				1486 (33)	$-B_2D_5$ (combination)
1471	1466 (95) A	1470 (94)			CH_3 as. and CH_2 def.
		1428 ssh		1428 (37i) b	B—D' sym. out-of-phase
			1428 (24) bsh		$-B_2H_5$
~1420	1414 (56i) C?	1404 (65i) C?			CH_3 def. sym.; or CH_3 as. and CH_2 def.
1408	1399 sh			1402 (41i)	$-B_2D_5$ (combination)
			1374 pip		
			~1321 (20)		
1310	1303 (72)	1294 (190) A?			CH_2 wag. and/or twist.
1295	1285		1280 wsh	1280 wsh	
		1250 sh		1250 sh	B—D' asym. out-of-phase? imp.
1259	1242 vw pip				
		1179 (~1300)		1193 (1300)	B—D' as. in-phase
1179	1176 pip				slight B_2H_6 and $Et_2B_2H_4$ imp.
	1172 pip		1200 sh		
1160	~1156 (300i) A		1179 (380)		BH_2 def.
1135	~1124 (620i) A				BH in-plane bend.
			1143 bsh		imp? $(EtBH_2)_2$? or BH bend.?
				1111 (70i) sh	
			1066 (140)	1063 sh	CD_3 as. and CD_2 def.
		1047 (270)		1050 (90)	BD in-plane bend.
~1072	~1065 (55) b				CH_3 rock.
~1020	~1015 (44) b				

TABLE II. (Continued)

"A_1" $C_2H_5B_2{}^{10}H_5$ cm^{-1}	"B_1" $C_2H_5B_2H_5$ cm^{-1} intensity[a]	"C_1" $C_2H_5B_2D_5$ cm^{-1} intensity[a]	"D_1" $C_2D_5B_2H_5$ cm^{-1} intensity[a]	"E_1" $C_2D_5B_2D_5$ cm^{-1} intensity[a]	Assignment[b]
978	973 pip C				B_2H_6 impurity
				~962 sh	prob. $(C_2D_5BD_2)_2$ imp.
~930	~930 sbsh	943 (84) A			C—C stretch?
				~950 A?	
			945–	938 A? (105)	CD_3 rock.
~917	~913 (60) C		–933 (82)		BH_2 wag. (out-of-plane) and BH out-of-plane bend.?
	889 w				v. slight $Et_2B_2H_4$ imp.
		881 (130) A		876 (190) A	BD_2 def.
			846 (55)		C—C stretch. in "D_1" and "E_1"
885	~870 (48i)				
?	857 (43i)				
?	851 sh	833 sh		837 sh	imp., $(EtBH_2)_2$
		806 pip			
~826	816 (43)	~800 (40) A?			CH_2 rock.
		751 (27i) C		781 ssh	BD out-of-plane bend.?
			742 (13) A?	760 (22) A?	CD_2 rock.
		735 (30i) C			
718	716 (20) C?				
		695 (35) C		695 (28) C	BD_2 wag. (out-of-plane)
			690 wvb		
				654 (28)	

[a] Approximate intensities expressed as absorbance × 10^3 divided by cell length in cm and sample pressure in mm. Abbreviations: w: weak; s: strong; sh: shoulder; b: broad; v: very; i: apparent intensity increased by overlap with other band(s); A, B, C: apparent band types.
[b] B—H′ and B—D′ refer to bridge stretchings.

In any event, the molecule is an asymmetric top, like methyldiborane, with the minor axis making a small angle with the B–B axis. Thus the clearly distinguishable *A*-type bands (see Fig. 1) represent vibrations having their dipole moments vary approximately along the B–B axis.

The frequencies of the C–H stretching vibrations in the 2900 cm^{-1} region (see Table II), as in triethylborane[2,3] are practically identical with those reported[6] for alkanes: 2962, 2926, 2872, and 2853 cm^{-1}. The ca 2920 cm^{-1} bands in "D_1" and "E_1" are due to the small amount of carbon-protium and lie slightly higher than C–H bands (2890±10 cm^{-1})[6] in tertiary alkanes (R_3CH). The C–D stretchings (2080 to 2230 cm^{-1}) have the same frequencies as in[3] $B(C_2D_5)_3$.

The terminal B–H and B–D stretching bands at 2500–2600 and 1850–1970 cm^{-1} are practically identical with those in the monomethyldiboranes but with somewhat better resolution between the two peaks representing the asymmetric and symmetric motions. The weak 2550 cm^{-1} peaks in "C_1" and "E_1" are due to boron-protium contamination.

The strongest band in each spectrum again belongs to the asymmetric in-phase bridge vibration, at ca 1600 cm^{-1} for B–H′ and 1200 cm^{-1} for B–D′. (For an explanation of our descriptions of the bridge vibrations see Fig. 3 of the previous paper[1].)

[6] L. J. Bellamy, *The Infrared Spectra of Complex Molecules* (John Wiley & Sons, Inc., New York, 1958).

The other three B–H′ vibrations are observed at ca 2115, 1920, and 1770 cm^{-1}, the frequencies and intensities being almost identical with those in the monomethyldiboranes. Likewise, two of the three B–D′ bands are located at ca 1530 and 1430 cm^{-1}. In "C_1" and "D_1" protium contamination is responsible for the B–H′ (single) band at 1658 cm^{-1}.

The frequencies and intensities of the BH_2 and BD_2 deformations and BH and BD bendings parallel closely those of the monomethyldiboranes. In "B_1" the BH_2 and BH bands are resolved slightly better, so that the lesser intensity and smaller B^{10} shift of the BH_2 absorptions are apparent.

The BH_2 and BD_2 wagging bands are located at ca 913 to 940 cm^{-1} and at 695 cm^{-1} as in the monomethyl compounds but without the same sharp *C*-type appearance (partly because of overlap with other bands). The BH_2 bands possibly are approximately coincident with BH out-of-plane bending modes, assigned to the 901–913 cm^{-1} region in monomethyldiboranes. The absorptions at 751 and 781 cm^{-1} in "C_1" and "E_1" may represent the corresponding BD motions.

The group [3] (i.e., $-C_2H_5$) bands in the 1470 to 1290 cm^{-1} region can readily be assigned by reference to triethylborane.[2,3] For the latter compound the following assignments have been made: 1471 cm^{-1} (strong) to CH_3 asymmetric and CH_2 deformations (shoulder at 1449 cm^{-1}), 1391 cm^{-1} (medium-weak) to CH_3 symmetric deformation, 1325 cm^{-1} (strong) to CH_2

wagging and/or twisting (shoulder at 1290 cm^{-1}); the first two bands exhibit no apparent B^{10}-isotope shift, but the 1325 cm^{-1} band shifts to 1333 cm^{-1} in triethylborane-b^{10}. The bands at ca 1470, 1410, and 1300 cm^{-1} in "B_1" and "C_1" have very similar relative intensities and apparent isotope shifts (e.g., ca 8 cm^{-1} for 1300 cm^{-1}) as the bands cited above and hence are assigned in the same manner. (Alternatively, the ca 1410 cm^{-1} bands could represent a companion to the CH_3 asymmetric and CH_2 deformations, analogous to the 1449 cm^{-1} shoulder in triethylborane.)

The corresponding CD vibrations in $B(C_2D_5)_3$ have been assigned[3] to 1067 (ms), 1028 (m), and 1238 (vs)—CH/CD frequency ratios of 1.38, 1.35, and 1.07. This enables us to assign the ca 1065 cm^{-1} bands in "D_1" and "E_1" to CD_3 asymmetric and CD_2 deformations (ratio of ca 1.38). The CD_2 wagging and/or twisting bands could quite well be masked by the strong bands at ca 1200 cm^{-1}. We are unable to arrive at an assignment for the CD_3 symmetric deformation, expected in the 1000 to 1060 cm^{-1} range, possibly because it is too weak to be observed or has been shifted by interaction with other vibrations (such as the CD_3 rockings at 940 cm^{-1}). In deuterated propane, both asymmetric and symmetric CD_3 deformations have been assigned[7] to 1070 cm^{-1}. The 1063 cm^{-1} band in "E_1" overlaps the BD in-plane bending at 1050 cm^{-1}; as in $CD_3B_2D_5$, the absorption in this region is surprisingly weak.

The weak 1065 and 1015 cm^{-1} bands in "B_1" are probably CH_3 rocking modes, masked in "C_1" by BD bending. The stronger absorptions in "D_1" and "E_1" at about 940 cm^{-1} could then represent CD_3 rocking modes (ratio of approximately 1.1). These assignments as well as the B^{10} shift of 5 to 7 cm^{-1} parallel closely those in $B(C_2H_5)_3$ and $B(C_2D_5)_3$ (1022 and 945 cm^{-1}, B^{10} shift of 5 cm^{-1}).

The bands at 826, 816, and 800 cm^{-1} in "A_1", "B_1", and "C_1", respectively, probably represent CH_2 rocking modes (in the CH_2 plane) shifted to 742 and 760 cm^{-1} for CD_2 in "D_1" and "E_1" (ratios of 1.10 and 1.05). For $B^{10}(C_2H_5)_3$, $B(C_2H_5)_3$, and $B(C_2D_5)_3$ these frequencies are 788, 779, and 725 cm^{-1} (CH_2/CD_2 ratio of 1.07).

The strong A-type band at 943 cm^{-1} in "C_1" has no obvious analog in "B_1", indicating tentatively that it is not a band characteristic of the $-C_2H_5$ group. Although the analog of this absorption could possibly occur in "E_1", hidden under the CD_3 rocking deformation, no such band is observed in[4] B_2D_5H nor in[1] $CH_3B_2D_5$; this eliminates it from consideration as a characteristic $-B_2D_5$ band. Thus, the assignment of this absorption is uncertain. A similar situation exists for the 846 cm^{-1} band in "D_1". It must be realized that considerable interaction can be expected among vibrations of such frequencies. Conceivably these various bands represent the C–C stretching mode coupled with other vibrations. In that case the aforementioned 943 cm^{-1} band in "C_1" may have the shoulder at 930 cm^{-1} in "B_1" as a parallel, and the analog of the 846 cm^{-1} band in "D_1" is hidden in "E_1" by the strong 876 cm^{-1} band. The C–C vibration has been assigned to 919 cm^{-1} in[2] $B(C_2H_5)_3$ and 881 cm^{-1} in[3] $B(C_2D_5)_3$.

As in the spectra of the monomethyldiboranes, no band is observed which can with certainty be assigned to the B–C stretching mode.

ACKNOWLEDGMENT

The authors are grateful to Dr. John C. Perrine of this laboratory for programming the ethyldiborane vapor-pressure equation on a Burroughs Model 205 Computer.

[7] H. L. McMurry and V. Thornton, J. Chem. Phys. **19**, 1014 (1951).

Effect of Chemical Etches on the Fast Germanium Surface States

Y. MARGONINSKI*

Department of Physics, The Hebrew University, Jerusalem, Israel

(Received October 21, 1959)

Simultaneous measurements of surface recombination velocity and added trapped charge density in the fast states as a function of surface potential were carried out on one and the same *n*-type filament which was subjected to three different etches: CP-4A, concentrated HNO_3 and HF. Most measurements were performed at various temperatures. It was found that (a) the reproducibility of surface state parameters after successive treatments with CP-4A was excellent; (b) the influence of the different etches was surprisingly small, with one exception: the average capture probability c_p for holes was found to undergo a more than threefold increase after treatment with HF; (c) the energy of the recombination center did not *always* decrease with increasing temperature, contrary to all previously reported measurements.

1. INTRODUCTION

ALTHOUGH the fast states on germanium surfaces are protected from the surrounding ambient gases by a germanium-oxide layer, it is a well-established fact[1] that this protection is not complete and hence the states are ambient sensitive. One is tempted to assume that chemical etches would have an even greater effect on these states than the ambients, the more so if etches are employed which either dissolve or strengthen this protective oxide layer. Consequently one and the same *n*-type germanium filament was subjected to three consecutive chemical etches: (1) CP-4A, which is known to yield a low surface recombination velocity, (2) Concentrated HNO_3 as an oxidizing agent, and (3) HF (40%), which dissolves the germanium oxide and greatly increases the surface recombination velocity. The results of these measurements are reported in this paper.

The effect of chemical etches on germanium surfaces has also been investigated by Wallis and Wang,[2] but they employed etches of different types irrespective of their action on the oxide and also baked their sample after each etch.

2. EXPERIMENTAL METHOD AND INTERPRETATION OF DATA

The chemical treatment varied with the different etches: the CP-4A treatment was carried out for 30 sec, that with HNO_3 for 10 min and etching with HF lasted for 10 sec only. After the CP-4A and HNO_3 etches the filament remained in air for about 15 hr to become stabilized, but after the HF treatment it was placed in vacuum as quickly as possible. All measurements were carried out in a vacuum of at least 10^{-4} mm Hg and many at two or even three different temperatures. After most surface treatments the filament stayed in vacuum for some days, so as to investigate the slow changes that were taking place. The different chemical treatments were mainly carried out in "cycles" consisting of three consecutive etchings: CP-4A, HNO_3, and HF, in that order. Altogether the filament underwent four etchings with CP-4A, three with HNO_3 and two with HF. The resistivity of the sample was 15 ohm cm.

The experimental procedure and interpretation of data were similar to those employed by Many and Gerlich[1]: the surface potential ϕ_s was changed by an alternating (50-cps) electric field, perpendicular to the filament, and simultaneous measurements of filament lifetime and resistivity were taken. From the experimental data two curves were constructed as functions of the surface potential $u_s=q\phi_s/kT$: (1) the fractional surface recombination velocity s/s_M, where s_M denotes the maximum value of the surface recombination velocity s, (2) the added trapped charge density ΔQ_s in the surface states relative to its value before application of the field, when $\phi_s=\phi_{s0}$. ΔQ_s is given by[3]:

$$\Delta Q_s=-\left[\frac{qN_t}{1+\exp[1/kT(E_t-E_i-q\phi_s)]}-\frac{qN_t}{1+\exp[1/kT(E_t-E_i-q\phi_{s0})]}\right], \quad (1)$$

where N_t=density of surface states per cm^2, q=electronic charge, E_t=energy of discrete surface states, and E_i=intrinsic energy level, T=temperature of measurement. (Throughout this paper the notation employed by Many and Gerlich[1] will be used.)

From the s/s_M vs u_s curve the energy $(E_t-E_i)/kT$ of the recombination center and the ratio c_p/c_n of the capture cross sections were derived. The analysis of

* Present address: Department of Physics, Brown University, Providence, Rhode Island.

[1] A. Many and D. Gerlich, Phys. Rev. **107**, 404 (1957).

[2] G. Wallis and S. Wang, J. Elektrochem. Soc. **106**, 231 (1959).

[3] Equation 1 assumes that the surface states are not spin degenerate. Statz *et al.* [Phys. Rev. **101**, 1272 (1956)] and Bardeen *et al.* [Phys. Rev. **104**, 47 (1956)] assumed a twofold degeneracy, i.e., each state can be occupied by one electron of either plus or minus spin but not by two electrons with plus and minus spin. This assumption would lead to the introduction of the factor 1/2 before the exponent in the denominator of Eq. 1. However, the changes caused by the inclusion of this factor lie within our experimental error; the analysis of the results reported in Fig. 1b assuming a twofold spin degeneracy yields the values $E_t'-E_i=(-2.1)kT$, $N_t=20\times10^{10}$, $N_t'=15\times10^{10}$.

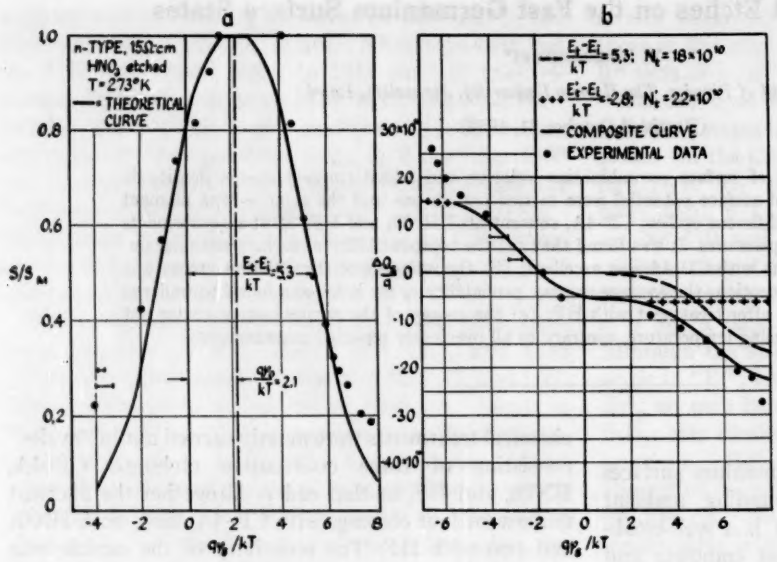

FIG. 1. (a) Fractional surface recombination velocity s/s_M and (b) added trapped charge density ΔQ_s vs surface potential $q\phi_s/kT$. Analysis of (b) indicates that besides the recombination center at least one additional "charge trap" is active within the range covered by the measurements.

the ΔQ_s vs u_s curve yielded the density N_t of the recombination centers as well as the energy $(E_t'-E_i)/kT$ and density N_t' of one additional surface state, not effective in recombination. In a few cases the experimental data was sufficient to measure the energy $(E_t''-E_i)/kT$ and density N_t'' of a second recombination-ineffective surface state. Figure 1 is typical of the type of curves encountered: 1(a) is the s/s_M curve and 1(b) the corresponding $\Delta Q_s(u_s)$ curve. The dashed line in 1(b) is the plot of Eq. (1) with $E_t-E_i=5.3kT$ [derived from Fig. 1(a)] and $N_t=18\times10$ cm^{-2}. In order to fit the experimental data the presence of an additional state with $E_t'-E_i=-2.8\ kT$ and $N_t'=22\times10^{10}$ had to be assumed; the theoretical ΔQ_s curve corresponding to these values is indicated by small crosses. The sum of the two theoretical curves is the solid "composite curve" of Fig. 1(b), which fits the experimental data over a range of 12 kT. As previously reported,[4] each s/s_M curve gives two values for the energy $(E_t-E_i)/kT$ of the recombination center, corresponding to the two values of u_s for $s/s_M=0.5$. In Fig. 1(a) these two energies are $E_{t1}-E_i=5.3\ kT$ and $E_{t2}-E_i=-1.1kT$. Only one of these two values has a physical meaning and this can be seen by inspecting Eq. (1) or its graphic plot in Fig. 1(b): For a range of $\mp2kT$ around $q\phi_s=E_t-E_i$ the slope of the ΔQ_s curve has to be fairly constant. This condition is met by the recombination center at $E_{t1}-E_i=5.3kT$ but not by the "virtual" center at $E_{t2}-E_i=(-1.1kT)$, where the experimental data clearly indicates a change of slope.

Figure 1(b) shows that within the range of measurements there are two surface states (the recombination center at 5.3 kT and the "charge trap" at $-2.8kT$) and indications of the presence of another two states, one near the valence and one near the conduction band. Figure 2(b) is remarkable in that within the range of measurements three centers could be covered and there is indication of only one additional state near the valence band. The recombination center is at $6.4kT$ and the other two surface states, not effective in recombination, are at $1.5kT$ and -4.7, respectively. Here too the slope of the $\Delta Q_s(u_s)$ curve is constant near $u_s=6.4$, but has a turning point near the virtual center at $-2.6kT$.

[4] A. Many, E. Harnik, and Y. Margoninski, *Semiconductor Surface Physics* (University of Pennsylvania Press, Philadelphia, 1957).

3. EXPERIMENTAL RESULTS

Some of the more significant results are summarized in Table I. This table is subdivided into three sections, according to the three temperature ranges. Each of the three sections has three horizontal divisions corresponding to the three surface treatments, and is subdivided into eight or nine columns, according to the following parameters: the temperature of the measurements in degrees centigrade, the maximum surface recombination velocity s_M, the energy of the recombination center E_t-E_i in units of kT, the ratio of the capture cross sections c_p/c_n, the capture cross section for holes c_p, the density of the recombination center N_t per cm^2, the energy $(E_t'-E_i)$ and density N_t' of the surface state which is not effective in recombination (a "charge trap") and similarly the values of $(E_t''-E_i)$ and N_t'' of the second "charge trap." The date of the measurements is also stated.

The estimated accuracy of the parameters appearing in Table I is as follows: s_M is accurate to $\mp10\%$. The error in the energy $(E_t-E_i)/kT$ of the recombination center is ∓0.3 and that in N_t about 20%. The corresponding data for the states ineffective in recombination is less accurate and depends somewhat on the shape of the $\Delta Q_s(u_s)$ curve: the error in $(E_t'-E_i)/kT$, $(E_t''-$

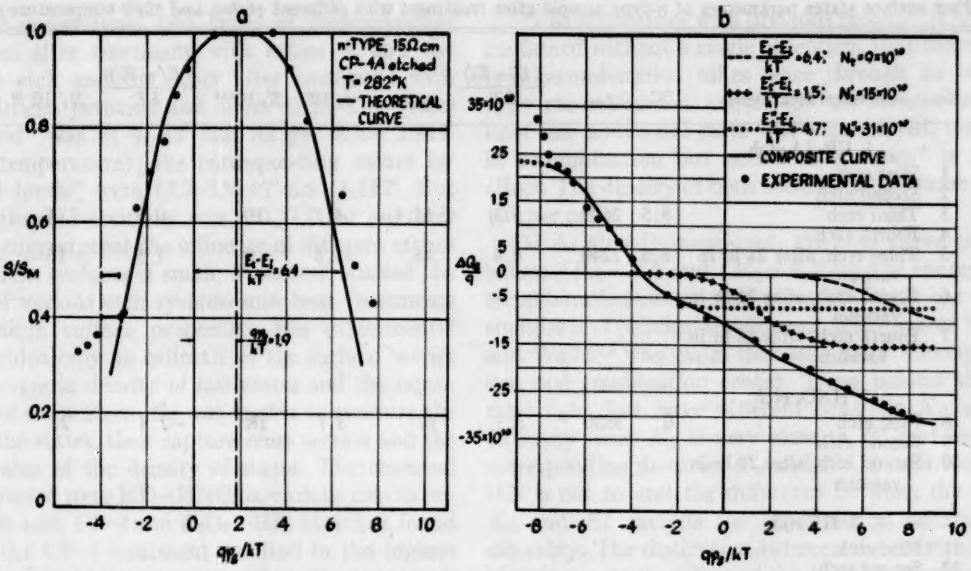

FIG. 2. (a) Fractional surface recombination velocity s/s_M and (b) added trapped charge density ΔQ_s vs surface potential $q\phi_s/kT$. Analysis of (b) indicates the presence of at least three centers within the range of measurements, only one of them active in recombination.

$E_t)/kT$ is about ∓ 1 and in N_t',N_t'' — $\mp 50\%$. The greatest errors are involved in c_p/c_n and c_p, because of their exponential dependence on the measured quantity $q\phi_0/kT$ (the displacement of the axis of symmetry of the s/s_M curve from the origin); the error in c_p/c_n may be as great as $\mp 50\%$ and the values quoted for the capture cross sections may differ by a factor of 2.

Three main results emerge from the experimental data represented in Table I:

1. The reproducibility of the surface parameters after successive treatments with CP–4A is very good, indicating that the same surface treatment always yields the same set of surface states. The mean values for $(E_t - E_i)$, c_p and N_t at about 20°C are $(4.9 \mp 0.3)kT$, $(2.2 \mp 0.4) \times 10^{-7}$ and $(17 \mp 1) \times 10^{10}$, respectively. As far as reproducibility is concerned it can be stated with certainty that the deviations of all surface parameters are chiefly due to the limitations of experimental accuracy. The same conclusion has been reached by Harnik and Margoninski,[5] who investigated the influence of chemical etches on unstabilized germanium surfaces.

2. The influence of the different chemical etches on the surface states is surprisingly small and usually within the limits of the experimental accuracy. There is, however, one important exception: the high value of s_M measured after treatment with HF is mainly due to a more than threefold increase in the average capture cross section c_p.

3. As already reported,[1,4] the energy of the recombination center is temperature dependent. But whereas *all* previous measurements indicated a decrease in energy with increasing temperatures, three measurements reported here (Nos. 3, 9, and 10) clearly show the opposite behavior. All three were carried out at 41°C; all previously reported data was taken at temperatures below 30°C. Within the experimental error runs 4 and 8 show no temperature dependence of the energy, run 7 shows a decrease and runs 3, 9, and 10 an increase of energy with temperature. Therefore, though the experimental data are insufficient to indicate a definite relation between temperature and energy of the states, they do throw some doubt on the previous assumption[1,4] that this relation is always monotonic. Hence, the energy of the real recombination center cannot be deduced solely from measurements taken at different temperatures, but must be determined with the help of the ΔQ_s curve.

Many and Gerlich[1] reported that E_t, N_t, and c_p/c_n decreased appreciably during the first few days in vacuum after etching. This behavior is not always verified in the measurements reported here: runs 12, 13 exhibit the same trend as reported in the work cited in footnote 1, whereas runs 3, 5 and 4, 6 indicate the opposite tendency. Regarding the changes in surface parameters during the sample's standing in vacuum the only result that can be stated with certainty is that N_t never increases during the stay in vacuum.

4. DISCUSSION

From the results of the measurements reported here the following conclusions can be drawn:

(1) With the exception of the effect of HF on the capture cross section c_p, the influence of the different chemical etches on the surface state parameters is within the limits of the experimental accuracy. Wallis

[5] E. Harnik and Y. Margoninski, J. Phys. Chem. Solids 8, 96 (1959).

TABLE I. Fast surface states parameters of n-type sample after treatment with different etches and their temperature dependence.

Date of measurement	No.	Chemical treatment	°C	s_M	$\frac{(E_t-E_i)}{kT}$	c_p/c_n	$c_p 10^7$	$N_t 10^{-10}$	$\frac{(E_t'-E_i)}{kT}$	$N_t' 10^{-10}$	E_t''	N_t''
		1. CP–4A etch										
3.4.58	1	First etch										
28.4	2	Second etch										
3.6.	3	Third etch	8.5	2600	5.3	13.4	4.1	10	0.5	14		
10.7.	4	Fourth etch										
4.6.	5	Third etch, after 24 hr in vacuum	8.5	2240	6.4	45	11.5	9	1.5	15	−4.7	31
11.7.	6	Fourth etch, after 24 hr in vacuum										
13.7.	7	Fourth etch, after 48 hr in vacuum										
		2. HNO_3 etch										
30.4.	8	First etch	0	5530	5.3	67	3.7	18	−2.8	22		
14.7	9	Second etch										
15.7.	10	Second etch, after 24 hr in vacuum										
		3. HF etch										
2.5.	11	First etch										
5.6.	12	Second etch										
9.6.	13	Second etch, after 100 hr in vacuum										

Date of measurement	No.	Chemical treatment	°C	s_M	$\frac{(E_t-E_i)}{kT}$	c_p/c_n	$c_p 10^7$	$N_t 10^{-10}$	$\frac{(E_t'-E_i)}{kT}$	$N_t' 10^{-10}$
		1. CP–4A etch								
3.4.58.	1	First etch	30	817	4.7	30	2.0	18	−1.0	25
28.4.	2	Second etch	20	1990	4.7	30	2.4	16	−3	18
3.6.	3	Third etch	20	1300	5.2	20	2.5	16	−0.7	25
10.7.	4	Fourth etch	20	1440	4.9	16.5	1.8	18	−2.1	26
4.6.	5	Third etch, after 24 hr in vacuum	20	1610	5.6	16.4	4.8	15	1.5	14
11.7.	6	Fourth etch, after 24 hr in vacuum	20	2710	6	148	10.2	18	−1.9	34
13.7.	7	Fourth etch, after 48 hr in vacuum	20	2710	6	148	10.2	18	−1.9	34
		2. HNO_3 etch								
30.4.	8	First etch	20	940	5.5	20	1.5	24	−2.1	18
14.7.	9	Second etch	20	2000	5	36.6	2.6	20	−1	24
15.7.	10	Second etch, after 24 hr in vacuum	20	3200	6.3	67	...	...	...	...
		3. HF etch								
2.5.	11	First etch								
5.6.	12	Second etch								
9.6.	13	Second etch, after 100 hr in vacuum								

Date of measurement	No.	Chemical treatment	°C	s_M	$\frac{(E_t-E_i)}{kT}$	c_p/c_n	$c_p 10^7$	$N_t 10^{-10}$	$\frac{(E_t'-E_i)}{kT}$	$N_t' 10^{-10}$
		1. CP–4A etch								
3.4.58.	1	First etch								
28.4.	2	Second etch								
3.6.	3	Third etch	41	670	6.2	148	8.6	20	2	18
10.7.	4	Fourth etch	41	1360	5	100	4.7	24	−0.6	30
4.6.	5	Third etch, after 24 hr in vacuum	41	800	5.2	81	3.9	20	−0.3	20
11.7.	6	Fourth etch, after 24 hr in vacuum								
13.7.	7	Fourth etch, after 48 hr in vacuum	41	1710	4.7	20	6.2	16	−2.5	46
		2. HNO_3 etch								
30.4.	8	First etch								
14.7.	9	Second etch	41	1210	6.7	221	5	100	−0.3	24
15.7.	10	Second etch, after 24 hr in vacuum	41	1450	7.8	270	...	...	...	...
		3. HF etch								
2.5.	11	First etch	41	2560	6.1	181	14.4	42	0.6	24
5.6.	12	Second etch	41	3980	5.7	330	16	42	−0.2	25
9.6.	13	Second etch, after 100 hr in vacuum	41	3400	5.3	270	17	23	−0.2	28

and Wang[2] encountered two types of recombination centers, one after treatment with iodine A and the electrolytic etch and the other after treatment with CP-4, hydrogen peroxide and silver etch. The "electrolytic level" was at $4.7kT$ and its $q\phi_0$ value $1.9kT$ (at room temperature); the corresponding values for the "CP-4 levels" were $(3.7\text{–}3.9)kT$ and $1.1kT$. But as their estimated accuracy was $\mp 0.3kT$ for $q\phi_0$ their results too suggest, that the influence of different etches on germanium surfaces is small. Morrison[6] studied the influence of various etch systems and heat treatments on germanium surface properties. His experimental method yielded only an estimate of the surface barrier height, changes in density of fast states and the reproducibility of the surface. He was unable to measure the energy of the states, their capture cross section and the absolute value of the density of states. The chemical etches employed were HF—HNO_3 in various concentrations, oxalic acid, CP-4 and H_2O_2—HF. Morrison found that: (a) the CP-4 treatment resulted in the highest density of recombination centers, but the reproducibility was poor. The source of the irreproducibility seemed to be the bromine, with the bromine absent the CP-4A acted just like an HF–HNO_3 etch. All the other chemical treatments did not change the surface characteristics appreciably, though the oxalic acid yielded a somewhat higher state density. (b) Very small amounts of impurity in the etch or rinse water had a controlling effect on the resulting surface characteristics, the most important impurities being copper, antimony, and silver. (c) Heat treatment (up to 100°C) in a dry atmosphere caused the density of states to increase, whereas the same treatment in a moist atmosphere decreased the density.

All hitherto reported measurements[7] seem to indicate, therefore, that at the germanium surface there exists a definite configuration of surface states whose parameters (energy, density, etc.) are not rigidly fixed but are confined to a range of values—conform to certain not too narrow specifications, so to speak. This "configuration of traps and recombination centers" consists of: (I) one state near the valence band, presumably of small capture cross sections and thus recombination ineffective; (II) two states near the intrinsic level, the lower [in the region between $+2$ and $-3)kT$] not effective in recombination and the upper [at $(3\text{–}8)kT$] an acceptor type recombination center; (III) one center near the conduction band. This "configuration" applies only at room temperature. Recent measurements[8] indicate that at liquid-air temperature the distribution of fast states is different: most of the states are found to lie near the conduction band edge and to have very small capture cross sections for electrons.

(2) In accordance with previous results[1,4] it was again confirmed without a single exception, that the electron-hole recombination takes place through an acceptor-type recombination center. In all measurements at least one additional state was encountered, not active in recombination but active as a "trap" in the field effect. The density of both states is of the same order—10^{11} per cm^2.

(3) As already mentioned, the s/s_M curve gives two values $(E_{t1}-E_i)$ and $(E_{t2}-E_i)$ for the energy of the recombination center. Our view, that only one of these energies is of physical significance, is not shared by Wang and Wallis[2,9] who claim that *each* value corresponds to one real combination center. These possess the same ratio c_p/c_n but have different densities N_{t1} and N_{t2}. In many cases E_{t2} is very close to E_t' and so are the corresponding densities N_{t2} and N_t', but in some cases this is not so and the difference between the energies E_{t2} and E_t' exceeds the experimental accuracy considerably. The distinction between the "virtual recombination center" at E_{t2} and the "charge trap" at E_t' is, therefore, important and we mention three points to support our view against that of Wang and Wallis: (a) the supposition $E_t'=E_{t2}$ is sometimes incompatible with the experimental results. As has already been stated, the slope of the ΔQ_s curve is nearly constant in the vicinity of a recombination center and this requirement is not always fulfilled by the center at E_{t2}, as illustrated in Figs. 1(b) and 2(b). For measurements taken at different temperatures, the inspection of the temperature dependence of the recombination center raises two further objections: (b) It can be seen from the experimental results that changes in temperature affect the two centers E_{t1} and E_{t2} in opposite directions, so that one center will approach the intrinsic level E_i while the other will recede from it. It is difficult to understand this contrary behavior, as E_i has no special physical significance. (c) Both the s/s_M and the ΔQ_s curves are temperature sensitive, hence the same change in E_{t2} should be derived from the two curves. But in some cases the change in E_{t2} as derived from s/s_M is opposite to that indicated by ΔQ_s: in measurement 5, at 20°C, $(E_{t2}-E_i)=-2.8kT$ and at 41°C $(E_{t2}-E_i)=-0.8kT$, hence E_{t2} increases with temperature. The corresponding ΔQ_s curves, on the other hand, are shifted towards lower energies [and hence the decrease in $(E_t'-E_i)$]. The same opposite behavior occurs in measurements 8, 9 and in Fig. 2 of Many and Gerlich's paper.[1]

ACKNOWLEDGMENTS

The author wishes to express his grateful thanks to Dr. E. Harnik, Dr. D. Gerlich, and Mr. N. Grover for most stimulating discussions and to Professor A. Many for his continued encouragement and interest during the progress of this work and his helpful comments in preparing the manuscript.

[6] S. R. Morrison, Second Conference on Semiconductor Surfaces held in December, 1959, at the Naval Ordnance Laboratory, White Oak, Maryland.

[7] A. Many, J. Phys. Chem. Solids **8**, 87 (1959).

[8] E. Harnik, N. B. Grover, Y. Goldstein, and A. Many, conference cited footnote 6.

[9] S. Wang and G. Wallis, Phys. Rev. **105**, 1459 (1957) and **107**, 947 (1957).

Brownian Motion in Liquids*

GERALD MANDEL AND FRANK C. COLLINS

Department of Chemistry, Polytechnic Institute of Brooklyn, Brooklyn, New York

(Received May 4, 1959)

The time derivative of the frictional force acting on a single molecule derived by Collins and Raffel was ambiguous with respect to a sign which left uncertain whether the calculated ensemble average velocity would decay exponentially in time or be initially sinusoidal in behavior. This point is now resolved and the exponential decay of the velocity is obtained for a molecule relaxing for an initial steady state. The frictional coefficient is also obtained by an alternative method involving an expansion of the conditional second-order phase density in powers of the distance that the representative molecule travels before its ensemble average velocity decays to zero. The alternative derivation enables the velocity dependence of the frictional coefficient to be examined. An approximate evaluation of the corrected velocity-dependent frictional coefficient for liquid argon averaged over all velocities is in improved agreement with the value calculated from the self-diffusion measurements of Corbett and Wang.

INTRODUCTION

THE statistical mechanical principles of molecular Brownian motion in liquids have been developed by Kirkwood[1] in terms of the intermolecular pair potential and the pair density function. A closed expression for the hydrodynamic frictional coefficient in terms of the pair potential was, however, not obtained. A plausible formula for the frictional coefficient as the square root of an average over the second space gradient of the pair potential was later suggested by Kirkwood, Buff, and Green[2] from dimensional considerations without detailed derivation. Collins and Raffel[3] have attempted to derive the Kirkwood, Buff, and Green equation for the frictional coefficient starting with the postulate that

$$\langle \mathbf{F}_1 \rangle = -\zeta \langle \mathbf{c}_1 \rangle, \tag{1}$$

where $\langle \mathbf{F}_1 \rangle$ is the ensemble average force acting on molecules having the ensemble average velocity $\langle \mathbf{c}_1 \rangle$ and ζ is the frictional coefficient.[4] By taking the time derivative of Eq. (1) following the motion of the molecule and then introducing Newton's second law of motion, they obtained

$$(d/dt)\langle \mathbf{F}_1 \rangle = (\zeta^2/m)\langle \mathbf{c}_1 \rangle. \tag{2}$$

There has been some question as to whether the Collins and Raffel developments of the time derivative $d\langle \mathbf{F}_1 \rangle/dt$ could be correct with respect to sign in view of the requirements of microscopic reversibility at equilibrium.[5] A negative sign for $d\langle \mathbf{F}_1 \rangle/dt$ would predict a sinusoidal dependence of the ensemble average velocity upon the time, at least in the region of the time of preparation of the subassembly rather than the exponential decay found by Collins and Raffel.

In this paper, the conditions necessary for a positive sign of $d\langle \mathbf{F}_1 \rangle/dt$ are established in terms of an ensemble relaxing from an initial steady state in which the ensemble average velocity of the given molecule is $\langle \mathbf{c}_1 \rangle$. Under this condition, the expected exponential decay of the ensemble average velocity $\langle \mathbf{c}_1 \rangle$ occurs. The expression previously found for the frictional coefficient remains valid.

The formula for the frictional coefficient thus derived holds strictly only in the steady state of constant $(\mathbf{c}_1)_{Av}$. The frictional coefficient for the case of decay of the velocity $\mathbf{c}_1$ under the frictional force may be expected to be somewhat larger and to exhibit velocity dependence. An approximate method for obtaining the frictional coefficient appropriate to the relaxation process is outlined and leads to a frictional coefficient which depends explicitly on the magnitude of the velocity $\mathbf{c}_1$. This method makes use of the mean correlation length defined as the distance that the representative molecule travels before the ensemble average velocity decays to zero. In the limit of low velocities the relaxation frictional coefficient converges to the same expression as that holding for that valid in the state of steady $(\mathbf{c}_1)_{Av}$.

CALCULATION OF THE FRICTIONAL COEFFICIENT

We will confine our considerations to systems in which the total potential is the superposition of molecular pair potentials which are functions of distance alone

$$\Phi = \sum_{j=2}^{N} \sum_{i=1}^{j-1} \phi(|\mathbf{r}_i - \mathbf{r}_j|) = \sum_{j=2}^{N} \sum_{i=1}^{j-1} \phi_{ij}. \tag{3}$$

* Part of the dissertation to be submitted by Gerald Mandel in partial fulfilment of the requirements for the Ph.D. degree at the Polytechnic Institute of Brooklyn. The research was supported by the Wright Air Development Center of the United States Air Force under contract.

[1] J. G. Kirkwood, J. Chem. Phys. **14**, 180 (1946).

[2] J. G. Kirkwood, F. P. Buff, and H. S. Green, J. Chem. Phys. **17**, 988 (1949).

[3] F. C. Collins and H. Raffel, J. Chem. Phys. **29**, 699 (1958).

[4] Equation (1) and the Kirkwood, Buff, and Green formula for the frictional coefficient have been obtained recently by S. A. Rice and J. G. Kirkwood by another method [J. Chem. Phys. **31**, 901 (1959)].

[5] R. C. Tolman, *Principles of Statistical Mechanics* (Oxford University Press, New York, 1938), p. 163.

It will be assumed that the system is in thermal equilibrium, except that the molecule labeled "1" has had the constant external force $\mathbf{x}_1$ exerted upon it for at least a time t_0 long compared to molecular fluctuation times. If the time t_0 is sufficiently long, by hypothesis the molecule 1 will have arrived at a limiting velocity at which the external force $\mathbf{x}_1$ will be exactly balanced by a frictional force $\langle \mathbf{F}_1 \rangle^s$ exerted by the $(N-1)$ other molecules of the system against the moving molecule 1. Thus we have

$$\mathbf{x}_1 + \langle \mathbf{F}_1 \rangle^s = \mathbf{x}_1$$

$$-\int\cdots\int \sum_{i=2}^{N} (\partial \phi_{i1}/\partial \mathbf{r}_1)\, {}^s f^{(N/1)} d\mathbf{c}_2 \cdots d\mathbf{c}_N d\mathbf{r}_2 \cdots d\mathbf{r}_N = 0, \tag{4}$$

where ${}^s f^{(N/1)}$ is the near-equilibrium phase density of the molecules 2 to N conditional upon the molecule 1 having been maintained in a steady state of average velocity $(\mathbf{c}_1)_{Av}$ for the time t_0.

The velocity $(\mathbf{c}_1)_{Av}$ is a time average

$$(\mathbf{c}_1)_{Av} = (\mathbf{c}_1)_\tau = \tau^{-1} \int_{t_0-\tau}^{t_0} \mathbf{c}_1(t)\, dt \tag{5}$$

in any given replica of the ensemble. Here τ is long compared to detailed molecular motion times but short compared to the time t_0 that the steady state has been maintained. In the following calculations, ensemble averages involving the molecule 1 will be constructed. The steady-state ensemble average time-smoothed velocity of the molecule is given by

$$\langle (\mathbf{c}_1)_{Av} \rangle = \int\cdots\int (\mathbf{c}_1)_{Av}\, {}^s f^{(N)} d\mathbf{c}_1 \cdots d\mathbf{c}_N d\mathbf{r}_1 \cdots d\mathbf{r}_N, \tag{6}$$

where ${}^s f^{(N)}$ is the Nth order phase density, related to the $(N-1)$ conditional density by

$${}^s f^{(N/1)}[\mathbf{c}_2 \cdots \mathbf{c}_N,\ \mathbf{r}_2 \cdots \mathbf{r}_N/\mathbf{r}_1,\ \mathbf{c}_1 - (\mathbf{c}_1)_{Av}] = \frac{{}^s f^{(N)}[\mathbf{c}_1 - (\mathbf{c}_1)_{Av},\ \mathbf{c}_2 \cdots \mathbf{c}_N,\ \mathbf{r}_1 \cdots \mathbf{r}_N]}{f^{(1)}[\mathbf{c}_1 - (\mathbf{c}_1)_{Av},\ \mathbf{r}_1]}, \tag{7}$$

where $f^{(1)} = n^{(1)} w^{(1)} = V^{-1} w^{(1)}$, V being the volume of the system. Consistent with the hypothesis that the system is in a state of near equilibrium, the velocity density $w^{(1)}$ will be assumed to be given by a Boltzmann distribution about the average $(\mathbf{c}_1)_{Av}$

$$w^{(1)} = {}^0 w^{(1)}[\mathbf{c}_1 - (\mathbf{c}_1)_{Av}] = (m/2\pi kT)^{\frac{3}{2}} \exp\{-m[\mathbf{c}_1 - (\mathbf{c}_1)_{Av}]^2/2kT\}. \tag{8}$$

Let us denote the position of the molecule 1 at the time t_0 by $\mathbf{r}_1^0$ and define

$${}^s f^{(N/1)} = {}^* f^{(N/1)} + {}^\prime f^{(N/1)} \tag{9}$$

with

$${}^* f^{(N/1)} = \frac{w^{(N/1)}(\mathbf{c}_2 \cdots \mathbf{c}_N) \exp(-\Phi^0/kT)}{\int\cdots\int \exp(-\Phi^0/kT)\, d\mathbf{r}_2 \cdots d\mathbf{r}_N} = w^{(N/1)}\, {}^* n^{(N/1)} \tag{10}$$

$$\Phi^0 = \sum_{j=2}^{N} \phi(\mathbf{r}_j - \mathbf{r}_1^0) + \sum_{j=3}^{N} \sum_{i=2}^{j-1} \phi(\mathbf{r}_j - \mathbf{r}_i), \tag{11}$$

where ${}^* f^{(N/1)}$ has been made explicitly independent of the time dependent position $\mathbf{r}_1$ of the molecule 1 by particularizing the configuration density to the fixed point $\mathbf{r}_1^0$. We will assume that the velocity densities of the molecules 2 to N are unaffected by the velocity of the molecule 1, and are hence given by the equilibrium density

$${}^0 w^{(N/1)} = (m/2\pi kT)^{\frac{3}{2}(N-1)} \exp(-m \sum_{i=2}^{N} \mathbf{c}_i^2/2kT). \tag{12}$$

The frictional force in Eq. (6) may now be written

$$\langle \mathbf{F}_1 \rangle^s = \langle \mathbf{F}_1 \rangle^* + \langle \mathbf{F}_1 \rangle^\prime \tag{13}$$

with

$$\langle \mathbf{F}_1 \rangle^* = -\int\cdots\int (\partial \Phi/\partial \mathbf{r}_1)\, {}^0 w^{(N/1)}\, {}^* n^{(N/1)} \times (\mathbf{r}_2 \cdots \mathbf{r}_N/\mathbf{r}_1^0)\, d\mathbf{c}_2 \cdots d\mathbf{c}_N d\mathbf{r}_2 \cdots d\mathbf{r}_N. \tag{14}$$

At the instant of time t_0,

$$\langle \mathbf{F}_1 \rangle^* = -\int\cdots\int (\partial \Phi/\partial \mathbf{r}_1)_{r_1^0}\, {}^0 w^{(N/1)}\, {}^* n^{(N/1)} \times (\mathbf{r}_2 \cdots \mathbf{r}_N/r_1^0)\, d\mathbf{c}_2 \cdots d\mathbf{c}_N d\mathbf{r}_2 \cdots d\mathbf{r}_N = 0 \tag{15}$$

because at this instant Eq. (14) is formally identical with that for the force on a molecule in the equilibrium ensemble. At other times, however, Eq. (14) does not correspond to the equilibrium expression because, except at the particular time t_0, $\partial \Phi/\partial \mathbf{r}_i$ is evaluated at a point other than $\mathbf{r}_1^0$ around which the density ${}^* n^{(N/1)}(\mathbf{r}_1^0,\ \mathbf{r}_2,\ \cdots,\ \mathbf{r}_N)$ is centered. Thus at times other than t_0, $\langle \mathbf{F}_1 \rangle^*$ is not necessarily zero.

Let us now consider the instantaneous time derivative of the frictional force acting on the molecule at the time t_0. According to Eq. (4), this time derivative must be zero,

$$(d/dt)\, \langle \mathbf{F}_1 \rangle^s = 0 \qquad t_0 - \tau \leq t \leq t_0 \tag{16}$$

and by Eq. (13),

$$(d/dt)\, \langle \mathbf{F}_1 \rangle^* + (d/dt)\, \langle \mathbf{F}_1 \rangle^\prime = 0 \qquad t_0 - \tau \leq t \leq t_0. \tag{17}$$

For later purposes, we wish to evaluate $d\langle \mathbf{F}_1\rangle'/dt$ in terms of $d\langle \mathbf{F}_1\rangle^*/dt$. The ensemble average force may be expressed directly as an average over the M replicas constituting the ensemble

$$\langle \mathbf{F}_1\rangle = M^{-1}\sum_{\mu}\mathbf{F}_{1\mu}. \tag{18}$$

The time derivative of the ensemble average force is then

$$(d/dt)\langle \mathbf{F}_1\rangle = (d/dt)(M^{-1}\sum_{\mu}\mathbf{F}_{1\mu}) = M^{-1}\sum_{\mu}(d/dt)\mathbf{F}_{1\mu} = \langle d\mathbf{F}_1/dt\rangle. \tag{19}$$

Thus we have, upon combining Eqs. (17) and (19),

$$\frac{d}{dt}\langle \mathbf{F}_1\rangle' = -\frac{d}{dt}\langle \mathbf{F}_1\rangle^* = \int\cdots\int\left(\frac{d}{dt}\sum_{i=2}^{N}\frac{\partial\phi_{i1}}{\partial\mathbf{r}_1}\right)_0 w^{(N/1)}\,{}^*n^{(N/1)}(\mathbf{r}_2\cdots\mathbf{r}_N/\mathbf{r}_1{}^0)\,d\mathbf{c}_2\cdots d\mathbf{c}_N d\mathbf{r}_2\cdots d\mathbf{r}_N$$

$$= -\int\cdots\int\left(\frac{d}{dt}\sum_{i=2}^{N}\frac{\partial\phi_{i1}}{\partial\mathbf{R}_{i1}}\right)_0 w^{(N/1)}\,{}^*n^{(N/1)}(\mathbf{R}_{21}{}^0\cdots\mathbf{R}_{N1}{}^0)\,d\mathbf{c}_2\cdots d\mathbf{c}_N d\mathbf{r}_2\cdots d\mathbf{r}_N, \tag{20}$$

where $\mathbf{R}_{i1}=\mathbf{r}_i-\mathbf{r}_1$, $\mathbf{R}_{i1}{}^0=\mathbf{r}_i-\mathbf{r}_1{}^0$, and $\partial/\partial\mathbf{R}_{i1}=-\partial/\partial\mathbf{r}_1$.

Noting that

$$\frac{d}{dt}\frac{\partial\phi_{i1}}{\partial\mathbf{R}_{i1}} = \frac{\partial}{\partial\mathbf{R}_{i1}}\frac{\partial\phi_{i1}}{\partial\mathbf{R}_{i1}}\cdot\left(\frac{d\mathbf{r}_i}{dt}-\frac{d\mathbf{r}_i}{dt}\right)$$

$$= \frac{\partial}{\partial\mathbf{R}_{i1}}\frac{\partial\phi}{\partial\mathbf{R}_{i1}}\cdot(\mathbf{c}_i-\langle\mathbf{c}_1\rangle), \tag{21}$$

substituting into Eq. (20), and integrating over the velocities, we obtain

$$\frac{d}{dt}\langle \mathbf{F}_1\rangle' = \int\cdots\int\sum_{i=2}^{N}\left(\frac{\partial}{\partial\mathbf{R}_{i1}}\frac{\partial\phi_{i1}}{\partial\mathbf{R}_{i1}}\right)_{\mathbf{R}_{i1}{}^0}\cdot\langle\mathbf{c}_1\rangle^* n(\mathbf{R}_{21}{}^0\cdots R_{N1}{}^0)\,d\mathbf{R}_{21}\cdots d\mathbf{R}_{N1}, \qquad t=t_0 \tag{22}$$

where now explicit note has been taken that at $t=t_0$, the second space gradient of the potential is to be evaluated at $\mathbf{r}_1{}^0$. By Eqs. (10) and (11) the density ${}^*n^{(N/1)}(\mathbf{R}_{21}{}^0, \cdots\mathbf{R}_{N1}{}^0)$ is equivalent to the equilibrium density if the first molecule is located at the point $\mathbf{r}_1{}^0$. Further, the $N-1$ integrations are all identical so that

$$\frac{d}{dt}\langle \mathbf{F}_1\rangle' = \langle\mathbf{c}_1\rangle\cdot(N-1)\int\frac{\partial}{\partial\mathbf{R}}\frac{\partial\phi}{\partial\mathbf{R}}{}_0 n^{(2/1)}d\mathbf{R} \qquad t=t_0. \tag{23}$$

Here ${}^0n^{(2/1)}$ is the equilibrium conditional second-order density, $\mathbf{R}=\mathbf{R}_{21}$, and $\phi=\phi_{21}$. The remaining integration over all orientations of the vector $\mathbf{R}$ is readily effected and yields

$$\frac{d}{dt}\langle \mathbf{F}_1\rangle' = \langle\mathbf{c}_1\rangle\frac{4\pi}{3}v^{-1}\int_0^\infty\left(\frac{d^2\phi}{dR^2}+\frac{2}{R}\frac{d\phi}{dR}\right)g_0{}^{(2)}(R)\,R^2dR,$$

$$= \langle\mathbf{c}_1\rangle I, \tag{24}$$

where the pair correlation or radial distribution function

$$g_0{}^{(2)} = {}^0n^{(2/1)}/n^{(1)} = v^0n^{(2/1)} \tag{25}$$

has been introduced and $v=V/N$.

Now let us suppose that the external force $\mathbf{x}_1$ acting on the molecule 1 is discontinuously cutoff at the time $t=t_0$. There is no corresponding instantaneous change in the density ${}^*f^{(N/1)}$ as the external force on the molecule affects the density of the other $(N-1)$ molecules only indirectly. The molecule 1, however, is now free to respond to the unbalanced frictional force exerted against it. If we differentiate Eq. (24) at the time $t=t_0$, we obtain

$$(d^2/dt^2)\langle \mathbf{F}_1\rangle' = I(d/dt)\langle\mathbf{c}_1\rangle, \tag{26}$$

where it has been noted that the time derivative of the integral I vanishes from symmetry:

$$dI/dt = -\langle \mathbf{c}_1 \rangle \langle \mathbf{c}_1 \rangle : (N-1) \int \frac{\partial}{\partial \mathbf{R}} \frac{\partial}{\partial \mathbf{R}} \frac{\partial \phi_0}{\partial \mathbf{R}} {}^{0}n^{(2/1)} d\mathbf{R} = 0. \quad (27)$$

By Newton's second law of motion

$$m(d/dt)\langle \mathbf{c}_1 \rangle = \langle \mathbf{F}_1 \rangle = \langle \mathbf{F}_1 \rangle' \qquad t = t_0, \quad (28)$$

the last equality following from Eq. (15). We thus obtain

$$(d^2/dt^2)\langle \mathbf{F}_1 \rangle' = (I/m)\langle \mathbf{F}_1 \rangle' \qquad t = t_0, \quad (29)$$

the general solution[6] of which is

$$\langle \mathbf{F}_1 \rangle' = \mathbf{A}_1 \exp[-(I/m)^{\frac{1}{2}}(t-t_0)] + \mathbf{A}_2 \exp[(I/m)^{\frac{1}{2}}(t-t_0)]. \quad (30)$$

The constant $\mathbf{A}_2$ may be set equal to zero on the grounds that the force $\langle \mathbf{F}_1 \rangle'$ should decay in time with the velocity $\langle \mathbf{c}_1 \rangle$. Irreversibility has been in fact introduced into the system by the use of Eq. (4) defining the frictional force on the molecule 1 resisting the constant external force $\mathbf{x}_1$. The particular solution satisfying the condition that $\langle \mathbf{F}_1 \rangle = \langle \mathbf{F}_1 \rangle_{t_0}$ at $t = t_0$ is then

$$\langle \mathbf{F}_1 \rangle' = \langle \mathbf{F}_1 \rangle_{t_0}' \exp[-(I/m)^{\frac{1}{2}}(t-t_0)]. \quad (31)$$

The rate of decay of the ensemble average velocity at $t = t_0$ is given by Eq. (28),

$$(d/dt)\langle \mathbf{c}_1 \rangle = (1/m)\langle \mathbf{F}_1 \rangle = (1/m)\langle \mathbf{F}_1 \rangle', \quad (32)$$

making use of Eq. (15). Upon combining Eqs. (31) and (28) and integrating, we obtain

$$\langle \mathbf{c}_1 \rangle = -(\langle \mathbf{F}_1 \rangle_{t_0}/m)(m/I)^{\frac{1}{2}} \exp[-(I/m)^{\frac{1}{2}}(t-t_0)]. \quad (33)$$

On evaluating Eq. (33) at the time $t = t_0$, we find that the frictional force acting on the molecule 1 in the steady state is

$$\langle \mathbf{F}_1 \rangle = \langle \mathbf{F}_1 \rangle_{t_0}' = -(mI)^{\frac{1}{2}} \langle \mathbf{c}_1 \rangle = -\zeta_s \langle \mathbf{c}_1 \rangle, \quad (34)$$

where we have defined the steady state frictional coefficient ζ_s. It may be remarked at this point that Eq. (34) is exact only for $t \leq t_0$ as the derivation of the integral I depends on Eq. (4), which is valid only for the steady state ensemble. At time $t > t_0$, the phase density will drift with the changing ensemble average velocity $\langle \mathbf{c}_1 \rangle$. Thus the frictional coefficient describing the decay of the velocity $\langle \mathbf{c}_1 \rangle$ will not necessarily be equal to that expressing the relation between the frictional force and velocity of the state of steady $\langle \mathbf{c}_1 \rangle$. An approximate method for evaluating the effective frictional coefficient for the relaxing velocity of the molecule will be developed in the next section of this paper.

MEAN CORRELATION DISTANCE

The equation for the frictional force may be used to define a mean correlation distance which has a statistical significance somewhat analogous to the mean free path in dilute gases but, unlike it, does not depend on a collisional model. Let us consider a representative molecule which is known to be decaying from some small velocity $\langle \mathbf{c}_1 \rangle_0$ at some starting time $t = t_0$ according to the law

$$\langle \mathbf{F}_1 \rangle = m(d/dt)\langle \mathbf{c}_1 \rangle = -\zeta_r \langle \mathbf{c}_1 \rangle, \quad (35)$$

so that

$$\langle \mathbf{c}_1 \rangle = \langle \mathbf{c}_1 \rangle_0 \exp[-(\zeta_r/m)t]. \quad (36)$$

We will now enquire as to the ensemble average distance traveled before this information decays to zero. By integrating Eq. (36) from $t = t_0$ to $t = \infty$, we obtain

$$\langle \mathbf{r}_1 \rangle_\infty - \langle \mathbf{r}_1 \rangle_0 = \boldsymbol{\lambda}_0 = (m/\zeta_r)\langle \mathbf{c}_1 \rangle_0, \quad (37)$$

where the magnitude of the vector $\boldsymbol{\lambda}_0$ may be identified with the mean correlation distance. The principal usefulness of the concept of the mean correlation distance is that it provides a method for evaluating approximately the relaxation frictional coefficient of Eq. (35). It may be of some further interest in the recombination kinetics of photochemical reactions and in other processes where the initial velocity distribution is known.[7]

As was earlier noted, the frictional coefficient for relaxation of the velocity $\langle \mathbf{c}_1 \rangle$ may not be the same as that for the steady state velocity. As the velocity $\langle \mathbf{c}_1 \rangle$ decays, the phase density $f^{(N/1)}$ drifts with the decreasing velocity $\langle \mathbf{c}_1 \rangle$. It may be expected, however, to lag behind that appropriate for the steady state $\langle \mathbf{c}_1 \rangle$ at any given instant, so that the effective frictional coefficient for the relaxation process may be somewhat higher than that for the steady state. Further, any lag in the response of the phase density to the changing $\langle \mathbf{c}_1 \rangle$ will be more pronounced the

[6] Strictly speaking, the solution to Eq. (29) may not be written down directly, since Eq. (29) is exact only at the point $t = t_0$. However, if a short time interval $(t-t_0$ is considered where $t > t_0$ and $(t-t_0) \ll m/\delta$, then we may express ${}^{*}n^{(2/1)}$ as follows:

$${}^{*}n^{(2/1)} = {}^{0}n^{(2/1)} + (\partial {}^{0}n^{(2/1)}/\partial \mathbf{r}_1) \cdot \langle \mathbf{c}_1 \rangle (t-t_0) + \cdots$$

and it may easily be shown that a correction term given as a power series in $(t-t_0)$ is to be added to Eq. (29). Integration of the "corrected" Eq. (29) followed by taking the limit as t goes to t_0 gives Eq. (30).

[7] Richard M. Noyes, University of Oregon (private communication).

larger the $\langle \mathbf{c}_1 \rangle$. Thus the relaxation frictional coefficient may be expected to display velocity dependence and to converge toward the steady state frictional coefficient in the limiting case of small $\langle \mathbf{c}_1 \rangle$.

The concept of the mean correlation distance now will be used to develop a perturbation series expression for the relaxation frictional coefficient expressing its dependence on the velocity $\langle \mathbf{c}_1 \rangle$. We begin by writing the velocity-dependent relaxation frictional coefficient as

$$\zeta_r = \zeta_0 + \zeta_1 \langle \mathbf{c}_1 \rangle^2 + \cdots. \tag{38}$$

It will later appear that terms in odd powers of $\langle \mathbf{c}_1 \rangle$ vanish from symmetry as might be anticipated from a physical argument. We now wish to integrate

$$(d/dt)\langle \mathbf{c}_1 \rangle = -(\zeta_r/m)\langle \mathbf{c}_1 \rangle. \tag{39}$$

The latter may be accomplished to a first-order approximation by neglecting terms in Eq. (38) in powers of $\langle \mathbf{c}_1 \rangle$ beyond the second and leads to

$$\lambda_0 = \frac{m\langle \mathbf{c}_1 \rangle}{(\zeta_0\zeta_1)^{\frac{1}{2}} |\langle \mathbf{c}_1 \rangle|}\left[\tfrac{1}{2}\pi - \tan^{-1}(\zeta_0/\zeta_1\langle \mathbf{c}_1 \rangle^2)^{\frac{1}{2}}\right]$$

$$= (m/\zeta_0)\left[1 - (\zeta_1/3\zeta_0)\langle \mathbf{c}_1 \rangle^2\right]\langle \mathbf{c}_1 \rangle, \tag{40}$$

where higher powers of $\langle \mathbf{c}_1 \rangle$ have been dropped in the expansion of $\tan^{-1}(\zeta_0/\zeta_1\langle \mathbf{c}_1 \rangle^2)^{\frac{1}{2}}$.

After the molecule has traversed the mean correlation distance λ_0, the velocity $\langle \mathbf{c}_1 \rangle$ on the average will have decayed to zero and the density $n^{(2/1)}$ around the molecule in its new position $\langle \mathbf{r}_1 \rangle'$ will be the equilibrium density. This suggests that the density at $\langle \mathbf{r}_1 \rangle$ be expanded in a Taylor series around the point $\langle \mathbf{r}_1 \rangle' - \lambda_0$:

$$n^{(2/1)} = {}^0n^{(2/1)} - (\partial {}^0n^{(2/1)}/\partial \mathbf{r}_1)\cdot\lambda_0$$

$$+ (1/2!)(\partial/\partial \mathbf{r}_1)\left[(\partial/\partial \mathbf{r}_1){}^0n^{(2/1)}\cdot\lambda_0\right]\cdot\lambda_0 - \frac{1}{3!}\cdots. \tag{41}$$

The ensemble average force acting on the first molecule is then

$$\langle \mathbf{F}_1 \rangle = -\int \frac{\partial\phi}{\partial \mathbf{r}_1} n^{(2/1)} d\mathbf{r}_2$$

$$= \int \frac{\partial\phi}{\partial \mathbf{r}_1}\frac{\partial {}^0n^{(2/1)}}{\partial \mathbf{r}_1}\cdot\langle \mathbf{c}_1 \rangle \frac{m}{\zeta_0}\left(1 - \frac{\zeta_1}{3\zeta_0}\langle \mathbf{c}_1 \rangle^2\right) d\mathbf{r}_2$$

$$+ \frac{1}{3!}\int \frac{\partial\phi}{\partial \mathbf{r}_1}\frac{\partial}{\partial \mathbf{r}_1}\left[\frac{\partial}{\partial \mathbf{r}_1}\left(\frac{\partial {}^0n^{(2/1)}}{\partial \mathbf{r}_1}\cdot\langle \mathbf{c}_1 \rangle\right)\cdot\langle \mathbf{c}_1 \rangle\right]$$

$$\cdot \langle \mathbf{c}_1 \rangle \frac{m^3}{\zeta_0^3}\left(1 - \frac{\zeta_1}{3\zeta_0}\langle \mathbf{c}_1 \rangle^2\right)^3 d\mathbf{r}_2, \tag{42}$$

where we note that integrals of the contributions from even terms of Eq. (41) vanish by symmetry. Upon the introduction of $\mathbf{R} = \mathbf{r}_2 - \mathbf{r}_1$ and repeated integration by parts, we have

$$\langle \mathbf{F}_1 \rangle = -\frac{m}{\zeta_0}\langle \mathbf{c}_1 \rangle\left(1 - \frac{\zeta_1}{\zeta_0}\langle \mathbf{c}_1 \rangle^2\right)\cdot\int \frac{\partial}{\partial \mathbf{R}}\frac{\partial\phi}{\partial \mathbf{R}}{}^0n^{(2/1)} d\mathbf{R}$$

$$- \frac{m^3}{6\zeta_0^3}\langle \mathbf{c}_1 \rangle\left(1 - \frac{\zeta_1}{\zeta_0}\langle \mathbf{c}_1 \rangle^2\right)^3$$

$$\cdot \int \frac{\partial}{\partial \mathbf{R}}\frac{\partial}{\partial \mathbf{R}}\frac{\partial}{\partial \mathbf{R}}\frac{\partial\phi}{\partial \mathbf{R}} : \langle \mathbf{c}_1 \rangle\langle \mathbf{c}_1 \rangle {}^0n^{(2/1)} d\mathbf{R}. \tag{43}$$

Integrating over all angles of the vector $\mathbf{R}$ and making use of the definition of the frictional coefficient of Eq. (30) leads to

$$\langle \mathbf{F}_1 \rangle = -\zeta_0\langle \mathbf{c}_1 \rangle\left[1 - (\zeta_1/\zeta_0)\langle \mathbf{c}_1 \rangle^2\right]$$

$$- (\langle \mathbf{c}_1 \rangle^2\langle \mathbf{c}_1 \rangle/\zeta_0^3)\left[1 - (\zeta_1/\zeta_0)\langle \mathbf{c}_1 \rangle^2\right]^3 S, \tag{44}$$

where $\zeta_0 = \zeta_s$ and

$$S = \frac{2\pi m^3}{15}\int_0^\infty \left(\frac{d^4\phi}{dR^4} + \frac{4}{R}\frac{d^3\phi}{dR}\right){}^0n^{(2/1)} R^2 dR. \tag{45}$$

On collecting the coefficients of $\langle \mathbf{c}_1 \rangle^2\langle \mathbf{c}_1 \rangle$ and comparing with Eqs. (38) and (39) we have as a first-order approximation to the velocity-dependent frictional coefficient

$$\zeta_r = \zeta_s + (3S/4\zeta_s^3)\langle \mathbf{c}_1 \rangle^2. \tag{46}$$

Where $\langle \mathbf{c}_1 \rangle$ has a Maxwell-Boltzmann distribution, we obtain for the frictional coefficient averaged over all velocities

$$\langle \zeta_r \rangle = \zeta_s + (9SkT/4\zeta_s^3 m). \tag{47}$$

This averaged relaxation frictional coefficient is related to the self-diffusion coefficient through the Einstein equation.

The foregoing development of the velocity dependence of the frictional coefficient ζ_r is not rigorous because no detailed justification is put forward for the use of the mean correlation length as an expansion parameter. While the question of its validity requires further examination, it is of interest now to compare it with available experimental data. Equation (46) has been numerically evaluated for the case of liquid argon at 89°K using the intermolecular potential energy and radial distribution function given by Kirkwood, Buff, and Green.[2] We find that $\langle \zeta_r \rangle = 5.55\times10^{-10}$ g sec^{-1} using the value of $\zeta_s = 4.84\times10^{-10}$ g sec^{-1} previously calculated from the same data.[2] These values compare with the experimental value of 5.93×10^{-10} g sec^{-1} found by Corbett and Wang[8] from measurements of the

[8] J. W. Corbett and J. H. Wang, J. Chem. Phys. **25**, 422 (1956).

self-diffusion coefficient. The second-order approximation to ζ_r involves the sixth space derivative of the potential. This has been found to lead to a correction of Eq. (46) of the order of 1%. Thus it appears that consideration of higher terms in the series in Eq. (41) will not notably improve the agreement with experiment.

Finally, it is of interest to determine the magnitude mean correlation distance averaged over all velocities:

$$\langle\lambda_0\rangle=(m/\langle\zeta_r\rangle)(8kT/\pi m)^{\frac{1}{2}}. \quad (48)$$

In the case of liquid argon at 89°K it is of the order of 0.24 A, where the Corbett and Wang value[8] has been used for the velocity-averaged frictional coefficient.

THE JOURNAL OF CHEMICAL PHYSICS VOLUME 32, NUMBER 6 JUNE, 1960

Electronic Structures and Spectra of Nitromethane and Nitrogen Dioxide

K. LENORE MCEWEN*

Department of Chemistry, University of Montreal, Montreal, P.Q., Canada

(Received April 29, 1959)

The electronic structures and spectra of nitromethane and nitrogen dioxide have been calculated by a semiempirical method. The self-consistent molecular orbitals and energies of the π-electron system have been calculated; however, for the nonbonding σ-electron system Hückel-type molecular orbitals are used. The nonbonding $2p$ oxygen orbitals of nitromethane are very slightly modified by mixing with the σ-electron system; in nitrogen dioxide, on the other hand, the totally symmetric combination of $2p$ oxygen orbitals and the sp^2 nonbonding nitrogen orbital mix strongly to form slightly bonding and slightly antibonding molecular orbitals. The calculated transition energies of nitromethane are in reasonable agreement with experiment. For nitrogen dioxide a series of transition energies are obtained which may illuminate experimental results; the complexity of the empirical data, however, and the multitude of calculated low-energy excited states, preclude definite assignment of the observed band systems at this stage.

INTRODUCTION

IN recent years a method has been evolved for calculating with some reliability the π-electronic spectra of conjugated hydrocarbons and many of their derivatives.[1–5] This work has been extended, furthermore, to include both the $\pi\rightarrow\pi^*$ and $n\rightarrow\pi^*$ spectra of a limited number of compounds containing hetero atoms.[6–8] The calculation of ionization potentials also comes within the framework of this theory[9,10]; however, although the relative values of a series of calculated ionization potentials are often very satisfactory, their absolute energies must as yet be adjusted somewhat artificially.

The method of calculation has two stages, the first being the choice of suitable one-electron orbitals for the π-electron system of the molecule, and the second the calculation of the linear combinations of many-electron configurations which are approximations to the stationary states of the molecule. The basic one-electron orbitals are taken as linear combinations of atomic orbitals (LACO), and may be either wave functions which are self-consistent under the complete one-electron Hamiltonian (SCF orbitals),[2] or they may be the simpler Hückel orbitals[1]; although in the two cases the configuration interaction conditions are somewhat different.

In order to obtain satisfactory energies for the various states of a molecule it is necessary to choose the various interaction terms of the Hamiltonian in a manner which takes some account of the σ-electron configuration. The choice of these terms has a semiempirical basis which is due originally to Moffitt[11] and to Pariser and Parr.[1] For example, integrals which involve the orbitals of only one atom are evaluated with the aid of atomic valence state ionization potentials. The sweeping simplification which is usually employed of ignoring differential overlap reduces the number of interaction terms required to a very few.

A further refinement takes account of the fact that the magnitude of the various interaction integrals, especially the one-center integrals, is a function of the

* National Research Council of Canada Postdoctorate Fellow. Present address: Department of Chemistry, University of Saskatchewan, Saskatoon, Saskatchewan, Canada.

[1] R. Pariser and R. G. Parr, J. Chem. Phys. **21**, (a) 466, (b) 767 (1953).

[2] J. A. Pople, Trans. Faraday Soc. **49**, 1375 (1953).

[3] R. Pariser, J. Chem. Phys. **24**, 250 (1956).

[4] J. N. Murrell and H. C. Longuet-Higgins, Proc. Phys. Soc. (London) **A68**, 329 (1955).

[5] J. A. Pople, Proc. Phys. Soc. (London) **A68**, 81 (1955).

[6] J. W. Sidman, J. Chem. Phys. **27**, 429 (1957).

[7] T. Anno. J. Chem. Phys. **29**, 1161, (1958).

[8] J. N. Murrell, Mol. Phys. **1**, 384 (1958).

[9] N. S. Hush and J. A. Pople, Trans. Faraday Soc. **51**, 600 (1955).

[10] R. G. Parr and R. Pariser, J. Chem. Phys. **23**, 711 (1955).

[11] W. Moffitt, Proc. Roy. Soc. (London) **A210**, 245 (1951).

electron density associated with the atoms concerned. This "self-consistent electronegativity" method has been applied to the electronic structure of formaldehyde,[12] and the results indicate that the usual SCF method overestimates the polarity of the π system of a hetero molecule.

The present work was undertaken with the hope of better understanding both the π-electronic and the nonbonding electronic properties of several compounds containing oxygen and nitrogen. The π orbitals employed are SCF-LCAO orbitals. For the nonbonding orbitals, however, a much rougher approximation is used. Not enough is known concerning the electronic properties of the compounds studied to justify a detailed variation of the interaction integrals with electron density. However, if the π-electron ground state structures which we calculate are very different from the structure assumed in choosing interaction integrals, some correction is made.

THEORY

A. π-Electron System

In the present calculation the usual approximation is made of evaluating the orbitals for the π-electron system in the presence of a core potential consisting of the nuclei and all electrons outside the π system.

The self-consistent orbitals ψ_i of a molecule are those for which the matrix

$$F_{ij}=H_{ij}^{\text{core}}+\sum_{l=1}^{m}\{2(ij\mid ll)-(il\mid lj)\} \qquad (1)$$

is diagonal, where

$$H_{ij}^{\text{core}}=\int\psi_i^*(1)H^{\text{core}}\psi_j(1)d\tau_1,$$

H^{core} being the potential of the molecular core, and where

$$(ij\mid kl)=\iint\psi_i^*(1)\psi_k^*(2)\,(e^2/r_{12})\psi_j(1)\psi_l(2)d\tau_1d\tau_2.$$

When the molecular orbitals are taken in the LCAO form

$$\psi_i=\sum_\nu c_{i\nu}\nu,$$

where μ, ν, etc., signify atomic orbitals, then, as has been shown by Hall[13] and Roothaan,[14] the equations for the ψ_i may be derived from Eq. (1), subject to the orthonormality constraint on the set of ψ_i, and, for a molecule with $2N$ electrons in a paired orbital configuration have the form

$$\sum_\nu F_{\mu\nu}c_{i\nu}=E_i\sum_\nu S_{\mu\nu}c_{i\nu}. \qquad (2)$$

The orbital energies E_i are the solutions of the secular determinant

$$|F_{\mu\nu}-ES_{\mu\nu}|=0,$$

the $F_{\mu\nu}$ being given by

$$F_{\mu\nu}=H_{\mu\nu}^{\text{core}}+\sum_{\eta\delta}P_{\eta\delta}[(\mu\nu\mid\eta\delta)-\tfrac{1}{2}(\mu\delta\mid\eta\nu)]. \qquad (3)$$

The $P_{\eta\delta}$ are expressions for the π-electron distribution, and are given by

$$P_{\eta\delta}=2\sum_i c_{i\eta}c_{i\delta},$$

where the various $c_{i\eta}$ are the LCAO coefficients of the self-consistent orbital ψ_i. In the present work we need only be interested in the case of real ψ_i.

In the approximation of zero-differential overlap the $F_{\mu\mu}$ and $F_{\mu\nu}$ have been shown by Pople[2] conveniently to reduce to expressions of the type

$$F_{\mu\nu}=\alpha_\mu+\tfrac{1}{2}P_{\mu\mu}(\mu\mu\mid\mu\mu)+\sum_{\nu\neq\mu}P_{\nu\nu}(\mu\mu\mid\nu\nu) \qquad (4)$$

and

$$F_{\mu\nu}=\beta_{\mu\nu}-\tfrac{1}{2}P_{\mu\nu}(\mu\mu\mid\nu\nu). \qquad (5)$$

In these expressions α_μ and $\beta_{\mu\nu}$ represent the interaction of an electron on one and two centers, respectively, with the core potential H^{core}. Here $\beta_{\mu\nu}$ is taken as zero unless μ and ν are on adjacent centers. The one-center integral α_μ is more completely given by the following expression:

$$\alpha_\mu=-I_\mu-\sum_{\nu\neq\mu}(n_\nu:\mu\mu)-\sum_{\nu\neq\mu}Z_\nu(\mu\mu\mid\nu\nu), \qquad (6)$$

where I_μ is the appropriate valence-state ionization potential, Z_ν is the number of electrons contributed by ν to the π-electron system, and $(n_\nu:\mu\mu)$ is the penetration integral of an electron in μ for the atom with orbital ν.

Turning now to the manner of approximating the various interaction integrals, we will choose all the required integrals assuming nonpolar σ-electron bonds. We will discuss the one-center quantities I_μ and $(\mu\mu\mid\mu\mu)$ together, the former being an empirically determined ionization potential and the latter being a coulomb repulsion integral, which is conveniently estimated by Pariser's approximation[15]

$$(\mu\mu\mid\mu\mu)=I_\mu-A_\mu \qquad (7)$$

where A_μ is the appropriate valence state electron affinity. With regard to the determination of I_μ and $(\mu\mu\mid\mu\mu)$ for nitromethane, we will consider two possibilities, first, that the nitrogen atom carries a positive charge of $+1$, and second, that it is neutral in the molecule (in which case the one-center integrals will be denoted by I^0, etc.) In the first case I_{N^+} and

[12] R. D. Brown and M. L. Heffernan, Trans. Faraday Soc. **54**, 757 (1958).
[13] G. G. Hall, Proc. Roy. Soc. (London) **A205**, 541 (1951).
[14] C. C. J. Roothaan, Revs. Modern Phys. **23**, 61 (1951).
[15] R. Pariser, J. Chem. Phys. **21**, 568 (1953).

$(NN \mid NN)$ may be taken from the energies associated with the processes

$$N^+(sxyzV_4) \rightarrow N^{++}(sxyV_3) \quad (8)$$

and

$$N(sxyz^2V_3) \rightarrow N^+(sxyzV_4). \quad (9)$$

If the nitrogen atom in nitromethane is neutral, however, the values of $I_{N^+}{}^0$ and $(NN \mid NN)^0$ will be rather different from those derived from the foregoing processes. The coulomb repulsion integral may be obtained from the energies of the following pair of processes, although these are not directly relevant to the N_π orbital in nitromethane,

$$N(sx^2yzV_3) \rightarrow N^+(sx^2yV_2) \quad (10)$$

$$N^-(sx^2yz^2V_2) \rightarrow N(sx^2yzV_3). \quad (11)$$

An artificial value for $I_{N^+}{}^0$ can be obtained which may be suitable for a neutral nitrogen atom, i.e.,

$$I_{N^+}{}^0 = E\{N(sxyz^2V_3) \rightarrow N^+(sxyzV_4)\} + (NN \mid NN)^0.$$

In this approximation the difference between the values for the one-center quantities for neutral or positively charged nitrogen is the same value δ_N for both I_{N^+} and $(NN \mid NN)$. A similar correction could be obtained for I_O and $(OO \mid OO)$ for the case when an oxygen atom has a negative charge. Although this is probably a very rough approximation, it allows us to write the total correction to $F_{\mu\mu}$ due to change of electronegativity in the convenient form $\delta_\mu[(P_{\mu\mu}/2)-1]$ [Eqs. (4) and (6)]. It is obvious that in an $-NO_2$ compound the correction to F_{OO} from such a term will be much smaller than the correction to F_{NN}, since δ_O arises from a net charge of only half the magnitude of that causing δ_N and furthermore, in a case of large negative charge on the oxygen atoms, when δ_O may be fairly large, $[(P_{OO}/2)-1)$ becomes very small. For this reason, and because of lack of data for oxygen negative ions, only the variation of I_{N^+} and $(NN \mid NN)$ will be considered; either those values suitable for neutral nitrogen or those for N^+ will be used, depending on which are more compatible with the resulting π-electronic distribution; it seems undesirable, in view of the roughness of the approximations used, to attempt to interpolate values of I_{N^+} and $(NN \mid NN)$ for intermediate electronic distributions.

The one-center integrals for nitrogen dioxide are calculated on the assumption that there is a doubly occupied nonbonding nitrogen sp^2 orbital. This means that the values of I_N and $(NN \mid NN)$ obtained from processes 10 and 11 should be combined with the values of these quantities obtained from the corresponding processes which apply to the nitrogen configuration $(s^2p^3V_3)$, i.e.,

$$N(s^2xyzV_3) \rightarrow N^+(s^2xyV_2);$$

$$N^-(s^2xyz^2V_2) \rightarrow N(s^2xyzV_3).$$

The required linear combination is of course $\{\frac{2}{3}E(sp^4) + \frac{1}{3}E(s^2p^3)\}$ where $E(sp^4)$ and $E(s^2p^3)$ are the energies of the desired quantity I_N or $(NN \mid NN)$ obtained assuming the nitrogen configuration (sp^4) and (s^2p^3), respectively. Unlike nitromethane, where a very polar π-electronic structure seems a distinct possibility, it is likely from dipole moment data that NO_2 is fairly nonpolar,[16] and that only parameters for neutral nitrogen and oxygen will be required.

The two-center integrals $(\mu\mu \mid \nu\nu)$ are estimated by the method of Pariser and Parr[10]: at large distances theoretically calculated values are used, while at shorter distances the values are adjusted downward so that at $r=0$ the magnitude of $(\mu\mu \mid \nu\nu)$ approaches $\frac{1}{2}\{(\mu\mu \mid \mu\mu) + (\nu\nu \mid \nu\nu)\}$.

One-center integrals of the type $(\mu\mu \mid \bar{\mu}\bar{\mu})$ and $(\mu\bar{\mu} \mid \bar{\mu}\mu)$, where $\bar{\mu}$ is a $2p$ orbital at right angles to μ, are readily estimated using atomic valence state ionization potentials, together with the identity[17]

$$(\mu\mu \mid \mu\mu) - (\mu\mu \mid \bar{\mu}\bar{\mu}) = 2(\mu\bar{\mu} \mid \bar{\mu}\mu).$$

The corresponding identity for two-center integrals is used to estimate $(\mu\mu \mid \bar{\nu}\bar{\nu})$, the value of $(\mu\bar{\mu} \mid \bar{\nu}\nu)$ being calculated theoretically from the tables of Roothaan.[18]

The contributions to F_{OO} and F_{NN} from penetration integrals are obviously very different, and are included in the calculation. The penetration integrals are calculated using the tables of Roothaan.[18]

The resonance integral $\beta_{NO}(\pi)$ is chosen by analogy with the values for the integral which have proved suitable for C=C and C=O bonds. For pure double bonds the values $\beta = -2.92$ ev[1] and $\beta = -3.0$ ev[6] have been found suitable for C=C and C=O, respectively. It may therefore be the case that the resonance integral for a pure N=O double bond is also approximately -3.0 ev. The length of a pure N=O double bond is approximately 1.18–1.20 A.[19] Now the two compounds in which we are interested have N—O bond lengths of 1.21 and 1.19 A for nitromethane[20] and nitrogen dioxide,[21] respectively. It therefore seems not unreasonable to use the value $\beta_{NO}(\pi) = -3.0$ ev in both cases.

---

[16] P. Gray and A. D. Yoffe, Chem. Revs. **55**, 1069 (1955).
[17] R. G. Parr and F. G. Fumi, J. Chem. Phys. **21**, 1265 (1953).
[18] C. C. J. Roothaan, (a) *Two-Center Coulomb Integrals* Special Technical Report of the Laboratory of Molecular Structure and Spectra, University of Chicago (1955); (b) J. Chem. Phys. **19**, 1445 (1951).
[19] G. W. Wheland, *Resonance in Organic Chemistry* (John Wiley & Sons, Inc., New York, 1955).
[20] L. O. Brockway, J. Y. Beach, and L. Pauling, J. Am. Chem. Soc. **57**, 2693 (1935).
[21] G. E. Moore, J. Opt. Soc. Am. **43**, 1045 (1953).

B. Nonbonding Orbital Wave Functions and Energies

In discussing the σ-electron system of

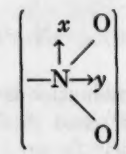

compounds, we shall treat the π electrons as part of the core. The $2p$ oxygen σ orbitals will be referred to as O_r and O_t, the former being parallel to the adjacent N—O bond, and the latter perpendicular to the N—O bond. The A_1 and B_2 symmetry orbitals $1/\sqrt{2}\{O_r \pm O_r'\}$ and $1/\sqrt{2}\{O_t \pm O_t'\}$ are conveniently designated $O_r^{\pm}$ and $O_t^{\pm}$. Similarly the oxygen $2s$ orbitals are taken in the form $O_s^{\pm}$. The nitrogen $2p$ orbitals are taken as N_y and N_x, with symmetry A_1 and B_2, respectively; that is, N_y is parallel to the axis of the molecule. The positive direction of N_y is toward the oxygen atoms, and the positive direction of O_r is toward the nitrogen. O_t and O_t' are taken with their positive directions toward one another.

If we consider for a moment the oversimplified case in which the B_2 orbitals O_t^- and O_r^- have equal diagonal matrix elements, then, neglecting for now O_s^-, we obtain a nonbonding orbital with energy and wave function as follows

$$E_{\text{nbo}}^- = \langle O_t^- \mid F_{\text{OO}} \mid O_t^- \rangle$$

and

$$\psi_{\text{nbo}}^- = c_1 O_r^- - c_2 O_t^-,$$

where

$$c_1/c_2 = \langle O_t^- \mid F_{\text{ON}} \mid N_x \rangle / \langle O_r^- \mid F_{\text{ON}} \mid N_x \rangle.$$

Besides ψ_{nbo}^- this simple system will include a bonding and an antibonding orbital containing N_x and $(c_2 O_r^- + c_1 O_t^-)$. Since the resonance integral for a σ bond is larger than that for a π bond, and since electron interaction increases $\langle O_r^- \mid F_{\text{ON}} \mid N_x \rangle$ but not

$$\langle O_t^- \mid F_{\text{ON}} \mid N_x \rangle,$$

it follows that $c_1 \gg c_2$.

This simplified example suggests that it may be possible to estimate $\psi_{\text{nbo}}^{\pm}$ and $E_{\text{nbo}}^{\pm}$ in an actual molecule. If the energy of the B_2 nonbonding orbital is calculated for the case when

$$\langle O_t^- \mid F_{\text{OO}} \mid O_t^- \rangle = \langle O_r^- \mid F_{\text{OO}} \mid O_r^- \rangle + \delta,$$

then the new energy E_{nbo}^- is of the form

$$E_{\text{nbo}}^- = \langle O_t^- \mid F_{\text{OO}} \mid O_t^- \rangle + \Delta$$

and the main contribution to Δ, for small δ, may be shown to be a term

$$\delta \langle O_t^- \mid F_{\text{ON}} \mid N_x \rangle^2 / \langle O_r^- \mid F_{\text{ON}} \mid N_x \rangle^2.$$

This indicates that although we may not be in a position to calculate reliably the various bonding and antibonding orbitals of the σ system, we may be able to obtain wave functions and energies of the $2p$ nonbonding orbitals on the oxygen atoms, since they may depend to a relatively small extent on the accuracy with which we can calculate the various off-diagonal matrix elements. The A_1 nonbonding orbitals, will, of course, become very dependent on the interatomic terms at very large angle ONO, since then the resonance integral $\beta(O_r N_y)$ becomes very small relative to $\beta(O_t N_y)$ because of the angular dependence of these terms.

The O_r orbitals of both A_1 and B_2 symmetry are engaged in strong σ bonding, the type of bonding varying as to the relative nitrogen s and p character with varying angle ONO. The O_t orbitals are capable of increasing π-type bonding as the angle ONO increases, but until this angle becomes very large there will be an A_1 and a B_2 orbital which are predominantly O_t, with energy rather removed from that of the bonding and antibonding σ orbitals. If therefore the secular determinant for the σ-electron system is set up, using Eqs. (2) and (3), and if all the diagonal elements except that for O_t are replaced by $(F_{\mu\mu} - \langle O_t \mid F_{\text{OO}} \mid O_t \rangle)$, then the resulting equation may be solved for E' which is closer than $\langle O_t \mid F_{\text{OO}} \mid O_t \rangle$ to the desired E_{nbo}. Similarly, E' may be substituted in the original determinant, and the final solution obtained by an iterative method.[22]

The method used to approximate the various electron interaction terms will be outlined subsequently. It should be pointed out, however, that in the case of the nitrogen dioxide nonbonding σ orbitals, certain difficulties arise because of the presence of an odd electron. The variation of Eqs. (2) and (3) which should be solved in such a case[23] will be discussed when nitrogen dioxide is dealt with specifically. The theory which has been presented up to now is adequate for discussing the manner in which the electron interaction terms arising from the σ bonds are to be estimated.

In our calculation of the nonbonding σ orbitals, Eq. (2) is to be solved using approximate wave functions to estimate the $P_{\mu\delta}$. In brief, σ-bonding molecular orbitals are initially assumed for nitromethane which may be derived from three identical nonpolar localized orbitals of the type $(\frac{1}{2})^{\frac{1}{2}}\{N_{sp^2} + \chi\}$, where χ is C_{sp^3} or O_r, and from substituent localized orbitals

$$(\tfrac{1}{2})^{\frac{1}{2}}(C_{sp^3} + H_{is}).$$

[22] H. Margenau and G. M. Murphy, *The Mathematics of Physics and Chemistry* (D. Van Nostrand and Company, Inc., Princeton, New Jersey, 1956).

[23] (a) J. A. Pople and R. K. Nesbit, J. Chem. Phys. **22**, 571 (1954); (b) G. Berthier, J. Chim. Phys. **51**, 363 (1954).

This simplified basic electronic structure, which will of course introduce some error, mainly at the carbon end of the molecule, allows a considerable simplification of the secular equations.

For nitrogen dioxide the various nonbonding molecular orbitals are calculated assuming a potential arising from nonpolar N—O σ bonds with the component nitrogen σ-bonding orbital pure sp^2. In addition the initial potential is assumed to include a doubly filled nonbonding molecular orbital which is adequately described by $(\frac{1}{3})^{\frac{1}{2}}(N_s-\sqrt{2}N_y)$. The basic structure described will have an A_1 σ-bonding molecular orbital $(\frac{1}{2})^{\frac{1}{2}}\{O_r+(\frac{1}{3})^{\frac{1}{2}}(\sqrt{2}N_s+N_y)\}$. It is clear that this orbital and the nonbonding sp^2 nitrogen orbital will mix; however, owing, to the disparity in the energies of the two orbitals, and the unfavorable bonding conditions between them, it seems likely that the mixing will be small enough to ignore in calculating the initial potential. The contributions to our final nonbonding orbital wave functions from the atomic orbital $(\frac{1}{3})^{\frac{1}{2}}(\sqrt{2}N_s+N_y)$ will provide some check on the suitability of the initial σ-bonding orbitals we have chosen.

Although the assumption of nonpolar N—O σ bonds seems rather arbitrary, a comparison of the relevant electroaffinities from the tables of Skinner and Pritchard[24] indicates that it may be not unreasonable. The electroaffinity of an oxygen (s^2p^4) $2p$ orbital is given as 9.95. If, however, the orbital in question has as much as 10% $2s$ character, then its electroaffinity is approximately 12. The electroaffinity of a nitrogen sp^2 orbital is also approximately 12.

Assuming the basic structure outlined before, we will proceed to simplify Eqs. (2) and (3). Differential overlap will be neglected, although this procedure is perhaps less justified in the treatment of σ bonds than for π-electron systems. The fact that various atoms have more than one orbital participating in the bonding system means that the matrix elements $F_{\mu\mu}$ and $F_{\mu\nu}$ are complicated by terms containing $P_{\nu\nu'}$, where ν and ν' are different orbitals on the atom n_ν. In the case of pure trigonal or tetrahedral hybridization of n_ν, however, where each hybrid orbital contains one electron, the value of $P_{\nu\nu'}$ will be zero. Furthermore, if one trigonal hybrid orbital contains two nonbonding electrons, then the resultant $P_{\nu\nu'}$ for this artificial system gives rise to terms in the diagonal matrix element $F_{\mu\mu}$ which may be included in the penetration integrals. We may then write for the diagonal matrix elements

$$F_{\mu\mu}=\alpha_\mu+\tfrac{1}{2}P_{\mu\mu}(\mu\mu\,|\,\mu\mu)+\sum_{\nu,\,\nu'\neq\mu}P_{\nu\nu}(\mu\mu\,|\,\nu\nu)+\sum_{\mu'\neq\mu}P_{\mu'\mu'}\{(\mu\mu\,|\,\mu'\mu')-\tfrac{1}{2}(\mu\mu'\,|\,\mu\mu')\},\quad(12)$$

where α_μ is given by Eq. (6), with the addition of terms $Z_{\mu'}\{(\mu\mu\,|\,\mu'\mu')-\frac{1}{2}(\mu\mu'\,|\,\mu\mu')\}$. It will be seen that some error in the $F_{\mu\mu}$ arising from the assumption of pure trigonal hybridization will tend to cancel between the second and fourth terms of $F_{\mu\mu}$, and also within the summation represented by the third term. For example in nitrogen dioxide the relative amount of N_s and N_y character in the N—O bonds and in the N_{sp^2} nonbonding orbital is likely to differ from that assumed, but the resulting errors in the $F_{\mu\mu}$ will cancel to some extent. Terms three and four of Eq. (12) provide a means of correcting the $F_{\mu\mu}$ for π-electron polarity.

The off-diagonal elements $F_{\mu\nu}$ are treated similarly to those for π-electron systems. In view of the neglect of differential overlap, the $F_{\mu\nu}$ are given by Eq. (5).

The final interactions to be considered are the $F_{\mu\mu'}$. When n_μ is trigonally or tetrahedrally bonded to equivalent atoms, then all the $F_{\mu\mu'}$ vanish. In the case of nitrogen dioxide, however, where there are assumed to be two nonbonding electrons on one side of the nitrogen atom, and two N—O σ bonds on the other side, there is a nonzero value for $F_{N_sN_y}$ which should be discussed briefly. The terms contributing to this matrix element are of two kinds. First, there are penetration-type integrals $(n_\nu:\mu\mu')$, which, since they are much smaller than ordinary penetration integrals $(n_\nu:\mu\mu)$, will be ignored. Second, there is an electron interaction term which is a sum of the interactions of an electron having distribution $NsNy$ with the electron density in the N_{sp^2} nonbonding orbital, and in the N—O σ bonds. In view of our neglect of differential overlap the latter electron repulsion should be ignored. It is, however, of such a magnitude as to roughly cancel the interaction (which is of opposite sign) with the electron density in the nonbonding orbital. For this reason the matrix element $F_{N_sN_y}$ will be ignored. There are also nonvanishing matrix elements of the type $F_{\mu\mu'}$ involving oxygen atomic orbitals; the largest of these will be $F_{O_rO_s}$, a term which might well be important in the calculation of σ-bonding orbitals. Since we are interested only in nonbonding orbitals, all the $F_{\mu\mu'}$ involving oxygen will be neglected.

The various one-center integrals are approximated in the same manner as was used for the π-electron system. The two-center integrals are treated somewhat differently, however. The resonance integrals $\beta_{\mu\nu}(\sigma)$ are taken as proportional to the corresponding overlap integrals obtained from the tables of Mulliken *et al.*,[25] and are calculated to correspond to $\beta_{\mu\nu}(\pi)$ for the same bond. The two-center coulomb integrals are taken from the tables of Roothaan.[18] There may be good reason to modify these Coulomb integrals so that at zero internuclear distance they would correspond to the empirical values for the one-center integrals. There is at present, however, no way of testing empirically the merits of such a procedure, so that the calculated integrals seem preferable.

[24] H. A. Skinner and H. O. Pritchard, (a) Trans. Faraday Soc. **49**, 1254 (1953); (b) Chem. Revs. **55**, 745 (1955).

[25] R. S. Mulliken, C. A. Rieke, D. Orloff, and H. Orloff, J. Chem. Phys. **17**, 1248 (1949).

TABLE I. Integrals involving π-atomic orbitals (ev).

I_{N^+}	28.86	$(NN \mid NN)$	16.77	$(O{:}NN)$	0.91	$(O_\pi O_\pi \mid O_t O_t)$	12.76
I_O	17.21	$(OO \mid OO)$	14.52	$(C{:}NN)$	0.52	$(N_\pi N_\pi \mid O_t O_t)$	9.46
$\beta_{NO}(\pi)$	−3.0	$(OO \mid NN)$	9.66	$(N{:}OO)$	1.14	$(N_\pi N_\pi \mid C_\pi C_\pi)$	8.33
		$(OO \mid O'O')$	6.38	$(O'{:}OO)$	0.05	$(O_\pi O_\pi \mid C_\pi C_\pi)$	5.95

NITROMETHANE

A. π-Orbitals

The structure of nitromethane which is used in calculating the various interatomic interaction integrals is that indicated by an electron diffraction study,[20] i.e.,

$r_{NO}=1.21$ A, $r_{CN}=1.46$ A and $\angle_{ONO'}{}^{26}=1.27°$.

A preliminary calculation of the π-electron structure using parameters appropriate to a neutral nitrogen atom results in a π-electron distribution in which the nitrogen atom has a positive charge of almost $+1e$. In view of this result, which is consistent with the fact that nitromethane has a high dipole moment, the π orbitals and their energies have been calculated using nitrogen integrals suitable for N^+. The penetration energies used are those for neutral atoms, since it is beyond the accuracy of the method to consider small changes in these quantities. The various required integrals involving π-atomic orbitals are found in Table I.

The values of I_{N^+} and $(NN \mid NN)_\pi$ are based on the empirical energy of $(N^+ s^2 p^2\,{}^3P_2 \rightarrow N^{+\,+} s^2\,p\,{}^2P)$[27] and promotional energies for the various valence states from the tables of Skinner and Prichard.[24] The latter sources were used for all the other empirical assignments of I_μ and $(\mu\mu \mid \mu\mu)$.

Also included in Table I are the Coulomb repulsion integrals of N_π and O_π with the various atomic orbitals which will appear in $\psi_{nbo}{}^{\pm}$. Since these are to be used in computing the $n\rightarrow\pi^*$ transition energies, semiempirical values are chosen. When μ and ν in $(\mu\mu \mid \nu\nu)$ are not p orbitals at right angles to one another and to the line joining μ and ν, as for instance when μ is N_π and ν is C_s or C_y, then the value for $\nu=C_\pi$ is used. This is not a serious approximation since the coefficients of these integrals in the expressions for the $n\rightarrow\pi^*$ transition energies are very small indeed.

The self-consistent π-orbitals and their energies are given below.[28] It is convenient to designate the orbitals according to their symmetry:

$$b_1=0.729N_\pi+(0.684/\sqrt{2})(O_\pi+O_{\pi'}) \quad -21.76 \text{ ev}$$

$$a_2=\sqrt{2}^{-1}(O_\pi-O_{\pi'}) \quad -15.51 \text{ ev}$$

$$b_1{}^*=0.684N_\pi-(0.729/\sqrt{2})(O_\pi+O_{\pi'}) \quad -3.61 \text{ ev}.$$

We shall adopt the following notation for the π-electron configurations:

$$\pi_0=|\cdots b_1\bar{b}_1 a_2\bar{a}_2|$$

$$=1/(n!)^{\frac{1}{2}}\,|\cdots b_1(n-3)\bar{b}_1(n-2)a_2(n-1)\bar{a}_2(n)|,$$

where a_2 and $\bar{a}_2$ differentiate orbitals containing electrons with α and β spin,

$$^{1,3}(a_2{}^{-1}b_1{}^*)=\sqrt{2}^{-1}\{|\cdots b_1\bar{b}_1 a_2\bar{b}_1{}^*| \pm |\cdots b_1\bar{b}_1 b_1{}^*\bar{a}_2|\}$$

and

$$^{1,3}(a_2{}^{-1}b_1{}^{-1}b_1{}^{*2})=\sqrt{2}^{-1}\{|\cdots b_1\bar{a}_2 b_1{}^*\bar{b}_1{}^*| \pm |\cdots a_2\bar{b}_1 b_1{}^*\bar{b}_1{}^*|\}$$

By allowing the various configurations with $^1A_1$ symmetry to interact, the ground state χ_0 for nitromethane is found to be

$$\chi_0=0.97\pi_0-0.23(a_2{}^{-2}b_1{}^{*2})+0.06(b_1{}^{-1}b_1{}^*)$$

$$-0.11(b_1{}^{-2}b_1{}^{*2}),$$

the stabilization achieved by this interaction being −0.60 ev. This ground state has a dipole moment of 2.40 debyes in the direction N^+—O_2^-. In addition to the π-electron moment there will be contributions to the dipole moment, also in the direction N^+—O_2^-, from the $2s$ oxygen orbitals (which have some $2p$ character) and from the C—N σ bond. The measured dipole moment of nitromethane vapor is 3.46 debyes.[29]

B. Nonbonding Orbitals

The A_1 and B_2 nonbonding orbitals are calculated in the manner already described, using the integrals

[26] In this section O, O′ will distinguish the two oxygen atoms. Different orbitals on one O atom will, when necessary, be specified O_t, O_π, etc.

[27] C. E. Moore, *Atomic Energy Levels*, Natl. Bur. Standards Circ. No. 467,.

[28] Similar orbitals to these were obtained in a semiempirical calculation by J. Tanaka (J. Chem. Soc. Japan 78, 1643 (1957). The B_1 orbital energies in that paper are appreciably less stable than those in the present work because they were calculated assuming the antisymmetric orbital π electrons to be part of the oxygen core, so that the B_1 orbital electrons were not allowed to exchange with them. The $\pi-\pi^*$ transition energies in the present work are therefore very different.

[29] E. Tannenbaum, R. J. Myers, and W. D. Gwinn, J. Chem. Phys. 25, 42 (1956).

TABLE II. Integrals involving σ-atomic orbitals (ev).

$I(O_s)=I(O_s^+)+(O_sO_s \mid O_sO_s)$	32.3	$(N_sN_s \mid O_sO_s)$	11.50	$(O':O_iO_i)$	0.04
$I(O_i)=I(O_i^+)+(O_rO_r \mid O_sO_s)$	14.71	$(C_sC_s \mid C_sC_s)$	12.23	$(O':O_rO_r)$	0.06
$I(O_r)$	17.21	$(N_sN_s \mid O_rO_r)$	13.65	$(O:N_xN_x)$	4.31
$I(N_{x,y})$	14.32	$(N_\perp N_\perp \mid O_rO_r)$	12.11	$(O:N_yN_y)$	1.60
$I(N_s)$	27.5	$(N_sN_s \mid O_rO_r)$	12.30	$(O:N_sN_s)$	2.27
$I(C_y)$	11.26	$(N_yN_y \mid C_yC_y)$	11.27	$(C:N_xN_x)$	0.52
$I(C_s)$	21.34	$(N_yN_y \mid C_sC_s)$	10.14	$(C:N_yN_y)$	2.43
$(O_rO_r \mid O_rO_r)$	14.52	$(N_sN_s \mid C_yC_y)$	10.45	$(C:N_sN_s)$	1.11
$(N_yN_y \mid N_yN_y)$	12.74	$(N_sN_s \mid C_sC_s)$	9.50	$(N:C_yC_y)$	3.27
$(N_sN_s \mid N_sN_s)$	13.6	$(N:O_iO_i)$	1.34	$(N:C_sC_s)$	1.45
$(C_yC_y \mid C_yC_y)$	11.08	$(N:O_rO_r)$	4.81	$(H:C_yC_y)$	0.81
$(N_sN_s \mid O_sO_s)$	12.62	$(N:O_sO_s)$	2.43	$(H:C_sC_s)$	1.29
$(N_\perp N_\perp \mid O_sO_s)$	10.93	$(O':O_sO_s)$	0.05		

tabulated in Tables II and III. The resonance integral $\beta_{CN}(\pi)$ is estimated using the formula suggested by Pariser and Parr for carbon-carbon bonds.[1] The resonance integral between O_i and $N_\perp$, a $2p$ nitrogen orbital oriented parallel to O_i, is taken the same as $\beta_{NO}(\pi)$. Instead of giving in Tables II and III Coulomb and resonance integrals involving N_x and N_y, it is more convenient to present values for $N_\perp$ and N_σ, the latter being parallel to an N—O bond. No account is taken of the polar π-electron structure in choosing the σ-electron integrals for nitrogen. The π-electron polarity is, however, included in the diagonal matrix elements $F_{\mu\mu}$ by the terms $\Delta F_{\mu\mu}$:

$$\Delta F_{\mu\mu}=-\delta\{(\mu\mu \mid N_\pi N_\pi)-\tfrac{1}{2}[(\mu\mu \mid O_\pi O_\pi)+(\mu\mu \mid O_{\pi'}O_{\pi'})]\},$$

where δ is the magnitude of π-electron positive charge on the nitrogen atom.

For convenience the A_1 carbon orbitals are taken in the form $C_1=\frac{1}{2}(C_s+\sqrt{3}C_y)$ and $C_2=\frac{1}{2}(\sqrt{3}C_s-C_y)$. The contributions of C_2 and the hydrogen $1s$ orbitals to the electron density of ψ_{nbo}^+ may be shown to be less than 0.01, so that for the present purpose the secular determinant may be approximately factored to exclude them.

TABLE III. Resonance and overlap integrals (ev).

N—O integrals			N—C integrals		
$\mu\nu$	$S_{\mu\nu}$	$\beta_{\mu\nu}$	$\mu\nu$	$S_{\mu\nu}$	$\beta_{\mu\nu}$
$O_\pi N_\pi$	0.18	(−3.00)	$N_\pi C_\pi$	0.18	(−1.6)
O_rN_s	0.32	−5.34	N_yC_y	0.32	−2.85
O_rN_s	0.31	−5.16	N_yC_s	0.31	−2.75
O_sN_s	0.40	−6.67	N_sC_y	0.40	−3.55
O_sN_s	0.33	−5.50	N_sC_s	0.33	−2.93

The two nonbonding orbitals $\psi_{nbo}^\pm$ and their energies are given below. The value of the diagonal matrix element $\langle O_i \mid F_{OO} \mid O_i\rangle$ is given in brackets.

$$\psi_{nbo}^+=a_1=0.95O_i^+-0.20O_r^+-0.02N_y-0.01N_S+0.24C_1+0.01O_S^+,$$

$$E^+=-16.11\text{ ev}(-16.19\text{ ev})$$

$$\psi_{nbo}^-=b_2=0.99O_i^--0.14O_r^--0.01N_x+0.004O_S^-;$$

$$E^-=-16.16\text{ ev}(-16.19\text{ ev}).$$

The $E_{nbo}^\pm$ and $\psi_{nbo}^\pm$ are found to be rather insensitive to changes in the values chosen for the σ-electron interatomic interaction integrals.

We will introduce a brief notation similar to that for the π system; the nonbonding electron contribution to the ground state is

$$n_0=|\cdots a_1\bar{a}_1b_2\bar{b}_2|,$$

and a configuration in which an a_1 electron has been excited into a π orbital will be written

$$^{1,3}(a_1^{-1}b_1^*).$$

TABLE IV. Ionization potentials and electron affinity of nitromethane.

Orbital	Calculated energy (ev)	Energy after zero adjusted (ev)
b_1	21.76	17.59
a_2	15.51	(11.34)[a]
a_1	16.11	11.94
b_2	16.16	11.99
b_1^* electron affinity	3.61	−.56

[a] See footnote 30.

TABLE V. Electronic transitions of nitromethane.

Symmetry	Excited state	Transition energy (ev)	f calc	Observed maximum (ev)	f obs
$^1B_2$	$0.94\ (a_2^{-1}b_1^*)-0.34\ (b_1^{-1}a_2^{-1}b_1^{*2})$	5.80	0.33	6.23[a]	0.15 ($\log\epsilon_{max}\sim4$)
$^1B_1$	$0.99\ (a_1^{-1}b_1^*)+0.17\ (a_1^{-1}b_1^{-1}b_1^{*2})$	4.41	0.0001	4.45[b]	0.0004 ($\log\epsilon_{max}\sim1.4$)[c]
$^1A_2$	$0.99\ (b_2^{-1}b_1^*)+0.15\ (b_2^{-1}b_1^{-1}b_1^{*2})$	4.56	0	...	
$^3B_2$	$^3(a_2^{-1}b_1^*)$	3.01	0	...	
$^3A_1$	$^3(b_1^{-1}b_1^*)$	7.64	0	...	
$^3B_1$	$^3(a_1^{-1}b_1^*)$	3.71	0	...	
$^3A_2$	$^3(b_2^{-1}b_1^*)$	4.60	0	...	

[a] R. A. McIvor and A. Grey (private communication).
[b] A. P. I. 104.
[c] P. A. D. de Maine, M. M. de Maine, and A. G. Goble, Trans. Faraday Soc. **53**, 427 (1957).

The ground state is of course χ_0, since the electron configuration n_0 is implied in all of the π configurations.

C. Ionization Potentials and Electronic Transition Energies

The orbital energies we have calculated represent approximations to the various ionization potentials of the molecule. In Table IV will be found the various predicted ionization potentials and the electron affinity based on the assumption that the lowest calculated ionization potential corresponds to the value observed at 11.34 ev,[30] and that the zero of energy for all the orbitals should be shifted accordingly. The small difference between the predicted ionization potentials for the a_2, a_1, and b_2 orbitals makes the assignment of the observed potential rather tentative.

If we turn now to the transition energies of nitromethane, it may be seen that, for reasons of symmetry, the effect of hyperconjugation with the methyl group will be to stabilize the ground state far more than the lowest excited states. It will be convenient to introduce this effect in the following simple manner. The stabilization of the ground state is assumed to arise from the interaction of χ_0, under a perturbing resonance integral, with the configuration $(m^{-1}b_1^*)$, in which an electron has been excited from an orbital m, with B_1 symmetry, on the methyl group into the orbital b_1^* of nitromethane. In a similar manner, all the excited configurations $(n^{-1}b_1^*)$ of nitromethane, where n is a_2, a_1, or b_2 will be stabilized by interaction with the configuration $(n^{-1}m^{-1}b_1^{*2})$. It has been shown that the required matrix elements are as follows[31,32]:

$$\langle\chi_0 \mid H^{\text{core}} \mid (m^{-1}b_1^*)\rangle=\sqrt{2}\int mH^{\text{core}}b_1^*d\tau;$$

$$\langle(n^{-1}b_1^*) \mid H^{\text{core}} \mid (n^{-1}m^{-1}b_1^{*2})\rangle=\int mH^{\text{core}}b_1^*d\tau.$$

where the only nonzero contribution to the integrals containing H^{core} arises from a resonance integral, β^*, between N_π and an orbital m with B_1 symmetry on the methyl group. It seems reasonable to employ a value for β^* which adequately accounts for the mesomeric shifts under methylation of the low energy transition of benzene. This value is $\beta^*=-2.6$ ev.[32] The energies of the various electron transfer configurations may readily be calculated using the ionization potential of methane (13.16 ev),[33] the electron affinity of nitromethane, from Table IV, and the various Coulomb repulsion integrals in Table I. The net mesomeric effect to the three lowest singlet-singlet transition energies is to raise them by 0.49 ev.

The calculated electronic transition energies of nitromethane which are lower than 9 ev are given in Table V, together with the calculated oscillator strengths. The $\pi\rightarrow\pi^*$ transition oscillator strengths are calculated assuming zero overlap, with the aid of the formula developed by Mulliken.[34] The $n\rightarrow\pi^*$ transition oscillator strengths are calculated employing values for the transition dipoles $\langle N_s \mid r \mid N_\pi\rangle$ and $\langle O_s \mid r \mid O_\pi\rangle$ which are derived using Slater orbitals for N_s, N_π, O_s, and O_π.

NITROGEN DIOXIDE

The location of the odd electron in nitrogen dioxide is open to question, since there are three nonbonding orbitals which might contain it. These include an orbital with A_1 symmetry, as well as a_2 and b_2, where $a_2=\sqrt{2}^{-1}(O_\pi-O_\pi')$; and $b_2=\sqrt{2}^{-1}(O_t-O_t')$, while the A_1 orbital contains a large contribution from $(\sqrt{2})^{-1}(O_t+O_t')$. As it has been pointed out, however,[35,36] this A_1 orbital, at the fairly large angle ONO which is found in nitrogen dioxide (134°),[21] will have some of the antibonding character it would have in a

[30] R. J. Kandel, J. Chem. Phys. **22**, 84 (1955).
[31] J. N. Murrell, Proc. Phys. Soc. (London) **A68**, 969 (1955).
[32] J. N. Murrell and K. L. McEwen, J. Chem. Phys. **25**, 1143 (1956).
[33] J. P. Morrison and A. J. C. Nicholson, J. Chem. Phys. **20**, 1021 (1952).
[34] R. S. Mulliken and C. A. Rieke, Repts. Progr. in Phys. **8**, 231 (1941).
[35] A. D. Walsh, J. Chem. Soc. **1953**, 2260.
[36] R. S. Mulliken, Can. J. Chem. **36**, 10 (1958).

TABLE VI. Integrals for nitrogen dioxide (ev).

I_N	14.16	$(N_\pi N_\pi \mid N_\sigma N_\sigma)$	11.31[a]	$(N{:}O_\pi O_\pi)$	5.09
$(N_\pi N_\pi \mid N_\pi N_\pi)$	12.81	$(N_\pi N_\pi \mid N_\sigma N_\sigma)$	12.81	$(N{:}O_i O_i)$	1.45
$(N_\pi N_\pi \mid O_\pi O_\pi)$	8.94	$(N_\pi N_\pi \mid O_i O_i)$	8.74	$(N{:}O_\sigma O_\sigma)$	2.70
$(N{:}O_\pi O_\pi)$	1.57				

[a] Estimated.

linear structure (it will therefore be denoted by a_1^*); the orbitals a_2 and b_2, on the other hand, remain nonbonding at any value of the angle ONO. For this reason we assume the wave function for the ground state to have as its main component the following configuration

$$^2\chi_0 = \mid \cdots b_1\bar{b}_1 a_2\bar{a}_2 a_1\bar{a}_1 b_2\bar{b}_2 a_1^* \mid,$$

where only the π orbitals and the low-energy σ nonbonding orbitals are mentioned explicitly; the symbol a_1 here denotes a nonbonding orbital which is expected to have a large contribution from $\sqrt{3}^{-1}(N_\sigma - \sqrt{2}N_y)$.

The presence of an unpaired electron in a molecule introduces the difficulty that the set of orbitals for electrons with α spin can no longer be assumed identical to that for electrons with β spin, so that two distinct sets of orbitals should be obtained.[23] If this is done, however, it will not in general be possible to write a single configuration approximation to the ground state, nor correspondingly simple approximations for the various excited states, since these will not be eigenfunctions of the operator S^2. Such sets of orbitals will therefore be inconvenient for discussing the various electronic transitions of the molecule. One way of dealing with this problem which has been suggested[27] is to obtain a set of orbitals assuming a Hamiltonian which is a mean of the correct Hamiltonians for α and β electrons. Single configurations may then be written which are eigenfunctions of S^2, and which may be used to calculate electronic transition energies; the various orbital energies do not, however, correspond directly to the various ionization potentials and electron affinities of the molecule.

In the present work we will take advantage of certain simplifying properties of the structure we have assumed for nitrogen dioxide. Since in our calculation of the nonbonding orbitals of the σ-electron system we do not attempt to obtain self-consistent orbitals, we will be interested in the Hamiltonian which is appropriate when the odd electron is in the simple orbital O_i^+. Turning first to the π-electron system, the Hamiltonian governing electrons with α and β spins differs only in the oxygen core potentials α_0^α and α_0^β, and only by an amount $\frac{1}{2}(O_\pi O_i \mid O_\pi O_i)$. The error introduced in the π-orbital energies by assuming an intermediate α_0 will then be rather small. Although we will not calculate the σ-bonding orbitals, it is worth noting that in the present approximation the difference between the σ-bonding orbitals containing α and β electrons will be of the same order as that for π-electrons, since it depends on the term $\frac{1}{2}(O_\sigma O_i \mid O_\sigma O_i)$ in the oxygen core potential of the Hamiltonian.

Turning now to the nonbonding σ orbitals, it is clear that if we hope to obtain orbital energies which correspond to ionization potentials we must use the correct Hamiltonian for the $O_i^\pm$ orbitals. This means that the diagonal matrix element for O_i^- will differ greatly depending on whether or not exchange with the electron in O_i^+ is possible. It will be shown, however, that the O_i orbital mixes so little with the σ-bonding system that the orbital $b_2 \simeq (\frac{1}{2})^{\frac{1}{2}}(O_i - O_i')$ is appropriate for electrons of both α and β spin. The orbital a_1, which is a solution of the same secular determinant as is the orbital a_1^*, is essentially the same for electrons of either spin, since in the present approximation only the diagonal matrix element of O_σ will be different depending on whether or not exchange is possible with the odd electron in O_i^+.

Thus it appears that we can obtain a ground configuration for nitrogen dioxide which is an eigenfunction of S^2, and hence can be used in calculating transition energies, and which at the same time is composed of one-electron orbitals whose energies may be reasonable approximations to the various ionization potentials of the molecule.

A. π-Electron Orbitals

Since we are assuming a nonpolar σ-bonding system, we will begin by calculating the SCF orbitals for the π-electron system of nitrogen dioxide.

Where possible the same integrals are used for nitrogen dioxide as for nitromethane: those which differ are tabulated in Table VI.

We have for the one-center core integrals α_N and α_O,

$$\alpha_N = -I_N - 2(O{:}N_\pi N_\pi) - (O_i O_i \mid N_\pi N_\pi) - 2(O_\pi O_\pi \mid N_\pi N_\pi)$$

$$\alpha_O = -I_O - (N{:}O_\pi O_\pi) - (O'{:}O_\pi O_\pi) - \tfrac{1}{2}\{(O_i O_i \mid O_\pi O_\pi) + (O_i' O_i' \mid O_\pi O_\pi)\} + \tfrac{1}{4}(O_\pi O_i \mid O_\pi O_i) - (N_\pi N_\pi \mid O_\pi O_\pi) - (O_\pi' O_\pi' \mid O_\pi O_\pi).$$

The SCF π orbitals of NO_2 are computed to have the

[27] H. C. Longuet-Higgins and J. A. Pople, Proc. Phys. Soc. (London) A68, 591 (1955).

following wave functions and energies,

$b_1 = 0.603N_\pi + (0.798/\sqrt{2})(O_\pi + O_\pi')$ $\quad -19.98$ ev.

$a_2 = \sqrt{2}^{-1}(O_\pi - O_\pi')$ $\quad -15.85$ ev.

$b_1^* = 0.798N_\pi - (0.603/\sqrt{2})(O_\pi + O_\pi')$ $\quad -2.23$ ev.

B. Nonbonding σ-Orbitals

The nonbonding orbitals of nitrogen dioxide are calculated in the same manner as for nitromethane. Except for certain of the penetration integrals, given in Table VI, the various interaction integrals used here are the same as those for nitromethane.

The A_1 and B_2 nonbonding orbital wave functions and their energies are given in the following. The original diagonal matrix element for O_i or N_{sp^2} is given in brackets. It is useful to express the nitrogen portion of the A_1 orbitals in terms of the functions $\sqrt{3}^{-1}(N_s - \sqrt{2}N_y)$ and $\sqrt{3}^{-1}(\sqrt{2}N_S + N_y)$:

$$a_1^* = 0.68\,O_i^+ - 0.41\,O_r^+ + 0.01\,O_s^+ + (0.60/\sqrt{3})(Ns - \sqrt{2}Ny) - (0.04/\sqrt{3})(\sqrt{2}Ns + Ny),$$

$$E(a_1^*) = -14.09 \text{ ev } \{E(O_i^+) = -16.93\},$$

$$a_1 = (0.67/\sqrt{3})(N_s - \sqrt{2}N_y) - (0.16/\sqrt{3})(\sqrt{2}N_s + N_y) - 0.18\,O_r^+ - 0.71\,O_i^+,$$

$$E(a_1) = -20.33 \text{ ev. } \{E(N_{sp^2}) = -19.02\},$$

$$b_2^\alpha = 0.99\,O_i^- - 0.14\,O_r^- + 0.01\,O_s^- - 0.02\,N_x;$$

$$E(b_2^\alpha) = -16.90 \text{ ev} \{E(O_i^{-\alpha}) = -16.93\},$$

$$b_2^\beta = 0.99O_i^- - 0.14\,O_r^- - 0.01\,O_s^- + 0.02N_x;$$

$$E(b_2^\beta) - = 12.89 \text{ ev } \{E(O_i^{-\beta}) = -12.86\}.$$

An examination of the wave functions a_1 and a_1^* shows that the nonbonding orbital on the nitrogen and the O_i^+ symmetry orbital mix strongly with one another, although mixing with the σ-electron bonding orbitals, $\sqrt{3}^{-1}(\sqrt{2}N_s + N_y)$ and O_r^+, takes place only to a small extent.

It is of interest that a study of the fine structure of the nitrogen dioxide electron spin resonance spectrum is reported to indicate that the density of odd electron in the nitrogen $2s$ orbital is 0.18.[38] This observation may be compared with the value of 0.10, the calculated odd electron density in N_s assuming the one-electron wave function a_1^* in the foregoing.

The difference between the spatial part of the b_2 wave functions obtained here for electrons with α and β spin is obviously negligible for the purpose of the present type of calculation. We can therefore include in the various many electron configurations an orbital

$$b_2 = 0.99O_i^- - 0.14O_r^-$$

which may be occupied by an electron of either spin, or by two electrons.

C. Electronic Transitions

The energies of the various excited configurations and the interactions between them have been computed using the molecular orbitals and energies given in the previous sections. The reduction of the many-electron integrals between determinantal wave functions is a standard procedure.[39]

The wave functions and energies of the various excited states are computed allowing all singly and doubly excited configurations to interact; however, any interaction between χ_i and χ_j such that

$$\langle \chi_i | H | \chi_j \rangle^2 / | E_i - E_j | < 0.1 \text{ ev}$$

has been ignored.

The many-electron wave functions of nitrogen dioxide are specified by a notation similar to that used for nitromethane. There are additional types of configuration to consider, however, the $n \rightarrow n^*$ and $\pi \rightarrow n^*$ excited configurations

$$(b_2^{-1}a_1^*) = | \cdots a_1\bar{a}_1 a_2\bar{a}_2 b_1\bar{b}_1 b_2 a_1^* \bar{a}_1^* |$$

and

$$(a_2^{-1}a_1^*) = | \cdots a_1\bar{a}_1 a_2 b_1\bar{b}_1 b_2\bar{b}_2 a_1^* \bar{a}_1^* |.$$

As well as simple doublet configurations such as the two preceding, there are wave functions containing three unpaired electrons. If the singly occupied orbitals are denoted by p, q, and r, and the other orbitals are all doubly filled, we can write two doublet configurations and a quartet, as follows;

$$^2\chi(1, r) = \sqrt{2}^{-1}\{| \cdots \bar{p}qr | - | \cdots p\bar{q}r |\}$$

$$^2\chi(2, r) = \sqrt{6}^{-1}\{2 | \cdots p\bar{q}r | - | \cdots \bar{p}qr | - | \cdots p\bar{q}r |\}$$

$$^4\chi = \sqrt{3}^{-1}\{| \cdots \bar{p}qr | + | \cdots p\bar{q}r | + | \cdots pq\bar{r} |\}.$$

In the case of the singly excited configurations where the orbital a_1^* remains singly occupied, and is represented by r in the preceding wave functions, it may be shown that a transition moment may exist between χ_0 and $\chi(1, r)$ but not between χ_0 and $\chi(2, r)$. However, $\chi(1, r)$ and $\chi(2, r)$ interact with one another,

[38] G. R. Bird, J. C. Baird, and R. B. Williams, J. Chem. Phys. 28, 738 (1958).

[39] E. U. Condon and G. H. Shortley *The Theory of Atomic Spectra* (Cambridge University Press, New York, 1935).

TABLE VII. The excited states of nitrogen dioxide.

Symmetry	Wave functions	Transition energy (ev)	f
$^2A_1$	$0.98\,\chi_0-0.10\,(a_2^{-2}\,b_1^{*2})+0.18\,(a_2^{-1}\,b_2^{-1}\,a_1^*\,b_1^*)\,(1, b_1)$	0	...
	$0.03\,\chi_0+0.71\,(b_1^{-1}\,b_1^*)\,(1, a_1^*)-0.30\,(a_2^{-2}\,b_1^{*2})-0.57\,(a_1^{-1}\,a_1^*)-0.30\,(a_2^{-1}\,b_2^{-1}\,a_1^*\,b_1^*)\,(1, b_2)$	7.49	0.008
	$0.06\,\chi_0-0.36\,(b_1^{-1}\,b_1^*)\,(1, a_1^*)+0.25\,(a_2^{-2}\,b_1^{*2})-0.80\,(a_1^{-1}\,a_1^*)+0.41\,(a_2^{-1}\,b_2^{-1}\,a_1^*\,b_1^*)\,(1, b_2)$	9.99	0.059
	$0.81\,(b_1^{-1}\,b_1^*)\,(2, a_1^*)-0.58\,(a_2^{-1}\,b_2^{-1}\,a_1^*\,b_1^*)\,(2, b_2)-0.03\,(b_1^{-1}\,b_1^*)\,(1, a_1^*)+0.04\,(a_1^{-1}\,a_1^*)$	7.32	0
$^4A_1$	$^4(b_1^{-1}\,b_1^*)$	7.81	0
$^2B_2$	$0.43\,(a_2^{-1}\,b_1^*)\,(1, a_1^*)+0.09\,(b_1^{-1}\,a_2^{-1}\,b_1^{*2})\,(1, a_1^*)-0.90\,(b_2^{-1}\,a_1^*)$	2.30	0.011
	$0.80\,(a_2^{-1}\,b_1^*)\,(1, a_1^*)+0.28\,(b_1^{-1}\,a_2^{-1}\,b_1^{*2})\,(1, a_1^*)+0.41\,(b_2^{-1}\,a_1^*)-0.34\,(b_1^{-1}\,b_2^{-1}\,a_1^*\,b_1^*)\,(1, b_2)$	6.75	0.192
	$(\phi)\,(a_1^{*-1}\,b_2^{-1}\,b_1^{*2})+0.15\,(b_2^{-1}\,a_1^*)-0.13\,(a_2^{-1}\,b_1^*)\,(1, a_1^*)$	5.67	0
	$(\phi)\,(a_2^{-1}\,b_1^*)\,(2, a_1^*)-0.07\,(b_2^{-1}\,a_1^*)-0.03\,(a_2^{-1}\,b_1^*)\,(1, a_1^*)$	6.19	0.001
$^4B_2$	$^4(a_2^{-1}\,b_1^*)$	3.93	0
$^2B_1$	$0.96\,(a_1^{*-1}\,b_1^*)-0.18\,(b_2^{-1}\,a_2^{-1}\,b_1^{*2})\,(2, a_1^*)-0.22\,(b_2^{-2}\,a_1^*\,b_1^*)$	1.20	0.0001
	$0.01\,(a_1^{*-1}\,b_1^*)-0.72\,(b_2^{-1}\,a_2^{-1}\,b_1^{*2})\,(2, a_1^*)+0.69\,(b_2^{-2}\,a_1^*\,b_1^*)$	7.87	0
	$(b_1^{-1}\,a_1^*)$	6.85	0.003
$^2A_2$	$0.91\,(a_2^{-1}\,a_1^*)-0.36\,(b_2^{-1}\,b_1^*)\,(1, a_1)+0.15\,(b_2^{-1}\,b_1^*)\,(2, a_1^*)-0.18\,(b_1^{-1}\,a_2^{-1}\,b_1^*\,a_1^*)\,(2, a_2)$	2.62	0
	$0.38\,(a_2^{-1}\,a_1^*)+0.81\,(b_2^{-1}\,b_1^*)\,(1, a_1^*)-0.45\,(b_2^{-1}\,b_1^*)\,(2, a_1^*)-0.08\,(b_1^{-1}\,a_2^{-1}\,b_1^*\,a_1^*)\,(2, a_2)$	3.54	0
	$0.03\,(a_2^{-1}\,a_1^*)+0.47\,(b_2^{-1}\,b_1^*)\,(1, a_1^*)+0.88\,(b_2^{-1}\,b_1^*)\,(2, a_1^*)-0.01\,(b_1^{-1}\,a_2^{-1}\,b_1^*\,a_1^*)\,(2, a_2)$	7.54	0
	$0.94\,(a_1^{*-1}\,a_2^{-1}\,b_1^{*2})-0.17\,(b_2^{-1}\,b_1^*)\,(1, a_1^*)+0.13\,(b_2^{-1}\,b_1^{-1}\,b_1^{*2})\,(1, a_1^*)+0.17\,(b_2^{-1}\,b_1^{-1}\,b_1^{*2})\,(2, a_1^*)$	7.31	0
$^4A_2$	$^4(b_2^{-1}\,b_1^*)$	2.57	0

and with other doublet configurations, so that both configurations are included in the calculation.

In Table VII will be found the wave functions and transition energies for the various states of nitrogen dioxide. In a few cases the restriction that small interactions are ignored results in a low-energy state represented by a single configuration of the type $^2\chi(2, a_1^*)$ or by a doubly excited configuration. If there are small interactions between these and allowed singly excited configurations, then the wave function has been corrected by perturbation theory, for the purpose of estimating transition probabilities. Wave functions which have been obtained by perturbation theory are marked (ϕ) in Table VII.

In order to compare intensities, calculated oscillator strengths are presented in Table VII. In this calculation it is assumed that the charge separations $r(O^+-O'^-)$ is the same whether the orbitals involved belong to the π or σ-electron system, and similarly for the charge separation $r(N^+-O_2^-)$.

The wave functions in Table VII may be seriously incomplete: since we have assumed throughout the calculation a fixed σ-bonding structure, it is likely that configurations involving σ-electron excitation would be important in many of the wave functions; furthermore, in this particular molecule it may not be justified to consider only singly and doubly excited configurations, since there will be other multiply excited configurations within the energy range studied. There would be a good argument for considering only interactions between singly excited configurations, a procedure which would have raised the energy of the strongly allowed $^2B_2$ state in Table VII from 6.75 to 7.8 ev., but would have altered the energies of the other states much less. It seems unlikely, however, that the spectrum of nitrogen dioxide will ever be well understood unless at least the low-energy multiply excited configurations are considered. This factor, and the desire that this calculation be carried out in a manner parallel to that used for nitromethane and for a group of related compounds the results of which will be reported subsequently, has led us to include doubly excited configurations in the calculation.

The electronic spectrum of nitrogen dioxide is extremely complex, and extends from 9000 A to the far ultraviolet. The approximate energies and intensities of the various transitions observed are summarized in Table VIII. There is very complex absorption from

TABLE VIII. Observed transitions of nitrogen dioxide.

Energy (ev)	Oscillator strength
2(?)[a]	$<<0.003$
3(max)[a]	0.003
5.3(max)[b]	0.0007 (B_2 transition density)
5.5–6(?)[b,c]	?
7.7–9.2[d]	strong

[a] See footnote 40.
[b] See footnote 42.
[c] See footnote 41.
[d] See footnotes 43 and 44.

4000 to 5200 A, with a maximum at 3 ev.; this absorption system continues to lower energy, but there is a sharp intensity decrease at 6200 A, which may indicate another transition (2 ev in Table VIII), and in this region a nonlinear excited state is indicated.[40] From 4000 A toward higher energy there is decreasing absorption to 2500 A[41] and then a series of bands between 2500 and 2300 A with transition density of B_2 symmetry, and about one-third the intensity of the absorption at 4000 A.[42] Beyond 2300 A the character of the absorption bands changes, indicating a new transition.[41] This band system which has been reported only to 2000 A, may have roughly comparable intensity to that of the system between 2300 and 2500 A. Between 2000 and 1600 A there is no absorption reported, and it is known that there are no strong bands in this region.[43] From 1600 to 1350 A there is absorption apparently composed of two distinct band systems, which are too far separated to be due to spin doublets.[44] The intensity in this region is described as strong.[43]

We will now attempt to identify some of the observed transitions of nitrogen dioxide. It seems probable that the excited state at 2.30 ev in Table VII, containing $^2(b_2^{-1}a_1^*)$ and $^2(a_2^{-1}b_1^*)(1, a_1^*)$, should be identified with the low-energy fairly strong band system at 3.0 ev. The weaker transition to $^2(a_1^{*-1}b_1^*)$, which we predict at 1.20 ev., may then be identified with the weak absorption system observed from about 2 ev toward longer wavelengths. The calculated excited state at 2.62 ev in which $^2(a_2^{-1}a_1^*)$ predominates, is forbidden, and may be obscured by the strong $^2B_2 \leftarrow {}^2A_1$ absorption in this area; there is, however, some evidence from fluorescence data indicating a low-energy $^2A_2$ excited state.[45]

The weak $^2B_2 \leftarrow {}^2A_1$ band system observed at 5.3 ev. may be to one of the last two $^2B_2$ states in Table VII. A further possibility is that there may be in this energy region a transition involving $b_2 \rightarrow \sigma^*$, where σ^* is an A_1 σ antibonding orbital. This transition would be weakly allowed, and should perhaps be considered. (In this case some of the complex absorption at 3–4 ev. would perhaps involve the $^2A_1 \leftarrow {}^2A_1$ transition $a_1^* \rightarrow \sigma^*$). It seems very unlikely that the weak absorption at 5.3 ev is to the strongly allowed $^2B_2$ state predicted at 6.75 ev. It is more probable that this strong transition, which is very sensitive to configuration interaction, occurs in the strong absorption region from 7.7–9 ev.

[40] G. W. Robinson, M. McCarty, and M. C. Keelty, J. Chem. Phys. **27**, 972 (1957).
[41] M. Lambrey, Ann. Physik, **14**, 95 (1930).
[42] L. Harris, G. W. King, W. S. Benedict, and R. W. Pearse, J. Chem. Phys. **8**, 765 (1940).
[43] W. C. Price and D. M. Simpson, Trans. Faraday Soc. **37**, 106 (1941).
[44] K. Mori, Science of Light **4**, 139 (1955).
[45] D. Neuberger and A. B. F. Duncan, J. Chem. Phys. **22**, 1693 (1954).

D. Ionization Potentials

Although we have chosen the one-electron wave functions of nitrogen dioxide so that the resulting many-electron configurations are eigenfunctions of S^2, we have shown that in the present approximation the molecular orbitals obtained differ very little from those which would arise using a different Hamiltonian for electrons with α and β spins. We may therefore take our orbital energies as approximations to the ionization potentials and electron affinities of the molecule.

The various configurations of the positive and negative ions are tabulated in Table IX, together with the corresponding ionization potential or electron affinity. In the case of singlet-triplet pairs of configurations the calculated orbital energies are used with the following corrections: for a π-electron ionization potential involving the orbital q the corrections for a singlet and triplet are respectively $\frac{3}{2}(a_1^*q \mid a_1^*q)$ and $-\frac{1}{2}(a_1^*q \mid a_1^*q)$; in the ionization potential of the orbital a_1 only the singlet requires a correction, of magnitude $2(a_1a_1^* \mid a_1a_1^*)$. One ionic configuration, namely $\mid \cdots a_1\bar{a}_1b_1\bar{b}_1a_2\bar{a}_2b_2\bar{b}_2 \mid$, is unique, in that it interacts very strongly with the low energy configuration $(b_2^{-2}a_1^{*2})$. Since no similar interaction occurs to the ground state of the radical nor to the other ionic configurations, it is desirable to include this interaction in the calculation.

Before comparing the ionization potentials in Table IX with experimental values it is important to realize that the radical ground state and the three lowest singlet configurations of the positive ion will be strongly stabilized by interaction with low energy doubly excited configurations, the interaction terms involving integrals of the type $(b_2a_1^* \mid a_2b_1^*)$. The corresponding interactions to the $^3B_2$ and $^3A_2$ triplet configurations are very much smaller, so that the ionization potentials to triplet states in Table IX should all be higher, relative to the doublet→singlet ionization potentials. This consideration would probably mean that the lowest ionization potential of the molecule is to an $^1A_1$ state of the ion, while the $^3B_2$ state appearing in Table IX as the lowest would be slightly higher.

The observed ionization potentials of nitrogen dioxide include one at 9.9 ev., estimated by an indirect method,[30] one with energy >11.7 ev., detected by a photoionization technique,[46] one at 12.3 ev. from a Rydberg series,[43] and one at 13.98 ev. detected by electron impact.[47]

The lowest ionization potential mentioned is thought to be to a low vibrational level of the linear ground state of the ion.[47] The corresponding vertical ionization potential might then be to a highly vibrationally excited state, perhaps much greater than 9.9 ev. It is perhaps possible that the transition reported at >11.7

[46] K. Watenabe, J. Chem. Phys. **26**, 542 (1957).
[47] J. Collin and F. P. Lossing, J. Chem. Phys. **28**, 900 (1958).

TABLE IX. Electron affinities and ionization potentials of nitrogen dioxide.

Symmetry	Wave function for ion	Ionization potential or electron affinity (ev)
$^{1,3}B_1$	$\sqrt{2}^{-1}\{\|\cdots a_1\bar{a}_1b_1\bar{b}_1a_2\bar{a}_2b_2\bar{b}_2a_1^*\bar{b}_1^*\|\pm\|\cdots a_1\bar{a}_1b_1\bar{b}_1a_2\bar{a}_2b_2\bar{b}_2b_1^*\bar{a}_1^*\|\}$	2.35 (S) 2.39 (T)
$^1A_1$	$\|\cdots a_1\bar{a}_1b_1\bar{b}_1a_2\bar{a}_2b_2\bar{b}_2a_1^*\bar{a}_1^*\|$	4.12
$^1A_1$	$.933\|\cdots a_1\bar{a}_1b_1\bar{b}_1a_2\bar{a}_2b_2\bar{b}_2\|-.359\|\cdots a_1\bar{a}_1b_1\bar{b}_1a_2\bar{a}_2a_1^*\bar{a}_1^*\|$	13.21
$^3B_2$	$\sqrt{2}^{-1}\{\|\cdots a_1\bar{a}_1b_1\bar{b}_1a_2\bar{a}_2b_2\bar{a}_1^*\|-\|\cdots a_1\bar{a}_1b_1\bar{b}_1a_2\bar{a}_2a_1^*\bar{b}_2\|\}$	12.89
$^1B_2$	$\sqrt{2}^{-1}\{\|\cdots a_1\bar{a}_1b_1\bar{b}_1a_2\bar{a}_2b_2\bar{a}_1^*\|+\|\cdots a_1\bar{a}_1b_1\bar{b}_1a_2\bar{a}_2a_1^*\bar{b}_2\|\}$	16.90
$^{1,3}A_1$	$\sqrt{2}^{-1}\{\|\cdots b_1\bar{b}_1a_2\bar{a}_2b_2\bar{b}_2a_1^*\bar{a}_1\|\pm\|\cdots b_1\bar{b}_1a_2\bar{a}_2b_2\bar{b}_2a_1\bar{a}_1^*\|\}$	25.76 (S) 21.32 (T)
$^{1,3}A_2$	$\sqrt{2}^{-1}\{\|\cdots a_1\bar{a}_1b_1\bar{b}_1b_2\bar{b}_2a_2\bar{a}_1^*\|\pm\|\cdots a_1\bar{a}_1b_1\bar{b}_1b_2\bar{b}_2a_1^*\bar{a}_2\|\}$	16.17 (S) 15.73 (T)
$^{1,3}B_1$	$\sqrt{2}^{-1}\{\|\cdots a_1\bar{a}_1a_2\bar{a}_2b_2\bar{b}_2b_1\bar{a}_1^*\|\pm\|\cdots a_1\bar{a}_1a_2\bar{a}_2b_2\bar{b}_2a_1^*\bar{b}_1\|\}$	20.26 (S) 19.72 (T)

ev could be to such a vibrationally excited state. The $^1A_1$ state of the ion corresponding to the calculated ionization potential 13.21 ev in Table IX is probably to be identified with the lowest ionization potential of the molecule.

The next ionization potential observed, at 12.3 ev., would then be to the $^3B_2$ ionic state. This state of the ion has not been reached by electron impact, and it may be forbidden by this process; however, a Rydberg series involving the b_2 orbital of nitrogen dioxide may well lead to a positive ion triplet state.

The final observed ionization potential to be tentatively assigned is that at 13.98 ev. The results of the present calculation would indicate an A_2 state of the ion for this transition.

The ionization potentials we have calculated are all too high, as was the case with the ionization potential of nitromethane. In view of the fact that configuration interaction is extremely important in the present case, however, and is largely ignored, it is not possible to find a correction for the α_μ which would yield satisfactor values for all the ionization potentials of the molecule.

DISCUSSION

The electronic structure we have calculated for nitrogen dioxide suggests a possible mode of bonding for its dimer, dinitrogen tetroxide. This molecule has been shown by electron diffraction on the vapor to have the following planar structure.

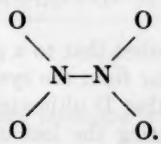

The interatomic distances within the NO_2 fragments are very similar to those in nitrogen dioxide itself, and the N—N distance is found to be 1.75 A.[48] In spite of the fact that the N—N bond is apparently very weak, infrared spectral data indicate that there is an internal rotation barrier of approximately 2.9 kcal/mole.[49]

The present calculation for nitrogen dioxide indicates appreciable odd electron density in the sp^2 atomic orbital of the nitrogen atom which is directed away from the oxygen atoms. Now if the two NO_2 fragments of dinitrogen tetroxide are in the relative positions suggested by the diagram, then the nitrogen sp^2 portions of the singly occupied orbitals will be available for σ-type bonding. It seems likely that the ground state of the dimer could be described by a nonbonding product of Slater determinants representing the ground states of the fragments stabilized by interaction with a low-energy charge transfer configuration in which one fragment has a doubly occupied a_1^* orbital and the other an empty a_1^* orbital.

At the large N—N distance of 1.75 A any π-type bonding would probably be a small effect; however, charge-transfer and dispersion-type interactions between the π-electron systems of the two fragments may account for the planarity of the molecule and for the barrier to internal rotation.

If the electronic structure outlined above for dinitrogen tetroxide is correct, then one would expect those electronic transitions of nitrogen dioxide which directly involve the orbital a_1^* to be modified upon dimer formation in the direction of higher energy; also there should be an additional low-energy transition involving an electronic excitation to a state composed largely of the electron transfer configuration mentioned above.

The electronic spectrum of dinitrogen tetroxide is

[48] D. W. Smith and K. Hedberg, J. Chem. Phys. 25, 1282 (1956).
[49] R. G. Snyder and I. C. Hisatsume, J. Mol. Spectroscopy 1, 139 (1957).

reported to show no absorption at lower energy than 4000 A.[50] Toward higher energy there are two broad bands: one with maximum at 3400 A, and the other with maximum beyond 2000 A; there is also a shoulder at 2600 A. As will be seen from Table VII, the nitrogen dioxide transitions predicted at very low energy (i.e., below 3.0 ev), are those which involve the orbital a_1^* and which therefore should be at higher energy in the dimer.

[50] A. P. Altshuller, D. Stephens, and C. M. Schwab, J. Phys. Chem. 62, 608 (1958).

ACKNOWLEDGMENT

I wish to express my appreciation to Professor C. Sandorfy for reading the manuscript of this paper. I should also like to thank Dr. R. A. McIvor and Mr. A. Grey, Defense Research Chemical Laboratories, Ottawa, for informing me of their unpublished results for the spectrum of nitromethane vapor.

THE JOURNAL OF CHEMICAL PHYSICS VOLUME 32, NUMBER 6 JUNE, 1960

Isotope Effect in the Hydrogen Atom-Formaldehyde Reaction*

JAMES R. McNESBY, MILTON D. SCHEER, AND RALPH KLEIN†

National Bureau of Standards, Washington, D. C.

(Received January 15, 1960)

The isotope effect in the hydrogen abstraction from formaldehyde by hydrogen atoms has been measured. The activation energy difference derived from relative rate measurements of the pair of reactions

$$H+H_2CO\rightarrow H_2+HCO \quad (2)$$

$$H+D_2CO\rightarrow HD+DCO \quad (5)$$

is $E_5-E_2=1.0$ kcal. The value for the corresponding pair

$$D+H_2CO\rightarrow HD+HCO \quad (6)$$

$$D+D_2CO\rightarrow D_2+DCO \quad (7)$$

$E_7-E_6=0.9$ kcal, is calculated from (5), (2), and the variation of the hydrogen-deuterium equilibrium constant with temperature. Application of the Bigeleisen theory of the isotope effect to these reactions suggests a loosely bound activated complex.

INTRODUCTION

THERE does not seem to be any recorded measurement of the isotope effect in metathetical reactions of H atoms in the gas phase. Such measurements are best made by a differential method where the attacking radical or atom abstracts H and D from substrate molecules. The photolysis of mixtures of H_2CO and D_2CO provides a convenient system for such a study.

The detailed mechanism of formaldehyde photolysis is rather well understood except for the chain terminating reaction:

$$(1) \quad H_2CO \xrightarrow{h\nu} H+HCO$$

$$(2) \quad H+H_2CO\longrightarrow H_2+HCO$$

$$(3) \quad HCO+M\longrightarrow H+CO+M$$

$$(4) \quad HCO \xrightarrow{\text{wall}} \text{termination}.$$

The quantum yield of hydrogen is in excess of 70 above 300°C and the pressures used here,[1] so that the termination reaction cannot contribute significantly to the hydrogen formed. It is permissible therefore to ascribe the formation of H_2 to reaction (2).

When mixtures of H_2CO and D_2CO are photolyzed, the following hydrogen forming reactions must be considered in addition to (2) and (3):

$$(5) \quad H+D_2CO\rightarrow HD+DCO$$

$$(6) \quad D+H_2CO\rightarrow HD+HCO$$

$$(7) \quad D+D_2CO\rightarrow D_2+DCO$$

$$(8) \quad DCO+M\rightarrow D+CO+M.$$

The mechanism requires that to a good approximation H can only disappear from the system by abstracting D from D_2CO and that D ultimately must abstract H from H_2CO. Neglecting the loss of H and D in the

* This research was performed under the National Bureau of Standards Free Radical Research Program, supported by the Department of the Army.

† Guest Scientist, Olin Mathieson Corporation.

[1] J. G. Calvert and E. W. R. Steacie, J. Chem. Phys. 19, 176 (1951).

termination steps, the stationary state concentrations of H and D are controlled entirely by (5) and (6):

$$d[H]/dt = k_6[D][F] - k_5[H][F_d] = 0 \quad (1)$$

$$[H]/[D] = k_6[F]/k_5[F_d]; \quad (2)$$

where $[F]$ and $[F_d]$ are the concentrations of H_2CO and D_2CO, respectively. The $[HD]/[H_2]$ ratio in the early stages of reaction is given by

$$\frac{[HD]}{[H_2]} = \frac{k_5[H][F_d] + k_6[D][F]}{k_2[H][F]} = \frac{2k_5[F_d]}{k_2[F]}. \quad (3)$$

Similarly,

$$[HD]/[D_2] = 2k_6[F]/k_7[F_d]. \quad (4)$$

It is upon this reaction sequence that the evaluation of the isotope effect, k_5/k_2 is based.

The apparatus employed in these studies has been described previously.[2] The light source, as before, was the full arc of a medium-pressure mercury lamp.

RESULTS AND DISCUSSION

It was first necessary to demonstrate that Eq. (3) is obeyed. Formaldehyde and formaldehyde-d_2 were prepared separately from their respective polymers.[3] Mixtures were made up over a range $F/F_d = 0.2$ to 5.2. Each mixture was photolyzed to about 1% destruction of formaldehyde at 305°. The light intensity was reduced by a factor of 10 in one experiment. In another experiment a Pyrex glass filter was inserted between the lamp and the reaction vessel to remove the shorter wavelengths. The H_2/HD ratio was found to be independent of intensity and wavelength under the conditions described. That Eq. (3) is obeyed is evident from Fig. 1.

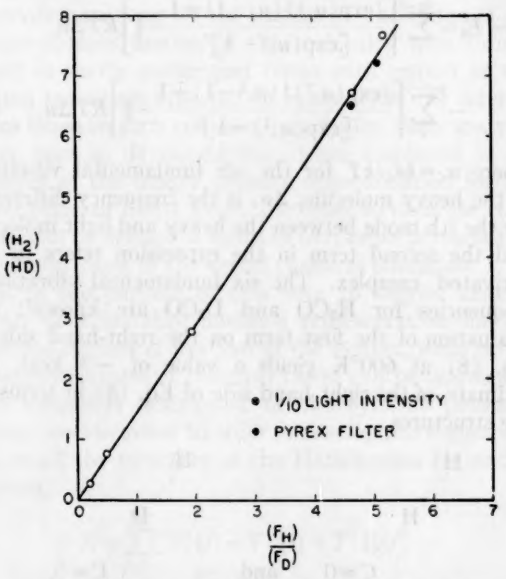

FIG. 1. Experimental verification of Eq. (3) at 305°.

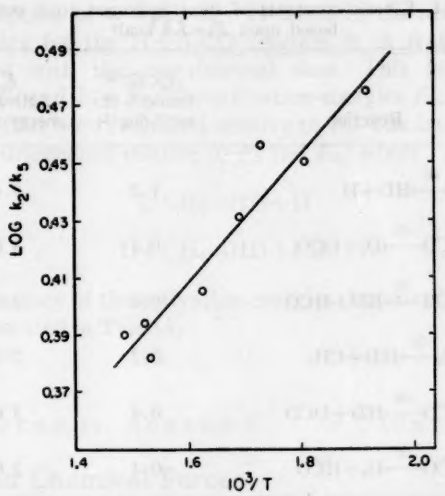

FIG. 2. Arrhenius plot for reaction of H atoms with H_2CO and D_2CO. $E_5 - E_2 = 1.0$ kcal, $A_2/A_5 = 1.1$.

Preliminary experiments, whose objective was to measure k_5/k_2 as a function of temperature; showed that the error in measuring the composition of the reaction mixture of one run relative to another was too large to reveal the small changes in k_5/k_2. Since D_2CO—H_2CO mixtures do not exchange[4] this problem was solved by mixing arbitrary amounts of the deuterated and undeuterated polymer, depolymerizing, and storing the mixture of monomers in a liquid-nitrogen-cooled storage vessel. This mixture was vaporized directly into the reaction vessel, and its composition determined from Fig. 1 by measuring the H_2/HD ratio after photolyzing at 305°. In order to be sure that the composition of the reaction mixture was not changing from run to run, the order in which experiments were carried out was staggered with respect to temperature. After several experiments at increasing temperatures, the reaction vessel was cooled to the original temperature and the H_2/HD ratio was found to return to its original value. The data are shown in Fig. 2. A least-squares treatment of the data gave

$$E_5 - E_2 = 1.01 \pm 0.08 \text{ kcal},$$

$$A_2/A_5 = 1.13 \pm 0.09.$$

The errors are probable errors and the quantities E and A are defined by

$$k_2/k_5 = (A_2/A_5)\exp[(E_5 - E_2)/RT].$$

Experimental evidence obtained previously on both the photo and thermal decomposition of mixed isotopic

[2] R. Klein, J. R. McNesby, M. D. Scheer, and L. J. Schoen, J. Chem. Phys. **30**, 58 (1959).
[3] R. Spence and W. Wild, J. Chem. Soc. **1935**, 338.
[4] R. Klein and L. J. Schoen, J. Chem. Phys. **24**, 1094 (1956).

TABLE I. Kinetic constants of some hydrogen atom reactions, based upon $E_8=5.4$ kcal[a]

Reaction	$A\times10^{-12}$ (mole^{-1} cc sec^{-1} deg^{-1})	E Activation energy (kcal)
$D+H_2\xrightarrow{(8)}HD+H$	1.2	5.4
$D+D_2CO\xrightarrow{(7)}D_2+DCO$	0.4	3.0
$D+H_2CO\xrightarrow{(6)}HD+HCO$	0.4	2.1
$D+CH_4\xrightarrow{(9)}HD+CH_3$	0.2	7.8
$H+D_2CO\xrightarrow{(5)}HD+DCO$	0.4	3.0
$H+H_2CO\xrightarrow{(2)}H_2+HCO$	0.4	2.0

[a] $k_8=1.2\times10^{12}T^{\frac{1}{2}}\exp(-5400/RT)$ mole^{-1} cc sec^{-1}.

formaldehydes[4,5] in a reaction vessel of small surface/volume ratio clearly indicates that the hydrogen isotopes are produced in ratios such that the expression $[HD]^2/[H_2][D_2]=K_{obs}$ closely approximates the value for the equilibrium constant K_e, of an equilibrated H_2, HD, D_2 system. It was shown that the equilibration does not arise from the reaction of H and D atoms with hydrogen and deuterium molecules but is already present in the molecular hydrogen species formed in the formaldehyde chain decomposition. In the present investigation K_{obs} was less than K_e (about 2 compared with 3.6) and approached the latter only at high F_D/F_H. In all other cases the rate of formation of D_2 was small relative to H_2 and HD. It is possible that in the large surface/volume reaction vessel employed in this work some D_2 (and H_2) was formed intramolecularly at the wall. This would be a considerable part of the total D_2, but a minor fraction of the H_2. Such a wall reaction would reduce K_{obs} less severely when the surface area was reduced. Such conditions were effected by means of a thin pencil of light traversing the reaction vessel axially. In this case the K_{obs} rose to within 10% of K_e. Because of a limited supply of D_2CO, such experiments were not further pursued. By choosing a high F_H/F_D ratio (1.7), large amounts of H_2 were generated chainwise and any contribution due to intramolecular wall formation was reduced to negligible proportions. That the ratio k_6/k_7 can be deduced from k_2/k_5 and the hydrogen-deuterium equilibrium constant K_e requires further justification.

The product of Eqs. (3) and (4) is given by

$$[HD]^2/[H_2][D_2]=4k_5k_6/k_7k_2=K \qquad (5)$$

where all the hydrogen isotopes arise from chain processes. K is given by

$$K=\frac{4F_5^{\ddagger}F_6^{\ddagger}}{F_7^{\ddagger}F_2^{\ddagger}}\exp\left(\frac{E_{0_7}^{\ddagger}+E_{0_2}^{\ddagger}-E_{0_5}^{\ddagger}-E_{0_6}^{\ddagger}}{RT}\right) \qquad (6)$$

according to the absolute reaction rate theory, where the F's and E's are the appropriate partition functions and zero-point energy differences. For a system consisting exclusively of hydrogen isotopes the equilibrium constant K_e is given by

$$K_e=(F_{HD}^2/F_{H_2}F_{D_2})\exp(-E_0/RT). \qquad (7)$$

A comparison of these two expressions, evaluated on the basis of translational, vibrational, and rotational partition functions and the approximate equality of the exponentials show that $K/K_e\cong1$. It is concluded that the hydrogen isotopes formed in the chain decomposition of mixed formaldehydes satisfy the relationship $[HD]^2/\{[H_2][D_2]\}=K_e$ where K_e is the true equilibrium constant for an H_2-D_2—HD system. It must be emphasized that for this requirement to be fulfilled, (1) the decomposition of the formaldehydes must be by long chains—that is, the ratio of hydrogen formed in the chain to that formed in termination or intramolecular reaction at the walls must be large; and (2) decomposition by intramolecular split must be negligible, compared to the chain processes. Since k_6/k_2 was measured directly, k_6/k_7 can be deduced from K_e. This leads to a value of $E_7-E_6=0.9$ kcal.

The theory of reaction velocities of isotopically substituted molecules has been discussed by Bigeleisen.[6] The activation energy difference of two reactions of the type considered here is given by

$$E_2-E_5=\sum_i^{3n-6}\left[\frac{\{\exp(u_i)\}(u_i-1)+1}{[\exp(u_i)-1]^2}-\tfrac{1}{2}\right]RT\Delta u_i$$
$$-\sum_i^{3n'-7}\left[\frac{\{\exp(u_i^{\ddagger})\}(u_i^{\ddagger}-1)+1}{[\exp(u_i^{\ddagger})-1]^2}-\tfrac{1}{2}\right]RT\Delta u_i^{\ddagger} \qquad (8)$$

where $u_i=h\nu_i/kT$ for the ith fundamental vibration of the heavy molecule, Δu_i is the frequency difference for the ith mode between the heavy and light molecule and the second term in the expression refers to the activated complex. The six fundamental vibrational frequencies for H_2CO and D_2CO are known[7]; the evaluation of the first term on the right-hand side of Eq. (8) at 600°K yields a value of -3 kcal. An estimate of the right hand side of Eq. (8) in terms of the structures

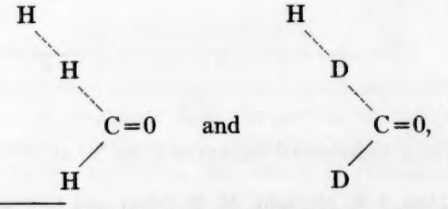

[5] R. Klein, M. D. Scheer, and L. J. Schoen, J. Am. Chem. Soc. **78**, 50 (1956).

[6] J. Bigeleisen, J. Chem. Phys. **17**, 675 (1949).

[7] E. S. Ebers and H. H. Nielsen, J. Chem. Phys. **6**, 311 (1938).

where H--H--C and H--D--C are weak bonds and make a negligible contribution, leads to a value of -2 kcal. Therefore, $E_5-E_2=1$ kcal compared with the experimental value of 1.0 kcal.

The preexponential factor for this pair of isotopic reactions can be calculated from the difference in the entropies of activation. Using the same loose complex as above and applying the expression derived by Bigeleisen[8] for the calculation of entropy differences between isotopic molecules, a value of 0.8 is obtained for A_2/A_5, 1.1 being obtained experimentally. The assumption of a weak H--H bond in the activated complex for the $H+H_2CO$ reaction is in reasonable accord with the experimental data. This leads to $E_5=E_7$ and $E_6=E_2$. The activation energies E_2, E_5, E_6 have thus been evaluated relative to E_7. The latter has been determined relative to E_8 and E_9,[2] where

(8) $$D+H_2\rightarrow HD+H$$

(9) $$D+CH_4\rightarrow HD+CH_3$$

A summary of the activation energies thus far obtained is presented in Table I.

[8] J. Bigeleisen, J. Chem. Phys. **21**, 1333 (1953).

THE JOURNAL OF CHEMICAL PHYSICS VOLUME 32, NUMBER 6 JUNE, 1960

Transport in Dilute Gases and Chemical Forces

RICHARD K. OSBORN

Department of Nuclear Engineering, University of Michigan, Ann Arbor, Michigan

(Received February 4, 1960)

It is shown that the theory of transport phenomena in gases may be so formulated that the potentials characterizing the cross sections, which account for intractions between molecules in the binary collision limit, are the same as those conventionally employed in investigations of molecular structure. Thus it is indicated that at least some of the essential features of chemical forces may be conveniently introduced into the description of such phenomena.

IN recent investigations Dahler[1] and von Roos[2] have formulated descriptions of transport phenomena for systems of polyatomic molecules taking explicit account of internal degrees of freedom. However, in both instances the effective potentials appearing in the Liouville equations for the statistical description of the center-of-mass motion of the molecules were formulated in slowly convergent terms with respect to the actual potentials expected to characterize the interactions between such systems. Specifically, these analyses have been so developed that, when employed in the context of the binary collision approximation for the description of dilute gases, the cross sections for collisions will be defined in terms of first-order perturbation approximations to the actual chemical potentials.

It is the purpose of this note to suggest that in terms of a suitably modified representation for the internal degrees of freedom of the system, some of the essential features of chemical forces can be retained in the statistical description of the systems presently under consideration. In order to develop this suggestion, we recall the structure of the Hamiltonian for such a system,

$$H=\sum_{j=1}^{N}[T(\xi^j)+V(\xi^j)+T(\mathbf{R}^j)]+\sum_{i<j}^{N}V(\xi^i,\xi^j,\mathbf{R}^{ij}), \quad (1)$$

where $T(\xi^j)$ is the kinetic energy of the internal degrees of freedom of the jth molecule; $V(\xi^j)$ the potential energy of same; $T(\mathbf{R}^j)$ the kinetic energy of the center-of-mass motion of the jth molecule, and $V(\xi^i,\xi^j,\mathbf{R}^{ij})$ is the potential energy of interaction between particles comprising the ith molecule and those of the jth molecule. We have here introduced the notation, $\mathbf{R}^{ij}=\mathbf{R}^i-\mathbf{R}^j$, where $\mathbf{R}^j$ is the position of the center-of-mass of the jth molecule. We now introduce two-molecule wave functions in the conventional manner appropriate to the description of the two molecules in strong interaction. On defining

$$H^{ij}=T(\xi^i)+T(\xi^j)+V(\xi^i)+V(\xi^j)+V(\xi^i,\xi^j,\mathbf{R}^{ij}), \quad (2)$$

we develop the set of eigenfunctions for our present purposes according to

$$H^{ij}\Phi_{\alpha_{ij}}(\xi^i,\xi^j,\mathbf{R}^{ij})=\mathcal{E}_{\alpha_{ij}}(\mathbf{R}^{ij})\Phi_{\alpha_{ij}}(\xi^i,\xi^j,\mathbf{R}^{ij}). \quad (3)$$

Clearly the Φ's have been assumed to be a diagonalizing representation in ξ space, and hence they—as well as their eigenvalues $\mathcal{E}$—depend parametrically upon the components of the center-of-mass displacements $\mathbf{R}^{ij}$. Noting that the potential $V(\xi^i,\xi^j,\mathbf{R}^{ij})$ vanishes when the ith and jth molecules are infinitely far apart, and defining molecular wave functions according to

$$H^i\phi_{\alpha_i}(\xi^i)=E_{\alpha_i}\phi_{\alpha_i}(\xi^i), \quad (4)$$

[1] J. S. Dahler, J. Chem. Phys. **30**, 1447 (1959).
[2] Oldwig von Roos, J. Chem. Phys. **31**, 1415 (1959).

where

$$H^i = T(\xi^i) + V(\xi^i); \tag{5}$$

we observe that

$$\lim_{|\mathbf{R}^{ij}|\to\infty} \Phi_{a_{ij}}(\xi^i, \xi_j, \mathbf{R}^{ij}) \to \phi_{\alpha_i}(\xi^i)\phi_{\alpha_j}(\xi^j), \tag{6}$$

if one chooses an unsymmetrized representation for the bimolecular states, or

$$\lim_{|\mathbf{R}^{ij}|\to\infty} \Phi_{a_{ij}}(\xi^i, \xi^j, \mathbf{R}^{ij}) \to [\phi_{\alpha_i}(\xi^i)\phi_{\alpha_j}(\xi^j) \pm \phi_{\alpha_i}(\xi^j)\phi_{\alpha_j}(\xi^i)]/\sqrt{2} \tag{7}$$

for a symmetrized representation. Symmetrization is here implied with respect to the simultaneous interchange of all of the coordinates of corresponding particles in the ith and jth molecules. Accordingly, one further expects that

$$\lim_{|\mathbf{R}^{ij}|\to\infty} \mathcal{E}_{a_{ij}}(\mathbf{R}^{ij}) \to E_{\alpha_i} + E_{\alpha_j}. \tag{8}$$

Both the bimolecular functions $\Phi_{a_{ij}}$ and the unimolecular functions ϕ_{α_i} are presumed to be unit vectors in their respective spaces.

The eigenvalues $\mathcal{E}_a$, considered as functions of the relative displacement of two interacting molecules, are the potentials which presumably characterize these interactions. It is part of our present purpose to indicate that transport theory in dilute gases may be so formulated that, in the binary collision approximation, the cross sections describing these collisions are to be computed (at least in part) within the context of a dynamical scheme characterized by these potentials.

We may now construct a complete orthonormal set of states in the space of the internal degrees of freedom of the system of N molecules, i.e.,

$$\{\Phi_{a_{12}}\Phi_{a_{34}}\cdots\Phi_{a_{N-1N}}\}, \tag{9}$$

and in terms of them exhibit the wave function for the totality of the degrees of freedom of the system as

$$\Psi(\mathbf{R}, \xi, t) = \sum_{a_{12}\cdots a_{N-1-N}} \chi_{a_{12}\cdots a_{N-1N}}(\mathbf{R}, t)\Phi_{a_{12}}\cdots\Phi_{a_{N-1N}}. \tag{10}$$

A distribution function for the external degrees of freedom may now be defined by[2]

$$\tilde{F}_{a|a'} = (2\pi)^{-3N/2}\chi_a C_{a'}{}^* e(-i\mathbf{K}\cdot\mathbf{R}). \tag{11}$$

In this expression the label a stands for the set of labels $\{a_{12}a_{34}\cdots a_{N-1N}\}$; the function $C_{a'}{}^*$ is the complex conjugate of the Fourier transform of $\chi_{a'}$, i.e.,

$$C_{a'}(\mathbf{K}^1\cdots\mathbf{K}^N, t) = (2\pi)^{-3N/2}\int d^{3N}R \exp(-i\mathbf{K}\cdot\mathbf{R})\chi_{a'}(\mathbf{R}^1\cdots\mathbf{R}^N, t), \tag{12}$$

and $\mathbf{K}\cdot\mathbf{R}$ is the $3N$ dimensional scalar product

$$\mathbf{K}\cdot\mathbf{R} = \sum_{j=1}^{N}\mathbf{K}^j\cdot\mathbf{R}^j. \tag{13}$$

Since the time derivatives of χ and C^* are directly deducible from the wave equation for Ψ, it is a straightforward matter to show that

$$D\tilde{F}_{a|a'} = (i/\hbar)\sum_b [\tilde{F}_{a|b}\Omega\{\mathcal{E}_b\delta_{ba'} + U_{ba'} + T_{ba'} + \nabla\cdot\mathbf{B}_{ba'} - i\mathbf{K}\cdot\mathbf{B}_{ba'}\}^\dagger - \{\delta_{ab}\mathcal{E}_b + U_{ab} + T_{ab} - \mathbf{B}_{ab}\cdot\nabla - i\mathbf{K}\cdot\mathbf{B}_{ab}\}\tilde{F}_{b|a}], \tag{14}$$

where all vectors are to be interpreted as $3N$-dimensional and we have introduced the symbols

$$D = [(\partial/\partial t) + (\hbar/M)\mathbf{K}\cdot\nabla - (i\hbar/2M)\nabla^2],$$
$$\Omega = \exp(-i'\nabla_K\cdot\nabla_R'), \tag{15}$$

where the nablas with primes at the upper left or right are to be interpreted as acting to the left or right, respectively. The matrix elements of T, U, and $\mathbf{B}$ are,

$$T_{ab} = (\Phi_{a_{12}}\cdots\Phi_{a_{N-1N}}, \sum_{j=1}^{N}[-(\hbar^2/2M)\nabla_{R^{j2}}]\Phi_{b_{12}}\cdots\Phi_{b_{N-1N}}),$$

$$U_{ab} = (\Phi_{a_{12}}\cdots\Phi_{a_{N-1N}}, \times\{(\sum_{\text{Odd } i}\sum_{j>i+1} + \sum_{\text{Even } i}\sum_{j>i})V(\xi^i, \xi^j, \mathbf{R}^{ij})\}\Phi_{b_{12}}\cdots\Phi_{b_{N-1N}})$$

and

$$\mathbf{B}_{ab} = (\Phi_{a_{12}}\cdots\Phi_{a_{N-1N}}, (\hbar^2/M)\nabla\Phi_{b_{12}}\cdots\Phi_{b_{N-1N}}), \tag{16}$$

and the eigenvalues $\mathcal{E}_a$ are explicitly

$$\mathcal{E}_a = \sum_{\text{Odd } i}\mathcal{E}_{a_{ii+1}}. \tag{17}$$

The distribution function defined by Eq. (11) and described by Eq. (14) is related to the conventional Wigner distribution function by

$$F_{a|a'} = \exp(\tfrac{1}{2}\nabla_K\cdot\nabla_R)\tilde{F}_{a|a'}. \tag{18}$$

This latter function satisfies the Liouville equation

$$[(\partial/\partial t) + (\hbar/M)\mathbf{K}\cdot\nabla]F_{a|a'} - (i/2\hbar)\sum_b[\mathbf{B}_{ab}\exp(\tfrac{1}{2}i'\nabla_R\cdot\nabla_K')\cdot\nabla F_{b|a'} + \nabla F_{a|b}e(-\tfrac{1}{2}i'\nabla_K\cdot\nabla_R')\cdot\mathbf{B}_{ba'}] = (i/\hbar)\sum_b[F_{a|b}e(-\tfrac{1}{2}i'\nabla_K\cdot\nabla_R') \times\{\delta_{ba'}\mathcal{E}_b + U_{ba'} - i\mathbf{K}\cdot\mathbf{B}_{ba'}\} - \{\delta_{ab}\mathcal{E}_b + U_{ab} - i\mathbf{K}\cdot\mathbf{B}_{ab}\}e(\tfrac{1}{2}i'\nabla_R\cdot\nabla_K')F_{b|a'}]. \tag{19}$$

At least one aspect of this relation is amusing. It is noted that the transport terms (left-hand side) are modified in a fashion peculiar to systems characterized

by velocity dependent potentials. That indeed the effective potentials in the present representation have this property is supported by the observation that the eigenfunctions χ_a satisfy an equation of the form

$$i\hbar(\partial\chi_a/\partial t)=\sum_b \mathcal{H}_{ab}\chi_b, \tag{20}$$

and

$$\partial\mathcal{H}_{ab}/\partial P_j=\delta_{ab}(P_j/M)-(i/\hbar)B_{jab}. \tag{21}$$

The issue of symmetrization of the total wave function is somewhat more complicated here than in the instance that the internal degrees of freedom are dealt with in the context of the representation, $\{\phi_{a_1}\cdots\phi_{a_N}\}$. However, this difficulty is not inconveniencing here. The implications of the present derivation are such that one would expect the resulting equations to be useful only in the limiting instance that the binary collision assumption is applicable. Under such circumstances, it is sufficient to be able to define a distribution function corresponding to an arbitrary ordering into pairs-appropriate symmetrization *within* a given bimolecular function being presumed.

We emphasize the content of these remarks by turning our attention to an investigation of the implications of Eq. (19) for the reduced distribution functions. To this end we define the densities

$$g^{(i)}(\mathbf{x},\mathbf{k})=\delta(\mathbf{R}^i-\mathbf{x})\,\delta(\mathbf{K}^i-\mathbf{k}),$$

$$g^{(ij)}(\mathbf{x},\mathbf{k},\mathbf{x}',\mathbf{k}')=\delta(\mathbf{R}^i-\mathbf{x})\,\delta(\mathbf{K}^i-\mathbf{k})\,\delta(\mathbf{R}^j-x')\,\delta(\mathbf{K}^j-\mathbf{k}'),$$

$$g^{(ijl)}(\mathbf{x},\mathbf{k},\mathbf{x}',\mathbf{k}',\mathbf{x}'',\mathbf{k}'')=\delta(\mathbf{R}^i-\mathbf{x})\,\delta(\mathbf{K}^i-\mathbf{k})\,\delta(\mathbf{R}^j-\mathbf{x}')\,\delta(\mathbf{K}^j-\mathbf{k}')\times\delta(\mathbf{R}^l-\mathbf{x}'')\,\delta(\mathbf{K}^l-\mathbf{k}''), \tag{22}$$

and the reduced distribution functions,

$$F_{a|a'}{}^{(i)}=\int d^{3N}Rd^{3N}K F_{a|a'}g^{(i)}, \quad \text{etc.} \tag{23}$$

If we concentrate our attention upon $F_{a|a'}{}^{(1)}$, we find that it satisfies the equation (neglecting terms which describe ternary collisions),

$$\begin{aligned}
&[(\partial/\partial t)+(\hbar/M)\mathbf{k}\cdot\nabla_x]F_{a|a'}{}^{(1)}\\
&=(i\hbar/2M)\int d^3x'd^3k'\sum_b[(\nabla_x\partial_{a|b}{}^{(12)})e(-\tfrac{1}{2}i'\nabla_k\cdot\nabla_x')\cdot\Delta_{ba'}{}^{(1)}+\Delta_{ab}{}^{(1)}e(\tfrac{1}{2}i'\nabla_x\cdot\nabla_k')\cdot(\nabla_x F_{b|a'}{}^{(12)}]\\
&+(i\hbar/2M)\int d^3x'd^3k'\sum_b[F_{a|b}{}^{(12)}e(-\tfrac{1}{2}i'\nabla_k\cdot\nabla_x')\,(\Delta_{ba'}{}^2)^{(1)}+(\Delta_{ab}{}^2)^{(1)}e(\tfrac{1}{2}i'\nabla_x\cdot\nabla_k')\,F_{b|a'}{}^{(12)}]\\
&+(\hbar/M)\int d^3x'd^3k'\sum_b[\{F_{a|b}{}^{(12)}e(-\tfrac{1}{2}i'\nabla_k\cdot\nabla_x')\,(\mathbf{k}\cdot\Delta_{ba'}{}^{(1)}+\mathbf{k}'\cdot\Delta_{ba'}{}^{(2)})\}\\
&\quad-\{(\mathbf{k}\cdot\Delta_{ab}{}^{(1)}+\mathbf{k}'\cdot\Delta_{ab}{}^{(2)})e(\tfrac{1}{2}i'\nabla_x\cdot\nabla_k')\,F_{b|a'}{}^{(12)}\}]\\
&+(i/\hbar)\int d^3x'd^3k'[F_{aa'}{}^{(12)}e(-\tfrac{1}{2}i'\nabla_k\cdot\nabla_x')\,\mathcal{E}_{a'}{}^{(12)}-\mathcal{E}_a{}^{(12)}e(\tfrac{1}{2}i'\nabla_x\cdot\nabla_k')\,F_{a|a'}{}^{(12)}].
\end{aligned} \tag{24}$$

Here we have introduced the notation

$$\Delta_{ab}{}^{(1),(2)}=(\Phi_{a12},\nabla_{1,2}\Phi_{b12}),$$

$$(\Delta_{ab}{}^2)^{(1),(2)}=(\Phi_{a12},\nabla_{1,2}{}^2\Phi_{b12}). \tag{25}$$

It is to be noted that having discarded terms characterizing three particle interactions (terms proportional to triplet densities) the issue of wave function symmetrization remains only in the ultimate treatment of the details of binary collisions and the reduction of the doublet densities to functionals of appropriate singlet densities.

Finally, it is recalled that the matrix elements (25) are in general expected to be small[3]; hence, if we ignore them entirely in Eq. (24), we obtain

$$\begin{aligned}
&[(\partial/\partial t)+(\hbar/M)\mathbf{k}\cdot\nabla_x]F_{a|a'}{}^{(1)}\\
&=(i/\hbar)\int d^3x'd^3k'[F_{a|a'}{}^{(12)}e(-\tfrac{1}{2}i'\nabla_k\cdot\nabla_x')\,\mathcal{E}_{a'}{}^{(12)}\\
&\quad-\mathcal{E}_a{}^{(12)}e(\tfrac{1}{2}i'\nabla_x\cdot\nabla_k')\,F_{a|a'}{}^{(12)}].
\end{aligned} \tag{26}$$

[3] M. Born and J. R. Oppenheimer, Am. J. Phys. 84, 457 (1927).

In this approximation, $\hbar\mathbf{k}=M\mathbf{v}$, where $\mathbf{v}$ is the velocity of the particles; and the equation for the diagonal elements of (26) may be written compactly as

$$\begin{aligned}
&[(\partial/\partial t)+\mathbf{v}\cdot\nabla_x]F_{a|a}{}^{(1)}\\
&=(2/\hbar)\int d^3x'd^3v'F_{a|a}{}^{(12)}\sin[(\hbar/2M)'\nabla_v\cdot\nabla_x']\mathcal{E}_a{}^{(12)}.
\end{aligned} \tag{27}$$

In the classical limit, (27) becomes

$$\begin{aligned}
&[(\partial/\partial t)+\mathbf{v}\cdot\nabla_x]F_{a|a}{}^{(1)}\\
&=M^{-1}\int d^3x'd^3v'(\nabla_x\mathcal{E}_a{}^{(12)})\cdot(\nabla_v F_{a|a}{}^{(12)}),
\end{aligned} \tag{28}$$

which is simply the familiar Liouville relation between a singlet density $F_{a|a}{}^{(1)}$ and a doublet density $F_{a|a}{}^{(12)}$ for a system of particles interacting according to the potentials, $\mathcal{E}_a{}^{(12)}$.

ACKNOWLEDGMENTS

The author gratefully acknowledges the considerable assistance and continuous stimulation of Dr. Oldwig von Roos throughout the course of these investigations. He is also grateful for the hospitality shown him by the Physics Section of the Jet Propulsion Laboratory, California Institute of Technology, during the period that this work was in progress.

THE JOURNAL OF CHEMICAL PHYSICS VOLUME 32, NUMBER 6 JUNE, 1960

Approximate Analytical Wave Functions for the $1sns\ {}^1S$ States of He and He-Like Ions*

Z. RITTER AND R. PAUNCZ†

Technion, Israel Institute of Technology, Haifa, Israel, Department of Physics

AND

Quantum Chemistry Group, Uppsala University, Uppsala, Sweden

(Received December 15, 1959)

Calculations have been made for the $1s2s$, $1s3s$, and $1s4s\ {}^1S$ states of He and He-like ions, assuming wave functions of the symmetrized product form, $u(1)\,v(2)+u(2)\,v(1)$. The results are the best obtained till now using such a functional form, and are even better than some recent calculations which, in addition, use angular correlations.

The energy values obtained for He are: 2.1430_7, 2.0603_6, and 2.0332_0 for the $1s2s$, $1s3s$, and $1s4s\ {}^1S$ states, respectively. The wave functions obtained were checked by other criteria besides the energy criterion.

1. INTRODUCTION

THE ground state of helium and He-like ions has been the subject of several investigations, but relatively little work has been done on the excited states of the same systems since the pioneer work of Hylleraas and Undheim,[1] Hylleraas,[2,3] and Coolidge and James.[4]

Recently, however, there seems to have been a renewed interest in this subject.[5–9] Our aim is to investigate the $1sns\ {}^1S$ states which present the greatest difficulties in a general treatment of the excited states of He.[1] We are looking for a relatively simple functional form for these wave functions which can be physically visualized and the use of which can be extended to more complex systems.

The most powerful method for obtaining approximate wave functions is the variation method. Its use for the excited states is complicated by the additional requirement that the trial function must be kept orthogonal to the *exact* wave functions belonging to the lower states. In the case of two-electron systems, reliable approximations have been obtained only for the ground state, so in practice the condition is replaced by the weaker requirement that the wave function must be orthogonal to the *approximate* trial functions corresponding to the lower states (e.g., Mariott and Seaton[5]) However, this does not ensure that the trial energy value should always be higher than the exact one, and it is very difficult to infer conclusions about the accuracy of the wave function (the trial energy value may coincide with the exact one, but the wave function may be very wrong). Essentially, the same holds for the Hartree-Fock treatment of the excited states (e.g., Vizbarite *et. al*, the energy values for the $1s2s\ {}^1S$ and $1s3s\ {}^1S$ of He lie *below* the experimental value).

There is, however, a variant of the variation method due to Ritz, which is free from this defect. The wave function is approximated by a trial function which is a linear combination of given functions, the coefficients are determined from the condition that $\langle H\rangle_{Av}$ should be stationary and the secular determinant, respectively, give roots I_0, I_1,⋯. Hylleraas and Undheim[1] and MacDonald[10] have shown that these roots are upper limits to the corresponding exact eigenvalues. Shull and Löwdin[11,12] obtained a criterion for the accuracy of the trial wave function and they have shown that the

* The research in this document has been sponsored in part by the King Gustaf VI Adolf's 70-Years Fund for Swedish Culture, Knut and Alice Wallenberg's Foundation, The Swedish Natural Science Research Council, and in part by the Wright Air Development Center of the Air Research and Development Command, U. S. Air Force through its European Office under a contract with Uppsala University.

† On leave from the Chemistry Department, Technion, Israel Institute of Technology, Haifa, Israel.

[1] E. A. Hylleraas and B. Undheim, Z. Physik **65**, 759 (1930).
[2] E. A. Hylleraas, Z. Physik **83**, 739 (1933).
[3] E. A. Hylleraas, Z. Physik **106**, 395 (1937).
[4] A. Coolidge and M. James, Phys. Rev. **49**, 676 (1936).
[5] R. Mariott and M. J. Seaton, Proc. Phys. Soc. (London) **A70**, 296 (1957).
[6] B. Kockel, Ann. Physik **20**, 53 (1957).
[7] Z. Horak, Czechoslov. J. Phys. **8**, 271 (1957).
[8] B. K. Gupta and V.S.R. Rao, Proc. Phys. Soc. (London) **A71**, 1015 (1958).
[9] Ya. I. Vizbaraite, V. I. Kaveckis, and A. P. Jucys, Optika i Spektroskopia **1**, 282 (1957).
[10] J. K. L. MacDonald, Phys. Rev. **43**, 830 (1933).
[11] H. Shull and P. O. Löwdin, Phys. Rev. **110**, 1466 (1958).
[12] P. O. Löwdin, Advances in Chem. Phys. **2**, 266 (1959).

upper bound for the mean-square error in the function is proportional to the difference $I_k - E_k$. This result can be used for the case when the basic set contains some nonlinear parameters, i.e., the matrix elements of the secular determinant depend upon these parameters. The energy will be a function of the linear coefficients and the nonlinear parameters. The minimization with respect to the former ensures that the ith root will be above the ith exact energy value. This result is true for every value of the nonlinear parameters, i.e., the minimization of the corresponding root with respect to the latter gives the best approximate function from the given class of functions. The result of Shull and Löwdin implies that we can look for the best values of the nonlinear parameters separately for each root. The functions obtained in such a way will be not strictly orthogonal to each other, but the nonorthogonality integrals also tend to zero as $(I_k - E_k) \to 0$.

If one of the nonlinear parameters can be chosen as a scale factor, the minimization with respect to this can be carried out easily, and we have the advantage that the virial theorem is fulfilled (Löwdin[13]).

In the case of the two-electron system, the space and spin variables can be separated, when H is spin-independent. For the singlet states we have the spin function $1/\sqrt{2}\{\alpha(1)\beta(2) - \alpha(2)\beta(1)\}$ and the space function must be symmetrical in the variables of the two electrons.

Adopting the method of calculation outlined in the foregoing, we have the following special cases for the form of the wave function (investigated in detail by Coolidge and James[4]).

(a) *Symmetrized-product form.* The spatial wave function can be written in the form

$$u(1)v(2) + u(2)v(1).$$

(b) *Best radial form* wave function which depends only on r_1 and r_2 but cannot be factorized in form (a).

(c) *Hylleraas form* which contains also the interelectronic distance r_{12} explicitly.

Of the three possibilities, the first one can be most easily physically visualized, but it can take into account only radial correlation if the two functions u and v correspond to functions with different radial maxima. In the ground state the angular correlation is certainly important, but in the excited states ($1sns$) we can try the simple physical picture that one electron moves in the neighborhood of the nucleus in a hydrogenlike orbital and that the second is far away from the first one and the nucleus. In this case we can anticipate that the angular correlation is less important, and we can investigate to what an extent the first form is useful.

The calculations of Coolidge and James[4] in the $(1s2s)\ {}^1S$ state of He have shown that there is only a small deviation from the hydrogenlike functional form for the inner orbital but that we can obtain good approximations to the energy, only if a greater flexibility is allowed for the outer orbital.

2. METHOD OF CALCULATION

We are looking for an approximate solution of the Schrödinger equation

$$[H_1 + H_2 + (1/r_{12})]\psi = E\psi$$
$$H_k = -\tfrac{1}{2}\Delta_k - (Z/r_k) \qquad \text{(A)}$$

under the assumption that $\psi(1, 2)$ is of the form

$$\psi(1, 2) = \varphi_1(1)\varphi_2(2) + \varphi_2(1)\varphi_1(2). \qquad (1)$$

As we are interested in solutions for the $1sns\ {}^1S$ states only for $n \geq 2$, we assumed further that the function φ_1 describing the inner electron is of the hydrogenlike type and may be written as

$$\varphi_1 = Ne^{-ar} \qquad N^2 = (2a)^3/8\pi \qquad (2)$$

with a as a variable parameter.

The unknown function φ_2 is expanded in a series of generalized Laguerre functions which depend on one free parameter α and are defined as

$$Z_n(r, \alpha) = e^{-\frac{1}{2}\alpha r} L_n(r, \alpha) N_n(\alpha)$$
$$L_n(r, \alpha) = e^{\alpha r} r^{-2} (d^n/dr^n)(e^{-\alpha r} r^{n+2}) \qquad \alpha > 0$$
$$N_n^2(\alpha) = \alpha^3/(n!)^2(n+1)(n+2) \qquad n = 0, 1, 2, 3, \cdots. \qquad (3)$$

The use of this basic set was suggested and used successfully in several applications by Shull and Löwdin.[14]

Insertion of (1) in Eq. (A) leads by a well-known treatment to the secular equation for the unknown coefficients a_k:

$$\sum_{k=0} a_k(\mathbf{H}_{ik} - E\mathbf{S}_{ik}) = 0 \qquad (i = 0, 1, \cdots) \qquad \text{(B)}$$

$$\mathbf{H}_{ik} = \{\delta_{ik}\mathcal{H} + (S_i\mathcal{H}_k + S_k\mathcal{H}_i) + \mathcal{H}_{ik} + C_{ik} + A_{ik}\}$$
$$\mathbf{S}_{ik} = \{\delta_{ik} + S_iS_k\}$$

$$\int \varphi_1 H \varphi_1 d\tau = \mathcal{H} \qquad \int \varphi_1^2 d\tau = 1$$

$$\int \varphi_1 H Z_i d\tau = \mathcal{H}_i \qquad \int \varphi_1 Z_i d\tau = S_i$$

$$\int Z_i H Z_k d\tau = \mathcal{H}_{ik} \qquad \int Z_i Z_k d\tau = \delta_{ik}$$

$$\int \varphi_1^2(1)(1/r_{12}) Z_i(2) Z_k(2) d\tau_1 d\tau_2 = C_{ik}$$

$$\int \varphi_1(1) Z_i(1)(1/r_{12}) \varphi_1(2) Z_k(2) d\tau_1 d\tau_2 = A_{ik}.$$

[13] P. O. Löwdin, J. Mol. Spectroscopy **3**, 46 (1959).

[14] H. Shull and P. O. Löwdin, J. Chem. Phys. **23**, 1362 (1955).

The free parameters a and α were fixed so as to make the energies of the systems minimum. Our calculations were based on determinants of order four only in order to make the calculations as simple as possible

The system (B) has solutions only if

$$\mathrm{Det}(\mathbf{H}_{ik}-E\mathbf{S}_{ik})=0.$$

By introducing a new parameter κ as $\alpha=\kappa a$, it is possible to write

$$\mathbf{H}_{ik}(a,\kappa,Z)=a^2T_{ik}(\kappa)+aV_{ik}(\kappa,Z)$$

$$\mathbf{S}_{ik}=S_{ik}(\kappa)$$

where $T_{ik}(\kappa)$ corresponds to the kinetic energy of the system and depends only on κ and $V_{ik}(\kappa,Z)$ corresponds to the potential energy and depends on κ and Z. The overlap matrix $\mathbf{S}_{ik}$ depends only on κ, and a may be called a scale parameter.[13]

An equivalent method of arriving at the set (B) is possible, starting from the well-known Fock equations for the He problem:

$$[H_0(r)-E+H_{22}+G_{22}(r)]\varphi_1(r)=-[I_{12}(H_0-E)+H_{12}+G_{12}(r)]\varphi_2(r) \quad (4)$$

$$[H_0(r)-E+H_{11}+G_{11}(r)]\varphi_2(r)=-[I_{12}(H_0-E)+H_{12}+G_{12}(r)]\varphi_1(r) \quad (5)$$

$$H_0(r)=-\tfrac{1}{2}\Delta-(Z/r)$$

$$H_{ik}=\int\varphi_i^*H_0\varphi_k d\tau \qquad (i,k=1,2)$$

$$I_{12}=\int\varphi_1^*\varphi_2 d\tau$$

$$G_{ik}(r)=\int\varphi_i^*(2)\,(1/r_{12})\varphi_k(2)d\tau_2.$$

By assuming that $\varphi_1(r)$ is given by (2) and by inserting this function in Eq. (5), one gets after integration over the angles the following integro-differential equation for the unknown function $r\varphi_2(r)=v(r)$ which describes the excited electron:

$$L(r,Z,a)[v(r)]+\int_0^\infty K(r,s,Z,a)v(s)ds-\lambda[v(r)+\int_0^\infty M(r,s,a)v(s)ds]=0$$

$$L(r,Z,a)=(d^2/dr^2)+\{[2(Z-1)/r]+2e^{-2ar}[(1/r)+a]+a(2Z-a)\}$$

$$M(r,s,a)=4a^3e^{-a(r+s)}rs \qquad \lambda=-2E \quad (6)$$

$$K(r,s,Z,a)=8a^3e^{-a(r+s)}[a^2rs+(Z-a)(s+r)-s\varphi(s)-r\psi(s)]$$

$$\varphi(s)=\begin{cases}1 & s\leq r\\ 0 & s>r\end{cases}$$

$$\psi(s)=\begin{cases}0 & s<r\\ 1 & s\geq r.\end{cases}$$

The approximate solution of Eq. (6) may be obtained by expanding $v(r)$ in a series of Laguerre functions (3). This leads after integration to the same set (B) of linear equations for the unknown coefficients a_l.

$$\sum a_l\{L_{jl}+K_{jl}-\lambda(\delta_{jl}+M_{jl})\}=0$$

$$L_{jl}=\int_0^\infty Z_j(r)\,L[Z_l(r)]r^2dr$$

$$K_{jl}=\int_0^\infty\int_0^\infty K(r,s)Z_j(r)Z_l(s)r^2s^2drds$$

$$M_{jl}=\int_0^\infty\int_0^\infty M(r,s)Z_j(r)Z_l(s)r^2s^2drds. \quad (7)$$

3. RESULTS AND DISCUSSION

In Table I we give the best energy values in atomic units for the states $1s2s$, $1s3s$, and $1s4s$ for He and He-like ions up to $Z=6$ in comparison with earlier works and experimental values as far as they are available.

The results for the ionization energy values obtained for the three excited states of He are better than those of B. Kockel[6] and Gupta and Rao[8] in spite of the fact that our approximation does not include terms containing r_{12} which they used in their work. This result is in accordance with the physical picture that the excited electron is already quite far from the electron in the $1s$ state, and therefore the term r_{12} is no longer as important as in calculations of the ground state of the He where the explicit inclusion of r_{12} terms in the wave function leads to considerably better approximation and lowering of the energy.

Gupta and Rao obtained improved energy values by including in their expansion one term containing configuration $(2p)^2$. But the explicit form of their wave function shows that the coefficient belonging to this term is significant only for the ground-state wave function, since for the first excited state this coeficient is 30 times smaller than the second smallest coefficient in their expansion, and for the second state even 40 times smaller. Therefore, one may conclude that the angular correlation is not very important for the $1sns$ ^1S excited states. This seems to be the explanation for the better results we obtained using radial correlation only by expanding in a series of $(1s1s')$ $(1s2s)$ $(1s3s)$ $(1s4s)$ configurations. The same seems to be correct by comparison with Kockel,[6] who included in his expan-

TABLE I. Energies of the $1sns\ ^1S$ states of the He-like ions.

	n	Exptl.[a]	Calc.[b]	Calc.[c]	Calc.[d]	Calc.[e]
He	2	-2.1459_9	-2.1430_7	-2.1424_1	-2.1430	-2.161
	3	-2.0612_8	-2.0603_8	-2.0580_4	-2.0598	-2.063
	4	-2.0335_8	-2.0332_0	...	...	...

	n	Exptl.[a]	Calc.[f]		n	Exptl.	Calc.
Li^+	2	(-5.0467_6)[f]	-5.0356_2	B^{3+}	2	not	-14.5709_1
	3	-4.7337_4	-4.7318_6		3	avail-	-13.4089_6
	4	-4.6298_0	-4.6289_6		4	able	-13.0083_8
Be^{++}	2	-9.1848_2[g]	-9.1781_9	C^{4+}	2	not	-21.2137_4
	3	not	-8.5147_8		3	avail-	-19.4144_2
	4	available	-8.2873_6		4	able	-18.7919_8

[a] Experimental energy values from C. E. Moore, Natl. Bur. Standards Circ. No. 467, I (1948).
[b] The slight differences between these values and those given in a preliminary publication [Bull. Research Council Israel 7F, No. 4 (1959)] are due to floating figures in the desk computer calculations made before.
[c] See reference 8.
[d] See reference 6.
[e] See reference 9.
[f] Not exactly known.
[g] See reference 15.

sion one function χ containing r_{12} explicitly. But again one can see from the explicitly given wave functions that the coefficient of χ is big in the ground-state wave function only and the smallest of all coefficients in the expansion of the excited state wave functions. For the $(1s1s')$ $(1s2s)$ $(1s3s)$ configurations, Kockel uses the hydrogenlike wave functions instead of Laguerre functions that we use. During our calculations we found that this last system gave improved results because it represents a complete system without the continuum, and this is in accordance with previous investigations made by Shull and Löwdin.[14]

The ionization potential obtained is about 1% different from the experimental value for the higher excited states and about 2% for the first excited state. According to the classical work of James and Coolidge,[4] we have reached the lowest possible value for $1s2s$ state of He with functions of the type (a) using the smallest number of expansion terms.

For Li II the results are even better; for the higher excited states the difference from the experimental value of the ionization energy is only 0.65–0.8%. For the first excited state no exact experimental value is available, but the difference seems to be near to 1%, since the experimental value given by Edlén[15] for the $1s2s\ ^1S$ state for Be III differs from our calculated value by only 0.55%.

For all Z values greater than four and for the excited states of $Z=4$ no experimental values are available, but it seems reasonable to assume that our calculated results differ by not more than 0.5% from the exact values.

A comparison of our results with those of the Russian authors[9] shows that our results are still better. They obtained, after numerically solving Fock equations for the excited states, energy values lower than the experimental values, a result which seems to be quite strange.

Slightly improved results of the energy values were reached by Hylleraas and Undheim[1] and Winther[16] for the first excited states of He and Li II by using functions not separable in r_1 and r_2, of the well-known type:

$$\psi(r_1, r_2) = \exp[-(\nu r_1+\mu r_2)](d_1+d_2 r_1+d_3 r_2) + \exp[-(\nu r_2+\mu r_1)](d_1+d_2 r_2+d_3 r_1). \quad (8)$$

(We introduce r_1, r_2 instead of s, t, and change the names of the constants in order to make comparison with our function easier.) As such calculations were not made for higher excited states, we do not know if functions of such a type also give still improved results for those states.

VALUE OF THE NONLINEAR PARAMETERS

In Table II we give the optimum values of the nonlinear parameter a and $\frac{1}{2}\alpha$. The parameter a is very close to the equivalent Z value in accordance with the physical picture that the effective charge of the inner electron is equal to the charge of the nucleus. The difference between a and Z is decreasing as the atom is more excited.

The second parameter α which is defined as $\alpha=a\kappa$ may be interpreted as the effective charge of the outer electron. It may be written as a linear function of the nuclear charge according to the formula

$$\begin{aligned} \tfrac{1}{2}\alpha &= 0.3351Z-0.3088 \quad \text{for the } 1s3s \text{ states} \\ &= 0.2510Z-0.2353 \quad \text{for the } 1s4s \text{ states} \end{aligned} \quad (9)$$

[15] B. Edlén, Arkiv Fysik 4, 441 (1952).
[16] A. Winther, Kgl. Danske Videnskab. Selskab. Mat. fys. Medd. 27, No. 2 (1952).

TABLE II. Optimum values of the parameters a and $\frac{1}{2}\alpha$.

	n	a	$\frac{1}{2}\alpha$	$\frac{1}{2}\alpha$ as computed from Eq. (9).
He	2	1.9945	0.7302	...
	3	1.9991	0.3614	0.3614
	4	1.9997	0.2668	0.2667
Li^+	2	2.9819	1.3784	...
	3	2.9956	0.6957	0.6965
	4	2.9982	0.5175	0.5177
Be^{++}	2	3.9738	1.9873	...
	3	3.9929	1.0328	1.0316
	4	3.9970	0.7688	0.7687
B^{3+}	2	4.9684	2.5885	...
	3	4.9911	1.3661	1.3667
	4	4.9963	1.0197	1.0197
C^{4+}	2	5.9648	3.1763	...
	3	5.9898	1.7020	1.7018
	4	5.9957	1.2708	1.2707

where the coefficient of Z converges towards $1/n$. This is in accordance with the general properties of approximate SCF functions, as pointed out by several authors.[17] No such good linear interpolation formula can be found for the $1s2s$ states.

In order to compare our normalized wave functions with the hydrogenlike wave functions, we have written down the explicit form of the functions for the outer electron for the three excited states of Li II.

$$\varphi_{2s}=\exp(-1.3784r)\,(2.0161-2.3024r+0.062\,874r^2-0.29577r^3)$$

$$\varphi_{3s}=\exp(-0.6957r)\,(0.97464-1.4931r+0.35924r^2+0.000\,115\,54r^3)$$

$$\varphi_{4s}=\exp(-0.5175r)\,(0.62624-1.0628r+0.38035r^2-0.033\,430\,r^3). \quad (10)$$

It is interesting to compute the overlap integrals between the functions belonging to different excited states. These must be zero for the exact wave functions and the same is true for the solutions of the *same* secular equations. As our functions are solutions of different secular equations, we cannot expect these integrals to vanish. But the calculation shows the integrals are quite small, e.g., for Li II they are as follows:

$$\int\psi_{1s2s}\psi_{1s3s}d\tau_1 d\tau_2=0.020$$

$$\int\psi_{1s3s}\psi_{1s4s}d\tau_1 d\tau_2=0.006. \quad (11)$$

The change in the nonlinear parameters does not greatly destroy the mutual orthogonality of the functions, but enables one to improve the minimization of the energy considerably.

The accuracy of the wave functions can be checked by the use of the criterion of Shull and Löwdin[11] according to which

$$\epsilon=1-C_{kk}^2=\int|\phi_k-\psi_k|^2d\tau$$

$$\leq[(I_k-E_k)/(E_{k+1}-E_k)]\{1+A^2\sum_{l=0}^{k-1}(E_{k+1}-E_l)\}$$

$$A=\sum_{l=0}^{k-1}(E_k-I_l)^{-1}. \quad (12)$$

This method seems to be suitable only for the first excited state, since for the higher states the coefficient A^2 increases so quickly that the upper bound turns out to be very high.

For the first excited states of He, Li II, and Be III we get

$$\epsilon(\text{He})\leq 0.075 \quad \epsilon(\text{Li II})\leq 0.075-0.040^{18}$$

$$\epsilon(\text{Be III})\leq 0.021. \quad (13)$$

It turns out that the mean-square deviation of our function from the exact one is decreasing from He to Be.

Functions of such a kind were used by Winther[16] in order to calculate transition probabilities of electrons to excited states, as consequence of β decay of radioactive nuclei. Comparison with this article will be made in a forthcoming publication.

ACKNOWLEDGMENTS

It is a real pleasure to thank Professor Per-Olov Löwdin for his generous hospitality in providing the stimulating environment in which our work, prepared partly in Israel, was completed. The authors also wish to thank F. M. Jan Nordling for carrying out many of the numerical computations in this paper using the electronic computer ALWAC III-E at the Quantum Chemistry Laboratory.

One of us (Z.R.) wishes further to express his gratitude to Professor H. M. Schwartz, University of Arkansas, for suggesting this investigation during his stay in Israel and to the Histadruth Haowdim Haklalith (Jewish labor organization in Israel) for financial assistance which made this research trip to Sweden possible.

APPENDIX I

Table III contains the eigenvectors belonging to every eigenvalue together with the normalization factor.

[17] See, e.g., P. O. Löwdin, Phys. Rev. **94**, 1600 (1954).

[18] The inexactness in the Li II value is due to the inexact knowledge of the experimental value of E_1.

TABLE III. Coefficients a_i in the expansion of φ_2.

Z	n	a_0	a_1	a_2	a_3	N^2
2	2	0.503 391	−1.000 000	0.362 211	−0.097 233	1.403 524
	3	0.015 389	0.848 071	−1.000 000	−0.000 276	1.722 387
	4	0.000 808	0.014 118	0.883 878	−1.000 000	1.782 620
3	2	0.442 023	−1.000 000	0.356 140	−0.095 694	1.336 853
	3	0.017 751	0.785 438	−1.000 000	0.000 892	1.618 930
	4	0.004 973	0.013 425	0.832 613	−1.000 000	1.694 145
4	2	0.429 355	−1.000 000	0.327 659	−0.082 442	1.301 785
	3	0.017 047	0.756 052	−1.000 000	0.001 931	1.572 918
	4	0.004 942	0.011 901	0.812 127	−1.000 000	1.660 131
5	2	0.423 519	−1.000 000	0.308 775	0.073 174	1.282 209
	3	0.013 909	0.746 372	−1.000 000	−0.001 306	1.557 921
	4	0.004 412	0.010 103	0.802 171	−1.000 000	1.643 869
6	2	0.422 871	−1.000 000	0.291 806	−0.065 375	1.269 745
	3	0.012 619	0.736 685	−1.000 000	0.000 103	1.543 318
	4	0.003 890	0.008 970	0.795 905	−1.000 000	1.633 747

APPENDIX II

During the calculation we found that our overlap matrix

$$S_{ik}=\delta_{ik}+S_iS_k$$

exhibited quite an interesting behavior. The elements S_{ik} are of a special kind, namely, each one (except the diagonal) may be written as

$$S_{ik}=S_iS_k \qquad S_i\neq S_k\neq 0.$$

We can prove that such a matrix of order n is highly degenerate and has $(n-1)$ eigenvalues equal to 1 and only one eigenvalue different from 1 which must be equal to $1+\sum S_i^2$.

A short calculation shows that the equation

$$\begin{vmatrix} (1+S_1^2)-\lambda & S_1S_2 & \cdots & S_1S_n \\ S_1S_2 & (1+S_2^2)-\lambda & \cdots & S_2S_n \\ \vdots & & & \\ S_1S_n & \cdot & \cdot & (1+S_n^2)-\lambda \end{vmatrix} =0$$

may be written as

$$(1-\lambda)^{n-1}[1-\lambda+\sum_i S_i^2]=0.$$

This can also be shown using a well-known theorem that the nonvanishing eigenvalues of two matrices $DD^\dagger$ and $D^\dagger D$ are the same; in our case $D=(S_1, S_2, \cdots, S_n)$.

This fact is of some significance for computational work since one knows immediately in such a case that the overlap matrix can not have eigenvalues lower than one. This fact assures the mathematical stability of the problem. Secondly, instead of solving the eigenvalue problem

$$|H_{ik}-\lambda S_{ik}|=0,$$

one may solve the much easier problem

$$|U^{-1}HU-\lambda S^*|=0$$

where U is the matrix transforming the overlap matrix S to diagonal form S^*, which is different from the identity matrix in only one element. It is quite easy to write down the eigenvectors belonging to the matrix S and therefore the transformation matrix U.

Composition Limits of Stability of PbTe

R. F. Brebrick and R. S. Allgaier

United States Naval Ordnance Laboratory, White Oak, Silver Spring, Maryland

(Received December 28, 1959)

Single crystals of PbTe have been heat-treated in evacuated silica tubes in the presence of Pb- or Te-rich ingots. At the heat-treatment temperatures, which ranged between 404° and 885°C, the ingot compositions were such that solid PbTe, liquid, and vapor phases coexisted. At a given temperature, the PbTe crystals were therefore as rich in Pb or Te as possible at equilibrium. After quenching the crystals, the resistivity and Hall constant were measured at room temperature and 77°K. Below about 860°C, crystals heated with Pb-rich ingots were *n* type. Those heated with Te-rich ingots were *p* type at all heat-treatment temperatures. The difference in the concentrations of electrons and holes at room temperature was taken as equal to the difference in concentration of lead and tellurium atoms at the heat-treatment temperature and was used to construct the PbTe solidus lines. The range of stability of PbTe is a maximum near 775°C and is between 49.994 and 50.013 at.% Te, corresponding to carrier concentrations of 3.3×10^{18} electron/cm^3 and 7.6×10^{18} holes/cm^3, respectively.

I. INTRODUCTION

In principle every compound crystal above absolute zero exists as a stable phase over a range of composition. This is possible through the incorporation of vacancy, interstitial, or place-exchange point defects into the crystal structure. In semiconductors, these point defects can introduce corresponding concentrations of donor or acceptor levels in the electronic energy-band structure so that ranges of composition too small to be detected by conventional chemical analysis can, in some cases, be detected by measurement of an electrical property such as the Hall effect. Two general methods have been employed to obtain the phase diagram of a compound semiconductor. In the more general method, the temperature and the partial pressure of one crystal component over a pure single crystal MN are held fixed. Part or all of the pressure-temperature-composition diagrams for CdS,[1] PbS,[2] Cu_2O,[3] and CdTe[4] have recently been established in this manner, while the pressure-temperature diagram has been established for InAs.[5] In the less general method, single crystals of the compound semiconductor are grown. The gradient of electronic-carrier concentration along the direction of growth is combined with the known liquidus lines to obtain the solidus lines in a temperature-composition or $T-X$ diagram. In this manner, the solidus lines or composition limits of stability have been established for PbSe[6] and Bi_2Te_3[7] between the invariant melting-point and a temperature some 30°C lower. We have applied another "equilibrium" technique to establish the composition limits of stability of PbTe between 404° and 885°C.

In the published phase diagram[8] for the Pb–Te system, the PbTe solidus lines are based upon room-temperature magnetic-susceptibility measurements of samples whose preparation was not described (Fig. 1). A range of stability some tens of at. % Te in width is indicated. In contrast, thermal analysis and microscopic studies suggested a negligible range of stability.[8] A desire to establish more accurate values for the stability limits for PbTe led to the investigation described in the following sections.

II. THEORY

For many binary systems, the $T-X$ projection of the phase diagram has been partially established. The solidus lines for any compounds that are formed, however, are often not known accurately. This is the case for many semiconducting compounds whose ranges of stability are at or below the limits of precision of conventional analytical methods. The information available in such an incomplete $T-X$ diagram can serve as a starting point for an accurate determination of the solidus lines (Fig. 1 for the Pb–Te system).

At any temperature except those close to the invariant melting-point, there are relatively wide ranges of composition where solid compound, liquid or second solid phase, and vapor phases coexist (Fig. 1, *AB* and *CD*). For these compositions, the equilibrium system has only one degree of freedom by the Gibbs Phase Rule. Fixing the temperature fixes all the intensive variables, including the composition of the phases. Moreover, the solid compound is as rich in one component or the other as possible, depending upon whether the average composition of the solid and liquid phases is on one or the other side of the solidus field. A practical problem arises in conveniently obtaining a portion of

[1] F. A. Kroger, H. J. Vink, and van den Boomgaard, J., Z. physik. Chem. (Frankfurt) **203**, 1 (1954).
[2] J. Bloem and F. A. Kroger, Z. physik. Chem. (Frankfurt) **7**, 1 (1956).
[3] J. Bloem, Philips Research Repts. **13**, 167 (1958).
[4] D. de Nobel, thesis, University of Leiden, May 1958.
[5] J. van den Boomgaard, and K. Schol, Philips Research Repts. **12**, 127 (1956).
[6] A. E. Goldberg, and G. R. Mitchell, J. Chem. Phys. **22**, 220 (1954).
[7] C. B. Satterthwaite, and R. W. Ure, Jr., Phys. Rev. **108**, 1164 (1957).
[8] Max Hansen, *Constitution of Binary Alloys* (McGraw-Hill Book Company, Inc., New York 1958), 2nd ed., p. 110.

the solid compound for examination. This can be solved by adding small single crystals to the system in such a way that they are in temperature equilibrium with the remaining material, but in contact with it only through the vapor phase. After equilibrium has been established, the crystals may be examined at the working temperature or, after quenching, at a more convenient lower temperature in order to determine their composition. Some melting of the samples can occur depending upon their initial composition and the exact positions of the solidus and liquidus lines. The fraction melted is very small, however, provided the compound has a narrow range of stability relative to the difference in the compositions of the compound and coexisting liquid or solid phase.

The method described is limited to those systems in which the vapor pressure of at least one crystal component is sufficiently large that the necessary transfer of material can occur in a reasonable length of time. When only the solidus lines remain to be fixed in a $T-X$ diagram, the more general temperature-pressure control method is less convenient because two variables rather than one must be accurately fixed. The method of analyzing a single crystal along the direction of growth is more easily applied near the invariant melting point. However, it is not an equilibrium method, is more liable to errors resulting from precipitation due to retrograde solubility, and gives results which depend upon the accuracy of the liquidus lines themselves.

The dependence of crystal composition upon the concentration of electronic carriers has been discussed elsewhere[9] and will be only briefly referred to in Sec. V.

III. EXPERIMENTAL

General

The experimental procedure consists of (1) preparation of a fairly homogeneous Pb-Te ingot that would be partly liquid and partly solid PbTe at the heat-treatment temperature, (2) preparation of small single-crystal samples (3) seal off of the ingot and a few crystals in an evacuated silica tube, (4) heat treatment and subsequent quench, and (5) examination of the crystals, including measurements of the Hall constant at 298° and 77°K. These steps are described in more detail in the following.

Ingot

Transparent fused-silica tubes, 16-mm o.d., were rinsed in hot nitric acid, then hydrofluoric acid, then distilled water, drained dry and outgassed at 1100°C for 17 hours. The final pressure was about 3×10^{-7} mm Hg. Spectroscopically pure stick Pb and Te (American Smelting and Refining Company, 99.999% pure) were individually weighed out to the nearest 0.1 mg so that the combined weight was about 10 grams and the average composition was between 29 and 62 at. % Te. The surface layer of lead was removed by cutting prior to weighing. The Pb and Te were then loaded into the silica tube. If the average composition was less than 50 at. % Te, the tube was coated with carbon by the thermal decomposition of tank propane prior to outgassing the empty tube as described above. The tube and contents were then outgassed for four hours at 200°C and the tube sealed off to a 4-in. length at a pressure of about 10^{-6} mm Hg. After a cautious initiation of the reaction between Pb and Te by application of a torch flame to the tube, the tube was put into a furnace. The temperature was quickly raised and held at 920–970°C for 10 minutes with occasional agitation of the tube. The tube was then quickly quenched in water so the water level was just higher than that of the melt. Evaporation and sublimation were thereby minimized and a compact, fairly homogeneous ingot obtained. The presence of a carbon coat inside the tube eliminated the cracking of the tube that occurred in the later stages of the quench with ingots richer in Pb than 50 at. %.

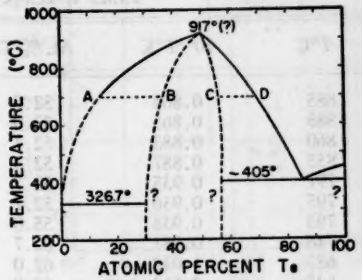

FIG. 1. $T-X$ diagram for Pb-Te system.

Single Crystals

Single crystals ranging between 3 and 6 mm in length and between 0.6 and 2.0 mm in the other two dimensions were cleaved from two large crystals grown by the Bridgman-Stockbarger method from spectroscopically pure Pb and Te. The lead was the same as that described in the foregoing but was converted into shot in H_2 at 1 atm by melting in a quartz crucible with a 10–15-mm diam hole in the bottom. Crystals of Te from two sources including that mentioned before were used. In one of the two PbTe crystals used, flecks of spectroscopically pure C were present during growth to minimize oxidation. In practically all cases, the cleavage planes of the small crystals appeared flat when viewed with the naked eye in oblique light. Etching of representative samples, however, invariably disclosed the presence of low-angle grain boundaries of the order of a few minutes of arc, grain sizes of a few tenths of a mm, and dislocation densities of about 10^5 per cm^2

[9] F. A. Kroger, and H. J. Vink, in *Solid State Physics*, edited by F. Seitz and D. Turnbull (Academic Press, Inc., New York, 1956), Vol. 3, pp. 310–438.

TABLE I. Temperature and duration of heat treatment and composition of ingot.

T°C	$10^3/T$°K	At. % Te	Hr	T°C	10^3 T°K	At. % Te	Hr
885	0.864	52.0	5	885	0.864	48.7	16
883	0.865	52.0	5.5				
860	0.883	52.4	4				
855	0.887	52.3	4.5	843	0.896	48.5	2.8
797	0.935	52.7	46.5				
795	0.936	52.7	17	795	0.936	48.6	11
793	0.938	55.0	21.5				
746	0.981	56.7	17.5	742	0.985	41.0	20.2
687	1.042	62.0	23.5	675	1.055	29.0	23
625	1.113	62.0	25.5	673	1.057	41.0	71.5
538	1.233	61.5	51.5	625	1.113	29.3	96
495	1.302	56.7	105.5	597	1.149	29.5	307
455	1.374	62.0	979	545	1.222	29.0	162
404	1.477	62.0	215.3	535	1.238	29.0	95
				455	1.374	28.3	979
				404	1.477	28.3	522.2

within the grain.[10] For any one run, crystals were taken at random from each of the larger as-grown crystals. In some cases, the dimensions of the crystals were measured to the nearest 0.05 mm before and after a run. The crystals could thereby be identified. Initially, the crystals were all p type and had room-temperature carrier concentrations between 3×10^{18} and 5×10^{18} per cm^3. Electrical properties of representative samples have been reported in more detail elsewhere.[11]

Seal-Off, Heat Treatment, and Examination

The heat-treatment ampoule was obtained from a 1.0-cm o.d. fused-silica tube which was 3 in. long between its test-tube bottom and a seal-off constriction. At a point about $\frac{3}{4}$ in. from the test-tube bottom, the i.d. of the tube was reduced to 4–6 mm by pushing in one side of the tube to form a dike. The tube was then cleaned as described previously. If an ingot richer than 50 at. % Pb was to be used, the surface of the tube to be in contact with the ingot was coated with carbon. In all cases, the empty tube was then outgassed as described above. Three to eight crystals of PbTe were then put into the tube in the pocket between the dike and test-tube bottom; the ingot was put into the tube between the dike and the seal-off constriction. So long as the tube was kept horizontal with the dike pointing upwards, the crystals and ingot were kept separated. The tube and contents were then outgassed for four hours between 240° and 280°C. A thin film of sublimate generally formed on the vacuum system side of the seal-off constriction in this time. The tube was then cooled and sealed off at about 3×10^{-6} mm Hg.

The tube and contents were then put into a horizontal furnace already at temperature and in which the temperature was constant over a 5-in. length to within 1.25°C. For runs below 600°C this gradient was reduced further by wrapping the tube in several thicknesses of aluminum foil. Temperatures were measured using Pt; Pt, 10% Rh thermocouples. Absolute values of the temperature were high by 3°C or less as judged by a Pt; Pt, 10% Rh thermocouple calibrated by the National Bureau of Standards and were not corrected. The furnace temperature used ranged between 404° and 885°C. After a period of time, the tube was quenched by immersion in water and was cool to the touch within a few seconds after removal from the furnace was started.

The tube was broken, the dimensions of the crystals measured, and the Hall constants and resistivities measured at 298° and 77°K. For n-type crystals, the Hall measurements were made within a few hours of the quench and repeated about a day later.

Criteria for Equilibrium

For crystals heated with Te-rich ingots, an upper limit for the time necessary to establish equilibrium substantially at the heat-treatment temperature was established at various temperatures by the use of one or all of three criteria: (1) agreement to within 20% or better of the Hall constants of crystals of varying thicknesses and origins, treated together; (2) the same agreement for crystals treated in runs identical except for the duration of the treatment; and (3) uniformity of the thermoelectric power across fresh cleave faces through the center of a treated crystal. The latter measurement was made at room temperature with a heated (4−10°C) tungsten probe of 20-mm wire that had been sharpened at one end. Iron-constantan thermocouples were attached close to the point of the probe and at a distant face of the crystal. This test was applied after the probe-crystal contact had been formed by discharge of a 3-μf condenser at 45 v. For crystals heated with Pb-rich melts, criteria (1) and (2) were used as before, but a spread of a factor of two in the carrier concentrations was considered acceptable.

The duration of heat treatment and the ingot compositions used at various temperatures are shown in

[10] Private communication from Dr. B. B. Houston of this Laboratory. The details of the etch have been given in J. Appl. Phys. **31,** 615 (1960).

[11] R. S. Allgaier, and W. W. Scanlon, Phys. Rev. **111,** 1029 (1958).

Table I. The ingot composition is very nearly the average composition of the system in every case, since the added single-crystal samples comprise at most 3% of the system by weight.

IV. RESULTS

General Observations

For heat treatments below 800°C, the added crystals showed no change in appearance; sharp edges were preserved, dimensions were unchanged within the experimental accuracy of about 6%, and the crystals still cleaved into rectangular parallelopipeds, though somewhat more poorly than before. Above 800°C, the crystal edges were somewhat rounded, and it was more difficult to prevent the crystals from melting or subliming away as a result of small temperature gradients across the tube. In contrast to the case of Pb-rich ingots, tubes with Te-rich ingots showed the characteristic yellow-green vapor of tellurium when drawn from the furnace and were covered inside with a thin film of sublimate on quenching. At 885°C, tubes with Pb-rich ingots also showed a sublimed film on quenching.

Electrical Properties

The Hall mobilities of carriers were calculated from the Hall-coefficient and resistivity measurements made on the quenched crystals at 298° and 77°K. For both n- and p-type crystals at 298°K and for n-type crystals at 77°K, the mobilities were approximately the same as in slowly cooled, as-grown crystals.[11] However, the mobilities at 77°K in the p-type crystals were only about half the usual values. Moreover, the Hall constant in the p-type crystals was 40% higher at 298° than at 77°K. For the higher resistivity n-type crystals, the Hall constant at 77°K was larger than that at 298°K, indicating some carrier freeze out.

Because of these complications at 77°K, the carrier concentrations were calculated from the room-temperature Hall constants, using the formula n or $p=1/Re$. In Fig. 2, the carrier concentration of the p-type crystals is plotted against the reciprocal of the heat-treatment temperature. The Hall constant in the p-type crystals showed no change over a period of weeks.

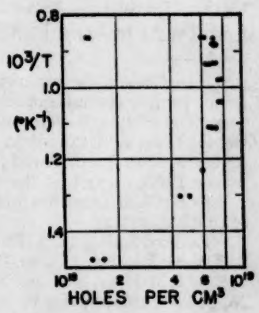

FIG. 2. Carrier concentration in p-type PbTe at 25°C as a function of heat-treatment temperature.

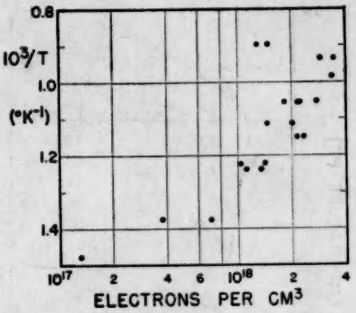

FIG. 3. Carrier concentration in n-type PbTe at 25°C as a function of heat-treatment temperature.

After quenching, the Hall constants of the n-type crystals were found to increase at room temperature. The logarithm of the carrier concentration varied linearly with the elapsed time. The proportionality constant in different crystals ranged from a value near zero to 0.6 day^{-1}. The extrapolated value of the carrier concentration at the end of the quench is plotted against the reciprocal of the heat-treatment temperature in Fig. 3. Along with the bulk changes, a golden-yellow surface layer, possibly yellow lead monoxide, developed on the exposed faces of the n-type PbTe, becoming visible in times ranging from hours to months. The same phenomenon has been observed in our Laboratory on the exposed faces of PbTe crystals grown from the melt, the yellow layer terminating at the $p-n$ junctions in these crystals. This layer is removed in a few seconds at room temperature using a HCl-thiourea etch.[12]

Carrier Sign

All of the crystals from runs in which the ingot contained excess Te were found to be p-type (Fig. 2), and all of the lead-rich ingots except one produced n-type crystals (Fig. 3). The single exception was a run at 885°C with an ingot consisting of 51.3 at. % Pb from which p-type crystals were obtained (the isolated points in the upper left-hand corner of Fig. 2).

V. DISCUSSION

Calculation of Carrier Concentration

A more accurate expression for the carrier concentration than the one which was used is n or $p=rf(K)/Re$, where r is a factor depending on the statistics and scattering law appropriate for the carriers, and $f(K)$ is a band-structure factor depending on the mass and scattering anisotropy. Recent magnetoresistance measurements[13] suggest that a $\langle 111 \rangle$ multivalley model is appropriate for p-type PbTe and that $f(K)$ is approximately 0.9. The value of r is not known accurately but is probably between 1.1 and 1.2 at room temperature. Thus the carrier concentrations for p-type PbTe,

[12] R. F. Brebrick, and W. W. Scanlon, J. Chem. Phys. **27**, 607 (1957).
[13] R. S. Allgaier, Phys. Rev. (to be published).

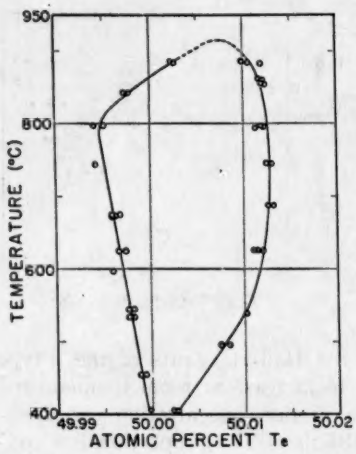

FIG. 4. PbTe solidus lines in $T-X$ diagram calculated from the data in Figs. 2 and 3 using the formula

$$(\text{at\% Te})/100 = \tfrac{1}{2}-(n-p)/4 \times 1.485\times 10^{23}.$$

calculated with $rf(K)$ equal to unity, are accurate to about $\pm 10\%$. The value of r for n-type PbTe is also between about 1.1 and 1.2, but the factor $f(K)$ is not known. However, barring an unsuspectedly complicated band structure, setting $rf(K)$ equal to unity should lead to carrier concentration accurate to within $\pm 20\%$.

Predominant Point Defects

The observed carrier sign of PbTe as a function of composition rules out the place-exchange type of point defect predominant in Bi_2Te_3. Only plausible arguments can be made to choose among the remaining four simple possibilities.[14] On the basis of published ionic radii, the two possibilities involving tellurium interstitials are unlikely. So the lead vacancy-tellurium vacancy and lead vacancy-lead interstitial combinations remain. The latter is favored by the observation that the n-type crystals changed more rapidly at room temperature than did the p-type crystals, since one expects the order of increasing mobility to be tellurium vacancy, lead vacancy, and lead interstitial.

The time dependence of carrier concentration in n-type PbTe at room temperature appears to be consistent with the theory of diffusion-limited precipitation.[15] Since it is not known whether the Hall measurements were made during the first or last half of the precipitation process, it is not possible to be certain on this point. In all cases, the carrier concentrations changed during observation by less than one-half of the extrapolated values at the end of the quench. The extent of precipitation during the quench itself is unknown, although the spread of carrier concentrations at any one temperature in Fig. 3 can be taken as one estimate of a lower limit. One would tentatively assume that interstitial lead atoms are precipitating on dislocations.

Calculation of PbTe Solidus Lines

The concentration of electrons, n, or holes, p, at 298°K is sufficiently larger than the intrinsic carrier concentration that it is equal to $|n-p|$ to an accuracy better than the precision of the values themselves. Using the equation

$$n-p=[\text{Pb}]-[\text{Te}], \qquad (1)$$

(where the brackets indicate concentrations of atoms), a value of 8.25 g/cm³ for the density of PbTe,[16] and a molecular weight of 334.8, the PbTe solidus lines can be obtained on a temperature-composition diagram from the data shown in Figs. 2 and 3. Equation (1) is based upon the observations that (a) PbTe is an exhaustion range semiconductor at room temperature, and (b) there is no evidence indicating multiple ionization of the donor and acceptor levels associated with deviations from the stoichiometric composition. The effects of impurities (discussed later), inadequate quench rate, and point-defect clusters are assumed negligible. Finally, lead or tellurium precipitated on dislocations, where it is electrically inactive as a donor or acceptor, is excluded in the determination of the crystal composition. The PbTe solidus lines are shown in Fig. 4. The liquidus lines have been omitted. The position of the dashed portion of the curve is somewhat arbitrary. The temperature at the invariant melting point is taken from the literature.[8] The composition is chosen to be consistent with observations made on single crystals grown from near stoichiometric melts by the Bridgman-Stockbarger method by a number of investigators.[17–20] On examination at room temperature, one finds that the first portions of PbTe to freeze are p type and range from 1×10^{18} to 5×10^{18} carriers/cm³. Since this is true whether an evacuated silica tube, a hydrogen-filled silica tube, or spectrographically pure carbon is used as the crucible,[17,18] it seems likely that the incorporation of oxygen into the PbTe lattice is not totally responsible for this behavior. The numbers above therefore impose a lower limit on the deviation from stoichiometry at the invariant melting point. The narrow range of stability above 875°C shown in Fig. 4 in conjunction with the published liquidus lines[8] accounts for the fact that pure PbTe crystals that are all n-type can only be obtained from melts very rich in Pb. The strong retrograde solubility indicates that crystals grown from the melt and cooled slowly are likely to contain an excess of one or the other components as a precipitate on grain boundaries and dislocations. The range of stability is comparable in magnitude to that found for PbS[2] and PbSe[6] and is much smaller than that

[14] F. A. Kroger, J. Phys. Chem. Solids **7**, 277 (1958).
[15] F. S. Ham, J. Phys. Chem. Solids **6**, 335 (1958).
[16] Based upon the experimental value of 8.25±.01 g/cm³ obtained for five crystals grown by Dr. B. B. Houston of our Laboratory. These crystals were pulled from a near stoichiometric melt, were p-type, and ranged in size from 14 to 25 g. This density agrees with that calculated from the lattice parameters of n and p-type PbTe quoted by Brady (see footnote 18).
[17] Unpublished experiments of R. F. Brebrick and B. B. Houston of this Laboratory.
[18] Edward L. Brady, J. Electrochem. Soc. **101**, 466 (1954).
[19] W. D. Lawson, J. Appl. Phys. **22**, 1444 (1951); **23**, 495 (1952).
[20] B. I. Boltaks, and In. N. Mokhov, J. Tech. Phys. U.S.S.R. **26**, 2448 (1956), Soviet Phys.-Tech. Phys. **1**, 2366 (1957).

indicated by magnetic-susceptibility measurements.[8] It is however consistent with thermal analysis and microscopic studies on the Pb-Te system.[8]

Comparison with Other Work

The room-temperature resistivities of polycrystalline ingots of PbTe containing 0.15 to 3.0% stoichiometric excess of lead have been measured as a function of annealing temperature up to about 760°C.[21] The ingots were annealed under hydrogen gas, then quenched to room temperature. The log resistivity vs reciprocal anneal temperature showed an "activation" energy of 0.51 ev. This is in fair agreement with the low-temperature slope of 0.40 ev in Fig. 3, as it should be if the electron mobility is essentially the same in the polycrystalline ingots and in our n-type single crystals. Single crystals of PbTe with an initial concentration of about 4×10^{18} holes/cm^3 have been annealed in evacuated tubes at temperatures between 200° and 500°C, quenched to room temperature and the Hall constant measured.[22] The results were reproducible. The carrier concentrations as a function of the reciprocal anneal temperature had an activation energy of 0.62 ev. The carrier concentrations at 400° and 500°C were 1.85×10^{18} and 4×10^{18}, respectively. The corresponding concentrations in Fig. 2 are 1.5×10^{18} and 4.6×10^{18}. The interpretation of this result was that the crystals contained an excess of Te as an internal precipitate, possibly on dislocations. This is consistent with the solidus lines shown in Fig. 4. As the anneal temperature was changed a redistribution of Te between the precipitate, where it is electrically inactive, and the crystal, where it introduces acceptor levels, occurred. The rapidity and reproducibility of the process are interconnected. Only short diffusion lengths are necessary, and, in the time required to reach internal equilibrium within the crystal, loss of material to the vapor phase affects only a negligible surface layer. No great effect was found,[22] however, on annealing single crystals of n-type PbTe in sealed, evacuated tubes.

Polycrystalline PbTe containing enough excess Pb or Te to insure the presence of a liquid phase has been annealed at 500°C quenched, and the room-temperature Hall constant measured.[22] For the purest material, maxima of 7×10^{17} electrons/cm^3 and 4×10^{18} holes/cm^3 were obtained in good agreement with our results at 500°C. For less pure material, the electron concentration was as high as 1.3×10^{19}, while the hole concentration remained almost unchanged.

Impurity Effects

The determination of PbTe-crystal composition at a limit of stability by the measurement of carrier concentration is affected in two ways by electrically active impurities. Firstly, the excess concentration of electrons or holes depends not only upon the difference in the concentration of Pb and Te, but also upon the concentration difference of foreign donors $[D]$ and acceptors $[A]$. If all donors and acceptors are ionized, we have

$$n-p=[\mathrm{Pb}]-[\mathrm{Te}]+[D]-[A]. \qquad (2)$$

Secondly, foreign impurities alter the chemical potentials of the Pb and Te and hence change the concentrations of these species at the limits of stability. Therefore, a necessary condition for the results given here to be characteristic of pure PbTe is that the concentration $[D]-[A]$ be small relative to the carrier concentrations observed. The Pb and Te used in making the ingots had an impurity concentration of the order of 1 ppm or less by weight as regards metals commonly detected by spectrographic analysis. The Pb and Te used in growing the crystals had an impurity concentration in the range 1 to 10 ppm. In PbTe, 1 ppm by weight corresponds to 7×10^{16} Cu or 2.5×10^{16} Bi atoms per cm^3. The range of carrier concentration obtained by heating crystals with Te-rich ingots is 1.4×10^{18} to 7.6×10^{18} and is well above these impurity concentrations. The range obtained with Pb-rich ingots is 1.3×10^{17} to 3.3×10^{18} and significant impurity-effects cannot be confidently ruled out. With regard to the effect of oxygen, the results of Koval'chik and Maslakovets are significant.[22] They found that polycrystalline PbTe with 7×10^{19} excess Te and that with 7×10^{19} excess TeO_2 when annealed at 500°C and quenched had essentially the same concentration of holes. Polycrystalline PbTe with up to 1×10^{20} excess Pb and that with 3×10^{19} to 1.5×10^{20} excess PbO had essentially the same electron concentration after annealing at 500°C. Therefore, the presence of oxygen does not significantly effect the limits of stability as calculated from Eq. (1). Either the solubility of oxygen in PbTe at 500°C is negligible relative to the maximum deviations from stoichiometry or the two effects mentioned at the beginning of the paragraph nearly compensate. The points at 495°C in Fig. 2 are of interest in this connection also. The crystals were heated with a Te-rich melt but in contrast to the usual procedure when using Te-rich melts, the silica container was coated with a carbon film. The points are in line with those at higher and lower temperatures although the partial pressure of oxygen would be expected to be considerably lower in the presence of carbon.

ACKNOWLEDGMENTS

The authors wish to thank G. L. Hammond and E. Gubner for their help in performing part of the experiments; Dr. B. B. Houston for providing us with data on the etch-pit density and making available several large single crystals for density measurements; and W. L. Clark for the fabrication of the silica tubes.

[21] R. W. Fritts, and S. Karrer, Bull. Am. Phys. Soc. **1**, 226 (1956).

[22] T. L. Koval'chik, and Iu. P. Maslakovets, J. Tech. Phys. U.S.S.R. **26**, 2417 (1956); Soviet Phys.-Tech. Phys. **1**, 2337 (1957).

Redetermination of the Intermolecular Potential for Krypton*

EDWARD A. MASON

Institute for Molecular Physics, University of Maryland, College Park, Maryland

(Received November 30, 1959)

The intermolecular potential for krypton has been redetermined from transport property data, including new experimental results on thermal diffusion and thermal conductivity. Both the Lennard-Jones (12–6) and the exp-6 potential functions have been used and reproduce the data about equally well. The parameter α of the exp-6 potential is not uniquely determined by the data, but a tentative selection of $\alpha=13.5$ has been made semiempirically on the basis of the theory of the dispersion energy and the consistency with the other rare-gas potentials. The most important conclusion is that there is a large discrepancy, not found for the other rare gases, between the present results and the experimental crystal properties and second virial coefficient. No amount of parameter adjustment has been able to reduce the discrepancy to a reasonably acceptable value. Possible explanations and implications of this unusual and unsatisfactory situation are discussed.

INTRODUCTION

A NUMBER of attempts to determine the intermolecular potential for krypton have previously been made, but without any very satisfactory results. It has not been possible to choose a single set of potential parameters which would reproduce all the experimental data with satisfactory accuracy. Furthermore, any potential parameters finally selected have not fitted in very smoothly with the corresponding parameters for the other rare gases. At the time of the previous work, the data available were rather scanty, and it was possible to hope that some of the data were in error and that subsequent experimental work would improve the situation. Since considerable new experimental results have now been accumulated, it seems reasonable to reconsider the problem at this time.

The intermolecular potential of krypton has previously been calculated by Mason and Rice[1] from crystal properties at 0°K together with viscosity and second virial coefficients for both the Lennard-Jones (12–6) and the exp-6 potential forms. They found it possible to select a set of potential parameters which reproduced the crystal data and second virial coefficients fairly well, but which did not appear to be satisfactory for the viscosity, thermal conductivity, and self-diffusion coefficient. The exp-6 parameters also did not appear very consistent with those for the other rare gases. Whalley and Schneider[2] performed similar calculations based on their new measurements of the second virial coefficient and used their potential parameters to calculate the crystal properties for comparison with experiment. The agreement was moderately good. Although they did not make the comparison, it was clear that their parameters also would not reproduce the transport properties satisfactorily. Srivastava and Srivastava[3] later redetermined the exp-6 parameters from thermal conductivity data alone. These data by themselves are not sufficient to permit the unambiguous determination of all three disposable parameters of the exp-6 potential, if any reasonable allowance for experimental error is considered. Furthermore, their parameters are not consistent with the crystal and second virial coefficient data, nor do they produce very good agreement with more recent thermal conductivity measurements at higher temperatures.[4] Madan[5] attempted to improve the situation by including the thermal diffusion measurements of Corbett and Watson,[6] but the results were inconclusive because of the experimental errors involved.

Recently, new experiments have become available which now make it possible to reach some unambiguous conclusions about the krypton intermolecular potential. The thermal diffusion factor has been remeasured more accurately by Moran and Watson[7] using a new technique, and the thermal conductivity has been measured at a higher temperature than before by von Ubisch,[4] who also measured a large number of mixtures of rare gases. It was, in fact, our attempts to analyze these mixture results theoretically that led to the present redetermination of the krypton potential, since none of the previous potentials was at all satisfactory.

In the present paper, the determination of potential parameters is first based entirely on transport property data, which form a consistent whole. The determinations of parameters based on crystal data and second virial coefficients are already adequate for these equilibrium properties.[1,2] It is not quite possible to determine as many as three disposable parameters uniquely from the transport data alone, and a final tentative selection is based semiempirically on the theory of the attractive dispersion energy term in the potential, and on the consistency with the results for the other rare gases. However, this selection is somewhat arbitrary, and all

* This research was supported in part by the U. S. Atomic Energy Commission.

[1] E. A. Mason and W. E. Rice, J. Chem. Phys. **22**, 843 (1954).

[2] E. Whalley and W. G. Schneider, J. Chem. Phys. **23**, 1644 (1955).

[3] B. N. Srivastava and K. P. Srivastava, Physica **23**, 103 (1957).

[4] H. von Ubisch, Arkiv Fysik **16**, 93 (1959).

[5] M. P. Madan, J. Chem. Phys. **27**, 113 (1957).

[6] J. W. Corbett and W. W. Watson, J. Chem. Phys. **25**, 385 (1956).

[7] T. I. Moran and W. W. Watson, Phys. Rev. **109**, 1184 (1958).

the potential parameters which reproduce the transport data are given. The ability of these parameters to reproduce the crystal and second virial coefficient data is then investigated and found to be quite unsatisfactory. Finally, the possibility of a compromise fit is investigated, in which one attempts to obtain only a fair overall fit of all properties, keeping in mind the possibility of experimental error in some of the properties. No such compromise fit proves to be possible. The implications of this eminently unsatisfactory and quite unusual (for a rare gas) situation are discussed.

DETERMINATION OF POTENTIAL PARAMETERS

Two forms of the potential energy function have been considered, the Lennard-Jones (12–6) potential,

$$\varphi(r)=\epsilon[(r_m/r)^{12}-2(r_m/r)^6], \tag{1}$$

and the exp-6 potential,

$$\varphi(r)=\epsilon\alpha(\alpha-6)^{-1}\{(6/\alpha)\exp[\alpha(1-r/r_m)]-(r_m/r)^6\}, \tag{2}$$

where $\varphi(r)$ is the potential energy of two molecules at a separation distance r, ϵ is the depth of the potential energy minimum, r_m is the position of the minimum, and α is a third parameter which determines the steepness of the repulsion energy.

The principal transport property data available for the determination of the parameters ϵ, r_m, and α are: (1) the reduced thermal diffusion factor (α_o); (2) the viscosity (η), and thermal conductivity (λ), which are essentially equivalent and can be considered together. The self-diffusion coefficient would also be suitable if more measurements were available, but the single available measurement can serve only as a check. The method used here for the determination of parameters is a graphical curve translation one, in which a plot of the experimental quantities $\log[10^7\eta/(266.93M^{\frac{1}{2}}T^{\frac{1}{2}})]$ or $\log[10^7\lambda M^{\frac{1}{2}}(f_\eta/f_\lambda)/(1989.1\,T^{\frac{1}{2}})]$ vs $\log T$ is moved to coincide as well as possible with plots of the theoretical quantities $\log[f_\eta/\Omega^{(2,2)*}]$ vs $\log T^*$, which form a family of curves. The amounts of motion parallel to each axis determine ϵ and r_m, and the choice of a particular theoretical curve determines α. The procedure has been described in detail elsewhere,[8] and need not be elaborated here. The quantity α_o is independent of r_m, and it is only necessary to plot α_o (exptl) vs $\log T$ and α_o (theor) vs $\log T^*$. Accurate values of α_o (theor) have recently been tabulated.[9]

The experimental error in α_o has been estimated to be about 10%.[7] The experimental error in η is probably not more than about 1% after the experimental values have been corrected to a uniform basis relative to the viscosity of air, which was taken as 1833.0×10^{-7} g/cm-sec at 23°C. The experimental error in λ is more difficult to estimate, but, on the basis of reproducibility and consistency among different investigators, an estimate of 2% appears reasonable. The measurements of von Ubisch are exceptions in that his results appear to be systematically high by about 4%, even though the precision of measurement is 2%.[4]

TABLE I. Potential parameters for krypton from transport properties.

Potential	α	ϵ/k, °K	r_m, A
Exp-6	12	173	4.169
	13	190	4.083
	13.5	200	4.036
	14	212	3.981
	15	234	3.890
12-6	...	225	3.926

Examination of the data readily showed that no one property determined all parameters uniquely, but, in general, could be considered to determine only a relation among the parameters. Thus η and λ yield a single relation among ϵ, r_m, and α; and α_o yields a single relation between ϵ and α. For the 12–6 potential, the parameter α does not appear, so that α_o determines ϵ uniquely, and then η and λ determine r_m. For the exp-6 potential, this procedure leaves one parameter still essentially undetermined, which has been chosen to be α. Thus a value of α was chosen, ϵ determined from α_o, and then r_m determined from η and λ. Within the limits of $\alpha=12$ to $\alpha=15$, there was no decided superiority in the fit, and all values determined are shown in Table I.

The problem remains of choosing a more definite value of α. This choice must be largely arbitrary in the absence of further experimental transport data and is made here purely as a convenience for future calculations of transport properties of krypton. A reasonable criterion might be that the parameter values fall reasonably smoothly in with the values for the other rare gases (excluding helium with its different electronic structure). The exp-6 parameters for the other rare gases are reproduced in Table II.[1] Comparison of Tables I and II shows that the variation is reasonably smooth for ϵ and r_m in all cases, but that one might reasonably expect the value of α for krypton to lie between 13 and 14. A similar conclusion follows from consideration of the ratio α/r_m, which is the coefficient of r in the exponential of the potential. This reasoning in itself is not very compelling, and, in the next section, comparison is made with various experimental quantities, including equilibrium data, in an attempt to establish a more definite choice of parameters.

COMPARISON WITH EXPERIMENT

It is first important to show how well the parameters of Table I reproduce the data used to determine them. Figure 1 shows a comparison of experimental and theoretical values of α_o as a function of temperature. Only one curve for the exp-6 potential is shown, since the others are not significantly different. The agreement

[8] E. A. Mason and W. E. Rice, J. Chem. Phys. **22**, 522 (1954).
[9] S. C. Saxena and E. A. Mason, J. Chem. Phys. **28**, 623 (1958).

TABLE II. Exp-6 potential parameters for other rare gases.

Gas	α	ϵ/k, °K	r_m, A
Ne	14.5	38.0	3.147
Ar	14.0	123.2	3.866
Xe	13.0	231.2	4.450

is just about within the experimental error estimate given by Moran and Watson.[7] Figure 2 shows a comparison of experimental[10] and theoretical values of η and λ. In this comparison, the theoretical ratio (f_η/f_λ) appears with the experimental quantities, but this ratio is so nearly unity in this case that only a rough theoretical estimation of it is adequate. Here again, only one exp-6 curve is shown, and no one potential gives a superior fit of the measurements. Several comments are suggested by Fig. 2. First, von Ubisch's measurements seem to be systematically high by a few percent, a fact which he himself has already pointed out. Secondly, the measurements of Kannuluik and Carman seem to be slightly low at their highest temperatures, a feature also previously noticed[8] in regard to their helium results. Thirdly, at the lowest temperatures, the experimental points are well above the calculated curves. This feature is not unique with krypton and has previously been pointed out for both argon[1] and xenon.[11] Amdur and Schatzki[11] have advanced some theoretical arguments suggesting reasons for this discrepancy.

A more important test of the parameters of Table I is their ability to reproduce properties not used in determining the parameters. The self-diffusion coefficient has been measured[12] only at 293.0°K, and the comparison between experiment and theory is given in Table III. It is evident that all the potentials give agreement within the experimental error.

The heat of sublimation E_o and the lattice spacing R_o of the crystal at 0°K can be readily calculated from the intermolecular potential on the assumption that the potentials are pairwise additive. The method of calculation has been summarized in detail elsewhere,[1,2] and it seems unnecessary to describe it again here. The results are given in Table IV and compared with the experimental values quoted by Whalley and Schneider.[2] It is seen that a value of α could be chosen which would give reasonable agreement for R_o, but there is a marked discrepancy for E_o in any case. If the experimental value of E_o is assumed to be in error, then there will be a marked discrepancy between the crystal data and the second virial coefficients, which are in moderately good agreement as they stand.[1] Another possibility is that the assumption of additivity of pair potentials is at fault.[13] If so, similar discrepancies should probably be found for argon and xenon, but, for both these substances, the transport properties, second virial coefficients, and crystal properties are all in reasonable accord.[1]

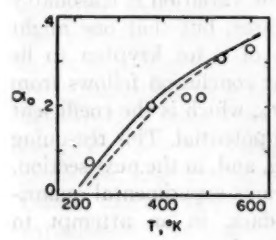

FIG. 1. Reduced thermal diffusion factor of krypton. Solid line, exp-6 potential ($\alpha=13.5$); dashed line, 12-6 potential.

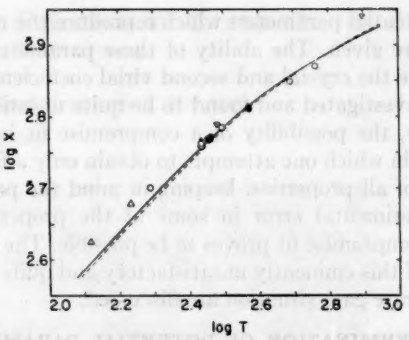

FIG. 2. Viscosity and thermal conductivity of krypton, where X is $(10^7\eta)(266.93M^{\frac{1}{2}}T^{\frac{1}{4}})^{-1}$ or $(10^7\lambda M^{\frac{1}{2}}/f_\eta)(1989.1\ T^{\frac{1}{2}}/f_\lambda)^{-1}$. Solid line, exp-6 potential ($\alpha=13.5$); dashed line, 12-6 potential. Experimental values: ●, Rankine; ▲, Nasini and Rossi; ◇, Curie and Lepape; ○, Kannuluik and Carman; △, Keyes; □, Srivastava and Saxena; ▽, von Ubisch. Filled points represent viscosities, open points represent thermal conductivities.

Finally, Fig. 3 shows a comparison of experimental[14] and calculated second virial coefficients as a function of temperature. The agreement here is also very poor. There is little probability that this can be blamed on experimental error, for the measurements have been

TABLE III. Self-diffusion coefficient of krypton at 293.0°K and 1 atm.

Source	D_{11}, cm²/sec
Exp-6, $\alpha=12$	0.0958
$\alpha=13$	0.0943
$\alpha=13.5$	0.0938
$\alpha=14$	0.0936
$\alpha=15$	0.0930
12-6	0.0926
Exptl	0.093±0.004

[10] (a) Viscosity: A. O. Rankine, Proc. Roy. Soc. (London) **A83**, 516 (1910); **A84**, 181 (1910); A. G. Nasini and C. Rossi, Gazz. chim. ital. **58**, 433, 898 (1928). (b) Thermal conductivity: M. Curie and A. Lepape, Compt. rend. **193**, 842 (1931); J. phys. radium **2**, 393 (1931); W. G. Kannuluik and E. H. Carman, Proc. Phys. Soc. (London) **B65**, 701 (1952); F. G. Keyes, Trans. Am. Soc. Mech. Engrs. **77**, 1395 (1955); B. N. Srivastava and S. C. Saxena, Proc. Phys. Soc. (London) **B70**, 369 (1957); H. von Ubisch, Arkiv Fysik **16**, 93 (1959).

[11] I. Amdur and T. F. Schatzki, J. Chem. Phys. **27**, 1049 (1957).

[12] W. Groth and P. Harteck, Z. Elektrochem. **47**, 167 (1941).

[13] B. M. Axilrod and E. Teller, J. Chem. Phys. **11**, 299 (1943); **19**, 719, 724 (1951); R. T. McGinnies and L. Jansen, Phys. Rev. **101**, 1301 (1956); **104**, 961 (1956); M. J. Sparnaay, Physica **25**, 219 (1959).

[14] Beattie, Brierley, and Barriault, J. Chem. Phys. **20**, 1613, 1615 (1952); E. Whalley and W. G. Schneider, Trans. Am. Soc. Mech. Engrs. **76**, 1001 (1954).

TABLE IV. Crystal properties of krypton.

Source	R_o, A	E_o, cal/mole
Exp-6, $\alpha=12$	4.040	2997
$\alpha=13$	3.981	3204
$\alpha=13.5$	3.944	3336
$\alpha=14$	3.899	3503
$\alpha=15$	3.822	3805
12-6	3.837	3845
Exptl	3.93±0.03	2733±50

made in two different laboratories by two different techniques.

Instead of a basis for a more definite choice of potential parameters, an unexpectedly large discrepancy has been found. The equilibrium data are reasonably concordant among themselves, and the transport data are also concordant among themselves, but there is a large discrepancy between the two. No amount of parameter adjustment was successful in bringing the two sets of data into even moderately reasonable concordance. The precision and variety of the experimental results further seem to preclude blaming the discrepancy on possible experimental errors. As a practical matter, however, it is still desirable to select a single exp-6 potential based on transport data which can be used for calculation of transport properties. Consideration of the dispersion energy makes such a selection possible, at least tentatively.

DISPERSION ENERGY

The starting point is taken to be the Slater-Kirkwood formula for the London dispersion energy between two like atoms,[15]

$$\varphi_{\text{dis}}(r)=3eh(N\alpha^3)^{\frac{1}{2}}/(8\pi m^{\frac{1}{2}}r^6), \qquad (3)$$

where e is the electronic charge, h is Planck's constant, m is the electronic mass, N is the number of electrons in the outer shell of one atom, and α is the atomic polarizability. According to Eq. (3), the coefficient C of the r^{-6} term in the potential should be proportional to $(N\alpha^3)^{\frac{1}{2}}$. Empirically, a plot of $\log C$ vs $\log(N\alpha^3)$ is indeed a good straight line, although the slope is about 0.56 for the rare gases, rather than the value of 0.5 required by the approximate theory.[16,17] A plausible tentative choice of the potential parameter α can therefore be made on the basis of the smoothness of a plot of $\log[\alpha(\alpha-6)^{-1}\epsilon r_m^6]$ vs $\log\alpha$, such as is shown in Fig. 4. On this basis, the most likely value of α is about 13.5, in agreement with the estimate of the previous section based on the smoothness of α itself and of α/r_m. It is perhaps of interest that on the basis of a plot of $\log(\epsilon r_m^6)$ vs $\log\alpha$, the new 12–6 parameters of Table I are in substantially better accord with the 12–6 parameters for the other rare gases[1] than are the previous 12–6 parameters[1] for krypton.

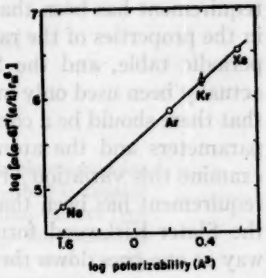

FIG. 4. Correlation of the coefficient of the dispersion energy with the polarizability for the rare gases. The point for Kr is for the parameter $\alpha=13.5$, and the extremes indicate the points for $\alpha=12$ and $\alpha=15$.

Pitzer[15] has suggested an alternative interpretation of Eq. (3) for the rare gases, in which the value of N is assigned to give agreement with the experimental dispersion energy. The excess of N over 8 (or 6) is then interpreted as an indication of contributions of inner-shell electrons to the polarizability. The values of N calculated in this way are found to increase smoothly with the atomic number. Thus a reasonable criterion on which to base the choice of potential parameters is the smoothness of N as a function of atomic number. Values of N calculated for the exp-6 potentials of Tables I and II are tabulated in Table V. The best value of the parameter α on this basis is again about 13.5.

It should be emphasized that there has been no requirement here that the coefficient of the dispersion energy satisfy the Slater-Kirkwood formula. The real

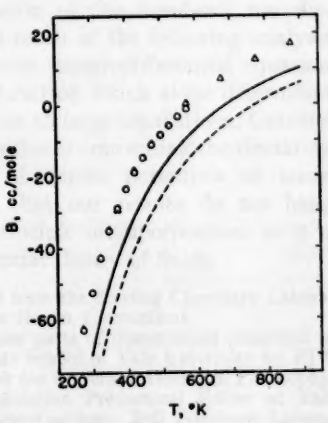

FIG. 3. Second virial coefficient of krypton. Solid line, exp-6 potential ($\alpha=13.5$); dashed, 12-6 potential. Experimental values: ○, Beattie, Brierley and Barriault; △, Whalley and Schneider.

TABLE V. Effective N values from Eq. (3) as a function of atomic number.

Gas	Z	N
Ne	10	8
Ar	18	14
Kr, $\alpha=12$	36	26
$\alpha=13.5$		19
$\alpha=15$		14
Xe	54	21

[15] A pertinent review has recently been given by K. S. Pitzer, J. Am. Chem. Soc. 78, 4505 (1956); Advances in Chem. Phys. 2, 59–83 (1959).

[16] J. S. Rowlinson, Quart. Revs. 8, 168 (1954).

[17] W. Brandt, J. Chem. Phys. 24, 501 (1956).

requirement has been that there be a smooth variation in the properties of the rare gases as one goes down the periodic table, and the Slater-Kirkwood formula has actually been used only in a semiempirical way to show that there should be a correlation between the potential parameters and the atomic polarizability in order to examine this variation (Fig. 4). Stated differently, the requirement has been that the rare gases deviate from the Slater-Kirkwood formula in the same systematic way as one goes down the periodic table (Table V).

DISCUSSION

The transport properties of krypton have been used to calculate exp-6 and 12-6 potential parameters. All the potentials reproduce the data about equally well, and a tentative selection of a single set of exp-6 parameters (with $\alpha=13.5$) and has been based on approximate theory. This selection can be easily changed to accommodate new experimental data. The most important result of the present work, however, is the establishment of a definite large discrepancy for krypton which does not seem to exist for any of the other rare gases. In the first place, none of the present potentials will reproduce the second virial coefficient of krypton, nor can any mutual adjustment of potential parameters be made which will secure a reasonable fit to both the second virial coefficient and the transport properties simultaneously. It seems impossible to doubt the essential accuracy of the experimental data. It would also be surprising if the forms used for the potential were so unrealistic as to produce this discrepancy, since these forms work reasonably well for all the other rare gases.

Furthermore, none of the present potentials will reproduce the experimental heat of sublimation of the crystal at 0°K. There is the possibility that the experimental value is in error, or that pairwise nonadditivity of potentials is important. However, the former possibility seems unlikely since the crystal properties are reasonably consistent with the second virial coefficient, and the latter possibility seems unlikely because the crystal calculations for argon and xenon seem all right.

This discrepancy seems to be unique for krypton, since none of the other rare gases exhibits it, except in such a mild form as to be reasonably attributed to oversimplification of the potential function. There seems to be no easy explanation, short of the rather depressing one that our fundamental understanding of intermolecular forces is more deficient than has been thought.

Theory of Fused Salts*†

FRANK H. STILLINGER, JR.,‡ JOHN G. KIRKWOOD, AND PETER J. WOJTOWICZ§

Sterling Chemistry Laboratory, Yale University, New Haven, Connecticut

(Received October 2, 1959)

The properties of ionic pair distributions are investigated for a simple fused-salt model. The short-range ion core forces are assumed to be identical for both anions and cations and, although the method is capable of handling mixtures of ions with different charges, only a single fused salt of the symmetrical-valence type is considered. A set of relations is developed to describe the asymptotic behavior (for large ion distances) of the ion pair distribution functions. These relations are obtained with benefit only of certain weak, plausible assumptions concerning the triplet superposition defects; as a consequence, the usual superposition approximation of liquid theory is circumvented. A significant feature of the results is prediction of concentric shells of average charge density surrounding a given ion in a manner suggesting local latticelike structure.

I.

IN this article we propose a simple model for understanding the equilibrium behavior of fused salts. The following analysis is perhaps of rather general interest in that, by slight elaboration, the technique outlined here may be adapted to handle concentrated electrolytic solutions. The important fact to be stressed in the following is that the ion Coulomb interactions, as well as the core interactions, are each equally influential in determining the characteristics of the fused salt near its melting point. Thus, for example, the short-range repulsive forces effectively provide geometrical constraints on the possible ion positions, resulting at least locally in a sort of close-packed latticelike structure; simultaneously, the electrostatic forces try to pair off ions of opposite charge. It is found that the result of these competing tendencies is to surround a given ion on the average by concentric shells of alternating charge density, similar to the charge ordering in ionic crystals where successive shells of neighbors differ in sign.

By varying the Coulombic coupling between the ions in a canonical ensemble, a set of integral equations is derived for determination of the fused-salt ion distributions. The central result of the following analysis is a linear inhomogeneous integrodifferential equation satisfied exactly by a function which alone determines the ion pair distributions at large separations. Granted certain reasonable hypotheses concerning the deviation from superposability of triplet potentials of mean force, it is significant that our results do not hang upon the restrictive principle of superposition as it is often used in the molecular theory of fluids.

The manner is quite clear in which the Debye-Hückel limiting theory is obtained at extremely high temperatures (or low ion number densities) in terms of our expressions for ionic distribution. Extension to larger values of the Debye-Hückel parameter κ necessarily involves in complicated fashion details of the short-range ion interactions.

II.

The fused salt to be considered will be restricted to the symmetrical-valence type, so that individual ions bear a small integral multiple ($\pm z$) of the electronic charge e. Furthermore, the total potential of interaction V_N for the assembly of N ions in a suitable container of volume $\mathcal{V}$ will be taken as pairwise additive

$$V_N = \sum_{i<j=1}^{N} V_{ij}. \tag{1}$$

Two contributions to each V_{ij} may immediately be distinguished, each of which we will take to be centrally symmetric[1]:

$$V_{ij}(r) = V_{ij}^{(0)}(r) + V_{ij}^{(1)}(r). \tag{2}$$

$V_{ij}^{(0)}$ represents the potential of short-range forces acting between the ion cores; its most noteworthy feature insofar as fused salts are concerned is inclusion of a strong repulsion at small distances r, reflecting improbability of ion interpretation. A reasonable choice for $V_{ij}^{(0)}$ would be at least qualitatively similar to the Lennard-Jones potentials often used to represent

* Contribution No. 1585 from the Sterling Chemistry Laboratory, Yale University, New Haven, Connecticut.

† This work is based upon parts of dissertations presented to the faculty of the Graduate School of Yale University by PJW (1956) and FHS (1958) for the degrees of Doctor of Philosophy.

‡ National Science Foundation Predoctoral Fellow at Yale University, 1955–1958; present address: Bell Telephone Laboratories, Murray Hill, New Jersey.

§ National Science Foundation Predoctoral Fellow at Yale University, 1953–1956; present address: RCA Laboratories, Radio Corporation of America, Princeton, New Jersey.

[1] The pairwise additive and central form of the total short-range interaction

$$V_N^{(0)} = \sum_{i<j=1}^{N} V_{ij}^{(0)}(r_{ij})$$

may be generalized somewhat without changing the following analysis. It is only necessary to demand, for a fixed set of N ion positions, that $V_N^{(0)}$ be invariant under the replacement of cations for anions, and vice versa. For present purposes this generalization is unimportant; a pairwise $V_N^{(0)}$ has the advantege of being easy to visualize.

interactions of noble gas atoms (which might be regarded as discharged ion cores). $V_{ij}^{(1)}$ is the Coulomb potential[2]:

$$V_{ij}^{(1)}(r)=\xi_i\xi_j[(ze)^2/Dr]. \tag{3}$$

The charging parameters ξ_i, ξ_j are $+1$ and -1 for cations or anions, respectively. Since the system as a whole is electrically neutral, the number of cations N_+ is equal to the number of anions N_-; equivalently,

$$\sum_{i=1}^{N}\xi_i=0, \qquad N=N_++N_-. \tag{4}$$

For the sake of mathematical convenience, we wish to restrict the fused salt model to having the simplest possible characteristics consistent with the general picture of ionic fluids. With this point of view, we demand that the potentials $V_{ij}^{(0)}$ be identical functions of r for all ion pairs.[1] At least as far as the notion of ionic radii is concerned, this condition is rather closely obeyed by salts such as KF, CsCl, and BaO. The significance of deviation from this ideal in the case of other salts is lessened by the fact that ion core interactions come most strongly into play between ions of opposite charge on account of Coulombic attraction. Assuming $V_{ij}^{(0)}$ to be this anion-cation potential will thereby minimize possible error.

The ultimate object of the following investigation will be an analysis of the fluid's macroscopic properties by means of ionic distribution functions. The result of the preceding remarks is that our simple model has been constrained to possess complete charge symmetry. There are consequently just two independent ion pair correlation functions to be determined[3]:

$$\begin{aligned} g_{++}^{(2)}(r)&=g_{--}^{(2)}(r),\\ g_{+-}^{(2)}(r)&=g_{-+}^{(2)}(r), \end{aligned} \tag{5}$$

which suffice to compute the fused salt thermodynamic functions as well as the x-ray scattering pattern. The first of Eqs. (5), stating that the correlation between pairs of cations and of anions is the same, follows directly from the model charge symmetry. The second relation (5) reflects isotropy of the fluid salt medium in the absence of external forces.

The correlation function $g_m(r)$ for particles of any type at a radial distance r from either a central anion or cation, is just the arithmetic mean of $g_{++}^{(2)}(r)$ and $g_{+-}^{(2)}(r)$,

$$\begin{aligned} g_m(r)&=\tfrac{1}{2}[g_{++}^{(2)}(r)+g_{+-}^{(2)}(r)]\\ &=\tfrac{1}{2}[g_{-+}^{(2)}(r)+g_{--}^{(2)}(r)]. \end{aligned} \tag{6}$$

Notice that whereas two like ions at a given distance of separation r might experience a mean repulsion, unlike ions would be expected to exhibit a mean attraction by virtue of charge sign change. The average correlation $g_m(r)$ consequently will show less fluctuation about unity than either $g_{++}^{(2)}(r)$ or $g_{+-}^{(2)}(r)$. Stated in another way, this amounts to concluding that the ionic charges (by virtue of the extreme range of Coulomb forces) will induce at fairly large distances fluctuations in the anionic and cationic number densities *relative to each other*, but that it is only in the immediate vicinity of a given ion that the *total* density varies. On this basis it is postulated that $g_m(r)$ approaches its asymptotic limit unity much more rapidly than do either $g_{++}^{(2)}(r)$ or $g_{+-}^{(2)}(r)$. In a later section, $g_m(r)$ will in fact be identified with the correlation function in a single-component fluid whose particles interact with only forces of considerably shorter range than the Coulomb forces.

A new function $\phi(r)$ is defined by the ratio

$$g_{++}^{(2)}(r)/g_{+-}^{(2)}(r)=\exp[-2\phi(r)/kT]. \tag{7}$$

$2\phi(r)$ is therefore the mean reversible work (at absolute temperature T) required to take an anion, at distance r from a cation, to "infinity" (though still within the fused salt medium), and subsequently to bring another cation in from "infinity" to the original position. For convenience in presentation, it is preferable to regard $g_m(r)$ and $\phi(r)$ as the two independent functions to be determined, rather than $g_{++}^{(2)}(r)$ and $g_{+-}^{(2)}(r)$. By solving (6) and (7), it is found that

$$\begin{aligned} g_{++}^{(2)}(r)&=\frac{2g_m(r)}{\exp[2\phi(r)/kT]+1},\\ g_{+-}^{(2)}(r)&=\frac{2g_m(r)\exp[2\phi(r)/kT]}{\exp[2\phi(r)/kT]+1}. \end{aligned} \tag{8}$$

We note in passing that the average electrostatic charge densities, $\rho_+^{(el)}(r)$ and $\rho_-^{(el)}(r)$ surrounding cations and anions are just

$$\begin{aligned} \rho_+^{(el)}(r)&=-\rho_-^{(el)}(r)\\ &=(ze)(N_+/\mathcal{V})g_{++}^{(2)}(r)-(ze)(N_-/\mathcal{V})g_{+-}^{(2)}(r)\\ &=-2zecg_m(r)\tanh[\phi(r)/kT],\\ c&=N_+/\mathcal{V}=N_-/\mathcal{V}. \end{aligned} \tag{9}$$

[2] Note here that the difficult problem of determining the appropriate dielectric constant D from individual ion polarizabilities is avoided. The form (3) will be regarded as an inherent characteristic of the fused salt model. Any deviations from the asymptotic dielectric constant D when r is small may be absorbed in $V_{ij}^{(0)}$. In practical cases, D will be estimated from the refractive index.

[3] For a comprehensive account of the elements of molecular distribution function theory see T. L. Hill, *Statistical Mechanics* (McGraw-Hill Book Company, Inc., New York, 1956), Chap. 6.

These charge densities are subject to local electroneutrality conditions, whereby the total average charge surrounding any ion must exactly counteract that ion's own charge. Therefore, $g_m(r)$ and $\phi(r)$ must satisfy the relation,

$$1/8\pi c=\int_0^\infty r^2 g_m(r)\,\tanh[\phi(r)/kT]dr. \quad (10)$$

The problem is to develop further relations between $g_m(r)$ and $\phi(r)$ from the fundamentals of statistical mechanics, since (10) alone is trivial and not particularly informative. For this purpose a coupling parameter technique is useful, wherein the electrostatic charge on one of the ions (chosen arbitrarily as ion 1) is allowed to vary continuously. Only at the end of our computation will it be necessary to set this ionic charge equal to its actual "physical" value $\pm ze$. This charging process is accomplished by considering changes in the parameter ξ_1.[4]

In the petit canonical ensemble theory, the nth-order fluid correlation functions $g^{(n)}$ and potentials of mean force $W^{(n)}$ are expressed as an integral of the canonical configuration density over the remaining $N-n$ particle positions,

$$g_{1\beta\cdots\nu}{}^{(n)}(\xi_1)=\exp\{-[W_{1\beta\cdots\nu}{}^{(n)}(\xi_1)]/kT\}$$
$$=\mathcal{V}^n\int_{\mathcal{V}}\cdots\int_{\mathcal{V}}\exp\{(kT)^{-1}[A_N(\xi_1)$$
$$-V_N(\xi_1)]\}d\mathbf{r}_{n+1}\cdots d\mathbf{r}_N,\quad \beta\cdots\nu=+,-, \quad (11)$$

where certain terms of negligible order $1/N$ have been disregarded. Here we have indicated explicitly only the dependence upon the parameter ξ_1. A_N is the normalizing factor,

$$\exp[-A_N(\xi_1)/kT]$$
$$=\int_{\mathcal{V}}\cdots\int_{\mathcal{V}}\exp[-V_N(\xi_1)/kT]d\mathbf{r}_1\cdots d\mathbf{r}_N. \quad (12)$$

A differentiation with respect to ξ_1 of the logarithm of Eq. (11) for $n=2$, followed by rearrangement and subsequent integration over ξ_1, leads to the integral equation,

$$W_{1\beta}{}^{(2)}(r_{12},\xi_1)-W_{1\beta}{}^{(2)}(r_{12},0)$$
$$=\xi_1\xi_2[(ze)^2/Dr_{12}]+\sum_{\gamma=+,-}\xi_3 c\int_0^{\xi_1}d\xi_1'\int_{\mathcal{V}}d\mathbf{r}_3$$
$$\times[(ze)^2/Dr_{13}]g_{1\gamma}{}^{(2)}(r_{13},\xi_1')$$
$$\times\left\{\exp\left[-\frac{W_{\beta\gamma}{}^{(2)}(r_{23})}{kT}-\frac{\epsilon_{1\beta\gamma}{}^{(3)}(123,\xi_1')}{kT}\right]-1\right\}. \quad (13)$$

The $d\mathbf{r}_3$ integration is over all positions of a third ion of type γ ($\xi_3=+1$ if $\gamma=+$, $\xi_3=-1$ if $\gamma=-$). The superposition defect function $\epsilon^{(3)}$ measures the extent to which triplet potentials of mean force may be represented by a sum of the three appropriate mean pair potentials,

$$\epsilon_{\alpha\beta\gamma}{}^{(3)}(123)=W_{\alpha\beta\gamma}{}^{(3)}(123)-W_{\alpha\beta}{}^{(2)}(r_{12})$$
$$-W_{\alpha\gamma}{}^{(2)}(r_{13})-W_{\beta\gamma}{}^{(2)}(r_{23}). \quad (14)$$

One approach to the theory of liquids is to obtain a closed set of equations for pair distributions by supposing all the $\epsilon^{(3)}$ to vanish; it will be seen that in the present context this hypothesis is unnecessarily stringent. $W_{1\beta}{}^{(2)}(r_{12},0)$ in (13) is the potential of mean force acting between a fully charged ion of type β, and the completely discharged ion 1; it is of course the same for β either $+$ or $-$.

Set β successively equal to $+$ and $-$ in (13), and let the difference of the results define $\phi(r_{12},\xi_1)$ [in Eq. (7) we have already introduced $\phi(r_{12})\equiv\phi(r_{12},1)$],

$$2\phi(r_{12},\xi_1)=W_{1+}{}^{(2)}(r_{12},\xi_1)-W_{1-}{}^{(2)}(r_{12},\xi_1)$$
$$=2\xi_1[(ze)^2/Dr_{12}]+[c(ze)^2/D]\int_0^{\xi_1}d\xi_1'\int_{\mathcal{V}}(d\mathbf{r}_3/r_{13})$$
$$\times\left\{g_{1+}{}^{(2)}(13,\xi_1')\left[\exp\left(-\frac{W_{++}{}^{(2)}(23)}{kT}-\frac{\epsilon_{1++}{}^{(3)}(123,\xi_1')}{kT}\right)\right.\right.$$
$$\left.-\exp\left(-\frac{W_{-+}{}^{(2)}(23)}{kT}-\frac{\epsilon_{1-+}{}^{(3)}(123,\xi_1')}{kT}\right)\right]$$
$$+g_{1-}{}^{(2)}(13,\xi_1')\left[\exp\left(-\frac{W_{--}{}^{(2)}(23)}{kT}-\frac{\epsilon_{1--}{}^{(3)}(123,\xi_1')}{kT}\right)\right.$$
$$\left.\left.-\exp\left(-\frac{W_{+-}{}^{(2)}(23)}{kT}-\frac{\epsilon_{1+-}{}^{(3)}(123,\xi_1')}{kT}\right)\right]\right\}. \quad (15)$$

The potentials of mean force $W_{\alpha\beta}{}^{(2)}(r_{12})$ have the property of becoming small as the distance r_{12} between ions 1 and 2 becomes large. Furthermore, the superposition defect function $\epsilon_{\alpha\beta\gamma}{}^{(3)}(123)$ decreases to zero when any one of r_{12}, r_{13}, r_{23} becomes large.[5] On the basis of these considerations, the asymptotic form of Eq. (15) is obtained, for large r_{12}, by linearizing the integrand with respect to the $\epsilon^{(3)}$'s. When $g_m(r_{13},\xi_1')$ is defined in analogy to Eq. (6), we find that the large r_{12}

[4] Violation of the over-all electroneutrality condition (4) to the extent of small arbitrary variations in ξ_1 may be disregarded, since the system has macroscopic size.

[5] One is not justified in assuming, however, that the rate of decrease to zero of $\epsilon^{(3)}$ with an increasing ion pair distance is of higher order than the corresponding decrease of $W^{(2)}$.

form of (15) is

$$\phi(r_{12},\xi_1)=\xi_1[(ze)^2/Dr_{12}]-E(r_{12},\xi_1)$$
$$+[c(ze)^2/D]\int_0^{\xi_1}d\xi_1'\int_{\mathcal{V}}(d\mathbf{r}_3/r_{13})g_m(r_{13},\xi_1')$$
$$\times\left\{\exp\left[-\frac{W_{++}^{(2)}(23)}{kT}\right]-\exp\left[-\frac{W_{+-}^{(2)}(23)}{kT}\right]\right\}$$

$$E(r_{12},\xi_1)=[c(ze)^2/2DkT]\int_0^{\xi_1}d\xi_1'\int_{\mathcal{V}}(d\mathbf{r}_3/r_{13})$$
$$\times\left\{g_{1+}^{(2)}(r_{13},\xi_1')\left[\exp\left(-\frac{W_{++}^{(2)}(23)}{kT}\right)\epsilon_{1++}^{(3)}(123,\xi_1')\right.\right.$$
$$\left.-\exp\left(-\frac{W_{+-}^{(2)}(23)}{kT}\right)\epsilon_{1-+}^{(3)}(123,\xi_1')\right]$$
$$+g_{1-}^{(2)}(r_{13},\xi_1')\left[\exp\left(-\frac{W_{++}^{(2)}(23)}{kT}\right)\epsilon_{1--}^{(3)}(123,\xi_1')\right.$$
$$\left.\left.-\exp\left(-\frac{W_{+-}^{(2)}(23)}{kT}\right)\epsilon_{1+-}^{(3)}(123,\xi_1')\right]\right\}$$

$$g_m(r_{13},\xi_1')=\tfrac{1}{2}[g_{1+}^{(2)}(r_{13},\xi_1')+g_{1-}^{(2)}(r_{13},\xi_1')]. \quad (16)$$

We have made use of the identities,

$$W_{++}^{(2)}(23)=W_{--}^{(2)}(23),$$
$$W_{+-}^{(2)}(23)=W_{-+}^{(2)}(23), \quad (17)$$

consistent with Eqs. (5).

It is now asserted that $E(r_{12},\xi_1)$ vanishes more strongly, as r_{12} increases, than does $\phi(r_{12},\xi_1)$. The conditions on the several $\epsilon^{(3)}$'s which ensure this behavior of $E(r_{12},\xi_1)$ are discussed in the Appendix. The implication, so far as the asymptotic Eq. (16) is concerned, is that $E(r_{12},\xi_1)$ may be dropped without destroying the validity of that relation

$$\phi(r_{12},\xi_1)=\xi_1[(ze)^2/Dr_{12}]+\xi_1[c(ze)^2/D]$$
$$\times\int_{\mathcal{V}}(d\mathbf{r}_3/r_{13})g(r_{13},\xi_1)\left\{\exp\left[-\frac{W_{++}^{(2)}(23)}{kT}\right]\right.$$
$$\left.-\exp\left[-\frac{W_{+-}^{(2)}(23)}{kT}\right]\right\}$$

$$g(r_{13},\xi_1)=\xi_1^{-1}\int_0^{\xi_1}g_m(r_{13},\xi_1')d\xi_1'. \quad (18)$$

The exponentials in the integrand of (18) may be linearized unless $W_{\alpha\beta}^{(2)}(23)$ is large, i.e., r_{23} is small. But having already demanded that r_{12} be large [since only asymptotic validity is claimed for (18)], this nonlinear region must have r_{13} large. It has already been remarked that $g_m(r_{13},\xi_1)$, and therefore $g(r_{13},\xi_1)$ for large r_{13} attain their asymptotic values unity very rapidly; for this reason, $g(r_{13},\xi_1)$ is taken to be identically unity for the troublesome region of small r_{23} values in (18). If, therefore, the Laplacian differential operator ∇_1^2 with respect to the position of ion 1 is applied to both sides of (18), the integrand then vanishes when r_{23} is small. Consequently, no error is incurred in the asymptotic equation by linearizing the exponentials for all positions of particle 3. If one uses the fact that $g(r_{13},\xi_1)$ is spherically symmetric, (18) may be transformed into the linear integrodifferential equation ($r_{12}\gg 0$),

$$\nabla_1^2\phi(r_{12},\xi_1)=-\xi_1[2c(ze)^2/DkT]\int_{\mathcal{V}}\phi(r_{23},1)$$
$$\times\{[g''(r_{13},\xi_1)r_{13}]-4\pi\delta(r_{13})g(r_{13},\xi_1)\}d\mathbf{r}_3. \quad (19)$$

The three-dimensional delta function arises when ∇_1^2 is applied to the Coulomb interaction.

A naive way of recovering the linearized Poisson-Boltzmann equation of the Debye-Hückel theory immediately suggests itself. If the correlation function $g(r_{13},\xi_1)$ were everywhere equal to the large r_{13} value unity, (19) would simplify ($\xi_1=1$)

$$\nabla_1^2\phi(r_{12},1)=\kappa^2\phi(r_{12},1),$$
$$\kappa^2=8\pi c(ze)^2/DkT. \quad (20)$$

The well-known solutions to this differential equation are without significance for fused salts near their melting points. In view of the facts that fused salts have dielectric constants on the order of 3, and concentrations around 50 moles per liter, the corresponding values of κ are enormous by comparison with typical dilute electrolytic solutions. The "diffuse" charge atmosphere around a central ion as predicted in this manner would be a thin skin of neutralizing charge only a few hundredths of an Angstrom unit thick. The ion core short-range forces implicit in $g(r_{13},\xi_1)$ play a preeminent role in establishing the fused-salt local structure, and they must be reckoned with in considerable detail to yield even a qualitatively correct picture of the fluid.

For realistic short-range interactions, $g(r_{13},\xi_1)$ will vanish at the origin because of the improbability of ion core interpretation. As a result, the second term of the integrand in (19) may be dropped. Because of the two-center nature of this integral, it is natural to transform to dipolar coordinates. One has, after performing an

elementary integration,

$$\chi''(R,\xi_1)=(\kappa^2/2)\int_0^\infty [g'(|R-s|,\xi_1) - g'(R+s,\xi_1)]\chi(s,1)ds,$$
$$\chi(R,\xi_1)=R\phi(R,\xi_1). \quad (21)$$

As before, it is justifiable to claim that the correct function χ satisfies (21) only as $R\to\infty$. By adding a suitable inhomogeneous function $h(R,\xi')$, an integrodifferential relation satisfied exactly by χ for all $R>0$ is formally obtained,

$$\chi''(R,\xi_1)=h(R,\xi_1) + (\kappa^2/2)\int_0^\infty [g'(|R-s|,\xi_1)-g'(R+s,\xi_1)]\chi(s,1)ds. \quad (22)$$

$h(R,\xi_1)$ must vanish for large R more rapidly than $\chi''(R,\xi_1)$ since (22) must reduce to (21). It may be recognized that $h(R,\xi_1)$ contains contributions arising not only from the superposition defects $\epsilon^{(3)}$, but also from the nonlinear portions of Eq. (18) disregarded in passing to Eq. (19).

III.

We proceed to construct the solutions to (22). For this purpose it is helpful to define $g'(R,\xi_1)$ to be an even function of R, and $h(r,\xi_1)$ to be odd. $\chi''(R,\xi_1)$ then becomes an odd function of R by satisfying the resulting extension of (22) onto the negative axis

$$\chi''(R)=h(R)+(\kappa^2/2)\int_0^\infty [g'(R-s)-g'(R+s)]\chi(s)ds, \quad (23)$$

where ξ_1 has been set equal to the "physical" value $+1$, and the dependence of χ, h, and g on this variable has been suppressed.

The physically admissible solution $R^{-1}\chi(R)$ for the fused salt must vanish at infinity because of a similar condition on the pair potentials of mean force. It will in fact be supposed that a positive constant ϵ exists such that $\exp(\epsilon R)\chi(R)$ is bounded as R increases; this exponential loss of order in pair space we shall take to be characteristic of fluids. It must be mentioned in this connection that the x-ray scattering patterns for all fluids, although clearly exhibiting maxima at certain angles, nevertheless do not show the sharp and distinctive Bragg reflections typical of crystalline solids, the latter having true long-range configurational order. A nonexponentially damped solution of (23) would yield scattering patterns of the crystalline solid, rather than the fluid, variety.

Introduce the following Fourier transforms:

$$Y_+(z)=\int_0^{+\infty}\chi''(R)\exp(izR)dR,$$
$$Y_-(z)=\int_{-\infty}^0\chi''(R)\exp(izR)dR,$$
$$H_+(z)=\int_0^{+\infty}h(R)\exp(izR)dR,$$
$$H_-(z)=\int_{-\infty}^0 h(R)\exp(izR)dR,$$
$$j(z)=\int_{-\infty}^{+\infty}g'(R)\exp(izR)dR. \quad (24)$$

If the first, second, and last of Eqs. (24) are integrated by parts, one finds

$$Y_+(z)=-\chi'(0)+i\chi(0)z-z^2X_+(z),$$
$$Y_-(z)=-Y_+(-z),$$
$$X_+(z)=\int_0^{+\infty}\chi(R)\exp(izR)dR,$$
$$i(z)=2+2z\int_0^{+\infty}\sin(zR)[g(R)-1]dR, \quad (25)$$

where the odd character $\chi(R)$, and the even character of $g'(R)$ have been used. In view of the condition on $\chi(R)$ at infinity already mentioned, we know that $X_+(z)$ is an analytic function of z for

$$\mathrm{Im}(z)>-\epsilon; \quad (26)$$

the same conclusion holds for $Y_+(z)$.

If A is the largest positive constant for which $\exp(AR)[g(R)-1]$ is bounded as $R\to+\infty$, then $j(z)$ is analytic in the strip

$$-A<\mathrm{Im}(z)<+A. \quad (27)$$

By virtue of our former observations concerning the asymptotic nature of $g(R)$ as contrasted with the corresponding behavior of the ionic correlation functions, we may suppose that $A>\epsilon$. The integrodifferential Eq. (23) is therefore equivalent to

$$\int_{-\infty+i\lambda}^{+\infty+i\lambda}[Y_-(z)-H_-(z)+(\kappa^2/2)j(z)X_+(-z)]\times\exp(-iRz)dz + \int_{-\infty+i\mu}^{+\infty+i\mu}[Y_+(z)-H_+(z)-(\kappa^2/2)j(z)X_+(z)]\times\exp(-iRz)dz=0,$$
$$-A<\lambda<+\epsilon, \quad -\epsilon<\mu<+A. \quad (28)$$

Appealing to a well-known theorem concerning Fourier transforms,[6] we write for the entire strip (27),

$$[Y_-(z)-H_-(z)+(\kappa^2/2)j(z)X_+(-z)]$$
$$+[Y_+(z)-H_+(z)-(\kappa^2/2)j(z)X_+(z)]=0; \quad (29)$$

the content of each square bracket is itself analytic in this strip. Insert the results (25) for Y_+ and Y_- in (29) to obtain

$$X_+(z)-X_+(-z)=\frac{2i\chi(0)z-H_+(z)-H_-(z)}{z^2+(\kappa^2/2)j(z)}. \quad (30)$$

The combination $X_+(z)+X_+(-z)$ is the Fourier transform of the odd extension onto the negative real axis of a function defined on the positive axis; since $\chi(R)$ has already been defined to be odd, this difference is just the transform of $\chi(R)$ itself. The inversion integral immediately yields $\chi(R)$

$$\chi(R)=(1/2\pi)\int_{-\infty}^{+\infty}\frac{2i\chi(0)z-H_+(z)-H_-(z)}{z^2+(\kappa^2/2)j(z)}$$
$$\times\exp(-iRz)dz. \quad (31)$$

The arbitrary constant $\chi(0)$ corresponds to the complementary solution of the homogeneous integrodifferential equation, and its value must eventually be determined by satisfying the local electroneutrality condition (10).

The general solution to the integrodifferential Eq. (23), besides the function (31), will contain solutions of the homogeneous equation of the form,

$$\chi_n(R)=\exp(iz_nR)-\exp(-iz_nR), \quad (32)$$

where the complex numbers z_n satisfy

$$d(z_n)\equiv z_n^2+(\kappa^2/2)j(z_n)=0 \quad (33)$$

and

$$-A<\mathrm{Im}(z_n)<+A. \quad (34)$$

That each $\chi_n(R)$ is in fact such a solution may be easily verified by substitution. However, since the $\chi_n(R)$ fail to satisfy the condition of vanishing exponentially at infinity, they cannot be included in constructing physically meaningful fluid correlation functions.

The desired solution $\chi(R)$ is therefore given alone by the contour integral (31) which, upon closing the contour along the appropriate infinite semicircle, may be evaluated by the calculus of residues. When $R>0$, $\chi(R)$ has the form

$$\chi(R)=\sum_k A_k\exp(-iz_kR),$$

$$A_k=i\lim_{z\to z_k}\left[(z-z_k)\frac{2i\chi(0)z-H_+(z)-H_-(z)}{z^2+(\kappa^2/2)j(z)}\right]. \quad (35)$$

The summation covers the poles z_k of the integrand of (31) in the lower half-plane, and the constants A_k are related as shown in the usual way to the residues at these poles. Among the z_k are the roots of the transcendental Eq. (33). Since the inhomogeneous function $h(R)$ is known to drop to zero rapidly with increasing R, any poles of $H_+(z)$ and $H_-(z)$ $[=-H_+(-z)]$ remain well off the real axis; the contribution of the corresponding terms in (35) therefore dies to zero rapidly. One anticipates, therefore, that the large R form of $\chi(R)$ arises from a root of (33) nearer the real axis. For these values of R, the inhomogeneous function $h(R)$ is in evidence only in establishing the proper values of the multiplicative constants A_k.

When the Debye-Hückel parameter κ is sufficiently small, all of the roots of (33) have nonvanishing imaginary parts, so that (35) gives a properly damped $\chi(R)$. By examining the expression (25) for $j(z)$, it becomes clear that the denominator $d(z)$ always has the roots $\pm i\kappa$ in the limit $\kappa\to 0$. $\chi(R)$ behaves asymptotically in this limit as $\exp(-\kappa R)$, so that the Debye-Hückel limiting theory has again been identified. Now, though, we see that this result is independent of the exact nature of $g(R)$, and therefore of the short-range ion forces.

As κ increases (corresponding, for example, to a decrease in temperature of the fused salt at constant density), the poles of the integrand in (31) due to the roots of $d(z)$ tend to move onto, and collect along, the real axis.[7] Under this circumstance it is mandatory to adopt the principle value definition of the contour integral (31) to insure that $\chi(R)$ remain an odd function of R, and a smooth function of κ (so long as the salt remains in a single fluid phase). The terms in the sum (35) corresponding to these poles along the real axis appear to give undamped contributions to $\chi(R)$, in contradiction to our condition on this function at $R=+\infty$. In addition, it may be shown that such contributions would give rise to Bragg-like x-ray scattering reflections.[8] It is necessary, as a consequence to recognize that A_k must vanish as z_k becomes real, to remove these spurious terms in $\chi(R)$. So far as (31) is concerned, we may infer that for each real z_k,

$$2i\chi(0)z_k-H_+(z_k)-H_-(z_k)=0. \quad (36)$$

Preliminary calculations on the remaining members of the sum (35) indicate that $\chi(R)$ oscillates in sign (and of course decays to zero), with a period roughly comparable to the nearest neighbor distance. By referring to the mean electrostatic charge densities $\rho_+^{(el)}(R)$ and $\rho_-^{(el)}(R)$, (9), it can be seen that every ion is surrounded on the average by concentric spherical shells of alternating sign. This characteristic un-

[6] E. C. Titchmarsh, *Introduction to the Theory of Fourier Integrals* (Oxford University Press, New York, 1950), p. 255.

[7] This typical behavior has already been noted and discussed in a similar computation in J. G. Kirkwood and J. C. Poirier, J. Phys. Chem. **58**, 591 (1954).

[8] P. J. Wojtowicz, unpublished thesis, Yale University, 1956.

doubtedly corresponds to a local ordering of the ions in a "smeared out" lattice type of structure similar to the lower temperature solid phase. In the latter as well, each ion has shells of neighbors of alternating charge.

IV.

The "hybrid" correlation function g_m has already been regarded as showing little of the rather long-ranged order induced by the ionic charges. By adapting some of the ideas of order-disorder theory,[9] we shall now find that it is possible to estimate g_m as the pair correlation function in a single-component fluid, the dominant part of whose particle interactions is just $V_N^{(0)}$.

In view of Eq. (11) and the last of Eqs. (16), $g_m(r, \xi_1)$ may be written as

$$g_m(r_{10}, \xi_1) = [\mathcal{V}^2/(N-1)]\sum_{i=2}^{N}\int_{\mathcal{V}}\cdots\int_{\mathcal{V}} \times\exp\left[\frac{A_N(\xi_1)-V_N(\mathbf{r}_1\cdots\mathbf{r}_N,\xi_1)}{kT}\right] \times\delta(\mathbf{r}_i-\mathbf{r}_0)d\mathbf{r}_2\cdots d\mathbf{r}_N, \quad (37)$$

to within terms of entirely negligible order. The delta function in the integrand of (37) constrains each ion of the set $2\cdots N$ to occupy in turn a position $\mathbf{r}_0$ at distance r_{10} from the variably charged ion 1. In the configuration integrations, not only are the positions of the remaining $N-2$ ion centers variable, but for a fixed set of such positions, the cations and anions may be distributed in a large number of distinct ways. Let us therefore perform first a thermal average over the various ways of occupying the $N-1$ sites at $\mathbf{r}_2\cdots\mathbf{r}_N$, and subsequently carry out the configuration integrations. It is by means of this artifice that the temperature dependent "potential" Ψ_N is introduced by the average, over the various modes of occupation, of $\exp[-(V_N/kT)]$.

$$\exp[-(kT)^{-1}\Psi_N(\mathbf{r}_1\cdots\mathbf{r}_N,\xi_1,T)] =[N_c!N_a!/(N_c+N_a)!]\sum_{\xi_2\cdots\xi_N=\pm1}' \times\exp[-(kT)^{-1}V_N(\mathbf{r}_1\cdots\mathbf{r}_N,\xi_1\cdots\xi_N)]. \quad (38)$$

The summation $\sum'$ is subject to the restriction[4]

$$\sum_{i=2}^{N}\xi_i=0, \quad (39)$$

and N_c and N_a denote the number of cations and anions among the members of the set of ions $2\cdots N$. After the averaging operation (39), the positions $\mathbf{r}_2\cdots\mathbf{r}_N$ are all equivalent in the sense that Ψ_N is invariant to interchange of any pair of them. Accordingly, each term of the sum (37) becomes identical when (38) is employed, so that

$$g_m(r_{12},\xi_1)=\mathcal{V}^2\int_{\mathcal{V}}\cdots\int_{\mathcal{V}} \times\exp\left[\frac{A_N(\xi_1)-\Psi_N(\mathbf{r}_1\cdots\mathbf{r}_N,\xi_1,T}{kT}\right]d\mathbf{r}_3\cdots d\mathbf{r}_N,$$

$$\exp[-A_N(\xi_1)/kT]=\int_{\mathcal{V}}\cdots\int_{\mathcal{V}} \times\exp\left[-\frac{\Psi_N(\mathbf{r}_1\cdots\mathbf{r}_N,\xi_1,T)}{kT}\right]d\mathbf{r}_1\cdots d\mathbf{r}_N. \quad (40)$$

When these last expressions are compared with the definitions (11), we conclude that g_m is exactly the correlation function in a system of N particles whose interaction potential is Ψ_N. These particles are all identical excepting particle 1 (it would be like the others if $|\xi_1|=1$).

A differential equation for Ψ_N follows directly from the definition of this quantity in (38),

$$\frac{\partial(\Psi_N(\xi_1,T)/kT)}{\partial(1/kT)}=\langle V_N(\xi_1)\rangle,$$

$$\langle V_N(\xi_1)\rangle=V_N^{(0)}+[(ze)^2/D]\sum_{i<j=1}^{N}r_{ij}^{-1}\langle\xi_i\xi_j\rangle,$$

$$\langle f\rangle=\frac{\sum_{\xi_2\cdots\xi_N=\pm1}' f\exp[-V_N(\xi_1\cdots\xi_N)/kT]}{\sum_{\xi_2\cdots\xi_N=\pm1}'\exp[-V_N(\xi_1\cdots\xi_N)/kT]}. \quad (41)$$

At infinite temperature, the Coulomb forces acting between the fused-salt ions are ineffective in discriminating between arrangements of the ions over the sites $\mathbf{r}_2\cdots\mathbf{r}_N$, i.e., the ions are randomly mixed. Each average value $\langle\xi_i\xi_j\rangle$, therefore, vanishes at infinite temperature due to equal probability of anionic and cationic occupation of neighboring sites. Consequently,

$$\Psi_N(\xi_1, T=\infty)=V_N^{(0)}, \quad (42)$$

so that Ψ has reduced to precisely the ion core interaction. In view of this boundary condition, the differential equation (41) may formally be integrated,

$$\Psi_N(\xi_1,T)=V_N^{(0)}+\frac{(ze)^2kT}{D}\sum_{i<j=1}^{N}\frac{1}{r_{ij}}\int_0^{1/kT}\langle\xi_i\xi_j\rangle_{T'}d\left(\frac{1}{kT'}\right). \quad (43)$$

[9] Z. W. Salsburg, P. J. Wojtowicz, and J. G. Kirkwood, J. Chem. Phys. 26, 1533 (1957).

Each of the $N(N-1)/2$ quantities $\langle \xi_i \xi_j \rangle$ depends upon all N positions $\mathbf{r}_1 \cdots \mathbf{r}_N$, including of course $\mathbf{r}_i$ and $\mathbf{r}_j$ themselves. We shall, however, replace this prohibitively complicated function by its value computed for a pair of neighboring sites in the fused-salt medium, separated by distance r_{ij}. Roughly speaking, this procedure effectively "homogenizes" the residual discrete set of $N-2$ ion sites, since in the fused salt their positions are not fixed. Thus,

$$\langle \xi_i \xi_j \rangle \cong \frac{g_{+\,+}^{(2)}(r_{ij}) - g_{+\,-}^{(2)}(r_{ij})}{g_{+\,+}^{(2)}(r_{ij}) + g_{+\,-}^{(2)}(r_{ij})}$$

$$= -\tanh[\chi(r_{ij}, 1)/kTr_{ij}] \quad i, j \neq 1,$$

$$= -\xi_1 \tanh[\chi(r_{ij}, \xi_1)/kTr_{ij}] \quad i, j = 1, \qquad (44)$$

where reference has been made to Eqs. (8) and (21). In this approximation, the electrostatic contribution to Ψ_N is therefore a sum of centrally symmetric, pairwise additive contributions,

$$\Psi_N(\xi_1, T) = V_N^{(0)} + \sum_{j=2}^{N} \psi(r_{1j}, \xi_1) + \sum_{i<j=2}^{N} \psi(r_{ij}, 1),$$

$$\psi(r_{ij}, \xi) = -[(ze)^2 kT\xi/Dr_{ij}] \int_0^{(1/kT)} \times \tanh[\chi(r_{ij}, \xi)/kT' r_{ij}] d(1/kT'). \qquad (45)$$

The particle interactions in the fictitious single component fluid for which g_m is the pair correlation function are thus nearly given by the short-range core forces supplemented by the $\psi(r_{ij})$[10]. Since χ for all temperatures in the fused-salt system is an exponentially damped function of distance, the pair interactions $\psi(r_{ij})$ also drop to zero very rapidly.[11] As a result, the correlations induced by these interactions will not possess the relatively long-range character of the ionic pair distribution functions.

As a practical matter, g_m is probably determined for the most part by the ion-core potential $V_N^{(0)}$ alone, since for the high temperatures encountered in fused salts, the $\psi(r_{ij})$ will not be very large. It is $V_N^{(0)}$ which leads one to picture the ion cores as a set of rather impenetrable spheres; $V_N^{(0)}$ then effectively forces the ions into local close-packed latticelike arrangements. An approximate g_m, computed by taking into account only $V_N^{(0)}$, implicitly contains the requisite geometrical restrictions on possible ion positions, and should be adequate to determine closely the ion distributions by the technique of Sec. III.

[10] In a formal way it is a simple matter to improve the estimate (45) of Ψ_N. To do so, it is necessary to correct systematically for the discrete nature of the environment of the sites $\mathbf{r}_i$ and $\mathbf{r}_j$ as it affects $\langle \xi_i \xi_j \rangle$. The result of the first step in this correction procedure is to add to (45) three-body interactions, whose computation requires knowledge of the fused-salt ion triplet correlations. Their inclusion should in no way modify our conclusions regarding the qualitative nature of g_m.

[11] It is elementary to verify for example that if $\chi(r)$ is the Debye-Hückel result $\chi(0) \exp(-\kappa r)$, $\psi(r)$ behaves for large r as r^{-6}.

APPENDIX

Since one has been up to the present in a position to state no more than the qualitative features of the superposition defect functions $\epsilon^{(3)}$, we shall attempt only to relate the supposed asymptotic behavior of $E(r_{12}, \xi_1)$ to a set of unproved, though not unreasonable, assumptions concerning the $\epsilon^{(3)}$. Complete justification must await future analysis of these assumptions in terms of general statistical theory.

Now since each $\epsilon^{(3)}(123)$ [like the triplet potentials of mean force $W^{(3)}$] will have an appreciable magnitude only when at least one of the three ion-pair distances (r_{12}, r_{13}, r_{23}) is small, there are just two significant regions of the $E(r_{12}, \xi_1)$ integration (16) to be considered (we already have made r_{12} large). These are characterized by:

1. r_{23} small (and hence r_{13} large),
2. r_{13} small (so that r_{23} must be large).

The curly-bracketed portion of the integrand of E in Eq. (16) reduces, in these two cases, essentially to

$$1.\ \{\ \} = \exp[-W_{+\,+}^{(2)}(23)/kT] \times [\epsilon_{1+\,+}^{(3)}(123, \xi_1') + \epsilon_{1+\,+}^{(3)}(123, -\xi_1')] - \exp[-W_{+\,-}^{(2)}(23)/kT] \times [\epsilon_{1-\,+}^{(3)}(123, \xi_1') + \epsilon_{1-\,+}^{(3)}(123, -\xi_1')] \qquad (A1)$$

$$2.\ \{\ \} = g_{1+}^{(2)}(13, \xi_1') \times [\epsilon_{1+\,+}^{(3)}(123, \xi_1') - \epsilon_{1-\,+}^{(3)}(123, \xi_1')] + g_{1+}^{(2)}(13, -\xi_1') \times [\epsilon_{1+\,+}^{(3)}(123, -\xi_1') - \epsilon_{1-\,+}^{(3)}(123, -\xi_1')]. \qquad (A2)$$

For case 1, regarding the vector $\mathbf{r}_{23}$ as fixed, it will be supposed that the quantities

$$\epsilon_{1+\,+}^{(3)}(123, \xi_1') + \epsilon_{1+\,+}^{(3)}(123, -\xi_1') \qquad (A3)$$

and

$$\epsilon_{1-\,+}^{(3)}(123, \xi_1') + \epsilon_{1-\,+}^{(3)}(123, -\xi_1') \qquad (A4)$$

each become zero faster than $\phi(r_{12}, \xi_1')$ as the vector $\mathbf{r}_{12}$ increases in length. Case 2 suggests one assume (for fixed $\mathbf{r}_{13}$ now) that the combinations

$$g_{1+}^{(2)}(13, \xi_1') \epsilon_{1+\,+}^{(3)}(123, \xi_1') + g_{1+}^{(2)}(13, -\xi_1') \epsilon_{1+\,+}^{(3)}(123, -\xi_1') \qquad (A5)$$

and

$$g_{1+}^{(2)}(13, \xi_1') \epsilon_{1-\,+}^{(3)}(123, \xi_1') + g_{1+}^{(2)}(13, -\xi_1') \epsilon_{1-\,+}^{(3)}(123, -\xi_1') \qquad (A6)$$

go to zero with increasing magnitude of r_{12} faster than $\phi(r_{12}, \xi_1')$. These hypotheses appear to be the weakest such set, consistent with the general ideas of molecular distributions, which will insure that $E(r_{12}, \xi_1)$ vanish more rapidly than $\phi(r_{12}, \xi_1)$, for each ξ_1, as r_{12} becomes infinite. If, incidentally, $E(r_{12}, \xi_1)$ did not have the stated asymptotic behavior, then it would not even appear possible to deduce the Debye-Hückel theory for high temperatures.

The nature of the quantities (A3) and (A4) may be given rough interpretation. The pair of ions 2 and 3 (which are close to each other) act, from the standpoint of the far removed ion 1, as a single-charge entity. We have claimed in effect that, first, the potential of average force acting between this double ion and ion 1 is not equal to the sum of the two single ion parts (potential of average force of ions 2 and 1, and of 3 and 1). Secondly (and this is the significant point) the excess of this double-ion effect over the sum of its separate ion effects is nearly opposite for opposite charges on ion 1. Therefore, at large distances r_{12}, the pairs of terms in (A3) and (A4) tend to cancel.

As regards (A5) and (A6), a similar crude interpretation may be drawn. Now, though, ions 1 and 3 are in close proximity (constituting the double ion), and ion 2 is isolated. Since ion 1 may have either charge $+\xi_1'ze$ or $-\xi_1'ze$, the double ion may have either greater, or less, total charge than ion 3 alone. The occurrence probabilities of charges $+\xi_1'ze$ and $-\xi_1'ze$ on ion 1 in the neighborhood of cation 3 are of course governed by $g_{1+}^{(3)}(13, \xi_1')$ and $g_{1+}^{(2)}(13, -\xi_1')$, respectively. (A5) and (A6) state that the superposition defect averaged over the two possible compositions of the double ion drops to zero sufficiently fast. Again it is presumed that at large r_{12} the pairs of terms in each of (A5) and (A6) cancel.

Nonstoichiometry and Ferroelectric Properties of $PbNb_2O_6$-Type Compounds*

E. C. SUBBARAO AND G. SHIRANE

Westinghouse Research Laboratories, Pittsburgh 35, Pennsylvania

(Received January 8, 1960)

The crystal structure of $PbNb_2O_6$ consists of a framework of NbO_6 octahedra linked through corners. The Pb^{2+} ions occupy 5 out of the 6 available interstitial sites in this framework. Single-phase compositions have been prepared by solid-state reactions to yield nonstoichiometric compounds of the form $A_{1+x}B_2O_6$ where A and B may consist of two ions of different valency and x has values between -0.08 and 0.15. In these materials, the number of unfilled interstitial sites inherently present in $PbNb_2O_6$ lattice has been varied. Lattice parameter and x-ray intensity data confirm that the additional ions introduced occupy the same sites as Pb^{2+} ions.

The ferroelectric Curie temperature has been studied as a function of the composition of these dielectric solids. For compositions with $x>0$, the Curie temperature is not very sensitive to composition. As the number of unfilled interstitial sites increases ($x<0$), the Curie temperature decreases sharply.

I. INTRODUCTION

In recent years there has been a growing interest in the structure and structure-sensitive physical properties of chemically imperfect solids. Defects which have a remarkable control over the properties of the host lattice may be induced in many inorganic compounds. The following may be cited as examples of oxides with induced departures from ideal composition:

(a) The lithium-substituted transition-metal oxides[1,2] which possess interesting electrical and magnetic properties. These oxide semiconductors contain the transition metal ion in two valence states. These materials which have the formula type $Li_xM_{1-x}O$ crystallize with the NaCl-type structure.

(b) The so-called alkali tungsten bronzes, A_xWO_3 with $x<1$.[3,4] Besides the presence of tungsten ions of mixed valency, these compounds are characterized by the introduction of alkali ions into vacant lattice sites. The electrical[5,6] and magnetic[7] properties of these compounds with variable composition have also been studied.

In substitutional solid solutions, crystallographically equivalent sites are occupied by different kinds of atoms. The foregoing examples differ from this simple case by possessing one or both of the following additional variables to control the composition (and thereby the properties) of the host lattice, (a) mixed valency (b) variable occupancy of lattice sites. In the case of dielectric solids, control of the number of filled lattice sites, without involving mixed valency of any of the ions, should be a fruitful means of achieving departures from stoichiometry (or simple atomic ratios). However, not much information seems to be available on insulating compounds with deviations from ideal composition. The recent reports on the role of lattice vacancies on the properties of perovskite-type compounds like $BaTiO_3$,[8,9] $NaNbO_3$,[10,11] and $PbTiO_3$[12] are a beginning in this direction. From this standpoint, lead metaniobate, $PbNb_2O_6$, which intrinsically has lattice vacancies, should be an interesting compound to study.

Lead metaniobate is orthorhombic at room temperature with the following lattice parameters[13]:

$$a=17.65,\ b=17.91,\ \text{and}\ c=7.736\ \text{A}.$$

There are 20 molecules in the unit cell. Due to the large size of the unit cell and the complexity of the x-ray patterns, no detailed structure analysis of $PbNb_2O_6$ is as yet available. $PbNb_2O_6$ has an orthorhombic-tetragonal transition at 570°C. The orthorhombic phase arises by a slight distortion of the tetragonal form. On the basis of the x-ray powder photographs, Francombe and Lewis[13] have pointed out the very close resemblance between the structure of some tetragonal alkali tungsten bronzes and that of the tetragonal modification of $PbNb_2O_6$. The projection of the structure[14] of tetragonal potassium tungsten bronze ($K_{0.57}WO_3$) along the [001] axis is shown in Fig. 1. The projection indicates a tetragonal cell dimension, a, of 12.5 A, which corresponds to [110] of the orthorhom-

* Research supported in part by contract with the Army Ordnance Corps.

[1] R. R. Heikes and W. D. Johnston, J. Chem. Phys. **26**, 582 (1957).

[2] W. D. Johnston, R. R. Heikes and D. Sestrich, J. Phys. Chem. Solids **7**, 1 (1958).

[3] G. Hägg and A. Magneli, Rev. Pure Appl. Chem. **4**, 235 (1954).

[4] A. Magneli, J. Inorg. Nuclear Chem. **2**, 330 (1956).

[5] E. J. Huibregtse, D. B. Barker, and G. C. Danielson, Phys. Rev. **84**, 142 (1951).

[6] D. B. Brown and E. Banks, Phys. Rev. **84**, 609 (1951).

[7] P. M. Stubbins and D. P. Mellor, Proc. Roy. Soc. New South Wales **82**, 255 (1948).

[8] G. A. Smolenskii, V. A. Isupov, and A. I. Agranovskaya, Doklady Akad. Nauk. S.S.S.R. **113**, 1053 (1957).

[9] E. C. Subbarao and G. Shirane, J. Am. Ceram. Soc. **42**, 279 (1959).

[10] B. Lewis and E. A. D. White, J. Electronics **1**, 646 (1956).

[11] M. H. Francombe and B. Lewis, J. Electronics **2**, 387 (1957).

[12] E. C. Subbarao, J. Am. Ceram. Soc. **43**, 119 (1960).

[13] M. H. Francombe and B. Lewis, Acta Cryst. **11**, 696 (1958).

[14] A. Magneli, Arkiv Kemi **1**, 213 (1949).

bic form. Along the c direction, WO_6 or NbO_6 octahedra are linked through corners to form O–metal–O chains, as in the case of perovskite-type structure. Also, the observed c (or $\frac{1}{2}c$, if the cell is doubled) parameter of $PbNb_2O_6$ (3.9 A) is close to the cell dimensions of perovskite-type compounds. Parallel to (001), the structure consists of WO_6 (or NbO_6 in the case of $PbNb_2O_6$) octahedra linked through the corners in a complicated manner forming rings of three, four, and five octahedra. The enclosed spaces possessing eight- and ten-fold oxygen coordination are designated "cages" and "tunnels," respectively.[15] The alkali ions (or Pb^{2+} ions) occupy these A-type sites. The similarity of the "cage" sites and the surrounding octahedra to the perovskite structure is noteworthy. There are two "cage" and four "tunnel" sites for occupancy by A-type ions. In $PbNb_2O_6$, only five out of the six available interstitial sites are occupied by Pb^{2+} ions. It is not known whether the unfilled sites are ordered or not.

Substitutional solid solutions based on $PbNb_2O_6$ in which Pb^{2+} is replaced by other divalent ions and Nb^{5+} by Ta^{5+} have been studied by several investigators.[13,16–18] On the other hand, the major purpose of this investigation was to study whether the fraction of the A-type sites occupied can be increased or decreased from that filled by Pb^{2+} ions in $PbNb_2O_6$. If variable composition can be achieved in $PbNb_2O_6$-type materials, it was proposed to determine the compositional limits beyond which the $PbNb_2O_6$ type structure collapses or a second phase appears. It would then be interesting to examine the influence of such departures from ideal composition and crystalline perfection on the physical properties of these materials. Thus, inasmuch as $PbNb_2O_6$ is ferroelectric[19] with a Curie temperature at 570°C, the dielectric properties and the phase transition from the orthorhombic to the tetragonal symmetry[20] at the Curie temperature may be studied as a function of the composition of these materials.

The following reactions were used in an effort to fill the vacant A-type sites:

$$\text{(i)}\quad (1-x)\ PbNb_2O_6 + x\ Pb_2Ti_2O_6 \rightarrow Pb_{1+x}(Ti_xNb_{1-x})_2O_6. \quad (1)$$

Instead of $Pb_2Ti_2O_6$, $Pb_2Zr_2O_6$ and "$Pb_2Sn_2O_6$" may also be used.

$$\text{(ii)}\quad (1-x)\ PbNb_2O_6 + x\ Na_2Nb_2O_6 \rightarrow (Pb_{1-x}Na_{2x})Nb_2O_6. \quad (2)$$

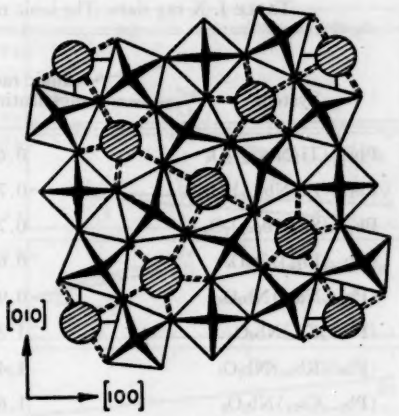

FIG. 1. Projection of the structure of tetragonal $K_{0.57}WO_3$ or paraelectric $PbNb_2O_6$ parallel to [001]. K^+ or Pb^{2+} ions (circles) are located ($Z=0$) in "tunnels" or "cages" formed by WO_6 or NbO_6 octahedra ($Z=\pm\frac{1}{2}$).

Here Li, K, Rb, and Cs may be employed in place of Na. An attempt to increase the number of unfilled A-type sites was made in the following manner:

$$(1-x)\ PbNb_2O_6 + x\ Y_{\frac{1}{3}}Nb_2O_6 \rightarrow (Pb_{1-x}Y_{\frac{1}{3}x})\ Nb_2O_6. \quad (3)$$

For the trivalent ion, Y, La, and Sm were tried. It may be expected that other trivalent rare earth ions behave in a similar manner.

$PbNb_2O_6$ prepared below about 1250°C, has rhombohedral symmetry[21,22] and is not ferroelectric. Sintering above 1250°C results in the ferroelectric phase which possesses orthorhombic symmetry at room temperature. The present study was concerned with the orthorhombic modification and the corresponding tetragonal phase.

2. EXPERIMENTAL

(a) Preparation

The compositions corresponding to the Eqs. (1) to (3) were prepared by solid state reaction of the appropriate oxides or carbonates of reagent grade. Niobium pentoxide, supplied by the Kennametal Company, was 99.5% grade. The largest impurities in this material, determined by spectrographic analysis are Fe(100 ppm) and Sn(500 ppm). The desired amounts of the materials were mixed under acetone in a glass mortar and sintered in powder form at temperatures between 1160° and 1290°C. The presintered material was ground, pressed into disks, and the disks resintered at 1230° to 1330°C. Appropriate sintering temperatures were chosen to ensure the absence of the rhombohedral phase of $PbNb_2O_6$ in the final product. The sintering was accomplished in covered platinum crucibles in a Globar furnace in air. Weight loss was determined at

[15] A. D. Wadsley, Rev. Pure Appl. Chem. **5**, 165 (1955).
[16] V. A. Isupov and V. I. Kosyakov, Zhur. Tekh. Fiz. **28**, 2175 (1958).
[17] K. E. Nelson and R. L. Cook, J. Am. Ceram. Soc. **42**, 138 (1959).
[18] E. C. Subbarao, G. Shirane, and F. Jona, Acta Cryst. **13**, 226 (1960).
[19] G. Goodman, J. Am. Ceram. Soc. **36**, 368 (1953).
[20] R. S. Roth, Acta Cryst. **10**, 437 (1957).
[21] M. H. Francombe, Acta Cryst. **9**, 683 (1956).
[22] R. S. Roth, J. Research Natl. Bur. Standards **62**, 27 (1959).

TABLE I. X-ray data. The ionic radii (after Ahrens[23]) of Pb^{2+} is 1.20 and Nb^{5+} 0.69 A.

System	Ionic radius of substituting ion, A	$\%(\Delta V/V)$ per 1% of Pb^{2+} or Nb^{5+} replaced	Value of x at the solubility limit	Phase appearing beyond the solubility limit
$Pb_{1+x}(Ti_xNb_{1-x})_2O_6$	0.68	+0.19	~0.10	cubic
$Pb_{1+x}(Zr_xNb_{1-x})_2O_6$	0.79	+0.23	0.05–0.10	cubic
$Pb_{1+x}(Sn_xNb_{1-x})_2O_6$	0.71	−0.14	0.02–0.05	cubic
$(Pb_{1-x}Li_{2x})Nb_2O_6$	0.68	−0.04	0.05–0.10	$LiNbO_3$
$(Pb_{1-x}Na_{2x})Nb_2O_6$	0.94	−0.06	~0.15	$NaNbO_3$
$(Pb_{1-x}K_{2x})Nb_2O_6$	1.33	+0.10	~0.25	N.D.[a]
$(Pb_{1-x}Rb_{2x})Nb_2O_6$	1.47	+0.29	0.05–0.10	cubic
$(Pb_{1-x}Cs_{2x})Nb_2O_6$	1.67	+0.47	<0.02	cubic
$(Pb_{1-x}Y_{2/3x})Nb_2O_6$	0.92	−0.11	~0.25	N.D.
$(Pb_{1-x}Sm_{2/3x})Nb_2O_6$	1.00	−0.11	~0.25	N.D.
$(Pb_{1-x}La_{2/3x})Nb_2O_6$	1.14	−0.07	~0.20	N.D.

[a] N.D. = Not determined.

the various stages of the preparation and the total loss was less than 1% in all cases.

(b) X-Ray Examination

Powder patterns and diffractometer tracings of the fired specimens were obtained on Norelco x-ray diffraction equipment using copper K-alpha radiation. The preparation procedures employed resulted in a single phase material with orthorhombic $PbNb_2O_6$-type structure. The second phase appearing beyond the solubility limit was identified in some cases (Table I).[23]

The orthorhombic lattice parameters for the investigated compositions were computed from the (820), (280), and (004) reflections, recorded with Norelco diffractometer. These reflections appear between 40° and 48°2θ.

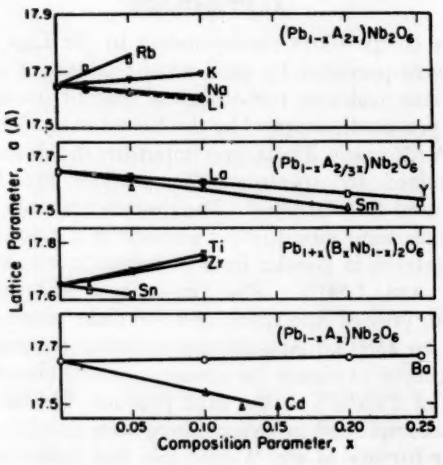

FIG. 2. Lattice parameter a vs composition in several $PbNb_2O_6$-type solid solutions.

[23] L. H. Ahrens, Geochim. Cosmochim. Acta **2**, 155 (1952).

(c) Dielectric Properties

The temperature dependence of dielectric constant was measured on silvered ceramic disks between 25° and 650°C using a capacitance bridge. The temperature corresponding to the dielectric constant maximum was designated as the Curie temperature. Since the dielectric behavior of compositions in the investigated systems was essentially similar to that of $PbNb_2O_6$, detailed dielectric data are not presented here.

3. RESULTS AND DISCUSSION

The small weight change (less than 1%) during the specimen preparation means that essentially all the starting materials were present in the final composition. X-ray powder diagrams showed that, up to the solubility limit, these compositions consist of a single phase of orthorhomibc $PbNb_2O_6$ type. Shifts in the lattice parameters and the Curie temperatures with composition substantiate the formation of solid solutions. On the basis of the similarity of ionic size (Table I), it may be expected that the tetravalent ions (Ti, Zr, and Sn) replace Nb^{5+} ions and the monovalent and the trivalent ions occupy the A-type sites in these solid solutions. The important characteristic of these compositions is that the fraction of the A-type sites filled either increased or decreased from that filled by Pb^{2+} ions in $PbNb_2O_6$. The observed changes in lattice parameters and x-ray intensities confirm that the occupancy of the A-type sites in $PbNb_2O_6$ can indeed be varied.

(a) Lattice Parameters

The variation of the lattice parameters a, b, and c with composition for the investigated systems is sum-

marized in Figs. 2 to 4. In these systems, the lattice parameters are influenced by two factors:

(1) Ionic size: As in substitutional solid solutions, the lattice expands or contracts, respectively, as the size of the substituting ion is larger or smaller than the ion being replaced.

(2) Stuffing: The introduction of ions into lattice sites, initially unoccupied, causes an expansion of the cell dimensions and unit cell volume (Table I).

These two factors may aid or oppose each other. It would, therefore, be instructive to compare the data for substitutional and "stuffed" systems containing ions of comparable size (e.g., Ba^{2+} and K^+; Cd^{2+} and Na^+). The lattice expands more in the potassium-containing samples than in the (Pb, Ba) Nb_2O_6 system. The lattice parameters of the sodium-containing specimens do not decrease with the composition parameter as rapidly as those of (Pb, Cd) Nb_2O_6. These results could be understood by considering that the additional alkali ions introduced occupy the vacant lattice sites. The same reasoning applies, as has recently been suggested,[24] to account for the expansion in the $Pb_{1+x}(Ti_xNb_{1-x})_2O_6$ system compared to the constancy of a and c parameters of $Pb(Ta_xNb_{1-x})_2O_6$ compositions.[18]

In these systems, the c increases more rapidly than a or b as the size of the alkali ion introduced increases (Figs. 2 to 4). This suggests that the stuffing of additional ions into the A-type sites brings about a straightening or "unpuckering" of the NbO_6 chains. On the basis of geometrical considerations, it appears reasonable to expect vacancies and the additional ions

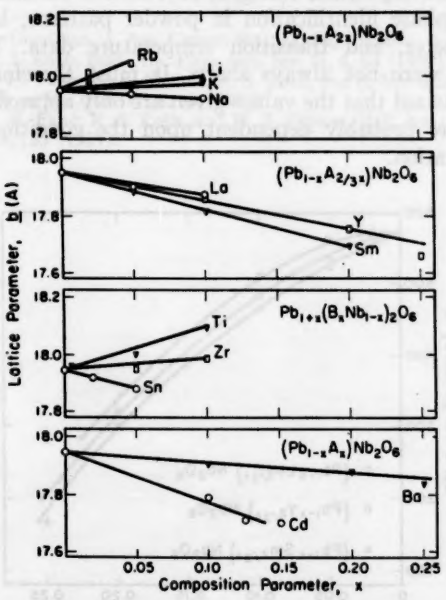

FIG. 3. Lattice parameter b vs composition in several $PbNb_2O_6$-type solid solutions.

[24] E. C. Subbarao, J. Am. Ceram. Soc. **42**, 448 (1959).

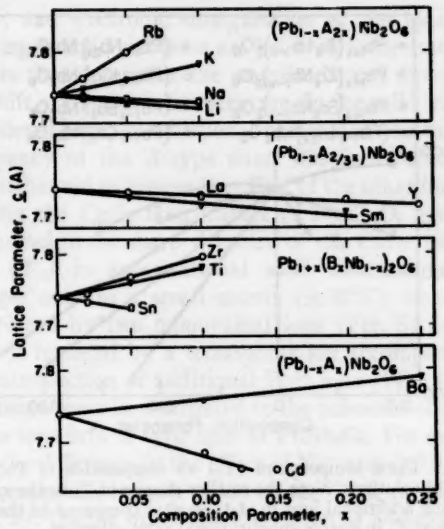

FIG. 4. Lattice parameter c vs composition in several $PbNb_2O_6$-type solid solutions.

to occupy the "cage" sites. It must be mentioned that the possibility of Li^+ ions going into the A-type sites formed by three NbO_6 octahedra or into the Nb^{5+} sites cannot be excluded on the basis of geometrical considerations.

In contrast to the large changes in the lattice parameters a and particularly c when additional ions are stuffed into $PbNb_2O_6$, these parameters are affected by composition only to a limited extent in the systems $(Pb_{1-x}A_{\frac{1}{3}x})Nb_2O_6$ where A is a trivalent ion (Fig. 2 and Fig. 4). However, the ferroelectric axis b shows a sharper decrease with composition in these systems, (Fig. 3) in agreement with the rapid drop of the Curie temperature (Fig. 6). On the other hand, b as well as the Curie temperature were found to be rather insensitive to composition in systems characterized by a higher fraction of filled A-type sites.

(b) X-Ray Intensities

The observed x-ray intensities for the (002) and (004) reflections of $PbNb_2O_6$ are consistent with those obtained by rather crude calculations assuming the relationship between the perovskite-type tungsten bronzes and $PbNb_2O_6$ suggested by Francombe and Lewis.[13] These intensities arise from $f_{Pb}-2f_{Nb}-f_O$ and $f_{Pb}+2f_{Nb}+3f_O$, respectively. Here, the f's are the scattering factors for the ions concerned. The structure factors for (002) and (004) of $PbNb_2O_6$ are 2.2 and 135.2, respectively. Actually the (002) reflection of $PbNb_2O_6$ is so weak that it could not be detected. However, when Pb^{2+} is partially replaced by a divalent ion of lower atomic number, such as Cd^{2+}, the $(1-x)f_{Pb}+xf_{Cd}$ would be less than f_{Pb} in $PbNb_2O_6$. Thus, replacement of 10% of Pb^{2+} by Cd^{2+} alters the structure factors of (002) and (004) to 4.3 and 132.5, respectively,

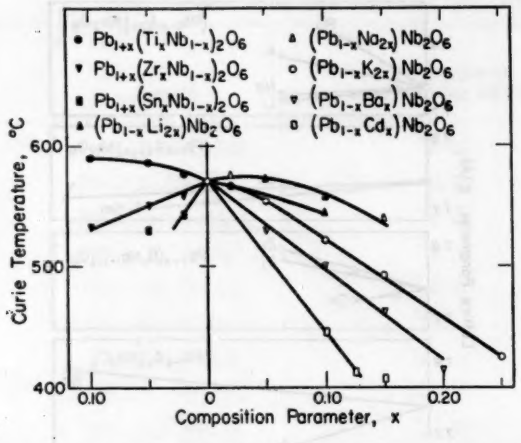

FIG. 5. Curie temperature (T_c) vs composition of $PbNb_2O_6$-type solid solutions. Note the smaller change of T_c in the systems containing additional ions in A-type sites compared to the rapid decrease of T_c in simple substitutional solid solutions.

in agreement with the observed trend in the intensities of these reflections. Similarly, replacement of 10% of Pb^{2+} by Na^+ leads to structure factors for (002) and (004) of 6.7 and 130.4, respectively. This is apparent in the increase of the observed intensity of (002) with Na^+. These data are not inconsistent with the assumption that the alkali ions introduced into these compounds occupy the A-type sites, some that were vacated by Pb^{2+} ions and others that were initially unfilled. The vacant sites and the additional Na^+ ions appear to be at the same level as the Pb^{2+} ions, referred to the c axis.

(c) Composition Limits

The evidence presented definitely shows that the composition of $PbNb_2O_6$ is variable within certain limits. The formula type of these compositions may best be represented by $A_{1+x}B_2O_6$ where A and B may consist of two ions of different valency and x can have both positive and negative values. The possibile variability of occupancy of the B-type and oxygen sites in this lattice were not studied in this investigation.

An attempt has been made to ascertain the limiting values of the composition parameter x. As in the case of divalent ion substitutions for Pb^{2+} in $PbNb_2O_6$, the ionic size seems to be the predominant factor in determining the extent of solid solubility of alkali ions in $PbNb_2O_6$. Thus the value of x in $(Pb_{1-x}A_{2x})Nb_2O_6$ varies (Table I) from less than 0.02 for $A=Cs^+$ to about 0.15 for $A=Na^+$. A limited amount of data on the $PbNb_2O_6$-type solid solutions was included in a study of the sodium-lead niobates by Francombe and Lewis.[11] They indicate that the solubility limit may be at about 30% Na and the corresponding transition temperature at about 280°C. The present study placed the solubility limit at somewhat below 15% Na with a Curie temperature of 550°C. At $x=0.25$, powder patterns showed a perovskite $NaNbO_3$-type phase besides the orthorhombic $PbNb_2O_6$-type solid solution. Also, this composition showed an additional dielectric anomaly at about 200°C corresponding to the $NaNbO_3$-type phase.

The data on the solid solutions where Nb^{5+} in $PbNb_2O_6$ was replaced by tetravalent ions show that, besides the size of ions in the A-type sites, the size of ions in Nb^{5+} sites may also influence the limiting value of the composition parameter x. Thus, the value of x decreased from about 0.10 for the case of Ti^{4+} to practically zero for Ge^{4+}. The lack of noble gaslike electronic shell in the case of Sn^{4+} may also be a factor in this instance.[25] (Ge^{4+} also lacks a rare gas shell.)

Thus, the upper limit of x in $A_{1+x}B_2O_6$ is about 0.15 (and somewhat higher in the case of K^+). Now let us examine the negative values of x, or the number of unoccupied A-type sites that can exist before a second phase appears. Trivalent ions in the form $A_{\frac{2}{3}}Nb_2O_6$ can be introduced into $PbNb_2O_6$ up to about 20% for $A=La$ and close to 25% for $A=Y$ or Sm, before a second phase appears. This leads to values of x between -0.07 and -0.08 in $A_{1+x}Nb_2O_6$. In summary, the composition of orthorhombic $PbNb_2O_6$-type materials may be described by $A_{1+x}B_2O_6$ with the occupancy of A-type sites varying between 0.92 and 1.15. These values may be compared with the composition limits for tetragonal potassium tungsten bronzes[14] which range from $K_{0.94}W_2O_6$ to $K_{1.14}W_2O_6$. The upper limit given above is in general agreement with the concept that only five out of the six available A-type sites are filled by Pb^{2+} ions in $PbNb_2O_6$.

The composition limits cited above were obtained from phase identification in powder patterns, lattice parameter, and transition temperature data. These limits were not always sharp. It must therefore be emphasized that the values given are only approximate and are probably dependent upon the conditions of preparation.

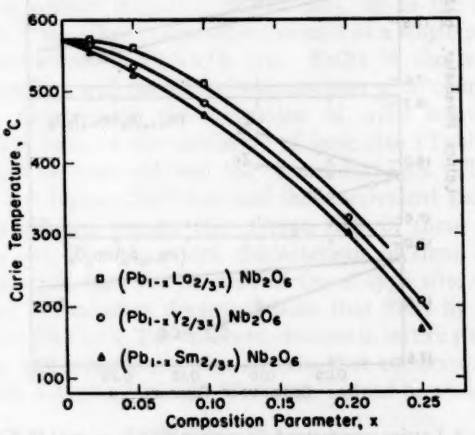

FIG. 6. Curie temperature vs composition in systems containing trivalent ions and additional unfilled A-type sites.

[25] S. Nomura, J. Phys. Soc. Japan **10**, 112 (1955).

Recently Goodman[26] and Roth and co-workers[27,28] reported ferroelectric behavior in compositions in the system $(BaNb_2O_6)_{1-x}(BaZrO_3)_x$ with x between 0.20 and 0.33. The formulas for the end members of these solid solution series are $Ba(Nb_{1.6}Zr_{0.2})O_{5.4}$ and $Ba(Nb_{1.34}Zr_{0.33})O_{5.0}$. Dielectric anomalies were observed as broad peaks in polycrystalline material in the vicinity of room temperature. These compositions are reported to have a tetragonal structure similar to that of $PbNb_2O_6$ above the Curie point. On the basis of these considerations, it may not be unreasonable to consider these compositions as members of the same family as $PbNb_2O_6$, but with a variable composition. The above formulas may be rewritten as $Ba_{1.11}(Zr, Nb)_2O_6$ and $Ba_{1.20}(Zr, Nb)_2O_6$ and are not far from the range assigned to $A_{1+x}B_2O_6$. Fang *et al.*[29] discussed a wide range of isomorphous substitutions possible in this type of systems.

(d) Ferroelectric Phase Transitions

In order to study the influence of the compositional variablity on the physical properties of $PbNb_2O_6$-type materials, the ferroelectric Curie temperature of these substances was chosen as the characteristic to examine. For purposes of comparison, a limited amount of data was obtained on the divalent ion substitutions for Pb^{2+} in $PbNb_2O_6$. These data are in substantial agreement with the results of others.[16-18]

All the attempted solid solutions of $PbNb_2O_6$ in which Pb^{2+} ions are replaced by other divalent ions, or Nb^{5+} by Ta^{5+} have resulted in a lowering of the Curie temperature of $PbNb_2O_6$ (Fig. 5). Ionic size, polarizability, and electronic configuration of the ions participating in solid solutions are believed to be among the factors that determine the magnitude and direction of the shift of the Curie temperature. In the solid solutions considered here, an additional parameter, the extent of occupancy of the A-type sites, was introduced. This may either aid or oppose the effect of the other factors in shifting the Curie temperature of $PbNb_2O_6$ materials. Compared to the sharp decrease of the Curie temperature (T_c) in substitutional solid solutions, the T_c changes only to a small extent ($\pm 30°C$) when Pb^{2+} is replaced by two monovalent ions (Fig. 5) or when Nb^{5+} is replaced by a tetravalent ion accompanied by the introduction of additional Pb^{2+} ions (Fig. 5). This difference must be attributed to the influence of stuffing excess ions into A-type sites of $PbNb_2O_6$. For example, note the difference in the effect of Na^+ and Cd^{2+} (which are comparable in ionic radii) on the Curie temperature (Fig. 5). On the other hand, creation of additional unfilled A-type sites appears to cooperate with the other factors in lowering the Curie temperature at a rapid rate (Fig. 6). These data demonstrate that the variation of the number of vacancies in the $PbNb_2O_6$-type lattice is a useful means of controlling the physical properties of this interesting family of ferroelectrics.

A phase change in addition to the one at the Curie temperature has been observed in compositions of the type $Pb_{1+x}(B_x^{4+}Nb_{1-x})_2O_6$ in the range 450–300°C depending on the value of x. This is discussed in detail elsewhere.[30]

ACKNOWLEDGMENTS

The authors wish to thank F. Jona and M. S. Lubell for helpful discussions. C. Merola and J. Hrizo took part in the preparation and dielectric measurements of this study.

[26] G. Goodman, J. Am. Ceram. Soc. **43**, 105 (1960).
[27] R. S. Roth, Bull. Am. Phys. Soc. Ser. II, **4**, 63 (1959).
[28] P. H. Fang, W. S. Brower, R. S. Roth, and S. Marzullo, Bull. Am. Phys. Soc. Ser. II, **4**, 64 (1959).
[29] P. H. Fang, R. S. Roth, and W. S. Brower, Bull. Am. Ceram. Soc. **38**, 183 (1959).
[30] E. C. Subbarao, J. Am. Ceram. Soc. (to be published).

Theory of Dilute Polymer Solution. III. Heterogeneous Polymer

HIROMI YAMAKAWA
Department of Textile Chemistry, Kyoto University, Kyoto, Japan
AND
MICHIO KURATA*
Department of Chemistry, Massachusetts Institute of Technology, Cambridge, Massachusetts
(Received January 11, 1960)

The second virial coefficients of osmotic pressure and light scattering of heterogeneous chain polymer solutions are calculated to the double-contact approximation. Two types are assumed for the molecular weight distribution: the Schulz distribution, and the distribution with two deltalike peaks.

Then, the heterogeneity corrections for intrinsic viscosity are evaluated on the assumption of the Schulz distribution. On the basis of the results obtained, a tentative attempt is made at interpreting the proportionality between the intrinsic viscosity at the Θ temperature and the square root of the molecular weight without discarding the hydrodynamic scheme, and the relation between the hydrodynamic and statistical radii of heterogeneous polymer coil is also examined.

Finally, the relation between the second virial coefficient A_2 and intrinsic viscosity $[\eta]$ is discussed somewhat in detail. And it is shown that the initial curvature of the curve of $[\eta]/[\eta]_\theta - 1$ vs $A_2M_w/[\eta]_\theta$ is concave upward for ordinary fractionated samples, where $[\eta]_\theta$ is the intrinsic viscosity at the Θ temperature, and M_w is the weight-average molecular weight. This statement is verified by comparison with experiment.

A. INTRODUCTION

IN the preceding papers,[1,2] we have treated theoretically various properties, related to the excluded volume effect, of dilute homogeneous polymer solutions. As a matter of fact, however, a completely homogeneous polymer can not be obtained even by fractionation. In this paper, therefore, we extend the previous theories[2] of the second virial coefficient and intrinsic viscosity to the case of heterogeneous polymers so that a thorough analysis of experimental data is made possible.

Now it is well known from a theoretical standpoint that the osmotic second virial coefficient A_2 coincides with the light-scattering second coefficient A_2' for homogeneous polymers,[3] but, in general, not for heterogeneous polymers,[4–7] and A_2 and A_2' depend on the molecular weight distribution in different manners from each other. We may say that the concrete expressions for A_2 and A_2' for heterogeneous polymers, nevertheless, have not yet been derived except in the investigation of Flory and Krigbaum,[7] in which the effect of heterogeneity on A_2 and A_2' has been examined by numerical calculations for mixtures of the two kinds of polymers differing in molecular weight. Thus, in Sec. B of this paper, we evaluate A_2 and A_2' on the assumption of an appropriate form of the molecular weight distribution, though only to the double-contact approximation.

The effect of heterogeneity on the intrinsic viscosity $[\eta]$ is of greater significance compared with that on the second virial coefficient, because the former has the direct and greater dependence on the molecular weight. This problem therefore has been discussed by many authors[8] both theoretically and experimentally, especially with respect to the viscosity average molecular weight. In Sec. C, we estimate the heterogeneity correction for the expression for intrinsic viscosity derived in Part II.[2] Now we know the experimental fact that the proportionality between the intrinsic viscosity $[\eta]_\theta$ at the Θ temperature and the square root of the molecular weight M holds over the wide range in M.[9] This is well interpreted by the Flory and Fox theory,[10] but not by the hydrodynamic theories.[11,12] Thus, using the results obtained for the effect of heterogeneity, we make a tentative attempt at interpreting the preceding relation without discarding the hydrodynamic scheme. Then, we examine also the relation between the hydrodynamic and statistical radii of heterogeneous polymer coils.

Finally, in Sec. D, we discuss the relation between the second virial coefficient and intrinsic viscosity somewhat in detail. In fact, this is one of the most important purposes of this paper. Recently, some attempts[13,14] have been made to deal with the experi-

* Sloan Foreign Post-Doctoral Fellow of the School for Advanced Study, Massachusetts Institute of Technology. Permanent address: Department of Industrial Chemistry, Kyoto University, Kyoto, Japan.

[1] M. Kurata, H. Yamakawa, and E. Teramoto, J. Chem. Phys. **28**, 785 (1958).

[2] M. Kurata and H. Yamakawa, J. Chem. Phys. **29**, 311 (1958).

[3] B. H. Zimm, J. Chem. Phys. **16**, 1093 (1948).

[4] H. C. Brinkmann and J. J. Hermans, J. Chem. Phys. **17**, 574 (1949).

[5] J. G. Kirkwood and R. J. Goldberg, J. Chem. Phys. **18**, 54 (1950).

[6] W. H. Stockmayer, J. Chem. Phys. **18**, 58 (1950).

[7] P. J. Flory and W. R. Krigbaum, J. Chem. Phys. **18**, 1086 (1950).

[8] See, for example, P. J. Flory, *Principles of Polymer Chemistry* (Cornell University Press, Ithaca, New York, 1953), Chap. VII, p. 311.

[9] See P. J. Flory, *Principles of Polymer Chemistry* (Cornell University Press, Ithaca, New York, 1953), Chap. XIV, p. 612.

[10] P. J. Flory and T. G. Fox, Jr., J. Am. Chem. Soc. **73**, 1904 (1951).

[11] J. G. Kirkwood and J. Riseman, J. Chem. Phys. **16**, 565 (1948).

[12] P. Debye and A. M. Bueche, J. Chem. Phys. **16**, 573 (1948).

[13] W. R. Krigbaum, J. Polymer Sci. **18**, 315 (1955).

[14] T. A. Orofino and P. J. Flory, J. Chem. Phys. **26**, 1067 (1957).

mental data by using a formula, such that $[\eta]/[\eta]_\theta - 1$ is expanded in powers of $A_2M/[\eta]_\theta$. For instance, Orofino and Flory[14] have obtained theoretically the result that the initial curvature of the curve of $[\eta]/[\eta]_\theta - 1$ vs $A_2M/[\eta]_\theta$ is concave downward. According to our theory[2] already developed, however, it appears that the initial curvature of the above curve is concave upward in contradiction to their theory. Now this curvature may possibly be affected by the effect of heterogeneity. Therefore, in order to obtain a final decision, we reexamine the relation mentioned above, taking care of the effect of heterogeneity, and also make comparison with experiment.

B. SECOND VIRIAL COEFFICIENT

B1. Basic Formulas

The osmotic pressure π and the intensity of scattering I of polymer solutions are related to the concentration c (in g per unit volume) by the following equations, respectively,

$$\pi/RTc = 1/M_n + A_2c + \cdots, \tag{B.1}$$

$$Kc/I = 1/M_w + 2A_2'c + \cdots, \tag{B.2}$$

where R is the gas constant, T is the absolute temperature, M_n is the number-average molecular weight, M_w is the weight-average molecular weight, K is a constant, and A_2 and A_2' are the second coefficients of osmotic pressure and light scattering, respectively.

According to the solution theory of McMillan and Mayer[15] and to the fluctuation theories,[5,6] A_2 and A_2' for heterogeneous polymers are written, respectively, as follows,

$$A_2 = \int_0^\infty \int_0^\infty A_{\alpha\beta} g(M_\alpha) g(M_\beta) dM_\alpha dM_\beta, \tag{B.3}$$

$$A_2' = (M_w^2)^{-1} \int_0^\infty \int_0^\infty A_{\alpha\beta} M_\alpha M_\beta g(M_\alpha) g(M_\beta) dM_\alpha dM_\beta, \tag{B.4}$$

where the function $g(M)$ represents the molecular weight distribution, such that $g(M)dM$ is the weight fraction of polymer of molecular weight M in the range dM, and $A_{\alpha\beta}$ is given by

$$A_{\alpha\beta} = -\frac{\mathbf{N}}{2VM_\alpha M_\beta} \int [F_2(\alpha, \beta) - F_1(\alpha) F_1(\beta)] d(\alpha) d(\beta), \tag{B.5}$$

which is one-half of the second virial coefficient for two polymers α and β of molecular weights M_α and M_β. Here, $\mathbf{N}$ is the Avogadro number, and V is the volume of the system. $F_1(\alpha)$, $F_1(\beta)$, and $F_2(\alpha, \beta)$ are the molecular distribution functions of McMillan and Mayer, and (α) or (β) denotes the total coordinate of each polymer.

In order to evaluate A_2 and A_2' given by Eqs. (B.3) and (B.4), respectively, first we calculate $A_{\alpha\beta}$. This can be easily performed by employing the procedure[2,16,17] of evaluating A_2 for homogeneous polymers, provided that the double-contact approximation is concerned. Here we merely outline the calculation.

Now we suppose that polymer molecule α consists of $N_\alpha + 1$ segments of diameter b, which are linearly connected by N_α links of a constant length a and are numbered from 0_α to N_α, and, similarly, molecule β consists of $N_\beta + 1$ segments. If we introduce a function $\chi(R_{ij})$ defined by

$$\chi(R_{ij}) \equiv \chi_{ij} = \exp(-u_{ij}/\mathbf{k}T) - 1, \tag{B.6}$$

where u_{ij} represents a short-range interaction potential as function of the distance R_{ij} between segments i and j, and $\mathbf{k}$ is the Boltzmann constant, we can express $A_{\alpha\beta}$ in the expanded form,

$$A_{\alpha\beta} = -(\mathbf{N}/2VM_\alpha M_\beta)(B_1 + B_2 + \cdots) \tag{B.7}$$

with

$$B_n = \sum \int [\prod_{n \text{ pairs}} \chi_{k_\alpha, k_\beta}] p_n\{n_\alpha\} p_n\{n_\beta\} d\{n_\alpha\} d\{n_\beta\}, \tag{B.8}$$

where the symbol $\prod$ represents the product of n different χ_{k_α, k_β}'s and the summation extends over all possible configurations. $p_n\{n_\alpha\}$ denotes the reduced segment distribution function defined by

$$p_n\{n_\alpha\} = \int F_1(\alpha) d\{N_\alpha + 1\}/d\{n_\alpha\}, \tag{B.9}$$

which is the probability of observing a particular set of n_α segments in $d\{n_\alpha\}$ at $\{n_\alpha\}$, irrespective of the coordinates of the remaining segments, where $\{n_\alpha\}$ represents the total coordinate of these n segments, and $\{N_\alpha + 1\} \equiv (\alpha)$. The n-fold intermolecular-contact term B_n given by Eq. (B.8) is the same as that for homogeneous polymers except the ranges of the running indices k_α, k_β, etc.

For the single-contact term B_1, we can readily obtain

$$B_1 = -VN_\alpha N_\beta (4\pi b^3/3)[1 - (\Theta/T)], \tag{B.10}$$

where the symbol Θ represents the Flory Θ temperature. Next, since the contributions of intramolecular

[15] W. G. McMillan and J. E. Mayer, J. Chem. Phys. **13**, 276 (1945).

[16] B. H. Zimm, J. Chem. Phys. **14**, 164 (1946).

[17] H. Yamakawa, J. Phys. Soc. Japan **13**, 87 (1958).

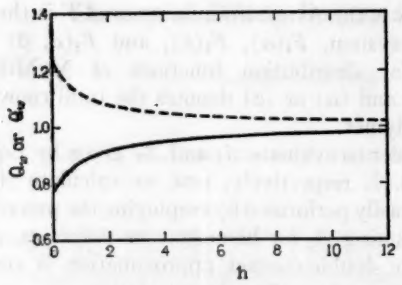

FIG. 1. The heterogeneity correction factors Q_w and Q_w' for the second virial coefficients vs the parameter h defined by $M_w/M_n=(h+1)/h$. Full curve: Q_w (for the osmotic second coefficient A_2); broken curve: Q_w' (for the light-scattering coefficient A_2').

contact to B_2 vanish to the double-contact approximation, B_2 can be evaluated as follows:

$$B_2=-2(6/\pi)^{\frac{1}{2}}B_1(b/a)^3[1-(\Theta/T)](N_\alpha N_\beta)^{-1}$$
$$\times\sum_{0\le k_\alpha<l_\alpha\le N_\alpha}\sum_{0\le k_\beta<l_\beta\le N_\beta}(l_\alpha-k_\alpha+l_\beta-k_\beta)^{-\frac{1}{2}}$$
$$=-(32/15)(6/\pi)^{\frac{1}{2}}B_1(b/a)^3[1-(\Theta/T)]$$
$$\times[N_\alpha^{\frac{1}{2}}/N_\beta+N_\beta^{\frac{1}{2}}/N_\alpha+\tfrac{5}{2}(N_\alpha^{\frac{1}{2}}+N_\beta^{\frac{1}{2}})$$
$$-(N_\alpha+N_\beta)^{5/2}/N_\alpha N_\beta]. \quad \text{(B.11)}$$

The substitution of Eqs. (B.10) and (B.11) into Eq. (B.7) leads to

$$A_{\alpha\beta}=\tfrac{2}{3}\pi N b_0^3(1-\Theta/T)[1-2.865\phi(M_\alpha,M_\beta)z_w+\cdots] \quad \text{(B.12)}$$

to the double-contact approximation. Here ϕ and z_w are given, respectively, by

$$\phi(M_\alpha,M_\beta)=(7-4\sqrt{2})^{-1}M_w^{-\frac{1}{2}}[M_\alpha^{\frac{1}{2}}/M_\beta+M_\beta^{\frac{1}{2}}/M_\alpha$$
$$+\tfrac{5}{2}(M_\alpha^{\frac{1}{2}}+M_\beta^{\frac{1}{2}})-(M_\alpha+M_\beta)^{5/2}/M_\alpha M_\beta], \quad \text{(B.13)}$$

$$z_w=(6/\pi)^{\frac{1}{2}}(b_0/a_0)^3[1-(\Theta/T)]M_w^{\frac{1}{2}} \quad \text{(B.14)}$$

with

$$a_0=a/M_0^{\frac{1}{2}}, \qquad b_0=b/M_0^{2/3}, \quad \text{(B.15)}$$

where M_0 is the molecular weight of segment.[18]

Therefore, from Eqs. (B.3), (B.4), and (B.12), we may write the second coefficient A_2 of osmotic pressure as

$$A_2=\tfrac{2}{3}\pi N b_0^3[1-(\Theta/T)](1-2.865Q_w z_w+\cdots) \quad \text{(B.16)}$$

with

$$Q_w=\int_0^\infty\int_0^\infty\phi(M_\alpha,M_\beta)g(M_\alpha)g(M_\beta)dM_\alpha dM_\beta \quad \text{(B.17)}$$

and the second coefficient A_2' of light scattering as

$$A_2'=\tfrac{2}{3}\pi N b_0^3[1-(\Theta/T)](1-2.865Q_w' z_w+\cdots) \quad \text{(B.18)}$$

with

$$Q_w'=\frac{1}{M_w^2}\int_0^\infty\int_0^\infty\phi(M_\alpha,M_\beta)M_\alpha M_\beta g(M_\alpha)g(M_\beta)dM_\alpha dM_\beta. \quad \text{(B.19)}$$

A_2 and A_2' differ in the expansion coefficients of the z_w series.

Now we are in a position to evaluate Q_w and Q_w', assuming an appropriate form for the molecular weight distribution. For convenience, in this section, we consider two types of distribution; one is the Schulz distribution,[19,20] and the other is the distribution with two deltalike peaks.

B2. Schulz Distribution

The generalized Schulz distribution[19,20] of molecular weight may be written in the form,

$$g(M)=(y^{h+1}/h!)M^h\exp(-yM) \quad \text{(B.20)}$$

with

$$y=h/M_n=(h+1)/M_w=(h+2)/M_z, \quad \text{(B.21)}$$

where M_z is the z-average molecular weight. $g(M)$ given by Eq. (B.20) is a function with a single peak whose width is determined by the parameter h; the large value of h corresponds to the sharp distribution, and the small value of h, to the broad one.

Performing the integrations (B.17) and (B.19) after substitution of Eqs. (B.13) and (B.20), we can obtain

$$Q_w=\begin{cases}(7-4\sqrt{2})^{-1}[5\Gamma(1.5)+4(\ln 2-\frac{4}{3})\Gamma(2.5)] & \text{if } h=0 \quad \text{(B.22)}\\ [(7-4\sqrt{2})h^2(h+1)^{\frac{1}{2}}]^{-1}\left[\dfrac{(7h+3)\Gamma(h+1.5)}{\Gamma(h)}-\dfrac{\Gamma(2h+2.5)}{\Gamma(2h)}\right] & \text{if } h>0,\end{cases}$$

$$Q_w'=[(7-4\sqrt{2})(h+1)^{5/2}]^{-1}\left[\frac{(7h+10)\Gamma(h+2.5)}{\Gamma(h+1)}-\frac{\Gamma(2h+4.5)}{\Gamma(2h+2)}\right], \quad \text{(B.23)}$$

[18] The parameter z_w does not differ from the z for homogeneous polymers except that M is replaced by M_w. In this paper, we employ the weight-average molecular weight rather than the number- or z-average.

[19] G. V. Schulz, Z. phys. Chem. **B43**, 25 (1939).
[20] B. H. Zimm, J. Chem. Phys. **16**, 1099 (1948).

where Γ is the gamma function. It can be easily shown that

$$\lim_{h\to\infty} Q_w = \lim_{h\to\infty} Q_w' = 1,$$

and hence, in the limit of $h=\infty$, both Eqs. (B.16) and (B.18) just give the second virial coefficient for homogeneous polymers already derived.[2,17] In Fig. 1, the variation of Q_w and Q_w' with h is shown, where the full curve represents Q_w, and the broken curve, Q_w'. It follows from the figure that Q_w is smaller than Q_w' for all values of h, and hence, the second coefficient A_2 of osmotic pressure is slightly greater than the second coefficient A_2' of light scattering in the vicinity of the Θ temperature.

B3. Distribution with Two Deltalike Peaks

The distribution with two deltalike peaks is given by

$$g(M) = w_1\delta(M-M_1) + w_2\delta(M-M_2), \quad \text{(B.24)}$$

where δ is Dirac's delta function. $g(M)$ given by Eq. (B.24) represents the molecular weight distribution for mixtures of two kinds of polymers of molecular weights M_1 and M_2, whose weight fractions are w_1 and w_2, respectively. Here we assume that the subscript 2 indicates the higher molecular weight component; i.e., $M_1<M_2$.

From Eqs. (B.13), (B.17), (B.19), and (B.24), we can readily obtain for Q_w and Q_w' in this case, respectively,

$$Q_w = M_w^{-\frac{1}{2}}\{w_1^2M_1^{\frac{1}{2}} + w_2^2M_2^{\frac{1}{2}} + (7-4\sqrt{2})^{-1}w_1w_2[2(M_1^{\frac{1}{2}}/M_2 + M_2^{\frac{1}{2}}/M_1) + 5(M_1^{\frac{1}{2}}+M_2^{\frac{1}{2}}) - 2(M_1+M_2)^{5/2}/M_1M_2]\}, \quad \text{(B.25)}$$

$$Q_w' = M_w^{-5/2}\{w_1^2M_1^{5/2} + w_2^2M_2^{5/2} + (7-4\sqrt{2})^{-1}w_1w_2 \times[2(M_1^{5/2}+M_2^{5/2}) + 5(M_1^{\frac{1}{2}}M_2 + M_1M_2^{\frac{1}{2}}) - 2(M_1+M_2)^{5/2}]\}. \quad \text{(B.26)}$$

Figure 2 gives the result of numerical calculations of A_2 and A_2', given by Eqs. (B.16) and (B.18) with (B.25) and (B.26), respectively, as functions of w_2, where the full curves represent A_2, and the broken curves, A_2'. The values are assumed that $a_0=0.7$ A, $b_0=0.1$ A, $1-(\Theta/T)=0.03$, $M_1=50\,000$, and $M_2/M_1=5$, 10, and 20 so as to satisfy the condition of convergence of the z_w series. Concerning this figure, it is of interest to make comparison with the result obtained by Flory and Krigbaum.[7] According to their result, both A_2 and A_2' take the respective maximum values, whereas in Fig. 2 both of them decrease monotonically with

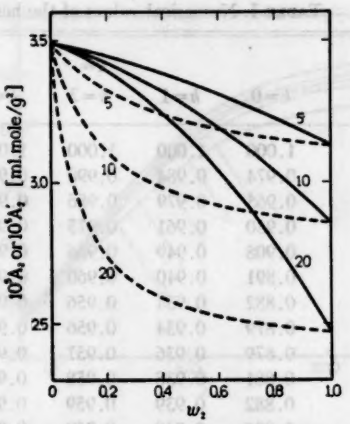

FIG. 2. A_2 and A_2' for mixtures of two kinds of polymers of molecular weights M_1 and M_2 vs the weight fraction w_2 of the higher molecular weight component. Numbers attached to the curves represent the ratio M_2/M_1 of the molecular weights. Full curves: A_2; broken curves: A_2'.

increasing w_2. This difference seems to arise from the fact that the expression for the second coefficient derived here is up to the double-contact term, that is, applicable only in the vicinity of the Θ temperature. It appears, however, that in accordance with their conclusion, the second coefficient of light scattering is more sensitive to the higher molecular-weight fraction than the osmotic second coefficient.

C. INTRINSIC VISCOSITY

C1. Basic Formulation

As is well known, the intrinsic viscosity $[\eta]$ for heterogeneous polymers is given by

$$[\eta] = \int_0^\infty [\eta]_M g(M)\,dM, \quad \text{(C.1)}$$

where $[\eta]_M$ represents the intrinsic viscosity for homogeneous polymers of molecular weight M. Substituting the expression for $[\eta]_M$ already derived[2,21] into Eq. (C.1), we may write $[\eta]$ (in 100 ml per g) in the form,

$$[\eta] = [\eta]_\theta[1 + (q_{1w}/q_{0w})p_1(X_w)z_w - (q_{2w}/q_{0w})p_2(X_w)z_w^2 + \cdots] \quad \text{(C.2)}$$

with

$$[\eta]_\theta = q_{0w}(\pi^{\frac{3}{2}}N/6^{\frac{3}{2}}\cdot 100)[X_wF_0(X_w)]a_0^3M_w^{\frac{1}{2}}, \quad \text{(C.3)}$$

$$X_w = (3/2\pi)^{\frac{3}{2}}(b_0/a_0M_0^{1/3})M_w^{\frac{1}{2}}. \quad \text{(C.4)}$$

Here, $[\eta]_\theta$ is the intrinsic viscosity at the Θ temperature, X_w is the draining parameter represented in terms

[21] H. Yamakawa and M. Kurata, J. Phys. Soc. Japan 13, 94 (1958).

TABLE I. Numerical values of the heterogeneity correction factors q_{0w} and q_{1w} for intrinsic viscosity.

X_w	q_{0w} $h=0$	$h=1$	$h=2$	$h=3$	$h=4$	q_{1w} $h=0$	$h=1$	$h=2$	$h=3$	$h=4$
0	1.000	1.000	1.000	1.000	1.000	1.329	1.175	1.119	1.090	1.073
0.1	0.974	0.984	0.990	0.994	0.996	1.277	1.149	1.101	1.078	1.063
0.2	0.963	0.979	0.986	0.991	0.994	1.257	1.140	1.094	1.074	1.059
0.5	0.930	0.961	0.975	0.982	0.986	1.185	1.102	1.070	1.054	1.044
1.0	0.908	0.949	0.966	0.975	0.980	1.132	1.074	1.049	1.038	1.031
2.0	0.891	0.940	0.960	0.970	0.975	1.085	1.049	1.033	1.025	1.019
5.0	0.882	0.934	0.956	0.966	0.972	1.044	1.025	1.016	1.012	1.009
10.0	0.879	0.934	0.956	0.967	0.973	1.027	1.014	1.008	1.005	1.003
20.0	0.879	0.936	0.957	0.968	0.974	1.015	1.008	1.005	1.003	1.002
50.0	0.881	0.938	0.958	0.969	0.974	1.007	1.005	1.003	1.002	1.001
100.0	0.882	0.939	0.959	0.969	0.975	1.004	1.003	1.002	1.001	1.000
∞	0.886	0.940	0.959	0.969	0.975	1.000	1.000	1.000	1.000	1.000

of the weight-average molecular weight, z_w is given by Eq. (B.14), q_{nw}'s are the heterogeneity correction factors, and the numerical values of $X_wF_0(X_w)$ and $p_1(X_w)$ are tabulated in Table I of Part II,[2] though the expression for $p_2(X_w)$ has not been derived.[22]

The intrinsic viscosity of mixtures of two fractions is linear in each weight fraction, and its behavior is rather simple. In this section, therefore, we consider only the Schulz distribution.[19,20] In this case, if variable M is transformed to t by $t=M/M_w$, the heterogeneity correction factors q_{nw}'s can be calculated by

$$q_{nw}=\frac{(h+1)^{h+1}}{\Gamma(h+1)}\int_0^\infty \frac{[(X_wt^{\frac{1}{2}})F_0(X_wt^{\frac{1}{2}})]p_n(X_wt^{\frac{1}{2}})}{[X_wF_0(X_w)]p_n(X_w)} \times t^{\frac{1}{2}(n+1)+h}\exp[-(h+1)t]dt, \qquad (p_0\equiv 1;\ n=0,1,2). \quad \text{(C.5)}$$

Remembering that the functions $F_0(X)$, $XF_0(X)$, and $p_n(X)$ tend to the finitely determinate values independent of the molecular weight as X approaches 0 or infinity, we can immediately obtain, from Eq. (C.5), the following asymptotic values for free- and nonfree-draining molecules,

$$\lim_{X_w\to 0} q_{nw}=\Gamma(h+\tfrac{1}{2}n+2)/(h+1)^{\frac{1}{2}(n+2)}\Gamma(h+1), \quad \text{(C.6a)}$$

$$\lim_{X_w\to\infty} q_{nw}=\Gamma(h+\tfrac{1}{2}n+\tfrac{3}{2})/(h+1)^{\frac{1}{2}(n+1)}\Gamma(h+1). \quad \text{(C.6b)}$$

Since it is impossible to perform the integration in Eq. (C.5) analytically for the intermediate values of X_w, the numerical integrations were carried out for several assigned values of X_w and h, though q_{2w} was not evaluated because of the absence of the expression for $p_2(X)$. The results are shown in Table I and Figs. 3 to 5. Figure 3 gives q_{0w} (full curves) and q_{1w} (broken curves) plotted against X_w, Fig. 4, the viscosity function $q_{0w}[X_wF_0(X_w)]$ for heterogeneous polymers plotted against X_w, and Fig. 5, the ratio q_{1w}/q_{0w}, the correction factor for $p_1(X_w)$, plotted against X_w. In these figures, numbers attached to the curves represent the values of h. It is easily seen from Fig. 4 that the viscosity function at the Θ temperature decreases with increasing heterogeneity, and from Fig. 5 that the coefficient of the linear term in z_w increases with increasing heterogeneity. Of course, all q_{nw}'s become unity as h approaches infinity, and hence, in this limit, Eq. (C.2) yields the intrinsic viscosity for homogenous polymers.

The effect of heterogeneity on the intrinsic viscosity has been dealt with by Newman *et al.*[23] and Krigbaum and Carpenter[24] concerning the value of Flory's universal constant Φ.[10] More recently, the detailed discussion about this value has been made by the present authors.[2,25] So it is merely noted here that the discrepancy of the theoretical value, 2.87×10^{21}, of Φ predicted by the Kirkwood and Riseman theory[11,26] from the experimental one, 2.1×10^{21}, may arise from both the effect of heterogeneity and the dependence of Φ on the linear expansion factor of polymer chain.

Thus we turn our attention to the intrinsic viscosity $[\eta]_\theta$ at the Θ temperature in connection with Fig. 4. According to the recent measurements,[9] the relation,

$$[\eta]_\theta=KM^{\frac{1}{2}}, \quad \text{(C.7)}$$

[22] In Part II, the notation $\mathfrak{p}(X)$ has been used in place of $p_1(X)$. The values of $X_wF_0(X_w)$ and $p_1(X_w)$ are equal to the respective values of $XF_0(X)$ and $p_1(X)$ at the same value of X as that of X_w.

[23] S. Newman, W. R. Krigbaum, C. Laugier and P. J. Flory, J. Polymer Sci. **14**, 451 (1954).

[24] W. R. Krigbaum and D. K. Carpenter, J. Phys. Chem. **59**, 1166 (1955).

[25] M. Kurata, H. Yamakawa and H. Utiyama, International Symposium on Macromolecules, Wiesbaden, 1959; Makromol. Chem. **34**, 139 (1959).

[26] The original value of Φ obtained by Kirkwood and Riseman is 3.62×10^{21}, instead of 2.87×10^{21}.

may hold for a variety of polymer-solvent systems over the wide range in M, where K is a constant independent of M. This relation is well interpreted by the Flory and Fox theory,[10] but not by the hydrodynamic theories[11,12]; that is, according to the latter, K must decrease with decreasing M. In Part II, we have emphasized that the draining effect is important for interpretation of the intrinsic viscosity as well as the excluded volume effect. We therefore make a tentative attempt to interpret the relation (C.7) without discarding the hydrodynamic scheme. Now it is known that the higher molecular-weight fraction is more heterogeneous than the lower molecular-weight one provided that the fractionation is carried out by the successive precipitation method[25,27] that is, the value of h of the fractionated sample decreases with increasing average molecular weight of the fraction. If such dependence of h on M_w or on X_w is taken into consideration, $q_{0w}[X_wF_0(X_w)]$ as function of X_w is shown schematically by the broken curve in Fig. 4. From the figure, the $q_{0w}[X_wF_0(X_w)]$ or K may be expected to be almost constant at least for the value of X_w greater than about 10 or 20.[28] This lower limit of X_w corresponds to the value of about 200 000 for M_w, when the value of M_0 is assumed as 52 in the case of a polystyrene molecule.

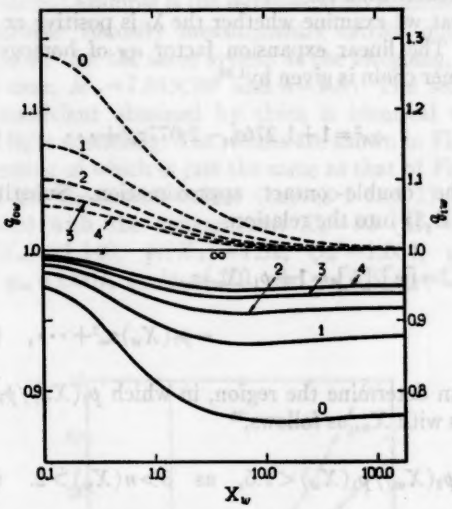

FIG. 3. The heterogeneity correction factors q_{0w} and q_{1w} for intrinsic viscosity vs the draining parameter X_w. Numbers attached to the curves represent the value of h. Full curves: q_{0w}. Broken curves: q_{1w}.

On the other hand, as suggested recently,[25] if we assume that the friction constant of a polymer segment is actually greater than that predicted by the Stokes law, the greater value could be assigned to X_w, and also thereby the relation (C.7) may be interpreted. Accordingly, in order to arrive at a final conclusion, we must await experimental investigations taking care of the effect of heterogeneity.

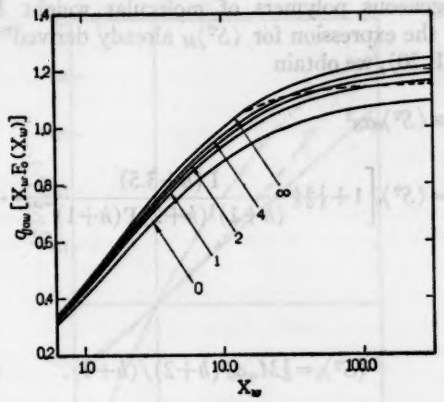

FIG. 4. The viscosity function $q_{0w}[X_wF_0(X_w)]$ for heterogeneous polymers at the Θ temperature vs the draining parameter X_w. Numbers attached to the curves represent the value of h. The broken curve gives a schematic representation of the

$$q_{0w}[X_wF_0(X_w)]$$

vs X_w for the case in which h decreases with increasing molecular weight or X_w.

C2. Relation to Gyration Radius

The mean-square radius of gyration $\langle S^2\rangle$ of a polymer chain obtained by light-scattering measurements is of the z average; that is,

$$\langle S^2\rangle = M_w^{-1}\int_0^\infty \langle S^2\rangle_M M g(M)\,dM, \qquad \text{(C.8)}$$

where $\langle S^2\rangle_M$ is the mean-square radius of gyration for

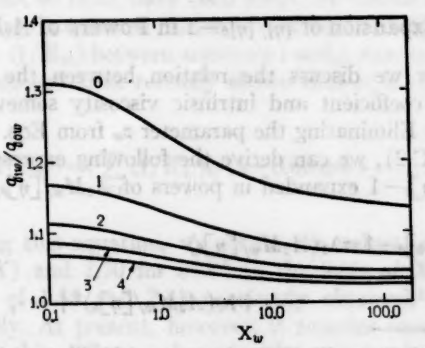

FIG. 5. The heterogeneity correction factor q_{1w}/q_{0w} for the coefficient of the linear term in z_w in the expression for intrinsic viscosity vs the draining parameter X_w. Numbers attached to the curves represent the value of h.

[27] G. V. Schulz, Z. phys. Chem. **B46**, 137 (1940); **B47**, 155 (1940).

[28] It must be remarked that the relation (C.7) is to be affected by the kind of the average of molecular weight, though the viscosity average molecular weight has been employed in most of the published works.

homogeneous polymers of molecular weight M. By using the expression for $\langle S^2\rangle_M$ already derived[29-31] and Eq. (B.20), we obtain

$$\langle S^2\rangle \equiv \langle S^2\rangle_0 \alpha_S^2 = \langle S^2\rangle_0\left[1+\tfrac{134}{105}\frac{\Gamma(h+3.5)}{(h+1)^{\frac{1}{2}}(h+2)\Gamma(h+1)}z_w-\cdots\right] \tag{C.9}$$

with

$$\langle S^2\rangle_0 = \tfrac{1}{6}M_w a_0^2(h+2)/(h+1). \tag{C.10}$$

In Part II, we proposed the relation

$$[\eta]=[\eta]_\theta \alpha_S^{n(X)}, \tag{C.11}$$

where, for homogeneous polymers, the value of $n(X)$ varies from 2.00 to 2.43 as X increases from 0 to ∞. $n(X_w)$ for heterogeneous polymers is obtained, from Eqs. (C.2), (C.9), and (C.11), as

$$n(X_w)=\frac{105}{67}\left(\frac{q_{1w}}{q_{0w}}\right)\frac{(h+1)^{\frac{1}{2}}(h+2)\Gamma(h+1)}{\Gamma(h+3.5)}p_1(X_w) \tag{C.12}$$

in the vicinity of the Θ temperature. For the polystyrene-cyclohexane system ($M_w=3.20\times10^6$, $h=4$) investigated by Krigbaum and Carpenter,[24] the theoretical value of $n(X_w)$ given by Eq. (C.12) is evaluated as 2.1, in place of 2.4 for homogeneous polymers. These are to be compared with the observed value, 2.2. Thus, it is noted here that the effect of heterogeneity makes the value of $n(X_w)$ decreased, though slightly, as well as the effect of the nonuniform expansion of polymer chain already discussed.[2,21]

D. RELATION BETWEEN THE SECOND VIRIAL COEFFICIENT AND INTRINSIC VISCOSITY

D1. Expansion of $[\eta]/[\eta]_\theta-1$ in Powers of $A_2M_w/[\eta]_\theta$

Now we discuss the relation between the second virial coefficient and intrinsic viscosity somewhat in detail. Eliminating the parameter z_w from Eqs. (B.16) and (C.2), we can derive the following expression for $[\eta]/[\eta]_\theta-1$ expanded in powers of $A_2M_w/[\eta]_\theta$,

$$[\eta]/[\eta_0]_\theta-1=\lambda_1(A_2M_w/[\eta]_\theta)+\lambda_2(A_2M_w/[\eta]_\theta)^2+\cdots, \tag{D.1}$$

where the coefficients λ_1 and λ_2 are given by

$$\lambda_1=q_{1w}p_1(X_w)[X_wF_0(X_w)]/400,$$

$$\lambda_2=[q_{0w}/q_{1w}p_1(X_w)][2.865Q_w-(q_{2w}/q_{1w})p_2(X_w)/p_1(X_w)]\lambda_1^2, \tag{D.2}$$

respectively, and the expansion in powers of $A_2'M_w/[\eta]_\theta$ can be obtained by replacing Q_w by Q_w'.

As easily seen from Fig. 3, if X_w exceeds about 10, q_{1w} becomes unity approximately irrespective of the value of h. It follows therefore that λ_1, the initial slope of the curve of $[\eta]/[\eta]_\theta-1$ vs $A_2M_w/[\eta]_\theta$, is substantially independent of heterogeneity for the value of X_w greater than 10.

Next we examine whether the λ_2 is positive or negative. The linear expansion factor α_S of homogeneous polymer chain is given by[1,30]

$$\alpha_S^2=1+1.276z_w-2.077z_w^2+\cdots \tag{D.3}$$

to the double-contact approximation. Substituting Eq. (D.3) into the relation,

$$\alpha_S^{n(X_w)}=[\eta]/[\eta]_\theta=1+p_1(X_w)z_w-p_2(X_w)z_w^2+\cdots, \tag{D.4}$$

we can determine the region, in which $p_2(X_w)/p_1(X_w)$ varies with X_w, as follows,[32]

$$1.3<p_2(X_w)/p_1(X_w)<1.6, \quad \text{as} \quad 3>n(X_w)>2. \tag{D.5}$$

Moreover, it can be shown from Eqs. (B.22), (B.23), (C.6a), and (C.6b) that the following inequalities may hold:

$$Q_w'>Q_w>0.875, \quad \text{if} \quad h>1, \tag{D.6}$$

$$1<q_{2w}/q_{1w}<1.5. \tag{D.7}$$

It therefore may be concluded from Eqs. (D.2) and (D.5) to (D.7) that if $h>1$, λ_2 is safely positive for all values of X_w; that is, the initial curvature of the curve (D.1) is concave upward. The condition, $h>1$, is ordinarily attained for fractionated samples.

D2. Comparison with Experiment

Now we ascertain the statement presented in the last subsection by comparison with experiment. The first example is the experiment of Krigbaum and Carpenter[24] already cited. In Fig. 6, the $[\eta]/[\eta]_\theta-1$ vs

[29] B. H. Zimm, W. H. Stockmayer and M. Fixman, J. Chem. Phys. **21**, 1716 (1953).
[30] M. Fixman, J. Chem. Phys. **23**, 1656 (1955).
[31] H. Yamakawa and M. Kurata, J. Phys. Soc. Japan **13**, 78 (1958).

[32] The upper limit of $n(X_w)$ does not exceed 3 at most, though it has been evaluated as 2.43 in our theory.[2,21]

$A_2'M_w/[\eta]_\theta$ plot is shown, where the circles represent the observed values and the curves 1 and 2 represent the theoretical values calculated by using Eq. (D.1) up to the leading term and the second term respectively, with the assignments; $X_w=60(M_0=52)$, $X_wF_0(X_w)=1.190$, $p_1(X_w)=1.52$, $Q_w'=1.048$, $q_{0w}=0.974$, $q_{1w}=1.001$, $q_{2w}/q_{1w}=1.1$, and $p_2(X_w)/p_1(X_w)=1.5$. In the figure the chain curve 3 represents the values obtained by Orofino and Flory's equations (D.1) and

$$\lambda_1=3^4\Phi/2^{5/2}\pi^{3/2}\mathrm{N},$$

$$\lambda_2=-(5-\pi^{\frac{1}{2}})3^7\Phi^2/2^8\pi^3\mathrm{N}^2 \qquad \text{(D.8)}$$

with $\Phi=2.1\times10^{21}$.

The second example is the sedimentation equilibrium and intrinsic viscosity measurements carried out by Fujita *et al.*[33] for the same system as the foregoing, but in this case, $M_w=7.84\times10^5$ and $h=1.85$. The second virial coefficient obtained by them is identical with that of light scattering. The results are shown in Fig. 7, the meaning of which is just the same as that of Fig. 6, though the theoretical values (curves 1 and 2) were calculated with the assignments: $X_w=30$ $(M_0=52)$, $X_wF_0(X_w)=1.140$, $p_1(X_w)=1.52$, $Q_w'=1.084$, $q_{0w}=0.956$, $q_{1w}=1.007$, $q_{2w}/q_{1w}=1.1$, and $p_2(X_w)/p_1(X_w)=1.5$.[34]

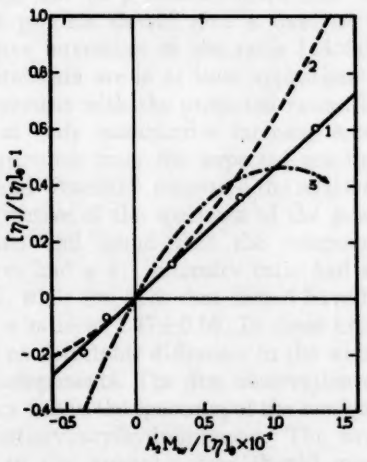

FIG. 6. Experimental test of the theoretical expression (D.1) with (D.2), $[\eta]/[\eta]_\theta-1$ vs $A_2'M_w/[\eta]_\theta$. Circles: experimental values for polystyrene in cyclohexane ($M_w=3.20\times10^6$, $h=4$) obtained by Krigbaum and Carpenter.[34] Full curve 1: present theory, Eq. (D.1) up to the leading term, with (D.2). Broken curve 2: present theory, Eq. (D.1) up to the second term, with (D.2). Chain curve 3: Orofino and Flory's equation with (D.8).

[33] H. Fujita, A. M. Linklater, and J. W. Williams, J. Am. Chem. Soc. **82**, 379 (1960).

[34] Since A_2' and $[\eta]$ had been measured at the different temperatures, we obtained the *observed* values of $[\eta]$ at the same temperature as A_2' had been measured, by the inter- and extrapolation of the original data.

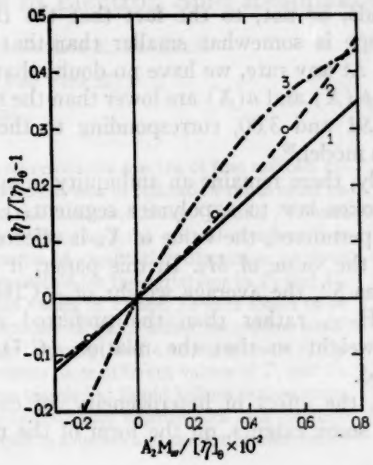

FIG. 7. Experimental test of the theoretical expression (D.1) with (D.2), $[\eta]/[\eta]_\theta-1$ vs $A_2'M_w/[\eta]_\theta$. Circles: experimental values for polystyrene in cyclohexane ($M_w=7.84\times10^5$, $h=1.85$) obtained by Fujita *et al.*[33] Full curve 1: present theory, Eq. (D.1) up to the leading term, with (D.2). Broken curve 2: present theory, Eq. (D.1) up to the second term, with (D.2). Chain curve 3: Orofino and Flory's equation with (D.8).

It is seen from Figs. 6 and 7 that indeed the initial curvature of the observed curves is concave upward as predicted by our theory, whereas the Orofino and Flory theory yields the curvature concave downward, and, moreover, the initial slope obtained by the latter is too large. These discrepancies may be attributed to the fact that in the Flory theories, the expansion coefficients of the second virial coefficient have been underestimated and those of the intrinsic viscosity have been overestimated, as already discussed in Part II.

In addition, it must be pointed out that the range of applicability of Eq. (D.1) is wider than that of the z_w series itself, perhaps because of the mutual cancellation of the two z_w series for A_2 and $[\eta]$.[35]

In conclusion, the following remarks may be given: First, in our viscosity theory,[2,21] some approximations, though not so fatal, have been made, for instance, for the average expansion factor of the mean reciprocal distance $\langle 1/R_{ij}\rangle$ between segments i and j. Stockmayer and Albrecht[36] have recently shown that it is exactly given by

$$\sum_{i<j}\langle 1/R_{ij}\rangle=(\sum_{i<j}\langle 1/R_{ij}\rangle_0)\,(1-0.609z+\cdots). \qquad \text{(D.9)}$$

On using this equation, we obtain the values of 1.72 for $p_1(X)$ and 2.70 for $n(X)$ in the limit of $X=\infty$, instead of 1.55 and 2.43 previously obtained,[2,21] respectively. At present, however, it remains uncertain whether this difference between the values of $p_1(X)$

[35] See Fig. 3 in Part II.

[36] W. H. Stockmayer and A. C. Albrecht, J. Polymer Sci. **32**, 215 (1958).

corresponds, or not, to the fact that the theoretical initial slope is somewhat smaller than that observed in Fig. 7. At any rate, we have no doubt that the true values of $p_1(X)$ and $n(X)$ are lower than the respective values, 1.91 and 3.00, corresponding to the uniform expansion model.[10]

Secondly, there remains an ambiquity in application of the Stokes law to a polymer segment. Even if it might be permitted, the value of X_w is affected by the choice of the value of M_0. In this paper, it has been assumed as 52, the average weight of —$CH(C_6H_5)$— and —CH_2—, rather than the preferred statistical segment weight so that the relation (C.7) may be interpreted.

Finally, the effect of heterogeneity, of course, depends, to some extents, on the form of the molecular weight distribution, but the results obtained here on the assumption of the Schulz distribution will not be altered so much even in the case of the other distributions except the precise numerical values.

ACKNOWLEDGMENTS

We are indebted to Professor Ichiro Sakurada of the Department of Textile Chemistry for his helpful discussion and kind encouragement. Thanks are tendered also to Professor Hiroshi Fujita of the Department of Fisheries for the opportunity of studying his manuscript prior to its publication, and to Miss Sadako Takeuchi for her help in numerical computations. One of us (MK) wishes to thank Professor Walter H. Stockmayer for his kind hospitality at Massachusetts Institute of Technology.

Anomalous Relaxation of Hyperfine Components in Electron Spin Resonance*

JAN W. H. SCHREURS, GEORGE E. BLOMGREN,† AND GEORGE K. FRAENKEL

Department of Chemistry, Columbia University, New York 27, N. Y.

(Received December 28, 1959)

It is shown that the different hyperfine components in the electron-resonance spectra of free radicals exhibiting proton hyperfine splitting saturate at different rates, and different sets of relaxation times must be used to describe the behavior of each component. The variations in the relaxation times (T_1 and T_2) were found to be approximately symmetric about the center of the spectrum, and the central component is the narrowest and saturates more readily than the outer components. A qualitative discussion is given of the relaxation and line-broadening mechanisms which may be responsible for the variations in T_1 and T_2. In solutions of the *p*-benzosemiquinone ion at room temperature, the values of T_1 and T_2 were found to be approximately 10^{-6} sec. An analysis is given of the experimental parameters which affect saturation measurements, including the effect of a nonuniform rf field in a rectangular cavity, and a study is made of the type of spectra to be expected when the individual hyperfine components have different values of T_1 and T_2. An appendix is included on the work of Jen *et al.* on deuterium atoms trapped at liquid helium temperature, which shows that the anomalous intensities obtained in these low-temperature experiments as a function of rf power is not the same as the phenomenon observed for free radicals in solution and cannot be adequately interpreted in terms of any currently proposed mechanisms.

I. INTRODUCTION

THE theory of the isotropic hyperfine splitting of electron spin resonance spectra of organic free radicals predicts definite relative intensities of the hyperfine components.[1,2] For example, if a radical contains equivalent protons, the intensities of the hyperfine components should be proportional to the binomial distribution, and thus a radical such as the semiquinone ion of *p*-benzohydroquinone with four equivalent protons should give a five-line spectrum with relative intensities in the ratio 1:4:6:4:1. The experimental data are in at least approximate quantitative agreement with the predicted ratios, but a few attempts at truly quantitative intensity studies have shown departures from the expected results. Venkataraman and Fraenkel[1] measured the relative maxima of the derivative of the spectrum of the *p*-benzosemiquinone ion and found that the components that should have had a 4:1 intensity ratio had a ratio of 3.61 ± 0.27, while the lines that should have had a 6:4 ratio had a ratio of 1.47 ± 0.06. In these experiments, there was no detectable difference in the widths of the different components. The first observation of a large discrepancy was in the spectrum of the semiquinone ion of 2,5-ditertiarybutylhydroquinone.[3] The two protons attached to the aromatic ring should give rise to three lines with intensity ratios 1:2:1, but, in the first observed spectrum, the peak-height ratios were 1:1.6:1, and again the widths of the different components appeared to be the same.

These results were at first sight rather startling since, on very general grounds, the ratios of the areas of the different components should be in the ratio of the statistical weights of the components. Further investigation[3,4] indicated, however, that the ratio of peak heights was not constant and depended on the level of the microwave power used in the experiment, i.e., some type of saturation phenomenon was taking place. When saturation occurs, it is no longer possible to conclude that the ratio of the areas of the components should be in the ratio of the statistical weights unless the saturation factors[5,6] of the components are all the same.

Saturation in electron spin resonance under typical experimental conditions in the microwave region has usually been considered to be important only at low temperatures. In fact, relaxation times at room temperature for many transition-metal ions in solids are so short that the lines are too wide to observe. Since the present study was initiated, however, it has become clear that free radicals in solution saturate readily. Saturation is important, for a given set of experimental conditions, whenever the product T_1T_2 of the spin-lattice relaxation time T_1 and the line-width parameter T_2 (the transverse relaxation time) is large. Even though T_1 is small for free radicals in solution (typical values are ca 10^{-6} sec, cf. *infra*), T_2 is large. A large value of T_2 corresponds to a small line width, and, in free radicals, line widths are often as narrow as 0.1 gauss (or sometimes even narrower), corresponding to a value of T_2 of about 10^{-6} sec.[7] A relatively small number of investigators have reported on saturation

* This research was supported in part by the United States Air Force through the Office of Scientific Research.

† Qincy Ward Boese Postdoctoral Fellow. Present address: National Carbon Company, Cleveland, Ohio.

[1] B. Venkataraman and G. K. Fraenkel, J. Am. Chem. Soc. **77**, 2707 (1955).

[2] S. I. Weissman, J. Chem. Phys. **22**, 1378 (1954).

[3] B. Venkataraman, thesis, Columbia University, New York, 1955.

[4] G. K. Fraenkel, Ann. N. Y. Acad. Sci., **67**, 546 (1957).

[5] E. R. Andrew, *Nuclear Magnetic Resonance* (Cambridge University Press, New York, 1955).

[6] J. P. Lloyd and G. E. Pake, Phys. Rev. **94**, 579 (1954).

[7] B. Venkataraman, B. G. Segal, and G. K. Fraenkel J. Chem. Phys. **30**, 1006 (1959).

in solutions of free radicals at high Zeeman fields: Hutchison[8] observed saturation in solutions of triphenylmethyl, Nilsen[9] observed it in solutions of thermochromic compounds at elevated temperatures, and substituted *p*-benzosemiquinone ions were found to saturate.[7] Lloyd and Pake studied the saturation at low Zeeman fields of the radical $(SO_3)_2NO^-$.[6]

During the course of the present study, it became clear that a proper description of the saturation behavior necessitated the assumption that the individual hyperfine components had different relaxation times T_1 and T_2. It therefore became of interest to study the spectra as a function of microwave power and attempt to elucidate the nature of the relaxation and line-broadening mechanisms that could cause a different T_1 and T_2 for the different components. In the following, the effects of a nonuniform microwave field on the observed saturation are analyzed, a study is made of the spectra to be expected if the relaxation times T_1 and T_2 differ from one component to another, and some preliminary experiments on the saturation behavior in solutions of two free radicals are described.

The only observation of a dependence of relative intensities of hyperfine components on power that has come to the authors' attention is in the work of Jen *et al*,[10] on the spectrum of deuterium atoms trapped at liquid helium temperature. The phenomena observed are quite different from those present in free radical spectra in solution, and a discussion of the data on the deuterium atoms is given in the Appendix.

II. EXPERIMENTAL PRINCIPLES

The output signal from any cavity-type electron spin resonance spectrometer is determined by the relative magnetic absorption, r,[11]

$$r=fQ_{LE}/Q_{M\perp}, \tag{2.1}$$

where f is the filling factor, Q_{LE} is the loaded Q of the cavity (with the sample in place), and $Q_{M\perp}$ is the effective magnetic Q of the sample. Explicit definitions of these quantities are given below. In the particular case of a crystal-mixer superheterodyne spectrometer employing a reflection cavity, the magnitude of the output signal is given by[11]

$$A(P_{\text{inc}}/2)^{\frac{1}{2}}(1\mp|\Gamma_{0E}|)r, \tag{2.2}$$

where A is the sensitivity of the crystal-amplifier-detector-recorder system, P_{inc} is the power incident on the cavity, and Γ_{0E} is the voltage reflection coefficient of the cavity at its resonant frequency in the absence of magnetic absorption and with the sample in place. The upper sign applies when $\Gamma_{0E}>0$ (undercoupled) and the lower sign when $\Gamma_{0E}<0$ (overcoupled). Equation (2.2) is only valid when the spectrometer is operated in such a way as to prevent the resonant magnetic dispersion from influencing the output signal.[11]

The expression for the effective magnetic Q, $Q_{M\perp}$, in Eq. (2.1) is

$$Q_{M\perp}^{-1}=4\pi\left(\int_s\chi''H_\perp^2dV\Big/\int_s H_\perp^2dV\right)=4\pi\chi_{eff}'', \tag{2.3}$$

where χ'' is the imaginary part (absorption) of the complex radio-frequency magnetic susceptibility, and $H_\perp$ is that component of the rf magnetic field which is perpendicular to the external steady field used to produce the Zeeman splitting. It is only this perpendicular component of the rf field which is effective in causing the resonance absorption. The integrations in Eq. (2.3) are taken over the volume of the sample. The effective rf absorption, χ_{eff}'', reduces to χ'' if the susceptibility is independent of rf field intensity, i.e., if no saturation occurs, or if the rf field is uniform over the sample. Under these conditions, the expression for $Q_{M\perp}$ reduces to the usual expression for the magnetic Q[12]:

$$Q_{M\perp}=(4\pi\chi_{eff}'')^{-1}=(4\pi\chi'')^{-1}=Q_M. \tag{2.4}$$

The filling factor f, determined by the fraction of the total rf magnetic field in the cavity that is effective in causing resonance absorption, is given by the expression[11]

$$f=\int_s H_\perp^2dV\Big/\int_c H^2dV, \tag{2.5}$$

where the denominator is the integral of the entire rf magnetic field H^2 over the volume of the cavity. Equation (2.5) is derived on the assumption that the field configuration inside the cavity is not appreciably affected by the presence of the sample, an assumption that is certainly not valid for a large sample with dielectric properties markedly different from the dielectric properties of the remainder of the space filling the cavity.

The loaded Q, Q_{LE}, is the Q of the cavity with the sample in place but with no magnetic resonance occurring. It is customary to write

$$Q_{LE}^{-1}=Q_{UE}^{-1}+Q_R^{-1}, \tag{2.6}$$

where Q_{UE} is the unloaded Q of the cavity with the sample in place but with no magnetic resonance occurring, and Q_R is the external or radiation Q. The first of these latter quantities is a measure of the losses in the walls and dielectric material filling the cavity, including the sample and its container, and the second

[8] C. A. Hutchison, private communication.
[9] W. G. Nilsen, thesis, Columbia University, New York, (1956).
[10] C. K. Jen, S. N. Foner, E. L. Cochran, and V. A. Bowers, Phys. Rev. **112**, 1169 (1958).
[11] G. K. Fraenkel in *Technique of Organic Chemistry. I. Physical Methods*, edited by A. Weissberger, (Interscience Publishers, Inc., New York), 3rd ed. (to be published).
[12] N. Bloembergen, E. M. Purcell, and R. V. Pound, Phys. Rev. **73**, 679 (1948).

is a measure of the losses arising from coupling the cavity to the waveguide.

Studies of saturation phenomena are most suitably made by employing an arrangement in which the rf magnetic field over the sample is uniform, because otherwise only an average saturation effect is observed. In a rectangular cavity operating in the lowest waveguide mode (TE_{10n}), the rf fields are constant across the narrow dimensions of the guide, and therefore a small-diameter cylindrical sample placed parallel to the narrow face through the midpoint of the broad face of a one-wavelength cavity is in an approximately uniform rf field. Under these conditions, in which the diameter of the sample is assumed to be very small compared to the guide wavelength, the filling factor is approximately $f=2(V_s/V_c)$ where V_s and V_c are the sample and cavity volume, respectively. A sample positioned in this manner will be called "type A filling." Type A filling, though feasible, is not as convenient for experiments with liquids as is a filling with a cylindrical sample placed in a one-wavelength rectangular cavity parallel to the broad face of the waveguide through the center of the narrow face. This latter type of sample placement will be called "type B filling." All the experiments performed to date have employed type B filling. As a rule, spectra reported in the literature have also been obtained with a nonuniform rf field over the sample.

Since type B filling has been employed, it is necessary, for proper interpretation of the experimental result, to calculate the saturation behavior of a sample subjected to a nonuniform rf field. The rf magnetic field over a small cylindrical sample in a one-wavelength rectangular cavity with type B placement is

$$H_\perp=H_x=H_{0x}\sin(\pi x/a), \tag{2.7}$$

where $0\leq x\leq a$, and a is the dimension of the broad face of the cavity. For type B filling, the average square of the field over the sample is one-half that for type A filling, but for standard X-band waveguide (with inside dimensions 0.9×0.4 in.), the type B sample is 0.9 in. long as compared to 0.4 in. for the type A filling. As a result, the filling factor for both types of filling is approximately the same.

When saturation is taking place, the calculation of the spectrometer output signal from Eqs. (2.1) and (2.2) is obtained from Eq. (2.3) by using the relation[5]

$$\chi''=(\tfrac{1}{2})\pi\chi_0\nu_0 g(\nu)Z, \tag{2.8}$$

where χ_0 is the static suceptibility, $g(\nu)$ is the normalized line-shape function (on a frequency scale), ν_0 is the resonant frequency, and Z is the saturation factor. The expression for the saturation factor can be written[5,6,13]

$$Z=[1+(\tfrac{1}{2})\gamma^2H_1^2g(\nu)T_1]^{-1}, \tag{2.9}$$

[13] M. J. Stephen and G. K. Fraenkel, J. Chem. Phys. **32**, 1435 (1960).

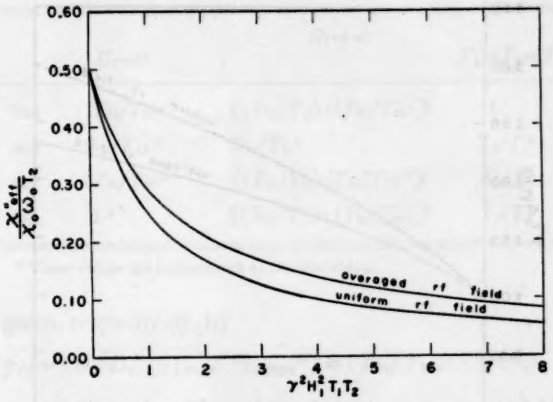

FIG. 1. Variation of absorption maximum (peak height) with rf field intensity (H_1^2) for a uniform rf field over the sample and for the averaged rf field obtained from the sinusoidal field dependence in a rectangular cavity.

where γ is the gyromagnetic ratio, $2H_1=H_{0x}$, and T_1 is the spin-lattice relaxation time.

For the purpose of evaluating the integrals in Eq. (2.3), we shall assume the line shape to be Lorentzian. The theory of Kubo and Tomita,[14] supplemented by that of Bloch,[15] shows this assumption is justified for the steady-state spectra from rapidly tumbling molecules in solution. The experimental evidence, although fragmentary, is also in accord with a Lorentz line shape.[5,6] Thus, the absorption can be written as

$$\chi''=(\tfrac{1}{2})\chi_0\omega_0T_2(1+(\omega-\omega_0)^2T_2^2+\gamma^2H_1^2T_1T_2)^{-1}, \tag{2.10}$$

where $\omega/2\pi$ is the frequency of the rf field, and $T_2=(\frac{1}{2})g(\nu_0)$. From Eqs. (2.3), (2.7) and (2.10), one obtains

$$X_{\rm eff}''=\frac{\chi_0\omega_0T_2}{q^2}\left[1-\left(\frac{1+u^2}{1+u^2+q^2}\right)^{\frac{1}{2}}\right], \tag{2.11}$$

where

$$q^2=\gamma^2H_1^2T_1T_2,$$

$$u=(\omega-\omega_0)T_2. \tag{2.12}$$

The absorption peak height $\chi''(u=0)$ obtained from Eq. (2.10) is plotted in Fig. 1 vs q^2 as the curve labeled "uniform rf field" and its effective value, $\chi_{\rm eff}''(u=0)$ obtained from Eq. (2.11), is plotted as the curve labeled "averaged rf field." The half-width at half-maximum absorption on a magnetic-field scale is, from Eq. (2.11),

$$\Delta_{\frac{1}{2}\cdot\frac{1}{2}}=(\gamma T_2)^{-1}\left[\frac{q^4-q^2-2+2(1+q^2)^{\frac{1}{2}}}{2+3q^2-2(1+q^2)^{\frac{1}{2}}}\right]. \tag{2.13}$$

Curves for the width vs q^2 for the uniform and averaged rf fields are shown in Fig. 2. The width between the points of extreme slope of the absorption spectrum

[14] R. Kubo and K. Tomita, J. Phys. Soc. Japan **9**, 888 (1954).
[15] F. Bloch, Phys. Rev. **102**, 104 (1956).

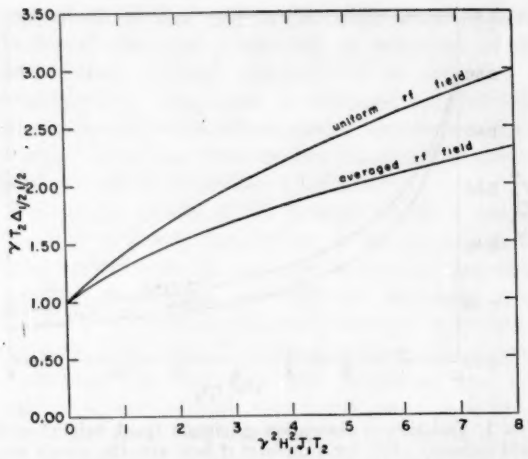

FIG. 2. Variation of the half-width at half-maximum absorption with rf field intensity (H_1^2) for a uniform rf field over the sample and for the averaged rf field obtained from the sinusoidal dependence in a rectangular cavity.

behaves in a qualitatively similar manner. The integral of Eq. (2.11) is

$$\int_0^\infty \chi_{eff}''d\nu=(\chi_0\omega_0/\pi q^2)(1+q^2)^{\frac{1}{2}} \times[E(k,\tfrac{1}{2}\pi)-(1+q^2)^{-1}F(k,\tfrac{1}{2}\pi)], \quad (2.14)$$

where $F(k, \frac{1}{2}\pi)$ is a complete elliptic integral of the first kind, $E(k, \frac{1}{2}\pi)$ is a complete eliptic integral of the second kind, and $k=q(1+q^2)^{-\frac{1}{2}}$. Equation (2.14) and the integral of Eq. (2.10) are plotted in Fig. 3.

The rf magnetic field strength is determined experimentally by measuring the incident power and making use of the relation, for a one-wavelength rectangular cavity,

$$H_1^2=(8Q_{LE}/\nu_0 V_c)\cdot[1+(c/2a)^2]^{-1}(1\mp|\Gamma_{0E}|)P_{\text{inc}}, \quad (2.15)$$

where ν_0 is the resonant frequency, c and a are the length and breadth, respectively, and V_c is the volume of the cavity. All quantities are expressed in emu. The loaded Q with the sample present, Q_{LE}, must be measured, and unless it is very small, the reflection coefficient Γ_{0E} must also be determined.

III. LINE-PARAMETER RATIOS

If the widths and saturation parameters of the different hyperfine components of a spectrum are not the same, it is helpful to examine the ratios of the line parameters for the different components as a function of power. Let D_i be the degeneracy of the ith component of the spectrum, let B_{0i} be the value of magnetic field at the center of this component, and let $g_i(B-B_{0i})$ be its normalized line-shape function on a magnetic field scale. Then the imaginary part of the rf susceptibility associated with the ith component is[13]

$$\chi_i''=\pi(D_i/\sum_i D_i)\chi_0(\omega_0/\gamma)g_i(B-B_{0i})Z_i, \quad (3.1)$$

where the saturation factor for the ith component is

$$Z_i=[1+\pi\gamma H_1^2 g_i(B-B_{0i})D_i\Omega_i]^{-1} \quad (3.2)$$

and Ω_i is the saturation parameter[13] of the ith component. For convenience in the following, we shall use the conventional notation T_{1i} in place of $D_i\Omega_i$, i.e., write

$$T_{1i}=D_i\Omega_i, \quad (3.3)$$

even though a spin-lattice relaxation time may not have physical significance for a single component in a spectrum with hyperfine structure and cross relaxation.[13]

The most readily determined experimental parameters are: (1) the maximum of the absorption curve (the peak height) $\chi_{i,\max}''$; (2) the half-width of the absorption at half-maximum Δ_i; (3) the maximum value of the derivative (the derivative peak height), $(\partial\chi_i''/\partial B)_{\max}$; and (4) the separation between points of extreme slope on the derivative of the spectrum, δ_i. It is also possible to obtain the area of the absorption curve A_i, but the area is not usually computed, and, since Lorentz-type lines have appreciable area in the wings, the determination of areas is often difficult and inaccurate. In the limit of low power ($Z_i \to 1$),

$$A_i^0=\int_0^\infty \chi''dB=\pi(D_i/\sum D_i)\chi_0(\omega_0/\gamma),$$

and the ratio of the area at low power for the ith and jth components is, of course,

$$A_i^0/A_j^0=D_i/D_j. \quad (3.4)$$

Although the result in Eq. (3.4) is independent of the line shape, the ratios of the areas when saturation

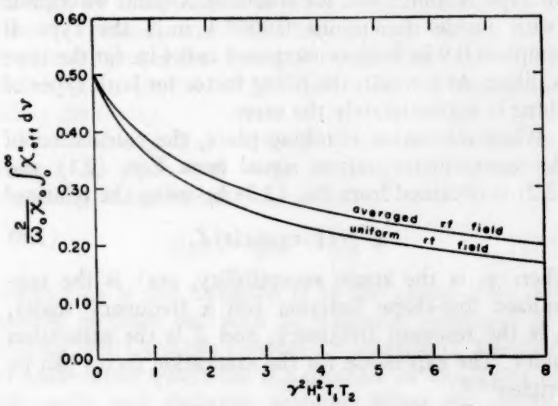

FIG. 3. Variation of the intensity (area) of the absorption with rf field intensity (H_1^2) for a uniform rf field over the sample and for the averaged rf field obtained from the sinusoidal field dependence in a rectangular cavity.

occurs are not independent of the shape, and the relative areas are therefore not simply proportional to the relative degeneracies when saturation is taking place. If the line shape is known, the areas can be computed even when saturation is occurring, but, if the shape is known, it is equally valid and much simpler to study the other four parameters instead of the area. To proceed further, it is thus necessary to assume a definite line shape, and, for the reasons given in Sec. II, we shall assume that the lines are Lorentzian.

For a Lorentz line, $T_2=(\frac{1}{2})g(\nu_0)$, and the half-width at half-maximum absorption on a magnetic field scale is

$$\Delta_i=\gamma^{-1}[(S_i)^{\frac{1}{2}}/T_{2i}], \tag{3.5}$$

where

$$S_i=(Z_i^{-1})_{B=B_{0i}}=1+\gamma^2H_1^2T_{1i}T_{2i} \tag{3.6}$$

is the reciprocal of the saturation factor at the center of the ith component. The separation between points of extreme slope, on a magnetic field scale, is

$$\delta_i=(2/\sqrt{3})\Delta_i. \tag{3.7}$$

For the peak heights, it is convenient to use quantities normalized for the degeneracy, and the normalized absorption is

$$(\chi_i''/D_i)=(\chi_{i,\max}''/D_i)\{1+[(B_0-B_{0i})/\Delta_i]^2\}^{-1}, \tag{3.8}$$

where

$$(\chi_{i,\max}''/D_i)=(\chi_0/\textstyle\sum D_i)\omega_0T_{2i}(1/S_i)$$
$$=(\chi_0/\textstyle\sum D_i)(\omega_0/\gamma)(1/\Delta_iS_i^{\frac{1}{2}}) \tag{3.9}$$

is the normalized absorption peak height. The normalized maximum value of the derivative is

$$D_i^{-1}(\partial\chi_i''/\partial B)_{\max}=(9/8\sqrt{3})(\chi_0/\textstyle\sum D_i)\omega_0\gamma T_{2i}^2(1/S_i^{\frac{1}{2}})$$
$$=(\sqrt{3}/2)(\chi_0/\textstyle\sum D_i)(\omega_0/\gamma)(1/S_i^{\frac{1}{2}}\delta_i^2), \tag{3.10}$$

and the normalized area is

$$A_i/D_i=\int_0^\infty\chi_i''dB=\pi(\chi_0/\textstyle\sum D_i)(\omega_0/\gamma)(1/S_i^{\frac{1}{2}})$$
$$=\pi\Delta_i(\chi_{i,\max}''/D_i)$$
$$=(2\pi/\sqrt{3})\delta_i^2(\partial\chi_i''/\partial B)_{\max}(1/D_i). \tag{3.11}$$

We shall be interested in the ratio of the widths of components i and j, $w_{i/j}$,

$$w_{i/j}=(\Delta_i/\Delta_j)=(\delta_i/\delta_j)=(T_{2j}/T_{2i})(S_i/S_j)^{\frac{1}{2}} \tag{3.12}$$

and the normalized ratios of the peak heights $p_{i/j}$, the derivative maxima $d_{i/j}$, and the areas $a_{i/j}$, which are given, respectively, by

$$p_{i/j}=(D_j/D_i)(\chi_{i,\max}''/\chi_{j,\max}'')=(T_{2i}/T_{2j})\cdot(S_j/S_i), \tag{3.13}$$

$$d_{i/j}=(D_j/D_i)\frac{(\partial\chi_i''/\partial B)_{\max}}{(\partial\chi_j''/\partial B)_{\max}}=(T_{2i}/T_{2j})^2(S_j/S_i)^{\frac{1}{2}}, \tag{3.14}$$

$$a_{i/j}=(D_j/D_i)\cdot(A_i/A_j)=(S_j/S_i)^{\frac{1}{2}}. \tag{3.15}$$

These ratios are interrelated:

$$(p_{i/j})(w_{i/j})^2=(T_{2j}/T_{2i})=(w_{i/j})(a_{i/j}), \tag{3.16}$$

and

$$p_{i/j}=(w_{i/j})(d_{i/j}). \tag{3.17}$$

The limiting values of the ratios are given in Table I. The second column applies when there is no saturation ($H_1\to0$), the third column when there is complete saturation ($H_1\to\infty$), and the last when there is complete saturation and $T_1=T_2=T$ for both components. The low-power values in this table also apply, of course, if a nonuniform rf field is employed, and it is readily shown from Eqs. (2.11)–(2.14) that the limiting values in the table for high power for $w_{i/j}$, $p_{i/j}$, and $a_{i/j}$, also hold for type B filling.

TABLE I. Limiting values of line-parameter ratios.[a]

	$H_1\to0$	$H_1\to\infty$	$T_1=T_2=T$
$w_{i/j}$	T_{2j}/T_{2i} [a]	$[(T_{1i}/T_{1j})\cdot(T_{2j}/T_{2i})]^{\frac{1}{2}}$	1
$p_{i/j}$	T_{2i}/T_{2j} [a]	T_{1j}/T_{1i} [a]	T_j/T_i [a]
$d_{i/j}$	$(T_{2i}/T_{2j})^2$	$[(T_{2i}/T_{2j})(T_{1j}/T_{1i})^2]^{\frac{1}{2}}$	T_j/T_i
$a_{i/j}$	1 [a]	$[(T_{1j}/T_{1i})\cdot(T_{2j}/T_{2i})]^{\frac{1}{2}}$	T_j/T_i

[a] These values are independent of the line shape.

The parameters are plotted in Fig. 4, where it is assumed, for simplicity, that $T_1=T_2=T$ for both components, and where

$$c=T_j/T_i \tag{3.18}$$

is the ratio of relaxation times. Figure 4 shows curves for $c=0.8$ and $c=0.9$. It follows from Eq. (3.16) that the width ratio is a constant (c) times the reciprocal of the ratio of areas, and from the curves it is seen that both the width ratio and the area ratio change very slowly at intermediate power. The peak-height ratio, however, changes from ($1/c$) at low power to (c) at high power, while the ratio of derivative maxima changes from ($1/c^2$) to (c).

The curves show that, if the relaxation times for two different components are different, the ratio of normalized peak heights or derivative maxima are, in general, not equal to unity. For $T_i>T_j$, the peak-height ratios $p_{i/j}$, and particularly the derivative-maxima ratios $d_{i/j}$, can be considerably larger than

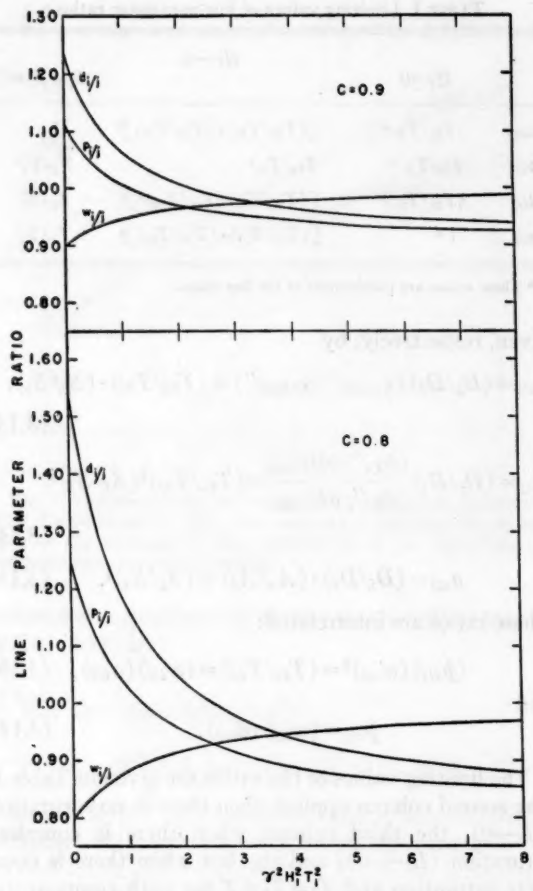

FIG. 4. Variation of line parameter ratios with rf field intensity (H_1^2). $p_{i/j}$ and $d_{i/j}$ are the normalized peak height and derivative maxima ratios, respectively, for components i and j, and $w_{i/j}$ is the ratio of half-width at half-maximum absorption. It is assumed that $T_1=T_2$ for both components, and

$$c=T_j/T_i=T_{1j}/T_{1i}=T_{2j}/T_{2i}.$$

unity at low power and become less than unity at high power. The width ratio $w_{i/j}$ starts below unity at low power and approaches unity at higher power, while the ratio of areas $a_{i/j}$ (not plotted) starts at unity and approaches a value greater than unity at high power.

A rather trivial error can be made in interpreting the results of saturation studies if measurements are not carried to sufficiently low power. A series of measurements of the width ratio as a function of power is likely to show little variation except at very low power. As a result, measurements that are not of high precision and do not extend to sufficiently low power may be misinterpreted as implying a width ratio that is independent of power. If one attempts to compute areas from the formula

$$a_{i/j}=\pi_{i/j}w_{i/j}, \tag{3.19}$$

using a constant value of $w_{i/j}$, the computed area ratio will vary as the peak-height ratio and will not approach unity at low power. Even more startling discrepancies are obtained if derivative-maxima ratios are used with an assumed constancy of $w_{i/j}$, for then

$$a_{i/j}=d_{i/j}w_{i/j}^2. \tag{3.20}$$

IV. RESULTS

Semiquantitative studies were made of the saturation characteristics of the spectra of the semiquinone ions of *p*-benzohydroquinone and 2,5-ditertiarybutylhydroquinone, using an X-band superheterodyne spectrometer previously described.[16] The power incident on the cavity was varied from about 0.04 to 30 mw, and the loaded Q of the cavity was estimated from rough measurements to be approximately $Q_{LE}=1650$. Most of the spectra were studied by taking photographs of an oscilloscope screen on which a particular component of the absorption spectrum was displayed. Type B filling of the cavity was employed (see Sec. II).

The *p*-benzosemiquinone ion is unstable and measurements were made using a flow system.[1,7] The tertiarybutyl compound is quite stable and thus it was examined using a stationary sample in a thin-walled capillary tube. All measurements were made at room temperature with ethanol or ethanol-water mixtures as solvent.

The photographs of the *p*-benzosemiquinone ion spectra showed that the components adhered closely to a Lorentz shape. The five lines in this spectrum have nominal intensities 1:4:6:4:1, and, for convenience, the components will be denoted by the numbers -2, -1, 0, 1, 2, respectively, with -2 signifying the line at the lowest field. It was found that the spectrum was essentially symmetric, i.e., the peak height of the $+2$ $(+1)$ line was essentially the same, at all rf powers employed, as the peak height of the -2 (-1) line. On the other hand, at low power, the normalized peak-height ratio of the central line to the ±1 lines was about $p_{0/\pm1}\cong1.02$, while at the highest power used, it was about $p_{0/\pm1}\cong0.94$. The ratio of normalized peak heights of the central component to the outside components was, at low power, about $p_{0/\pm2}\cong1.06$, while, at the highest power, it was about 0.8. The general behavior of the data for peak-height ratios was similar to the curve in Fig. 4, but since the data were not corrected for the effects of the nonuniform rf field, quantitative agreement with the curves is not to be expected. It was found that T_1 and T_2 are both of the order of magnitude of 10^{-6} sec.

The 2,5-ditertiarybutyl semiquinone ion spectrum consists of three lines with nominal intensity ratios 1:2:1 separated from each other by 2.13 gauss. Each of these components is further split by the eighteen protons on the tertiarybutyl groups into nineteen incompletely resolved lines with a splitting constant of about 0.06 gauss.[3,4] This spectrum behaved in a

[16] J. M. Hirshon and G. K. Fraenkel, Rev. Sci. Instr. 26, 34 (1955).

manner similar to the *p*-benzosemiquinone ion spectrum: the two outside components saturated to the same extent, and, at low power, the normalized peak-height ratio was about $p_{0/\pm 1} \cong 1.1$, while, at the highest power, it was about 0.65. A smooth curve drawn through the data is shown in Fig. 5, where m is used as a symbol to designate the middle component (in place of 0) and s (in place of ± 1) to designate the side components. The normalized peak-height ratio $p_{m/s}$ is plotted vs relative power incident on the cavity, the unit of power being taken as P_1, the lowest power used. It was found by trial and error that the values $T_1^s/T_1^m = 0.65$ and $T_2^m/T_2^s = 1.17$ gave a calculated curve which, when corrected for the effects of nonuniform rf field, was of a form very close to that of the experimental curve. Plots of the calculated normalized peak-height ratio for the uniform and averaged rf fields are shown in Fig. 6 for this choice of parameters.

V. DISCUSSION

At low power, the results show that the normalized peak height of the central component is higher than any other. The normalized heights of symmetrically placed components on either side of the center are the same and decrease uniformly, the smallest normalized height occurring for the two outside components. These data imply that the central component has the narrowest width.

At high power, the normalized peak height of the central component is the smallest, and the normalized height of the other components increases uniformly towards the extremities of the spectrum.

If the components are numbered, from low field to high field, in the sequence $-n, -(n-1), \cdots, -1, 0, 1, \cdots, (n-1), n$, the symmetrical behavior implies that

$$\begin{aligned} p_{i/-i} &= 1, \\ T_{2i} &= T_{2,-i} \\ T_{1i} &= T_{1,-i}. \end{aligned} \tag{5.1}$$

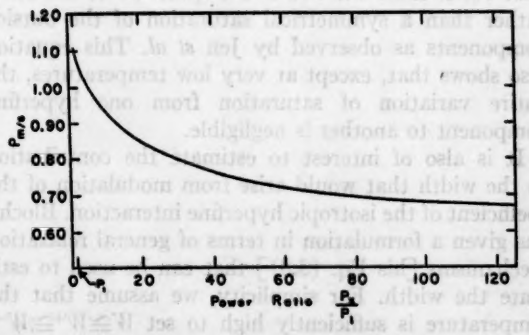

FIG. 5. Curve drawn through experimental points for the variation of the ratio of the peak height of the middle component to the side components ($P_{m/s}$) vs rf power (P_x) for the 2,5-ditertiarybutylsemiquinone ion. The power is given as the ratio of the power (P_x) to the lowest power at which an experiment was performed, (P_1).

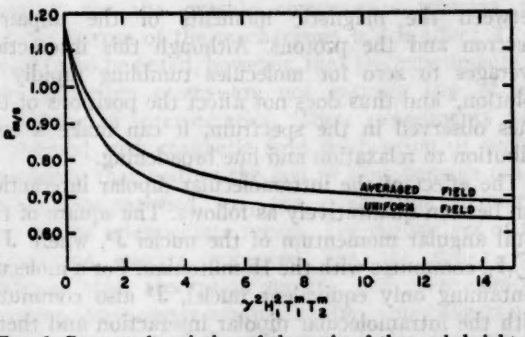

FIG. 6. Computed variation of the ratio of the peak height of the middle component to the side components ($P_{m/s}$) as a function of the rf field intensity (H_1^2) for the 2,5-ditertiarybutylsemiquinone ion. The curves are given for a uniform rf field over the sample and for the averaged rf field obtained from the sinusoidal dependence in a rectangular cavity and are computed for a ratio of side to middle values of T_1 of $T_1^s/T_1^m = 0.65$ and for a ratio of middle to side values of T_2 of $T_2^m/T_2^s = 1.17$. The abscissa is in terms of the relaxation times for the middle component.

Since, at low power, the normalized peak-height ratio is inversely proportional to the width ratio (see Table I), the low power data implies that

$$T_{2n} < T_{2,n-1} \cdots < T_{2,0}. \tag{5.2}$$

The high power results show that

$$T_{1n} < T_{1,n-1} \cdots < T_{1,0}. \tag{5.3}$$

Although it is possible that $T_{1i} = T_{2i}$, or perhaps that $T_{1i} = \alpha T_{2i}$, where α is a constant independent of i, the data are not sufficiently precise to draw a conclusion of this type.

Equations (5.2) and (5.3) show that the mechanisms which cause line broadening and relaxation of the central component are weaker than the mechanisms which affect the outer components, and, therefore, one of the significant mechanisms of line broadening and relaxation is intramolecular in origin. This conclusion arises from the following considerations. At any instant, a particular radical molecule contributes to only a single one of the component lines observed in the spectrum, and a particular component arises from the magnetic resonance contributed by a large number of different radicals which all have the same number of (equivalent) nuclei oriented in the direction of the external magnetic field. The only difference between radicals which, at any instant, give rise to different hyperfine components is the number of nuclei aligned in the field direction, and it is therefore extremely unlikely that radicals contributing to different hyperfine components interact with the external surroundings in an appreciably different manner. The relevant interaction must thus be internal rather than external. A mechanism which might account for the observed behavior, suggested by Bloembergen,[17] is the action of the intramolecular anisotropic dipolar interaction

[17] N. Bloembergen (private communication).

between the magnetic moments of the unpaired electron and the protons. Although this interaction averages to zero for molecules tumbling rapidly in solution,[2] and thus does not affect the positions of the lines observed in the spectrum, it can make a contribution to relaxation and line broadening.

The effect of the intramolecular dipolar interaction can be seen qualitatively as follows. The square of the total angular momentum of the nuclei $\mathbf{J}^2$, where $\mathbf{J}=\sum_i \mathbf{I}_i$, commutes with the Hamiltonian. For a molecule containing only equivalent nuclei, $\mathbf{J}^2$ also commutes with the intramolecular dipolar interaction and therefore this interaction does not cause transitions between different J states. For example, a molecule with two protons can have the values $J=0$ and $J=1$; the dipolar interaction can cause transitions among the three states for $J=1$, but cannot affect the state with $J=0$. The central component will therefore be relaxed less strongly by the dipolar interaction than the outside components. Similar reasoning can be extended to systems with any number of equivalent nuclei. The actual calculations of the saturation parameters Ω_i arising from this and other mechanisms is being carried out by Stephen and Fraenkel,[13] and a calculation of the width (T_2^{-1}) is being made by Kivelson.[18]

APPENDIX

The experiments of Jen *et al.*[10] referred to in the introduction showed too large a value of the intensity of the central component as compared to the two outer components in the spectrum of deuterium atoms trapped in a solid matrix at liquid helium temperature for all levels of microwave power investigated. These experiments, in contrast to the data obtained in the present study, showed a greater degree of saturation for the outside components than for the central component. Jen suggested that the saturation in the deuterium atoms could at least in part be explained by relaxation arising from a modulation, or time dependence, of the factor A in the term in the Hamiltonian $A\,\mathbf{I}\cdot\mathbf{S}$ giving rise to the hyperfine splitting. Modulation of A would cause relaxation through terms like $\frac{1}{2}A(I^+S^-+I^-S^+)$. A mechanism of this type was used by Abragam[19] to explain unsymmetrical behavior in the spectrum of arsenic-doped silicon. In these experiments of Abragam and Combrisson, the relaxation time was quite long and the spectra were observed before the system had time to come to equilibrium in the applied field. Jen's experiments, however, involved relaxation times of the order of milliseconds and were therefore steady-state experiments. But for steady-state experiments, as the following analysis shows, this mechanism cannot account for the experimental results.

The proposed mechanism causes transitions from a state (m_s, m) to $(m_s\pm1, m\mp1)$ where m_s and m are the quantum numbers denoting the field-direction component of the electron and nuclear spin, respectively. The transition probability is proportional to $(I\pm m)\times(I\mp m+1)$ which, for a nucleus with spin $I=1$, is independent of m, and we shall denote the transition probability for the transition $(m_s, m)\rightarrow(m_s\pm1, m\mp1)$ by $X^\pm$. Transitions of the type $(m_s, m)\rightarrow(m_s\pm1, m)$ must also take place, and if the assumed mechanism accounts for the dependence on m, these $\Delta m_s=\pm1$, $\Delta m=0$ transitions must be taken to be independent of m. We denote the probabilities of these latter transitions by $W^\pm$. The ratio of the upward to the downward transition probabilities, W^+/W^- (or X^+/X^-) is given by[20]

$$W^+/W^-=\exp(-\epsilon) \qquad \text{(A.1)}$$

where $\epsilon=(h\nu/kT)$ and $h\nu$ is the energy separation between the states with $m_s=-\frac{1}{2}$ and $m_s=+\frac{1}{2}$. Differences in energy arising from the hyperfine interaction have been neglected in writing Eq. (A.1) and are also neglected in the ensuing development. It is readily shown that the saturation parameters Ω_m, the quantities appropriate for the description of the saturation in a steady-state experiment,[13] are given by:

$$\begin{aligned}
2W^-\Omega_1&=\tfrac{2}{3}\cdot\frac{1+2e^\epsilon}{1+e^\epsilon}\cong1+(\epsilon/6),\\
2W^-\Omega_0&=\tfrac{1}{3}\cdot\frac{1+4e^\epsilon+e^{2\epsilon}}{1+e^\epsilon}\cong1+(\epsilon/2),\\
2W^-\Omega_{-1}&=\tfrac{2}{3}\cdot\frac{2+e^\epsilon}{1+e^\epsilon}e^\epsilon\cong1+(5\epsilon/6),
\end{aligned} \qquad \text{(A.2)}$$

where the subscript on the saturation parameters signifies the value of m and the approximate forms given on the right hold for $\epsilon\ll1$. Equation (A.2) shows that a cross-relaxation mechanism arising from modulation of the coefficient of the isotropic hyperfine interaction causes an effect in a steady-state experiment that varies from one end of the spectrum to the other rather than a symmetrical saturation of the outside components as observed by Jen *et al.* This equation also shows that, except at very low temperatures, the entire variation of saturation from one hyperfine component to another is negligible.

It is also of interest to estimate the contribution to the width that would arise from modulation of the coefficient of the isotropic hyperfine interaction. Bloch[15] has given a formulation in terms of general relaxation mechanisms [his Eq. (3.8)] that can be used to estimate the width. For simplicity, we assume that the temperature is sufficiently high to set $W\cong W^+\cong W^-$, and similarly for X, and assume that the relaxation mechanism causing the W-type transitions ($\Delta M_s=\pm1$, $\Delta m=0$) arises from a term in the Hamiltonian of

[18] D. Kivelson (private communication).
[19] A. Abragam and J. Combrisson, Nuovo cimento 6, Series X, Supplement 3 1197 (1957).
[20] Y. Ayant, J. phys. radium 16, 411 (1955).

the form $\mathbf{H}'(t)\cdot\mathbf{S}$. $\mathbf{H}'(t)$ is taken to be an isotropic fluctuating magnetic field with mean value zero and with no correlation between the x, y, and z components. Application of the Bloch formulation to the present problem gives

$$T_{2,0}^{-1}=2W+X,$$
$$T_{2,\pm 1}^{-1}=2W+(3/2)X, \qquad \text{(A.3)}$$

where the second subscript on the relaxation times denotes the value of m. In the limit of large cross relaxation (large X/W), Eq. (A.3) shows that the ratio $T_{2,0}/T_{2,\pm 1}$ approaches 3/2. This is the value of the ratio of peak heights of the central to outside components observed by Jen *et al.* at low power.

The deuterium atom experiments at low power imply that $T_{2,0}>T_{2,\pm 1}$, while those at high power imply that $T_{1,0}<T_{1,\pm 1}$. The experimental results indicate that $T_1\sim 10^4 T_2$, a result which is consistent, according to the above mechanism, with the requirement that $X/W\gg 1$. One must therefore conclude that the magnitude of T_1 and its variation from one component to another arises from a much weaker relaxation mechanism than the mechanisms affecting T_2, and one which is largest for the central component and smallest for the outside components whereas the reverse is true of the mechanisms which affect T_2. It should also be noted, however, that the experiments on the deuterium atoms are not entirely free of any ambiguity of interpretation. These experiments were performed with magnetic field modulation of such a frequency that neither the fast or slow passage conditions were satisfied, i.e., the modulation frequency was in the intermediate region. The derivatives of the absorption spectra appeared like the direct, undifferentiated, absorption spectra, and these complex intermediate-passage modulation-frequency effects may account for part of the difficulties in interpreting the saturation behavior.

It should be noted that a modulation of the coefficient of indirect hyperfine interaction would not be expected to have a significant effect for free radicals in solution. Variations in this coefficient that might occur on collision with solvent molecules would be too rapid (of the order of the vibrational frequencies) to influence the relaxation appreciably, and, in addition, the above arguments show that the saturation behavior arising from this mechanism cannot account for the experimental results on solutions.

Letters to the Editor

THE Letters to the Editor section is subdivided into three parts entitled Communications, Comments and Errata, and Notes. These three sections are all subject to the same limitations on length. The textual material of each Letter is limited to a number of words equal to 950 minus the following: (a) 200 words for each average-sized figure; (b) 50 words for each displayed equation; (c) 7 words for each line of table including headings and horizontal rulings. No proof will be sent to the authors of "Communications" and "Comments and Errata." Proof will be sent to the authors of "Notes." The publication charge for Letters is $30 per page, with a minimum of $30 per Letter. If honored, the Institution will be entitled to 100 reprints without covers. See issues of May–September, 1957, for descriptions of categories.

Communications

Detection of Short-Lived Transients in Radiation Chemistry*

MAX S. MATHESON AND LEON M. DORFMAN

Argonne National Laboratory, Lemont, Illinois

(Received March 23, 1960)

DIRECT detection of short-lived transients in radiation chemistry by methods analogous to those of flash photolysis has heretofore not been possible because of the unavailability of a source of a high-energy radiation pulse of sufficiently high intensity. We report here the results of a series of experiments in which short-lived transients have been observed by synchronized flash absorption spectroscopy in solutions irradiated with a 5-μsec pulse of 15-Mev electrons at an average current of 0.1 amp obtained from an Applied Radiation Corporation linear accelerator.

The solutions were irradiated with a single electron pulse in an 8-cm-long cylindrical quartz cell. The front window, through which the electron beam entered, was coated on the outside with a thin aluminum mirror. The analyzing light beam from a Xenon flash lamp entered through the rear window collinearly with the electron beam, and was reflected twice from the front window and once from a concave mirror at the rear, being finally directed to the slit of a Jarrell-Ash 2.25-m grating spectrograph after thus traversing an absorption path of 32 cm. The spectroflash lamp, which had a pulse half-width of about 10 μsec, was fired electronically through a thyratron from a condenser bank after a preselected delay following the electron pulse.

The following solutions, carefully degassed and sealed off in the cells, were irradiated: (1) 0.01 *M* benzyl chloride in cyclohexane; (2) 0.01 *M* allyl chloride in triply distilled water (as well as 0.01 *M* allyl alcohol in water); (3) 0.004 *M* 1,4-cyclohexadiene in cyclohexane; (4) 0.007 *M* KI in water; (5) 0.04 *M* $KBrO_3$ in water. The transient absorption spectra shown in Fig. 1 were obtained. They are: (1) An absorption undoubtedly due to the benzyl radical, with a strong maximum at 3171 A and a weaker band at 3055 A, the spectrum corresponding with that obtained previously by flash photolysis.[1] The half-life under our conditions was less than 30 μsec. (2) A broad band beginning at 2420 A and cut off at lower wavelengths by the absorption of the allyl compounds themselves, and possibly due to the allyl radical. (3) A broad band beginning at 2625 A, overlying the banded absorption of the cyclohexadiene itself and cut off at lower wavelengths by the absorption of that compound. (4) A band at 3700 A, probably due to the I_2^- ion, the spectrum corresponding to that observed in flash photolysis,[2] and the 3530-A band of I_3^- found as a permanent product.[3] (5) A broad, very short-lived absorption at 3600 A, with a half-life of approximately 10 μsec, suggested in previous photochemical work[4] to be the BrO_3 radical; and a weaker, longer-lived transient with peaks at

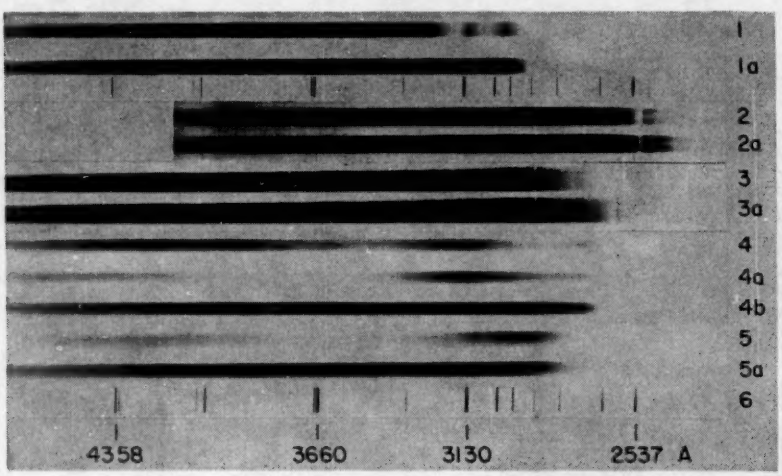

FIG. 1. Transient absorption spectra following electron pulse irradiation. (1) benzyl chloride, 10 μsec delay (1a) blank; (2) allyl chloride, 5-μsec delay (2a) blank; (3) 1,4-cyclohexadiene, 7-μsec delay, (3a) blank; (4b) initial blank (4a) potassium iodide, 6-μsec delay (4) blank after electron pulse; (5) potassium bromate, 5-μsec delay (5a) blank; (6) Hg calibration spectrum. The structure in all the spectra, and the two repeated absorption bands in sets (2) and (3) are due to the spectroflash lamp itself.

about 4500 and 3300 A, previously suggested[4] to be BrO.

These investigations on a variety of systems are continuing and will be detailed in a forthcoming publication.

We are indebted to a number of our associates whose invaluable assistance has made this work possible. They are H. Cremer of the Electronics Division and W. Ramler, L. Rawson, K. Johnson (who achieved accelerator performance in excess of specifications), W. Mulac, and D. Dement of the Chemistry Division. We are grateful for the encouragement Dr. O. C. Simpson gave us in the initiation of this work.

* Based on work performed under the auspices of the U. S. Atomic Energy Commission.

[1] G. Porter and M. W. Windsor, Nature **180**, 187 (1957).
[2] L. I. Grossweiner and M. S. Matheson, J. Phys. Chem. **61**, 1089 (1957).
[3] A. D. Awtrey and R. E. Connick, J. Am. Chem. Soc. **73**, 1842 (1951).
[4] N. K. Bridge and M. S. Matheson, J. Phys. Chem. (to be published).

Paramagnetic Resonance of Co^{2+} with Four- and Eightfold Coordination

T. P. P. HALL AND W. HAYES
Clarendon Laboratory, Oxford

(Received March 22, 1960)

DVIR and Low[1] recently reported an electron spin resonance line in CaF_2 with $g_{max}=2.010$ and $g_{min}=2.0035$ which they assigned to Co^{2+}. We have made measurements on cobalt present in 0.05% M concentration in CaF_2 and CdF_2 which have the fluorite structure with eightfold coordination, and in CdTe which has the zincblende structure with fourfold coordination. Cobalt spectra with cubic symmetry are observed in CdF_2 and CdTe and the measurements are fitted to the spin Hamiltonian

$$\mathcal{H}=g\beta\mathbf{H}\cdot\mathbf{S}+A\mathbf{I}\cdot\mathbf{S}$$

with $S=\frac{3}{2}$ and $I=\frac{7}{2}$. In CdF_2 the cobalt hyperfine structure is resolved at 20°K and we find $g=2.278\pm0.005$ and $A=23.0\pm0.6\times10^{-4}$ cm^{-1}. In CdTe the cobalt hyperfine structure is resolved at 4°K and we find $g=2.30\pm0.01$ and $A=23\times10^{-4}$ cm^{-1}. With CaF_2 a slight anisotropy occurs which makes it difficult to measure A accurately, but we estimate A to be 23×10^{-4} cm^{-1} and $g=2.31\pm0.02$. In both CaF_2 and CdF_2 a fluorine hyperfine splitting parameter A_F of 6×10^{-4} cm^{-1} is measured with some orientations of the magnetic field. In view of these results it would appear that the line observed by Dvir and Low does not arise from Co^{2+}. Paramagnetic resonance of four-coordinated cobalt was also observed by Owen[2] in Cs_3CoCl_5; he observed a broad line with no resolved hyperfine structure. The measured g values ($g_{||}=2.32$, $g_{\perp}=2.27$) are in agreement with the susceptibility measurements of Holm and Cotton[3] on Cs_3CoCl_5.

The ground state of Co^{2+} is ^4F and with four- or eightfold coordination the orbital F level splits into a singlet (Γ_2) and two triplets (Γ_4, Γ_5) with the singlet lowest. The cubic field and spin-orbit coupling do not raise the fourfold spin degeneracy, and the calculated g value is $2-8\lambda/\Delta$ where λ is the spin-orbit coupling constant and $\Delta=10Dq$ is the separation of the first excited triplet Γ_5 from the Γ_2 ground state. A preliminary investigation of the optical absorption spectrum of Co^{2+} in CdF_2 (Hayes, unpublished) indicates a value of 4200 cm^{-1} for Δ. Using this value of Δ and the free ion λ value (-180 cm^{-1}) one calculates g to be 2.343. This is greater than the measured g value suggesting, in agreement with previous measurements,[4] that the value of the spin-orbit coupling constant in the solid environment is less than that of the free ion. In the present case a reduction in λ of about 20% would explain the observed g value.

The hyperfine structure constant A may be written

$$A=N^2P(g_L-\kappa)$$

where N is a normalization factor, $P=2g_n\beta\beta_n/h^3$, $g_L=-8\lambda/\Delta$ is the second-order orbital contribution to the g value, and κ is determined by the admixture of configurations containing unpaired s electrons.[5] Abragam and Pryce[6] find good agreement between the observed and calculated hyperfine structures of Co^{2+} in the sixfold coordinated zinc fluosilicate and the ammonium and potassium Tutton salts using $P=0.225$ cm^{-1} and $\kappa=0.325$. In the cubic field of MgO (sixfold coordinated) Low[7] finds $g=4.278$ and $A=98.7\times10^{-4}$ cm^{-1} for Co^{++}, but in this case the sign of the cubic field splitting is reversed, leaving Γ_4 as the ground state, and the large A value arises from the large orbital contribution to the hyperfine structure ($g_L\simeq1.0$). With four- or eightfold coordination the orbital contribution is a second-order effect ($g_L=0.278$ in CdF_2) and is comparable in size with the contribution from unpaired s electrons. Since the contributions are of opposite sign the value of A is considerably reduced. These measurements provide further evidence for the presence of a κ term in Co^{2+} of the size suggested by Abragam and Pryce[6] since the orbital contribution alone would give an A value more than twice too large. A determination of the sign of A would decide whether κ is larger or smaller than g_L and hence lead to an accurate value of κ. This is not possible in the present case, however, by the usual method.

We are indebted to Dr. R. W. H. Stevenson of the University of Aberdeen, who supplied the CaF_2 and CdF_2 crystals and to Dr. D. A. Wright and Dr. J. Woods of the General Electric Company, Webmley,

for the CdTe crystals. This work was supported by the Board of Admiralty and the United States Air Force.

[1] M. Dvir and W. Low, Proc. Phys. Soc. (London) **75**, 136 (1960).
[2] K. D. Bowers and J. Owen, Repts. Progr. Phys. **18**, 348 (1955).
[3] R. H. Holm and F. A. Cotton, J. Chem. Phys. **31**, 788 (1959).
[4] J. Owen, Proc. Roy. Soc. (London) **A277**, 183 (1955).
[5] A. Abragam and M. H. L. Pryce, Proc. Roy. Soc. (London) **A205**, 135 (1951).
[6] A. Abragam and M. H. L. Pryce, Proc. Roy. Soc. (London) **A206**, 173 (1951).
[7] W. Low, Phys. Rev. **109**, 256 (1958).

MO Treatment of Acetylene Including All Electrons

LOUIS BURNELLE*
Department of Chemistry, Indiana University, Bloomington, Indiana

(Received March 28, 1960)

THE electronic structure of acetylene has already been the object of numerous theoretical investigations.[1–4] However, the Roothaan SCF procedure[5] has to our knowledge never been applied to the entire molecule, taking the H atoms explicitly into account. We have undertaken the present work with the purpose of filling this gap. In view of the importance of inner-shell electrons in molecular structure, we have considered all the electrons of the molecule. Due to the complexity of an exact treatment, however, simplifications have had to be introduced. The following approximations have seemed appropriate to the problem:

(1) The three- and four-center integrals involving the 1*s* orbitals of the carbons have been neglected; all other three- and four-center integrals have been evaluated by the Mulliken approximation.[6]

(2) No configuration interaction has been taken into account.

We have used nodeless Slater orbitals with the following orbital exponents: *h*, 1; *c*, 5.7; *s*, *x*, *y*, *z*, 1.59. Here, *h* and *c* refer to 1*s* orbitals on hydrogen and carbon, respectively, and *s*, *x*, *y*, *z* refer to *L*-shell carbon orbitals. The molecular axis is taken as the *z* axis, and the $2p_z$ orbitals have their positive lobes oriented toward the opposite carbon atom.

From this basis we have constructed normalized symmetry orbitals in the usual fashion. For example, $h_g=(h_1+h_2)/(2+2S_h)^{\frac{1}{2}}$, and $h_u=(h_1-h_2)/(2-2S_h)^{\frac{1}{2}}$, etc.

The expressions for the occupied SCF MO's as well as the corresponding orbital energies are given in Table I. The first excited orbital (π_g) has an energy of 0.283 a.u.

The general features of the results, for instance, the order of the various levels and the signs of the LCAO coefficients, are in agreement with what one would predict on a simple MO basis.[4] The first ionization potential, if taken equal to the orbital energy of the π_u orbital, is 10.34 ev, which can be compared with the experimental value of 11.41 ev.[7] The excitation energy corresponding to the first singlet $\pi\rightarrow\pi^*$ transition ($^1\Sigma_g^+\rightarrow{}^1\Sigma_u^-$) is found to be 6.24 ev, which also compares fairly well with the experimental value of 5.23 ev.[8] It is to be mentioned that, by considering the six-electron system C≡C, Ross has found for the first $\pi\rightarrow\pi^*$ transition an energy of 8.02 ev.[1] The explicit introduction of the inner-shell electrons and of the CH bonds brings thus a sizable improvement of the result.

The calculated total molecular energy is −77.95 a.u., which is 0.56 a.u. lower than the experimental value. The apparent violation of the variation theorem is a consequence of the approximation of the integrals. A comparable result was found in the case of Be_4, where the Mulliken approximation has been shown to lower the total energy by an appreciable amount.[9]

TABLE I.

Molecular wave functions	Orbital energies (a.u.)
$(1\sigma_g)=0.00263\,h_g+0.99614\,c_g+0.01380\,s_g+0.00388\,z_g$	−11.592
$(1\sigma_u)=0.00078\,h_u+0.99685\,c_u+0.017977\,s_u+0.00630\,z_u$	−11.588
$(2\sigma_g)=0.42589\,h_g-0.19421\,c_g+0.71275\,s_g-0.17702\,z_g$	−1.064
$(2\sigma_u)=0.47504\,h_u-0.15780\,c_u+0.36194\,s_u-0.27328\,z_u$	−1.001
$(3\sigma_g)=0.28105\,h_g+0.14097\,c_g-0.35225\,s_g-0.78500\,z_g$	−0.862
$(\pi_u)=x_u$	−0.380

We have carried out an electron distribution analysis, according to Mulliken's definitions.[10] The overlap population of each CH bond is found to be 0.87, that of the CC σ bond 0.82. Both values are larger than the corresponding ones in ethylene,[11] in agreement with the current views on hybridization. The gross atomic population on the hydrogens is 0.895, on the carbons 6.105. A charge of 0.92 *e* is found to be promoted from the carbon 2*s* orbital, which corresponds to a degree of hybridization very close to *sp*.

A detailed amount of the present work will be published later, including the application of the SCF procedure to various *cis*- and *trans*-bent configurations, and calculation of the quadrupole moment.

The present study was started at the University of Liege, Belgium, and the author wishes to acknowledge help in programing from the staff of IBM Belgium. He is also deeply indebted to the members of the Quantum Chemistry Group of Indiana University for use of their programs and for numerous valuable discussions.

* Chercheur Qualifié du Fonds National Belge de la Recherche Scientifique. Appointment at Indiana University supported by the International Cooperation Administration under the Visiting Research Scientists Program administered by the National Academy of Sciences of the U.S.A. This work was also supported in part by a grant to Indiana University from the National Science Foundation.

[1] I. G. Ross, Trans. Faraday Soc. **48**, 973 (1952).
[2] J. Serre and A. Pullman, J. Chim. Phys. **50**, 447, (1953).
[3] T. Nakamura, K. Ohno, M. Kotani, and K. Hijikata, Prog. Theoret. Phys. **8**, 387 (1952).
[4] R. S. Mulliken, J. Chem. Phys. **3**, 517 (1935); A. D. Walsh, J. Chem. Soc. **1953**, 2288.
[5] C. C. J. Roothaan, Revs. Modern Phys. **23**, 69 (1951).
[6] R. S. Mulliken, J. Chim. Phys. **46**, 500 (1949).
[7] K. Watanabe, J. Chem. Phys. **26**, 542 (1957).
[8] C. K. Ingold and G. W. King, J. Chem. Soc. **1953**, 2702.
[9] R. D. Cloney and J. S. Dooling, J. Chem. Phys. **29**, 425 (1958).
[10] R. S. Mulliken, J. Chem. Phys. **23**, 1833 (1955).
[11] H. Berthod, Compt. rend. **249**, 1354 (1959).

Charge Distribution, Hybridization, and Bonding in Acetylene and Carbon Dioxide*

A. D. McLEAN, B. J. RANSIL, AND R. S. MULLIKEN

University of Chicago, Chicago 37, Illinois

(Received March 31, 1960)

COMPARISON of Burnelle's[1] SCF-LCAO-MO wave functions for C_2H_2 with these of McLean[2] shows qualitative agreement, but very appreciable quantitative differences. These are understandable in view of the fact that all integrals were evaluated accurately by McLean, whereas the three- and four-center integrals in Burnelle's treatment were approximated or in fact (where small) omitted. The general agreement of the two calculations is gratifying.

With reference to the electron population analysis[3] reported by Burnelle, a comparison with corresponding results based on McLean's wave functions taken from a paper in course of preparation, seems of interest. Following are our numbers compared with those of Burnelle, in parentheses. Overlap populations of CH and CC σ bonds, 0.79 e (0.87 e) and 0.89 e (0.82 e). Gross charge on each H atom, $+0.21$ e ($+0.105$ e) providing the first calculated numbers which correlate with the acidic character of H in acetylene. Promotion out of the $2s$ carbon AO, 0.92 e (0.92 e), indicating hybridization close to sp in the σ bands, as also concluded by Burnelle. Of interest also is the π overlap population, for which we find 1.05 e in total for the two π bonds (π_x plus π_y); Burnelle does not report this, although his value should be the same as ours. Comparison with the isoelectronic molecule N_2 is interesting; there[4] the net total σ overlap population is 0.395 e, while for the two π bonds the overlap population is 0.880 e. The much smaller σ population in N_2 than in C_2H_2 is attributable to lone-pair repulsions which are absent in C_2H_2.

A similar population analysis on McLean's CO_2 wave function yields the following major features: σ and π overlap populations per C═O bond, 0.21 e and 0.52 e, respectively. Gross charges, $+0.43$ e on the carbon and -0.22 e on each oxygen atom. Promotion out of $2s_C$ into $2p\sigma_C$ (plus some transfer to the O atoms), 1.08 e, indicating hybridization means sp in the σ bonds, as in C_2H_2. In the O atoms in CO_2, we find $2s_O \rightarrow 2p\sigma_O$ promotion of 0.14 e, about the same[3] as for the O atom in CO and in H_2O.

* Supported in part by a grant from the National Science Foundation, by Air Force contracts, and by the Office of Ordnance Research.

[1] L. Burnelle, J. Chem. Phys. **32**, 1872 (1960), preceding communication.
[2] A. D. McLean, J. Chem. Phys. **32**, 1595 (1960).
[3] R. S. Mulliken, J. Chem. Phys. **23**, 1833 (1955).
[4] C. W. Scherr, J. Chem. Phys. **23**, 569 (1955).

ESR Spectrum of the Cyclooctatetraenyl Radical Anion*

THOMAS J. KATZ AND HERBERT L. STRAUSS†

Department of Chemistry, Columbia University, New York 27, New York

(Received April 1, 1960)

CYCLOOCTATETRAENE has attracted considerable attention since Willstätter, in an attempt to create a new nonbenzenoid aromatic system, synthesized the molecule and found it devoid of aromatic stability. The molecule is now known to exist in a nonplanar tub conformation (D_{2d}), and the basis of its olefinic properties clearly resides in the absence of conjugation between the nearly orthogonal double bonds.[1] On inquiring into the fundamental means by which aromatization could be effected in the eight-membered ring, we considered the addition of electrons to the molecule and noted that the process of adding electrons to the antibonding orbitals of the tetraolefin might well be superseded by ring flattening and the entrance of electrons into the nonbonding π orbital associated with the D_{8h} conformation if the greatly increased resonance energy in the new frame of reference were sufficiently great to overcome the compressional strain required to flatten the ring. The facile reaction of cyclooctatetraene with alkali metals seems incompatible with the known chemistry of unconjugated olefins and seems clearly indicative of the change suggested. We have examined the species resulting on reaction of cyclooctatetraene with lithium or potassium in tetrahydrofuran and have shown that such treatment results in the establishment of an equilibrium between a small amount of a radical, which we will name the cyclooctatetraenyl radical anion, and a preponderant amount of the corresponding divalent anion and unchanged hydrocarbon.[2] These

results will be discussed in detail elsewhere, but we wish to report here a portion of our studies on the cyclooctatetraenyl radical anion.

Considerable interest has recently attended the study of radical ions derived from benzenoid aromatic compounds. Although physical measurements of electronic spectra[3] and redox potentials[4] have resulted in satisfying correlations with theoretical calculations,[5] a particularly sensitive and valuable method by which the validity of theoretical inferences of their molecular structure has been assessed involves the examination of their electron spin resonance spectra.[6] The usefulness of the observation that coupling can occur between the magnetic moment of an unpaired electron occupying a carbon $2p$ π orbital and the nuclear moment of the attached hydrogen atom as a result of σ-π exchange interactions has been greatly enhanced as a result of the extended theoretical treatment owing to McConnell.[7] The fundamental consequence of these theoretical considerations lies in the prediction that the hyperfine splitting (a) owing to a proton attached to a carbon atom of the aromatic nucleus is proportional to the average spin density on that carbon (ρ), so that $a = Q\cdot\rho$, where Q is a negative constant. The difficulties associated with the theoretical estimation of the unpaired electron densities in the complex, often polycyclic aromatic systems for which the proton hyperfine spectra have been analyzed,[8] and the complications arising when account is taken of negative spin densities have impeded progress in the field. These obstacles have been surmounted in the study of the benzene radical anion,[9] a molecule in which symmetry considerations alone define the unpaired electron density on each carbon atom as one-sixth of an odd electron, and of the methyl radical,[10] in which the odd electron resides in a p orbital on the lone carbon atom. However, the lack of other molecules which provide this rare opportunity has thus far limited exact study to these two.

The cyclooctatetraenyl radical anion provides a new system in which ρ is defined independently of any arbitrary theoretical assumptions. Solutions prepared by treatment of cyclooctatetraene in tetrahydrofuran with up to two moles of lithium were examined by the electron spin resonance method, which reveals a spectrum of nine equally spaced lines in the expected intensity ratios attributable to the hyperfine interaction of the eight equivalent protons. No splitting due to the nuclear moment of the cation was observed in such solutions. If the cyclooctatetraenyl radical anion is planar, the observed equivalence of the protons implies that Jahn-Teller distortions are averaged in a time short compared with the hyperfine splitting frequency.[9,11,12]

The splitting of the peaks due to the proton hyperfine interaction was determined to be 3.209 ± 0.007 gauss.[13] Although the geometry of the molecule cannot be precisely specified, symmetry considerations require that one-eighth of the odd electron reside on each carbon atom, and thus the proton hyperfine splitting constant Q is here found to be -25.67 ± 0.07 gauss. The values previously established are -22.5 gauss for the benzene radical anion and -22.9 gauss for the methyl radical.

The g value was found to be 2.0025 ± 0.0001, remarkably close to the free-electron value. The determination was made by comparison with a sample of diphenylpicrylhydrazyl, the g value of which was measured as 2.0036 ± 0.0001.

The presence of the radical anion in solutions prepared by treatment of cyclooctatetraene in tetrahydrofuran with potassium metal was similarly indicated by the electron spin resonance spectrum. Here, however, an exchange reaction broadened the hyperfine structure considerably. The observation that such structure could be resolved in solutions of constant cyclooctatetraene concentration (approximately 0.7 M) only when trace amounts of potassium metal were employed, whereas broadening to a single unsplit resonance occurred as larger amounts of potassium were used, revealed that rapid exchange of the electrons of the radical anion was occurring not with the hydrocarbon, cyclooctatetraene, but with the divalent anion. These findings support the view that the anion radical and the dianion are similar in geometry and unlike the parent hydrocarbon, for the electron exchange between the molecules is subject to the restrictions of the Franck-Condon principle.

The spectra were determined using an improved spectrometer similar to that of Hirshon and Fraenkel[14] equipped with a Varian 6-in. magnet. The frequency of a proton oscillator[15] was measured with a Hewlett Packard model 524B counter checked against a standard oscillator.

* Supported in part by the U. S. Air Force through the Office of Scientific Research.

† National Science Foundation Predoctoral Fellow, 1957–1960.

[1] For recent reviews of the chemistry of cyclooctatetraene see R. A. Raphael, *Non-Benzenoid Aromatic Compounds*, edited by D. Ginsburg (Interscience Publishers, Inc., New York, 1959), p. 465 ff. and R. A. Raphael, *Chemistry of Carbon Compounds*, edited by E. H. Rodd (Elsevier Publishing Company, New York, 1953), Vol. IIB, p. 260 ff.

[2] The disproportionation equilibrium constant at room temperature was estimated by electron spin resonance as 10^{9}–10^{10}.

[3] P. Balk, S. DeBruijn, and G. J. Hoijtink, Rec. trav. chim. **76**, 907 (1957); P. Balk, G. J. Hoijtink, and J. W. H. Schreurs, *ibid.* **76**, 813 (1957).

[4] G. J. Hoijtink, Rec. trav. chim. **77**, 555 (1958), and earlier papers.

[5] P. Balk, S. DeBruijn, and G. J. Hoijtink, Mol. Phys. **1**, 151 (1958); P. Balk, S. DeBruijn, and G. J. Hoijtink, Rec. trav. chim. **76**, 860 (1957).

[6] G. K. Fraenkel and B. Segal, Ann. Rev. Phys. Chem. **10**, 435 (1959).

[7] H. M. McConnell and D. B. Chesnut, J. Chem. Phys. **28**, 107 (1958).

[8] A. Carrington, F. Dravnieks, and M. C. R. Symons, J. Chem. Soc. **1959**, 947; E. DeBoer and S. I. Weissman, J. Am. Chem. Soc. **80**, 4549 (1958).

[9] T. R. Tuttle, Jr., and S. I. Weissman, J. Am. Chem. Soc. **80**, 5342 (1958).

[10] C. K. Jen, S. N. Foner, E. L. Cochran, and V. A. Bowers, Phys. Rev. **112**, 1169 (1958); T. Cole, H. O. Pritchard, N. R. Davidson, and H. M. McConnell, Mol. Phys. **1**, 406 (1958).

[11] Weissman,[12] however, has suggested that Jahn-Teller effects manifest themselves in a broadening of paramagnetic resonance lines. The half-width at half maximum of the central line in our spectrum is 0.41 gauss.

[12] M. G. Townsend and S. I. Weissman, J. Chem. Phys. **32**, 309 (1960).

[13] Standard deviation.

[14] J. M. Hirshon and G. K. Fraenkel, Rev. Sci. Instr. **26**, 34 (1955).

[15] D. J. E. Ingram, *Free Radicals Studied by Electron Spin Resonance* (Academic Press, Inc., New York, 1958), p. 63.

Comments and Errata

Luminosity of Shock Waves in Xenon

JOHN N. BRADLEY

Department of Inorganic and Physical Chemistry, University of Liverpool, Liverpool, England

(Received November 23, 1959)

IN order to explain the luminosity behind shock waves in xenon, Roth and Gloersen[1] have postulated the initial formation of an excited xenon atom Xe^*, which undergoes a radiative transition to the metastable state Xe^m. This then reacts with another xenon atom to form the stable excited molecule Xe_2^*, which gives an emission continuum in the visible on dissociating.

The kinetic scheme which they employed did not include reverse collision processes, the steady-state concentrations of Xe^* and Xe^m being maintained entirely by radiative deactivation. As the collision frequency of Xe^* atoms in these experiments was of the same order of magnitude as the radiative transition probability, such an approximation may require further justification. However, the most serious objection to the kinetic scheme is that it predicts a time dependence of the Xe_2^* concentration of the form: $a(1-e^{-b,t})$ with a maximum gradient at $t=0$. The oscilloscope records of the light emission displayed a finite induction period followed by a steep rise in concentration. It is obvious that the steady-state approximation cannot be applied to both portions of the experimental curve. If the approximation were valid during the induction period, then a further reaction mechanism would be required to explain the subsequent increase in the rate of production of xenon molecules.

New experimental data[2] show that resonance radiation from xenon appears at the same time as the visible continuum so that the same induction period applies to both types of emission. The uv continuum displayed the same time dependence as the resonance radiation while the visible continuum gave a symmetrical emission-time curve. The latter behavior has been explained on the basis of severe radiation cooling, the other types of emission persisting owing to the imprisonment of radiation.

Previous measurements of radiative cooling[3] were made in argon at higher temperatures and provided no evidence to support a symmetrical emission curve. For such behavior to persist over a range of temperatures, it is necessary that the rate of buildup of Xe_2^* should show a similar temperature coefficient to the radiative loss, which seems very unlikely. The work with argon indicated an approximately exponential decay, which should lead to a pronounced "tail" at lower temperatures.

The fact that the intensity of resonance radiation does not increase linearly with time after passage of the shock shows that resonance-state atoms are not formed by simple binary collisions. As the intensity-time behavior of the visible continuum corresponds very closely to the first derivative of the intensity-time curve for the resonance radiation, it is postulated that the rate of formation of resonance-state (or metastable) atoms is proportional to the concentration of Xe_2^* producing the continuum. The results therefore suggest a standard consecutive reaction sequence of the type

$$A \rightarrow Xe_2^* \rightarrow Xe + Xe^* + h\nu \text{ (visible)}.$$

The Xe_2^* species here now represents a higher excited state of the molecule. In this system, the visible continuum will be produced by the breakdown of the higher excited-state molecules to give excited atoms. This explains why the resonance radiation continues to increase in intensity even after the visible continuum has passed through a maximum but ceases to rise as soon as continuum emission disappears. The uv continuum can still be produced from the resonance state (or metastable) atoms by a mechanism similar to that proposed by Roth and Gloersen.

A scheme of this type leaves unsettled the route by which higher excited states of Xe_2 are populated. One possible explanation may be that small concentrations of electrons are built up at the front, where impurity emission is observed. These will have low translational energies initially[4] so that the induction period may correspond to the time during which the electron temperature is raised by elastic collisions. At these higher energies, the electrons may participate in the formation of excited xenon atoms or molecules. The formation of the Xe_2^+ ion by electron impact is known to involve an excited xenon atom rather than a xenon ion.[5]

Although these suggestions are quite speculative, it seems certain that different species must be responsible for the different continua and that the mechanism for the production of these species is more complicated than was thought hitherto.

[1] W. Roth and Per Gloersen, J. Chem. Phys. **29**, 820 (1958).
[2] W. Roth, J. Chem. Phys. **31**, 844 (1959).
[3] H. E. Petshek, P. H. Rose, H. S. Glick, A. Kane, and A. Kantrowitz, J. Appl. Phys. **26**, 83 (1955).
[4] H. E. Petshek and S. Byron, Ann. Phys. (N. Y.) **1**, 270 (1957).
[5] J. A. Hornbeck and J. P. Molnar, Phys. Rev. **84**, 621 (1951).

Reply to "Luminosity of Shock Waves in Xenon"

WALTER ROTH

Armour Research Foundation, Physics Research Division, Chicago, Illinois

(Received December 1, 1959)

BRADLEY[1] points out correctly that the time dependence of Xe_2^* concentration predicted by the proposed mechanism[2] is not in accord with experimental observations. However, reverse collisional processes are still considered unimportant by this author, inasmuch as equilibrium emission is never reached but only a steady-state emission is attained. The steady-state condition was not applied during the induction period. The time to reach a steady state in Xe_2^* concentration was equated with the induction period for visible continuum emission.

It seems clear that Xe does not absorb its own visible continuum radiation but does absorb its resonance and uv continuum radiation.[3] Thus, the radiation is optically thick in the uv but optically thin in the visible, and cooling must occur via visible continuum radiation. Radiative cooling behind shocks in Ar has been found to be the dominant cooling mechanism.[4] The difference in emission decay rates in Xe and Ar may merely reflect a difference in transition probabilities in Xe_2^* and Ar_2^*.

Resonance-state atoms, formed in binary collisions, are imprisoned by reabsorption and by formation of metastable-state atoms. It was assumed[2] that the latter ultimately formed Xe_2^* molecules upon interaction with ground-state atoms. It is known that resonance- and ground-state atoms interact to form molecules which radiate uv continua.[5] This combination of processes would not be expected to result in a linear increase of resonance radiation intensity with time.

The fact remains, however, that despite the validity of individual steps in the proposed mechanism,[2] the over-all mechanism does not successfully account for the observed approach to steady-state emission. Therefore the mechanism must either be revised or an alternative mechanism must be offered.

The suggestion by Bradley that a higher excited state of Xe_2^* is involved in visible continuum emission than that found for the uv continuum is certainly worth investigating. The same suggestion has been advanced by others.[6,7] However, when a mechanism involving formation of the higher excited state is forthcoming, it should, when applied to the experimentally determined induction period, give an activation energy which is consistent with the energy of formation of the higher-excited-state molecule. In addition, it would be of value to have other spectroscopic evidence of the existence of the proposed molecular state. It should be pointed out that a band system has been observed for the first excited state[4] of Xe_2^* but has not been observed yet for any higher state.

[1] J. N. Bradley, J. Chem. Phys. **32**, 1875 (1960), preceding comment.
[2] W. Roth and P. Gloersen, J. Chem. Phys. **29**, 820 (1958).
[3] W. Roth, J. Chem. Phys. **31**, 844 (1959).
[4] H. E. Petschek *et al.*, J. Appl. Phys. **26**, 83 (1955).
[5] P. G. Wilkinson and Y. Tanaka, J. Opt. Soc. Am. **45**, 344, 710 (1955).
[6] R. S. Mulliken, University of Chicago (private communication).
[7] P. Gloersen (to be published).

Self-Diffusion in the Primary Alcohols

DAVID W. MCCALL AND DEAN C. DOUGLASS

Bell Telephone Laboratories, Incorporated, Murray Hill, New Jersey

(Received March 18, 1960)

POWLES and Cutler[1] have recently reported measurements of the coefficients of self-diffusion for some normal alcohols at 25°C. The nuclear magnetic resonance spin-echo method[2,3] was employed, but the nature of the field gradient was not well defined; in particular, it was not constant over the sample. Owing to calibration difficulties, their figures were reported as the ratio $D(\text{alcohol})/D(\text{water})$.

The ratios $D(\text{alcohol})/D(\text{water})$ were found[1] to be significantly greater than those previously obtained by Partington, Hudson, and Bagnall[4] from tracer measurements. Powles and Cutler[1] suggested the possibility that adsorption of the glass frits employed in the tracer studies might be responsible for this discrepancy. At Dr. Powles' suggestion, we have measured the self-diffusion coefficients for *n*-propanol and *n*-butanol by the spin-echo method[3] in an attempt to resolve the discrepancy experimentally. Our technique differs from that of Powles and Cutler in that we apply a constant field gradient to the sample when making

TABLE I.

Substance	This study $10^5 D$ (cm²/sec)	This study $D/D(H_2O)$	Powles and Cutler $D/D(H_2O)$	Partington *et al.* $D/D(H_2O)$
H_2O	21[5]	[1.00]	[1.00]	[1.00]
n-C_3H_7OH	5.12	0.24	0.6[5]	0.27
n-C_4H_9OH	4.26	0.20	0.6[0]	0.21
n-$C_8H_{17}OH$	1.38	0.066		

our diffusion measurements. Our results are listed in Table I. These results were obtained at 24°C; *n*-octanol was also measured for comparison.

It is apparent that the present measurements confirm the tracer studies adequately. We suggest that the use of a decay term of the form $\exp(-2\gamma^2G^2Dt^3/3)$ lies at the root of the difficulty. This decay applies only to a constant field gradient G. It appears that even relative diffusion coefficients determined in a non-constant gradient are incorrect. The analysis of the experiment in the presence of higher-order field terms, $H=H_0+G_x+G_1x^2+\cdots$, is sufficiently complicated that we have been unable to include even the square term.

[1] J. G. Powles and D. Cutler, Arch. Sci. (Geneva) **12**, 135 (1959).
[2] H. Y. Carr and E. M. Purcell, Phys. Rev. **94**, 630 (1954).
[3] D. C. Douglass and D. W. McCall, J. Phys. Chem. **62**, 1102 (1958).
[4] J. R. Partington, R. F. Hudson, and K. W. Bagnall, J. Chim. Phys. **55**, 77 (1958).
[5] J. H. Simpson and H. Y. Carr, Phys. Rev. **111**, 5 (1958).

Erratum: Theory of Phase Transitions in Solid Heavy Methane

[J. Chem. Phys. **31**, 12 (1959)]

HUBERT M. JAMES
Purdue University, Lafayette, Indiana
AND
THOMAS A. KEENAN
University of Rochester, New York

(Received March 25, 1960)

A PROOFREADING error in our paper with the above title seems to deserve notice, since it might be troublesome to someone making use of our results. In the caption to Table V, read $d=-255/32$ [cf. Eq. (4.2)], rather than $d=255/32$.

Notes

Spin-Lattice Relaxation and Molecular Structure. I. The Major Importance of Intermolecular Contributions

F. A. BOVEY
Central Research Laboratories, Minnesota Mining and Manufacturing Company, St. Paul, Minnesota

(Revised manuscript received March 15, 1960)

IN organic liquids of not too high viscosity, i.e., where the molecular reorientation rate is much greater than the observing rf frequency, the following

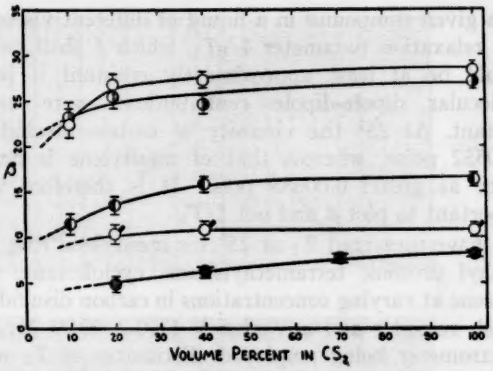

FIG. 1. The dependence of $\beta(=1/\eta T_1)$ for solute protons on vol % of solute in CS_2. Open circles: mesitylene methyl groups; circles shaded on right: tetramethylsilane; circles shaded on left: cyclohexane; circles with projections: mesitylene ring; fully shaded circles: benzene.

relationship describes the rate of intramolecular spin-lattice relaxation produced by the interaction of neighboring pairs of protons,[1] if it be assumed that the reorientation rate may be expressed by the Stokes-Einstein approximation:

$$\frac{1}{T_1}=\frac{h^2\gamma^4}{2\pi kT}\cdot\frac{a^3}{b^6}\cdot\eta. \qquad (1)$$

Here γ is the proton gyromagnetic ratio, a is the radius of the molecule (taken as being at least approximately spherical), b is the distance between the two protons, and η the viscosity (in poises) of the liquid or of its solution in another liquid. Where two protons relax a third, as in methyl groups or benzene rings, Eq. (1) requires modification,[2] but its general form may be expected to hold.

The calculation of intermolecular relaxation rates is somewhat more uncertain. Bloembergen *et al.*[1(a)] indicated that this process may be important in water, but in larger molecules, particularly of less highly associated or non-associated liquids, it is not clear that it is important. Reilly *et al.*[3,4] have approached this question experimentally by measuring the T_1 of a compound at various dilutions in carbon disulfide, which contains no magnetic nuclei. On plotting $1/T_1$ for the methyl groups and ring protons of mesitylene against weight percent of mesitylene in carbon disulfide solution, they obtained approximately straight lines having markedly positive slopes and having intercepts on the zero-concentration axis which were less than half the values for pure mesitylene. It was concluded (Table I of reference 4) that intermolecular dipole-dipole interaction contributes the major share of the spin-lattice relaxation in this molecule, particularly for the ring protons. (It should be noted that in a recent textbook,[5] this work of Reilly *et al.* is quite erroneously described as dealing with T_2, the spin-spin relaxation time.)

From Eq. (1), it would be expected that, for solutions

of a given compound in a liquid of different viscosity, the relaxation parameter $1/\eta T_1$, which I shall call β, would be at least approximately constant if intermolecular dipole-dipole contributions were unimportant. At 25° the viscosity of carbon disulfide is 0.00352 poise, whereas that of mesitylene is nearly twice as great: 0.00638 poise. It is therefore very important to plot β and not $1/T_1$.

I have measured T_1 at 25° for mesitylene ring and methyl protons, tetramethylsilane, cyclohexane, and benzene at varying concentrations in carbon disulfide, a Brush recorder and a Varian V-4300-2 40.00 Mc/sec spectrometer being employed. Estimates of T_1 were made by the direct method [method I of reference 1(a)]. The samples were first saturated by using high rf power for 5–10 sec; the power was then quickly reduced to levels corresponding to only slight saturation. Semi-log plots of the regrowth of the signal were made at four rf power levels. The values of T_1 estimated by extrapolation to zero power appeared to be reproducible within ± 2–3% for pure liquids and about ± 5–10% at the higher dilutions. Viscosity measurements were made at 25° using Ostwald pipettes of long flow time (about 6 min for water), no kinetic energy correction being made. Figure 1 shows plots of β *vs* volume percent of the compound in carbon disulfide. The curves are in general nonlinear and (somewhat surprisingly) show a rather abrupt decrease of β below 40 vol % solute, making extrapolation to infinite dilution uncertain. There appears to be no doubt, however, that the contributions of intermolecular and intramolecular dipole-dipole interactions depend strongly on molecular structure. In benzene, the protons are relatively far apart, and this is reflected in a small β and an intermolecular contribution of at least 50–60%. The mesitylene ring protons interact with the methyl groups and show less intermolecular contributions. Methyl group protons, having two near neighbors, show a large β and a small (ca 15–20%) intermolecular contribution. There appear to be some grounds for assigning a value of about 5–6 for the intermolecular contribution to β in neat non-associated liquids. These results appear to me to indicate that, contrary to the conclusions of Reilly *et al.*,[3,4] intramolecular interaction is commonly the dominant contribution to spin-lattice relaxation in such liquids.

The samples were prepared and their viscosities measured by Miss Lucetta Stifter. The spectrometer was operated by Mr. George Filipovich and Mr. Donald Hotchkiss. I am grateful to Dr. G. V. D. Tiers for many stimulating conversations, and am particularly indebted to Dr. C. A. Reilly for very helpful suggestions and discussion.

[1] (a) N. E. Bloembergen, E. M. Purcell, and R. V. Pound, Phys. Rev. **73**, 679 (1948); (b) R. Kubo and K. Tomita, J. Phys. Soc. Japan **9**, 888 (1954); (c) I. Solomon, Phys. Rev. **99**, 559 (1955).

[2] See, for example, P. S. Hubbard, Phys. Rev. **109**, 1153 (1958).

[3] G. W. Nederbragt and C. A. Reilly, J. Chem. Phys. **24**, 1110 (1956).

[4] C. A. Reilly and R. L. Strombotne, J. Chem. Phys. **26**, 1338 (1957).

[5] J. D. Roberts, *Nuclear Magnetic Resonance* (McGraw-Hill Book Company, New York, 1959), pp. 17–18.

Potential Energy Barrier to Rotation in Methyl Nitrite Measured by PMR

PETER GRAY* AND LEONARD W. REEVES

Chemistry Department, University of British Columbia, Vancouver 8, B. C., Canada

(Received July 29, 1959)

THE potential energy barrier to rotation in methyl nitrite was determined by Gray and Pratt[1] as $V_b = 7800$ cal mole^{-1}. Uncertainties in calorimetric data limited the accuracy of this estimate. The work reported here was complete when Piette and Anderson[2] published a comprehensive study of alkyl nitrites.

A Varian V-4300 high-resolution spectrometer (with flux stabilizer) operating at 40 Mc was used. The methyl nitrite, prepared from methanol in the usual way,[3] and purified to better than 99.95% is contained as a liquid under its own vapor pressure in a 5-mm o. d. glass tube. These tubes and their bearings are accurately made on a microglass lathe[4] to ensure that spinning is free from wobble. The sample temperature is controlled by a modification[4] of the equipment used by Bernstein *et al.*[5] and it is measured to 0.1° with a copper-constantan couple connected to a Rubicon potentiometer. With this apparatus it is easy to keep constant (better than 1°C) temperatures down to −80°C. Signal halfwidths are independent of sweep rates and deviations are not greater than $\pm 2\%$ from the average at the lower temperatures (below 0°C).

Potential barrier from broadening of high temperature signal. The single resonance signal observed at 28°C has a $T_2 = 0.21$ sec. As the temperature is lowered, broadening of this line sets in as the rate of isomerization diminishes. It is noticeable at +15°C and by −30°C the width $\Delta\nu_{\frac{1}{2}}$ is about 25 cps though the line is still symmetrical. From the line widths measured at temperatures between 10° and −35°C the barrier height V_b is determined by means of the Eq. (24) of reference 2. The value $V_b = 10\,500 \pm 2000$ cal mole^{-1} to which these measurements lead may be compared with the "thermodynamic" value[1] $V_b = 7800$ cal mole^{-1} and with the other NMR value 9000 ± 2000 cal mole^{-1} reported[2] by Piette and Anderson.

The "coalescence" temperature. At −32.5°C a shoulder is apparent; this shoulder is pronounced at −36°C and by −40.4°C appears as a broad, nearly horizontal point of inflexion. Figure 1 shows the appearance of the signal at ∼3°C intervals in the neighborhood of −27° to −44°C. As well as fixing the "coalescence"

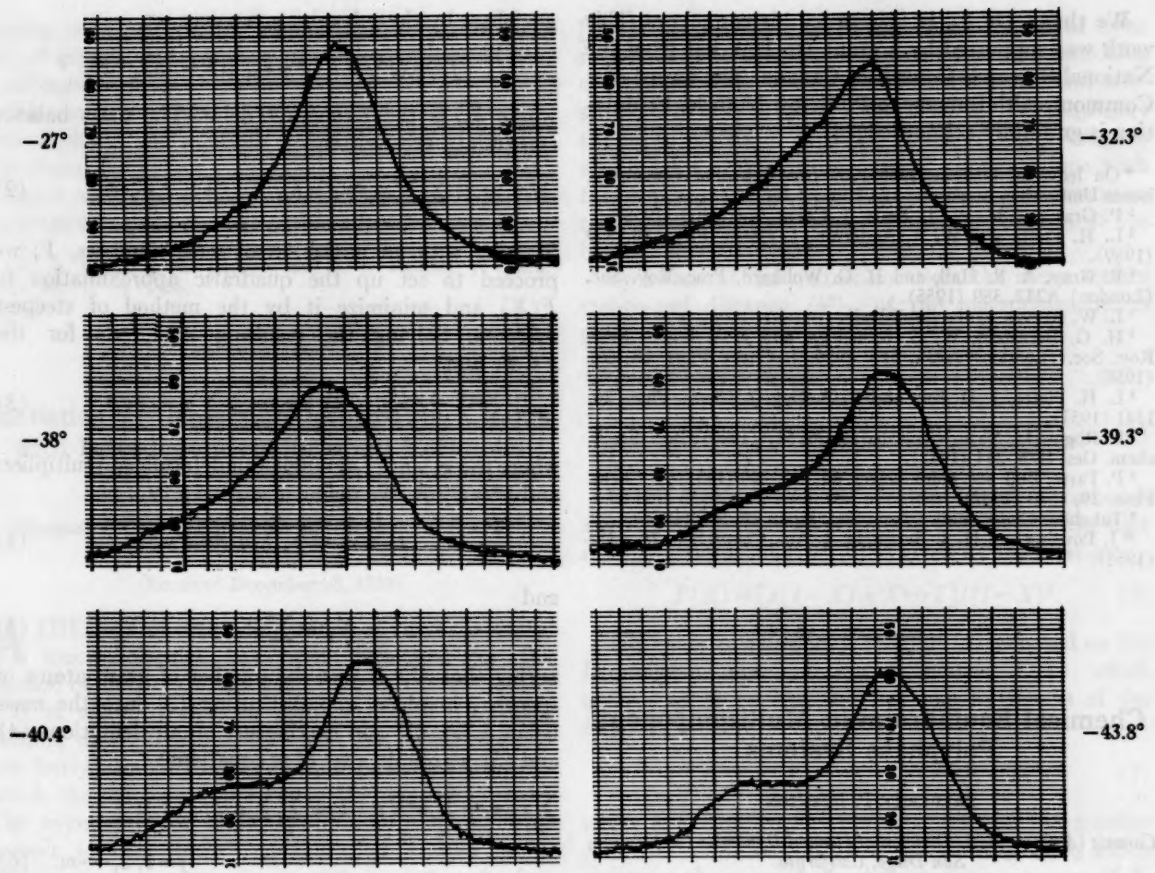

FIG. 1. The appearance of the signal at ~3°C intervals in the neighborhood of −27° to −44°C.

temperature, T_c, at −38±1° (previously reported[2] as −43±3°C) these spectra, which were not obtained consecutively but on different days, serve as an indication of the internal consistency and accuracy of the temperature control.

Since $\Delta\nu$=43±2 cps at 40 Mc and 32±2 cps at 30 Mc,[6] the value of τ at −38°C (235°K) is 5.23 msec. If the velocity constant of isomerization is taken as $k=A\exp(-V_b/RT)$, then these values of T_c, τ_c, and V_b lead to $A=1.2\times10^{12}$ sec^{-1}, close to the value of $KT/h=4.7\times10^{12}$ sec^{-1} at T_c.

Isomer abundance and heat of isomerization from the low-temperature spectrum. Below −40°C the broad inflexion on the low field side becomes a second peak and by −53°C the two peaks are almost completely separated: their maxima are 37±1 cps apart. At 75°C there is no appreciable broadening of the constituent peaks which are separated completely and are 43±2 cps apart[2] (cf. separation[6] 32±2 cps at 30 Mc). From the areas under the two peaks the relative abundance of the *cis* and *trans* isomers may be evaluated. We find, at −52°C (*cis*/*trans*)=0.377±0.025. A *cis*/*trans* ratio of ca 0.29 has been reported[6] "near −60°C" and of 0.303 at −75°C. These values are consistent with an enthalpy of isomerization (from *trans* to *cis*) in the liquid phase, ΔH_l=ca 800 cal mole^{-1}. If the observation of Piette *et al.* that at 21° the coalesced peak lies midway between the low temperature locations of the separated peaks is correct so that at 21°C *cis*/*trans*=1, then ΔH_2 would be still positive but numerically larger. These numerical estimates of ΔH_2 are subject to large errors.

Electron-diffraction patterns[7] indicate (*cis*/*trans*)=4 in the vapor, a figure which receives qualitative support[1,8] from infrared spectroscopic evidence. The contrast is not a conflict but is readily interpreted in terms of the dipole moments[9] of the two species, since the *trans* form with the larger dipole moment will have the larger heat of solution. The enthalpy of isomerization in a solvent of dielectric constant ϵ and molecular volume $V=(M/\rho)$ is related[10] to that in the gas phase by the equation:

$$\Delta H_l-\Delta H_g=[(\epsilon-1)\rho/(2\epsilon+1)M]\cdot N_0^2(\mu_t^2-\mu_c^2).$$

Inserting the values ΔH_g= ca −350 cal mole^{-1},[8,9] μ_t=3.0 debyes[9], μ_c=1.3 debyes[9] and ϵ= ca 7 appropriate to methyl nitrite we have ΔH_l= ca 100 cal mole^{-1}, small but opposite in sign to that in the gas.

We thank Dr. L. H. Piette for his comments. This work was supported by a grant (to L.W.R.) from the National Research Council of Canada. The award of a Commonwealth Bursary to P. G. by Nuffield Foundation is gratefully acknowledged.

* On leave of absence 1958–1959 from School of Chemistry, Leeds University, England.

[1] P. Gray and M. W. T. Pratt, J. Chem. Soc. 3403 (1958).
[2] L. H. Piette and W. A. Anderson, J. Chem. Phys. **30**, 899 (1959).
[3] P. Gray, A. R. Hall, and H. G. Wolfhard, Proc. Roy. Soc. (London) **A232**, 389 (1955).
[4] L. W. Reeves (to be published).
[5] H. G. Bernstein, W. G. Schneider, and J. A. Pople, Proc. Roy. Soc. (London) **A236**, 515, 1956; J. Chem. Phys. **28**, 601 (1958).
[6] L. H. Piette, J. D. Ray and R. A. Ogg, J. Chem. Phys. **26**, 1341 (1957).
[7] F. Rogowski, Naturwissenshaften **28**, 517 (1940); Ber. dirsch. chem. Ges. **B75**, 244 (1942).
[8] P. Tarte, Bull. soc. chim. belges. **60**, 227, 240 (1951); J. Chem. Phys. **20**, 1570 (1952).
[9] Takehiko Chiba, Bull. Chem. Soc. Japan **28**, 505 (1955).
[10] J. Powling and H. J. Bernstein, J. Am. Chem. Soc. **73**, 4353 (1951).

Chemical Equilibrium in Multicomponent Polyphase Systems

FREDERICK P. BOYNTON

Convair (Astronautics), Division of General Dynamics Corporation, San Diego, California

(Received November 23, 1959)

A RECENTLY proposed method[1] of calculating the equilibrium composition of a mixture of ideal gases at constant temperature and pressure proceeds by minimizing the free energy of the system. The method of steepest descents and the minimization of free energy may also be applied to a system of many phases, since the criterion of equilibrium is exactly the same. The derivation of a method of handling a polyphase system in which condensed phase solutions may occur is presented below. Only ideal systems will be specifically considered, although the method may also be applied to those nonideal systems where the activity coefficients are known functions of a composition by adding another iterative loop.

Consider a mixture containing n molecular species, formed from m different atoms, and distributed among ϕ phases. Following the notation of White *et al.*[1] we define the free-energy function of the system:

$$F(X)=\sum_i\sum_\alpha x_i^\alpha f_i^\alpha \tag{1}$$

where x is the number of moles of the ith molecular species in phase α. The effect of pressure upon condensed phases is usually very small, so that if we identify the gas phase by the subscript g, we may set

$$f_i^\alpha=(F^0/RT)_i^\alpha+\delta_{g\alpha}\ln P+\ln x_i^\alpha/\bar{x}^\alpha$$

where $\delta_{g\alpha}$ is the Kronecker delta. The mass balance constraints are written:

$$\sum_i\sum_\alpha a_{ij}^\alpha x_i^\alpha=b_j, \qquad j=1,2,\cdots m. \tag{2}$$

Starting with an initial set of mole numbers, Y, we proceed to set up the quadratic approximation to $F(X)$ and minimize it by the method of steepest descents. Solving the resulting equations for the x's, we find

$$x_i^\alpha=f_i^\alpha(Y)+y_i^\alpha u^\alpha+\sum_j \pi_j a_{ij}^\alpha y_i^\alpha \tag{3}$$

where the π_j's are Lagrangian undetermined multipliers and $\bar{u}^\alpha=\bar{x}^\alpha/\bar{y}^\alpha$. We define

$$r_{jk}=r_{kj}\equiv\sum_i\sum_\alpha a_{ij}^\alpha a_{ik}^\alpha y_i^\alpha \tag{4}$$

and

$$N_j^\alpha\equiv\sum_i a_{ij}^\alpha y_i^\alpha \tag{5}$$

noting that N_j^α is just the number of gram atoms of species j in phase α. Substituting (3) into the mass balance Eq. (2) and making use of our definitions (4) and (5) we obtain a set of m equations:

$$\sum_k r_{jk}\pi_j+\sum_\alpha u^\alpha N_j^\alpha=b_j+\sum_i\sum_\alpha a_{ij}^\alpha f_i^\alpha(Y), \qquad j=1,2,\cdots m. \tag{6}$$

Another group of ϕ independent equations may be obtained by summing the equations (3) over all j for each phase:

$$\sum_j \pi_j N_j^\alpha=\sum_i f_i^\alpha(Y)=F^\alpha(Y) \quad \alpha=1,2,\cdots\phi \tag{7}$$

where F^α is the free-energy function of the phase α. We then have a set of $m+\phi$ linear equations for the π's and u's. The coefficient matrix of these equations is symmetrical about the major diagonal, as may be seen by expanding (6) and (7). Comparison of this development with that of White *et al.*[1] shows immediately that the set of $m+1$ equations derived therein is simply a specialization, for the case where $\phi=1$, of that given here.

The numerical computation of composition is generally straightforward, provided that the chemical species and phases chosen are those that should be present. Phases not included in the initial assumptions will not spontaneously appear; therefore, it is necessary to provide for every condensed phase whose presence is suspected. If a phase that should not be present is included (such as a solid which should be a gas), those species in other phases which can react directly with the extra phase will tend to disappear. In any case a false result will be obtained. One method of correcting this

answer is to perform the computation for a different set of phases and compare the free energies of the resulting system.

One must be careful to use standard states for condensed phases and solutions which are compatible with the above derivation.

Good results have been obtained from an IBM 704 program using the method outlined here.

[1] W. B. White, S. M. Johnson, and G. B. Dantzig, J. Chem. Phys. 28, 751–55 (1958).

Statistics of Isotactic Deformable Chains with Interdependent Internal Rotations

V. Magnasco and C. Rossi

Instituto di Chimica Industriale dell'Università di Genova, Genova, Italy

(Received December 28, 1959)

A THEORY of mean dimensions of vinylic isotactic macromolecules has been developed by the method of matrices of rotation.[1,2]

It is assumed that in consequence of Brownian motion, the N bonds of the chain can rotate more or less freely around the equilibrium positions, the ones which the macromolecule has in the crystalline state. The asymmetry of these equilibrium positions with respect to the "trans" configuration enables us to explain the asymmetrical potentials hindering the free rotation of the bonds. The calculations have been performed in the case of a periodic structure with period two, where the rotations of odd place (all equal among them) are different from the rotations of even place (all also equal among them).

That enables us to define $R_1=\langle R_{2j-1}\rangle$ ($j=1, 2, \cdots, N/2$) the mean matrix of odd rotations, and $R_2=\langle R_{2j}\rangle$ [$j=1, 2, \cdots, (N-2)/2$] the mean matrix of even rotations. The interdependence of internal rotations, determined from the interactions among lateral substituents of vinylic chain, is described by $X=\langle R_{2j}R_{2j-1}\rangle$ the mean matrix of even-odd product. The average is effected by averaging on over-all configurations with the proper statistical weight the trigonometric functions that characterize the state of internal rotation of the bonds.

By means of the matrix notation, the mean square end-to-end distance $\langle h^2\rangle_N$ of the macromolecule, is given by

$$\langle h^2\rangle_N=2l^2[x(I+R_1)_{11}+\sum_{p,q=1}^{3}(I+R_1)_{1p}F(X)_{pq}(X+R_2)_{q1}]. \quad (1)$$

In this expression l is the constant length of the bond, $x=N/2$ the number of periods of the chain, I the unit matrix of third order. $F(X)$ is given by the relation

$$F(X)=[x(I-X)+X^x-I]/(I-X)^2. \quad (2)$$

The exact calculation of relation (1) is based on the Lagrangean representation of matrix $F(X)$ which enables us to express this last one by means of the following quadratic expression in X,

$$F(X)=aX^2+bX+cI, \quad (3)$$

where a, b, c are coefficients depending on the number N of the bonds and on the eigenvalues λ_1, λ_2, λ_3 which represent the roots of the characteristic equation of X.

Having established the mean values of angular parameters, one can perform numerically the exact calculation of the mean molecular dimensions for every N value.

When the chain is flexible and $N\gg1$ (Gaussian chain) in the case of interdependence of rotations, we have

$$\frac{\langle h^2\rangle_N}{Nl^2}=\frac{1+\alpha}{1-\alpha}\frac{[1-\sigma-(1-\alpha)\eta_1\eta_2][1-\rho+(1-\alpha)\epsilon_1\epsilon_2]+[\omega+(1-\alpha)\epsilon_1\eta_2][\tau+(1-\alpha)\eta_1\epsilon_2]}{(1-\eta_1)[(1-\eta_2)(1-\rho)+\omega\epsilon_2]+\epsilon_1[(1-\eta_1)\tau+(\sigma-\alpha)\epsilon_2]}, \quad (4)$$

where α is the cosine of the supplement of the valence angle and

$$\begin{cases}\eta_1=\langle\cos\phi_{2j-1}\rangle & \eta_2=\langle\cos\phi_{2j}\rangle & \epsilon_1=\langle\sin\phi_{2j-1}\rangle & \epsilon_2=\langle\sin\phi_{2j}\rangle\\ \rho=\langle\cos\phi_{2j}\cos\phi_{2j-1}\rangle-\alpha\langle\sin\phi_{2j}\sin\phi_{2j-1}\rangle & \sigma=\alpha\langle\cos\phi_{2j}\cos\phi_{2j-1}\rangle-\langle\sin\phi_{2j}\sin\phi_{2j-1}\rangle\\ \tau=\alpha\langle\sin\phi_{2j}\cos\phi_{2j-1}\rangle+\langle\cos\phi_{2j}\sin\phi_{2j-1}\rangle & \omega=\langle\sin\phi_{2j}\cos\phi_{2j-1}\rangle+\alpha\langle\cos\phi_{2j}\sin\phi_{2j-1}\rangle.\end{cases} \quad (5)$$

If the interactions among the lateral substituents are weak, the rotations can be considered statistically independent. Then $X=\langle R_{2j}\rangle\langle R_{2j-1}\rangle$, and we have

$$\frac{\langle h^2\rangle_N}{Nl^2}=\frac{1+\alpha}{1-\alpha}\frac{1-2(\eta_1\eta_2-\epsilon_1\epsilon_2)+(\eta_1^2+\epsilon_1^2)(\eta_2^2+\epsilon_2^2)}{(1-\eta_1)(1-\eta_2)-(\eta_1^2+\epsilon_1^2-\eta_1)(\eta_2^2+\epsilon_2^2-\eta_2)}, \quad (6)$$

which coincides with the result of Kazuo Nagai.[3] It is easy to obtain from Eq. (4) all the results known in the literature.

Numerical applications of Eq. (1) have been performed in the case of the isotactic polystyrene, where the equilibrium positions are alternatively the gauche and the trans positions, by means of different potential models. Detailed calculations and these applications will be published elsewhere.[4]

We wish to thank Professor Antonio Borsellino for many useful suggestions and discussions.

[1] S. Lifson, J. Chem. Phys. **29**, 80, 89 (1958).
[2] A. Borsellino, Ric. Sci. **29**, 496 (1959); J. Chem. Phys. **30**, 857 (1959).
[3] Kazuo Nagai, J. Chem. Phys. **30**, 660 (1959).
[4] V. Magnasco, Ric. Sci. **30**, 405 (1960); Makromol. Chem. (to be published).

Quadrupole Resonance Spectrum of Chloranil and Its Hexamethylbenzene Complex*

DEAN C. DOUGLASS†
Department of Chemistry, Cornell University, Ithaca, New York

(Received February 4, 1960)

THE nuclear quadrupole resonance spectrum of chlorine in chloranil (tetrachloroquinone) and the 1:1 complex of chloranil with hexamethylbenzene have been obtained by means of a regenerative spectrometer[1] and a recording system.[2] The resonant frequencies and approximate line widths obtained are given in Table I.

The crystal structure of chloranil is such that the four chlorine atoms in a given chloranil molecule are crystallographically different. The four molecules per unit cell are, however, equivalent.[3] Therefore, the chloranil may have up to four lines in its spectrum.[4] The crystal structure of the complex may be obtained from that of the pure chloranil by replacing two chloranil molecules by hexamethylbenzene molecules in each unit cell.[5] In this structure each remaining chloranil molecule has a center of symmetry. The two chloranil molecules are equivalent, therefore, the complex has a two-line spectrum.

Since the quadrupole resonance frequency of the chlorine depends strongly on the ionic character of the bond, the quadrupole resonance frequency may be used as a quantitative measure of the ionic character of the chlorine-carbon bond in chloranil. For a purely ionic bond, the resonant frequency would be very low and for a pure covalent bond, 55 Mc. The ionic character of the halogen-carbon bond, in term, depends on the electron density at the carbon; therefore, one expects the quadrupole resonant frequency of the chlorine to give a quantitative measure of the charge density on the carbon atom to which it is bonded. This expectation is borne out by the experiments of Bray[6] and the calculations of Jaffé.[7] Bray has shown that the quadrupole resonant frequencies of substituted benzenes may be correlated with the Hammett σ function. Jaffé has calculated charge density in the π system of substituted benzenes and correlated these charge densities with the Hammett σ function. Using the results of these two papers, one concludes that the chlorine resonance frequency should decrease about 12 Mc for an increase of one electronic charge on carbon bonded to the chlorine.

If the chloranil:hexamethylbenzene complex is a charge-transfer complex, one expects the electronic transfer to take place from the hexamethylbenzene to the chloranil. Such a transfer would result in a decrease of the chlorine resonant frequency in the complex relative to the pure chloranil. Table I shows that in fact the average of the observed frequencies increases slightly (100 kc). It is known that crystalline field effects frequently shift quadrupole resonance frequencies by ± 200 kc. These crystal field effects are extraneous and would have to be eliminated in order to determine any shift arising from charge transfer. Unfortunately, these extraneous effects are not obtainable, at present, from either experiment or calculation; therefore, one can only estimate an upper limit to the amount of charge transfer allowed by this experiment. In order to make such an estimate suppose that a crystal field effect raises the resonance frequency of the chlorine in the complex relative to chlorine in pure chloranil by 200–300 kc.[6] In this case the downward shift from the electron transfer would have to be about 100–200 kc. If the electron which is transferred from the hexamethylbenzene is more or less uniformly distributed in the chloranil π system, this shift is accomplished by a transfer of at most 5–10% of an electronic charge. This upper limit of 5–10% of an electronic charge for the amount of charge transfer is in keeping with the amount of charge transfer inferred from dipole moment data.[8]

Complexes of picrylchloride (2, 4, 6 trinitrochlorobenzene):hexamethylbenzene and parachloroaniline: *sym*-trinitrobenzene were also prepared but no resonances could be detected. X-ray scattering from the picrylchloride:hexamethylbenzene complex shows a somewhat disordered structure.[9] Instead of alternate

TABLE I. Quadrupole spectra of chloranil and its hexamethylbenzene complex.

	77°K	Width	Room temp	Width
Chloranil	37.5851 Mc	2.7 kc	...	...
	37.5148	2.0	...	...
	37.4698	0.94	36.7885	1.1 kc
	37.4417	1.5	36.8596	1.2
Chloranil-hexamethyl-benzene	37.5042	1.9	No resonance observed	
	37.7161	very broad		

layers of picrylchloride and hexamethybenzene molecules, one occasionally finds more than one layer of one type of molecule. This disorder might well account for the failure to observe a resonance in this compound.

The author wishes to acknowledge the assistance and guidance of Professor R. Bersohn in this work.

* This work was supported by the U.S. Atomic Energy Commission.

† Present address, Bell Telephone Laboratories, Inc., Murray Hill, New Jersey.

[1] T. C. Wang, Phys. Rev. **99**, 566 (1955).
[2] D. C. Douglass, thesis, Cornell University, 1957.
[3] S. L. Chorghade, Z. Krist. **101**, 418 (1939).
[4] The previously reported spectrum [D. W. McCall and H. S. Gutowsky, J. Chem. Phys. **21**, 1300 (1953)] is the spectrum of an old sample which may have experienced reduction.
[5] T. T. Harding and S. C. Wallwork, Acta Cryst. **8**, 787 (1955).
[6] P. J. Bray and R. G. Barnes, J. Chem. Phys. **27**, 551 (1957).
[7] H. H. Jaffé, J. Chem. Phys. **20**, 279 (1952).
[8] G. Briegleb, and J. Czekalla, Z. Elektrochem. **59**, 184 (1955).
[9] H. M. Powell and G. Huse, J. Chem. Soc. 435, 1943.

Raman Spectrum and Structure of Perchlorylfluoride

FRANCIS X. POWELL AND ELLIS R. LIPPINCOTT

Department of Chemistry, University of Maryland, College Park, Maryland

(Received February 1, 1960)

THE infrared spectrum of perchlorylfluoride, ClO_3F, has been reported by Lide and Mann[1] and an analysis of the spectrum indicates that it has a structure with C_{3v} symmetry. The structure may be derived by replacing one of the oxygen atoms in the perchlorate ion, ClO_4^-, by a fluorine atom.[1,2] We have recently obtained the Raman spectrum of this substance and find that the assignment of the Raman frequencies is in essential agreement with the assignment made for the infrared spectrum thus furnishing additional evidence for the C_{3v} symmetry.[4]

Raman spectra were recorded using a two-prism Huet spectrograph (aperture $f/8$) with a dispersion of 18 A/mm at 4358 A. Excitation was accomplished with a low-pressure Toronto arc using the 4358-A mercury line with potassium nitrite and rhodamine dye as optical filters for radiation above and below this wavelength, respectively. The sample was condensed in a Raman tube at dry-ice temperature and during the experiment the temperature was maintained at approximately $-50°C$ by means of a heat exchanger. Standard techniques were used in photographing and recording the spectrum. The observed Raman frequencies and assignment are given in Table I, along with the observed fundamental infrared spectrum from Lide and Mann.[1]

A comparison of Table I with the infrared frequencies given by Lide and Mann[1] show that all Raman frequencies are coincident with infrared frequencies within experimental error. C_{3v} symmetry calls for three (a_1)-type fundamentals and three (e)-type doubly degenerate fundamentals. In the (a_1) species there are: $\nu_1(ClO_3$ symmetric stretch), ν_2(ClF stretch), and $\nu_3(ClO_3$ symmetric deformation). The degenerate modes are ν_4(ClO stretch), $\nu_5(ClO_3$ deformation), and ν_6(rock). All six modes are Raman- and infrared-active. The lines at 549 and 1061 cm^{-1} were assigned $\nu_3(ClO_3$ symmetric deformation) and ν_1(ClO symmetric stretch), respectively, because their sharpness and intensity are consistent with their interpretation as polarized lines. The degenerate modes should be assigned higher frequencies than their symmetric counterparts, in which case the 587-cm^{-1} line is $\nu_5(e)$ (ClO_3 deformation) and the 1312-cm^{-1} line is $\nu_4(e)$ (ClO stretch). The choice of 1312 cm^{-1} over the other observed Raman lines in this region was made because it coincides with a very strong infrared frequency at 1315 cm^{-1}. The lowest Raman frequency at 410 cm^{-1} was assigned $\nu_6(e)$ (rock). The band at 685–724 cm^{-1} was assigned ν_2(ClF stretch). The presence of Cl^{35} and Cl^{37} isotopes could account for the relative broadness of this band. The remaining lines can be assigned as combination or overtone frequencies.

TABLE I. Raman spectrum of ClO_3F (cm^{-1}).

Raman frequencies[a]	Assigned infrared fundamentals[b]	Interpretation
410 m	405	$\nu_6(e)$ rock
549 ms	549	$\nu_3(a_1)$ deformation
587 m	589	$\nu_5(e)$ deformation
695–724 m	704	$\nu_2(a_1)$ stretch $Cl^{37}F$
	714	$\nu_2(a_1)$ stretch $Cl^{35}F$
1061 s	1061	$\nu_1(a_1)$ ClO stretch
1175 w (broad)		$2\times587(e)=1174(A_1+E)$
1312 w (broad)	1315	$\nu_4(e)$ ClO stretch
1346 w		
1460 w (broad)		$1061+410=1471(E)$

[a] s=strong, ms=medium strong, m=medium, w=weak.
[b] For the infrared frequencies in addition to the fundamentals see reference 1.

We wish to thank Dr. William C. Purdy for calling our attention to this problem and for furnishing us with a sample of perchlorylfluoride.

[1] D. R. Lide and D. E. Mann, J. Chem. Phys. **25**, 1138 (1956).
[2] R. P. Madden and W. S. Benedict, J. Chem. Phys. **25**, 594 (1956).
[3] D. R. Lide and D. E. Mann, J. Chem. Phys. **25**, 59 (1956).
[4] It has been brought to our attention that an unpublished Raman spectrum of this substance was obtained by J. L. Dunlap and E. A. Jones. (Abstract K6 of Southeastern meeting of APS, Lexington, Kentucky, April, 1957.)

Ionization Potential of Fluorine*

JOHN T. HERRON AND VERNON H. DIBELER

Mass Spectrometry Section, National Bureau of Standards, Washington, D. C.

(Received February 8, 1960)

ACCURATE measurements of thermochemical constants of fluorine are made difficult by the highly reactive nature of this element and many of its compounds. Nevertheless, acceptable values for the dissociation energy of the molecule, ionization potential, and electron affinity of the atom, and other constants are now well established. There is, however, some uncertainty as to the ionization potential of F_2.

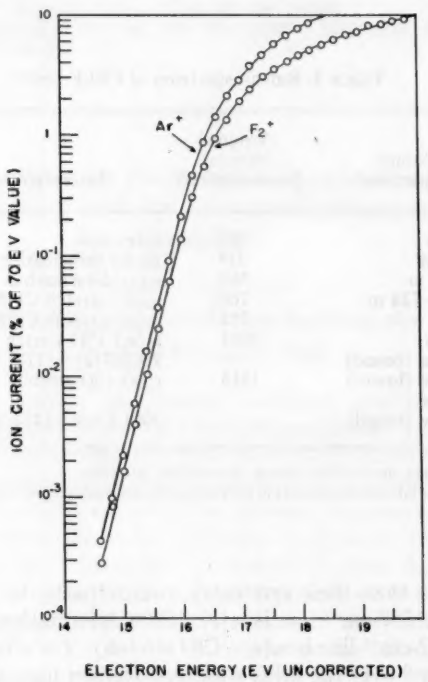

FIG. 1. Ionization efficiency curve for F_2^+.

Burns[1] and Thorburn[2] have reported mutually consistent values for $I(F_2)$ from electron-impact studies. However, their values are considerably greater than a value based on a Rydberg series, recently reported by Iczkowski and Margrave.[3]

We have repeated measurements of the ionization potentials of F_2, Cl_2, and Br_2 by electron impact. We find good agreement with recent electron-impact and photoionization measurement in all cases except F_2.

The mass spectrometer and the method used to measure appearance potentials are described elsewhere.[4]

The sample handling system was all glass and used greaseless metal valves in place of the usual lubricated stopcocks. Nevertheless the introduction of the halogen gases always resulted in the formation of some hydrogen halides.

In the case of the doubly charged ions, measurements were made on the isotopically mixed species, suitably corrected for any contributions from the hydrogen halides occurring at the same m/e.

The results are shown in the table along with other recent experimental values. Unless otherwise indicated, the values refer to electron-impact experiments. Standard deviations are included.

The results for the second ionization potentials of chlorine and bromine have not been reported previously.

For the first ionization potentials of Cl_2 and Br_2, the results of various workers are in reasonable agreement. In the case of fluorine, however, our result is 0.7 to 0.8 ev lower than the previous electron impact measurements, but is consistent with the spectroscopic value.

If the low value for the ionization potential of F_2 is accepted, then from

$$D(F_2^+)+I(F_2)=D(F_2)+I(F)$$

using $D(F_2)=1.59$ ev[5] and $I(F)=17.42$ ev,[6] $D(F_2^+)=3.18$ ev.

The ionization efficiency curve for the F_2^+ ion, shown in the figure, gives no indication of more than one ionization process within several volts of threshold.

As no electronically excited state is expected in this region we are at a loss to explain the discrepancy between the present and the previous electron-impact data for F_2.

TABLE I. Ionization potentials of F_2, Cl_2, and Br_2.

Ionization potential (ev)			
F_2	Cl_2	Br_2	Reference
16.5			Burns[a]
16.6±0.2			Thorburn[b]
	11.80	10.92	Morrison and Nicholson[c]
	11.63±0.04	10.69±0.03	McDowell and Frost[d]
	11.48±0.01	10.55±0.02	Watanabe (photoionization)[e]
15.7			Iczkowski and Margrave (Rydberg series)[f]
15.83±0.05	11.64±0.05	10.58±0.08	This work
	$Cl_2 \rightarrow Cl_2^{++}$	32.6 ev	
	$Br_2 \rightarrow Br_2^{++}$	30.0 ev	

[a] Footnote reference 1.
[b] Footnote reference 2.
[c] J. Chem. Phys. 20, 1021 (1952).
[d] Can. J. Chem. (to be published).
[e] J. Chem. Phys. 26, 542 (1957).
[f] Footnote reference 3.

* This research was supported in part by the Department of the Army under the National Bureau of Standards' Free Radical Research Program.

[1] J. F. Burns, Carbide and Carbon Chemicals Company, K-25 Plant, Ph.D. thesis: University of Tennessee, August, 1954, Report K-1147, October 8, 1954.
[2] R. Thorburn, Proc. Phys. Soc. (London) **73**, 122 (1959).
[3] R. P. Iczkowski and J. L. Margrave, J. Chem. Phys. **30**, 403 (1959).
[4] J. T. Herron and V. H. Dibeler, J. Am. Chem. Soc. **82**, 1555 (1960).
[5] W. H. Evans, T. R. Munson, and D. D. Wagman, J. Research Natl. Bur. Standards **55**, 147 (1955).
[6] C. E. Moore, Natl. Bur. Standards Circ. No. 467 (1949).

Optical Absorption of *F* Bands in Thallium-Doped Potassium Halides

JORDAN J. MARKHAM* AND HERBERT N. HERSH

Research Department, Zenith Radio Corporation, Chicago 39, Illinois

(Received February 12, 1960)

ONE would like to know the environment of *F* centers in Tl-doped alkali halides. Is it the same as in "pure" crystals, or are the negative-ion vacancies near thallous ions? Foreign ions near *F* centers will distort the ground and excited-state electron-wave functions. The nearby thallous ion could also change the local vibrational modes about the negative-ion vacancies. These two effects will influence the width of the absorption band at half-height *H*. (For a detailed theoretical justification of these statements see the Appendix of work cited footnote 1.) *H* could also be changed due to the formation of additional centers with absorption bands which overlap the *F* band. An unchanged *H* would indicate that the band is not altered by the formation of additional centers and that the environment of the negative-ion vacancies has not been influenced by additional imperfections. This is the case in x-rayed crystals that have been plastically deformed at room temperature.[2]

Smakula[3] studied the dependence of *H* on the presence of Tl^+ in NaCl at room temperature. Here *H* is quite large (0.46 ev) and it cannot be measured with great accuracy. A small bandwidth, less than 0.2 ev, means that the sides of the band are quite steep and that the points at half-height can easily be determined. This is not the case when *H* is large. Even making this allowance the variations in Smakula's data seem excessive. Nevertheless, a conclusion obtained from his data is that the presence of Tl^+ does not influence the width.

We herewith present measurements of *H* and the point of maximum absorption ϵ_m on *F* bands in single crystals of KCl, KBr, and KI, both "pure" and thallium-doped (see Table). The concentration of Tl^+ in the doped KI crystal was about 0.01 mole %. Comparable concentrations were found in the other materials. Hence, the concentration of Tl^+ ions is of the order of 10^{18} cm^{-3}, approximately 10 times the concentration of *F* centers. Statistically, the probability of having a negative-ion vacancy next to a thallium ion is small if both are randomly distributed. The possibility of nonrandom distributions exists.

TABLE I. *F* band in thallium-containing potassium halides.[a]

Crystal	Temp °K	*H* ev±.01	ϵ_m ev±.01
KI	5	0.14	1.88
KI:Tl	5	0.14	1.88
KI	78	0.19	1.87
KI:Tl	78	0.19	1.87
KI and *U* centers	78	0.19	1.87
KI	300	0.35	1.81
KI:Tl	300	0.36	1.82
KBr	78	0.19	2.07
KBr:Tl	78	0.19	2.07
KBr	193	0.29	2.02
KBr:Tl	193	0.31	2.02
KBr	300	0.36	1.99
KBr:Tl	300	0.36	1.99
KCl	78	0.19	2.31
KCl:Tl	78	0.19	2.31

[a] The *F* band is essentially the same whether the *F* centers are produced by x raying (at any temperature) or by additive coloration (with proper quenching). *F* centers cannot be formed in heavily doped crystals by additive coloration.

The data show that *H* and ϵ_m in thallium-doped potassium halides are no different than in the "pure" crystals. Most probably, the shapes of the *F* bands are identical. We tentatively conclude that the *F* center in Tl^+ doped crystals is in a "perfect" crystal environment (not near Tl^+). This is also the case in plastically deformed crystals.[2]

Doping produces new color centers and radically changes the thermal and optical behavior of the *F* centers.[4,5] The doping affects the type of *V* centers formed. It does not, however, influence the *F* centers directly. The optical and thermal bleaching properties of the *F* centers are different in doped crystals because of the release of holes or electrons into the conduction—or the valence band—from centers that form primarily in doped crystals.

We would like to thank R. Jarka and J. D. Konitzer for taking the data.

* Now at Physics Research Division, Armour Research Foundation, Chicago 16, Ill.

[1] J. D. Konitzer and J. J. Markham, J. Chem. Phys. **32**, 843 (1960).
[2] H. N. Hersh and J. J. Markham, J. Phys. Chem. Solids **12**, 207 (1959).
[3] A. Smakula, Z. Phys. **59**, 603 (1930).
[4] J. H. Schulman, J. Phys. Chem. **57**, 749 (1953).
[5] H. N. Hersh, J. Chem. Phys. **30**, 790 (1959) and **31**, 909 (1959).

Correlation of Molecular Yields in Hydrocarbon Radiolyses with Mass Spectral Data*

LEON M. DORFMAN AND MYRAN C. SAUER, JR.
Argonne National Laboratory, Lemont, Illinois

(Received February 4, 1960)

CORRELATION of radiation chemical yields with mass spectral data has recently been attempted for over-all product formation in the case of hexane,[1] and has previously been suggested for individual products.[2] In spite of the reasonable questions which may be raised concerning the theoretical validity of such calculations, the G values obtained, solely from information on ionic processes (unimolecular and bimolecular) and a knowledge of the energy requirement for ionization, seem to show good agreement with experiment.

We have carried out such a correlation for the molecular detachment yields of H_2, CH_4 and C_2H_2 in the gas-phase radiolyses of methane, ethylene, ethane, and propane, and have obtained exceedingly close agreement between calculated and observed values. Molecular detachment yields, which have been established for a number of compounds,[2-5] were chosen for the correlation, rather than total product yields, for two reasons. The correct experimental value of the initial total yield may be in doubt in many cases, since it appears[6-8] that radical yields of products are very much dependent on percent conversion, and decrease from the true initial yields (with which comparison should be made) as the reaction proceeds. Molecular detachment yields, on the other hand, seem to be independent of percent conversion[8] and thus representative of initial yields. In calculating total yields, the broad selection among elementary processes which may contribute to radical yields weakens the significance of the correlation. The suggested elementary ionic processes contributing to molecular yields, based on mass spectral information, are limited in number, so that the calculation is not readily subject to adjustment by selection. Thus, the comparison for molecular yields would seem to be a more stringent test.

The experimental molecular yields, taken from published and recent, unpublished work, are listed below.

TABLE I. Comparison of calculated and observed molecular yields.

Reactant	Molecular product	Molecular yield (molecules/100 ev) Obs[a]	Calc
CH_4	H_2^M	3.3±0.2	3.4
C_2H_4	H_2^M	1.3±0.1	1.2
C_2H_4	$C_2H_2^M$	2.3±0.3	1.9
C_2H_6	H_2^M	3.3±0.2	3.3
C_2H_6	CH_4^M	0.4±0.1	0.6
C_3H_8	H_2^M	2.1±0.3	1.7
C_3H_8	CH_4^M	0.9±0.2	0.9

[a] Values obtained at room temperature.

The molecular yield of H_2 from methane is obtained from the over-all yield[2,5,9,10] of 5.9±0.5 and the determination of molecular contribution by both scavenger and isotopic techniques.[2,5,11] The molecular yields of H_2 and C_2H_2 from ethylene correspond to the over-all yields[12,13] since both isotopic[13] and scavenger[14] experiments show these products to be completely molecular. The molecular yields of H_2 and CH_4 from ethane are obtained from the over-all yields[4,5] and molecular contribution estimates by both scavenger and isotopic techniques[3,5] at 0.3 to 1% conversion, as well as at very low conversion.[8] The molecular yields of H_2 and CH_4 from propane are obtained from scavenger studies[4,5] alone.

The calculated values are based on W values of 27.3, 26.5, 24.6, and 24 ev per ion-pair for CH_4, C_2H_4, C_2H_6, and C_3H_8, respectively,[15] and on the mass-spectral patterns for 70-v electrons listed in the API Tables. The elementary reactions involved have, for the most part, been observed in the mass spectrometer[16,17] and have in many cases already been suggested as the contributing processes. These are: H_2 from methane by the reaction $CH_3^+ + CH_4 = C_2H_5^+ + H_2$ and neutralization of the CH_5^+ ion as suggested,[2] along with a minor contribution from $CH_4^+ = CH_2^+ + H_2$; H_2 from ethylene by the unimolecular dissociations[12] to give $C_2H_2^+$ and C_2H^+; C_2H_2 from ethylene by the reaction[12] $C_2H_3^+ + C_2H_4 = C_2H_5^+ + C_2H_2$ and the charge transfer† $C_2H_2^+ + C_2H_4 = C_2H_4^+ + C_2H_2$; H_2 from ethane[3] by the dissociation to give $C_2H_4^+$, $C_2H_3^+$, $C_2H_2^+$, and C_2H^+; CH_4 from ethane[3] by the reaction $C_2H_3^+ + C_2H_6 = C_3H_5^+ + CH_4$; and H_2 and CH_4 from propane by the dissociations which give $C_3H_6^+$, $C_3H_5^+$, $C_3H_4^+$, etc., and $C_2H_4^+$ and $C_2H_2^+$.

In the foregoing selection, all observed pertinent ion-molecule reactions are included. Neutralization of fragment ions or parent molecule ions is uniformly excluded. CH_5^+-ion neutralization is a unique case in that the neutralized species has an extra, nonbonded hydrogen to begin with, so that detachment of H_2 rather than H may be different from the case of fragment ions or parent molecule ions.

The values calculated on this basis show a striking correlation with the observed values. It is a consequence of this correlation (unless the agreement is purely fortuitous) than un-ionized excited states, produced by electron impact, contribute little to the above molecular yields.

The agreement shown here supports the validity of such calculated values. The major uncertainty concerns the identification of the fragmentation pattern for 70-v electrons with the pattern obtained in an irradiation where the electron degradation spectrum includes all energies up to E_0, the energy of the incident primaries. Experiments[18] covering a limited energy range, show that the fragmentation pattern does not undergo major change with increase in electron energy above 30 v. Thus the 70-v pattern may be representative of

that produced by electrons over a somewhat broader energy range. The distribution of fragment ions changes drastically as the electron energy falls below about 30 v and approaches the appearance potentials of the fragments. The secondary electron spectrum[19] does consist, to a large extent, of low-energy electrons, but those below about 10 v do not result in positive ion formation. And the smaller number of electrons in the long high-energy tail of this spectrum produces many ionizations as the degradation proceeds, so that a large part of the ionization is produced by electrons with energies above 30 v. But it is difficult to say exactly how large the contribution to ionization may be by 10- to 30-v electrons. If this contribution exceeds about 15%, the correlation is probably fortuitous.

A less serious question concerns the competition between unimolecular dissociation and ion molecule reaction of the parent ion. The case of ethylene is a matter of contention, but for ethane, propane and more complex alkanes the dissociation competes favorably[20] with ion-molecule reaction of the parent ion.

* Based on work performed under the auspices of the U. S. Atomic Energy Commission.

† *Added in Proof:* Recent results of C. E. Melton and P. S. Rudolph, kindly sent to us in advance of publication, show clearly that the charge transfer does not compete with ion-molecule reactions of $C_2H_2^+$ to form $C_2H_3^+$ and $C_3H_3^+$. The $C_2H_3^+$ will give acetylene; the ultimate fate of the $C_3H_3^+$ is not certain.

[1] J. H. Futrell, J. Am. Chem. Soc. **81**, 5921 (1959).
[2] G. G. Meisels, W. H. Hamill, and R. R. Williams, Jr., J. Phys. Chem. **61**, 1456 (1957).
[3] L. M. Dorfman, J. Phys. Chem. **62**, 29 (1958).
[4] W. H. T. Davison, (The Chemical Society, London, 1958), Special Publication No. 9, pp. 151–164.
[5] K. Yang and P. J. Manno, J. Am. Chem. Soc. **81**, 3507 (1959).
[6] R. A. Back and N. Miller, Trans. Faraday Soc. **438**, 911 (1959).
[7] W. S. Guenther, T. J. Hardwick, and R. P. Nejak, J. Chem. Phys. **30**, 601 (1959).
[8] R. A. Back (private communication, to be published).
[9] S. C. Lind and D. C. Bardwell, J. Am. Chem. Soc. **48**, 2335 (1926).
[10] F. W. Lampe, J. Am. Chem. Soc. **79**, 1055 (1957).
[11] L. M. Dorfman (unpublished work).
[12] F. W. Lampe, Radiation Research **10**, 691 (1959).
[13] M. C. Sauer, Jr., and L. M. Dorfman, Abstracts, 137th Meeting Am. Chem. Soc., April, 1960.
[14] K. Yang and P. J. Manno, J. Phys. Chem. **63**, 776 (1959).
[15] W. P. Jesse and J. Sadauskis, Phys. Rev. **97**, 1668 (1955).
[16] D. O. Schissler and D. P. Stevenson, J. Chem. Phys. **24**, 926 (1956).
[17] F. H. Field, J. L. Franklin, and F. W. Lampe, J. Am. Chem. Soc. **79**, 2419 (1957).
[18] D. P. Stevenson and J. A. Hipple, J. Am. Chem. Soc. **64**, 1588 (1942).
[19] J. L. Magee and M. Burton, J. Am. Chem. Soc. **73**, 523 (1951).
[20] D. P. Stevenson, Radiation Research **10**, 610 (1959).

Spectrum of K_2ReCl_6

J. C. Eisenstein

National Bureau of Standards, Washington, D. C.

(Received February 22, 1960)

Stephens and Drickamer[1] have recently reported observing a pressure-induced peak in the absorption spectrum of K_2ReCl_6 at 16 100 cm^{-1}. Peaks at 14 200 and 15 700 cm^{-1} were already known to exist, and have been interpreted by Jørgensen[2] as due to transitions from the $^4A_2$ ground state to ^2E, $^2T_1$ or $^2T_2$ states. If the ligand field has cubic symmetry, and if off-diagonal elements of the interaction matrices are neglected, both the ^2E and $^2T_1$ states lie $9B+3C$ above the ground state. B and C are the Racah[3] parameters. Off-diagonal elements remove the degeneracy of the two states.

Stephens and Drickamer suggested that the third peak might be due to transitions from $^4A_2$ to a $^2T_2$ state whose separation from $^4A_2$ is $15B+5C$ if off-diagonal elements are neglected. However, even if one takes a sanguine view of the effect of perturbations on the relative positions of ^2E, $^2T_1$, and $^2T_2$ it is unlikely that these three levels all lie near one another.

It is possible that the new peak is also due to a transition to a $^2T_1$ state. States whose orbital designation is $^2T_1$ are contained in both the Γ_6 and Γ_8 representations of the complete Hamiltonian (inclusive of spin). The perturbations due to other states will be slightly different for the two representations. Consequently the $^2T_1$ level will be split.

A trial calculation was made with $B=711$ cm^{-1}, $C=3200$ cm^{-1}, and roughly estimated values for the other relevant parameters. The following results were obtained for the positions of the levels of interest here.

$2E$	14 983 cm^{-1}
$^2T_1(\Gamma_8)$	15 243
$^2T_1(\Gamma_6)$	16 038.

Despite the respectable agreement of theory and experiment it seems much more likely that the transitions in question are all to $^2T_2$ states. If the ligand field has strict cubic symmetry there are two of these. One belongs to the Γ_7 representation that is spanned by the complete wave functions, the other to the Γ_8 representation. Again one can expect a splitting of the two states because these states belong to different representations. The values of B and C required to put these states near 16 000 cm^{-1} are close to the values used by Moffitt *et al.*[4] in their interpretation of the absorption spectra of ReF_6, OsF_6, IrF_6, and PtF_6.

A difficulty with this interpretation is that there are only two low-lying $^2T_2$ states, whereas three absorption peaks are observed. However, the $^2T_2$ state which belongs to the Γ_8 representation will probably be split by a ligand or crystal field of low symmetry. It is interesting to note, in this connection, that the third peak only appears when pressure is applied to a crystal of K_2ReCl_6. This fact suggests that the interpretation given here is the correct one, and also that the fields of low symmetry in the uncompressed crystal are small.

I am indebted to Irene Stegun and Ruth Zucker, who did the numerical calculations for me.

[1] D. R. Stephens and H. G. Drickamer, J. Chem. Phys. **30**, 1364 (1959).
[2] C. K. Jørgensen, Acta Chem. Scand. **9**, 710 (1955).
[3] G. Racah, Phys. Rev. **62**, 438 (1942).
[4] Moffitt, Goodman, Fred, and Weinstock, Mol. Phys. **2**, 109 (1959).

Photochromotropism of *gamma*-(2,4-Dinitrobenzyl)-Pyridine in Solution

HARRY S. MOSHER AND CLARK SOUERS

Department of Chemistry and Chemical Engineering, Stanford University, Stanford, California

AND

R. HARDWICK

Department of Chemistry, University of California, Los Angeles, California

(Received February 22, 1960)

THE striking photochromotropic property of crystalline *alpha*-(2,4-dinitrobenzyl)pyridine, which was discovered by Chichababin *et al.*,[1] has recently been shown[2] to be characteristic also of the solutions of the compound under certain conditions. The fact that this phenomenon is shown in solution reveals that the underlying cause is molecular in nature and not solely a property of the crystalline state.

We have begun an investigation of analogous compounds in order to determine: (1) if the effect is much more widespread than has been commonly realized; (2) if it can be associated with any particular molecular structure and; (3) if the mechanism of the effect can be elucidated more fully. This note is a preliminary report on one other such compound.

Chichababin investigated various analogs without finding another substance showing phototropic behavior. During this process he prepared the γ isomer of (2,4-dinitrobenzyl)pyridine and reported that it too was devoid of photochromic properties. We have repeated the preparation of this compound and find that, although the *crystalline solid* indeed is inactive, alcohol *solutions* at lower temperatures turn a deep violet color on exposure to radiation in the blue and ultraviolet regions. For example, a solution of a few milligrams of the compound in 10 ml of a 1:1 mixture of absolute ethanol-*t*-butyl alcohol turns a faint purple in sunlight at room temperature; when the solution is slightly cooled, a deeper color results. At $-180°$, irradiation of an ethanol glass gives intense purple color. The maximum absorption of an irradiated alcohol solution of the γ isomer falls at about 575 mμ and is somewhat more stable than the corresponding 568 mμ peak of the α compound. In the dark, all of these solutions fade rapidly when warmed.

Although the lack of photochromism in the crystalline γ isomer indicates that a special mechanism may make the behavior of crystals of the α isomer unique, a more general mechanistic conclusion may be drawn from the results in solution. The original proposal of Chichababin that the colored α isomer was formed by a shift of a hydrogen from the methylene bridge to the ring nitrogen can hold for the γ isomer only if the the process I→II is bimolecular, since the γ configuration precludes the unimolecular process,

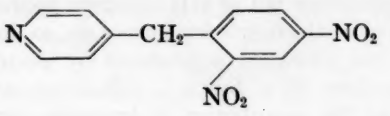

I

⇅

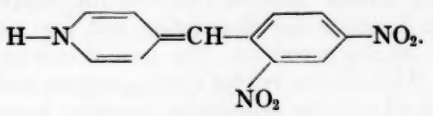

II

If, as one might suppose, solutions of the colored γ isomer fade with the same unimolecular kinetics which we have found[3] for the α form, then the process III→IV seems an attractive alternative.

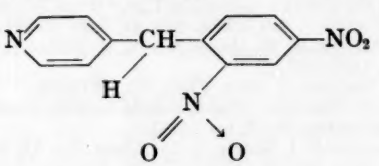

III

Colorless

⇅

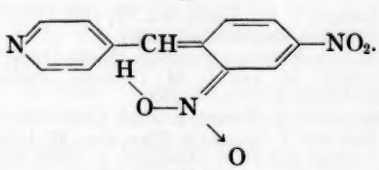

IV

Colored

Since the hydrogen transfer in III⇄IV may take place via a six-membered ring, this process can easily be unimolecular. This reaction, which involves a nitro group and results in the conjugation of the two aromatic rings, should give a product whose spectra closely resemble that of the methylene base[4] as we have indeed observed.

We are now engaged in a flash photolysis study of the kinetics of the bleaching reaction in various solvents and are continuing our search for analogous compounds that may show the characteristic photochromic behavior in solution.

One of us, CS, wishes to acknowledge his indebtedness to the United States National Science Foundation for support via its Undergraduate Summer Research Program.

[1] A. E. Chichababin, B. Kuindshi, and S. V. Benevalenskii, Ber. **588**, 1580 (1925).
[2] R. Hardwick, H. S. Mosher, and P. Passailaigue, Trans. Faraday Soc. **56**, 44 (1960).
[3] R. Hardwick, H. S. Mosher and David Benhur (to be published).
[4] W. C. Clark and G. P. Lothian, Trans. Faraday Soc. **54**, 1790 (1958).

Ionization Potentials of B_5H_9, B_5H_8I, $B_{10}H_{14}$, and $B_{10}H_{13}C_2H_5$ from Electron Impact Studies

JOHN L. MARGRAVE

Department of Chemistry, University of Wisconsin Madison, Wisconsin

(Received February 23, 1960)

THE ionization potential for the simplest boron hydride, B_2H_6 has been reported as 12.1±0.2 ev by Margrave,[1] and as 11.9±0.1 ev by Koski and coworkers[2] from mass-spectrometric appearance potential studies. In addition, the ionization potential has been set between 11 and 12 ev by the vacuum ultraviolet absorption spectrum of Price.[3] Because of the more complicated structures of the higher boron hydrides, it is of interest to establish their ionization potentials for comparison with B_2H_6.

The modified Consolidated Model 21-103B mass spectrograph of the Callery Chemical Company was used in this work. The same techniques for measurement and plotting of data were applied as in previous studies of BF_3, $B(CH_3)_3$, etc.[1,4] The appearance potential was obtained from semilog plots of ion current vs voltage, with Ne, Ar, and Xe as calibrating gases.

Samples of high-purity boron hydrides were made available from the Callery Chemical Company and were used without further treatment. In all cases the patterns obtained on routine traces at 70 ev energies agreed with established standard patterns. These materials have extremely complicated mass spectra because of the many possibilities of B^{10} and B^{11} combinations, and the possibility of forming a series of ions differing by only one mass unit as hydrogens are removed. The mass spectrum of pentaborane has been reported.[5] Shapiro and Keilin have also reported typical patterns for boranes.[6] In the present work appearance potentials were determined for the heaviest ion peak of each molecule that could only be associated with the completely B^{11}-substituted molecule, and could not show interferences from overlapping lighter ions. As the ionizing voltages were decreased, the mass patterns tended toward those of the parent ions with the relative abundances as predicted for a B^{11}/B^{10} isotope ratio of about 4.0 by standard calculations.[7]

TABLE I.

Boron hydride	Ionization potentials (ev)	References
B_2H_6	12.1, 11.9, 11–12	1, 2, 3
B_2D_6	12.1	2
B_5H_8I	11.1±0.5	This work
B_5H_9[a]	10.8±0.5	This work
$B_{10}H_{14}$[a]	11.0±0.5	This work
$B_{10}H_{13}C_2H_5$	9.0±0.5	This work

[a] In a private communication, V. H. Dibeler of the National Bureau of Standards, Washington, D. C. has cited unpublished work of R. M. Reese of the NBS which yields $I(B_5H_9)=10.9\pm0.5$ ev and $I(B_{10}H_{14})\approx10.7$ ev in agreement with the data reported here.

The ionization potentials determined are listed in Table I.

The author wishes to acknowledge the cooperation of the research staff of the Callery Chemical Company in this work.

[1] J. L. Margrave, J. Phys. Chem. **51**, 38 (1956).
[2] W. S. Koski, J. Kaufman, C. F. Pachucki, and F. J. Shipko, J. Am. Chem. Soc. **80**, 3202 (1958).
[3] W. C. Price, J. Chem. Phys. **16**, 894 (1948).
[4] R. W. Law and J. L. Margrave, J. Chem. Phys. **25**, 1086 (1956).
[5] V. Dibeler, F. Mohler, L. Williamson, and R. Reese, J. Research Natl. Bur. Standards **43**, 97 (1949).
[6] B. Keilin and I. Shapiro, Olin Mathieson Tech. Rept. MCC-1023-TR-165 (1955).
[7] R. B. Polansky and J. L. Margrave, University of Wisconsin (unpublished work).

Photodissociation in the Schumann-Runge System of Oxygen

D. W. O. HEDDLE

Physics Department, University College, London, England

(Received February 26, 1960)

A DETERMINATION of the band oscillator strengths of the Schumann-Runge system of oxygen has been reported by Ditchburn and Heddle.[1] The published oscillator strengths were computed from measured absorption data by assuming that the dispersion-form breadth of the lines was due to radiation damping. The demonstration by Wilkinson and Mulliken[2] that predissociation broadening occurs certainly in the (12,0) band and probably in other bands invalidates this assumption of constant, calculable line breadth. Absorption strengths of the Schumann-Runge bands have recently been determined by Bethke[3] under conditions of severe pressure broadening that reduce the effects of natural broadening and spectrometer resolving power to a negligible degree. Absolute Frank-Condon factors for the system are now available[4] and have been used by Bethke to obtain the electronic oscillator strength. These experimental[3]

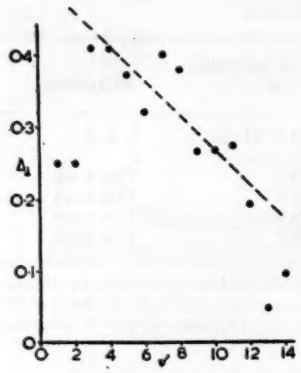

FIG. 1. Dispersion-form breadths of lines in the (v', 0) progression of the Schumann-Runge system. ord: line breadth Δ_d in cm^{-1}; abs: vibrational quantum number v'.

and theoretical[4] results can be used to derive true line breadths from the measurements of Ditchburn and Heddle.[1] From Fig. 3 of their paper it is clear that the oscillator strength computed for a line showing a given peak absorption will depend inversely on the assumed damping ratio provided that this damping ratio is greater than 10^{-4}. The dispersion-form breadth is related to the damping ratio by the equation

$$\Delta_d = [\Delta_D/(\ln 2)^{\frac{1}{2}}]\rho\gamma$$
$$= 0.14\rho_d \text{ cm}^{-1}$$

where Δ_d and Δ_D are the dispersion-form and Doppler breadths, respectively, and ρ_d is the damping ratio.

Values of Δ_d are shown in Fig. 1. These values are subject to a systematic uncertainty of $\pm 25\%$ because of uncertainty in the true resolving power of the spectrograph. The general increase of line breadth towards low values of v' is probably due to collision damping because the pressure required for observation of a band is greater at low v'. It does not seem probable that the sudden increases between $v'=2$ and $v'=3$ and between $v'=13$ and $v'=12$ can be due to this effect alone and taken in conjunction with other evidence[2] supports the view that predissociation occurs for the (3,0) through (12,0) bands. If this explanation is correct we can estimate the line breadth due to predissociation as approximately 0.15 cm^{-1} with an upper limit of 0.25 cm^{-1}. This limit corresponds to a lifetime against predissociation of 2×10^{-11} sec that can be compared with the radiative lifetime of 2.5×10^{-9} sec to assess the probability of predissociation as about 99%. Similar values are obtained from measurements of Fig. 2 of the paper by Wilkinson and Mulliken.[2]

Nicholls[5] has estimated the probable accuracy of the Frank-Condon factors as about 20% and Bethke's results do not, therefore, resolve the uncertainty in the value of the oscillator strength of the Schumann-Runge transition. Values obtained by various methods are listed in Table I. The absorption coefficients at five wavelengths in the continuum have been measured by James[6] using a double-beam photoelectric method. These values are consistent with an oscillator strength somewhat greater than 0.20.

I wish to thank Professor R. W. Ditchburn whom I have consulted with regard to this note. I gratefully acknowledge correspondence with Professor R. W. Nicholls and Dr. P. G. Wilkinson.

TABLE I. Oscillator strength of the $B\,^3\Sigma_u^- \leftarrow X\,^3\Sigma_g^-$ transition in O_2.

Oscillator strength	Wave number of centroid (cm^{-1})	Method of determination
0.161	68 430	Absorption in continuum (photoelectric)[a]
0.177		Absorption in continuum (photoelectric)[b]
0.193		Absorption in continuum (photographic)[c]
0.202	68 100	Dispersion of oxygen[d]
0.215	68 330	Absorption in continuum (photographic)[e]
0.230	68 370	Electron scattering[f]

[a] K. Watanabe, E. C. Y. Inn, and M. Zelikoff, J. Chem. Phys. **21**, 1026 (1953).
[b] W. A. Rense and R. Mercure, Bull. Am. Phys. Soc. **30**, (January 27, 1955).
[c] R. Ladenburg and C. C. Van Voorhis, Phys. Rev. **43**, 315 (1933).
[d] R. Ladenburg and G. Wolfson, Z. Physik. **79**, 42 (1932).
[e] R. W. Ditchburn and D. W. O. Heddle, Proc. Roy. Soc. (London) **A220**, 61 (1953).
[f] E. N. Lassetre, S. Silverman, and M. E. Krasnow, Phys. Rev. **95**, 635 (1954).

[1] R. W. Ditchburn and D. W. O. Heddle, Proc. Roy. Soc. London **A226**, 509 (1954).
[2] P. G. Wilkinson and R. S. Mulliken, J. Appl. Phys. **125**, 594 (1957).
[3] G. W. Bethke, J. Chem. Phys. **31**, 669 (1959).
[4] R. W. Nicholls, P. A. Fraser, and W. R. Jarmain, Combustion and Flame **3**, 13 (1959).
[5] R. W. Nicholls (private communication).
[6] J. F. James, thesis, Reading 1957.

Sedimentation of Polydisperse Macromolecules

PREM R. GUPTA*
Department of Chemistry, McGill University
AND
D. A. I. GORING
Pulp and Paper Research Institute, Montreal

WE have observed an interesting and hitherto unreported anomaly in the ultracentrifugal analysis of certain alkali lignins.[1] Maximum-ordinate sedimentation coefficients (s_m) when measured on the same fraction at different centrifugal fields differed by as much as an order of magnitude.

Runs were done in a Spinco ultracentrifuge at 12 600 rpm and 52 600 rpm corresponding to fields of 11.5×10^3 g and 200×10^3 g, respectively. In all cases a single clear-cut maximum was found in the gradient diagram but peaks did not leave the meniscus completely. Sedimentation coefficients s_{m1} and s_{m2} (at 12 600 and 52 600 rpm, respectively) were obtained by the usual linear

plot of the logarithmic displacement of the maximum ordinate against time. The concentration dependence was found to be small for s_{m1} and negligible for s_{m2}. All runs were then made at a concentration of 0.5 ($\pm$0.02) g/deciliter.

In various fractions, the range of s_{m1} was 5S to 28S while s_{m2} varied only from 2S to 3S. Detailed distribution analyses based on peak spreading indicated that in any one fraction, the true sedimentation coefficients of the components could range from 0.5S to over 100S. As shown in Fig. 1 the ratio s_{m1}/s_{m2} increased with increase in the root-mean-square deviation σ of the true sedimentation coefficients from the weight-average sedimentation coefficient. This behavior differs considerably from the constancy of s_m with change in field found for certain naturally occurring polymers.[2] It also emphasizes the well-known uncertainty in using the movement of the maximum ordinate to calculate the sedimentation coefficient.

Our studies have shown alkali lignin to be a highly polydisperse, water-soluble, degraded product of lignin in wood.[3] The molecule is rather compact, giving the small dependence of s_m on concentration. Such a system would be expected to contain very small and very large particles. In sedimentation, the small particles conform to the Archibald solution of the Lamm equation in which no maximum is found, and the gradient slopes down from the meniscus, decreasing as the run proceeds. The large particles would obey Faxen's solution in which the characteristic Gaussian peak moves away from the meniscus and down the cell. The pattern observed will consist of a super-position of many such types of gradient distribution. The relative number of particles that conform to Faxen's solution will depend on the centrifugal field. At low rotor speeds the peak will be made up of high-molecular-weight material giving a large s_{m1}. At higher speeds, the more slowly sedimenting components will contribute to the peak, thereby causing s_{m2} to be small. The effect would be expected to be greater the greater the polydispersity of the sample, and this is confirmed by the increase of s_{m1}/s_{m2} with σ in Fig. 1.

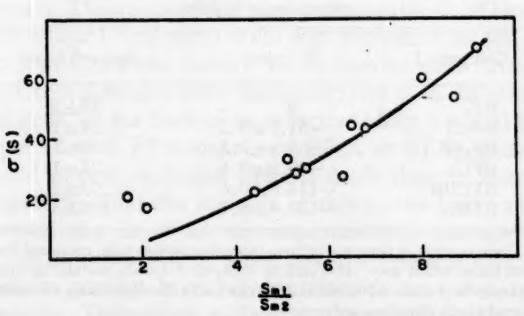

FIG. 1. Increase of ratio s_{m1}/s_{m2} with increase in σ.

The validity of the above explanation was tested by comparing over a range of rpm maximum-ordinate sedimentation coefficients for alkali lignin and Armour's bovine serum albumin. For the alkali lignin (Table I) s_m increased markedly at low fields in contrast to the relatively constant values found for the monodisperse serum albumin. These data support the view that the previously noted differences in s_{m1} and s_{m2} are due to the polydispersity of the alkali lignin. Thus, the phenomenon will probably be of general occurrence and should be found in any widely polydisperse system in which the concentration dependence of s_m is small (e.g., glycogen).[4]

TABLE I. Variation of sedimentation coefficient with field for 0.5% serum albumin and alkali lignin in $NaHCO_3$-NaOH buffer (ρH=9.65; $\Gamma/2$=0.1). Temperature=26°C.

Serum albumin		Alkali lignin	
Field (1000 g)	s_m(S)	Field (1000 g)	s_m(S)
260	4.9	260	2.0
113	4.7	202	2.0
56	4.7	113	2.1
30	4.6	30	3.9
11.5	4.5	11.5	8.4

In a recent theoretical paper, Fujita and MacCosham[5] presented an approximate solution to the Lamm equation for homogeneous solutes of intermediate molecular size. These authors proposed that the sedimentation coefficient can be computed approximately from the movement of the maximum ordinate for monodisperse particles sedimenting under conditions such that the peak does not move completely away from the meniscus. The data for serum albumin in Table I support this prediction because there was no layer of pure solvent between the boundary and the meniscus for fields of 56 000 g and under. Extension of the treatment of Fujita and MacCosham[5] to polydisperse systems might elucidate the observed changes in s_m and might permit a rapid determination of polydispersity based on the easily measured changes of s_m with centrifugal field.

The authors wish to thank Dr. R. F. Robertson for the use of the ultracentrifuge.

* Holder of a studentship from the National Research Council of Canada. Present address: Indian Aluminium Company, Ltd., Calcutta, 16, India.

[1] P. R. Gupta, R. F. Robertson, and D. A. I. Goring, Can. J. Chem. **38**, 259 (1960).
[2] D. A. I. Goring and C. Chepeswick, J. Phys. Chem. **60**, 506 (1956).
[3] P. R. Gupta and D. A. I. Goring, Can. J. Chem. **38**, 270 (1960).
[4] W. A. J. Bryce, C. T. Greenwood, and I. G. Jones, J. Chem. Soc. **1958**, 3845.
[5] H. Fujita and V. J. MacCosham, J. Chem. Phys. **30**, 291 (1959).

Possible Ion-Molecule Reaction in the Gamma Radiolysis of C_3 Hydrocarbons

KANG YANG

Radiation Laboratory, Continental Oil Company, Ponca City, Oklahoma

(Received February 8, 1960)

IN this note experimental evidence is presented showing that radiolysis of gaseous hydrocarbons may involve ion-molecule reactions of the hydride-ion transfer type

$$C_2H_5^+ + C_mH_n \rightarrow C_2H_6 + C_mH_{n-1}^+. \quad (1)$$

Field and Lampe[1] reported occurrences of these reactions with various ions in a mass spectrometer at slightly elevated pressure. The importance of such reactions in the radiolysis of hydrocarbons has been shown very clearly in two recent publications.[2,3] Lampe[2] demonstrated how isobutene, while still producing a free radical with a G value of 3.7, could undergo radiation-induced polymerization by an ionic mechanism[4,5] based on the reaction

$$i\text{—}C_4H_8^+ + i\text{—}C_4H_8 \rightarrow C_4H_9^+ + C_4H_7. \quad (2)$$

Futrell[3] succeeded in explaining quantitatively the product distribution in the radiolysis of n-hexane by assuming the extensive occurrence of reactions of the type (1) together with various free-radical processes.

Reactions of the same type seem to explain the relative yields of ethane, recently obtained in this laboratory, for the radical-free radiolysis of gaseous propane, propylene, and cyclopropane.[6] In Table I, $G(C_2H_6)$ values in the nitric-oxide inhibited radiolysis of C_3 hydrocarbons were compared with the percent intensity of the $C_2H_5^+$ ion in the mass spectra[7] of corresponding hydrocarbons. The $G(C_2H_6)$ in the radiolysis of propane-nitric oxide system was constant within the range of energy absorption, $(0.2 \leftrightarrow 2) \times 10^{21}$ ev/g of propane. As much as 2×10^{21} ev/g of energy was given to propylene-nitric oxide and cyclopropane-nitric oxide systems, but ethane formation was negligible.

A simple explanation for the results described in Table I is that reaction (1) plays a predominant role in the formation of ethane by nonradical processes. It should further be noted that the $C_2H_5^+$ ion is the major peak in the mass spectrum of propane; thus, one would predict ethane to be the major product in the radical-free radiolysis of propane in accordance with the experimental observation.[6]

TABLE I. $G(C_2H_6)$ in the nitric-oxide inhibited radiolysis of C_3-hydrocarbons and percent intensity of $C_2H_5^+$ ion.

Comp. irradiated	$G(C_2H_6)$ Molecules/100 ev	Percent intensity of $C_2H_5^+$ ion
$CH_3CH_2CH_3$	1.5	30.8
$(CH_2)_3$	0.0	0.1
$CH_3CH{=}CH_2$	0.0	0.0

[1] F. H. Field and F. W. Lampe, J. Am. Chem. Soc. **80,** 5587 (1958).
[2] F. W. Lampe, J. Phys. Chem. **63,** 1986 (1959).
[3] J. H. Futrell, J. Am. Chem. Soc. **81,** 5921 (1959).
[4] E. Collinson, F. S. Dainton, and H. A. Gills, J. Phys. Chem. **63,** 909 (1959).
[5] W. H. T. Davison, S. H. Pinner, and R. Worrall, J. Polymer Sci. **252,** 187 (1959).
[6] Experimental conditions and procedures were similar to those described in K. Yang and P. J. Manno. J. Am. Chem. Soc. **81,** 3507 (1959).
[7] *Catalog of Mass Spectral Data*, A.P.I. Project **44,** Carnegie Institute of Technology, Pittsburgh, Series Nos. **3, 24,** and **115.**

NMR Studies on Mixed Boron Halides. Detection of the New Halide BBrClF*

T. D. COYLE† AND F. G. A. STONE

Department of Chemistry, Harvard University, Cambridge, Massachusetts

(Received March 4, 1960)

IN the course of studies on compounds in which two or more different halogens are bonded to a central atom, we have been particularly concerned with mixed boron halides. A recent study[1] of exchange reactions in phosphorus halide and ester systems, using the nuclear magnetic-resonance technique, prompts us to adumbrate our results on the F^{19} NMR spectra of boron halide mixtures.

Although binary mixtures of boron trihalides equilibrate to form mixtures of all possible halides, rapid disproportionation to the symmetrical BX_3 compounds prevents isolation of the mixed species.[2] Nevertheless, these systems may be investigated by techniques which do not perturb the labile equilibria. The vibrational spectra of some of the mixed boron halides have been reported,[3] and infrared and Raman spectroscopy have been used to evaluate equilibrium constants[4,5] and reaction rates.[6]

TABLE I. F^{19} chemical shifts and B^{11}-F spin coupling constants for mixed boron halides.

Compound	δ[a] (ppm)	$J_{B^{11}-F^{19}}$[b] (cps)
BF_3	0	15±2
BF_2Cl	−51.5±0.2	34±1
BF_2Br	−68.4±0.3	56±1
$BFCl_2$	−99.0±0.6	74±1
$BFClBr$	−114.8±0.6	92±2
$BFBr_2$	−130.4±0.7	108±3

[a] Chemical shift in parts per million, increasing to high field, measured from chart traces which were calibrated by applying a known modulating audio frequency to produce sidebands on all major peaks. Average values for several sweeps in both directions are reported.
[b] Average peak-to-peak separations in the quartets. Error limits are standard deviations of the measurements.

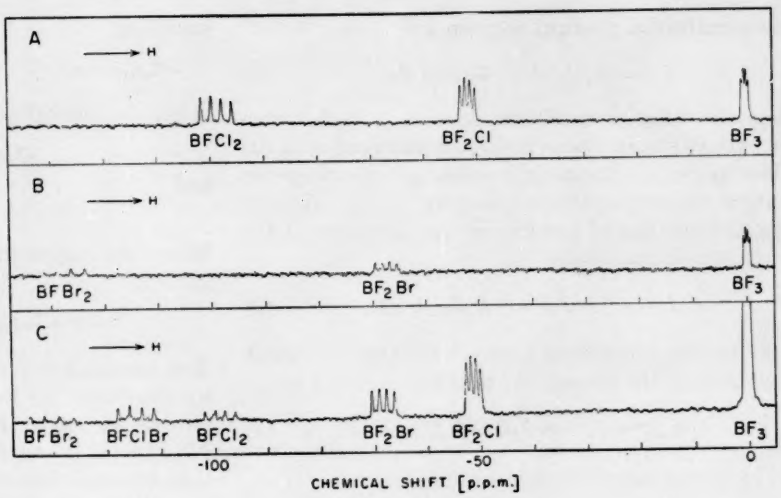

FIG. 1. F^{19} NMR spectra of boron halide mixtures. A: BF_3 (19%)+BCl_3 (81%); B: BF_3 (19%)+BBr_3 (81%); C: BF_3 (38%)+BCl_3 (25%)+BBr_3 (37%).

These equilibria can also be studied by the nuclear magnetic resonance technique. Figure 1 shows typical F^{19} NMR spectra of binary mixtures of BF_3 with BCl_3 and BBr_3, and of a ternary mixture. The particular spectra shown were recorded at room temperature using a Varian V-4300B NMR spectrometer operating at 40 Mcs. In the BF_3–BCl_3 and the BF_3–BBr_3 mixtures, three quartets typical of compounds containing B—F bonds are observed, corresponding to BF_3 and the expected mixed species. In the ternary system (C, Fig. 1) the strong resonance due to BF_3 is accompanied by four quartets which may be correlated with those observed in the binary mixtures. The sixth quartet that appears in the ternary mixture must be attributed to the expected but hitherto unreported BBrClF.

The position of the BF_3 resonance has been previously established,[7] and the assignment of the BBrClF peak is unequivocal. Assignment of the remaining F^{19} resonances has been made on the basis of variations of intensity with BF_3 concentration, shifts of RBF_2 and R_2BF compounds,[7] and the position of the BBrClF peak. Chemical shifts, relative to the BF_3 resonance, vary slightly with concentration. Values for the ternary mixture (C, Fig. 1) are given in Table I.

The shifts to lower field upon substitution of fluorine in boron trifluoride by chlorine or bromine are of special interest. Theoretical work[8] and experimental data[9] have shown that F^{19} chemical shifts may frequently be correlated with electron density at the fluorine atom. Since fluorine is normally more electronegative than the other halogens, on the basis of an inductive effect it would be expected that F^{19} resonance in BF_2X or BFX_2 species would appear at higher applied fields than in boron trifluoride. That the opposite of this occurs lends support to the idea[10] of the importance of mesomeric effects in boron halides, which should decrease in magnitude in passing from boron trifluoride to boron tribromide. Decreasing π-electron donation in the sequence F>Cl>Br is probably responsible for the Lewis acidity order $BBr_3>BCl_3>BF_3$,[11] recently the subject of a theoretical treatment.[12]

* We are indebted to the National Science Foundation for support of this work.

† Edwin W. Rice, Jr., Fellow of the General Electric Educational and Charitable Fund, 1959–1960.

[1] E. Fluck, J. R. Van Wazer, and L. C. D. Groenweghe, J. Am. Chem. Soc. **81**, 6363 (1959).
[2] L. H. Long and D. Dollimore, J. Chem. Soc. 1954, 4457.
[3] L. P. Lindeman and M. K. Wilson, J. Chem. Phys. **24**, 242 (1956).
[4] T. H. S. Higgins, E. C. Leisegang, C. J. G. Raw, and A. J. Rossouw, J. Chem. Phys. **23**, 1544 (1955).
[5] J. Goubeau, D. E. Richter, and H. J. Becker, Z. anorg. Chem. **278**, 12 (1955).
[6] R. E. Nightingale and B. Crawford, J. Chem. Phys. **22**, 1468 (1954).
[7] T. D. Coyle and F. G. A. Stone, J. Am. Chem. Soc. (to be published).
[8] A. Saika and C. P. Schlichter, J. Chem. Phys. **22**, 26 (1954).
[9] See, for example, J. A. Pople, W. G. Schneider, and H. J. Bernstein, *High-Resolution Nuclear Magnetic Resonance* (McGraw-Hill Book Company, Inc., New York, 1959).
[10] L. Pauling, *The Nature of the Chemical Bond* (Cornell University Press, Ithaca, New York, 1959), 3rd ed., p. 318.
[11] H. C. Brown and R. R. Holmes, J. Am. Chem. Soc. **78**, 2173 (1956).
[12] F. A. Cotton and J. R. Leto, J. Chem. Phys. **30**, 993 (1959).

Diffusion and Heterogeneous Reaction. III. Atom Recombination at a Catalytic Boundary*

HANS MOTZ† AND HENRY WISE

Department of Chemical Physics, Stanford Research Institute, Menlo Park, California

(Received January 11, 1960)

IN a preceding paper[1] the diffusion and heterogeneous reaction of labile species in a cylinder of finite length and catalytic activity were examined. Under steady-state conditions the number flux of particles i in the positive and negative directions relative to

the concentration gradient is given by[2]

$$J_i^{\pm}=\tfrac{1}{2}n_i(\tfrac{1}{2}c_i+w)\mp\tfrac{1}{2}D_i|\nabla n_i| \quad (1)$$

where the diffusion coefficient $D_i=\frac{1}{3}\lambda_i c_i$; λ_i the mean free path of species i with respect to collisions with the unlike species, c_i, the mean random velocity of species i, and w the mean particle transport velocity. Accordingly the net flux of particles in the direction of the concentration gradient is

$$J_i=J_i^{+}-J_i^{-}=-D_i\nabla n_i+n_i w. \quad (2)$$

If the species i represents atoms, a fraction γ of which recombines at the surface, the next flux of atoms is

$$J_1=J_1^{+}-J_1^{-}=\gamma J_1=-D_i\nabla_s n_1+n_1 w_s \quad (3)$$

and by proper substitution in Eq. (1)

$$n_1c_1\gamma/4=-D_1[1-(\gamma/2)]\nabla_s n_1+n_1w_s[1-(\gamma/2)]. \quad (4)$$

Equation (4) represents the boundary condition at a catalytic surface with a recombination coefficient γ, and the subscript s denotes the component normal to the boundary.

In the model chosen[1] the resultant mass flow is zero, and

$$m_1\mathbf{J}_1+m_2\mathbf{J}_2=0. \quad (5)$$

where m_1 is the atomic and m_2 the molecular mass. For a chemical reaction involving the recombination of two atoms with a diatomic molecule as a product $\mathbf{J}_1+2\mathbf{J}_2=0$, or

$$-D_1\nabla n_1+n_1w=2(D_2\nabla n_2-n_2w). \quad (6)$$

Since the total gas pressure is constant throughout

$$\nabla n_1+\nabla n_2=0 \quad (7)$$

and from Eq. (6)

$$w=[(D_1-2D_2)/(n_1+2n_2)]\nabla n_1. \quad (8)$$

By substitution into (4) one obtains for the boundary condition

$$-\nabla_s n_1=(n_1c_1\gamma)[2-(n_1/n)]/\{8D_{12}[1-(\gamma/2)]\} \quad (9)$$

where the interdiffusion coefficient D_{12} is defined[2] by

$$D_{12}\equiv(n_1D_2+n_2D_1)/n$$

and

$$n\equiv n_1+n_2.$$

When the concentration of atoms is small so that $n_1/n\ll 1$

$$-\nabla_s n_1\approx(n_1c_1\gamma)/\{4D_{12}[1-(\gamma/2)]\}. \quad (10)$$

This condition differs from the one cited in footnote 1 by the factor $1/[1-(\gamma/2)]$. As a result the dimensionless parameter δ should be modified to read $\delta\equiv 4D_{12}[1-(\gamma/2)]/\gamma c_1 R$. It is apparent that this correction becomes important for surfaces with large recombination coefficients. For $\gamma=0.2$ as observed for various metals[3] the correction amounts to 10%.

It should be noted that Eqs. (1) and (2) are derived on the assumption that the mean particle transport velocity is small compared with the random velocity. This assumption is justified when $n_1\ll(n_1+n_2)$. For high atom concentration more accurate transport equations might be required.

Also it can be shown that the diffusion equation in the presence of a catalytic boundary is of the form

$$\Delta n_1+(\nabla n_1)^2/(2n-n_1)=0. \quad (11)$$

A solution of this nonlinear differential equation has recently been published.[4] It shows that the linear form of the diffusion equation $\Delta n_1=0$ is a satisfactory approximation for $n_1/n_2<0.2$.

* One of us (HW) wishes to acknowledge sponsorship of this work by Project Squid, supported by the Office of Naval Research, Department of the Navy.

† International Fellow, summer 1959; present address: Oxford University, Oxford, England.

[1] H. Wise and C. M. Ablow, J. Chem. Phys. **29**, 634 (1958).
[2] J. Jeans *The Dynamical Theory of Gases* (Dover Publications, New York, 1954), p. 309.
[3] B. J. Wood and H. Wise, J. Chem. Phys. **29**, 1416 (1958).
[4] J. C. Greaves and J. W. Linnett, Trans. Faraday Soc. **55**, 1338 (1959).